UNIVERSITA' DEGLI STUDI DI SIENA
DIPARTIMENTO DI BIOTECNOLOGIE, CHIMICA E FARMACIA

DOTTORATO DI RICERCA IN
BIOCHEMISTRY AND MOLECULAR BIOLOGY BiBiM 2.0

CICLO XXXIV

COORDINATORE: PROF. Dr. LORENZA TRABALZINI

DNA-ENCODED CHEMICAL LIBRARIES: ADVANCES AND APPLICATIONS TO DRUG DIFFICULT TARGETS

SETTORE SCIENTIFICO-DISCIPLINARE: DRUG DISCOVERY

DOTTORANDO: ADRIÁN GIRONDA MARTÍNEZ

TUTOR: PROF. Dr. DARIO NERI

ANNO ACCADEMICO: 2021/2022

UNIVERSITA' DEGLI STUDI DI SIENA
DIPARTIMENTO DI BIOTECNOLOGIE, CHIMICA E FARMACIA

DOTTORATO DI RICERCA IN
BIOCHEMISTRY AND MOLECULAR BIOLOGY BiBiM 2.0

CICLO XXXIV

COORDINATORE: PROF. Dr. LORENZA TRABALZINI

TITOLO DELLA TESI: **DNA-ENCODED CHEMICAL LIBRARIES: ADVANCES AND APPLICATIONS TO DRUG DIFFICULT TARGETS**

SETTORE SCIENTIFICO-DISCIPLINARE : DRUG DISCOVERY

DOTTORANDO: ADRIÁN GIRONDA MARTÍNEZ

TUTOR: PROF. Dr. DARIO NERI

ANNO ACCADEMICO: 2021/2022

"Nothing in life is to be feared, it is only to be understood.
Now is the time to understand more, so that we may fear less"

Maria Salomea Skłodowska-Curie

To my beloved ones

This page is intentionally blank.

1. Summary

The discovery of small organic ligands or biologics capable of modulating biological processes remains one of the biggest challenges in developing new medicines. Different technologies have been implemented over the last decades to ease this process and make it more efficient. In this regard, encoded display technologies have played a major role in the discovery of new antibodies, peptides, and proteins. However, the efficient exploitation of automated high-throughput screening to discover small organic ligands has mainly been limited to big pharmaceutical companies. DNA-Encoded Chemical Libraries (DELs) have emerged as a powerful and cost-effective alternative to solve this issue. The technology has been established during the last 25 years and has become one of the best methods to synthesize and screen libraries of unprecedented size, promising a bright future in the early drug discovery stages.

DELs are collections of small molecules individually coupled to oligonucleotide fragments, serving as amplifiable identification barcodes. In the first part of this thesis new DEL designs, displaying molecules capable of targeting challenging therapeutic targets while keeping library-quality at the highest grade, were investigated. A novel single-pharmacophore library, termed AG-DEL, was synthesized. The library was constructed using split-and-pool procedures on single-stranded DNA. The modularity of this library design allowed the creation of different dual-pharmacophore libraries in an encoded self-assembling chemical library format (ESAC 2+1 and ESAC Plus). Furthermore, the new AG-DEL facilitated the use of novel screening methodologies (e.g., photo-crosslinking) to efficiently discover new small organic ligands.

DEL synthesis mainly relies on the chemical diversity of building blocks and the efficiency of the chemical reactions to link them. Following this trend, many different groups have made great efforts during the last years to develop new mild and efficient DNA-compatible reactions. One of the most used reactions for DEL synthesis is the amide bond formation, thanks mainly to various reliable reaction protocols and the big commercially available collections of amino acids. Nevertheless, the current availability of DNA-compatible post-functionalization of amino acids is still quite limited due to some restrictions inherent to the presence of the DNA. In the second part of this thesis, a new DNA-compatible diazo-transfer reaction was successfully optimized and implemented. This reaction has shown to be efficient, both in reaction times and reaction yields, as well as to be mild and fully compatible with DNA, as demonstrated by subsequent enzyme-mediated ligation of the oligonucleotide template to a new fragment, and has served for the synthesis of new ESAC Plus libraries within our group.

The modulation of protein-protein interactions (PPIs) represents another formidable challenge. These interactions are often characterized by large and flat protein surfaces that are composed of many different interacting groups. Therefore, these interactions are usually targeted using large macrocyclic peptides or antibodies. Notwithstanding this challenge, some examples have been reported during the last years in which small organic ligands or peptidomimetics were specifically designed for targeting this class of proteins. Some of these examples have successfully reached clinical trials and even marketing authorization, showing the critical importance of PPI modulators and indicating broad prospects.

In PPI modulation, the discovery of ligands targeting cytokines is even more challenging, due to the small size and particularly flat surface of these proteins. Nevertheless, different small molecule ligands targeting cytokines have been described over the years. Among all these proteins, Interleukin-2 (IL2) represents one of the best examples. IL2 is a pro-inflammatory cytokine, that plays a crucial role in immunity, and different therapeutic approaches using IL2 are increasingly being used for the treatment of a variety of malignancies, like melanoma and renal cell carcinoma. However, the use of IL2 has been limited due to strong side effects related to the high doses of cytokine necessary to achieve a pharmacological effect. Side effects have been linked to the release of pro-inflammatory cytokines as well as to CD25-mediated endothelial damage induced by IL2 binding to endothelial surface receptors, leading to a vascular leak syndrome. The interaction between IL2 and its alpha subunit receptor (IL2Rα or CD25) activates immunosuppressive regulatory T cells (T$_{regs}$) and reduces its antitumor activity. Thus, avoiding the formation of the multimeric IL2/IL2R complex can enhance the antitumor response.

The last chapter of this thesis was focused on the development of novel DEL-derived IL2 ligands capable of interacting at the CD25 binding domain of IL2. During these studies, a tumor-targeting antibody-IL2 fusion protein, L19-IL2, was used to find ligands masking the IL2 moiety. The ligands were optimized by a medicinal chemistry approach and characterized by fluorescence polarization. Furthermore, the best ligand showed binding at the CD25 binding epitope of IL2, as evidenced by competition experiments using an anti-IL2 antibody. The use of one of the discovered compounds or an affinity matured derivative can allow the generation of a new class of biopharmaceutical-small molecule complexes that localize at the site of the disease and regain activity of the cytokine only at the tumor site.

2. Introduction

Understanding the origin of diseases represents a scientific challenge that implies a perfect knowledge of all the biological processes. Despite over the last decades, the scientific community has made tremendous progress on understanding the biology of all organisms, most of the interactions and processes are still not well characterized. Moreover, diseases caused by the interaction of other organisms with the human body steps up one level of complexity due to the necessity of understanding both the human and pathogen biology and the interactions between them.[1,2]

Drugs are exogenous agents able to modify temporarily or permanently the normal biological functions of any organism. Historically, drugs were typically identified from natural sources (e.g., plants, microorganisms.) without a clear understanding of the biomolecular structure or process that was modified and/or modulated upon drug administration. Over the last century, scientists have focused their efforts on understanding the biological process modulated by natural products and isolating the molecules responsible for those interactions, trying to mimic some of these agents to improve their effects and lower the undesired effects associated with non-specific interactions with other biomolecules (**Figure 2.1**).[3–5]
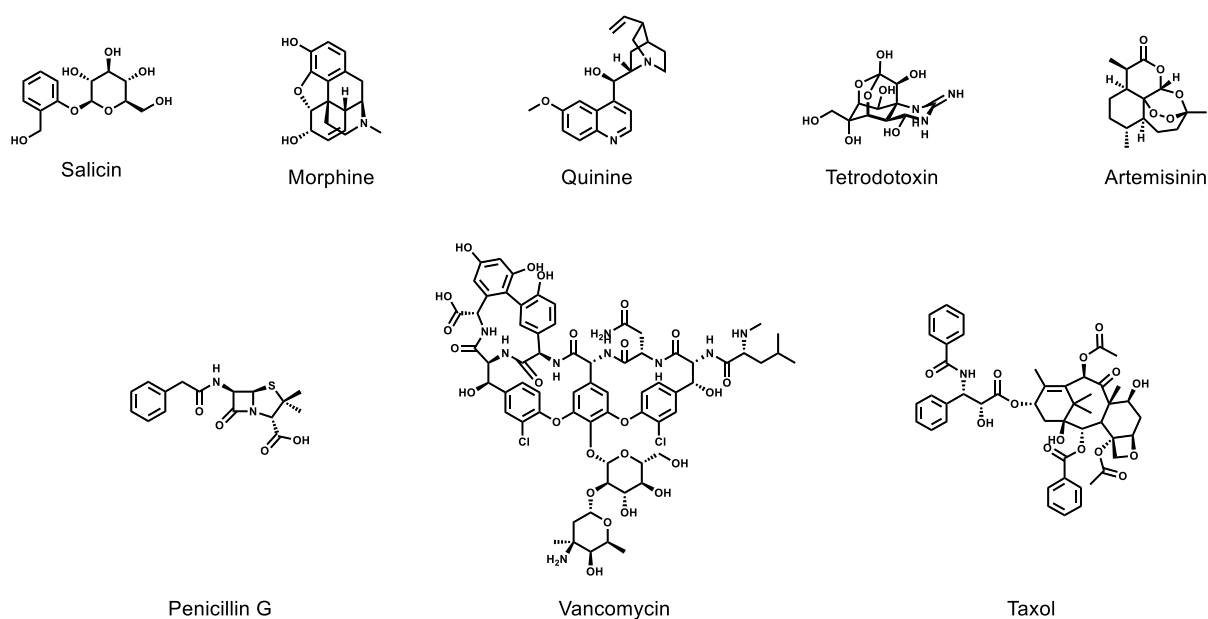
Figure 2.1. Examples of natural products. Salicin, a precursor of salicylic acid (Aspirin), is an anti-inflammatory agent, isolated for the first time in 1829 from the bark of the willow tree *Salix alba*. Morphine, one of the most potent opiates, was first isolated in 1805 from the opium poppy *Papaver somniferum*. Quinine was first isolated in 1820 from the bark of a cinchona tree *Cinchona officinalis*. Nowadays Quinine is used as a medication to treat malaria, but it was traditionally used to stop shivering. Tetrodotoxin, isolated from the pufferfish *Tetraodon*, in 1909, is one of the most potent toxins and it has been investigated as a possible treatment for cancer-associated pain. Artemisinin, the treatment of choice for malaria, first introduced as Artemisin, was isolated from the plant *Artemisia annua* in 1972. Penicillin G is an antibiotic that was first discovered in 1928 from the Penicillium mold *P. rubens*. Vancomycin, another antibiotic drug, was isolated in 1953 from the soil bacterium *Amycolatopsis orientalis*. Taxol or Paclitaxel was first isolated in 1971 from the pacific yew *Taxus brevifolia*. It is extensively used as a chemotherapeutic agent for the treatment of various malignancies.

Drug discovery has evolved and currently relies on identifying biological targets (e.g., enzymes, receptors) that cause a predetermined pathological condition. Once

the target causing the disease is identified, scientific efforts are needed to find molecular entities (e.g., small organic molecules, peptides, antibodies) able to interact with the target and to bring a therapeutic benefit.[6,7]

The current process for the discovery, characterization, and approval of medicines for human use represents a long process that usually lasts over ten years. Even excluding the long time-lines of the process, there are other complications when generating a new drug, such as high costs and multidisciplinary approaches that have to cooperate.[6] Latest studies have calculated that the mean investment in research and development to bring a new medicine to the market is about \$1.3 billion.[8] As represented in **Figure 2.2**, only one compound out of more than 10,000 enters into research stages after target identification, reaches the market, and becomes a medicine.[6,8] The still not well-established translation from animal models to humans, makes the process poor in success rate.[6,9,10] In this regard, the scientific community has focused efforts on developing new techniques and models which can efficiently reduce these times by screening multiple small molecules or biologics at the same time; and which efficiently translate experimental results from the laboratory to the clinic.[6,11,12]

Drugs can be classified in different ways (e.g., by their size, the function they modulate).[13] Looking at the molecular weight, drugs can be divided into three categories:

- **Small molecules**. These drugs are typically lower than 1kDa in molecular weight.
- **Peptides and Oligopeptides**. Their molecular weight usually ranges from 1 to 10 kDa.
- **Biomacromolecules or biologics**. Very large classes of molecules or cell-based therapeutics, whose molecular weights are above 10kDa.

Due to their different size and nature, all these classes of drugs have characteristic properties and are often discovered using different approaches and techniques.[12] The discovery of small molecules relies on the use of synthetic libraries, *in silico* models, or can be identified from natural extracts and organisms.[4,14–18] Small molecules have excellent pharmacokinetic profiles, and toxicities can often be predicted using *in vitro* models. Most of the small molecules adhere to certain rules proposed by Lipinski and collaborators in 1967.[19] According to these rules, so-called Lipinski's rule of five (RO5), small molecule drugs should not be bigger than 500 Da and should have a partition coefficient between octanol and water lower than five. Moreover, the number of hydrogen bond acceptors should be below five, and the number of hydrogen bond donors less than ten. Nevertheless, certain classes of small molecules (e.g., antibiotics, chemotherapeutic agents) may violate these rules but have still become successful drugs.[20] Small molecules can interact with other targets besides the target of interest and are traditionally less specific than other classes of drugs.[13] Furthermore, the success rate for the discovery of small molecules is typically low and represents a bottleneck in the drug discovery process. Therefore, the development of new screening methodologies is of key importance for future drug development.[6,10]
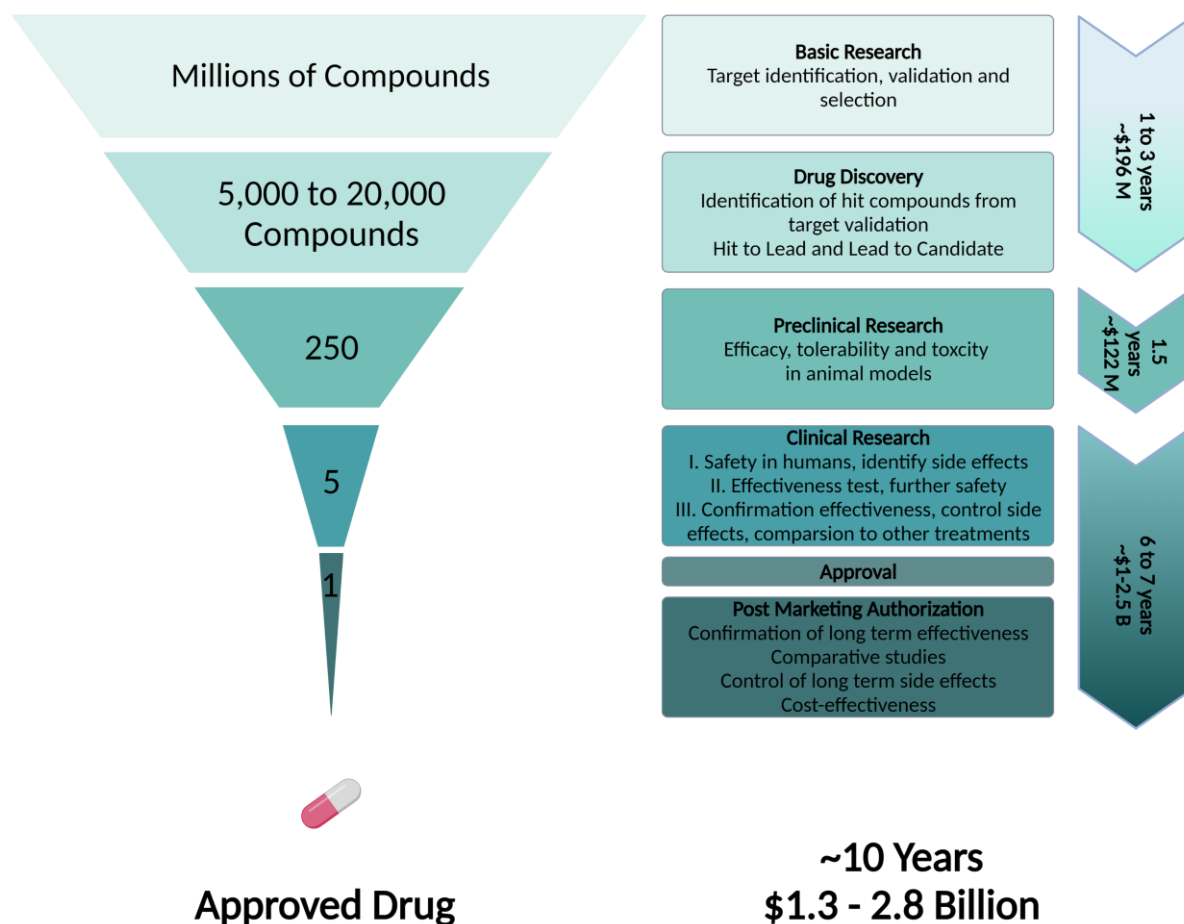
Figure 2.2. Drug discovery process overview. Companies usually start their programs with millions of compounds looking for target identification and validation in basic research stages. During drug discovery and preclinical stages, identified potential hits are studied and evolved into lead compounds that are tested, first *in vitro* and then *in vivo*, to determine a drug candidate. This part of the process usually takes 1 to 3 years, and the average cost is around $196 million. During the preclinical stage, candidates are extensively tested *in vivo* to determine pharmacokinetic properties, efficacy, tolerability, and toxicity; spending on average 1.5 years and $122 million. Once the final candidates enter clinical trials, the safety, effectiveness, and side effects are confirmed in humans. The average time until approval and post-marketing authorization range between 6 to 7 years, costing around $1 to 2.5 billion. Data obtained from Taconic Bioscience "The Drug Discovery Process" April 2019 and references[6,8,9]. Created with BioRender.com

In contrast to small molecules, peptides, oligopeptides, and biomacromolecules are often discovered using encoded combinatorial libraries (e.g., phage display, ribosome display).[21,22] These classes of drugs are usually very specific, and the associated off-target toxicity is minimized. On the other hand, the poor oral bioavailability makes them difficult to administer (typically parenteral administration). Peptides and oligopeptides often lack stability in plasma and can accumulate in other organs, being kidneys the most prominent one. In this respect, the investigation of proteolytically stable peptides for oral administration may improve the characteristics of this class.[23] While peptides and oligopeptides can be resynthesized using chemical approaches and have low production costs, biomacromolecules are difficult to produce and require well-controlled and expensive manufacturing processes (**Table 2.1**).[13]

Table 2.1. Characteristic comparison between small molecules and biologics

	Small molecules	Biologics
Molecular Weight	~200 to 500 Da	~150 kDa
Physicochemical properties	Mostly well defined	Complex (e.g., tertiary structures, stability)
ADME tools	Available/Extensive understanding	Understanding of ADME still evolving
Dosing route	Oral often possible	Usually parenteral (IV, SC and IM)
Dose interval	Daily (typically)	Intermittent dosing
Half-life ($t_{1/2}$)	Short (typically less than 24h)	Long (typically days or weeks)
Distribution (V_d)	High, distribution to organs/tissues. Potential substrate of transporters	Lower distribution, mainly plasma and extracellular space
Metabolism	Mainly by CYP enzymes and phase II enzymes. Metabolized to non-active and active metabolites	Catabolism. Degraded to peptides or amino acids
Metabolite's safety evaluation	Yes	No
Excretion	Mainly biliary and renal	Mostly recycled by body
Clearance (CL)	Mostly linear PK	Slow clearance
PD	Short acting	Long acting
PK/PD	PK usually not driven by PD	PK and PD mechanistically connected
Immunogenicity	No	Yes
Toxicity	On- and off-target related	Typically exaggerated pharmacology
Formulation	Complex and diverse	Simple
Production Process	Synthesized (uniform single entity)	Culture-derived (generally nonuniform)

Modified from[13]. Note: Peptides and oligopeptides have characteristics that lay between small molecules and biologics.

Despite their manufacturing and poor oral bioavailability, biomacromolecules represented 12 out of the top 20 best-selling drugs in 2020, comparable numbers to small molecules (**Table 2.2**).

Table 2.2. Top 20 best-selling drugs in 2020

Rank	Name	Type	Sales ($M)	Company	Use
1	Humira	Antibody	20,390	AbbVie	Rheumatoid arthritis, psoriatic arthritis, Crohn's disease, and others
2	Keytruda	Antibody	14,380	Merck & Co.	Melanoma, small and non-small cell lung cancer, other cancers.
3	Revlimid	Small molecule	12,150	Bristol Myers Squibb	Multiple myeloma, myelodysplastic syndromes, and others
4	Eliquis	Small molecule	9,170	Bristol Myers Squibb and Pfizer	Nonvalvular atrial fibrillation
5	Imbruvica	Small molecule	8,430	AbbVie, Johnson and Johnson	Mantle cell lymphoma, Waldenstrom's macroglobulinemia, and other
6	Eylea	Biologic	8,360	Regeneron and Bayer	Wet age-related macular degeneration, diabetic macular edema, and others
7	Stelara	Antibody	7,940	Johnson and Johnson	Plaque psoriasis, psoriatic arthritis, Crohn's disease, ulcerative colitis
8	Opdivo	Antibody	7,920	Bristol Myers Squibb	Melanoma, non-small and small lung cancer, Hodgkin lymphoma, other cancers

9	Biktarvy	Small molecules combination	7,260	Gilead Sciences	HIV
10	Xarelto	Small molecule	6,930	Bayer, Johnson and Johnson	Stroke prevention in non-valvular atrial fibrillation, and others
11	Enbrel	Biologic	6,370	Amgen	Rheumatoid arthritis, plaque psoriasis, ankylosing spondylitis, and others.
12	Prevnar 13	Vaccine	5,950	Pfizer	Pneumococcal disease
13	Ibrance	Small molecule	5,390	Pfizer	HR-positive, HER2-negative breast cancer
14	Avastin	Antibody	5,320	Roche	Cervical cancer, colorectal cancer, epithelial ovarian, and others
15	Trulicity	Biologic	5,070	Eli Lilly	Type 2 diabetes
16	Ocrevus	Antibody	4,610	Roche	Multiple sclerosis
17	Rituxan	Antibody	4,520	Roche and Pharmstandard	Chronic lymphocytic leukemia, non-Hodgkin's lymphoma, pemphigus vulgaris, and others
18	Xtandi	Small molecule	4,390	Astellas Pharma	Metastatic and non-metastatic castration-resistant prostate cancer, and others
19	Tagrisso	Small molecule	4,330	AstraZeneca	Non-small cell lung cancer
20	Remicade	Antibody	4,195	Johnson and Johnson	Chron's disease, ulcerative colitis, rheumatoid arthritis, and others

Data obtained from [24,25] and fiercepharma.com.

Nowadays, peptides and biomacromolecules can be discovered against virtually any target of interest.[21] The development, during the last decades, of encoded combinatorial libraries and new screening methodologies, have made this process easier, drastically improving the outcome of drug discovery programs related to these drug classes.[21] Therefore, it is of high interest to the scientific community, the advancement of new encoded combinatorial procedures suitable for small organic ligands identification, in analogy to biologics; which promises a better success rate during drug discovery campaigns.

2.1 Conventional strategies for small molecule ligand identification in drug discovery

The discovery of small organic molecules capable of interacting with biomolecular entities is an essential step in drug discovery programs.[6,18] Often, the identification of these molecules starts with the screening of vast virtual collections of compounds or moderate-size collections of already synthesized small molecules that are tedious and expensive to test.[14,17,18,26,27] Screening campaigns aim to find "lead" compounds that can be subsequently optimized through medicinal chemistry. Nevertheless, screening campaigns often lead only to "hit" compounds, far away from turning into drug candidates, increasing the cost of these programs.

Another frequently practiced methodology for the discovery of small molecules is the identification of naturally occurring ligands that can serve as an inspiration for the design of potential lead compounds. However, identifying natural ligands is not cost-effective and is very time-consuming due to the complex synthetic transformations needed to produce the naturally derived products.[3,4]

7

2.1.1 High-throughput screening

In the era of process automation, one of the most employed methodologies for ligand identification is the high-throughput screening (HTS) of big collections of synthetic small molecules and/or natural products.[26,28] The effective exploitation of HTS requires the individual synthesis, storage, and testing of hundreds of thousands to millions of compounds.[26,28–30] HTS activities are typically carried out on multi-well triter plates (384 or 1536) in the presence of the protein target of interest or living organisms (e.g., cells).[26,28–30] Notwithstanding the progress in the HTS field, the identification of high-quality ligands, even from libraries comprising more than 1 million molecules, remains challenging. Large repertoires are laborious and expensive to produce, store, and screen. On the other hand, the individual testing of every single compound requires large amounts of protein target or cells, which, despite the advances of recombinant protein production, drastically increases the cost of these campaigns.[28]

HTS activities are virtually only possible in big pharmaceutical companies, which can afford the prohibitive costs to run these platforms. Increasing further the overall expenses of the screening campaigns, hit compounds identified have often low to medium activity (i.e., in the micromolar range) and demand extensive medicinal chemistry optimizations to generate lead molecules, which can potentially become a drug candidate.[26]

As previously mentioned, large chemical libraries (>1 million compounds) are costly to produce and store; and the low success rate of HTS campaigns (typically around 50%) may be due to the poor chemical space covered by these collections. Due to the extremely high cost of expanding chemical libraries by iterative synthesis of new compounds, other methodologies have been proposed to improve the chemical diversity of these collections. For example, parallel synthesis and combinatorial chemical approaches have enhanced the success rate of HTS campaigns.

2.1.2 Fragment-based drug discovery

Another commonly used approach for generating small molecule ligands is fragment-based drug discovery (FBDD).[14,31,32] FBDD makes use of different biophysical, biochemical, and functional assays for the screening and detection of short fragments, whose activities usually range in the high micromolar to the millimolar range. The so-called fragments can provide excellent information and can serve as a good starting point for the design and synthesis of more complex molecules, with enhanced activities and better physicochemical properties.[31–33]

During FBDD campaigns, libraries of small molecules are screened against a particular target of interest. The isolated fragments should be small enough to allow for their expansion or linkage with other fragments and avoid steric clashes, but also enable a sufficient number of interactions to be detected by biophysical techniques.[14,31–33] Libraries are normally constructed following a modification of Lipinski's rule of five, also called "the rule of three" (RO3). The molecular weight of the fragments is usually below 300 Da, the number of hydrogen-bond donors and acceptors is also typically below three, as well as the logP.[19,34,35]

Several approaches to turn a binding fragment into a lead compound have been established. Among them, the most straightforward is fragment growing. The main objective is to move from fragments obeying the rule of three to more sophisticated and high-affinity compounds that could potentially exceed the rule of five. To reach this goal, it is essential to identify the main functionalities in the initial fragment and generate the so-called growth vectors. A growth vector represents a position of the fragment to install additional modifications (e.g., heteroatoms, functional groups) which can improve the activity of the ligand (**Figure 2.3a**).[32,36] A second approach relies on merging different fragments that bind to adjacent pockets on the target of interest. This strategy allows the generation of more complex molecules whose binding properties can be enhanced due to synergistic interactions to close-proximity regions (**Figure 2.3b**).[32,37] The third most common method for fragment evolution is fragment linking. This approach relies on the same principles as fragment merging. The main difference with fragment merging is the introduction of another level of complexity in the final molecule; a linker (**Figure 2.3c**).[32,38,39] The selection of the linker is often very challenging since it must orientate both fragments in the appropriate conformation to have the best binding affinity.

The most common biophysical techniques employed during FBDD programs are surface-plasmon resonance (SPR), thermal shift assays (TSA), microscale thermophoresis (MST), isothermal titration calorimetry (ITC), X-Ray methods, or nuclear magnetic resonance (NMR) methods.[32,33] Because of the high false-positive rate during FBDD, mostly due to the low activity and high degree of sensitivity necessary for interaction detection, ligands have to be confirmed by orthogonal methodologies. Other pre-screening techniques, such as virtual screenings and pan-assay interference compounds filters, are often applied to discard possible false-positive fragments and to focus the attention on the most promising libraries available.[32,33]

During the last decades, FBDD has become a useful alternative to HTS, mainly because of the ease of implementation and cost-effectiveness. FBDD platforms can be run both in pharmaceutical companies and academic groups. Nevertheless, highly interdisciplinary teams are necessary to overcome the possible challenges one may face using this approach. These challenges are mainly associated to the confirmation of fragment activity, and fragment evolution.[32,33,35]
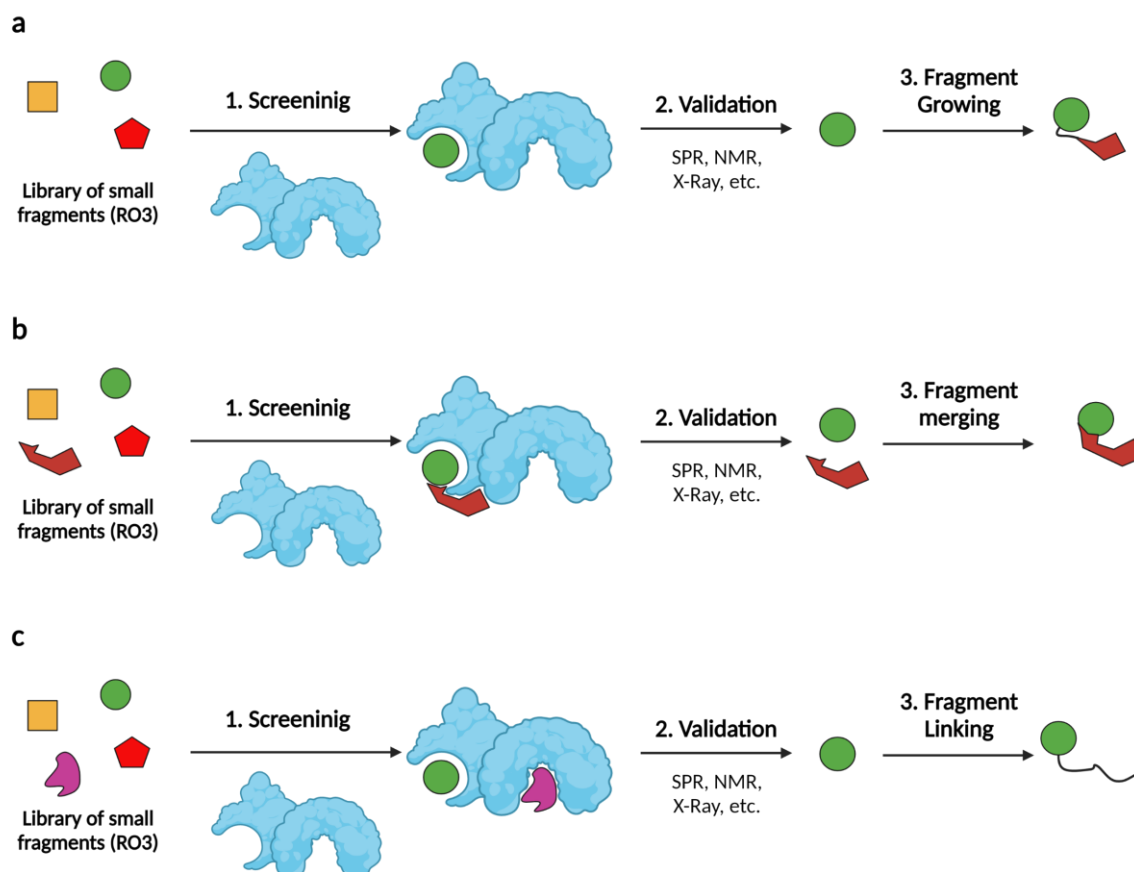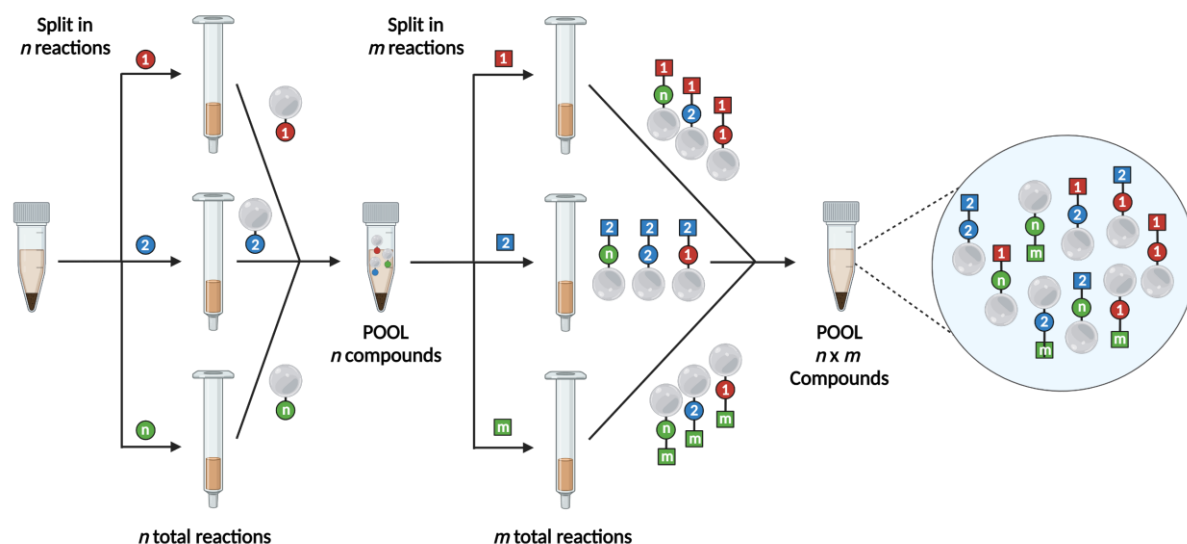
Figure 2.3. Schematic representation of fragment-based drug discovery approaches. **a**. Fragment growing. Identification and validation of small binding fragments from the library are followed by the growth of the fragment using growth vectors. **b**. Fragment merging. Two different fragments with adjacent binding sites are validated and merged into a single molecule. **c**. Fragment linking. In a similar manner to fragment merging, two different fragments with different binding pockets are linked using an appropriate linker, which is optimized to obtain the correct orientation of the fragments. Created with BioRender.com

2.1.3 Combinatorial chemistry

In 1963, Bruce Merrifield, later awarded the Nobel Prize in chemistry, set up the foundations of modern combinatorial chemistry and diversity-oriented synthesis by introducing the automated and parallel synthesis of peptides on solid phase.[40–44] During the early sixties, the chemical synthesis of small peptides became rapidly popular due to the ease of the procedures and the development of new coupling reagents. Nevertheless, the synthesis of long linear polypeptide chains represented a challenge because of the solubility of the intermediates and the isolation of the final molecules. The automated synthesis of peptides, linked to solid supports (solid-phase peptide synthesis) revolutionized the construction of this type of compound.[40] The polymeric resin (solid phase) facilitates the purification of every intermediate since the excess of reagents and coupling agents can be removed by filtration. The isolation of the final product can be achieved by simply breaking up the linkage between the peptide and the solid support.[40]

The method employed by Merrifield became very attractive. Later, other groups implemented similar approaches for the construction of oligonucleotides, oligosaccharides, and small molecules.[45–47] The first report highlighting the potential of solid-phase synthesis for the construction of small molecules was published by Ellman *et al.* in 1992.[47] This work was remarkably important, not only because of the type of drug-like structures synthesized but also because of the type of transformations. In addition to amide bond formations, other reactions like carbonyl-amine condensations and *N*-alkylation were implemented.[47] Since that time, tremendous efforts have been applied to develop elegant and elaborated procedures which allow the synthesis of drug-like molecules on solid supports.[48]

It is also important to remark that, between 1988 and 1991, Furka and collaborators elaborated the early stages of one of the most popular approaches in recent chemical synthesis, combinatorial chemistry.[41] The first approach relied on the use of "split-and-pool" procedures (**Figure 2.4**). In this strategy, the chemical synthesis of small organic molecules, using solid supports or magnetic beads, is performed through iterative steps of chemical reactions, deprotections, washings, and pooling. The final pool, containing all the individual elements of every reaction can be split again to follow the same procedure in a new synthetic cycle. This approach rapidly generates a vast amount of chemically diverse small molecules.[41] The theoretical approach attracted much attention, and the first publications employing this methodology promptly appeared.[49,50] Despite the popularity of this procedure, different challenges needed to be addressed. Identifying every individual molecule on the final library mixture becomes more and more difficult as soon as the library size drastically increases. The use of robust and sensitive analytical techniques becomes essential at this step to identify the molecules that potentially interacted with the target of interest after the screening of the libraries.[51]

Figure 2.4. Schematic representation of a split-and-pool procedure for the creation of combinatorial libraries. In this figure, *n* different reactants are coupled to a solid support (grey balls) to create the first pool of *n* different compounds. The mixture is split into *m* different reactions to react with *m* different reactants. After pooling again all the reactions, a library of *n* x *m* compounds is generated. The procedure can be iterated as many cycles as desired, exponentially increasing the number of final molecules and the complexity of the library. Created with BioRender.com

The problem of ligand identification among all the library members can be efficiently solved using encoded combinatorial methodologies, such as display technologies (e.g., phage display, ribosome display). These approaches inspired the theoretical hypothesis of constructing encoded combinatorial libraries of small molecules on beads. This idea was later implemented, originating the DNA-Encoded Chemical Libraries technology, which will be deeply discussed in chapter 2.3.
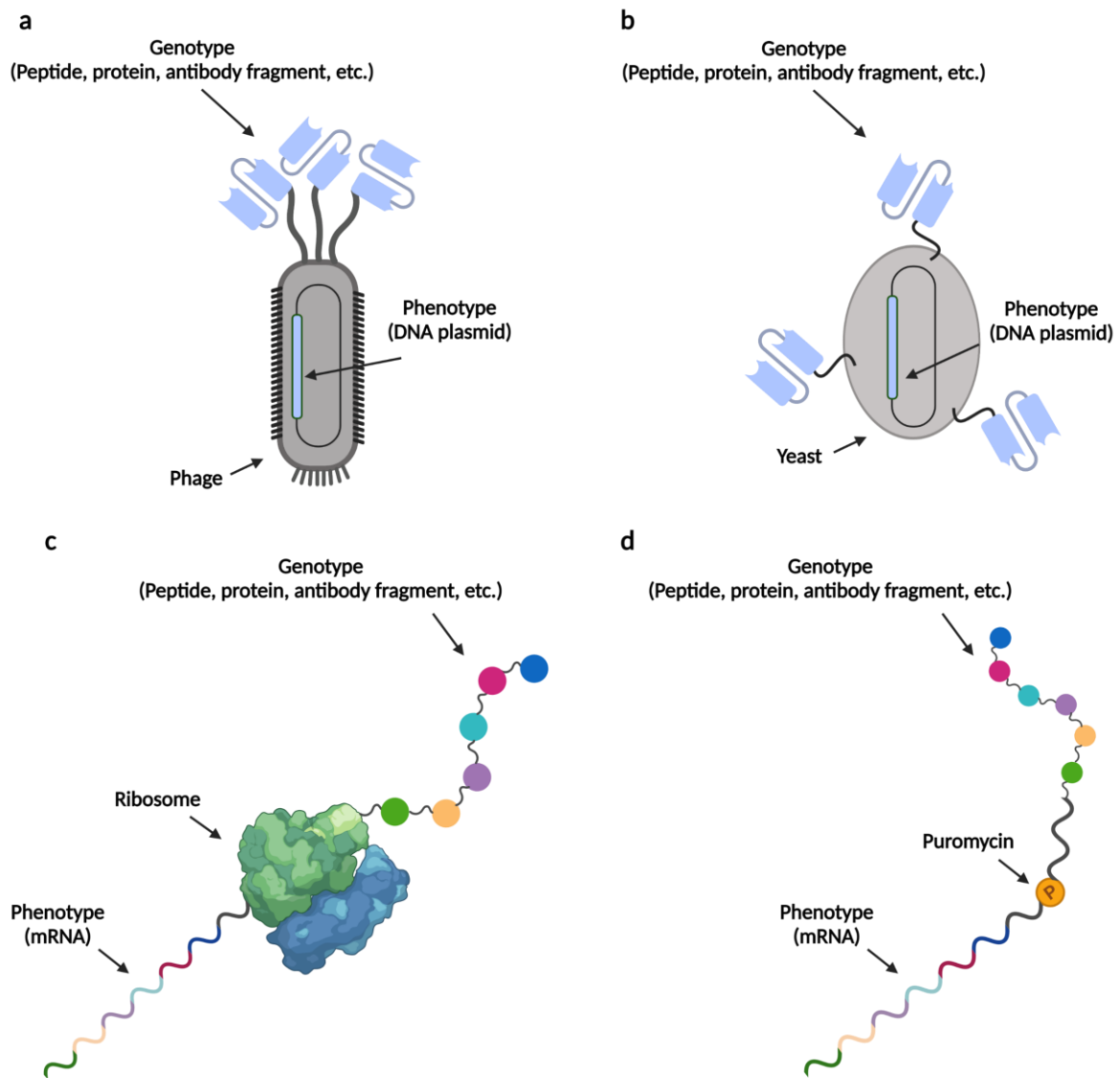
2.2 Encoded display technologies

Emulating the production of proteins or polypeptides through transcription of DNA into mRNA deputed to the cell machinery represented the inspiration for the development of encoded display technologies. Display technologies represent collections of genetically encoded biomolecules (e.g., antibodies, peptides) via directed evolution.[22,52] Directed evolution requires compartmentalization of the systems or physical linkage between the encoding structures (i.e., genotype) and the displayed molecules (i.e., phenotype). Regardless of the format, a display library consists of modularly encoded molecules, each of which contains three components: displayed entities, a common linker, and the corresponding unambiguous sequence.[22,53] Encoded combinatorial libraries can be screened by affinity capture and yield high-affinity ligands towards virtually any target of interest. The genetic tag not only allows the biosynthetic protein production but also encodes for the library members, allowing employing PCR reaction for the structural assessment of the binding moieties.[22,52,53]

The expression of proteins on the surface of different organisms (e.g., bacteria, yeast, or filamentous phages) has successfully been applied.[54,55] Nevertheless, during the last decades, other display technologies, which do not make use of cells, have also been developed (e.g., mRNA display or ribosome display) leading to full *in vitro* display technologies (**Figure 2.5**).[22,53,56–61]

Display libraries and affinity selections involve three steps. First, the generation of a large collection of variants (the library); second, multiple rounds of enrichment (biopanning), which ensures the selection of variants with the desired properties; and the characterization of the selected variants via appropriate assays and genetic information decoding.[22]

A major limitation of using Sanger sequencing for the identification of binding members is the relatively low fraction of the library that can be sampled (typically 10 to 10^2 sequences). The development of next-generation sequencing technologies (NGS) has impacted display technologies and the selection processes profoundly. NGS offers a much greater number of sequencing reads ($>10^6$), thus increasing the capacity to obtain the sequence information of all clones of each selection round. This capacity allows for a comprehensive analysis of the selection process and the library members.[62]

In the following sections, the main display technologies will be described in more detail.

Figure 2.5. Schematic representation of display technologies. **a**. Phage display, **b**. Yeast display, **c**. Ribosome display, **d**. mRNA display. The encoding information (genotype) is contained in the genome sequence (phage or yeast) or the ribosome-mRNA complex or mRNA alone. The displayed moiety (phenotype) could be a peptide, a protein, or an antibody fragment. Created with BioRender.com

2.2.1 Phage display libraries

For the past 45 years, hybridoma technology represented for the scientific community a valuable method for the isolation of monoclonal antibodies.[53] However, the generation of murine antibodies through hybridoma technology has some limitations (e.g., immunogenicity) when moving these biomolecules to advanced drug research stages.[53]

In 1985, George P. Smith introduced the revolutionary concept of phage display, in which a foreign DNA fragment is inserted into the filamentous phage gene III. The insertion of this DNA fragment creates a fusion protein that is incorporated into the virion and the foreign peptide sequence is displayed in immunological accessible regions. The virion retains infectivity and can be enriched more than 1000-fold over non-fusion phages by affinity purification using an antibody recognizing the displayed region.[63]

In the following years, the concept was further expanded by Smith and Sir Gregory Winter (Nobel Prize in Chemistry 2018 together with Frances Arnold), and several publications were reported in which different proteins, peptides, and antibody fragments were displayed on the surface of phages.[64–67]

The concept is based on the possibility to display different fragments (phenotypes) on the surface of the bacteriophages, by introducing the encoding information for each particular phenotype into the phage genome (genotype). Every single different peptide, protein, or antibody fragment is unambiguously encoded allowing for the construction of libraries of unprecedented size (>10^{10} different fragments), which can be screened against a target of interest to identify the best binding partner.[63–67] In a typical affinity selection procedure, the target of interest is immobilized onto a solid support. The library is incubated with the immobilized target allowing for the binding members to interact with it. The non-binding members are removed, and the selected ones are isolated and amplified by bacterial infection.[22,53,68,69] To enrich the best binding members, the libraries can be interrogated for several selection rounds (biopanning) thanks to the high stability of phages to acidic, basic, and proteolytic conditions. Finally, the selected library members can be identified by DNA sequencing (**Figure 2.6**).[22,53,68,69]
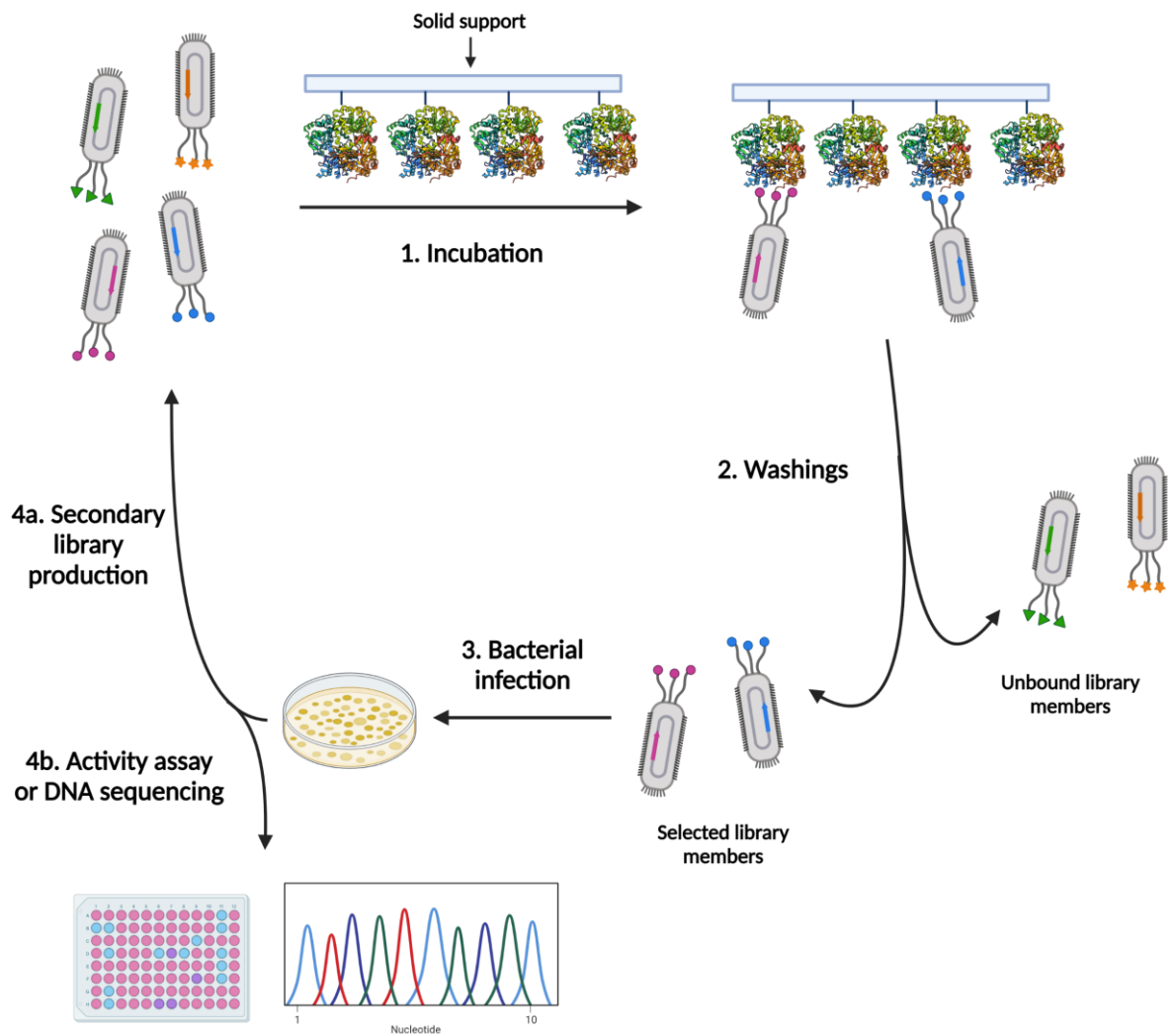
Figure 2.6. Schematic representation of phage display affinity selection procedures. The library containing all the different members is incubated with the target protein immobilized onto the solid support. After washing away the unbound library members, the selected members are isolated and amplified by bacterial infection. The binding members can be characterized by activity-based assays or DNA sequencing, or the procedure can be repeated iteratively (biopanning) for the selective enrichment of the best library members. Created with BioRender.com

2.2.2 Yeast display libraries

In analogy to phage display, in 1996 Schreuder and collaborators postulated for the first time the possibility to immobilize proteins on the surface of yeast cells.[70] But it was in 1997 when Boder and Wittrup introduced the concept of yeast display.[55]

Yeasts possess two related cell-surface receptors (*a*-agglutinin and α-agglutinin), which mediate cell-cell adhesion. Unlike α-agglutinin, *a*-agglutinin is a two-subunit glycoprotein (Aga1 and Aga2). Aga1 subunit anchors the assembly to the cell wall interacting with the β-glucan via covalent linkage, while Aga2 is linked to the Aga1 via two disulfide bridges. The Aga2 C-terminus is responsible for the binding activity and represents a useful position to display macromolecules (e.g., peptides or antibodies).[55] By introducing the genetic information of the displayed macromolecule into the C-terminus of the Aga2 gene, the desired protein can be displayed on the surface of *Saccharomyces cerevisiae*. The induction of production of Aga1 and Aga2-fusion gene products is achieved by the addition of galactose to the medium, avoiding the overexpression of a single library member. With these conditions, the desired peptides or antibodies are displayed at a density of about 10^4-10^5 copies per cell.[55]

Multiple advantages characterize the use of yeast display over phage display, but the most important one is the possibility to directly detect the bound library members via cell sorting using flow cytometry. This technique allows for the screening of fluorescently-labeled targets in solution, without the need of immobilizing them onto a solid support, as well as for precise quantitative discrimination, better control, and avoiding the accumulation of weak binders. Another advantage of cell cytometry-based selection methods is the possibility to quantify certain binder properties directly (e.g., binding kinetics) (**Figure 2.7**).[58]
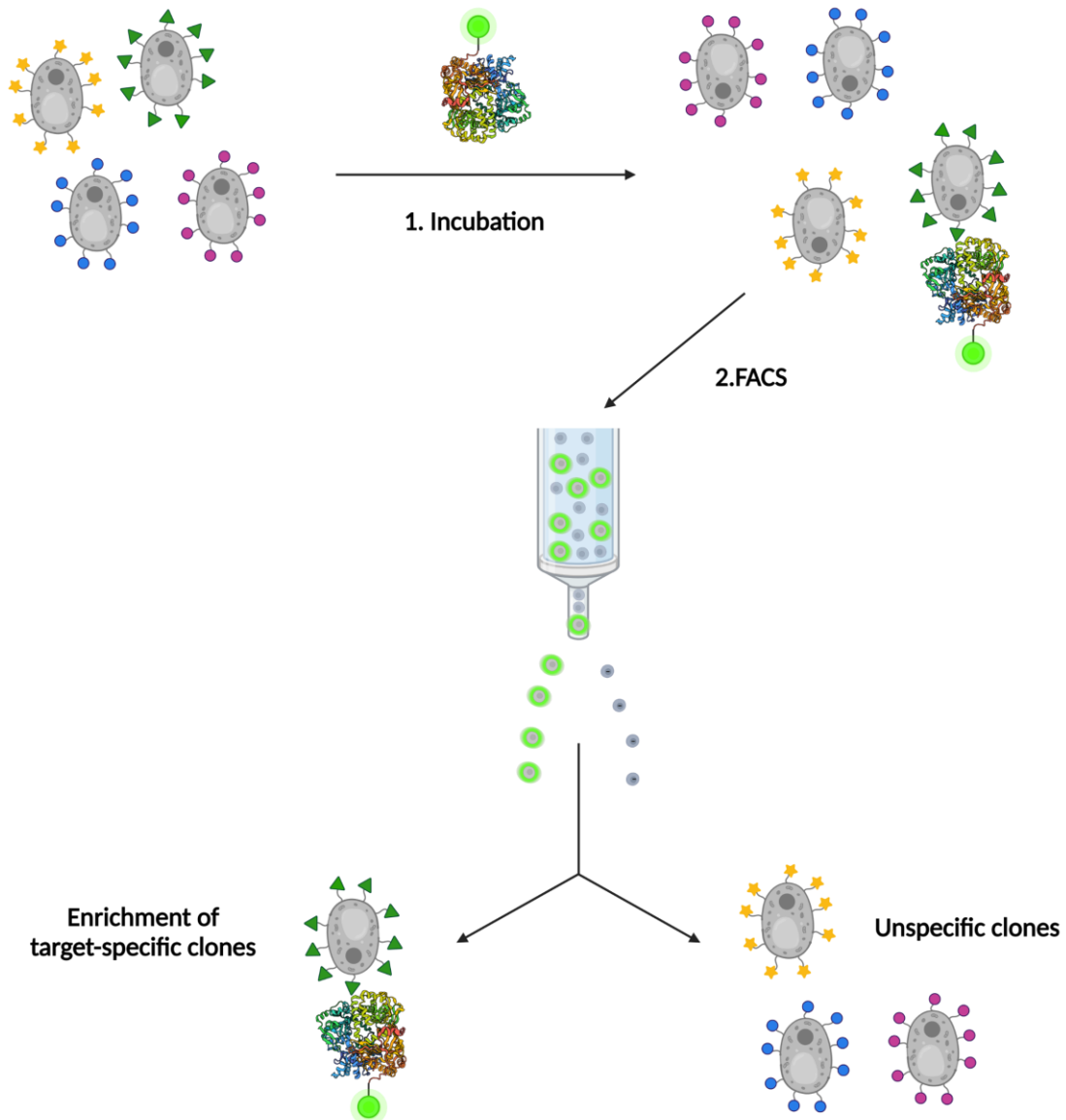
Figure 2.7. Schematic representation of yeast display affinity selection procedures. The library containing all the different members is incubated with a fluorescently-labeled target of interest. Fluorescent activated cell sorting (FACS) allows for the separation of enriched specific library members over unspecific ones. Created with BioRender.com

2.2.3 Ribosome display libraries

Full control over the specific mutations, where and how many should occur, can be achieved by PCR-based randomization techniques (i.e., Darwinian evolution), without the use of cells. This idea led to the development of full *in vitro* display technologies.[57,59,60]

Ribosome display was one of the first full *in vitro* technology platforms developed. This methodology was introduced by Mattheakis and co-workers in 1994. The concept proposed was similar to those in cell-based display systems but using the isolated S30 transcription/translation system from *Escherichia coli*.[60]

Ribosome display connects the protein (phenotype) to its encoding mRNA (genotype) through the stabilization of the complex protein-ribosome-mRNA by stalling the translating ribosome at the 3'-end of the mRNA. The procedure involves the deletion of the stop codon. Alternative methods for stabilizing the protein-ribosome-mRNA complex have been reported, which use different antibiotics or incubation with high concentrations of Mg^{2+} in the buffer. To allow the synthesized protein to fold correctly outside of the ribosome tunnel, a spacer of about 20 to 30 amino acids should be included in the sequence. Usually, the synthesis also starts with a typical protein detection tag (e.g., His6 tag or FLAG tag).[60,71,72]

In a typical ribosome display system, a pool of different DNA sequences is transcribed into the corresponding mRNA using a T7 promoter. Polypeptide synthesis starts with ribosome reading and translation, and once the mRNA is read, the deletion of the stop codon enables the protein to remain linked to the tRNA. The complex is used for affinity selection procedures on immobilized targets, and after isolation of binding members, washing steps allow for the mRNA to be released by complex dissociation. A reverse transcription-polymerase chain reaction (RT-PCR) step yields a PCR product, which can be incubated again with the transcription/translation system for a new round of selection. After several rounds, highly specific binders can be isolated and characterized (**Figure 2.8**).[22,60,71–73]

The main advantage of ribosome display over cell-based display technologies, apart from the control on mutations, is the possibility to screen libraries of much higher size (10^{12} to 10^{14} members) in a few PCR reactions, contrary to the, at least, 1,000 transformations necessary to achieve similar library sizes in cell-based systems.[74]
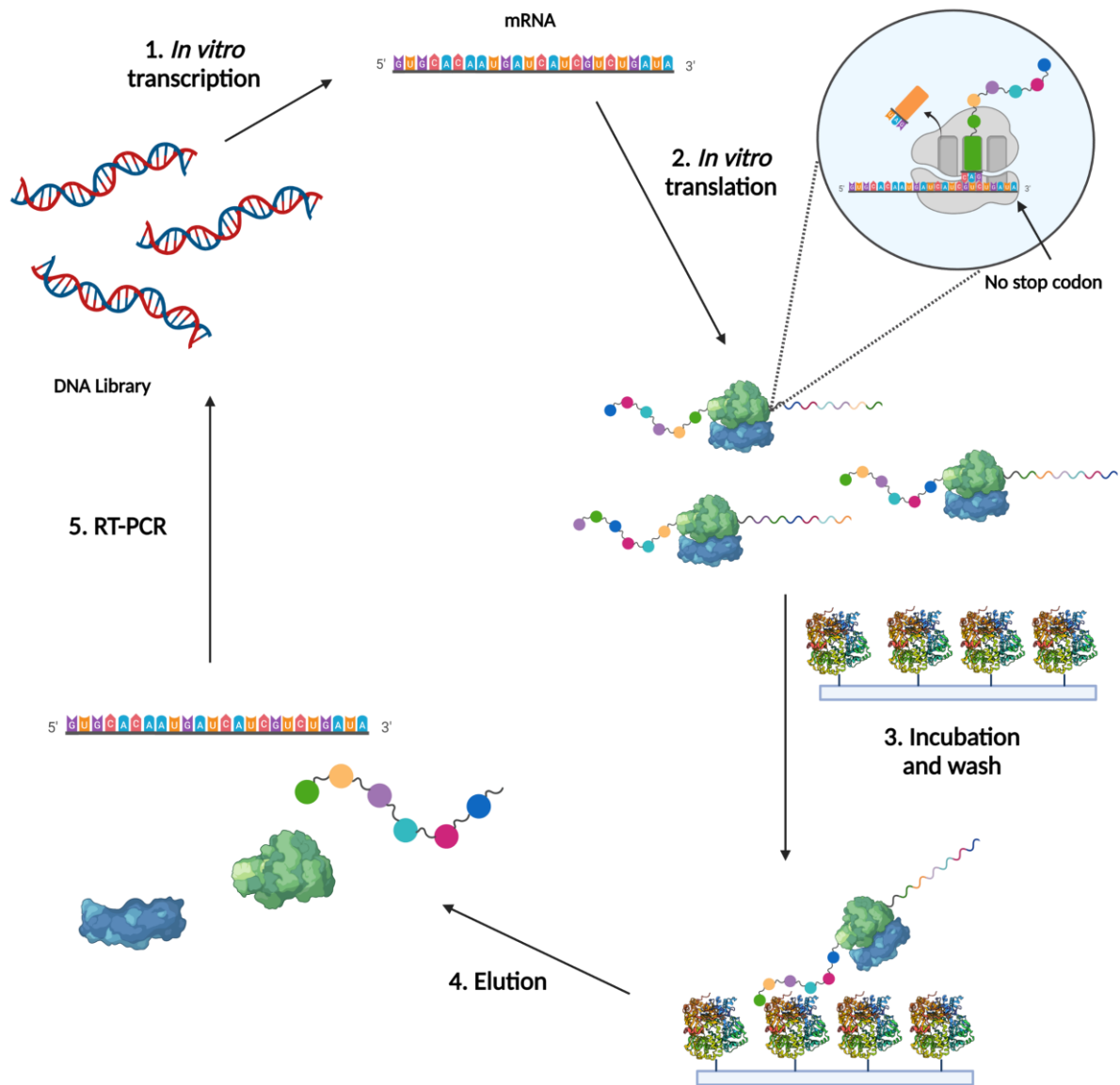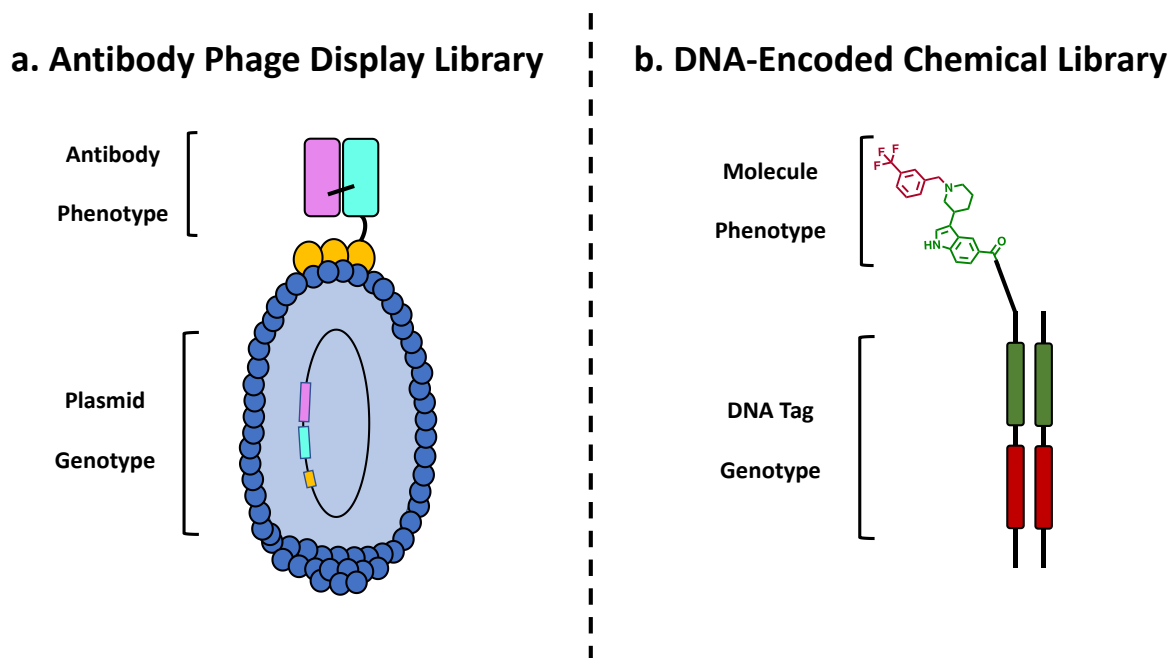
Figure 2.8. Schematic representation of ribosome display affinity selection procedure. The library containing all the DNA sequences is transcribed into mRNA and translated into the corresponding proteins, peptides, or antibody fragments. The ternary complex protein-ribosome-mRNA is stabilized by deletion of the stop codon. After incubation with the target of interest and washing away non-binding members, the elution step dissociates the complex into their corresponding subunits. The mRNA is then reverse transcribed and PCR amplified to follow another round of selection or identification of binding members through DNA sequencing. Created with BioRender.com

2.2.4 mRNA display libraries

In analogy to ribosome display, in 1997, Richard W. Roberts and the Nobel Prize in Physiology or Medicine, Jack W. Szostak, described for the first time a system called mRNA display.[75]

In this setting, large libraries of polypeptides or proteins can be generated and covalently linked to their corresponding encoding mRNA without the necessity to stabilize the ternary complex with the ribosome. Instead, a pool of DNA sequences undergoes *in vitro* transcription and addition of the antimicrobial natural product puromycin at 3'-end of the corresponding mRNA. Puromycin inhibits the translation by mimicking the natural substrate of the ribosome (the 3'-end of an aminoacyl-tRNA). Puromycin resembles the amino acid tyrosine linked by a stable amide bond to the 3'-end of a modified adenine nucleoside of the mRNA. After *in vitro* translation, the ribosome encounters the puromycin moiety, is recognized by the peptidyl transfer center at the ribosome, and inhibits the translation by forming a covalent bond between the peptide and the modified tyrosine, enabling the transfer of the nascent peptide to the puromycin-modified mRNA.[56,75] Before affinity selection procedures, the conjugate mRNA-peptide fusion is subjected to another modification. The mRNA is reverse transcribed into cDNA. The cDNA/mRNA-peptide fusion pool is incubated with the target of interest, immobilized on magnetic beads. After washing out the non-binding members, the cDNA of the active members is PCR amplified and serves as a template for another round of selection (**Figure 2.9**).[56,75]

As for ribosome display, one of the major advantages of mRNA display is the much bigger library size compared to cell-based systems. On the other hand, both ribosome display and mRNA display are monovalent display systems. Only one copy of each polypeptide or protein is attached to its corresponding ribosome-mRNA complex or puromycin-modified mRNA. This feature allows for the enrichment of the displayed biomolecule to be based solely on their intrinsic affinity to the target of interest, thus avoiding avidity effects.[22,59,76]

The discovery of small peptides, in contrast to antibodies or antibody fragments, has been much less efficient. The inability of small peptides to undergo stable folding, as well as the limitation of using only the 20 natural amino acids, have impacted the productivity of these libraries profoundly. To tackle this issue, two main approaches have been developed over the last years. First, the introduction of non-canonical amino acids is now possible thanks to the contributions of Hiroaki Suga and Szostak.[77,78] On the other hand, through spontaneous disulfide bridges, it has been possible to create cyclic peptides which have more chances to find an adequate tridimensional conformation upon approaching the target of interest.[79,80] In parallel, Heinis, and Winter developed a strategy to create cyclic and bicyclic peptide libraries using post-translation modifications. The libraries are produced using phage display technology, incorporating two or more cysteine amino acids. Upon oxidation or addition of certain bi- or tri-functional symmetric scaffolds, the formation of the cyclic peptides is allowed via reaction with the free cysteines.[23,81,82]
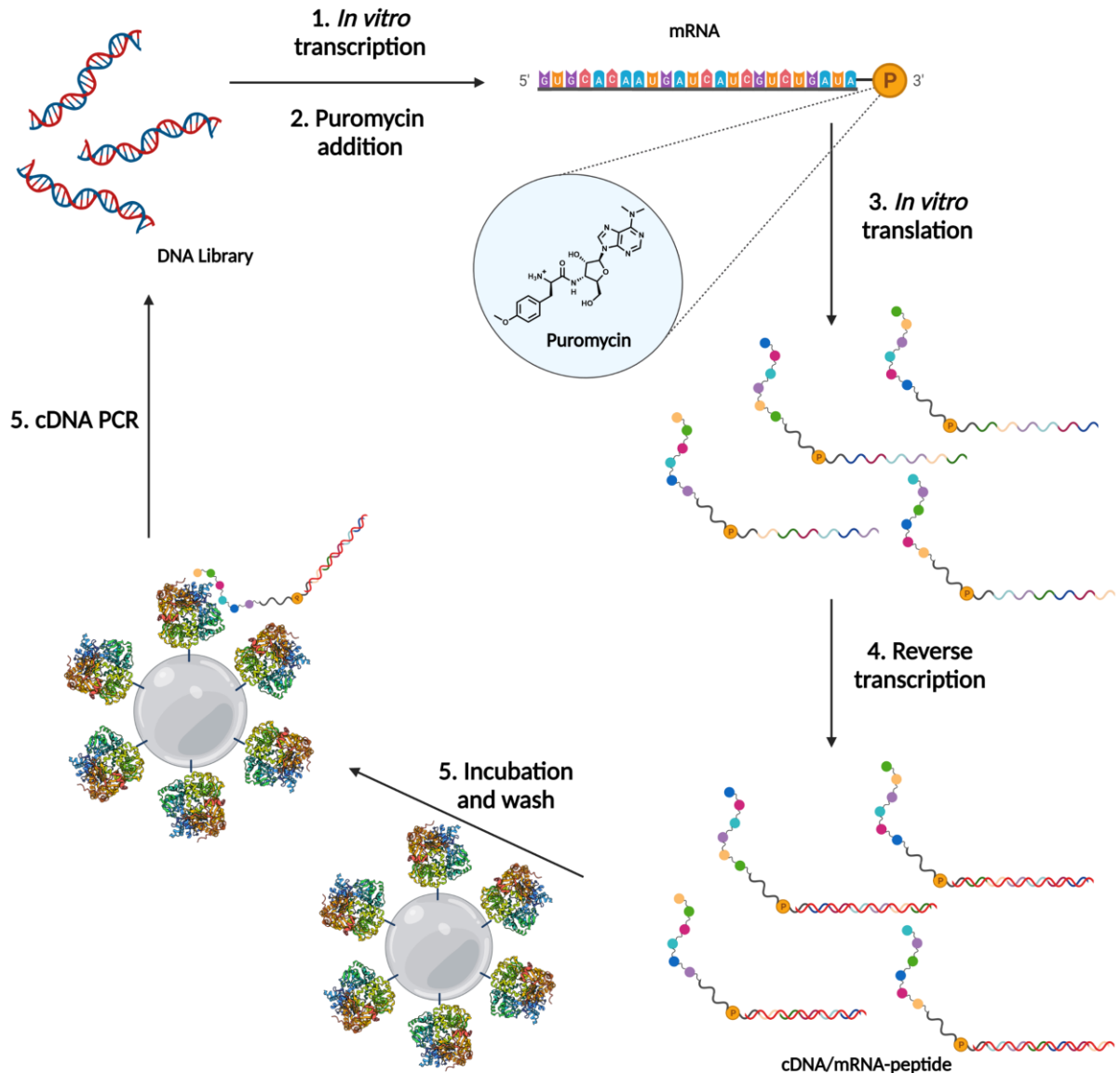
Figure 2.9. Schematic representation of mRNA display affinity selection procedure. The library containing all the DNA sequences is transcribed into mRNA and puromycin is added at 3'-end. The sequences are translated into the corresponding proteins, peptides, or antibody fragments, and the mRNA is reverse transcribed, forming a cDNA/mRNA-peptide complex. After incubation with the target of interest, immobilized on magnetic beads, and washing away non-binding members, the binding members are isolated. The cDNA is then subjected to PCR amplification and serves as a template for the next round of selection. Created with BioRender.com

2.3 DNA-Encoded Chemical Libraries (DELs)

Some parts of this chapter have been adapted from "DNA-Encoded Chemical Libraries: A Comprehensive Review with Successful Stories and Future Challenges" by Adrián Gironda-Martínez, Etienne J. Donckele, Florent Samain and Dario Neri, published in *ACS Pharmacology and Translational Science*, **2021**, *4*, 1265–1279. Copyright 2021 American Chemical Society.

Display technologies have played a tremendous role in the discovery of new antibodies, proteins, and polypeptides for therapeutic and diagnostic uses, to virtually any target of interest.[21] Despite progress in the HTS field, it is still difficult to identify high-quality ligands even from libraries comprising more than 1 million molecules. In principle, virtual libraries could be analyzed using computational approaches, but reliable ligand binding predictions remain challenging.[83] For this reason, substantial efforts have been committed to the development of alternative methodologies for ligand discovery such as DNA encoded chemical libraries (DELs). Improved methodologies are particularly needed for the identification of specific binders towards more difficult targets, such as those involved in protein-protein interactions.[84,85]

Progress in the field of encoded protein libraries inspired Brenner and Lerner to propose the construction of encoded chemical libraries, in which synthetic chemical entities on beads would be linked to individual DNA fragments, acting as identification barcodes (**Figure 2.10**).[86,87] Further elaborations of this original proposal have led to a variety of different experimental schemes, for the synthesis of DNA-encoded libraries (DELs), even in the absence of beads.[88–95]

Figure 2.10. Schematic representation of **a**. Antibody phage display library and **b**. DNA-Encoded Chemical Library. In both setting, the displayed entities, antibody fragments or small molecules respectively (phenotype) are unambiguously encoded by the genetic information, phage plasmid or oligonucleotide fragment respectively (genotype).

Shortly after the conceptual scheme proposed by Brenner and Lerner, the synthesis and screening of encoded peptide libraries comprising positive control peptides of known binding properties was experimentally implemented.[96,97] However, for more general applications, the bead-based approach was limited by the lack of efficient orthogonal strategies for the simultaneous synthesis of both peptides and oligonucleotides on solid phase. Two years later, Kinoshita and colleagues demonstrated the possibility to enzymatically ligate oligonucleotides for DEL applications, a feature that has later been frequently used for library encoding purposes.[98] In 2004, three methodologies for DEL construction were proposed and experimentally implemented, which featured the direct coupling of chemical matter to double-stranded DNA fragments, without the use of beads.[99–103] Avoiding beads may be important, both in terms of library size (there is a physical limit for the number of solid particles that can be suspended in a given volume) and in terms of versatile procedures for synthesis and screening. Liu and co-workers, from Harvard University, introduced an approach called DNA-templated synthesis.[99] Neri and colleagues, from ETH Zürich, developed an encoding strategy based on the self-assembly of partially complementary DNA strands (ESAC).[100] A few years later, they also reported the first library based on DNA-recorded synthesis strategies.[104] Finally, the group of Harbury reported a strategy, named DNA-routing, in which DNA-conjugates are sequentially captured on sepharose resin coated with complementary oligonucleotides, allowing an iterative procedure of sequential chemical transformations in organic solvents.[101–103]

While the basic ideas behind DEL technology had been postulated in 1992, it took approximately 15 years before an increasing number of groups started reporting alternative methods for library construction and screening. Those methodologies have crucially contributed to the popularity that DEL enjoys today, both in industry and in academia.[88–91,94] In the following sections, some of the most frequently used strategies for library encoding, synthesis, and screening will be presented.

2.3.1 Encoding Strategies

When considering strategies for DEL encoding, it may be convenient to make a distinction between "single-pharmacophore libraries" and "dual-pharmacophore libraries". In single-pharmacophore libraries, individual chemical moieties (no matter how complex) are coupled to distinctive DNA fragments (either in single-stranded or double-stranded format). In dual-pharmacophore libraries, two different chemical moieties are attached to the extremities of complementary DNA strands, acting synergistically for specific protein recognition. Moreover, it is convenient to distinguish between predefined DNA sequences that drive library construction ("DNA-templated chemistry"), and synthetic procedures in which the identity of individual building blocks that make up the final molecule is encoded by the iterative ligation of small DNA fragments ("DNA-recorded chemistry"). This latter procedure was first introduced in a 2008 publication, describing the synthesis and screening of DEL comprising 4000 members.[104] Shortly afterward, scientists at GSK reported the construction and screening of a library comprising 800 million compounds.[105]

2.3.1.1 Single-Pharmacophore libraries

Single-pharmacophore libraries are most commonly constructed using DNA-recorded synthesis, which relies on the use of split-and-pool procedures.[41] Libraries

are built up through a series of chemical transformations in multiple steps, each of which is encoded by the addition of either double-stranded or single-stranded DNA fragments (dsDNA or ssDNA) that uniquely identify them (**Figure 2.11**).[88–91,94] In a typical construction procedure, *n* different chemical building blocks are encoded using the same number of DNA fragments. In general, DNA fragments only differ from a short sequence, typically 6 to 7 base pairs, which serve as a barcode. After the first step, all the individual DNA-conjugated small molecules are pooled together, which can be subsequently split into *m* different wells allowing for the second cycle of chemical transformation and DNA tag elongation to yield *n x m* library compounds. The split-and-pool procedure can be iterated multiple times (most of the DELs typically consist of 2-3 cycles). In the case of dsDNA, DNA fragments are ligated using overhang tags, while ssDNA fragments can be assembled using splint-mediated ligations.[88,106] If desired, ssDNA DEL encoding can be converted into the corresponding dsDNA format by the use of Klenow polymerization with a complementary oligonucleotide primer.[107,108] Alternative strategies such as chemical ligation have also been developed.[109] Chemical modifications during this approach are performed using a large excess of reagents and reactants to ensure high conversions, therefore minimizing the amount of remaining starting materials and the so-called truncated libraries.

Alternative procedures for DNA-recorded synthesis of DELs
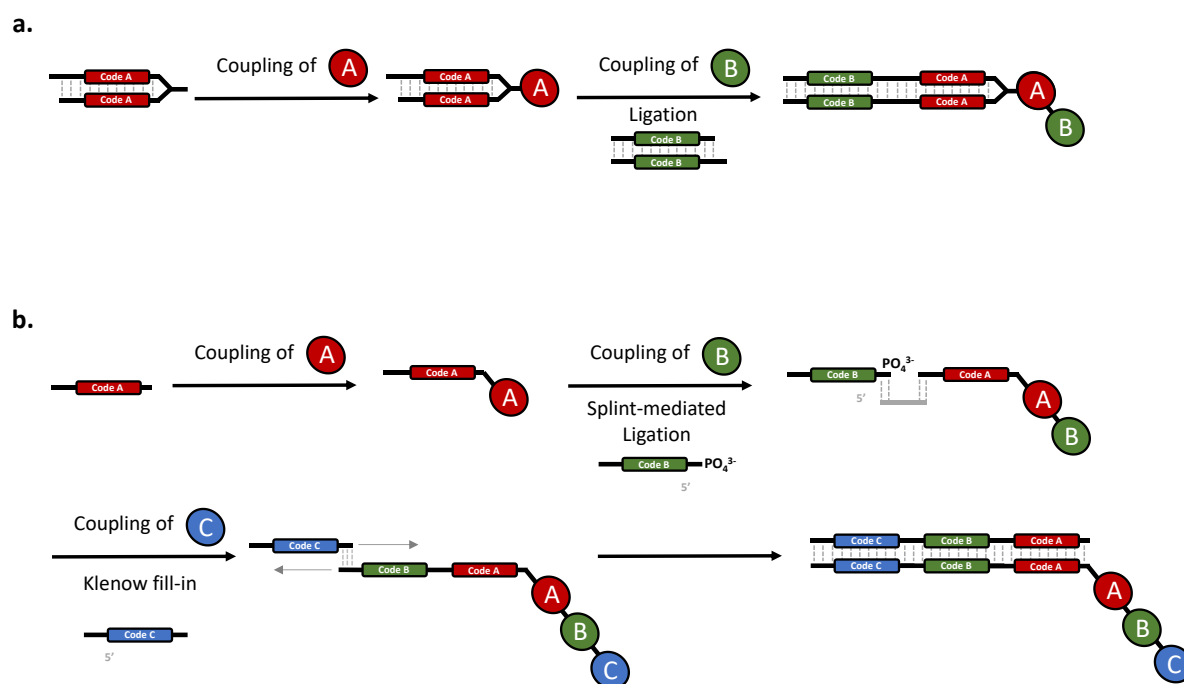
Figure 2.11. Schematic representation of alternative procedures for DNA-recorded chemical libraries. **a**. The small molecules are appended to the dsDNA by a linker (head-piece) which are encoded by subsequent DNA ligations using overhang DNA heteroduplexes. **b**. Building blocks A and B are encoded by splint-mediated ligation, in which the additional DNA fragment is ligated to the nascent DNA structure. Building block C is encoded by the annealing of a partially complementary DNA fragment followed by a Klenow polymerization procedure.

Liu and co-workers designed and implemented library construction methodologies using pools of pre-encoded DNA templates (**Figure 2.12a**).[99] This methodology relies

on DNA-directed chemical reactions to promote the coupling of diverse sets of building blocks. The interaction of two nucleobases through hydrogen bonds is known to increase the local concentration of the reactants in solution and to accelerate bimolecular reactions. The authors described the use of a 48-mer DNA-linked lysine derivative used as a DNA template to mediate three steps of DNA-directed amine acylation reactions with building blocks linked onto 10-mer or 12-mer biotinylated complementary oligonucleotides. After each coupling, suitable cleavage steps are required, and the reagent oligonucleotides are biotinylated for purification by affinity capture with streptavidin-linked magnetic beads.[99]

The group of Xiaoyu Li optimized the encoding method by using a single universal template code, which is capable of directing chemical reactions with multiple small molecule-DNA conjugates displaying various encoding sequences (**Figure 2.12b**).[110] The universal DNA oligonucleotide contains a polyinosine segment that serves as promiscuous hybridization stretch for short oligonucleotides including transferrable chemical moieties.[110]

A tridimensional extension of the classical linear DNA-templated encoding strategy was developed and implemented by scientists at Vipergen (**Figure 2.12c**).[111,112] This methodology, named YoctoReactor®, relies on the annealing and subsequent enzymatic ligation of three-way DNA-hairpin-looped junctions carrying chemical moieties. In the first step, two single-stranded DELs are mixed with a third oligonucleotide, which assists the self-assembly of the libraries. Upon the formation of a three-way junction construct, two sets of building blocks are then coupled by a DNA-templated reaction. The resulting library is then purified by polyacrylamide gel electrophoresis, which confers high fidelity to the process. All incomplete intermediates are removed, and truncations are eliminated from the combinatorial library. After cleavage of the linker and DNA ligation, a PCR primer extension is carried out to generate the complementary strand. After hybridization, the building blocks are transferred onto a core acceptor site, and the final library is obtained in a double-stranded format.[111,112]

Harbury and co-workers described an alternative synthetic approach known as "DNA-routing" (**Figure 2.12d**). This technology requires, at the start of the library construction process, the availability of as many pre-synthesized DNA oligonucleotides as the final complexity of the library. In a sequential fashion, the mixture of oligonucleotides is captured on resin coated with partially complementary DNA fragments, allowing the selective modification of captured oligonucleotides on the solid phase.[102,103] The technology may become difficult to implement if large libraries are desired, given the numerous capture steps that would be required and for the risk of suboptimal fidelity in the hybridization process. Nonetheless, in principle, DNA-routing procedures may facilitate the Darwinian evolution of library complexity, as the oligonucleotides recovered at the end of a selection experiment could be used to drive the synthesis of chemical variants of preferentially enriched compounds. Similar considerations have also been made for DNA-templated synthesis strategies.

a. Classical DNA-directed Synthesis

b. DNA-directed Synthesis with General Template

c. YoctoReactor™ Technology

d. DNA Routing
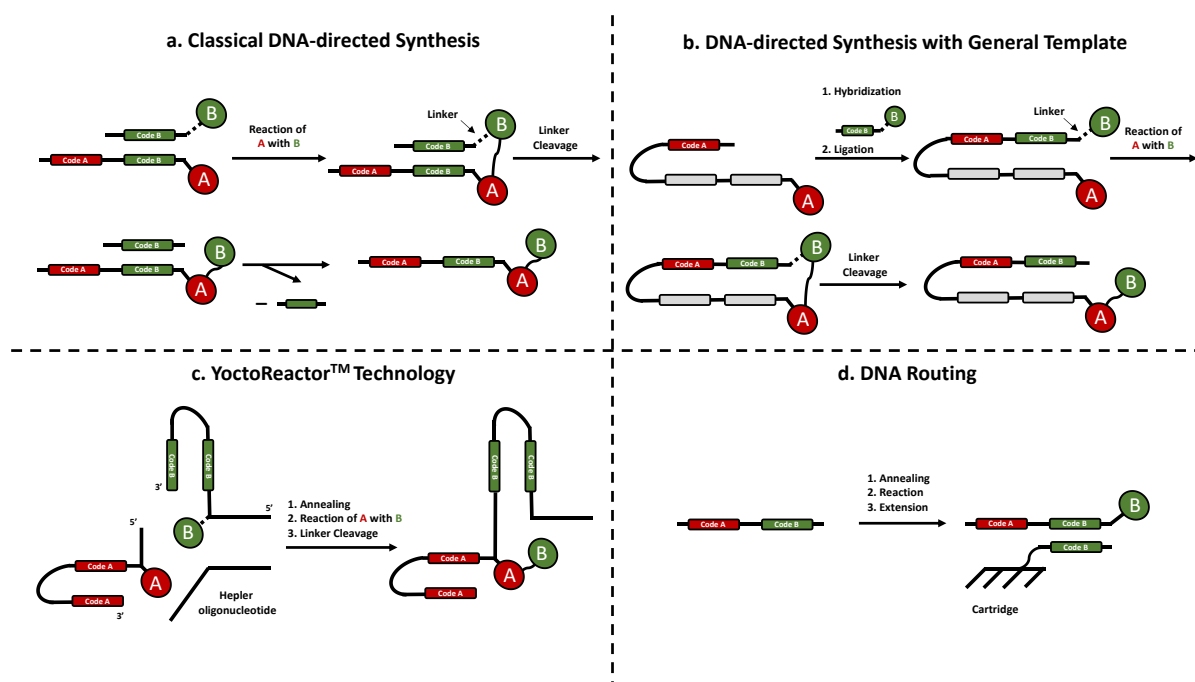
Figure 2.12. Schematic representation detailing the encoding strategies for DNA-templated synthesis of chemical libraries. **a**. During classical DNA-templated synthesis, short oligonucleotides bearing small molecule reactants are annealed with the DNA to promote the reaction between the two chemical entities. After the reaction is completed, the linker between the oligonucleotide and the reactant is cleaved and the oligonucleotide is removed by affinity capture. **b**. Using a polyinosine segment, Universal DNA-templated synthesis avoids the use of high fidelity annealing between the oligonucleotide promoter and the DNA. **c**. The YoctoReactor® technology promotes highly efficient intermolecular reactions by close proximity, using 3D DNA junctions. **d**. On-Resin immobilized DNA complementary codons are used to promote annealing with the different DNA-conjugated small molecules and subsequent reaction and elution.

2.3.1.2 Dual-Pharmacophore libraries

In 2004, the Neri group developed an encoding strategy based on the self-assembly of partially complementary DNA strands, leading to the so-called Encoded Self-Assembling Chemical libraries (ESAC; **Figure 2.13**). In essence, two mutually complementary sub-libraries are annealed in order to create large combinatorial diversity.[100,113] In this dual-pharmacophore library setting, the first sub-library displays chemicals at the 5' extremity of a tagged-oligonucleotide, whereas the second sub-library has chemical moieties attached at the 3' extremity and features abasic portions to facilitate the hybridization of complementary strands.[100,113–115] The strategy for the construction of ESAC libraries makes use of Klenow polymerization in order to transfer code information from one sub-library to the other one.

ESAC libraries feature the simultaneous display of pairs of building blocks that could synergistically interact with the target protein of interest. The flexible linkers between chemical moieties and DNA may facilitate the protein recognition procedure but create an element of complexity when ESAC binders are converted into small organic molecules devoid of DNA. Individual members of ESAC sub-libraries are HPLC purified, which contributes to an extremely high quality of the resulting assembled library. By comparison, library construction using split-and-pool

procedures features a purification step only after the first building block coupling, which may lead to insufficient library purity due to low reaction yields.
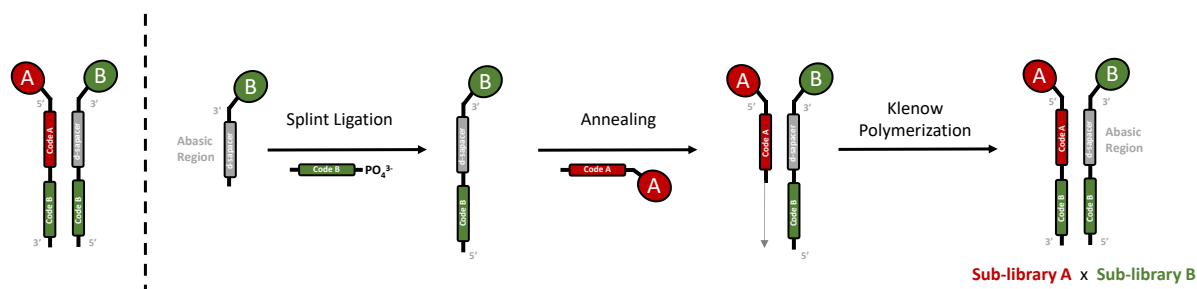
Figure 2.13. Encoding strategies for dual-pharmacophore encoded chemical libraries. During Encoded Self-Assembling Chemical libraries (ESAC) synthesis, both strands A and B bearing the two distinct chemical moieties are prepared and purified individually, offering an extremely high degree of purity to the final library. Upon annealing between code A and the d-spacer oligonucleotide, code B is transferred onto the complementary strand by Klenow polymerization.

The practical use of ESAC allows the identification and recognition of adjacent binding fragments (chelate-binding effect), which can be exploited in FBDD programs, where every single moiety can be engaged in two distinct non-overlapping binding events. In analogy with FBDD, the two chemical moieties must be linked to yield a single organic molecule. Bigatti *et al.* reported an optimized process to expedite the fragment-linking strategy on ssDNA using a set of predefined bi-functional scaffolds.[116] The DNA-conjugate is hybridized with a complementary locked nucleic acid (LNA) bearing a fluorescent molecule (fluorescein or bodipy) and used in fluorescence polarization (FP) assays to determine their dissociation constant with the target protein. From this screen, the best candidates are resynthesized by conventional off-DNA organic synthetic methods and the binding affinity confirmed by orthogonal methodologies.[117,118]

Reddavide *et al.* reported the application of "dynamic recombination" for the synthesis of "ESAC-type" libraries (**Figure 2.14a**).[119] The principle, based on "dynamic combinatorial chemistry" (DCC), employs a reversible covalent bond (e.g., disulfide bond, Schiff-base formation) to construct dynamic systems of transient small molecule adducts in thermodynamic equilibrium. In analogy to ESAC, the two sub-libraries have a short complementary DNA strand, which allows the formation of a heat-induced DNA-encoded dynamic combinatorial chemical library (hi-EDCCL). Due to thermodynamic instability, the two sub-libraries can hybridize to form unstable dsDNA interactions. Upon addition of the target, the equilibrium is shifted towards the high-affinity duplexes. Thus, the protein can be considered as a template for the *in-situ* generation of potent binders via the chemical stabilization of unstable adducts. After a round of selection, the non-binding pairs can be "shuffled" by heating and used for a second round of selection to identify the best combinations. Zhou *et al.* described a conceptually similar method, generating EDCCL libraries from two sub-libraries that could be covalently connected after a binding event to the target protein of interest, thanks to a *p*-stilbazole moiety (**Figure 2.14b**).[120] Upon UV irradiation, an intermolecular [2+2] cycloaddition locks the dynamic exchange of each binding pair. The resulting duplexes, which synergistically interact with the target protein, are then isolated, PCR amplified, and decoded by high-throughput DNA sequencing.

In 2019, the second generation of EDCCL libraries was reported, in which a Y-shaped DNA construct was designed for the dynamic enrichment of synergistic binding pairs (**Figure 2.14c**).[121] The approach features the use of a third DNA strand that anneals to the complementary ESAC components, contains the code information for the pair of chemical moieties, and can be PCR amplified and sequenced at the end of the selection procedure.

Alternative procedures for self-assembling synthesis of DELs

a. hi-EDCCL Approach

b. EDCCL with photo-crosslinking

c. Y-shaped EDCCL
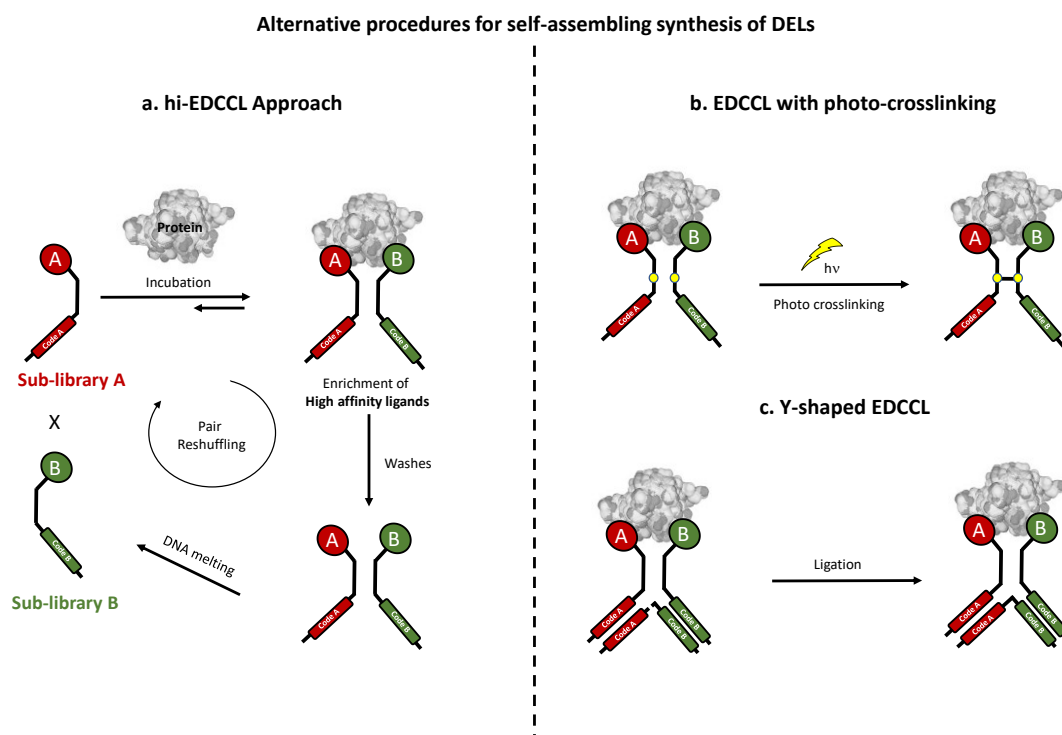
Figure 2.14. Schematic representation of different EDCCL approaches. **a**. hi-EDCCL are based on partial annealing of two complementary sub-libraries. The DNA duplex is unstable until the addition of the target displaces the equilibrium towards the high-affinity combinations. The non-binding moieties can be re-shuffled to identify the best combinations. **b**. An evolution of hi-EDCCL is based on the generation of a physical linkage ([2+2] UV-promoted cycloaddition) between both DNA strands once the equilibrium gets shifted upon addition of the target. **c**. The latest advancement on EDCCL relies on the formation of Y-shaped DNA constructs to facilitate the dynamic enrichment of synergistic binding pairs.

In principle, peptide nucleic acids (PNAs) could be considered as an alternative to DNA for the construction of DELs. PNAs are more stable than DNA and may enable a broader set of chemical reactions. However, PNAs are not compatible with PCR amplification and may require the use of complementary DNA fragments for the hybrid formation and subsequent library decoding. Winssinger and co-workers have pioneered the design, synthesis, and screening of PNA-encoded libraries.[122,123] For many applications, DNA microarrays have been used for the hybridization of PNA-based ligands recovered at the end of affinity capture procedures, followed by a fluorescent readout detection.[122]

2.3.2 DNA-compatible reactions for DEL synthesis

The efficient exploitation of DELs depends on several crucial parameters (e.g., library size, library diversity, encoding strategy, screening methods, sequencing

power). Even though some of them are already addressed, library diversity remains a factor that can be improved.

The construction of DELs and the chemical diversity covered highly depend on the availability of a sufficient number of individual building blocks, as well as on the development of DNA-compatible reactions. The current commercial and on-demand availability of mono-, di- and tri-functional building blocks would, in principle, be sufficient to cover a big part of the chemical space using simple reactions like amide bond formation, or reductive amination/alkylation. However, the multiple possible ways to connect DEL building blocks would highly influence the properties of the final library members and the quality of the molecules obtained.[124–129]
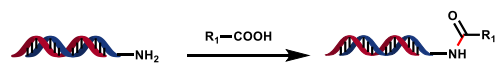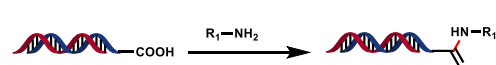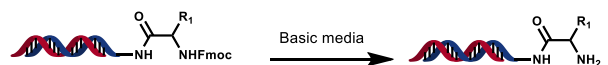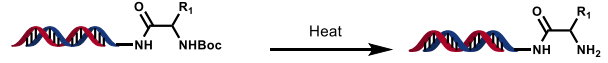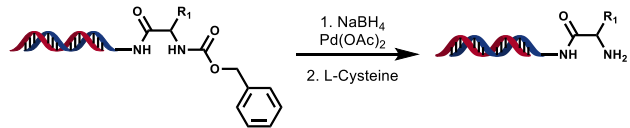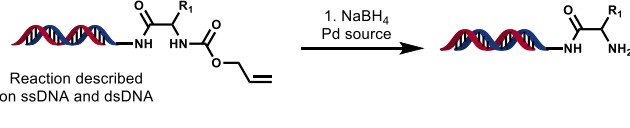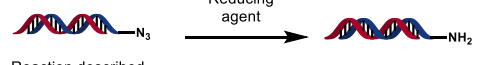
Historically, DNA-compatible reactions were thought to be limited to the insolubility of DNA in organic solvents, as well as its instability to harsh reaction conditions (e.g., acidic and oxidizing conditions).[127,130] The degradation of the DNA influences profoundly the outcome of DELs since the identification of small molecule binders depends on the ability to efficiently amplify the encoding information *via* PCR, and on the readability of the templates when performing NGS.[131,132] On the other hand, the performance of DELs is also influenced by the different by-products that can be formed during the chemical reaction steps.[133] Therefore, it is also important to consider the average conversion of DEL reactions for efficient library synthesis and affinity selection campaigns. Even with these limitations in hand, in recent years, the number of new compatible transformations reported has increased exponentially, together with new reaction methodologies for protecting the DNA from harsh conditions.[124,134–138]

Chemical transformations for the formation of new carbon-carbon, carbon-heteroatom, and heteroatom-heteroatom bonds have attracted most of the attention in recent years. Several new reaction conditions for Suzuki, Sonogashira, or Buchwald-type cross-coupling reactions have been described, among others.[135,139–143] On the other hand, photocatalysis and C-H activation are among the other classes of reactions that have been reported in the last few years.[144–151] Even if new chemical transformations have attracted most of the attention, the modification of pre-existing functional groups (e.g., carboxylic acids, amines) or the *in-situ* formation of heterocycles and non-aromatic heterocyclizations (e.g., oxadiazoles, thiazoles, benzimidazoles) is still an active research field in DEL, since these transformations may also increase the availability of new DEL-compatible building blocks.[152–171]

Table 2.3 illustrates some of the classical and most recent DNA-compatible transformations and DNA-compatible modalities reported, but a full comprehensive revision is available in a recent publication from Hupp *et al.* (X-Chem Inc.).[134]

A new DNA-compatible diazo-transfer reaction is described in entry 10 of **Table 2.3**. This new transformation is part of the research work described in this thesis (section 4.2) and was published in 2019.[170] The new reaction has served as a tool for the generation of a new DEL design, for which a patent application was filed in 2019. Moreover, the publication was highlighted on Synfacts, showing the importance of this transformation.[172] In 2021, researchers from Bayer AG have expanded the scope, including anilines. Nevertheless, the use of copper salts for the efficient transformation of anilines into their corresponding azides may influence the readability of the DNA fragment and influence the selection output and the NGS results.[171]

Table 2.3. Classical and most recent DNA-compatible reactions

Entry	On-DNA Reaction	Reaction Conditions
1	R_1—COOH → amide formation. Reaction described on ssDNA and dsDNA	Different reaction conditions. **a.** DMT-MM in borate buffer, pH = 9.4; **b.** s-NHS/EDC in MOPS buffer pH = 8; **c.** EDC/HOAt/NMM in MOPS buffer pH = 8 at room temperature over 16 h
2	—COOH, R_1—NH$_2$ → HN—R_1. Reaction described on ssDNA and dsDNA	Different reaction conditions. **a.** Activation of carboxylic acid with DMT-MM at 30 °C for 30 min, then addition of amine, at 30 °C over 16h. **b.** Amine, HCl and DMT-MM at room temperature over 48 h. Addition of DMT-MM after 48 and 60 h. Total reaction time 72h
3	NHFmoc, Basic media → NH$_2$. Reaction described on ssDNA and dsDNA	Different reaction conditions. **a.** 20% Piperidine in Water at room temperature for 2 h **b.** Triethylamine at 37 °C over 16 h.
4	NHBoc, Heat → NH$_2$. Reaction described on ssDNA and dsDNA	Different reaction conditions. **a.** borate buffer pH = 9.4, 90 °C over 16h; **b.** bicarbonate buffer pH = 8.5, NaOAc, MgCl$_2$, 75 °C over 24 h; **c.** borate buffer pH = 9.5, 80 °C over 48h; **d.** water, block copolymer containing sulfonic acid moiety, 40 – 50 °C, 4 – 18 h
5	1. NaBH$_4$ Pd(OAc)$_2$ 2. L-Cysteine → NH$_2$	**1.** Water, NMP, DMA, at room temperature 1 h. **2.** L-Cysteine at room temperature 4 h
6	1. NaBH$_4$ Pd source → NH$_2$. Reaction described on ssDNA and dsDNA	Different reaction conditions. **a.** on ssDNA Water, ACN, DMA, Pd(PPh$_3$)$_4$ at room 2 h; **b.** on dsNDA **1.** Water, NMP, DMA at room temperature 1 h. **2.** L-Cysteine at room temperature 4 h
7	—N$_3$, Reducing agent → NH$_2$. Reaction described on ssDNA and dsDNA	Different reaction conditions. **a.** on ssDNA Tris buffer, TCEP, 40 °C for 3 h; **b.** on ssDNA 9:1 ACN:Water [Ru(bpy)$_3$]Cl$_2$, 26 W CFL irradiation, 25 °C for 1 h; **c.** on dsDNA tris buffer pH = 8, TCEP, 25 °C for 12 h **d.** on dsDNA **1.** Water, NMP, DMA, Pd(OAc)$_2$, NaBH$_4$ at room temperature for 1h, **2.** L-Cysteine at room temperature 4 h

30

Table 2.3. Classical and most recent DNA-compatible reactions. Continuation

Entry	On-DNA Reaction	Reaction Conditions
8	Reaction described on ssDNA and dsDNA R = Me, Et, tBu	Different reaction conditions. **a.** for Me and Et esters, NaOH, borate buffer pH = 9.4, 60 °C for 2 h **b.** for Me and Et esters, water, LiOH at room temperature for 2 h; **c.** for tBu ester, borate buffer pH = 9.4, at 80 °C for 2 h
9	R = Bn, Allyl	**1.** Water, at room temperature 1 h. **2.** L-Cysteine at room temperature 4 h
10	X = BF$_4$, HSO$_4$ Reaction with BF$_4$ was described on ssDNA. Reaction with HSO$_4$ was described on dsDNA	Different reaction conditions. **a.**on ssDNA for alkylic and benzylic amines, borate buffer pH = 9.4, 37 °C for 1 h **b.** on dsDNA for akylic, benzylic and anilines, water, K$_2$CO$_3$, CuSO$_4$ at room temperature for 16 h;
11	Reaction described in ssDNA and dsDNA X = Cl, Br, I, OSO$_2$F	Different reaction conditions. **a.** on ssDNA for Aryl iodides, carbonate buffer, Pd(OAc)$_2$, TPPTS at 60 °C for 3 - 24 h; **b.** on dsDNA for Aryl iodides, phosphate buffer pH = 9.2, EtOH, ACN, Pd(dppf)Cl$_2$, at 90 °C for 1 h; **c.** on dsDNA for Aryl chlorides, bromides and iodides, water, dioxane, sSPhos Pd G2, CsOH, at 80 °C for 15 min; **d.** on dsDNA for Aryl bromides and iodides, water, TPGS-750-M, THF, Pd(dtbpf)Cl$_2$, K$_3$PO$_4$, at 60 °C for 5 h; **e.** on dsDNA for Aryl fluorosulfonates, water, DMA, Pd(OAc)$_2$, TEA, at room temperature for 2h
12	Reaction described in ssDNA and dsDNA X = I, OSO$_2$F	Different reaction conditions. **a.** on ssDNA for Aryl iodides, carbonate buffer, DMA, [PdCl(allyl)]$_2$, TPPTS at 70 °C for 3 h; **b.** on dsDNA for Aryl fluorosulfonates,water, DMA, Pd(OAc)$_2$, Xantphos, TEA, at 60 °C for 2 h
13	X = Br, I	NiBr$_2$ Diglyme, dtbbpy, K$_2$CO$_3$, Ruben's silane, NaI (for Aryl bromide reactions only), quaternary ammonium resin, DMA at room temperature for 3 - 18 h

31

Table 2.3. Classical and most recent DNA-compatible reactions. Continuation

Entry	On-DNA Reaction	Reaction Conditions
14		Borate buffer pH = 9.4, DMSO, KOH, at 30 °C for 1 h
15	 Reaction described in ssDNA and dsDNA X = Cl, Br, I, OSO$_2$F for dsDNA X = I for ssDNA	Different reaction conditions. **a.** on ssDNA for Aryl iodides, water, DMSO, Cu(OAc)$_2$, 2,6-dimethoxyanilino(oxo)acetic acid, sodium ascorbate, K$_3$PO$_4$, at 40 °C for 3 h; **b.** on dsDNA for Aryl iodides, water, DMA, tBuXPhos Pd G1, CsOH at 100 °C for 3 h; **c.** on dsDNA Aryl iodides and aliphatic amines only, water, DMA, CuSO$_4$, proline, sodium ascorbate, KOH, at 100 °C for 2 h; **d.** on dsDNA water, DMA, tBuXPhos Pd G3, NaOH, at 30 °C (Aryl iodides) or 60 °C (Aryl bromides) for 1h **e.** on dsDNA for Aryl fluorosulfonates, water, DMA, tBuBrettPhos Pd G3, TEA, at 60 °C for 2 h **f.** on dsDNA for Aryl chlorides and bromides, water, DMA, Pd-PEPPSI-iPent^{Cl}-pyr, sodium ascorbate, CsOH, at 95 °C for 15 min **g.** on dsDNA for Aryl iodides, NiBr$_2$(bipy)$_3$, TBAB, DBU (only some reactions), quaternary ammonium resin, graphite electrodes 4 mA, 4 A MS, at room temperature for 3 h
16		Different reaction conditions. **a.** Water, DMA, CuBr, 1,10-Phen, nBu$_4$NOH, at 80 °C for 4 h
17	 Reaction described in ssDNA and dsDNA X = Br, I	Different reaction conditions. **a.** on ssDNA PEG+ resin, DMSO, Ir[dF(CF$_3$)ppy]$_2$(dtbbpy)PF$_6$ or Ir[dF(Me)ppy]$_2$(dtbbpy)PF$_6$, NiCl$_2$(dme), 4,4'-di-tert-butyl-2,2'-bipyridine, Cs$_2$CO$_3$, blue LED, at room temperature for 5 - 60 min; **b.** on dsDNA MOPS buffer pH = 8, DMSO, Ir[dF(CF$_3$)ppy]$_2$(dtbbpy)PF$_6$, TMHD)$_2$, TMG, blue LED, at room temperature for 10 - 30 min. Also possible with α-Boc amino acids **c.** on dsDNA Water, DMSO, Ir[dF(CF$_3$)ppy]$_2$(dtbbpy)PF$_6$, NiCl(o-tolyl)(TMEDA),4-(CF$_3$)picolinimidamide, K$_2$HPO$_4$, blue LED, at room temperature for 10 - 30 min. Also possible with α-Boc amino acids
18	 A = carbonyl or (hetero)aryl	Water, DMSO, Ir[dF(CF$_3$)ppy]$_2$(bpy)PF$_6$, K$_2$HPO$_4$, blue LED, at room temperature for 6 h
18	 A = carbonyl or (hetero)aryl	Water, DMSO, Ir[dF(CF$_3$)ppy]$_2$(dtbbpy)PF$_6$, K$_2$HPO$_4$, blue LED, at room temperature for 2 h

32

Table 2.3. Classical and most recent DNA-compatible reactions. Continuation

Entry	On-DNA Reaction	Reaction Conditions
19		Morpholine, aq. DMA, at 45 °C for 16 h
20		Borate buffer pH = 9.5, at room temperature for 24 h
21		1) Borate buffer pH = 9.4, TEA, at room temperature for 5 h, then room temperature or 80 °C for 16 h 2) Borate buffer pH = 9.4, at room temperature for 30 min
22		Borate buffer pH = 9.4 at 60 °C for 1 h
22		Borate buffer pH = 9.4 at 60 °C for 1 h
23	 Reaction described on ssDNA and dsDNA Also described as intermolecular reaction	Different reaction conditions. **a**.on ssDNA (intermolecular) borate buffer pH = 9.4, TBTA, CuSO$_4$, sodium ascorbate, at 30 °C for 3 h **b.** on dsDNA (intramolecular) borate buffer pH = 9.4, CuSO$_4$, sodium ascorbate, at 60° C for 30 min
24		Different reaction conditions. **a. 1.** Water, TMSCN, TBHP, at 50 °C for 10 h; **2.** 50 °C for 20 min **b. 1.** HEPES buffer pH = 7.0/ACN, K$_2$CO$_3$, TBHP, at 50 °C for 10 h; **2.** 50 °C for 20 min **c. 1.** HEPES buffer/ACN, TBHP, at 50 °C for 10 h; **2.** 50 °C for 20 min **d. 1.** Water/ACN, at 70 °C for 10 h; **2.** 50 °C for 20 min

33

2.3.3 Screening Methodologies

Compared to traditional HTS, DEL technology offers the possibility to screen billions of molecules in a single experiment by affinity selection procedures.[173,174] The outcome of a DEL selection campaign may serve as a starting point for a complete drug discovery program or may directly deliver a lead compound that can be slightly modified or not before entering into clinical trials.[175–178] Since the selection of binders from DELs represents such an important step, many different academic and industrial groups have focused their efforts on the development of new screening methodologies. Screening methodologies can be separated into three main groups: selections on solid phase, selections in solution, and cell-based selections. In the following sections, the main features and recent advances on each procedure will be discussed.

2.3.3.1 Screenings on solid phase

In a typical selection procedure on solid phase, affinity-based selections rely on the immobilization of the proteins of interest on solid supports, which are successively incubated with a library.[179–185] Preferentially enriched binders are separated from other library members after affinity capture by stringent washing steps. Suitable solid supports for affinity capture include magnetic beads (**Figure 2.15a**) and resin-filled tips (**Figure 2.15b**). Proteins may be immobilized either by covalent modification of lysine residues or by non-covalent capture of suitable tags (e.g., Biotin, His-tag, or other peptide-tags). Washing conditions and the use of detergents may significantly influence the selection output. In rare cases, immobilization of the protein of interest on solid support may impair its folding, thus contributing to the isolation of false positives. Non-specific binding with the matrix may also lead to an increase in the noise level of the selections, thus hindering the discrimination between real binders and artifacts.[186] Non-specific binding events can be avoided using Herring sperm DNA, bovine serum albumin, biotin, or imidazole as blocking agents. After washing out the non-binders, the binding members can be eluted from the protein (e.g., by heat elution). The DNA obtained is PCR amplified and sent for high-throughput DNA sequencing to identify all the possible hit compounds (**Figure 2.15c**).

In analogy to phage display, our group recently published a methodology to efficiently quantify the recovered DNA employing quantitative PCR. This new procedure allows for the quantification of the DNA before and after affinity selection, thus providing fair confidence in the affinity capture efficiency and the quality of the selection campaign.[187]

The simplicity of affinity capture methodologies has made it attractive for many screening campaigns and has successfully been used for the identification of DEL-derived hits.
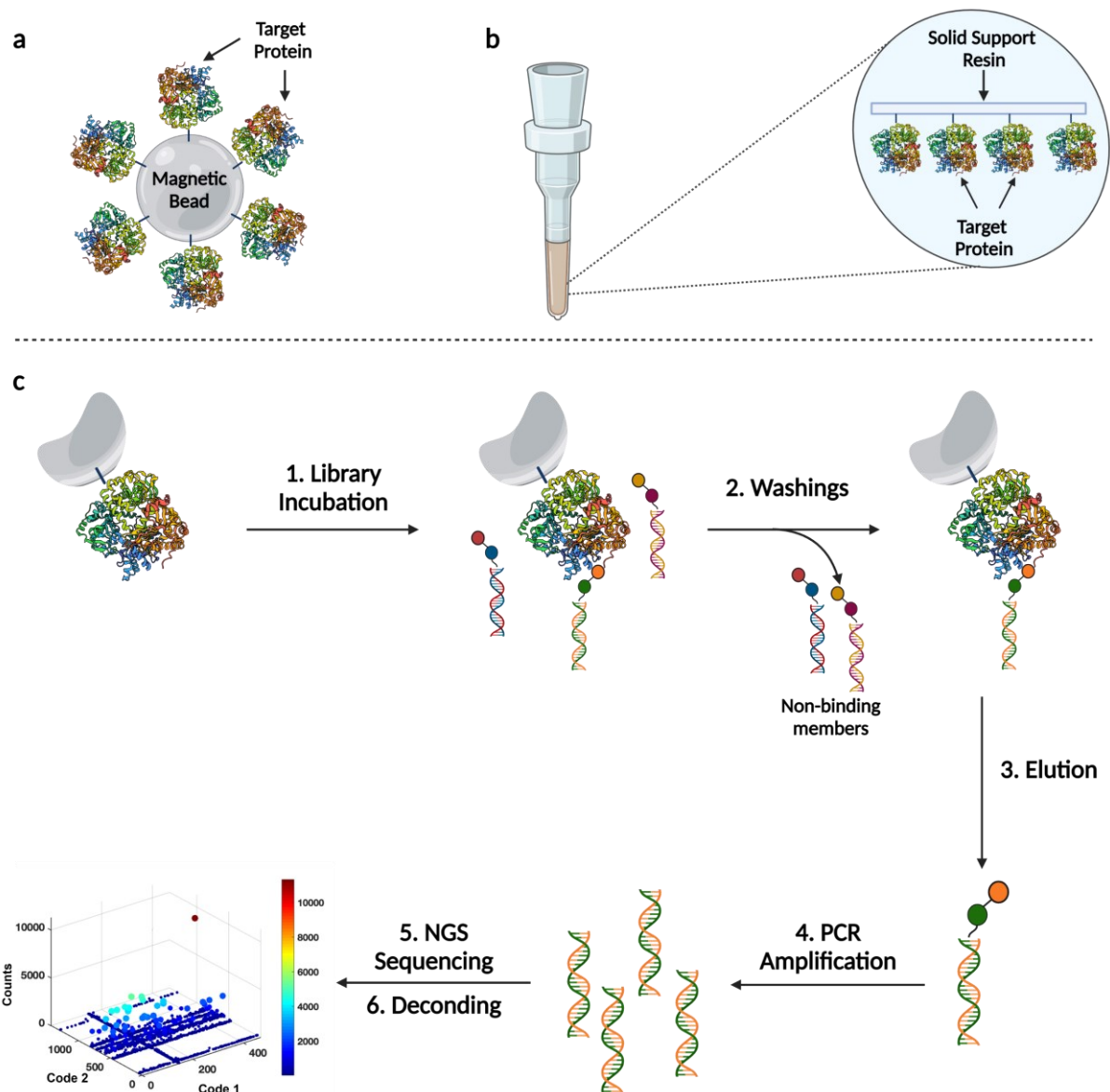
Figure 2.15. Schematic representation of solid-phase screening procedures. **a**. Immobilization of the target protein into functionalized-magnetic beads. **b**. Immobilization of target protein into functionalized-resin tips. **c**. The library is incubated with the immobilized target. After the incubation step, several stringent washings are performed to wash away non-binding members. After washing, binding members are eluted from the protein; the DNA is amplified by PCR and sent to high-throughput DNA sequencing. The results of the sequencing can be plotted as a function of both encoding fragments (Code 1, x-axis; Code 2, y-axis) and the number of sequence counts of each combination (Counts, z-axis). Created with BioRender.com

2.3.3.2 Screenings in solution

In principle, it would be desirable to perform selections in solution, without the need to immobilize the target on a solid support. In 2010, Liu and co-workers described the use of Interaction-Dependent PCR (IDPCR) for the identification of small-molecule binders of oligonucleotide-tagged proteins (**Figure 2.16a**).[188] In this approach, single-stranded DNA DELs are used, and the target protein is covalently tagged with an oligonucleotide, which is complementary to the DEL tags and may stabilize the ligand-protein interaction. Such oligonucleotide can also act as a primer for the selective PCR amplification of library members which preferentially interact with the protein target.[188]

Pseudo-hairpin structures may be particularly suited for IDPCR. Later, the same group developed an extension of their first in-solution selection methodology named "Interaction Determination using Unpurified Proteins" (IDUP).[189] Using cell lysates, they were able to identify binders for targets that are otherwise very difficult to purify, enhancing the potential uses of in-solution methodologies. Instead of covalently attaching oligonucleotides to the protein of interest, DNA can be coupled to an antibody or a SNAP-tagged protein.[190]

Vipergen developed Binder Trap Enrichment (BTE) as a screening methodology that occurs in water-in-oil emulsions. In the first step, a DNA-tagged protein target is incubated with a library. By subsequently forming water-in-oil emulsions at high dilution of target protein, the simultaneous incorporation of the protein target and bound DEL member within the same water droplet can be promoted. A ligation step can be performed within the droplet, thus leading to a hybrid DNA molecule that contains both the DEL barcode and the DNA fragment originally coupled to the protein. The resulting ligation product can be PCR amplified and sequenced (**Figure 2.16b**).[112]
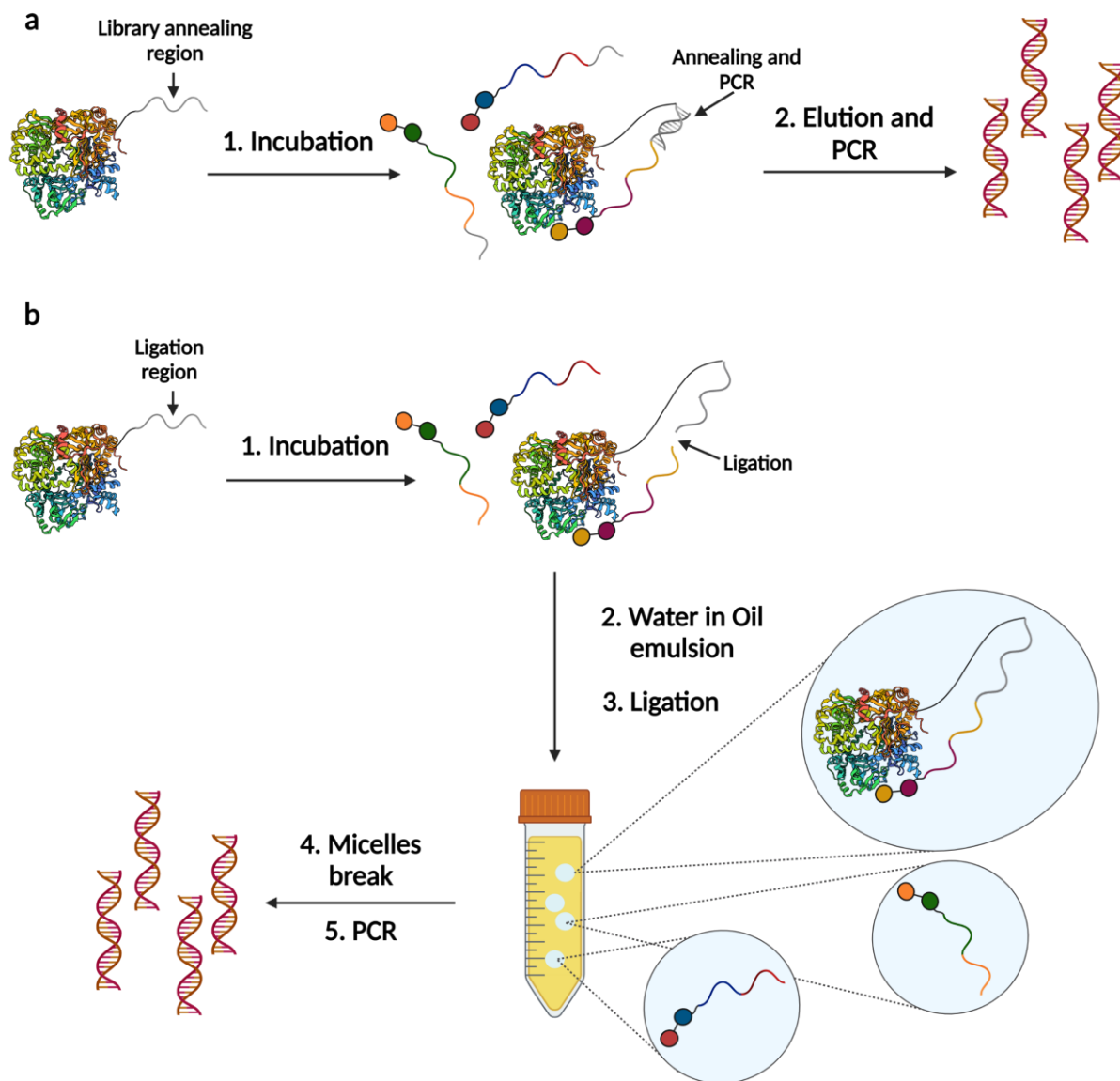
Figure 2.16. Schematic representation of screening procedures in solution. **a**. Interaction dependent PCR (IDPCR). The library is incubated with the pre-tagged protein of interest. Only binders that ensure close proximity between both DNA regions are subjected to annealing and PCR amplification. **b**. Binder trap enrichment (BTE). The library is incubated with the pre-tagged protein of interest. Once binders have bound the protein, dilution, and water in oil emulsion are performed. The complex protein-binder is trapped inside the micelles and is subjected to DNA ligation between the library and the protein DNA fragments. The micelles are broken, and the ligated DNA is PCR amplified. Created with BioRender.com

Li *et al*. described an innovative methodology so-called "DNA-programmed photoaffinity labeling" (DPAL) to select binders from a DELs without the need of tagging or immobilizing the protein before the screening.[191–193] DNA-conjugates are capable of forming a stable heteroduplex with a short complementary oligonucleotide containing a photoreactive group that reacts with proteins of interest. When DNA-conjugates bind to the target protein in solution, an irradiation step ensures that preferential binders are captured on the target protein by photo-crosslinking. The same approach has been followed by our group, in which a critical evaluation of different parameters of photo-crosslinking methodologies using model selections against Carbonic Anhydrase IX (CAIX) was investigated (**Figure 2.17**).[194]
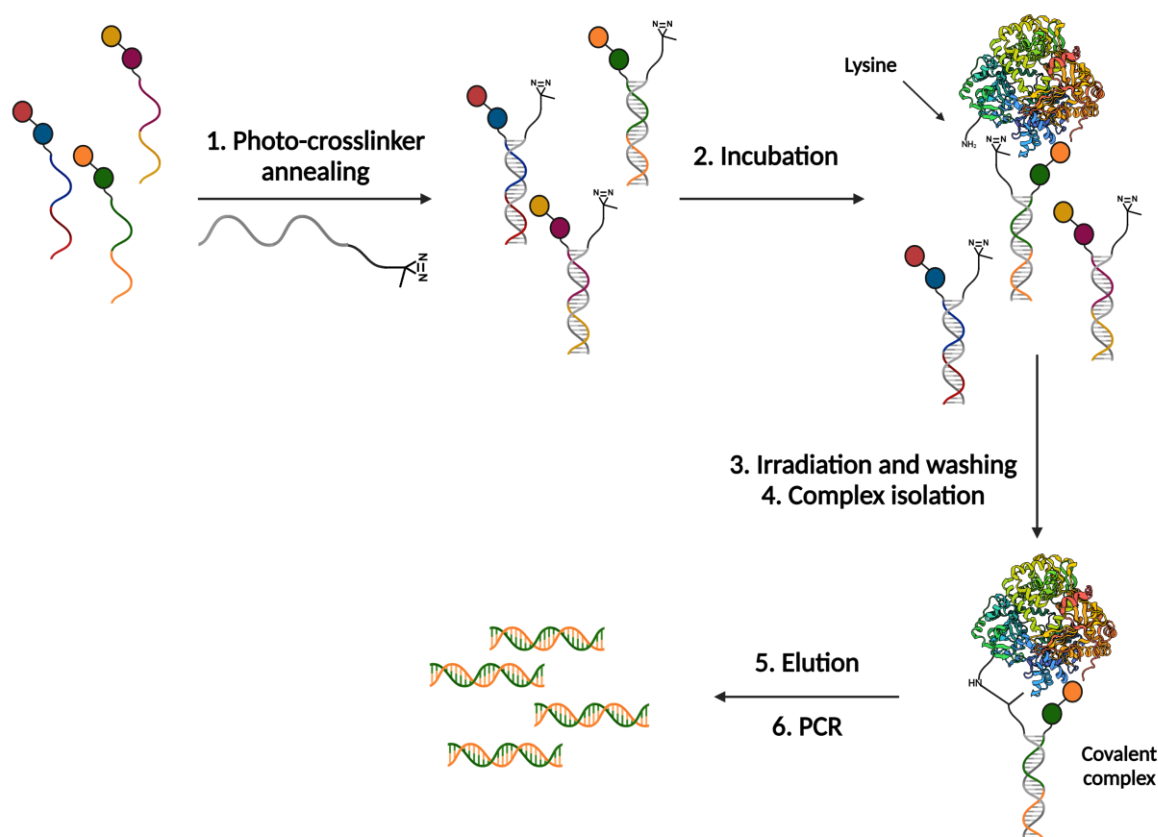
Figure 2.17. Schematic representation of screening procedures in solution mediated by photo-crosslinking (DPAL). The ssDNA library is pre-annealed with a complementary oligonucleotide bearing a photo-reactive group. After incubation with the target, the mixture is irradiated at 365 nm to promote the crosslinking between the photo-reactive group and the target, stabilizing the preformed complex. The complex is captured (e.g., using magnetic beads) and the binding members are eluted, and PCR amplified. Created with BioRender.com

2.3.3.3 Cell-based screenings

Although DEL screenings on immobilized targets and in solution have demonstrated to be a successful approach for the identification of new chemical entities, certain targets may be difficult to stabilize in those conditions, or the isolation of them, out of the context of the living cells, can lead to a loss of their biological activity (e.g., misfolding). It may therefore be desirable to develop new methodologies for the execution of DEL selections against targets in their natural environment (e.g., membrane proteins on cells). In 2015, scientists at GSK described the first cell-based DNA-encoded library screening. In this report, transduced HEK293 cells overexpressed the tachykinin receptor neurokinin-3 (NK3). A DEL repertoire

containing approximately 15 billion compounds was incubated with the living cells, using reagents to avoid target internalization and unspecific binding (sodium azide and sheared salmon sperm). After a series of washing steps, binding molecules were eluted by heat denaturation of the cells and the resulting supernatant was collected after centrifugation. The authors were able to identify a series of different NK3 antagonists, from 4 different DEL libraries, which display different structural motives from one to another. Moreover, some of these compounds have potencies and specificities comparable to other known NK3 antagonists optimized by medicinal chemistry campaigns (Talnetant and Osanetant).[195]

In 2019, the group of Krusemark reported DEL screening experiments against protein targets located either in the cytosol or on the surface of live cells. The authors used a cyclic cell-penetrating peptide (cCPP) conjugated to DNA-linked molecules to facilitate the penetration of the DEL members into the cytosol. A photo-reactive group was used to enrich DEL members capable of selective interaction with the protein target of interest.[196] In spite of these encouraging results, the absence of more reports on successful DEL selections on cells makes it difficult to evaluate how generally applicable such procedures may be. In principle, the binding interaction of two binding partners present at very low concentrations (i.e., the target protein on the cell surface and a DEL member) could be challenging.

To improve the performance of cell-based selections, Xiaoyu Li and co-workers have recently described the possibility to specifically label cell membrane proteins with a DNA tag, in a similar manner as previously described by Liu *et al*.[188] The presence of such DNA tags on the target protein of interest may be able to promote a specific hybridization of libraries based on ssDNA, thus increasing the local concentration of DEL compounds in the cell proximity. The affinity of the DNA guide for the library members should not be too high, to allow for a further affinity gain as a result of ligand-protein interaction. After suitable washing steps, preferential binders could be recovered, PCR amplified, and sequenced (**Figure 2.18**).[197]
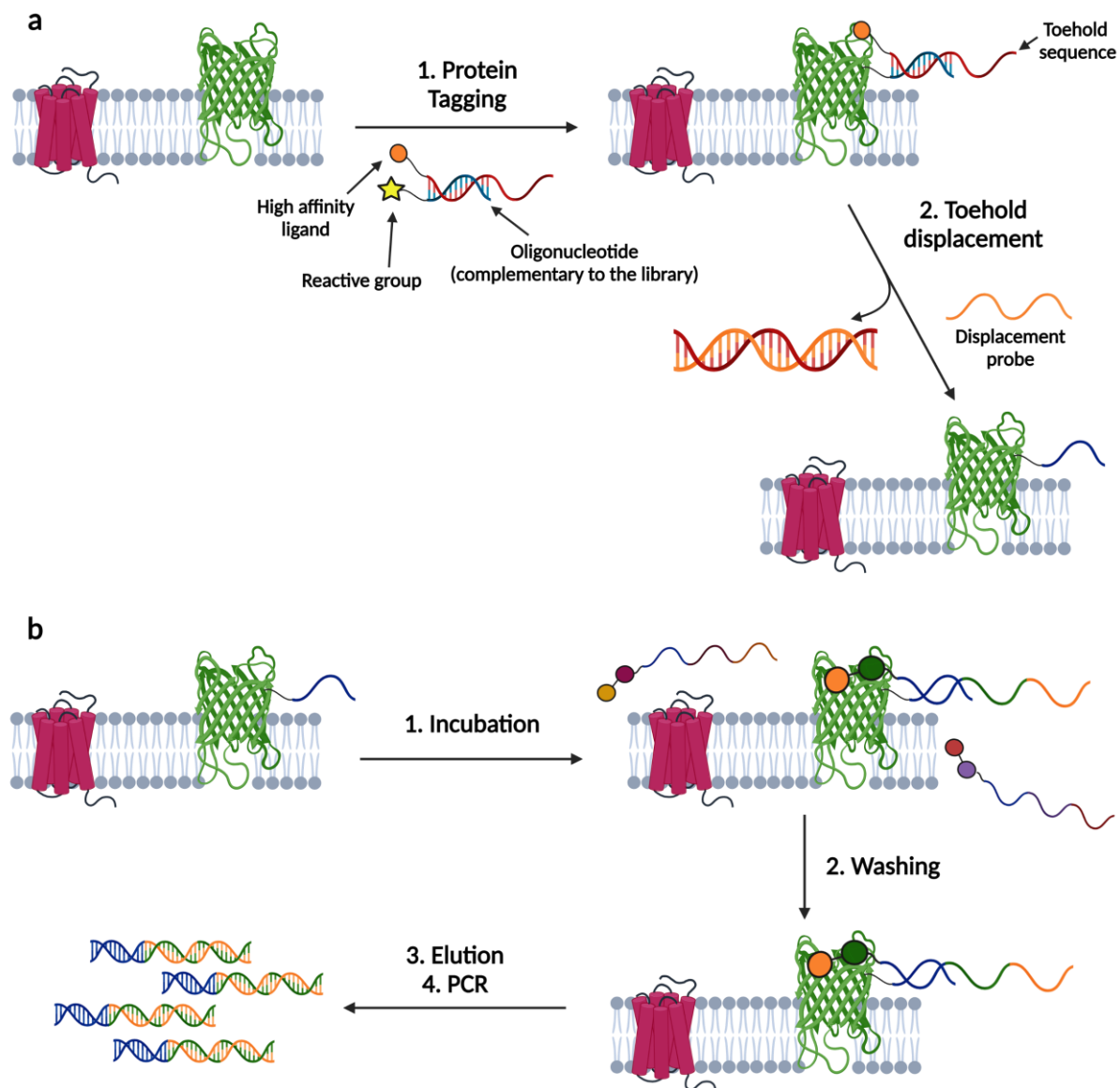
Figure 2.18. Schematic representation of the work of Xiaoyu Li and co-workers. **a**. The protein of interest can be specifically tagged with an oligonucleotide, using DNA-programmed photoaffinity labeling methodologies. After labeling, the tagged-high affinity ligand is removed using a fully complementary oligonucleotide displacement probe. **b**. Cells with the specifically labeled target of interest are incubated with the library. The oligonucleotide attached to the targets facilitates the interaction with binding members by increasing the affinity. After washing away the non-binding members, the ligands are eluted from the protein and the DNA is PCR amplified. Created with BioRender.com

Early this year, scientists at Vipergen have described a new methodology for DEL screening on live cells. The authors reported the use of oocytes, which are more than 100,000 times bigger than typical somatic cells, to specifically express the protein target of interest in the cytosol. The target protein of interest (POI) is expressed in the oocytes fused to a prey protein domain. A bait DNA-conjugate (a specific binder for the prey protein) is co-injected with the library into the oocytes. The purpose of the bait-prey complex is to ensure the subsequent PCR amplification of the library binders to the POI. Using their proprietary BTE methodology, a water-in-oil emulsion is formed by high dilution, thus isolating the complex between POI-prey fusion protein, bait, and library member. A ligation step can then be performed to form a hybrid that contains

40

both the bait DNA barcode and the DEL member barcode. The resulting DNA hybrid can be PCR amplified and sequenced (**Figure 2.19**).[198]
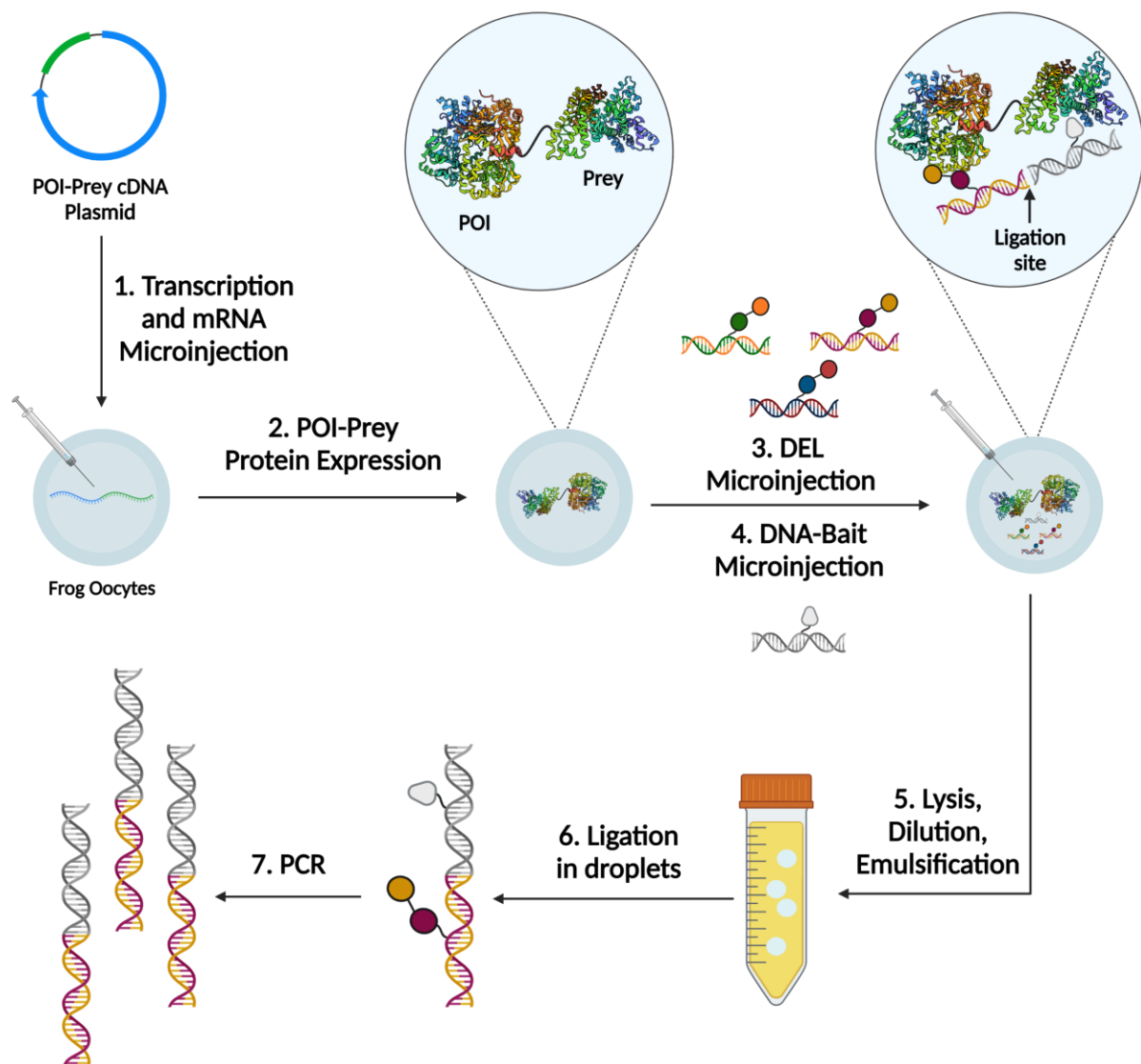
Figure 2.19. Schematic representation of the work of Vipergen. The POI-Prey (Protein of Interest-Prey Protein) protein complex cDNA plasmid is transcribed into mRNA to perform microinjections into frog oocytes. The expression of the POI-Prey is performed in the live oocytes. The library and the DNA-bait conjugate are microinjected into the oocytes and let interact with the POI-Prey complex. The complex between POI-Prey protein, the DNA-bait and, the binding members is isolated following the binder trap enrichment procedure. The proximity between the DNA-bait conjugate and the binding members to the POI enables a DNA ligation between the two fragments, followed by a final PCR amplification step. Created with BioRender.com

2.3.4 Decoding of DEL selections

In analogy to other display technologies like phage display, the power of DNA-encoded libraries technology relies on the possibility to amplify and sequence the genetic information unambiguously associated with all the different library members.[88,104,105,199]

Before the development of next-generation sequencing technologies, DNA sequencing was performed using laborious and tiring processes (e.g., Sanger sequencing). Although Sanger sequencing and other sequencing technologies have provided an invaluable tool in the early genomics era, the necessity for a high-throughput methodology for sequencing millions of different oligonucleotides made DEL decoding a complicated process at its conception.

The early works of the Neri group on the synthesis and selection of ESAC libraries showed how microarray decoding and concatemer formation and sequencing could efficiently decode the genetic information associated with the library members.[100,186,200] Nevertheless, the use of these technologies was limited to libraries with a small number of members. It was in 2008 when the same group demonstrated the practical use of one of the first NGS methods (454 Life Sciences) for decoding a library of 4,000 members.[104] One year later, the seminal work of GSK established the potential of new NGS methods for the successful decoding of large DNA-encoded chemical libraries.[105] Later, in 2010, the Neri group reported again the use of new sequencing technology, Illumina, comparing it with the previous 454 system and showing its better performance in terms of sequencing power.[199] Ever since then, Illumina sequencing has become the preferred methodology for the decoding of DEL libraries (**Figure 2.20**).

The development of NGS technologies also offers a powerful method to quantitatively evaluate the distribution of each library member before and after affinity selection. This comparison allows for the calculation of relative enrichment factors, which can be correlated with the binding affinity of every hit. Moreover, it also facilitates the comparison between selections performed in different experimental conditions (e.g., buffers, temperature) or the comparison between different targets (e.g., isoforms), which gives information about the specificity of the ligands discovered using DEL.[187,201–203]

Despite some efforts on normalizing the procedures for the efficient deconvolution of affinity selection experiments, the evaluation of DEL screening results is typically performed using *in-house* software and statistical methods. To study how to efficiently decipher the sequencing output, researchers in academia have focused their efforts on studying the DNA integrity, which may influence the PCR outcome during the whole process.[133,204–208] One could assume that the number of counts for a particular compound identified after affinity selections can be correlated with the binding affinity, but is important to understand all the possible variables that can determine the selection outcome, such as selection parameters, chemical yields, library size, library PCR amplifiability, sequencing depth, and sequencing errors. In 2017, Satz *et al.* showed that libraries above 10^8 members lead to a higher rate of false negatives due mainly to the higher amount of truncates and by-products during library synthesis.[133] More recently, Sannino *et al.* and Chen *et al.* concluded that a minimum of 10^4 copies per library member may be required to efficiently identify potential binders with dissociation constants below 10^{-6} M, which may be lost in the selection process.[187,209] Those aspects may be essential to consider if one is attempting to build up very large libraries (e.g., $>10^{11}$ library members).

1. Library preparation

DEL Library after affinity selection

PCR Amplification

Illumina adapter

DNA library for sequencing

2. DNA library bridge amplification

Library hybridization
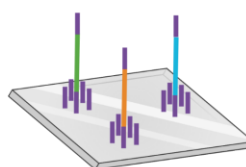
Bridge amplification cycles

Amplified clusters
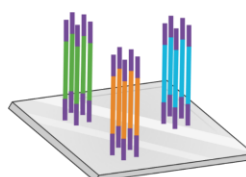
3. DNA library sequencing

Fluorescently labeled nucleotides

A G T C
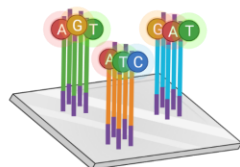
Sequencing cycles

Data collection

4. Alignment and data analysis

Contigs (overlapping regions)

Reads cluster 1   Reads cluster 2   Reads cluster 3

Assembled sequence
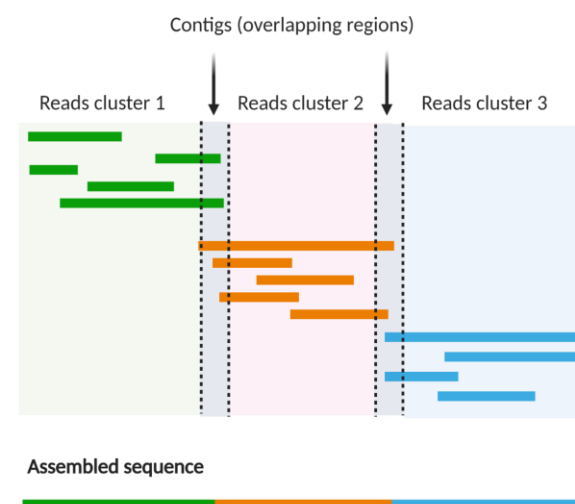
Figure 2.20. Schematic representation of the Illumina sequencing procedure. After affinity selection using DELs, the recovered DNA is subjected to PCR amplification, introducing Illumina adapters. The separation of both DNA strands allows for the hybridization on the surface of the chip, followed by several bridge amplification cycles. The amplified clusters are then subjected to DNA sequencing using fluorescently labeled nucleotides. After data collection and alignment of the different cluster reads, the assembled sequences are enumerated. Created with BioRender.com

The development of statistical methods for the evaluation and comparison of DEL experiments is likely to gain importance in the future. The Neri group first described the use of the negative binomial distribution as a model for the analysis of the sequencing readouts after affinity selection experiments.[210] Further work on the statistical evaluation of selection suggests that the determination of the relative enrichment of sequence counts over the noise may rely on alternative data-processing solutions.[204–207] While most DEL selections are performed in solution, library construction and screening on beads bring certain attractive features. For instance, Paegel and co-workers first reported the use of the Poisson distribution for the calculation of the false-negative rate.[205] In 2018, Kuai *et al.* from GSK reported similar results using the same model for the classical DEL screening platform.[204] In 2019,

Faver *et al.* implemented an attractive z-score metric approach to determine the enrichment of compounds during DEL screening, which heeds the selection sampling bias.[206] More recently, Kómár and Kalinić have reported the use of machine learning (open-source Deldenoiser) to empower the determination and discrimination of real potential binders from the background noise.[207] The fidelity of DNA sequencing has been inspected with algorithms to assess and integrate sequencing errors or PCR duplicates in analytical models, thus enhancing the detection, quantification, and informativeness.[211] Other methods aim to efficiently determine the chemical yields and estimate the binding affinity of ligands coming from DEL selection primary data.[212,213]

Typically, DELs are subjected to DNA sequencing before performing affinity selections to analyze the distribution of every combination in the final pool. This represents the so-called Naïve library and serves as a one-to-one comparison with results from DEL screenings to assess the relative enrichment of every combination. As previously shown in **Figure 2.15**, the representation of DEL screening results is usually plotted in a tridimensional cube, where the axes represent the identity of every building block and the number of sequence counts of every compound. Alternatively, when three building blocks libraries are analyzed, the representation of the sequence counts can be displayed in a color code or by the size of every single combination.

2.3.5 Successful stories using DEL technology

DEL technology offers the ability to screen large collections of molecules of unprecedented size and functionality, which opens new opportunities for drug discovery.[88–94] Over the years, the design and construction of novel DELs have led to the discovery of high-affinity binders against a wide range of proteins of pharmaceutical interest (**Figures 2.21 and 2.22**).[107,108,125,165,169,195,214–227] DEL-derived molecules may possess analogous physical properties to those obtained from traditional screening platforms. Moreover, the increasing number of DNA-compatible reactions combined with the availability of a large panel of building blocks provide higher chemical diversity and complexity for more drug-like structures.[88]

When considering DEL synthesis and screening approaches over the last two decades, two main strategies can emerge. On one side, certain DELs were constructed by split-and-pool procedures, aiming at "drug-like molecules" which would be compliant with the RO5. From such libraries, binders were isolated against various types of targets, including proteins with defined pockets such as kinases, phosphatases, or proteases. In some cases, libraries with three sets of building blocks were screened, but only one or two chemical moieties contributed to specific protein recognition. For this reason, even if the parental compounds were larger than 500 Da, DEL results served as a basis for the discovery of drug-like hits. One often finds molecules comprising two large building blocks (average MW > 200 Da) or three smaller ones (average MW < 160) (**Figure 2.20**).[15,125,176]

DEL-Derived Small Molecule Ligands

RIPK1 $IC_{50} = 1.3$ nM	**sEH** $IC_{50} = 8$ nM	**Autotaxin** $K_i = 12$ nM	**PDE12** $IC_{50} = 0.8$ nM	**PARP1** $IC_{50} = 180$ nM
p38 MAPK $IC_{50} = 7$ nM	**Wip1** $IC_{50} = 6$ nM	**SARS-CoV-2 M^{PRO}** $K_i = 45$ nM	**IL2** $K_d = 2.5$ μM	**FAN1** $K_d = 330$ nM
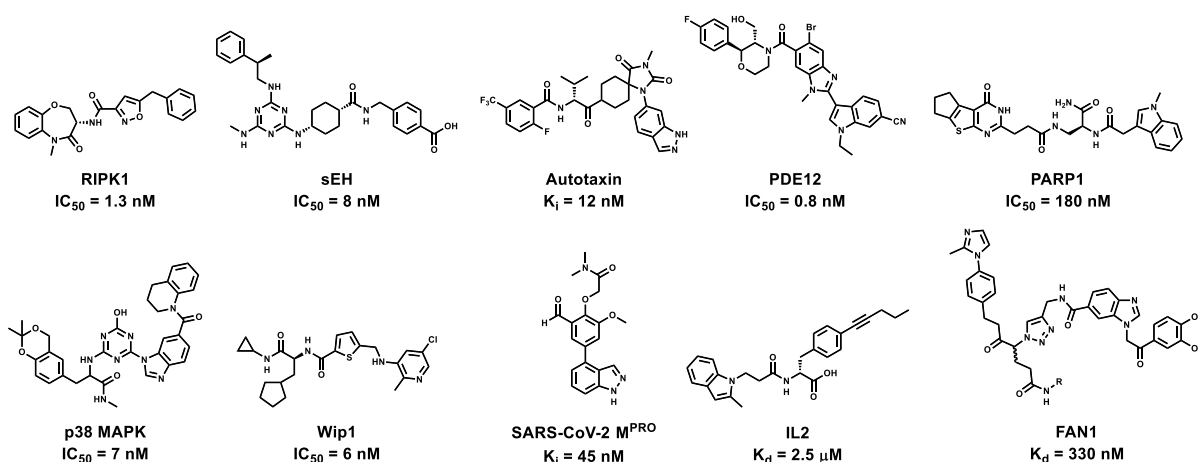
Figure 2.21. Hit small molecules derived from DEL screening campaigns.

To the other extreme, certain DELs have been synthesized with the specific goal of stepping outside of the RO5 chemical space. The synthesis of larger molecular entities (e.g., macrocyclic compounds) may facilitate the recognition of large and flat protein surfaces, which are otherwise difficult to drug with small ligands.[88,115] Several reports of macrocyclic DELs, based on peptidic structures or natural products derivatives, have demonstrated promising properties against targets that would typically be targeted by larger macromolecular binders such as antibodies.[165,226,228,229] Alternatively, macrocyclic peptides have been used as scaffolds for the combinatorial modification of side chains.[107] These repertoires have been screened against dozens of different proteins and have yielded binders with affinities between the low micromolar and the low nanomolar range (**Figure 2.21**).

DEL-Derived Macrocyclic Ligands

Skp2-Skp1 $K_d = 7.5$ μM	**IDE** $IC_{50} = 50$ nM	**CaM** $K_d = 5$ μM	**Streptavidin** $K_d \sim 30$ nM	**AGP** $K_d = 4.1$ μM
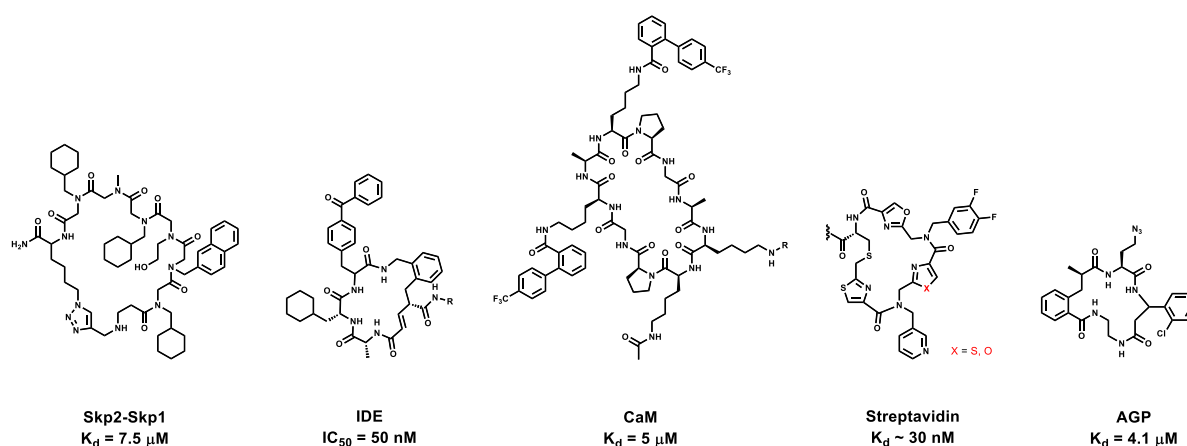
Figure 2.22. Hit macrocyclic ligands derived from DEL screening campaigns.
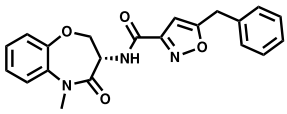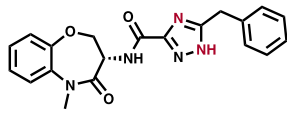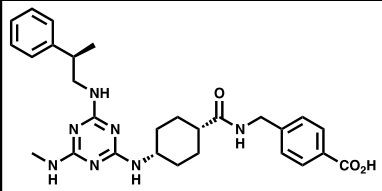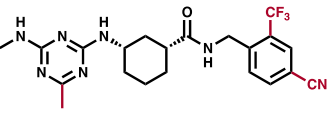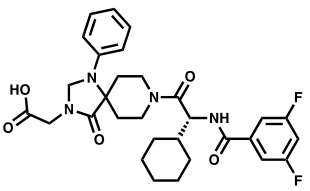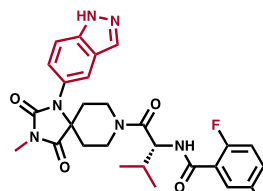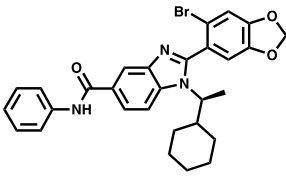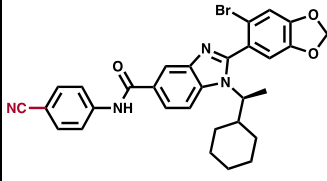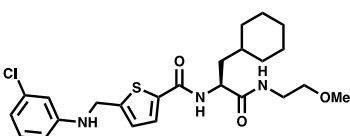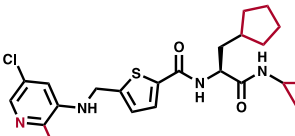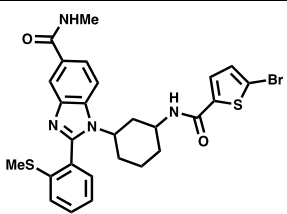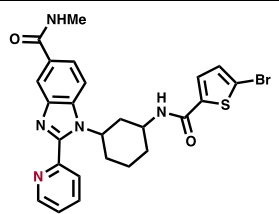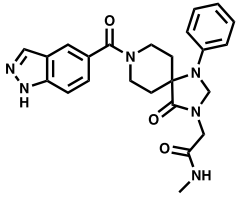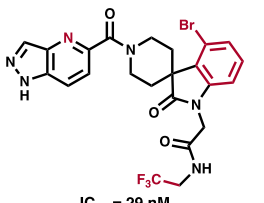
Despite an extensive effort in the field, chemical optimizations of initial hits from DEL screening campaigns are typically required.[15,176–178] **Table 2.4** summarizes the different chemical transformations of DEL hit structures for the generation of lead molecules, which have progressed to late industrial developments. Six out of seven hits display dissociation constants in a single- or double-digit nanomolar range and

optimization studies were performed with few structural alterations, mainly with unvaried or decreased molecular weight and lower cLogP (entries 1, 2, 4–6). Three DEL-derived molecules are currently in clinical trials, inhibitors of receptor-interacting protein 1 (RIP1) kinase (entry 1), soluble epoxide hydrolase (sEH; entry 2), and autotaxin (ENPP2; entry 3).[176–178,222] Removal of unnecessary chemical moieties from the initial hits regularly led to improvement of physicochemical properties. Some examples reported in **Table 2.4** (entries 2, 3, and 7) indicate that DEL-derived hits undergo a different chemical approach during their structure optimization but give a broad space of maneuver during subsequent chemical transformations.

One common feature that can be observed when considering hit to lead conversion of DEL-derived binders is the relatively small number of chemical transformations which were needed to substantially improve binding affinity and potency. For example, scientists at GSK described a RIP1 kinase inhibitor from a library comprising three sets of building blocks, in which only two of the chemical moieties were necessary for binding (entry 1). The confirmed DEL-hit displayed sufficient activity (IC_{50} 1.4 nM) and only a few chemical modifications were performed to improve pharmacokinetic properties.[176] Analysis of medicinal chemistry activities from entry 2 revealed that by eliminating certain chemical features, tuning the regiochemistry of the central core, and judicious substitutions in other parts of the molecule, the authors were able to strikingly increase the activity of the hit compound (IC_{50} 0.027 nM) and reduce its molecular weight by almost 100 Da.[177,178] Recently, AstraZeneca has described the discovery of a potent protease-activated receptor-2 (PAR2) ligand from DEL campaigns. Rapid optimization of the hit compound (entry 4), by the introduction of a nitrile group in para-position, led to the isolation of a lead compound (IC_{50} 23 nM), which acts as a negative allosteric modulator of PAR2.[230] Roche reported a novel and selective inhibitor (entry 7) against Discoidin Domain Receptor 1 (DDR1) from two different library pools of 83 and 85 billion compounds, respectively. Structure-guided optimization of DEL-derived hits resulted in few modifications and the generation of an optimized lead compound with 50-fold IC_{50} improvement (IC_{50} 29 nM).[231]

Direct applications of DEL technology also led to the development of small molecule-drug conjugates (SMDCs) and small molecule-radio conjugates (SMRCs) for oncology applications (treatment and imaging).[115,232–234] Our group reported a high-affinity acetazolamide-derived ligand for carbonic anhydrase IX (CAIX), a well-known tumor-associated antigen overexpressed in renal cell carcinoma and hypoxic tumors.[115] The discovery of such ligand served for the development of a [99mTc]-radiolabeled ligand, which is currently in Phase I clinical trials for the imaging of clear renal cell carcinoma and hypoxia.[235]

Table 2.4: Optimized compounds derived from DEL screens

Entry	Target	DEL Hits	Optimized Structures	Status
1	RIPK1 GSK	IC$_{50}$ = 1.6 nM Mw = 377.4; cLogP = 1.83; tPSA = 80.23	IC$_{50}$ = 1.0 nM Mw = 377.4; cLogP = 0.81; tPSA = 95.39	Phase 2a
2	sEH GSK	IC$_{50}$ = 8 nM Mw = 517.6; cLogP = 0.04; tPSA = 139.57	IC$_{50}$ = 0.027 nM Mw = 447.2; cLogP = −0.22; tPSA = 114.03	Phase 2a
3	ENPP2 X-Chem	IC$_{50}$ = 86 nM Mw = 568.6; cLogP = 4.13; tPSA = 110.26	IC$_{50}$ = 55 nM Mw = 624.6; cLogP = 3.69; tPSA = 97.35	Phase 1
4	PAR2 AstraZeneca / X-Chem	IC$_{50}$ = 90 nM Mw = 546.5; cLogP = 7.23; tPSA = 63.16	IC$_{50}$ = 23 nM Mw = 571.5; cLogP = 6.67; tPSA = 86.95	Lead
5	Wip1 GSK	IC$_{50}$ = 13 nM Mw = 478.1; cLogP = 4.70; tPSA = 79.46	IC$_{50}$ = 6 nM Mw = 461; cLogP = 3.30; tPSA = 82.59	Lead
6	BCATm GSK	IC$_{50}$ = 251 nM Mw = 583.6; cLogP = 4.76; tPSA = 73.8	IC$_{50}$ = 13 nM Mw = 538.0; LogP = 2.92; tPSA = 86.16	Lead
7	DDR1 Roche	IC$_{50}$ = 1.5 μM Mw = 466.5; LogP = 0.79; tPSA = 97.35	IC$_{50}$ = 29 nM Mw = 565.3; LogP = 0.54; tPSA = 106.47	Lead

2.4 Drugging difficult targets

Until today, there are more than 2,000 drugs approved by the FDA and more than 700 protein targets for FDA-approved drugs. Moreover, more than 4,000 genes in the UniProt database have been identified with experimental evidence of being involved in disease conditions. From all these, more than 1,300 might be of particular interest to investigate as they can serve as drug targets, and they belong to known drug target classes (i.e., enzymes, transporters, receptors).[236–239]

The concept of druggability refers to the likelihood of being able to modulate a target with a small molecule. Druggability is a crucial concept in drug discovery programs since it will determine whether a hit compound will progress to a lead compound.[240–242] The most common approach to assessing the druggability of a certain target is to classify it in terms of the gene family it belongs to and understand if other targets of this family have previously been drugged. Certain gene families are known to be "easily" druggable (e.g., kinases, G protein-coupled receptors) and drug discovery programs aiming at drugging these classes have successfully delivered medicines to the market.[240] However, other classes of targets are known to be "undruggable" or, more appropriate, "difficult to drug" or "yet to be drugged".[85] Many of the most interesting and promising targets in cancer have fallen into this category (e.g., RAS and MYC oncogenes) and have encouraged many pharmaceutical companies and academic research groups to develop new techniques and methodologies to characterize these targets and identify new molecular entities capable of modulating their activities.[84,85,243,244]

Novel chemical entities are now being investigated, aiming at addressing the difficult task of developing therapeutics for these classes of targets. Some examples are protein-protein interaction (PPI) modulators, proteolysis targeting chimeras (PROTACs), and nucleic acid-based therapeutics.[244] Among these classes of targets, those involved in protein-protein interactions have been particularly difficult to study and to drug.

2.4.1 Protein-protein interactions

Some of the most critical biological processes (e.g., DNA replication, transcription) are governed by specific proteins that are regulated through protein complexes and controlled via PPIs.[245–249] Targeting PPIs, previously regarded as undruggable targets, represents a significant challenge compared to designing small molecules targeting enzymes or other classes of targets. Certain characteristics make the design of small-molecule modulators of PPIs such a particular challenge. Compared with binding pockets, the interface of PPIs is likely to be a flat surface and contains few cavities. These interfaces are also typically large (1,500–3,000 Å) and are highly hydrophobic. The interaction between both proteins involves amino acid residues resulting in high-affinity binding events, making it even more challenging for small molecules to disrupt them. Moreover, PPIs lack endogenous small-molecule ligands that can serve as a reference for drug design.[246,249]

PPIs usually involve several amino acid residues in the interaction region, which have particular and critical roles in the interaction. These regions are called "hot spots" and as the area of the interaction expands, the number of hot spots increases. A typical approach for characterizing hot spots in PPIs involves the specific mutation of

certain amino acids. Usually, the amino acids on the interface are systematically mutated into alanine residues and changes in the binding-free energy are measured. Changes higher than 2.0 kcal/mol on the binding-free energy upon a specific mutation are taken into account to define what can be considered a hot spot. The most common amino acids that appear in PPI hot spots are tyrosine, tryptophan, and arginine, therefore are usually considered for the design of small-molecule PPI modulators.[246,249]

PPIs can be classified into different classes (**Figure 2.23**): Pairs of globular proteins that interact through a discontinuous epitope without having substantial structural changes upon binding (e.g., Trypsin/BPTI); pairs of globular proteins in which one or both undergo significant changes upon binding (e.g., IL2/IL2R); a globular protein interacting with a single polypeptide chain (e.g., BCL-2/BAX BH3 peptide); and PPIs between two polypeptide chains (e.g., MYC/MAX).[249]

In general, PPIs involving two globular proteins are considered a formidable challenge in drug discovery. One clear example is the interaction between Interleukin-2 (IL2) and its receptor (IL2R). The interaction surfaces on these proteins are flatter (on average) than those involved in other PPIs, and thus potentially less suitable for finding a small molecule binding partner.[249–251] On the other hand, interactions between two single polypeptide units display different challenges. One example of this interaction is the MYC-MAX complex. The lack of defined binding sites, together with the intrinsically disordered structure of both peptides when uncomplexed makes it very difficult to define any potential binding site.[249,252] By contrast, interactions between a single polypeptide chain and a globular protein have been defined to be more druggable. In this class of PPIs, the peptide usually adopts one or more secondary structural elements which define the interaction with the surface of the globular protein. Structural examination of these PPIs has revealed a direct interaction between the hot spots of both partner proteins. Nevertheless, typically the polypeptide hot spot is the one that accesses the globular protein hot spot, and discovery programs targeting this class have yielded ligands that bind to the globular protein, displacing the polypeptide binding partner.[249,253,254]

Despite all the obstacles mentioned above, in recent years progress has been made towards the modulation of PPIs, and in general, towards the druggability of difficult targets. Some of these proteins include the BCL-2 family, integrins, KRAS, and IL2.[244,246,249,251,253,254] A perfect example representing one of these novel compound types is Venetoclax, a recently approved (2016) first-in-class inhibitor for the BCL-2 protein for the treatment of chronic lymphocytic leukemia. It took more than 20 years, extensive efforts, and many leads and clinical trials, but its approval demonstrates the possibility of targeting PPIs with small molecules and represents the first approved modulator of PPIs.[244,253,254] Another recent example is the successful targeting of KRAS[G12C]. Extensive efforts on X-ray crystallography and NMR characterization showed that some particular mutations may create pockets that are considered druggable. This breakthrough science effort led to the development of Sotorasib. The use of this molecule has resulted in absolute or partial responses in 32% of the patients with small-cell lung cancer having KRAS[G12C] mutations and control of the disease in more than 88%, and 73% in colorectal cancer.[244,255–258] Moreover, IL2 has been among the first successful demonstrations that small molecules could inhibit PPIs and it remains as one of the few examples of small molecules able to mimic a

highly discontinuous epitope. The knowledge gained in the exploration of the IL2/IL2R small molecule-mediated inhibition has revealed many interesting features and surprising complexity at the PPI interaction interface and still serves as major guidance for the design of new PPI modulators.[108,244,251,259–262]
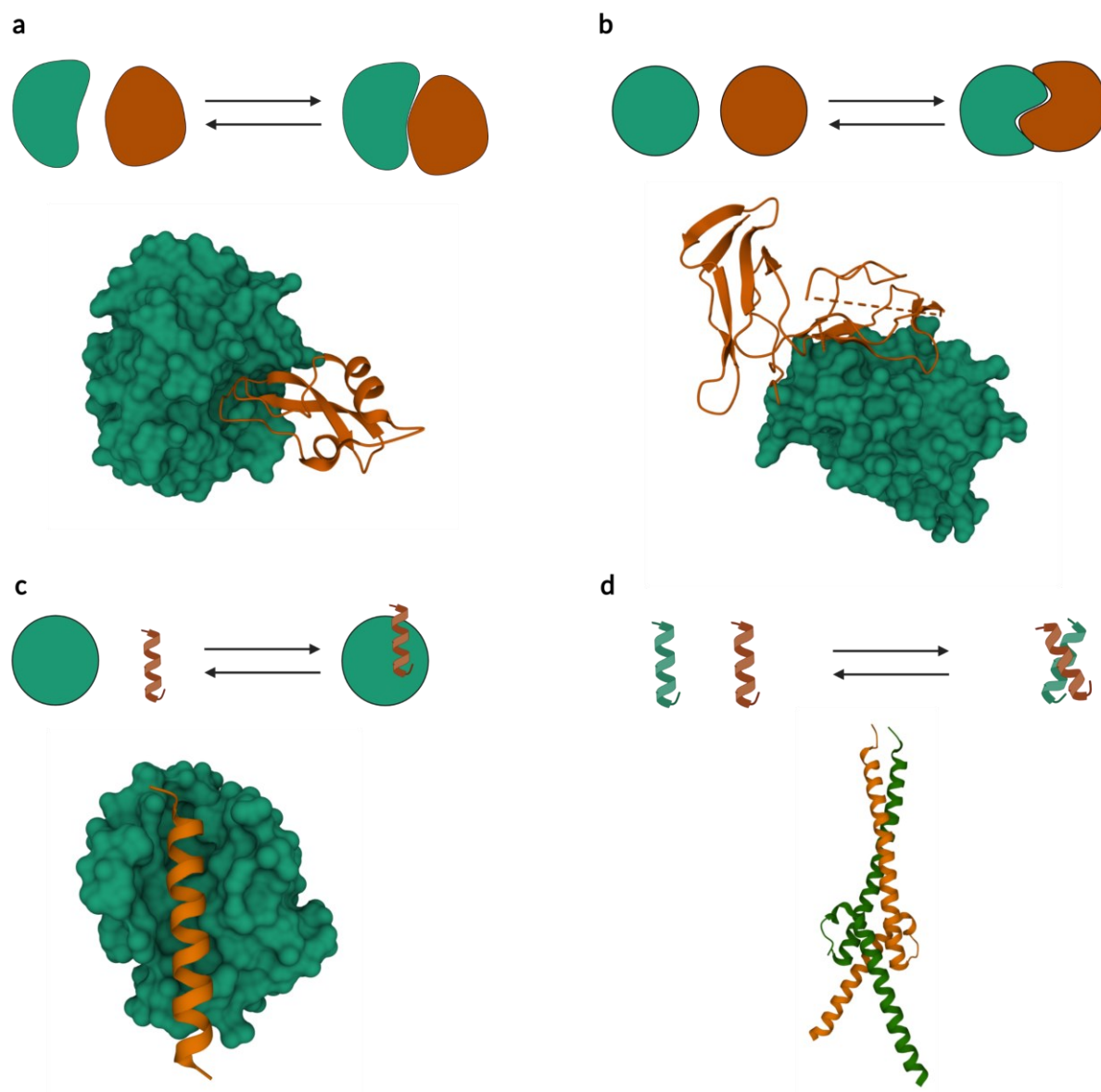
Figure 2.23. Structural classification of protein-protein interactions. A simplified illustration of the protein or peptide partners and representative examples are illustrated. **a**. Interaction between two globular proteins which do not undergo substantial structural changes (Trypsin/BPTI complex; PDB ID 3fp6). **b**. Interaction between two globular proteins undergoing substantial structural changes (IL2/IL2Rα; PBD ID 1z92). **c**. Interaction between a globular protein and a single polypeptide chain (BCL-2/BAX BH3 peptide; PDB ID 2xa0). **d**. Interaction between two single polypeptide chains (MYC/MAX; PDB ID 1nkp). Adapted from[249]. Created with BioRender.com

Drug discovery programs aiming at tackling PPIs typically make use of different hit identification methodologies. Among them, FBDD, rational design of peptides and peptidomimetics, and computational approaches have been demonstrated to be more efficient when investigating this class of interactions. In recent years, the development of DNA-encoded libraries has been postulated as an alternative and/or complement

to all these methodologies for the discovery of PPI modulators. During the last part of this thesis, new IL2 ligands binding at the CD25 recognition site of IL2, which has traditionally been considered a considerable challenge in drug discovery, have been found using DEL technology.

2.4.2 Interleukin-2 (IL2)

Cytokines are essential membrane-bound or secreted proteins (e.g., interleukins, interferons, chemokines) that regulate the growth, differentiation, and activation of immune cells, allowing communication between the cells.[263,264] Cytokines can be divided into two classes: those with a pro-inflammatory effect (e.g., IL2, IL1, TNF, or IFN-γ); and those with an anti-inflammatory effect (e.g., IL3, IL4, IL14, and IFN-α). On the other hand, cytokine receptors can be classified into homodimeric, or heterodimeric; and those in which the ligand can trimerize forming homotrimeric structures (TNF receptor family). In some cases, certain cytokines can share one or more of the different subunits from the heterodimeric or heterotrimeric forms respectively. The most representative case is the common polypeptide gamma chain (γc or CD132) family (IL2, IL4, IL7, IL9, IL15, and IL21). All these cytokines bind to the CD132 subunit and cytokine-specific subunits and activate different signaling pathways, which promote differentiation and activation of the immune cells (**Figure 2.24**).[263,264]
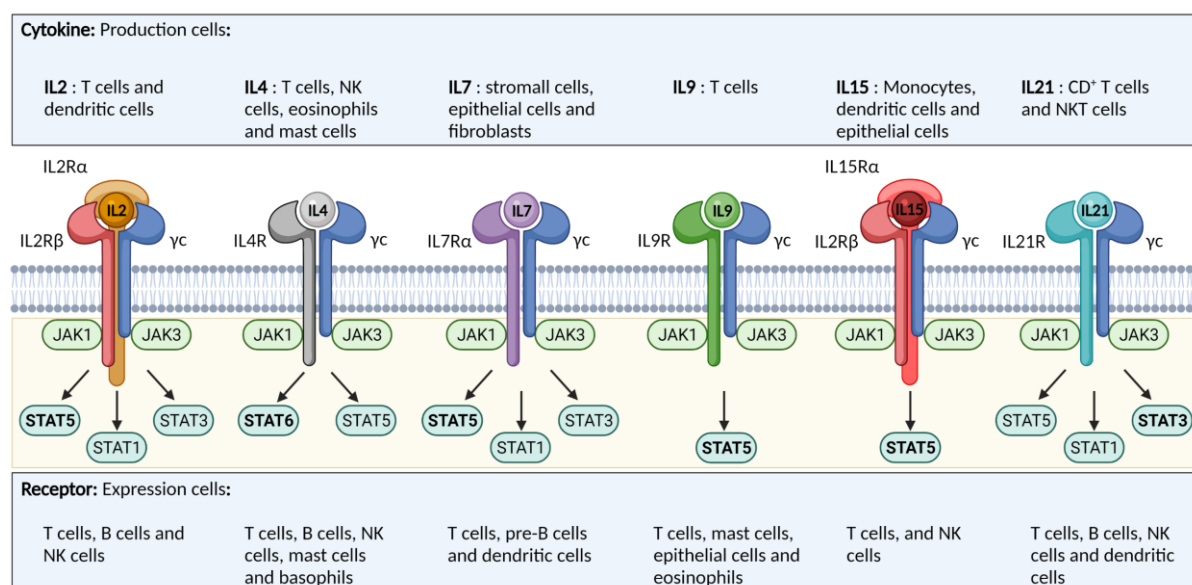
Figure 2.24. Cytokines of the common gamma chain family and their receptors. Interaction with the common gamma chain subunit will activate the Janus kinase 3 (JAK3), while the interaction with other corresponding cytokine-specific receptors will activate the Janus kinase 1 (JAK1). The activation of JAK1 and JAK 3 will primarily activate the STAT signaling pathway. Adapted from[263]. Created with BioRender.com

Cytokines are involved in the development of many autoimmune diseases (e.g., rheumatoid arthritis, psoriasis). Some efforts have been carried out during the last decade to generate antibodies that may be able to block certain pro-inflammatory cytokines.[265–267] On the other hand, due to its immune-stimulatory activity, certain cytokines have been investigated as a potential treatment for diseases like renal cell

carcinoma, soft tissue sarcoma, multiple sclerosis, or metastatic melanoma. From all these cytokines, the most studied one is IL2.[268–272]

IL2 is a 15.5–16 kDa, four-α-helix bundle cytokine comprising 153 amino acids and is a member of the γc cytokine family, whose receptor comprises certain specific subunits and the γc.[273] IL2 is a unique cytokine not only for its prominent role in immunity but also because of the various interaction modalities of this protein with its cognate receptor (IL2R). Indeed, the IL2R is composed of three different subunits, which are not always present on the cell surface, and which may contribute to different signaling outcomes.[273,274] Monomeric IL2Rs, comprising IL2Rα (CD25), are usually cell membrane-associated, but can also exist in soluble form. The affinity of CD25 towards IL2 has a dissociation constant $K_d \sim 10^{-8}$ M.[273–275] In resting T cells, the IL2R is mainly heterodimeric, consisting of a beta subunit (IL2Rβ or CD122) which can associate to the γc. The binding of IL2 to the heterodimeric IL2R consisting of CD122 and γc, with an affinity of $K_d \sim 10^{-9}$ M, activates JAK1 and JAK3, leading to the subsequent activation of STAT5.[273,274] The alpha subunit of the IL2R is not involved in signaling but, when present, CD25 enhances the binding affinity to IL2 by as much as 100-fold (**Figure 2.25**).[273,274,276–279] Association of IL2 with the IL2R causes internalization of the quaternary complex. IL2, CD122, and γc become degraded in vesicles, and by contrast, CD25 is recycled to the cell surface via endosomes.[280]

Several immune cells have been reported to produce IL2. Among all these, IL2 is continuously produced on resting CD4$^+$ T cells.[273,277] Other cells like T cell receptors α,β^+ and $\gamma\delta^+$ T cells, natural killer (NK) cells, and dendritic cells can produce IL2 upon activation.[273,277] IL2 is also produced to some extent by CD8$^+$ T cells. On the other hand, dimeric IL2Rs are highly expressed on antigen-experienced (memory) CD8$^+$ T cells and NK cells. This cytokine is also expressed at a certain extent on naïve CD8$^+$ T and memory CD4$^+$ T cells, and lower extent on naïve CD4$^+$ T cells.[273,277,278,281] The trimeric IL2R is expressed on activated B cells.[273,282] It has been reported that innate lymphoid cells and endothelial cells also express low levels of the trimeric IL2R.[273,283,284] Dendritic cells express CD25 and use it to present it to T cells (trans presentation) expressing the dimeric IL2R.[273,279]

Signal transduction upon triggering IL2R occurs via three major pathways. First, the Janus kinase (JAK)-signal transducer and activator of transcription (STAT); second, phosphoinositide 3-kinase (PI3K)-AKT; and third, mitogen-activated protein kinase (MAPK) (**Figure 2.25**).[273,277,281] IL2 signaling also actives the transcription factor B lymphocyte-induced maturation protein 1 (Blimp1), which serves as a negative feedback loop by repressing the production of IL2.[273,277] The regulation of IL2 production also occurs at the cellular level, where an equilibrium between CD4$^+$ T cells producing IL2, and regulatory T (T$_{reg}$) cells consuming IL2 is essential.[273,277,281] T$_{reg}$ cells cannot produce IL2, so they maintain peripheral immune tolerance by dampening effector T cells. Upon binding IL2 and subsequent signaling on T$_{reg}$ cells, the suppressive capacity of T$_{reg}$ cells is promoted by upregulation of CD25 and FoxP3.[273,277,281] IL2 production is increased upon upregulation of T cell receptors, which leads to terminal differentiation, followed by CD25 upregulation, of CD4$^+$ and CD8$^+$ T cells into short-lived effector T cells. Lower IL2 signals preferentially stimulate CD4$^+$ T cell differentiation into long-lived T$_{FH}$ cells or central memory T cells.[273,277,281]
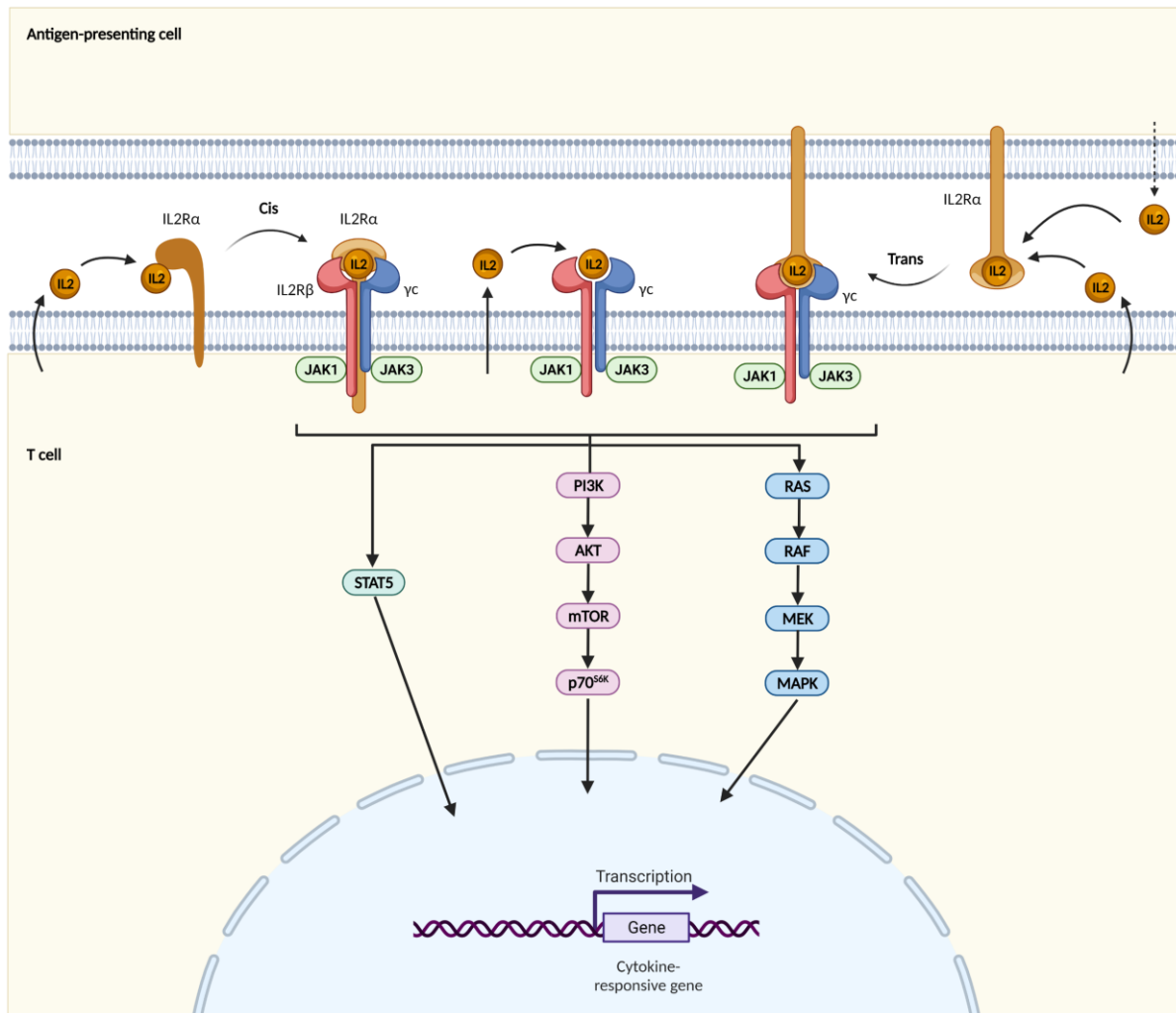
Figure 2.25. The IL2 receptor system and signaling. IL2 is secreted by activated T cells and dendritic cells (antigen-presenting cells). IL2 can bind to IL2Rα (CD25) and this interaction increases the affinity of IL2 for the other two receptor subunits (IL2Rβ or CD122 and γc or CD132). The IL2-CD25 complex can bind to the heterodimeric receptor, or the complex can be presented by dendritic cells to neighboring T cells. Cells that lack expression of CD25 can form a trimeric complex IL2-IL2Rβ-γc. Upon binding to the IL2Rβ and γc, IL2 activates different signaling pathways, including JAK1 and 3, STAT5, PI3K-AKT, or MAPK, leading to the subsequent transcription of target genes. Created with BioRender.com

2.4.3 Recombinant IL2 as anti-cancer therapeutic agent

IL2 is essential for the homeostasis and suppressive activity of T$_{reg}$ cells and efficient stimulation of cytotoxic T cells. A balance between these subtypes is necessary to maintain immune tolerance and immunity.[273,277,278] A lack of IL2 and CD25 has been linked to certain pathologies such as type 1 diabetes, multiple sclerosis, or rheumatoid arthritis, while the complete lack of IL2 or CD25 is extremely rare in humans.[285–288]

The immunological relevance of IL2 is best illustrated by the fact that pharmaceutical agents which inhibit IL2 production, such as cyclosporine or Tacrolimus (FK506), represent some of the most potent immunosuppressive agents known so far.[289] IL2 can potently activate both T cells and NK cells and, for this reason, the protein has attracted considerable interest for the therapy of cancer. Indeed,

recombinant IL2 has received marketing authorization (Proleukin®) for the treatment of renal cell carcinoma (1992) and metastatic melanoma (1998).[290] However, these treatments have been limited by the IL2-related side effects and its short half-life which makes it fast to be cleared off by the kidneys. Side effects related to the therapeutic use of IL2 have been linked to the release of pro-inflammatory cytokines (TNF) by NK cells, as well as to CD25-mediated endothelial damage induced by IL2 binding to endothelial surface receptors, leading to a vascular leak syndrome.[291]

Recently, several efforts have been made to render IL2 therapeutics more potent and selective, for example, by fusion with tumor-targeting antibodies.[269,292–300] Philogen S.p.A. has developed Darleukin (L19-IL2), a fully human antibody fusion protein consisting of the anti-EDB antibody L19 fused with IL2. L19-IL2 has demonstrated better tumor localization and striking superiority compared to non-targeted IL2.[294–296] Darleukin is currently under phase II clinical trials in combination with radiation and anti-PD-1 therapy for the treatment of non-small cell lung cancer.[294] Moreover, the combination of Darleukin with the other immunocytokine L19-TNF (Fibromun) is currently under phase III clinical trials for the treatment of melanoma and nonmelanoma skin cancer (Nidlegy®).[269] Roche has developed antibody fusion proteins composed of mutated versions of IL2 (IL2v or muteins) and certain antibodies targeting specific antigens like anti-fibroblast activation protein (FAP); anti-carcinoembryonic antigen (CEA), or anti-programmed cell death protein (PD-1). IL2 muteins can reduce the affinity of IL2 to CD25, while the antibodies are intended to localize the drug at the tumor site.[292,293,300,301] Nevertheless, from all the three IL2-fusion proteins only the IL2v-anti-PD1 remains in clinical trials.[301,302] The IL2v-anti-CEA was discontinued after the company observed a lack of efficacy.[293,302] On the other hand, the IL2v-anti-FAP fusion protein was discontinued after showing immunogenicity in some patients.[292,302]

The preferential expression of CD25 on immunosuppressive T_{regs} may limit the therapeutic potential of IL2-based biopharmaceuticals, as low doses of cytokine may preferentially interact with those cells.[303] In an attempt to limit T_{reg} binding, antibodies masking the IL2 epitope involved in CD25 binding, multi-PEGylation, or site-specific PEGylation of engineered IL2 residues at the CD25 binding interface, have been proposed and moved into clinical development activities.[304–310] The group of Professor Boyman, at the University of Zurich, described and extensively studied NARA1, a CD25-mimobody that binds IL2 at the CD25 recognition site, thus reducing the activation of T_{reg} cells and enhancing the antitumor response.[309] The discovery of this molecule led to the foundation of Anaveon and to the development of ANV419, an engineered fusion protein that has demonstrated fewer toxic effects in preclinical models, requires less frequent dosing and has better selectivity towards CD8^{+} T cells, respect to native IL2. ANV419 has recently entered phase I/II clinical trials for the treatment of metastatic tumors.[310] Nektar Therapeutics has developed Bempegaldesleukin (NKTR-214), a prodrug of human IL2 composed of a multi-PEGylated IL2 version with an average of 6 PEG units, close to the CD25 binding site.[304,305] Bempegaldesleukin slowly releases the PEG units regaining full activity. The PEG molecules are intended to block the interaction with CD25, reducing the activation of T_{reg} cells while the activation of CD8^{+} T cells is not affected.[304,305] Multi-PEGylation has also demonstrated an increased half-life of IL2. Nektar Therapeutics is advancing Bempegaldesleukin to different clinical trial stages, in combination with other agents (nivolumab or pembrolizumab) for the treatment of different tumors

(previously untreated melanoma, unresectable melanoma, metastatic melanoma, previously untreated advanced renal cell carcinoma, or metastatic urothelial cancer).[304,305] Synthorx, now part of Sanofi, has developed a similar approach to Nektar. In this case, a specifically PEGylated version of IL2 at the CD25 binding site was engineered using a microbial organism with a six-letter semi-synthetic DNA code.[308] The product, termed THOR-707 (now SAR444245), selectively binds to IL2Rβ and γc but does not bind to CD25.[307,308] In mice, THOR-707 resulted in large-scale activation of CD8^{+} T cells and NK cells without expansion of T$_{reg}$ cells. The product enhances drug accumulation at the tumor site, stimulates tumor-infiltrating CD8^{+} T cells and NK cells, and leads to a dose-dependent tumor growth reduction. SAR444245 has recently entered phase I clinical trials as monotherapy and in combination with immune checkpoint inhibitors (anti-PD-1) and epidermal growth factor receptor (EGFR) inhibitors.[307,308]

In principle, it would be attractive to develop selective small-molecule IL2 binders rather than monoclonal antibodies, that could abolish the interaction of IL2 with the alpha subunit of the IL2R. Several efforts in this direction have been undertaken over the years, despite the formidable challenge of discovering small ligands which disrupt protein-protein interactions (PPIs).[246,249] In 1997, scientists at Hoffmann-LaRoche successfully identified the first small molecule (Ro26-4550) capable of modulating the interaction between IL2 and its alpha subunit receptor.[259] Previous studies of the IL2 structure, using X-ray crystallography and NMR techniques, revealed that IL2 is formed by four α-helixes with an up-up-down-down configuration.[311–313] Moreover, site-directed mutagenesis studies showed critical residues in the AB loop (K35, R38, T41, F42, K43, Y45) and the B helix (E62 and L72) for the interaction between IL2 and its alpha subunit receptor.[314] Ro26-4550 was designed as a peptidomimetic of the IL2 hot spot, mimicking the residues R38 and F42 of IL2 and was intended to bind the IL2Rα. ^{15}N-NMR studies with uniformly labeled IL2 revealed that the molecule was instead an IL2 binder which served as an inhibitor of the IL2/IL2Rα interaction. Ro26-4550 was claimed to have a dissociation constant K$_d$ = 22 μM against IL2 and IC$_{50}$ = 3 μM for the inhibition of the IL2/IL2Rα interaction and represented the first example of nonpeptide inhibitor of a cytokine/cytokine receptor interaction.[259] Later in 2002, the same group of scientists presented a study in which they described the NMR characterization of the interaction between Ro26-4550 and IL2.[315] Surprisingly, Roche did not continue with the development of Ro26-4550. In 1998, James A. Wells, a founding member of the protein engineering department at Genentech Inc., founded Sunesis Pharmaceuticals. In 2000, scientists at Sunesis described a novel fragment discovery platform known as disulfide trapping or Tethering.[316] Subsequent optimization of Ro26-4550, by Sunesis, based on the combined use of X-ray crystallography, tethering approaches, and fragment assembly, led to the discovery of a series of potent IL2 binders, in which the best ligand SP4206 was characterized to have a dissociation constant K$_d$ = 0.10 μM, and to be able to inhibit the IL2/IL2Rα interaction with a half-maximal inhibitory constant IC$_{50}$ = 0.06 μM.[251,260,261,317–321] Later in 2012, our group reported the discovery of a small organic IL2 ligand ($A_{17}B_{284}$) using DEL technology, with a K$_d$ = 2.5 μM, as measured by fluorescence polarization techniques. The molecule was predicted to bind to the CD25 interaction site based on modeling studies.[108]

3. Aims and structure of the thesis

As previously described, the efficient exploitation of small molecule libraries remains a major challenge in drug discovery. Thanks to the implementation, in the last decades, of DNA-encoded libraries, now libraries of unprecedented size and diversity can be screened in a single experiment to accelerate drug discovery programs. In the first part of this thesis, section 4.1, a new single-stranded DNA-encoded library, termed AG-DEL, which comprises 669,240 members, has been synthesized and screened against multiple pharmaceutically and biologically relevant targets. The design of this library allows for the screening of *de novo* ssDNA or dsDNA and the implementation of new photo-crosslinking-mediated affinity selections. Moreover, this library could be annealed with a different sub-library generating the so-called ESAC 2+1 format. The last part of this chapter presents the synthesis of a new type of ESAC libraries, termed ESAC plus, aiming at expanding our library portfolio. The new design resulted in a patent application filed in 2019 and published in 2020.

We soon realized that the efficient exploitation of DEL-macrocyclic libraries could be enhanced by the synthesis of new ESAC plus libraries. The ESAC plus format relies on the availability of different reactions to connect both sub-libraries. Amino acids and amines are common types of building blocks used for DEL synthesis, mainly due to their availability and relatively affordable cost. However, the availability of different DNA-compatible reactions that allow facile functionalization and derivatization of amino acids and amines remains quite limited. On the other hand, reactions like copper-catalyzed azide-alkyne cycloaddition represent an attractive and DNA-compatible approach for generating new chemical libraries, but the poor availability of bi-functional azides results in low diversity libraries. In section 4.2, a new DNA-compatible diazo-transfer reaction has been investigated and optimized. The reaction proceeded in very mild conditions, without the use of metals. The reaction scope was investigated using different types of primary amines, efficiently converted into their corresponding azides. Moreover, the stability and structural integrity of the DNA tags was confirmed by ligating a subsequent DNA fragment to the nascent oligonucleotide, showing the potential of this new reaction for the synthesis of new DELs.

DEL technology has also promised to enhance the productivity of drug discovery programs aiming at tackling undruggable targets, like those involved in protein-protein interactions. In this direction, traditionally one of the most challenging proteins to be drugged with small molecules has been IL2, which has a prominent role in immunity and is being used as a therapeutic approach for the treatment of different types of tumors. Nevertheless, the activation of regulatory T cells induced by administration of low doses of IL2, which preferentially binds to these cells by the trimeric form of the IL2 receptor, and toxicity associated with therapeutic (high) doses have limited its therapeutic applications. Ideally, small molecule inhibitors of the interaction between IL2 and its alpha subunit receptor may be desirable to enhance the anti-tumor response of IL2-based therapeutics, which can also be enhanced by specific localization at the tumor site using antigen-specific IL2 fusion proteins. In section 4.3, a new series of small molecule ligands of IL2 has been discovered by screening the previously synthesized AG-DEL. The molecules had originally single-digit micromolar to nanomolar affinity for IL2. One of these hits was carefully studied by medicinal chemistry approaches and optimized to a new compound that preserves IL2 binding

and improves selectivity towards albumin (HSA) and alpha-1-acid glycoprotein (AGP). This molecule was tested against a panel of different proteins, including non-related cytokines (IL15 and TNF), demonstrating a good selectivity profile. This compound was also able to form a kinetically stable complex with IL2 in size-exclusion chromatography and recognized the CD25-binding site, evidenced by competition with the previously described NARA1 antibody.

The last part of this thesis includes appendixes containing all the materials and methods and supplementary information used throughout the different projects, and related bibliography.

4. Results

4.1 Design, synthesis and screening of different DELs

As the first part of this thesis, different DNA-encoded libraries were synthesized and screened against multiple targets of pharmaceutical interest. Moreover, a new ESAC-type library was introduced and led to a patent application which was published in 2020.[322]

The main objective of this project was the synthesis of a new single-stranded DEL (AG-DEL). The major advantage of this new library is the modularity of its single-stranded format. Our group has previously demonstrated that libraries constructed in this format are particularly interesting for the implementation of new encoded self-assembling chemical libraries (ESAC), bearing two distinct pharmacophores in each DNA strand.[115,116,200,225,323,324] Up to now, the use of ESAC has focused on two strategies. First, the coupling of single building blocks in each strand, for the discovery of *de novo* ligands exploiting the chelate effect.[115,116,200] Second, the annealing of previously identified hit compounds with a more complex single-pharmacophore library for the construction of affinity maturation libraries.[225,323,324] On the other hand, the utility of the single-stranded DEL format for the efficient implementation of photo-crosslinking-mediated affinity selections has also been demonstrated by our group and others.[191–194] This new screening methodology exploits the covalent binding of a photo-reactive moiety aided by the inherent affinity of the hit displayed on the main library. The study of photo-crosslinking parameters and the implementation of this methodology for DEL screenings was mainly performed by Dr. Alessandro Sannino using the AG-DEL described in this thesis. This work was part of his doctoral thesis and was published in *ACS Combinatorial Science.* **2020**. *22*. 204–212, therefore it will not be described here.[194]

In this work, the new AG-DEL served as a single-pharmacophore single-stranded DEL for the identification of *de novo* ligands and the construction and screening of a new ESAC 2+1 library.

4.1.1 Single-Pharmacophore AG-DEL

Some parts of this section, the related materials and methods, and supporting information included in chapter 6 "Appendix" have been adapted from "Identification and Validation of New Interleukin-2 Ligands Using DNA-Encoded Libraries" by Adrián Gironda-Martínez, Émile M. D. Gorre, Luca Prati, Jean-François Gosalbes, Sheila Dakhel, Samuele Cazzamalli, Florent Samain, Etienne J. Donckele and Dario Neri, published in *Journal of Medicinal Chemistry*, **2021**, *64*, 17496–17510. Copyright 2021 American Chemical Society.

Library Synthesis

DELs can be constructed in a modular fashion, by the stepwise assembly of sets of building blocks employing suitable chemical reactions. After each incorporation of a building block in the nascent molecule, the ligation of a suitable oligonucleotide allows the unambiguous identification of the chemical moiety that had been coupled.

The construction of the AG-DEL was inspired by a similar library design, which had been published by the Neri group in 2012 and which featured the use of a set of amino acids as the first building blocks in the library construction scheme, followed by the capping of amino groups with carboxylic acids serving as the second set of building blocks.[108]

The first step for the construction of the AG-DEL was performed by coupling 468 different Fmoc-amino acids (BB1) to 468 distinct 45-mer 5'-amino-modified oligonucleotides (Code 1) as represented in **Figure 4.1.1**.
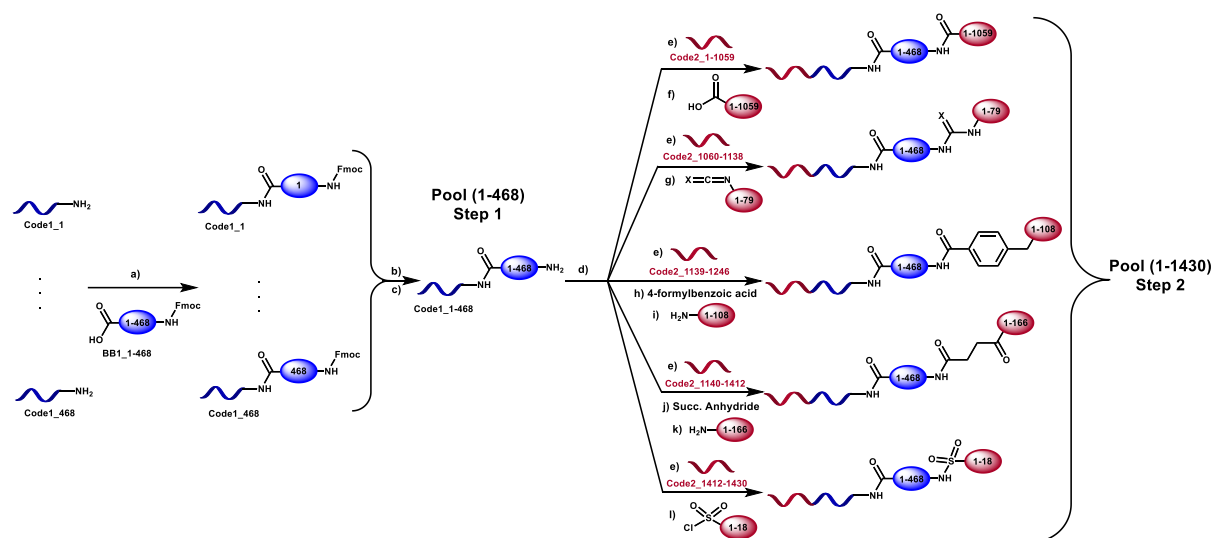
Figure 4.1.1. Schematic representation of the design and construction of AG-DEL. Two sets of building blocks and encoding oligonucleotides are represented in blue (Code 1 and BB1) and red (Code 2 and BB2). The first set of building blocks (Fmoc-amino acids) was encoded by amide bond formation between them and the corresponding 5'-amino-modified oligonucleotide. The second set of building blocks reacted with the corresponding encoded aliquot of the Pool 1 through amide bond formation, (thio)urea formation, reverse amide bond formation, reductive amination and sulfonylation. **a**) Three different conditions were used for Fmoc-amino acid coupling. Method 1: DMT-MM 300 mM in H_2O, MOPS buffer 50 mM, pH 8.0, 500 mM NaCl, overnight at 37 °C. Method 2: EDC/s-NHS 55:150 mM in DMSO/H_2O 5:1, MOPS buffer 50 mM, pH 8.0, 500 mM NaCl, overnight at 30 °C. Method 3: EDC/HOAt/NMM 100:20:100 mM in DMSO, MOPS buffer 50 mM, pH 8.0, 500 mM NaCl, 1 h at room temperature, twice. **b**) Each of the conjugates was individually HPLC-purified and pooled together in an equimolar concentration (5 nmol/conjugate) to obtain Pool 1. **c**) Fmoc-deprotection of Pool 1: triethylamine in H_2O overnight at 37 °C. **d**) Split in 1,430 different wells. **e**) Encoding by splint-mediated ligation: Pool 1 aliquot (1 equiv), Code 2 (1.5 equiv) and DNA-adaptor (2 equiv), T4 DNA-ligase buffer and T4-DNA ligase, for 16 h at 16 °C, then 65 °C for 10 min. **f**) Amide bond formation with 1,059 carboxylic acids was performed using the three different conditions described above. **g**) (Thio)urea formation with 79 iso(thio)cyanates: borate buffer 400 mM, pH 9.4, overnight at 40 °C. **h**) 4-formylbenzoic acid coupling: DMT-MM 300 mM in H_2O, MOPS buffer 50 mM, pH 8.0, 500 mM NaCl, overnight at 37 °C. **i**) Reductive amination with 108 amines: $NaCNBH_3$ 400 mM in MeCN, in phosphate buffer 1 M, pH 5.5, overnight at 40 °C. **j**) Succinic anhydride coupling: DMAP 200 mM in TEA HCl buffer 300 mM, pH 10, 3 h at 60 °C. **k**) Reverse amide bond formation with 166 amines: DMT-MM 200 mM, MOPS buffer 100 mM, pH 8.0, 500 mM NaCl, overnight at 37 °C. **l**) Sulfonylation with 18 sulfonyl chlorides: borate buffer 400 mM, pH 9.4, overnight at 40 °C.

The resulting DNA-conjugates were individually characterized and HPLC-purified. The HPLC purification of each individual library member ensures a high-quality library construction, both in terms of encoding and homogeneous distribution of sequence counts in the final library. After HPLC purification, a normalized amount of each individual DNA-conjugate was pooled in a single fraction (Pool 1, **Figure 4.1.2**).
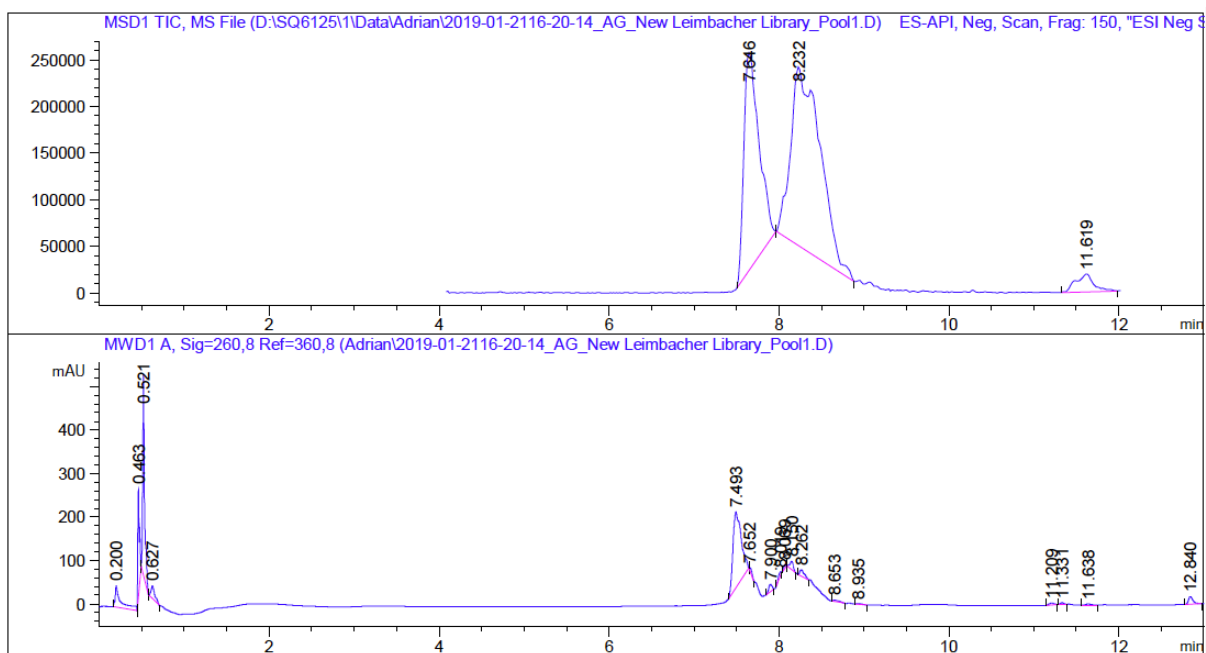
Figure 4.1.2. UV and MS traces of the purified intermediate Pool 1 of the AG-DEL before Fmoc deprotection. Fmoc-protected pool can be observed between 7.900 min to 8.935 min (DAD), 8.232 min (TIC). A fraction of Pool 1 already deprotected after lyophilization of the single conjugates can be observed at 7.493 min (DAD), 7.646 min (TIC).

Pool 1 was subjected to complete Fmoc deprotection leaving a free amino group for the subsequent coupling of the building block 2 (**Figure 4.1.3**)
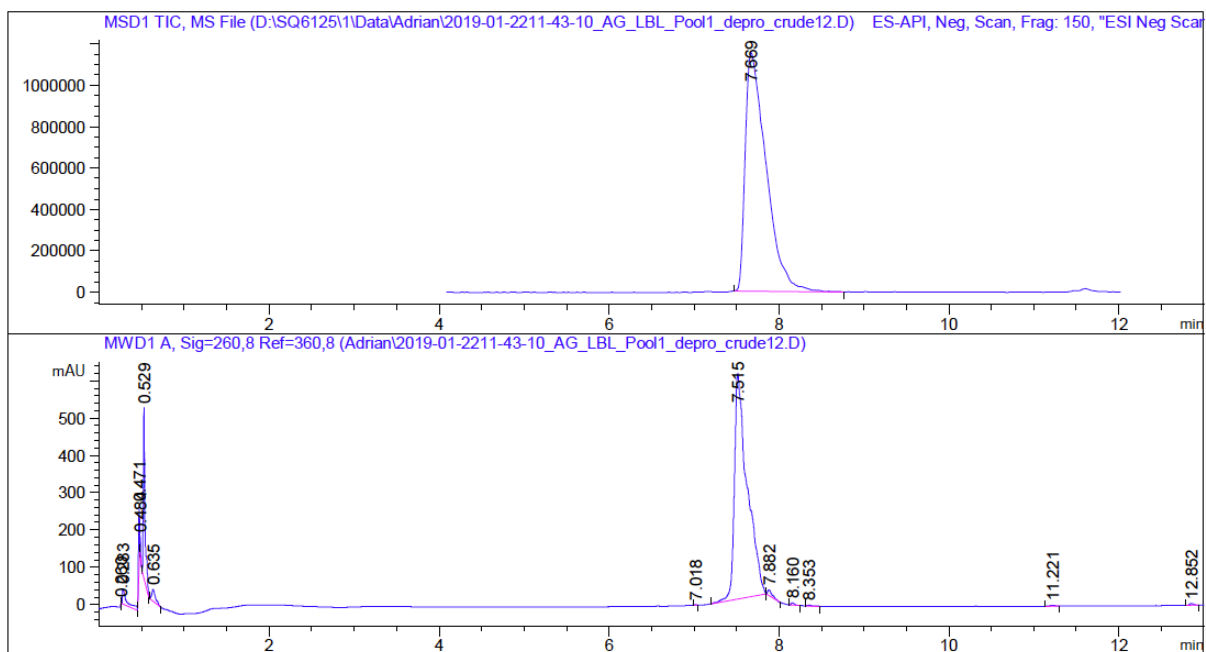
Figure 4.1.3. UV and MS traces of the purified intermediate Pool 1 of the AG-DEL after Fmoc deprotection. Deprotected pool can be observed at 7.515 min (DAD), 7.669 min (TIC) and no remaining protected Pool 1 can be observed.
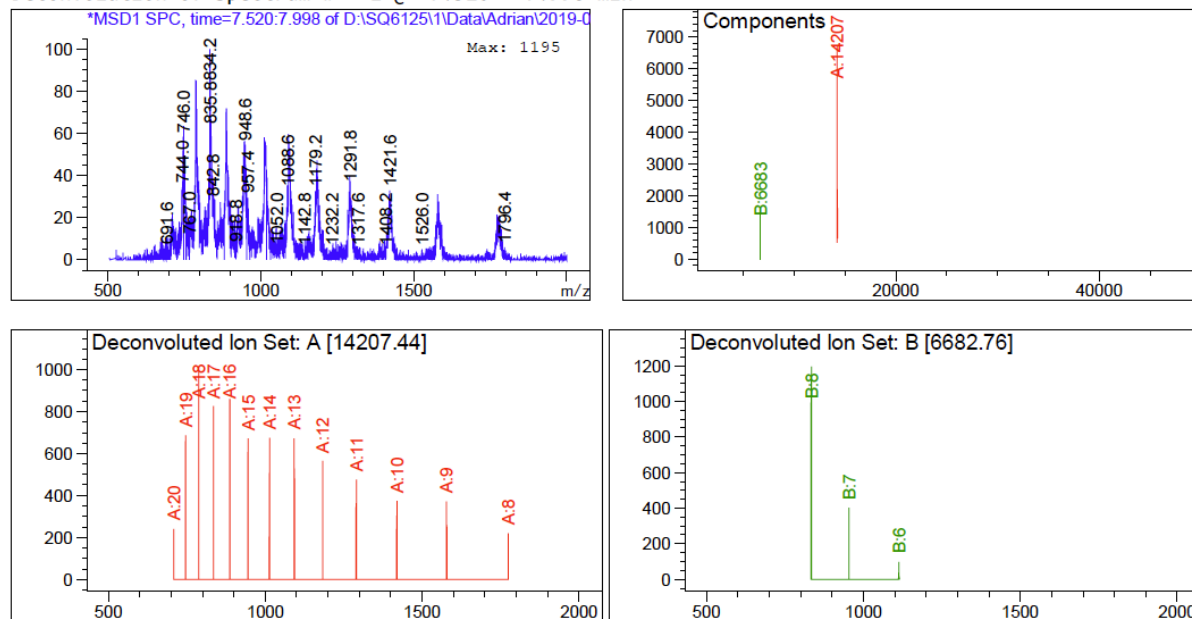
Figure 4.1.4. Non-deconvoluted MS spectrum of the purified intermediate Pool 1 of the AG-DEL after Fmoc deprotection. Different *m/z* values can be observed, corresponding to the average molecular weight of the intermediate Pool 1, composed of 468 different molecules.

Figure 4.1.5. Deconvoluted MS spectrum of the purified intermediate Pool 1 of AG-DEL after Fmoc deprotection. The molecular weight indicated represents an average of the whole Pool 1, composed of 468 different molecules.

The second encoding step was performed by splint-mediated ligation of 1,430 distinct 29-mer 5'-phosphorylated oligonucleotides (Code 2) and reaction with 1,426 different chemical building blocks (BB2) including carboxylic acids, amines, iso(thio)cyanates, and sulfonyl chlorides; and 4 different controls (**Figure 4.1.1**). At this point, the ligation efficiency must reach close to 100% to ensure a perfect encoding of all the library compounds for a subsequent good sequencing profile.

The ligation of Pool 1 to new encoding fragments, Code 2, was investigated and optimized, and the optimized protocol can be found in chapter 6 "Appendix". A representative example of all the possible scenarios after splint-mediated ligation is illustrated in **Figure 4.1.6**. Lane 1 represents the DNA ladder, lanes 2–4 and 8 represent the oligonucleotide controls and "no sample" control (Pool 1, Code 2, DNA adaptor, and "no sample" respectively), and lanes 5–15 represent different ligation reactions. Lanes 5, 7, and 10 represent examples of successful encoding of Pool 1 (~30 bp), which was correctly ligated to Code 2 (~19 bp) as shown in the band at approximately 50 bp (ligation product). In lanes 5 and 10, a minor excess of Code 2 (~19 bp) and DNA adaptor (~17 bp) can be found, while in lane 7 only the DNA adaptor is remaining. Lanes 6, 11, 14, and 15 represent examples of unsuccessful encoding with only Pool 1 and DNA adaptor present in the mixture. A pipetting error could explain the absence of Code 2 in the mixture. In lanes 9, 12, and 13 the encoding of Pool 1 proceeded with medium conversion. In lanes 9 and 13 Code 2 cannot be detected (~19 bp), meaning that the quantity added was not sufficient for a full conversion. On the other hand, lane 12 represents a situation in which the encoding

was not efficient, but all the oligonucleotides were still present in the mixture. All the unsuccessful reactions were restarted adding the corresponding necessary oligonucleotides and a fresh amount of ligase. With the optimized conditions, less than 10% of the ligations needed to be repeated.
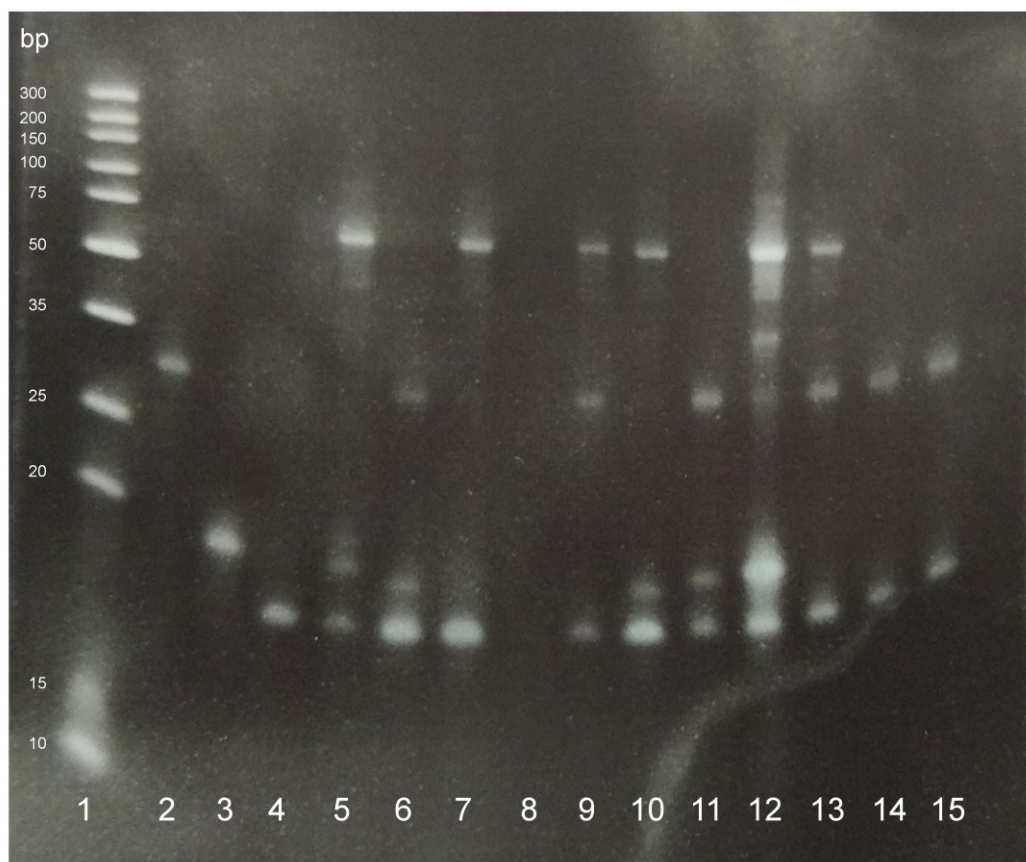
Figure 4.1.6. Representative 15% TBE-Urea gel electrophoresis analysis of different ligation reactions. Lane 1, DNA ladder (size expressed in base-pairs); lane 2, Pool 1 before ligation with Code 2; lane 3, Code 2; lane 4, DNA adaptor; lanes 5–15, representative examples. As depicted in the gel, ligations that did not proceed to completion (lanes 6, 9, 11, 12, 13, 14, and 15) show a band at approximately 30 bp (remaining Pool 1) and other bands at the size of the Code 2 (~19 bp) and at the size of the adaptor (~17 bp). Ligation reactions that proceed to completion (5, 7, and 10) show a band at approximately 50 bp (ligated product) and other bands at the size of the Code 2 and the DNA adaptor (excess of reagents).

Only building blocks which showed more than 75% conversion in model reaction experiments were used in this second step. The validation of these building blocks was part of previous internal activities of our group and is not described in this thesis. Either 4-formylbenzoic acid or succinic anhydride was conjugated to aliquots of Fmoc-deprotected Pool 1 to allow for reductive amination or reverse-amide bond formation with the BB2s amine (**Figure 4.1.1**). The experimental procedure for all the different reactions can be found in chapter 6 "Appendix".

All the final 1,430 different sub-pools were mixed in a single aliquot for the subsequent final purification. Different purification tests were conducted using revers-phase high-performance liquid chromatography (RP-HPLC). During this investigation, different mobile phases, gradients, and temperatures were tested. However, none of these conditions provided a good separation between the final library and the DNA

adaptor (**Figure 4.1.7a**). With these results in hand, the possibility of using ion-exchange high-performance liquid chromatography (IE-HPLC) was investigated. During IE-HPLC all the different species in the mixture can be separated in terms of the total number of charges, which is defined by the negatively charged oligonucleotide backbone. As shown in **Figure 4.1.7b**, using IE-HPLC, the efficient separation of the different oligonucleotide species in the final pool (Final library, excess of Code 2, non-encoded by-products, and DNA adaptor) could be achieved.
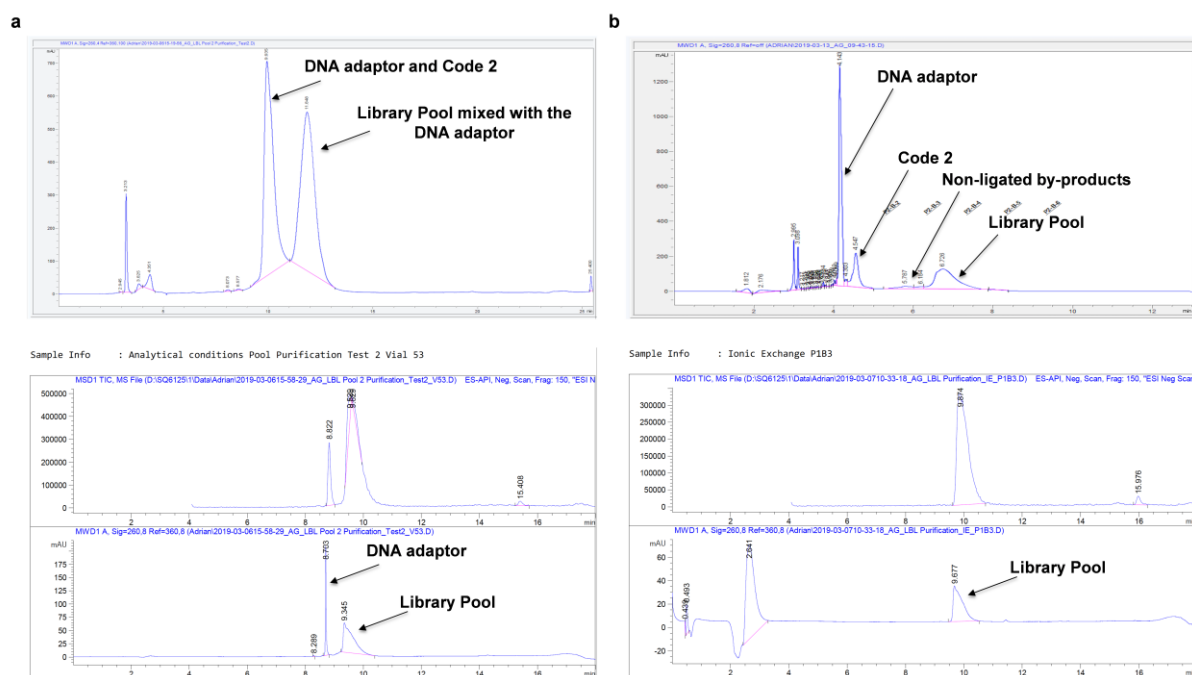
Figure 4.1.7. HPLC traces of AG-DEL final library purification tests. **a**. (up) RP-HPLC purification traces; (down) LC-MS analysis of the recovered peak from RP-HPLC. As observed, the peak recovered contains impurities which correspond to the DNA adaptor. **b**. (up) IE-HPLC purification traces; (down) LC-MS analysis of the recovered peak from IE-HPLC. As observed, all the different species can be efficiently separated using IE-HPLC and the final library can be obtained with the desired high purity.

After desalting using molecular weight cut-off filter devices (Amicon®) the final AG-DEL, composed of a total of 669,240 encoded small molecules, was characterized by LC-MS and gel electrophoresis for assessing the final purity (**Figures 4.1.8** and **4.1.9**).
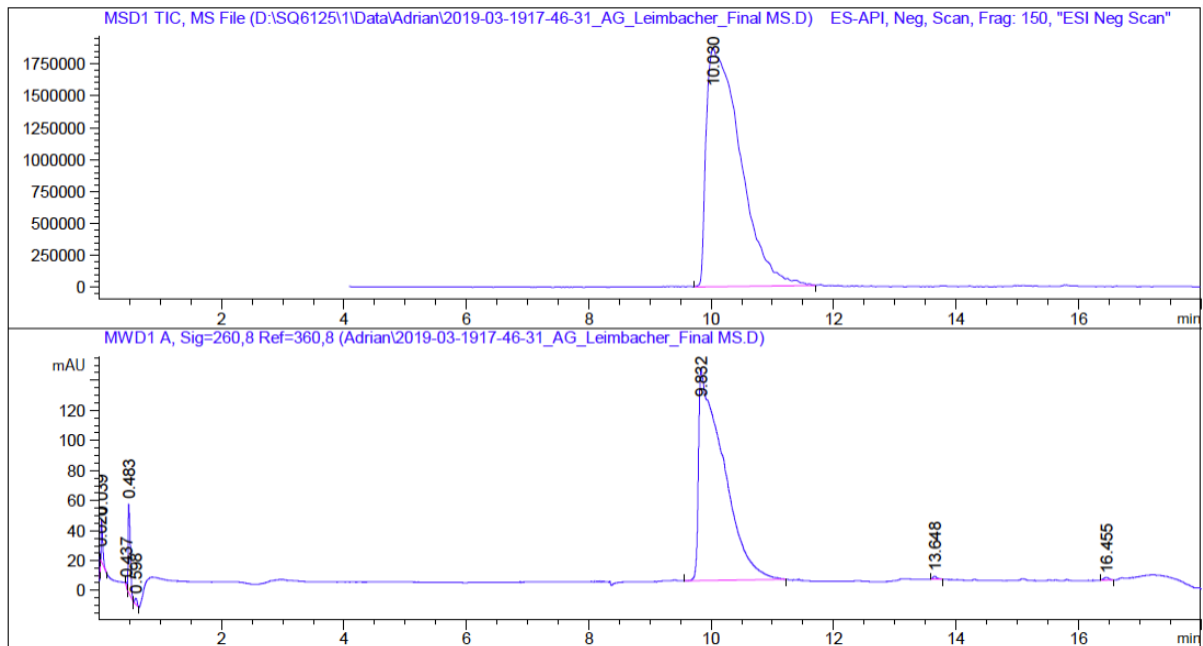
Figure 4.1.8. UV and MS traces of the final AG-DEL after purification and desalting. As observed, a single peak can be detected in both traces, and the DNA adaptor and excess of codes were discarded.
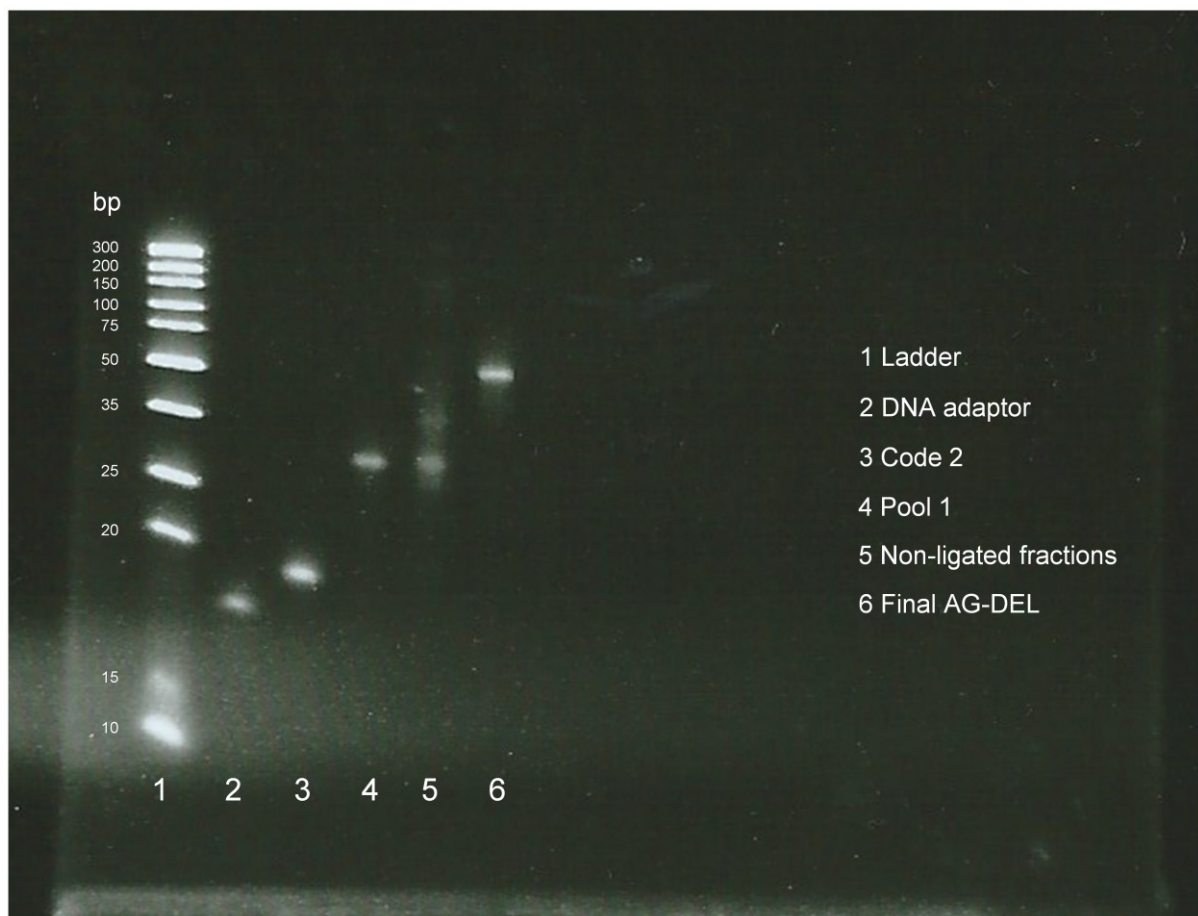
Figure 4.1.9. Representative 15% TBE-Urea gel electrophoresis of the final AG-DEL with the corresponding controls. Lane 1, DNA ladder (size expressed in base-pairs); lane 2, DNA adaptor; lane 3, Code 2; lane 4, Pool 1 before ligation of the Code 2; lane 5, non-ligated products recovered from IE-HPLC purification; lane 5, final AG-DEL after purification and desalting.

Screenings using AG-DEL can be performed both in ssDNA and/or dsDNA format. Screenings in ssDNA format have been described to enhance the enrichment factor of preferentially selected combinations.[203] Nevertheless, for comparison and reproducibility with screenings of ESAC 2+1 and ESAC Plus libraries, AG-DEL was screened in dsDNA format. Before the affinity selection experiments, the library needs to be converted into a dsDNA library by a Klenow polymerization procedure. This procedure has already been described in other publications of our group and was used without further optimization.[325] In essence, the AG-DEL ssDNA library (5' overhang) was annealed with a 34-mer complementary oligonucleotide (Code 3). The addition of deoxynucleotide triphosphates (dNTPs) and DNA polymerase I, Large (Klenow) fragment allows for the polymerization of the ssDNA AG-DEL, filling in from 5' to 3' direction, as well as the polymerization of the Code 3, in the same direction. After Klenow polymerization, the library was obtained as a 96-base pair dsDNA (**Figure 4.1.10**). A quality control gel electrophoresis can be found in chapter 6 "Appendix" (**Figure 6.2.6**)
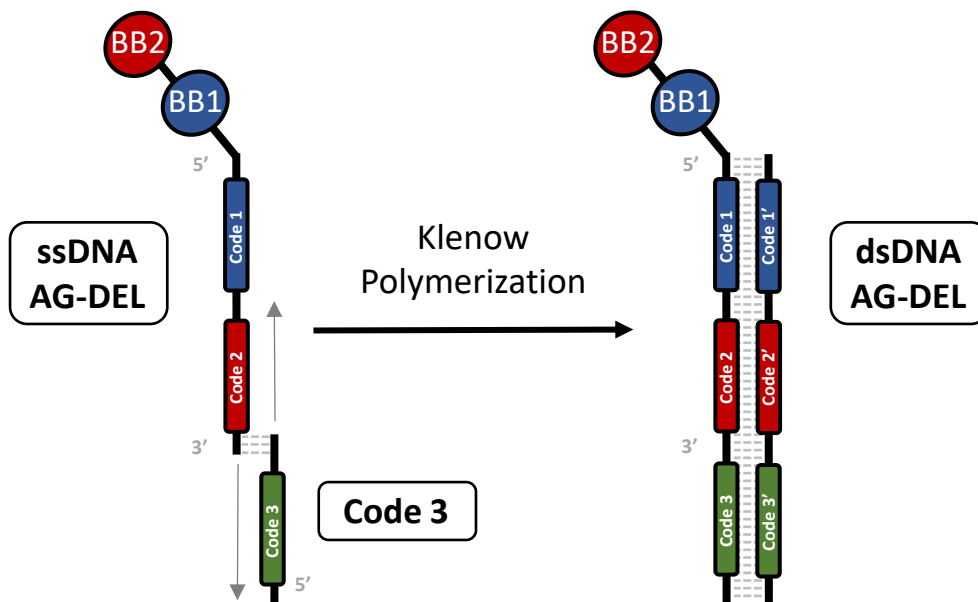
Figure 4.1.10. Schematic representation of the Klenow polymerization reaction step. The single-stranded AG-DEL is annealed with a partially complementary 34-mer oligonucleotide (Code 3). After the addition of dNTPs and Polymerase Klenow fragment, the library is converted into the corresponding double-stranded AG-DEL.

Affinity selection experiments were performed against several biotinylated relevant targets, in duplicates or triplicates (depending on the availability of the target protein), using solid-phase affinity capture methodologies.[95] The library was also screened against empty beads, serving as a "No protein" control (**Figure 4.1.11b**) for the discrimination of specifically enriched combinations. Moreover, prior to selection experiments, the library was characterized by high-throughput DNA sequencing (Naïve library). All library members are visible as dots in a three-dimensional space, in which the x- and y-axes correspond to the identity of the individual building blocks used for AG-DEL construction, while the relative abundance of individual library members (determined on the basis of DNA sequence counts) is displayed on the z-axis. Sequence counts are also indicated by a color code. Naïve library sequencing

reveals a uniform distribution of sequence counts for all the library members. This parameter serves as a confirmation for library quality (**Figure 4.1.11a**). In the next paragraphs, different selections against some pharmaceutically and biologically relevant targets are going to be described. A representative example of each affinity selection for every target is going to be disclosed in the figures, but all the replicates can be found in chapter 6 "Appendix".
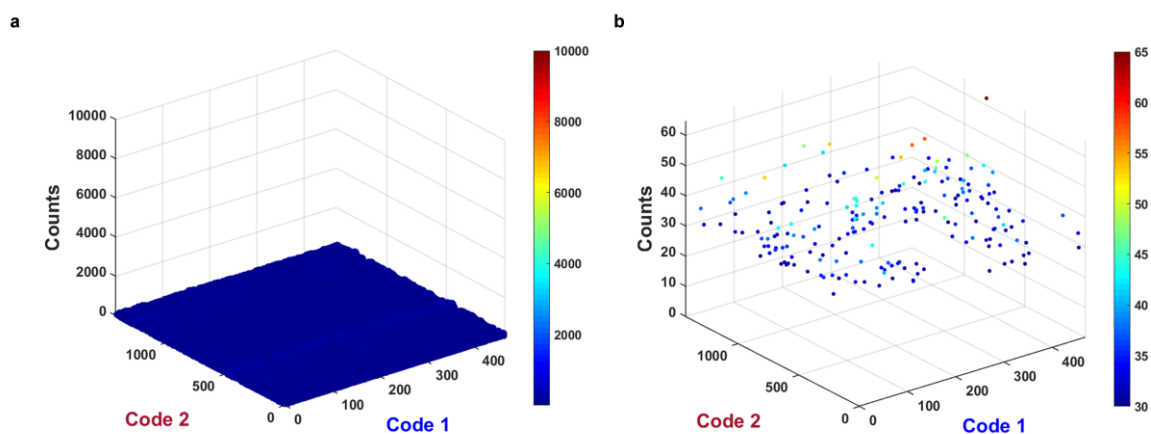
Figure 4.1.11. Representative fingerprints of the AG-DEL naïve library and selections against empty beads. The x-and y-axes represent the identification barcode of every BB1 and BB2, respectively, while the z-axis represents the relative abundance of every library member. Relative abundance is also represented in a color code. **a**. Naïve library before affinity selection experiments shows a homogeneous distribution of sequence counts. **b**. Selections against empty beads reveal certain promiscuous structures which would be carefully considered if appear in selections against other targets.

Carbonic anhydrase IX (CAIX) represents a very well-characterized tumor-associated antigen highly expressed in renal cell carcinomas and hypoxia.[326,327] Several ligands in the micromolar and nanomolar range have been described over the years by different research groups, including ours.[115,194,328–330] The most characterized types of ligands for CAIX are aromatic sulfonamides. This class of molecules reversibly interacts with the Zinc anion in the catalytic site.[329,330] Affinity selection experiments against CAIX usually serve as a positive control since several sulfonamide ligands are included as building blocks during library construction. **Figure 4.1.12a** shows affinity selection fingerprints against biotinylated CAIX. Lines representing different aromatic sulfonamides can be observed (e.g., BB1_146, BB2_49, 461, 586, and 803), as well as different combinations (e.g., **356/586**, **201/586**, **105/586**, **80/586**, **146/586**). Interestingly, out of the 5 most enriched combinations (**Figure 4.1.12b**), only one of them represented a bivalent sulfonamide compound (i.e., **146/586**) which could suggest that other combinations may have better dissociation constants compared to compounds that might take advantage of avidity effects. Some of these compounds were identified and confirmed as CAIX binders, with dissociation constants in the nanomolar range, during another selection campaign using photo-crosslinking methodologies. This work was published in 2020 and represents part of the results of the doctoral thesis of Dr. Alessandro Sannino.[194]

Affinity selection results against CIAX are also described in chapter 4.3 as part of our publication in the *Journal of Medicinal Chemistry*. **2021**, *64*, 17496–17510.
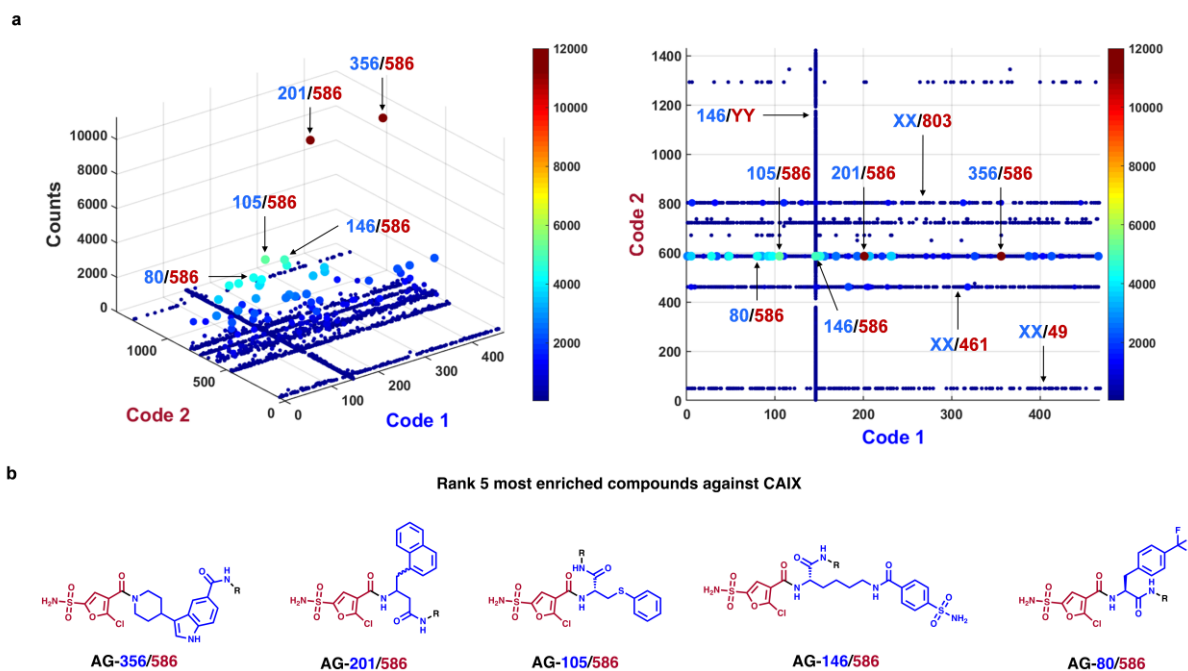
Figure 4.1.12. **a**. A representative fingerprint of affinity selections against CAIX. Different lines and combinations representing different aromatic sulfonamide compounds could be identified. **b**. The 5 most enriched compounds. Only one of them represents a bivalent sulfonamide molecule. Some of these compounds were already validated in a previous work of our group.[194]

As previously mentioned, different pharmaceutically and biologically relevant targets were screened using AG-DEL. Some of these targets include human alpha-aminoadipic semialdehyde synthase (AASS), which catalyzes the first two steps of lysine catabolism and has been associated with pyridoxine-dependent epilepsy in neonates; carcinoembryonic antigen (CEA), a glycoprotein involved in cell adhesion that has been related with different adenocarcinomas; human serum albumin (HSA), which represents the most abundant protein in plasma and is involved in the circulation and distribution of many drugs and endogenous substrates; and L19-IL2, a clinical-stage antibody fusion protein used for the treatment of different malignancies.[294–296,331–339]

Figure 4.1.13 shows affinity selection fingerprints against two different constructs of AASS. The first one, the full human AASS protein (**Figure 4.1.13a**), and the second one, AASS$_{454-926}$, only the saccharopine dehydrogenase domain (**Figure 4.1.13b**). The fingerprints of the three replicates for each construct were remarkably reproducible (see chapter 6 "Appendix"), showing enrichment factors (EF) over 100 for both proteins. Interestingly, combination **13/1013** was highly enriched in selections against the full construct (EF = 190 ± 43) while the enrichment factor in selections against the saccharopine dehydrogenase domain was lower (EF = 72 ± 6). On the other hand, BB1_326 was preferentially enriched in both proteins, which may suggest a possible specific fragment for the saccharopine dehydrogenase domain. Moreover, the combination **326/232** represented the most enriched combination in the three replicates for AASS$_{454-926}$ selections, and the first one and second one for one and two replicates, respectively, for the AASS full construct.
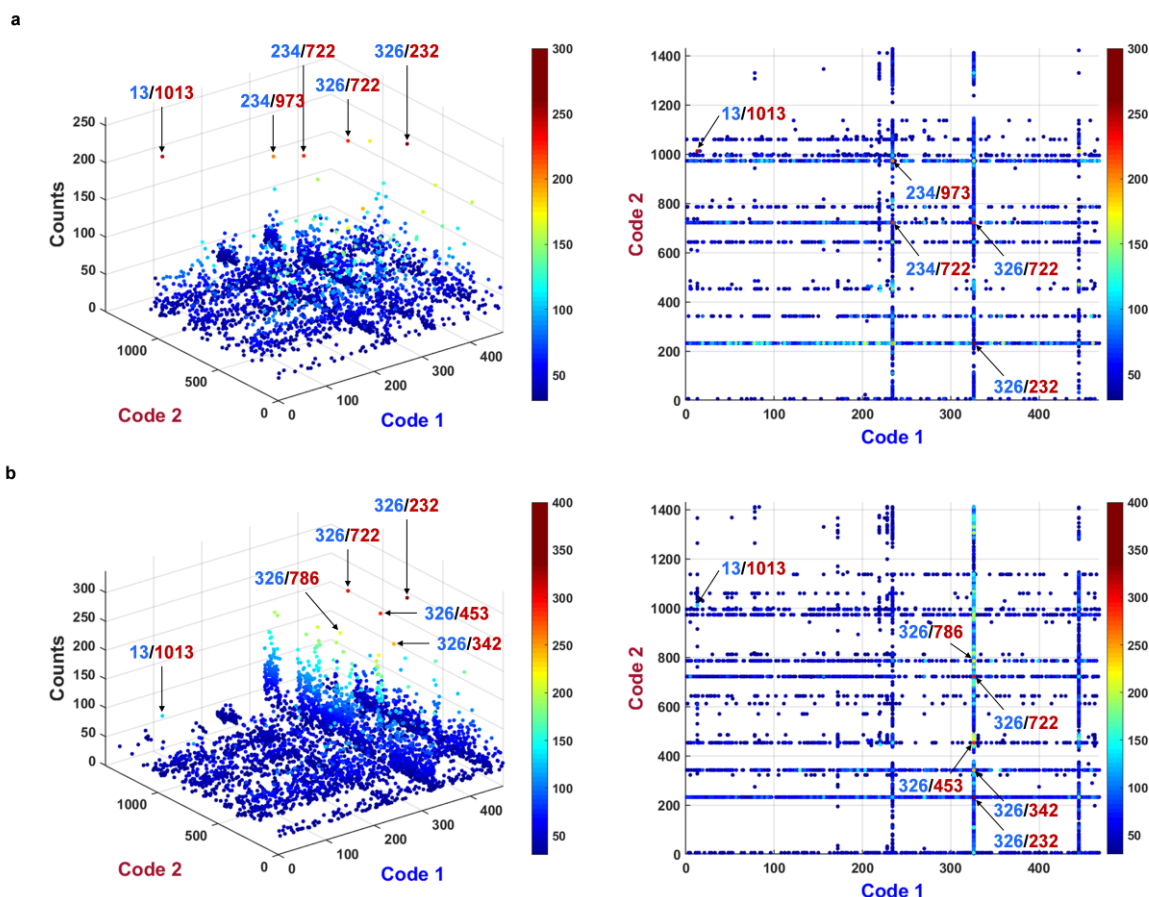
Figure 4.1.13. **a**. A representative fingerprint of affinity selections against the full AASS protein. **b**. A representative fingerprint of affinity selections against the saccharopine dehydrogenase domain of AASS (AASS$_{454-926}$). In both selections, the combination **326/232** was preferentially enriched, as well as some lines for which line BB1_326 represents the most populated and enriched.

Affinity selection fingerprints against CEA and HSA are displayed in **Figure 4.1.14**. **Figure 4.1.14a** shows fingerprints against CEA, in which BB2_722 was preferentially enriched. All the 5 most enriched combinations bear this moiety. Nevertheless, the validation of these combinations would need to be carefully considered since BB2_722 also showed enrichment in no protein affinity selection controls. On the other hand, HSA fingerprints are shown in **Figure 4.1.14b**. Using the same threshold to evaluate all the selections (30 counts), HSA selections were much less populated than any other, showing only 13 combinations. However, these combinations had enrichment factors over 1,000, being the most enriched combination over 8,000. Notably, BB1_214 and 251 do not represent populated lines, which may suggest that the combination of this building block with the BB2 might be crucial for the interaction with the protein.
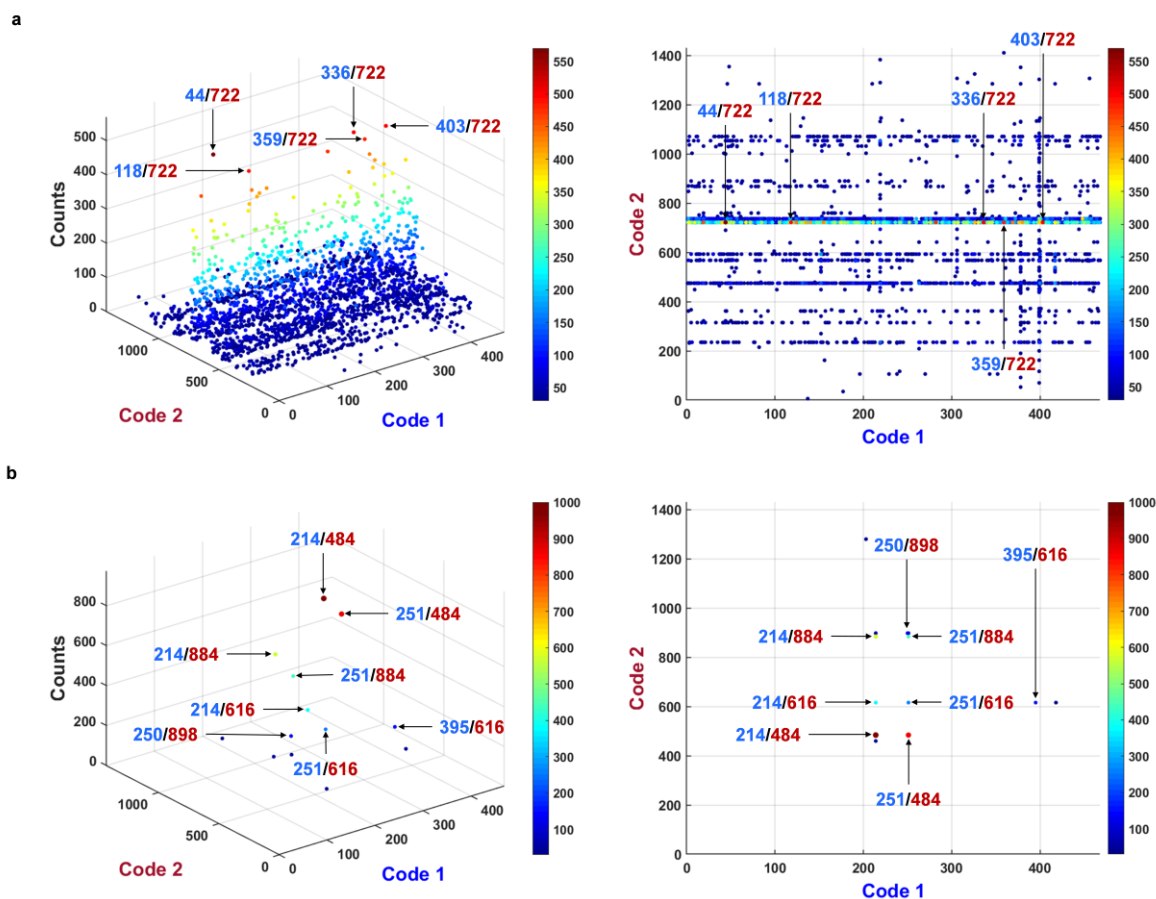
Figure 4.1.14. **a**. A representative fingerprint of affinity selections against CEA. BB2_722 is particularly enriched producing a highly populated line. Nevertheless, the validation would need further consideration due to enrichment of the same building block in no protein affinity selection controls **b**. a representative fingerprint of affinity selections against HSA. The preferential enrichment of certain compounds bearing BB1_214 and 251 may suggest that a particular combination with BB2 is necessary for protein recognition.

Finally, a representative example of selection fingerprints against L19-IL2 is depicted in **Figure 4.1.15**. As shown in this figure, some combinations were preferentially enriched over the rest, with EFs over 200. The analysis of the fingerprints, the validation of the identified hits, and an extensive characterization and medicinal chemistry campaign are described in chapter 4.3, as part of our publication in the *Journal of Medicinal Chemistry*. **2021**, *64*, 17496–17510.
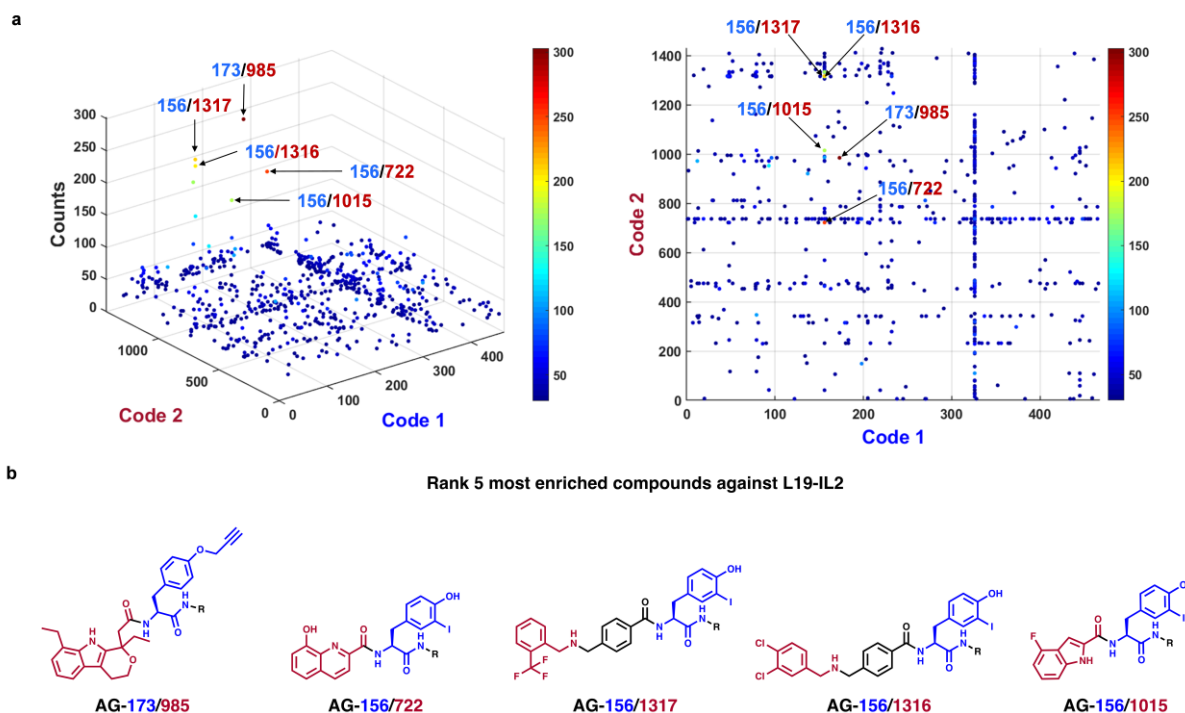
Figure 4.1.15. **a**. A representative fingerprint of affinity selections against L19-IL2. Different combinations are identified, having enrichment factors over 200. **b**. The 5 most enriched compounds. Some of these combinations were validated and confirmed as IL2 ligands and subsequently optimized through medicinal chemistry approaches.

4.1.2 Dual-Pharmacophore ESAC 2+1

The dual-pharmacophore ESAC 2+1 format was first described by our group in a patent application in 2014 and designed and presented in the doctoral thesis of Dr. Willy Decurtins.[340] The ESAC 2+1 format relies on the same concept as the original ESAC libraries. The first sub-library is annealed with a second sub-library bearing an abasic (d-spacer) portion which ensures the correct random combinatorial assembly of both sub-libraries. Moreover, the use of ESAC 2+1 format, in an affinity maturation fashion, was investigated by Bassi *et al*. for the discovery of new potent ligands against targets like CREB-binding protein (CREBBP), HSA, CAIX and tyrosinase.[225]

Library Synthesis

The format of the new ESAC 2+1 library is based on the combination of AG-DEL, in ssDNA format, and a second complementary sub-library (Elib6). The oligonucleotides sequence design was slightly modified from the original one. In the original patent, the first sub-library comprises 72 nucleotides, while AG-DEL comprises 74 nucleotides. On the other hand, the original second sub-library is composed of 103 nucleotides (including abasic sites) while the new Elib6 is composed of 106 nucleotides. The final size of the original ESAC 2+1 library was 103-base pairs, while the new ESAC 2+1 is a 106-base pairs library. The exact sequences and designs of the new ESAC 2+1 library can be found in chapter 6 "Appendix".

Originally, the second sub-library was constructed by the subsequent ligations of the d-spacer (41-mer) with a second d-spacer (31-mer) and a Code 3 (31-mer). In this new adapted format, different 65-mer oligonucleotides, bearing an abasic region for

the annealing with the AG-DEL, and a Code 3 region encoding the Elib6 chemical moiety, were directly purchased from an external provider. The creation of the Elib6 library was achieved using the same ligation procedure optimized for the ssDNA AG-DEL.

256 already derivatized d-spacer conjugates were obtained from previous ESAC libraries from our group. These conjugates were individually HPLC purified. All the different members were individually ligated to 256 distinct 3'-phosphorylated 65-mer oligonucleotides to obtain the final library members. As for AG-DEL, all the individual members were pooled in a single fraction, in an equimolar amount, and purified by IE-HPLC to separate the final library from the excess of codes and DNA adaptor.

The final ESAC 2+1 library, comprising more than 171 million members, was constructed by annealing and Klenow polymerization of AG-DEL and Elib6 as previously performed before affinity selection experiments using AG-DEL (**Figure 4.1.16**). A quality control gel electrophoresis can be found in chapter 6 "Appendix" (**Figure 6.2.13**).
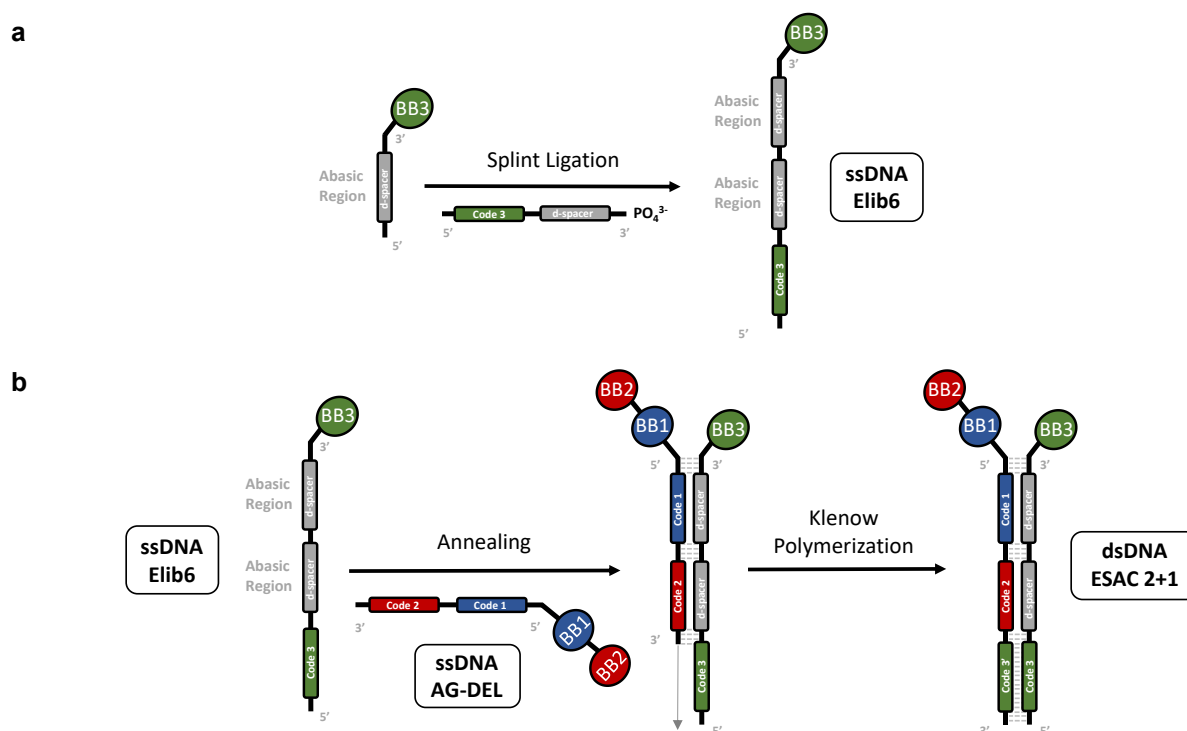
Figure 4.1.16. Schematic representation of the construction of Elib6 sub-library and final ESAC 2+1 library. **a**. The 256 different conjugated-d-spacer molecules were ligated to 256 distinct 65-mer 3'-phosphorylated oligonucleotides and the final pool was purified by IE-HPLC. **b**. The final ESAC 2+1 library comprising more than 171 million members, was constructed by annealing the ssDNA AG-DEL with the Elib6 sub-library, followed by Klenow polymerization.

Affinity Selection Experiments

As for the single-pharmacophore AG-DEL, affinity selection experiments using the dual-pharmacophore ESAC 2+1 library were performed in duplicates using solid-phase affinity capture methodologies.[95] In this case, only selections against empty beads, CAIX, and L19-IL2 were performed. The Naïve library was also characterized

by high-throughput DNA sequencing, revealing a uniform distribution of sequence counts (**Figure 4.1.17**).
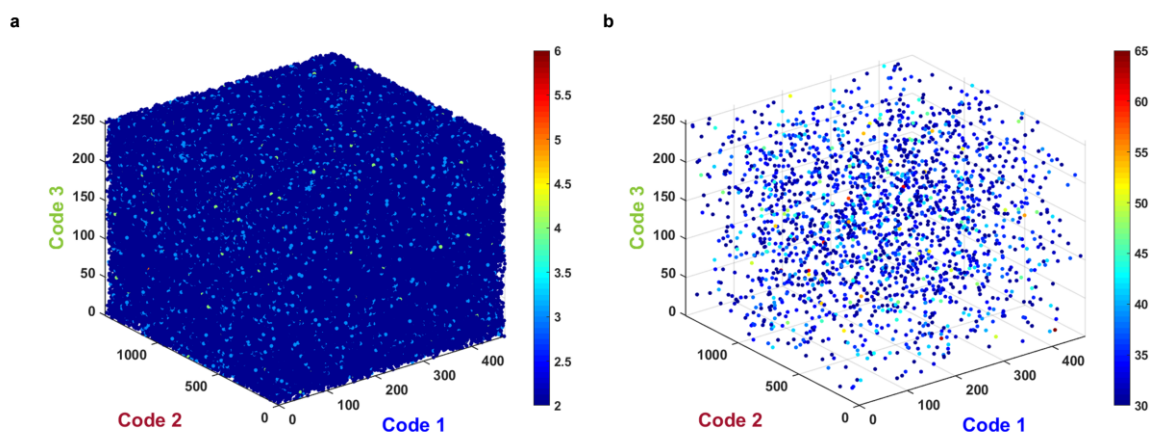
Figure 4.1.17. Representative fingerprints of the ESAC 2+1 naïve library and selections against empty beads. The x-, y-, and z-axes represent the identification barcodes of every BB1, BB2, and BB3, respectively. The relative abundance of every library member is represented by a color code. **a**. ESAC 2+1 Naïve library before affinity selection experiments shows a homogeneous distribution of sequence counts. **b**. Selections against empty beads reveal certain promiscuous structures which would be carefully considered if appear in selections against other targets.

Following the same approach as for AG-DEL, the new ESAC 2+1 was interrogated against CAIX, as a positive control selection experiment. **Figures 4.1.18** and **4.1.19** show fingerprints for CAIX selections, at threshold 350 and 50, respectively. Aromatic sulfonamides were again highly enriched. In this case, the first and second most enriched compounds for both replicates showed combinations of three different aromatic sulfonamide moieties, thus representing a good example of a high avidity effect. Nevertheless, other combinations bearing two or only one aromatic sulfonamides were identified. As shown in **Figure 4.1.19** highly populated lines and planes could be identified for building blocks including BB1_80, 146, 201, 356, and 466; BB2_49, 461, 586, and 803; and BB3_1 and 119. The identification of these combinations serves as a quality control and validation of the ESAC 2+1 library design and construction.
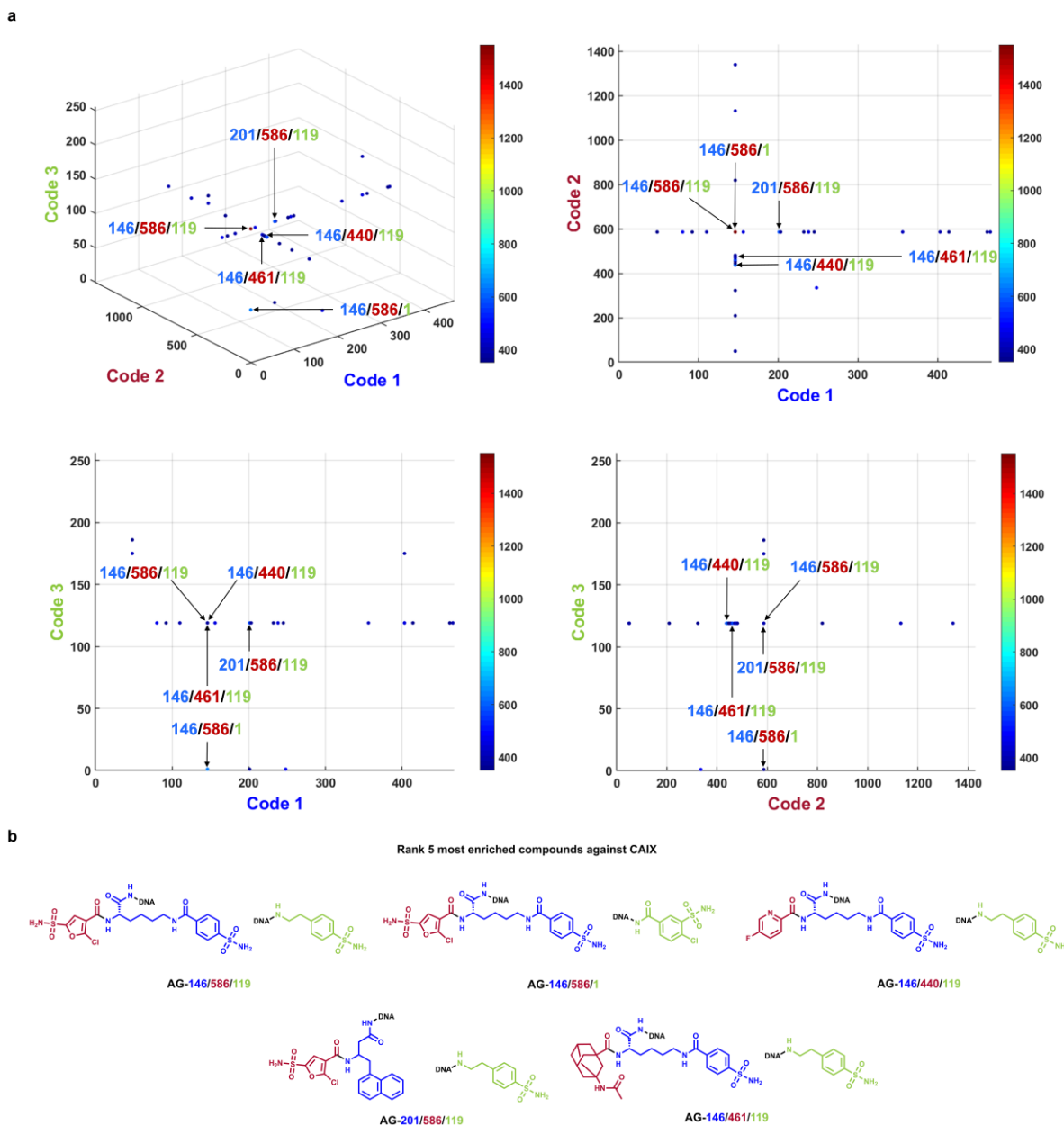
Figure 4.1.18. **a**. A representative fingerprint of affinity selections against CAIX. Different lines and combinations representing different aromatic sulfonamide compounds could be identified. **b**. The 5 most enriched compounds. Some of these molecules are composed of three different aromatic sulfonamide moieties, representing an example of the enhanced avidity effect.
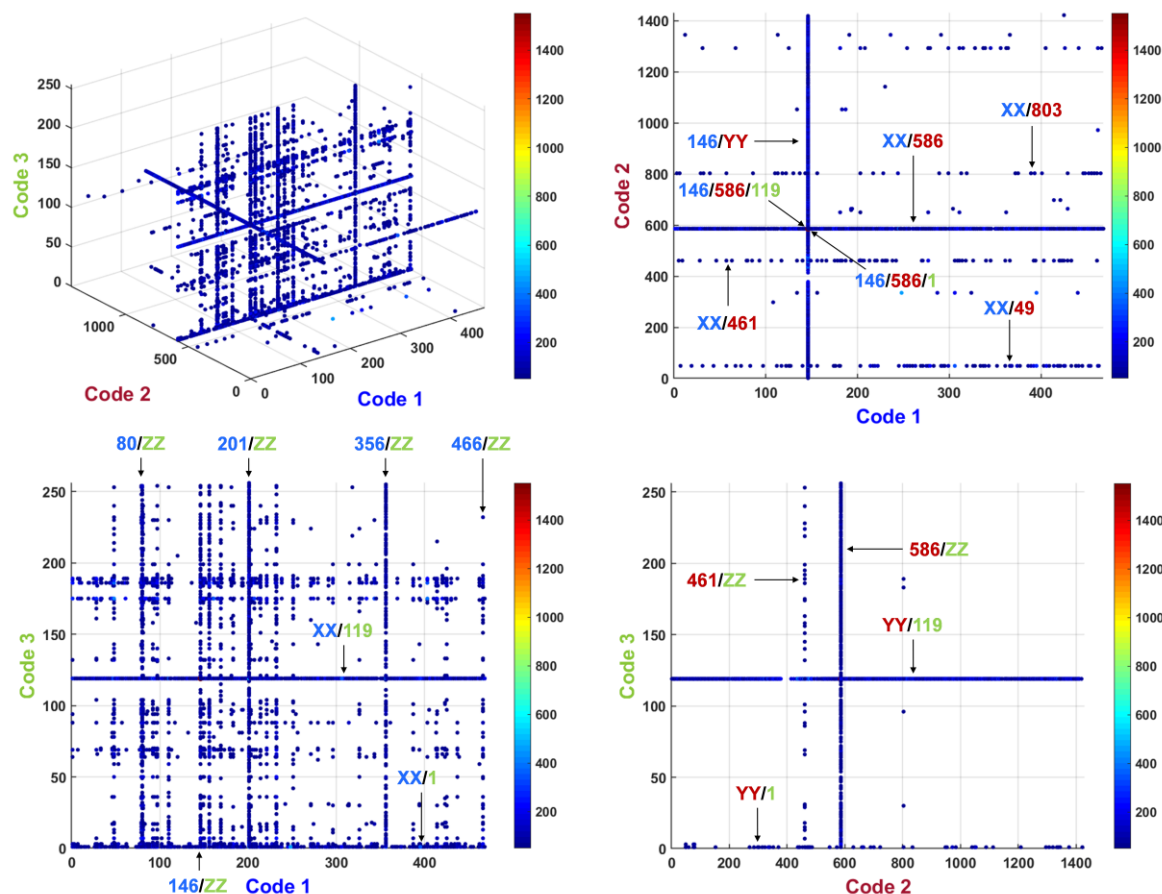
Figure 4.1.19. A representative fingerprint of affinity selections against CAIX. Threshold evaluation of 350 counts. Different lines and combinations representing different aromatic sulfonamide compounds could be identified, which serves as a validation of the ESAC 2+1 library design and construction.

Affinity selection experiments were then performed against L19-IL2. The combinations depicted in **Figure 4.1.20** show a clear structure-activity relationship (SAR) with those obtained during the selection campaign using the single-pharmacophore AG-DEL. The most enriched combinations of these selection experiments have enrichment factors over 2,500. To understand if the selection results of the ESAC 2+1 library were real, one of the combinations was resynthesized off-DNA and validated using fluorescence polarization techniques. The combination (i.e., **AG-326/44/209**) was resynthesized using *L*-2,3-diaminopropionic acid (Dap) and the original succinyl linker used for the attachment of BB3_209 to the DNA. Fluorescence polarization experiments showed a dissociation constant $K_d = 1.5 \pm 0.3$ μM. Even if the selection results may be encouraging, the validation of hits from ESAC 2+1 libraries should be carefully considered. As for classical ESAC libraries, the linkage between the DNA barcode and the pharmacophore offers high flexibility to the small molecules to find and bind the protein target of interest. Nevertheless, both pharmacophores need to be linked in classical off-DNA validation. As previously demonstrated by our group, there is a critical impact on the geometry and flexibility of the linkers used to attach both pharmacophores for the validation of these hits, and the selection of the linker may be a complicated process that increases the time and cost for hit validation activities.[116] Therefore, and based on the results of hits identified

using both libraries, the attention was focused on the validation of the ligands found in selections using AG-DEL, as will be discussed in chapter 4.3.
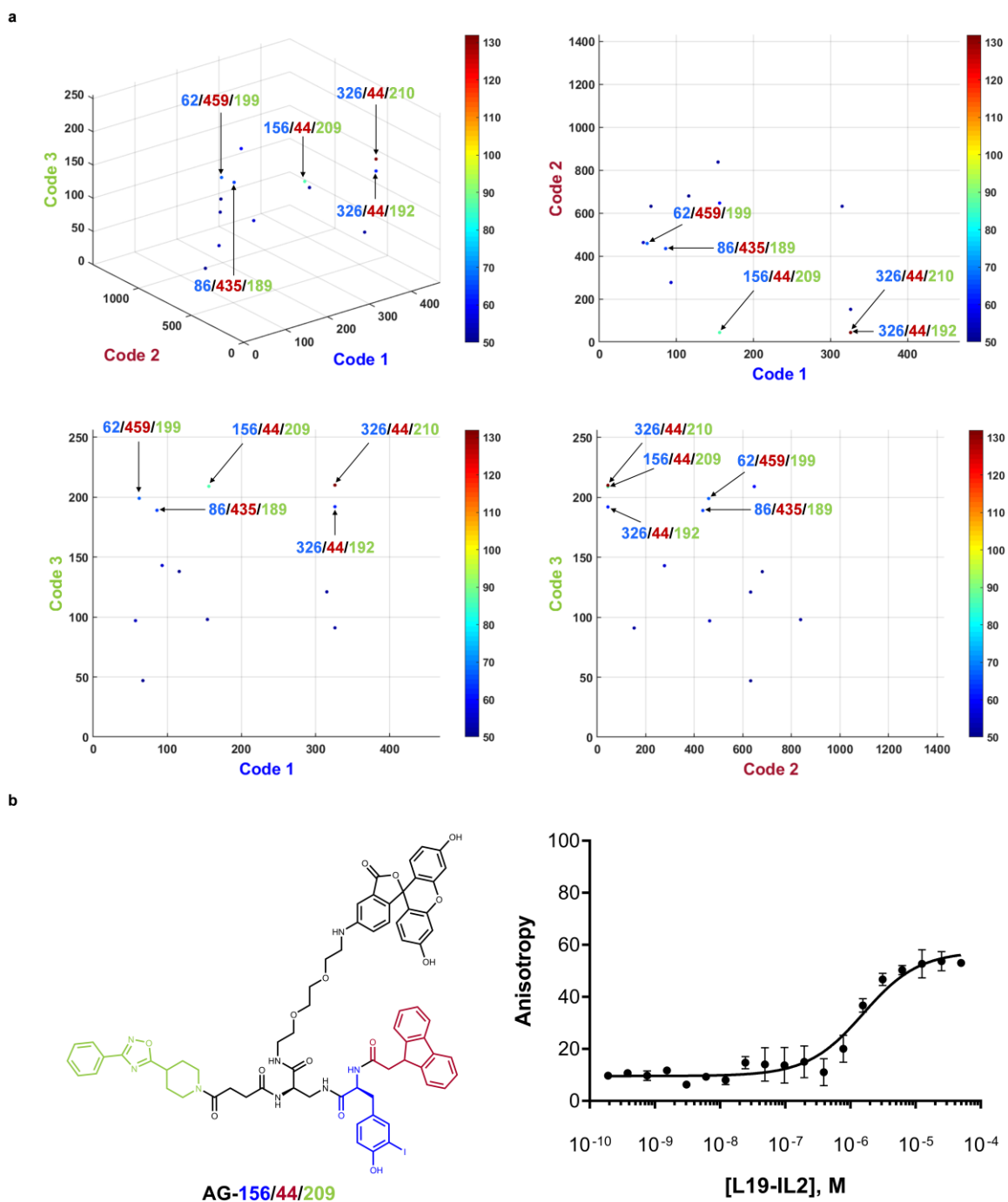
Figure 4.1.20. **a**. A representative fingerprint of affinity selections against L19-IL2. Different combinations are identified, having enrichment factors over 2000. **b**. The combination **156/44/209** was resynthesized using a Dap-Succinyl linker to link both pharmacophores, and tested in fluorescence polarization experiments giving a dissociation constant of 1.5 μM. The results are encouraging and demonstrate a structure-activity relationship between selections performed with AG-DEL and ESAC 2+1.

4.1.3 Dual-Pharmacophore ESAC Plus

This section and the related supporting information included in chapter 6 "Appendix" has been adapted from "Nucleic acid encoded chemical libraries" by Florent Samain, Émile Gorre, Jacopo Millul, Etienne Donckele, and Adrián Gironda Martínez, patent application with International Publication Number **WO 2020/128064 A1**, published on June 25th, 2020.

Motivated by the possibility of drugging different classes of biological targets, for example with extended surfaces, a new ESAC format was hypothesized. In the format, called ESAC Plus, both pharmacophores would be linked through a covalent bond, thus relatively locking the conformation of the final displayed molecules. One way to achieve the covalent bond between both pharmacophores would be *via* copper-catalyzed alkyne-azide cycloaddition (CuAAC) "click" reaction. CuAAC reaction was first described in 2002 by the groups of Meldal, and Fokin; and Sharpless, independently, as one of the best examples of the concept of "click" chemistry.[341–343] CuAAC reaction has been extensively studied in the context of bioconjugation, thus representing a perfect methodology for application in DEL.[124,344,345]

The first part of this work was focused on establishing good conditions for the efficient reaction between a DNA-conjugated azide and a complementary DNA-conjugated alkyne. A 5'-amino-modified 48-mer oligonucleotide (Elib2 Code) was reacted with 5-hexynoic acid using DMT-MM as a coupling reagent. On the other hand, a 3'-amino-modified 41-mer d-spacer oligonucleotide was reacted with 4-azidobenzoic acid, using the same coupling reagent. Both DNA-conjugates (**A** and **B**) were individually HPLC purified to obtain pure material for the optimization of the CuAAC reaction conditions.

Reaction conditions for CuAAC were slightly adapted from internal procedures. Both oligonucleotides were dissolved in basic borate buffer and incubated with Tris(benzyltriazolylmethyl)amine (TBTA), copper sulfate, and sodium ascorbate (chapter 6 "Appendix). The reaction was analyzed by LC-MS. To have control over the procedure, a separated reaction without the addition of TBTA, copper sulfate, and sodium ascorbate was performed. **Figure 4.1.21** shows a comparison between both reactions. Analysis of the MS traces revealed a total conversion of the CuAAC reaction for the formation of the corresponding triazole (**C**).
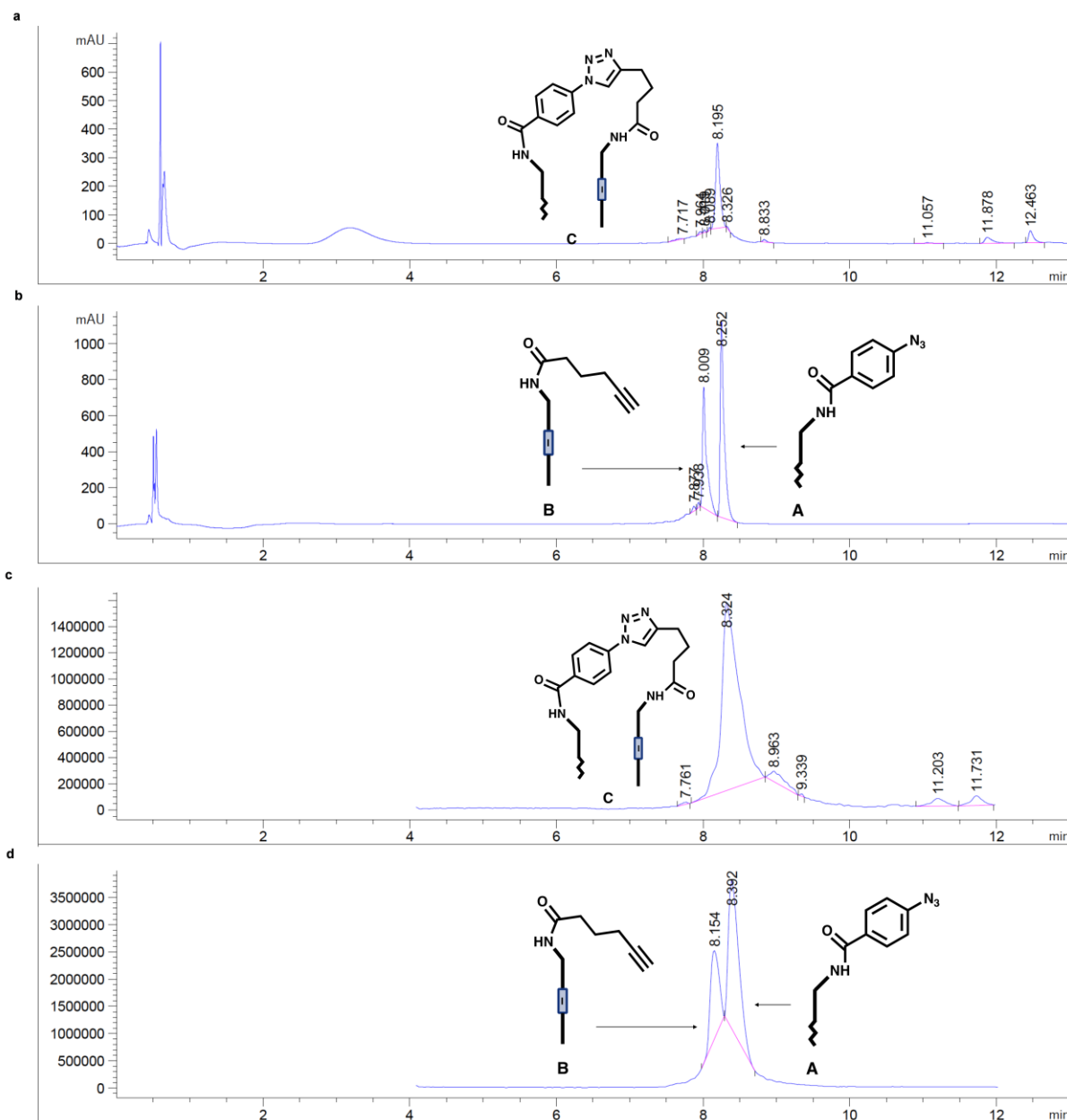
Figure 4.1.21. UV (**a** and **b**) and MS (**c** and **d**) traces for the CuAAC reaction between two partially complementary DNA-conjugates. The formation of the 1,2,3-triazole can be confirmed by the formation of a single peak (**a** and **c**), compared with the two peaks observed in the reaction without TBTA, CuSO$_4$, and sodium ascorbate (**b** and **d**).

Different designs and experimental conditions were tested to select the best synthetic scheme for the production of ESAC Plus libraries. In the next experimental setup, a 5'-amino-modified 48-mer oligonucleotide (Elib2 Code) was reacted with azidoacetic acid, using EDC/s-NHS as coupling reagents, and a 3'-amino-modified 41-mer d-spacer oligonucleotide was reacted with 6-heptynoic acid using DMT-MM as coupling reagent. Both DNA-conjugates were purified by RP-HPLC and CuAAC reaction was performed using the same procedure. The reaction was analyzed by LC-MS and compared with the control without cyclizing reagents (**Figure 4.1.22**).
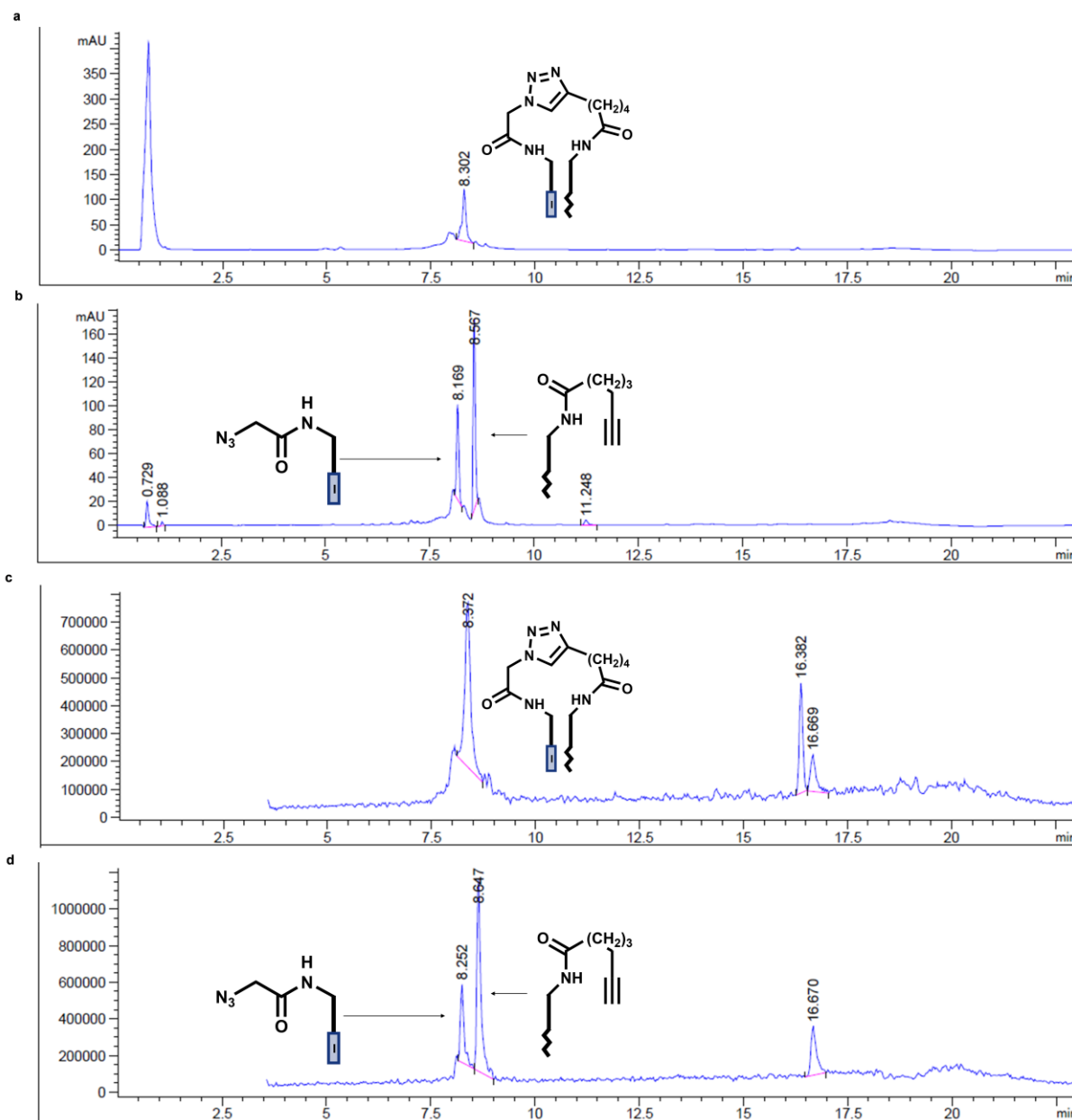
Figure 4.1.22. UV (**a** and **b**) and MS (**c** and **d**) traces for the CuAAC reaction between two partially complementary DNA-conjugates. The formation of the 1,2,3-triazole can be confirmed by the formation of a single peak (**a** and **c**), compared with the two peaks observed in the reaction without TBTA, $CuSO_4$, and sodium ascorbate (**b** and **d**).

To ensure a good conversion using fully encoded DNA-conjugates, the DNA-conjugated alkyne from the previous experiment was ligated to a new 38-mer oligonucleotide (Elib4 code) using a 21-mer oligonucleotide chimeric DNA/RNA adaptor. The use of a chimeric DNA/RNA adaptor may facilitate the subsequent separation of the fully encoded DNA-conjugate from other oligonucleotides by prior degradation of the adaptor using RNases.[115] **Figure 4.1.23** shows the LC-MS analysis after cyclization reaction and the mixture of the complementary DNA-conjugates without cyclization.
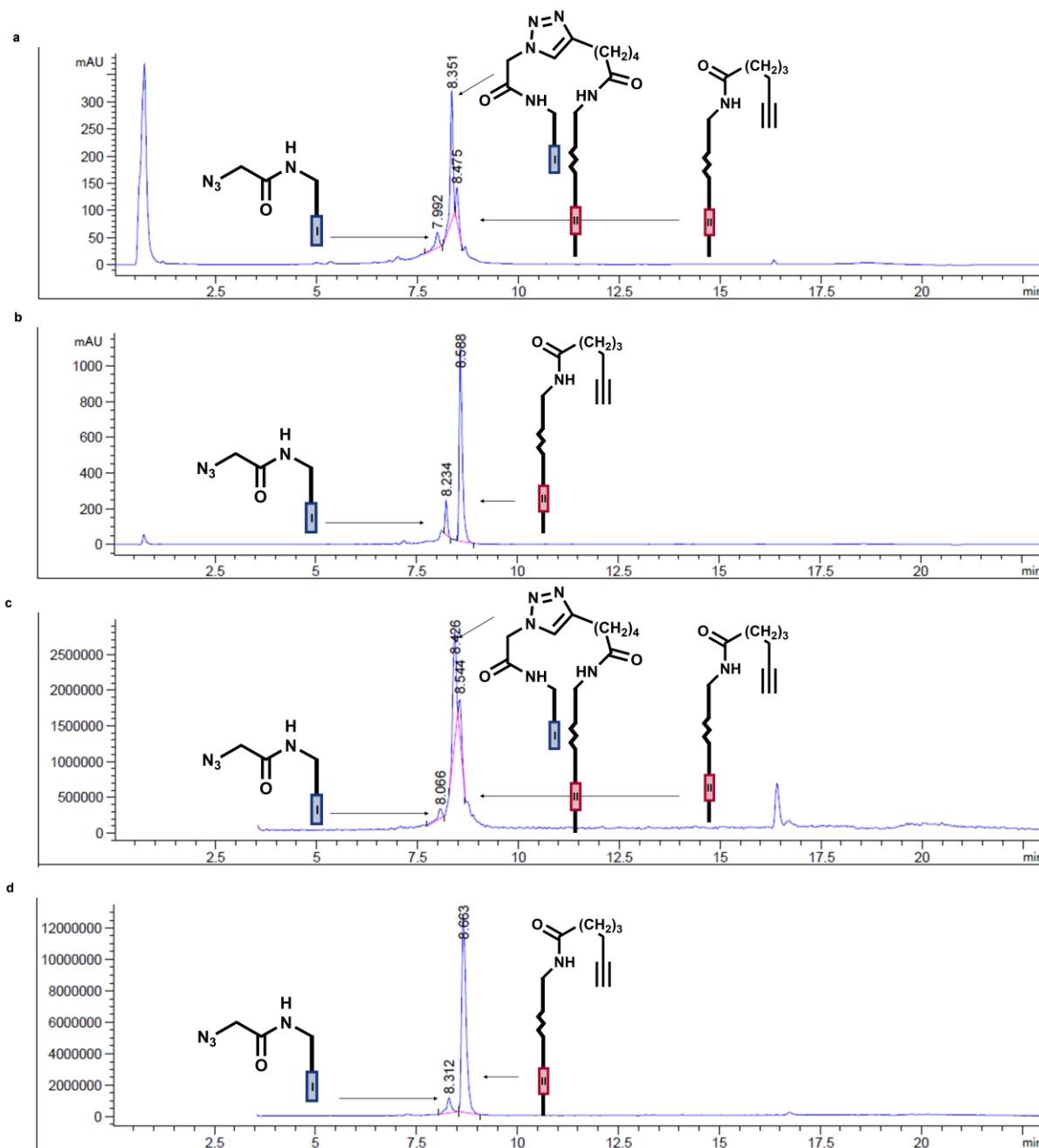
Figure 4.1.23. UV (**a** and **b**) and MS (**c** and **d**) traces for the CuAAC reaction between two partially complementary DNA-conjugates. The formation of the 1,2,3-triazole can be confirmed by the formation of a single peak (**a** and **c**), compared with the two peaks observed in the reaction without TBTA, CuSO$_4$, and sodium ascorbate (**b** and **d**). Some remaining starting materials can be detected.

Klenow polymerization is a critical step for transferring the encoding regions of one of the ESAC sub-libraries to the complementary one, thus allowing for efficient DNA sequencing. Performing Klenow polymerization before the cyclization step may avoid possible degradation of the nascent oligonucleotides and inefficient encoding. Moreover, the higher complementary of the full constructs, after the Klenow step, may increase the local concentration and proximity between the azide and alkyne moieties, thus allowing for a more efficient cyclization reaction. The same single DNA-conjugates used in the last experimental setup were mixed in equimolar concentrations and annealed. Then, a Klenow polymerization step was performed,

transferring the encoding region of the Elib4 code to the Elib2 strand. Prior to the cyclization step, cartridge purification was performed to eliminate the dNTPs and the Klenow polymerase. The cyclized double-stranded DNA construct was achieved using the same experimental conditions for CuAAC reaction (**Figure 4.1.24**).
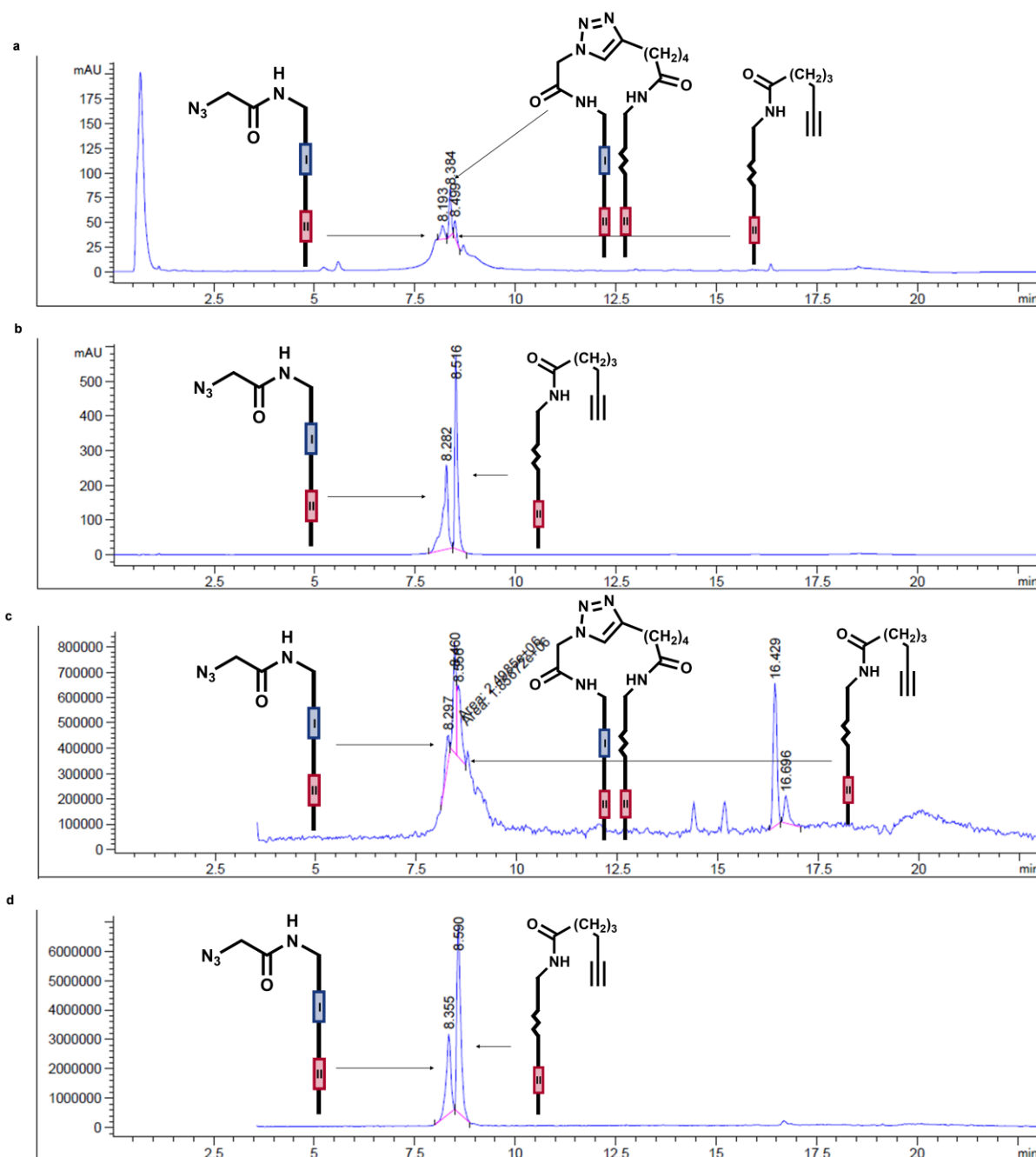
Figure 4.1.24. UV (**a** and **b**) and MS (**c** and **d**) traces for the CuAAC reaction between two partially complementary DNA-conjugates. The formation of the 1,2,3-triazole can be confirmed by the formation of a single peak (**a** and **c**), compared with the two peaks observed in the reaction without TBTA, CuSO₄, and sodium ascorbate (**b** and **d**). Klenow polymerization step was performed before cyclization to transfer the information of the Elib4 code to the Elib2 sub-library. Some remaining starting materials can be detected.

Library Synthesis

After setting up the appropriate synthetic scheme and reaction conditions, a small ESAC Plus library composed of 41,020 members was constructed. The first sub-library (Elib5) was constructed by the combinatorial assembly of 14 different tri-functional scaffolds, containing a carboxylic acid, an *N*-Fmoc/Boc protected amine and an azide moiety; with 293 different carboxylic acids. The complementary sub-library (Elib6) was synthesized by conjugation of 10 different bi-functional acid/alkyne building blocks. Both sub-libraries were purified by HPLC and subjected to Klenow polymerization and subsequent CuAAC cyclization reaction to obtain the final ESAC Plus library (**Figure 4.1.25**). A quality control gel electrophoresis can be found in chapter 6 "Appendix" (**Figure 6.2.17**).
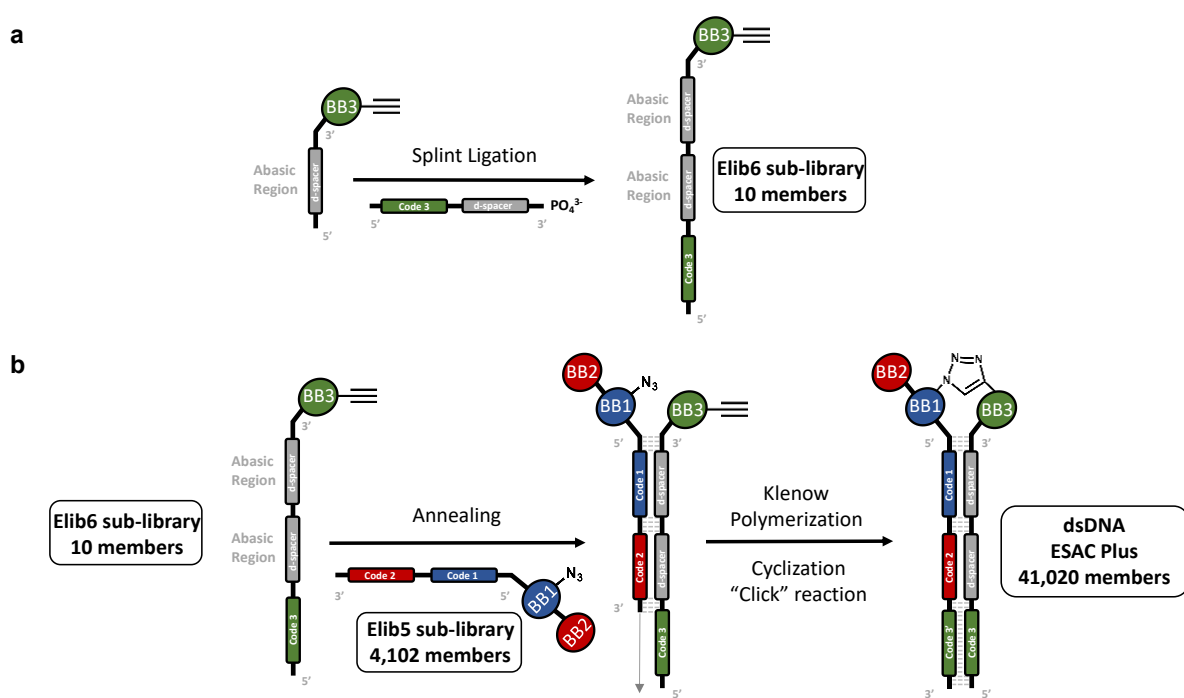
Figure 4.1.25. Schematic representation of the ESAC Plus library construction. **a**. Construction of the Elib6 sub-library by amide bond formation between the d-spacer oligonucleotide and 10 different acid/alkyne building blocks; followed by splint mediated ligation using 10 distinct 65-mer 3'-phosphorylated oligonucleotides. **b**. The final ESAC Plus library, comprising 41,020 members, was constructed by annealing the ssDNA Elib5 sub-library, previously synthesized by our group, with the Elib6 sub-library, followed by Klenow polymerization and cyclization via "click" reaction.

Affinity Selection Experiments

Affinity selections experiments were performed against CAIX as a positive control, together with no protein controls and naïve sequencing. The Elib5 sub-library, the intermediate non-cyclized ESAC library, and the final cyclized ESAC Plus library were interrogated. To compare the results obtained for the three different libraries affinity selection experiments were performed with the libraries in dsDNA format. The Elib5 sub-library in dsDNA format was already available in our laboratory. An aliquot of the ESAC Plus library intermediate, after Klenow polymerization and before the CuAAC reaction, was separated and used as the intermediate non-cyclized ESAC library in dsDNA.

Figure 4.1.26 shows fingerprints for naïve and no protein controls for the three libraries. Naïve sequencing showed a homogeneous distribution of sequence counts, confirming library quality, while no protein controls showed preferentially enriched combinations that may be carefully considered in subsequent hit validation campaigns.
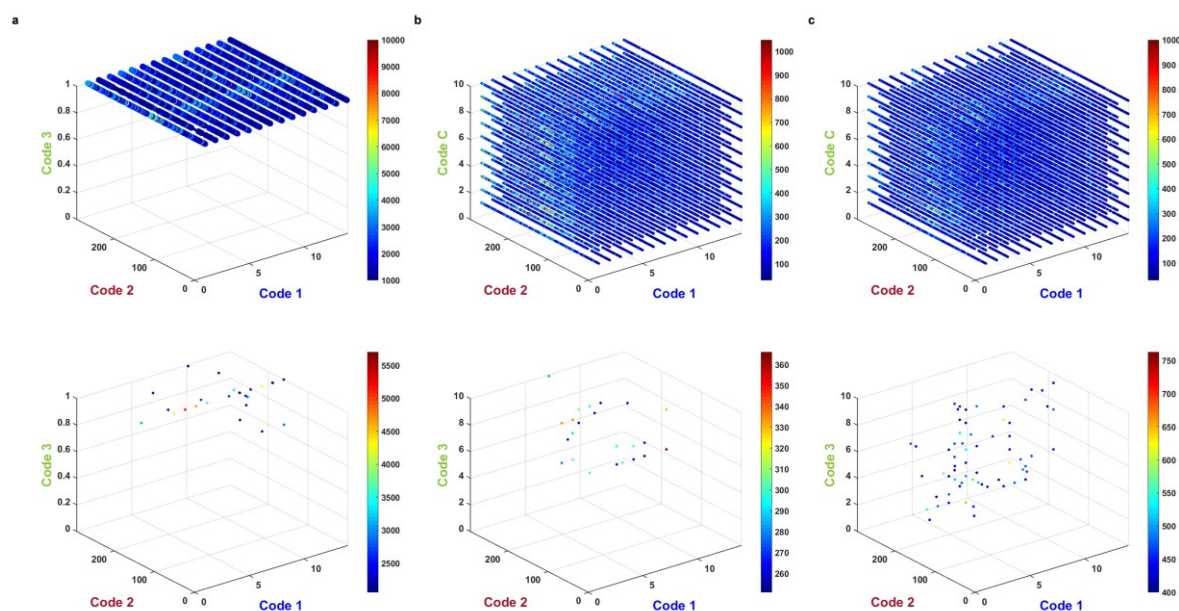
Figure 4.1.26. Naïve libraries before affinity selection experiments (up) show a homogeneous distribution of sequence counts. Selections against empty beads (down) reveal certain promiscuous structures for every library. **a**. Elib5, **b**. non-cyclized ESAC, and **c**. ESAC Plus.

Different combinations and enrichment factors can be observed for every library against CAIX (**Figure 4.1.27**). As for AG-DEL and ESAC 2+1, the ESAC Plus library was constructed including aromatic sulfonamides as positive control binders of CAIX. Preferentially enriched combinations in the three different libraries represent mono-, di-, or tri-valent sulfonamide compounds. The most enriched compounds corresponded to the combinations between BB2_6 and different BB1 and BB3. Combinations bearing BB3_5 and 9 (corresponding to secondary aromatic sulfonamides) were particularly enriched. ESAC Plus library selections showed lower enrichment factors than non-cyclized ESAC library, and preferentially enriched combinations locked both BB1_4 and BB2_6. The differences between the enriched combinations using the intermediate non-cyclized ESAC library and the final ESAC

Plus library may suggest a possible influence on the rigidity of the final displayed molecules. These results confirm that the new ESAC Plus library may serve as an important tool for ligand discovery against pharmaceutically and biologically relevant targets in which the three-dimensional conformation of the binders may play a crucial role in protein recognition.
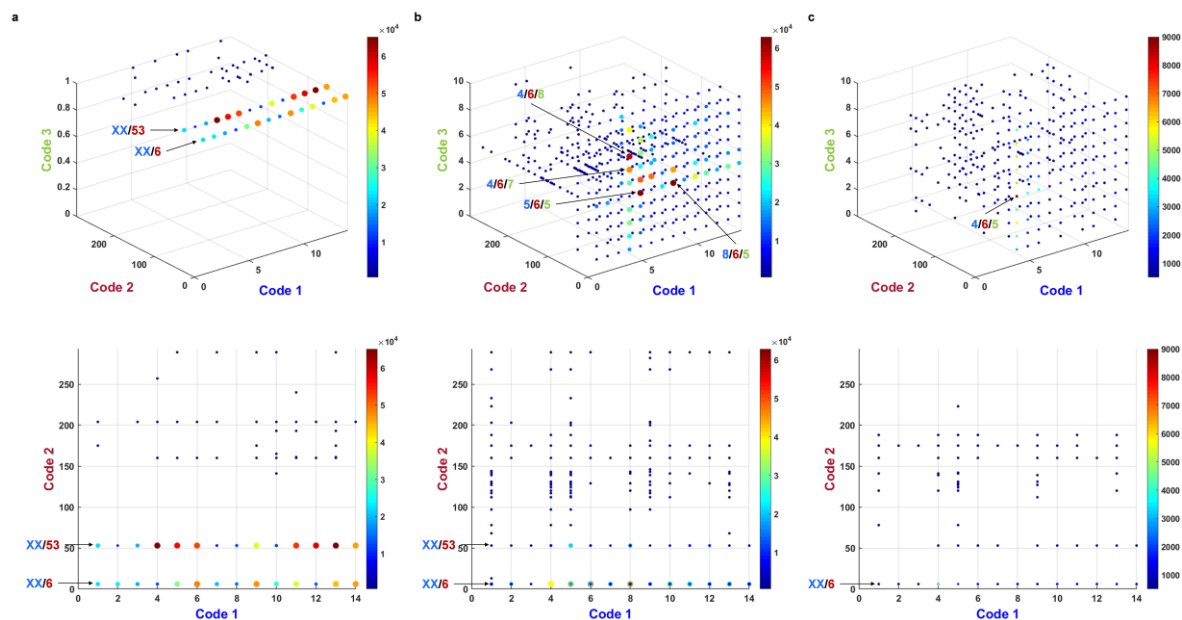
Figure 4.1.27. Representative fingerprints of affinity selections against CAIX. **a**. Elib5 selections. Two preferentially enriched building blocks can be observed (BB2_6 and 53) corresponding to aromatic sulfonamides, in combination with several BB1. **b**. Non-cyclized ESAC selections. The most enriched compounds correspond to the combinations between BB2_6 and different BB1 and BB3. Combinations bearing BB3_5 and 9 (corresponding to secondary aromatic sulfonamides) are particularly enriched. **c**. ESAC Plus library selections show lower enrichment factors than non-cyclized ESAC library, being the combinations bearing both BB1_4 and BB2_6 the most enriched compounds.

4.2 DNA-compatible diazo-transfer reaction in aqueous media suitable for DNA-encoded chemical library synthesis
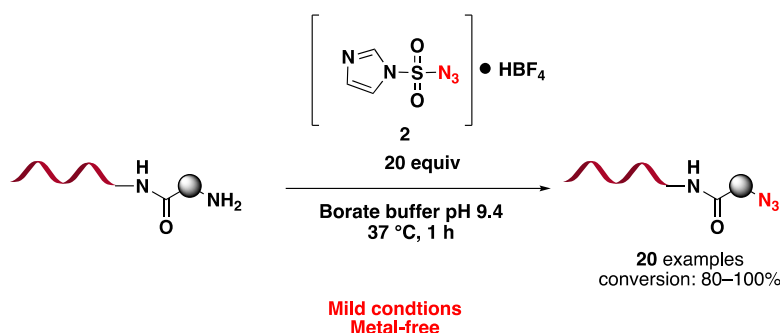
This section and the related supporting information included in chapter 6 "Appendix" has been adapted from "DNA-Compatible Diazo-Transfer Reaction in Aqueous Media Suitable for DNA-Encoded Chemical Library Synthesis" by Adrián Gironda-Martínez, Dario Neri, Florent Samain and Etienne J. Donckele, published in *Organic Letters*, **2019**, *21*, 9555–9558. Copyright 2019 American Chemical Society.

4.2.1 Abstract

DNA-encoded chemical libraries (DELs) are increasingly being used for the discovery of ligands to proteins of interest. Protected amino acids are the most commonly used building blocks for the construction of DELs; therefore, the expansion of reaction scope with the subsequent free amine is highly desired. Here, we developed a robust DNA-compatible diazo-transfer reaction using imidazole-1-sulfonyl azide tetrafluoroborate salt converting a wide range of primary amines into their corresponding azides in good to excellent yields.

4.2.2 Introduction

DNA-encoded chemical libraries (DELs) have become a powerful technology platform for the discovery of ligands against targets of pharmaceutical interest and have made notable progress for the identification of high affinity ligands in the last decade.[86,88,89,92,346,347] DELs are collections of organic molecules, covalently conjugated to a distinctive and amplifiable DNA tag, that lead to the generation and screening of chemical libraries comprising millions to billions of compounds. The chemical and structural diversity of tagged-molecules is essential to the successful hit identification of drug-like chemical features.[125,130] Despite the growing interest in the field, DNA-compatible reactions, which cover a wider chemical space, remain a formidable challenge.[140,145,149,162,348–357] One of the most used reactions for the construction of DELs is the amide bond formation thanks to various reliable protocols and the availability of a large panel of amino acids at reasonable cost.[348,358] Currently, the availability of DNA-compatible methodologies that allow facile post functionalization and derivatization of amino acids attached to DNA is quite limited due to several restrictions in the presence of the oligonucleotide.[130] Herein, we describe a diazo-transfer reaction of DNA-conjugated amino acids into their corresponding azides in solution. Azide is a versatile intermediate extensively employed in organic synthesis for the construction of triazoles (CuAAC "click" reaction), carbamates (Curtius rearrangement), or amides (Schmidt reaction).[359–362] Thus, azides became very

attractive for the generation of DNA-encoded macrocyclic peptide libraries, the implementation of azides-based scaffolds to explore the ligand geometry, and the construction of benzodiazepine and pyrazolopyrimidine libraries featuring azides as diversity elements.[229,363,364]

Alkyl azides are commonly prepared by S_N2 substitution using azide ions and various electrophiles.[365] However, this approach can lead to the formation of elimination products or with incorrect stereochemical configuration. The diazo-transfer reaction to primary amines utilizing trifluoromethanesulfonyl azide (TfN$_3$) as a "diazo-donor" has emerged to be a popular method due to its high reactivities using mild reaction conditions and for the retention of any preexisting stereochemistry.[366–368] Nevertheless, this procedure suffers from several problems. The reaction needs excess TfN$_3$ and requires long reaction time even in the presence of a metal catalyst, thus inducing damage to the DNA. In addition, the preparation of TfN$_3$ poses a risk of toxicity and explosion due to the excess of sodium azide under acidic media.[369] Recently, imidazole-1-sulfonyl azide salt (ISA salt) was reported as an economical, shelf-stable, and suitable substitute to TfN$_3$.[370–373] However, despite its possible applications, diazo-transfer reaction has not been studied in the context of DELs. At present, few examples have been reported for the conversion of aminated oligodeoxyribonucleotides (ODNs) into their corresponding azides and on Novapeg Rink resin for the design of peptide nucleic acid PNA-encoded libraries.[374,375]

4.2.3 Results and discussion

To initiate our studies, DNA-tagged glycine (**1**) was synthesized and used as a model substrate in the presence of imidazole-1-sulfonyl azide (ISA; **2**) and CuSO$_4$ for the optimization of the diazo-transfer reaction, as initially described in literature (**Table 4.2.1**).[369,371]

We decided to use ISA·HBF$_4$ as diazo-donor due to its high thermostability, long life storage at ambient conditions, and its being reported as the safest-to-handle ISA salt.[371] The integrity and purity of the DNA-conjugated products were analyzed by liquid chromatography−mass spectrometry (LC−MS). Throughout the manuscript, this approach has been used to identify conversion yields and optimized conditions. Foremost, we tested the influence of the quantity of diazo-transfer agent **2** in the presence of CuSO$_4$ as catalyst to promote the azide formation. In this case, 60 equivalents of the diazo-transfer reagent is sufficient to obtain the desired DNA-conjugated azido product (**3**) in excellent yield (**Table 4.2.1**, entry 2). Surprisingly, DNA damage was observed by MS despite good conversion to the corresponding product **3**. To tackle this issue, we noticed that the absence of copper in more basic buffer in the media led to similar reactivity without any DNA damage (**Table 4.2.1**, entries 4 and 5).

Furthermore, the use of catalyst, such as CuSO$_4$, proved to be completely ineffective for the transformation. We then explored the effect of temperature and reaction time (**Table 4.2.1**, entries 5−8) on single-stranded DNA-conjugated **1**. The diazo-transfer reaction gave similarly high conversion at lower temperature and reaction time using 20 equivalents of ISA·HBF$_4$ (**2**) without significant DNA degradation. While epimerization of chiral centers may occur under basic media, the diazo-transfer reaction was investigated by Samuelson and co-workers, who reported the evidence of retention of the stereocenter upon addition of ISA·HCl.[376]

Table 4.2.1. Selected results for optimization of DNA-compatible diazo-transfer reaction[a]
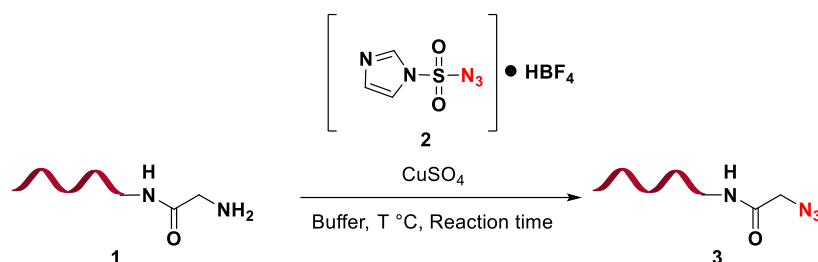
entry	2 (equiv)	CuSO$_4$ (equiv)	buffer (pH)	temperature (°C)	reaction time (h)	conversion[b] (%)
1	120	120	MOPS (8.0)	60	16	95[c]
2	60	60	MOPS (8.0)	60	16	95[c]
3	60	–	MOPS (8.0)	60	16	95
4	60	–	Borate (9.4)	60	16	95
5	60	–	Carbonate (11.5)	60	16	95
6	60	–	Borate (9.4)	37	16	95
7	60	–	Borate (9.4)	37	1	95
8	**20**	**–**	**Borate (9.4)**	**37**	**1**	**95**

[a]All the reactions were conducted at 0.4 mM in 2 nmol scale. [b]Conversion observed by LC–MS. [c]DNA degradation observed by mass spectrometry.

The new developed conditions were then used to explore the reactivity of structurally diverse amino acids (**1**, **4−22**; **Figure 4.2.1**). To our delight, the reaction delivered azido DNA-conjugated products in good to excellent conversion yields. Diazo-transfer reaction of DNA-conjugated benzyl amine **4** gave **23** in excellent conversion. The same trend was observed with DNA-conjugated cyclic derivatives (**5−9**), in which the desired azido products (**24−28**) were obtained in good conversions between 80 and 100%. Interestingly, steric hindered DNA-conjugated amine **10** underwent functionalization to the corresponding azidocyclopentyl DNA product **29** in 90% conversion.

The generality of our synthetic protocol was then investigated with electron donating groups on the benzyl rings (**Figure 4.2.1**, entries **9−12**), which could be useful reagents for further derivatization such as alkylation, Suzuki, or Sonogashira reaction. Diazo-transfer reaction of DNA-conjugated amines gave the corresponding azides **30−33** in excellent conversion. Different electron withdrawing groups (nitrile, nitro, or amide) were well tolerated; azido products **34−37** were obtained with a conversion greater than 90%. We were delighted to see that diazo-transfer reaction of DNA-conjugated urea **19** provided **38** in excellent conversion yield. In addition, DNA-

conjugated amino acid **20** containing a sulfonamide moiety yielded **39** upon addition of ISA·HBF$_4$ (**2**) in 70% conversion. It is noteworthy that the diazo-transfer reaction with **20** afforded sulfonyl azide as side product in 30% conversion. Surprisingly, reaction of DNA-conjugated anilines yielded the desired azido product in very low conversion. Compared to DNA-conjugated benzyl amine derivative **4**, **21** and **22** are more electron releasing groups and thus make the π system more electrophilic, which inhibits the insertion of the azide moiety.
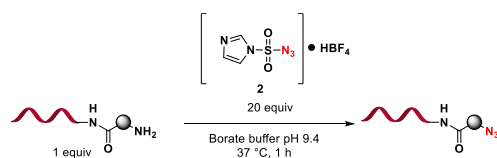
entry	Substrate	Product	Conversion[a]	entry	Substrate	Product	Conversion[a]
1	1	3	95%	11	13	32	94%
2	4	23	90%	12	14	33	97%
3	5	24	95%	13	15	34	90%
4	6	25	100%	14	16	35	93%
5	7	26	90%	15	17	36	100%
6	8	27	80%[b]	16	18	37	92%[b]
7	9	28	90%	17	19	38	97%
8	10	29	90%	18	20	39	70%
9	11	30	92%	19	21	40	< 5%
10	12	31	85%	20	22	41	< 5%

Figure 4.2.1. Scope of the diazo-transfer reaction of DNA-conjugated amino acids. All the reactions were conducted at 0.4 mM in 2 nmol scale. [a]Conversion observed by LC–MS. [b]Reported conversion after 3 h.

It was previously described by Defrancq *et al.* that the diazo-transfer reaction proceeds only on the desired amine and not over the pendant amino group of the nucleobases, even in harsher reaction conditions (65 °C, highly concentrated reagents, over 2 days).[374] The efficiency of the ligation was studied to demonstrate

the compatibility of the methodology with DEL synthesis (**Scheme 4.2.1**). A 45-mer single-stranded DNA (ssDNA) containing glycine **42** gave DNA-conjugated **44** in excellent conversion upon addition of ISA·HBF$_4$ as reported earlier (**Table 4.2.1** and **Figure 4.2.1**). Purification of the DNA-conjugated product was done at each chemical step. The obtained ssDNA azido **44** was then ligated to a 29-mer ssDNA to yield the 74-mer ssDNA-conjugated product **45**. Oligonucleotide azido conjugate **45** was further functionalized by click reaction, using hex-5-ynoic acid (**46**), yielding **47** in full conversion.

Scheme 4.2.1. DNA-Compatible Chemistry Validation Process
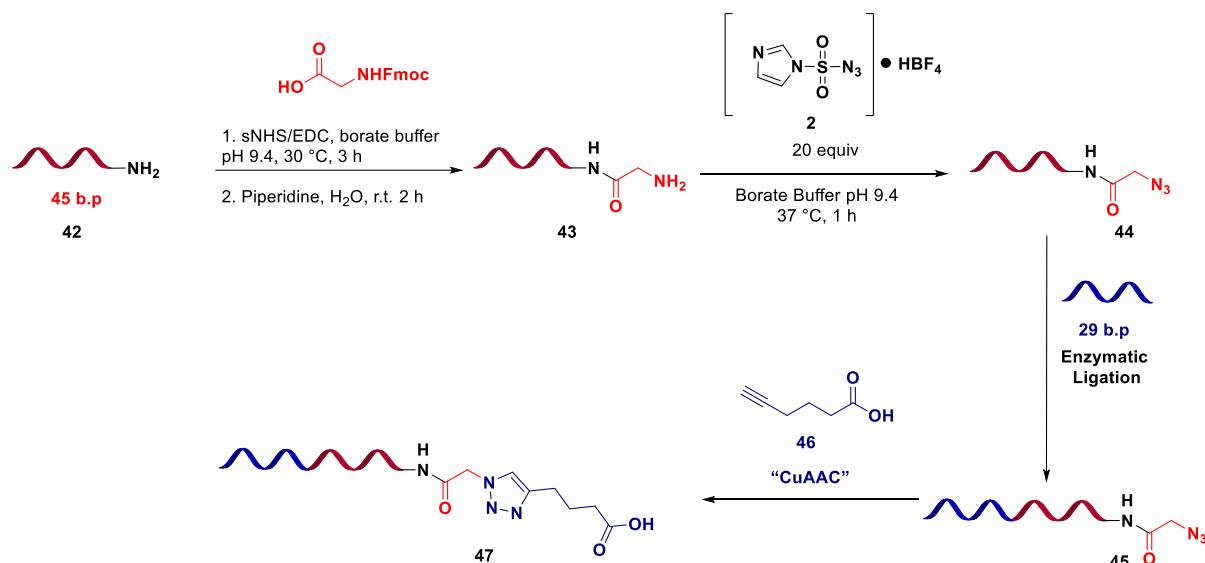
4.2.4 Conclusions

In summary, we have presented a robust, mild, and efficient protocol for the diazo-transfer reaction to convert on-DNA primary amines of high diversity into their corresponding azides, using ISA·HBF$_4$ in solution. Remarkably, the ligation efficiency and the structural integrity were preserved with the diazo-transfer reaction protocol. This simple DNA-compatible transformation with a wide range of amino acids enhanced the chemical diversity for the construction of DELs.

As previously mentioned in chapter 3 "Aim of the thesis" and in chpater 4.1.3 "Dual-Pharmacophore ESAC Plus", the optimized diazo-transfer reaction serves as a valuable tool for enhancing the diversity of DNA-conjugated azides. Thanks to this optimization, an efficient implementation of the ESAC Plus library concept was achived in our group, leading to several macrocyclic dual-pharmacophore libraries. However, the synthesis of such libraries and the subsequent affinity selection experiments are out of the scope of this thesis and will be disclosed in subsequent publications by our group.

4.3 Identification and validation of new interleukin-2 ligands using DNA-encoded libraries
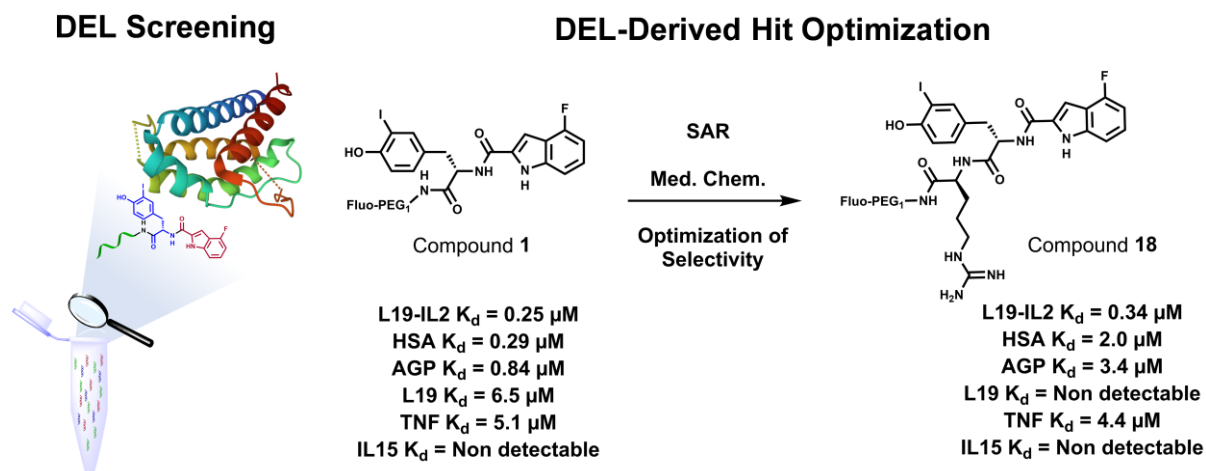
DEL Screening

DEL-Derived Hit Optimization

Compound **1**

L19-IL2 K_d = 0.25 μM
HSA K_d = 0.29 μM
AGP K_d = 0.84 μM
L19 K_d = 6.5 μM
TNF K_d = 5.1 μM
IL15 K_d = Non detectable

SAR
Med. Chem.
Optimization of Selectivity

Compound **18**

L19-IL2 K_d = 0.34 μM
HSA K_d = 2.0 μM
AGP K_d = 3.4 μM
L19 K_d = Non detectable
TNF K_d = 4.4 μM
IL15 K_d = Non detectable

Some parts of this section, the related materials and methods, and supporting information included in chapter 6 "Appendix" have been adapted from "Identification and Validation of New Interleukin-2 Ligands Using DNA-Encoded Libraries" by Adrián Gironda-Martínez, Émile M. D. Gorre, Luca Prati, Jean-François Gosalbes, Sheila Dakhel, Samuele Cazzamalli, Florent Samain, Etienne J. Donckele and Dario Neri, published in *Journal of Medicinal Chemistry*, **2021**, *64*, 17496–17510. Copyright 2021 American Chemical Society.

4.3.1 Abstract

Interleukin-2 (IL2) is a pro-inflammatory cytokine that plays a crucial role in immunity, which is increasingly being used for therapeutic applications. There is growing interest in developing IL2-based therapeutics which do not interact with the alpha subunit of the IL2 receptor (CD25), as that protein is primarily found on immunosuppressive regulatory T cells (T$_{regs}$). Screenings of a new DNA-Encoded Library, comprising 669,240 members, provided a novel series of IL2 ligands, subsequently optimized by medicinal chemistry. One of these molecules (compound **18**) bound to IL2 with a dissociation constant of 0.34 μM, was able to form a kinetically stable complex with IL2 in size-exclusion chromatography and recognized the CD25-binding site as evidenced by competition experiments with the NARA1 antibody. Compound **18** and other members of the series may represent the starting point for the discovery of potent small-molecule modulators of IL2 activity, abrogating the binding to CD25.

4.3.2 Introduction

Interleukin-2 (IL2) is a four-α-helix bundle cytokine comprising 153 amino acids and is a member of the so-called common gamma chain cytokine family, whose receptor comprises certain specific subunits and one common polypeptide chain, termed γc or CD132.[273] IL2 is a unique cytokine not only for its prominent role in immunity but also because of the various interaction modalities of this protein with its cognate receptor (IL2R). Indeed, the IL2R is composed of three different subunits, which are not always present on the cell surface, and which may contribute to different signaling outcomes.

In resting T cells, the IL2R is mainly heterodimeric, consisting of a beta subunit (IL2Rβ or CD122) which can associate with the common gamma chain. The binding of IL2 to the heterodimeric IL2R consisting of CD122 and γc activates JAK1 and JAK3, leading to the subsequent activation of STAT5.[273,274] The alpha subunit of the IL2R (IL2Rα or CD25) is not involved in signaling but, when present, CD25 enhances the binding affinity to IL2 by as much as 100-fold.[273,274,277,278]

IL2 is mainly produced by activated CD4^{+} T cells and dendritic cells and plays a crucial role in the homeostasis and efficient activation of T cells.[273,274,277–279] The immunological relevance of IL2 is best illustrated by the fact that pharmaceutical agents which inhibit IL2 production, such as cyclosporine or Tacrolimus (FK506), represent some of the most potent immunosuppressive agents known so far.[289] Interleukin-2 can potently activate both T cells and Natural Killer cells and, for this reason, the protein has attracted considerable interest for the therapy of cancer. Indeed, recombinant IL2 has received marketing authorization for the treatment of metastatic melanoma and renal cell cancer.[290] Recently, several efforts have been made to render IL2 therapeutics more potent and selective, for example, by conjugation to hydrophilic polymers or by fusion with tumor-targeting antibodies.[296–300,304–306,308] However, the preferential expression of CD25 on immunosuppressive T$_{regs}$ may limit the therapeutic potential of IL2-based biopharmaceuticals, as low doses of cytokine may preferentially interact with those cells.[303] In an attempt to limit T$_{reg}$ binding, antibodies masking the IL2 epitope involved in CD25 binding, or site-specific PEGylation of engineered IL2 residues at the CD25 binding interface, have been proposed and moved into clinical development activities.[273,308,310]

In principle, it would be attractive to develop selective small-molecule IL2 binders rather than monoclonal antibodies, that could abolish the interaction of IL2 with the alpha subunit of the IL2R. Several efforts in this direction have been undertaken over the years, in spite of the formidable challenge of discovering small ligands which disrupt protein-protein interactions (PPIs).[249,250] In 1997, scientists at Hoffmann-LaRoche successfully identified the first small molecule (**Ro26-4550**) capable of modulating the interaction between IL2 and its alpha subunit receptor.[259] **Ro26-4550** was claimed to have a dissociation constant K_d = 22 μM against IL2 and IC$_{50}$ = 3 μM for the inhibition of the IL2/IL2Rα interaction.[319] Subsequent optimization of the molecule, based on the combined use of X-ray crystallography, tethering approaches, and fragment assembly, led to the discovery of SP4206 (K_d = 0.10 μM, IC$_{50}$ = 0.06 μM) by the group of James A. Wells at Sunesis Pharmaceuticals.[260,261,317–319]

In 2012, our group reported the discovery from a DNA-encoded chemical library (DEL) of a small organic IL2 ligand ($A_{17}B_{284}$) with K_d = 2.5 μM, as measured by fluorescence polarization techniques. The molecule was predicted to bind to the CD25 interaction site on the basis of modeling studies.[108] DELs are collections of organic compounds, individually attached to distinctive DNA fragments, serving as amplifiable identification barcodes. Ever since the original postulation of DEL technology by Brenner and Lerner, DELs have become increasingly popular tools for the construction of large combinatorial libraries and the discovery of protein ligands.[16,86,88] The library which we had synthesized and used for the discovery of $A_{17}B_{284}$ featured a set of amino acids as the first group of building blocks, which was then capped with a second set of amine-reactive moieties.[108] This design has later been widely adopted, both in

industry and in academia, because of ease of synthesis and availability of building blocks.

Here we describe the construction of a novel, versatile, and Lipinski-compliant DEL based on the use of amino acids as the first set of building blocks in library synthesis, followed by the reaction of the amine function with a set of capping reagents (carboxylic acids, iso(thio)cyanates, amines, and sulfonyl chlorides), in analogy to the original report of Leimbacher *et al.*[108] The library (termed AG-DEL), which comprised 669,240 members, was synthesized using DNA in single-stranded format, as this procedure has recently been found to be versatile for ligand discovery and compatible with various screening techniques, including the conventional use of affinity capture procedures and the use of oligonucleotide-assisted cross-linking methods.[187,194,225] AG-DEL was screened against several proteins, including IL2. Here we describe the discovery and optimization of a series of IL2 binders. The best ligand (compound **18**) bound to IL2 with $K_d = 0.34$ μM at the CD25 binding site, as evidenced by competition experiments performed with the clinical-stage NARA1 antibody.[309]

4.3.3 Results and discussion

The synthesis of AG-DEL was first described as part of the results of this manuscript. However, for convenient reasons these results have been included and extended in chapter 4.1 of this thesis, therefore the synthesis of the library will not be repeated in this section.

Affinity selection experiments

Affinity selection experiments were performed with the AG-DEL in dsDNA format after a Klenow polymerization step, which converted the single-stranded DNA barcode into the corresponding double-stranded structure.[325] The library was screened against multiple proteins, including carbonic anhydrase IX (CAIX, which was used as a positive control) and the clinical-stage IL2-based L19-IL2 fusion protein.[377] Prior to selection experiments, the library was also characterized by high-throughput DNA sequencing, revealing a uniform distribution of sequence counts for all the library members (**Figure 4.3.1a**). Before selections, all library members are visible as dots in a three-dimensional space, in which the x- and y-axes correspond to the identity of the individual BBs used for AG-DEL construction, while the relative abundance of individual library members (determined on the basis of DNA sequence counts) is displayed on the z-axis (**Figure 4.3.1a**).[104,199] Sequence counts are also indicated by a color code. In the rest of this section, compound numbers are indicated as **AG-XX/YY**, where XX corresponds to the numbering of BB1, while YY represents the numbering of BB2.

Figure 4.3.1 shows fingerprints of the AG-DEL before and after affinity-based selections against CAIX, a validated tumor-associated antigen that is expressed in renal cell carcinomas and hypoxic tumors. As expected, screenings against CAIX provided selective enrichment of aromatic sulfonamide compounds, thus validating the synthesis and encoding of the library.[95,187,194]
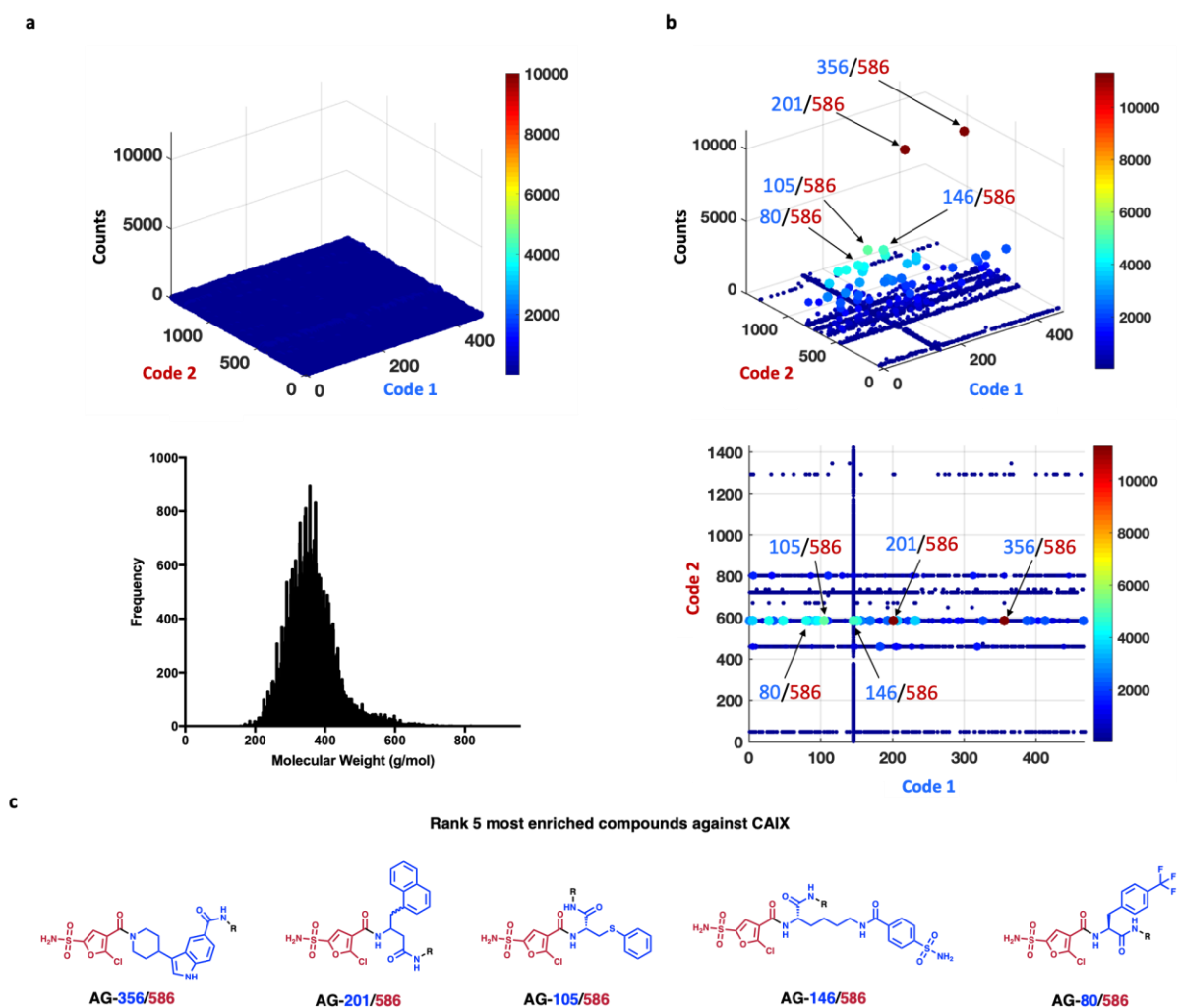
Figure 4.3.1. **a**. (up) High-throughput DNA sequencing results of the unselected AG-DEL. (down) Molecular weight distribution of final compounds in the library. **b**. (up) 3D plot of the sequencing analysis of CAIX selections. (down) 2D plot of the sequencing analysis of CAIX selections. Two different combinations of building blocks showed EFs over 10,000. These combinations represent, as expected for this target, aromatic sulfonamides which serve as a validation of the library screenings. **c**. Rank 5 most enriched compounds in CAIX selection experiments. R: codifying oligonucleotide strand. In blue is indicated the corresponding Code 1; in red is indicated the corresponding Code 2.

Our main goal was to identify new small organic ligands against IL2 that could potentially serve as a starting point for the development of "not-alpha" IL2-based therapeutics.[309,310] Selections were performed with L19-IL2 (an IL2-based fusion protein, which is currently investigated in Phase III clinical trials) rather than recombinant IL2, as the L19-IL2 is easier to produce, store and formulate than recombinant IL2, which is normally stored in the presence of SDS for clinical use.[377] A biotinylated version of the protein was immobilized on streptavidin-coated magnetic beads. Screenings against empty beads were also performed as a control. All the screening experiments were performed in duplicates, as for the CAIX control. For simplicity, only one fingerprint is shown in **Figure 4.3.2** (for all the fingerprints see chapter 6 "Appendix"). Preferentially enriched amino acids were identified, BB1_156 (3-iodo-*L*-tyrosine) and BB1_173 (*O*-Propargyl-*L*-tyrosine) (**Figure 4.3.2a**). The five most enriched compounds showed enrichment factors (EF) over 200, as calculated using the equation in **Figure 6.4.1** (chapter 6 "Appendix").
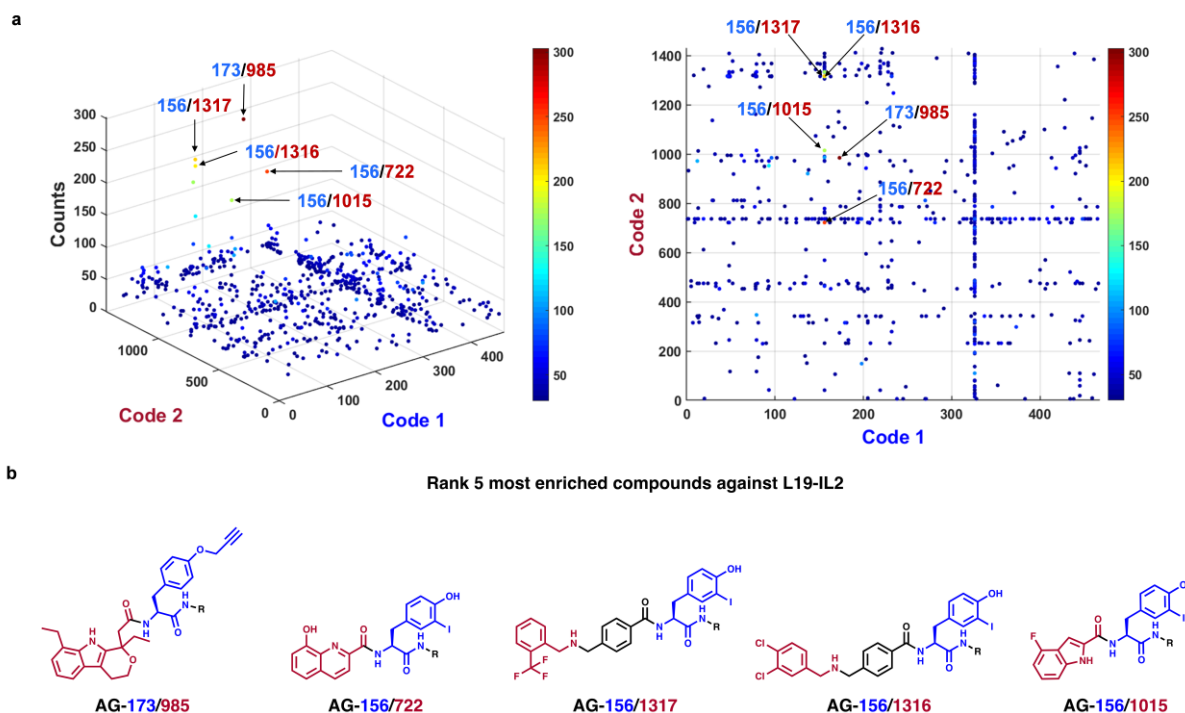
Figure 4.3.2. **a**. 2D and 3D plots of the sequencing analysis of L19-IL2 selections. Preferential enriched combinations bearing the BB1_156 and BB1_173 were selected **b**. Rank 5 most enriched compounds in L19-IL2 selections. R: codifying oligonucleotide strand. In blue is indicated the corresponding Code 1; in red is indicated the corresponding Code 2.

Hit validation

Encouraged by these results, three of the most enriched combinations were resynthesized on a 12-mer amino-modified oligonucleotide following the same procedures as described for the library synthesis. According to the methodology previously reported by our group, this strategy may serve for the validation of the ligands via enzyme-linked immunosorbent assay (ELISA), fluorescence polarization assay (FP), or by surface-plasmon resonance (SPR).[116–118]

We decided to perform fluorescence polarization assays of compounds **AG-173/985**; **AG-156/1317** and **AG-156/1015** against L19-IL2. Despite the combination **AG-156/722** represented the second most enriched molecule, previous experience with the 8-hydroxyquinoline moiety and the presence of this building block highly enriched in the no protein controls, encouraged us to discard it for hit validation. As shown in **Figure 4.3.3**, two of the compounds displayed a sub-micromolar affinity against L19-IL2 (**AG-156/1015** and **AG-156/1317**). Compound **AG-173/985** was synthesized using a racemic mixture of BB2, and we were able to separate both diastereoisomers On-DNA (**AG-173/985_1** and **AG-173/985_2**). Both molecules were tested separately (no identification of stereocenters was done) and while **AG-173/985_1** did not show binding to the protein target, the other diastereoisomer showed a single-digit micromolar affinity (**AG-173/985_2**).

Based on these results, we further proceeded with the validation of the hits Off-DNA. The compounds were synthesized on resin, as fluorescein derivatives, using a PEG$_2$ linker between the ligand and the fluorophore (see detailed procedures in section 6.4.1.). All the molecules could be confirmed as binders of L19-IL2 (**Figure**

4.3.3). Compound **AG-156/1317** showed a ten-fold reduced binding profile in Off-DNA measurements.

Due to the compactness of the ligand **AG-156/1015** and its better binding performance, the compound was selected for medicinal chemistry optimization. An extensive investigation on the linker between the ligand and the fluorophore was performed (data not shown).
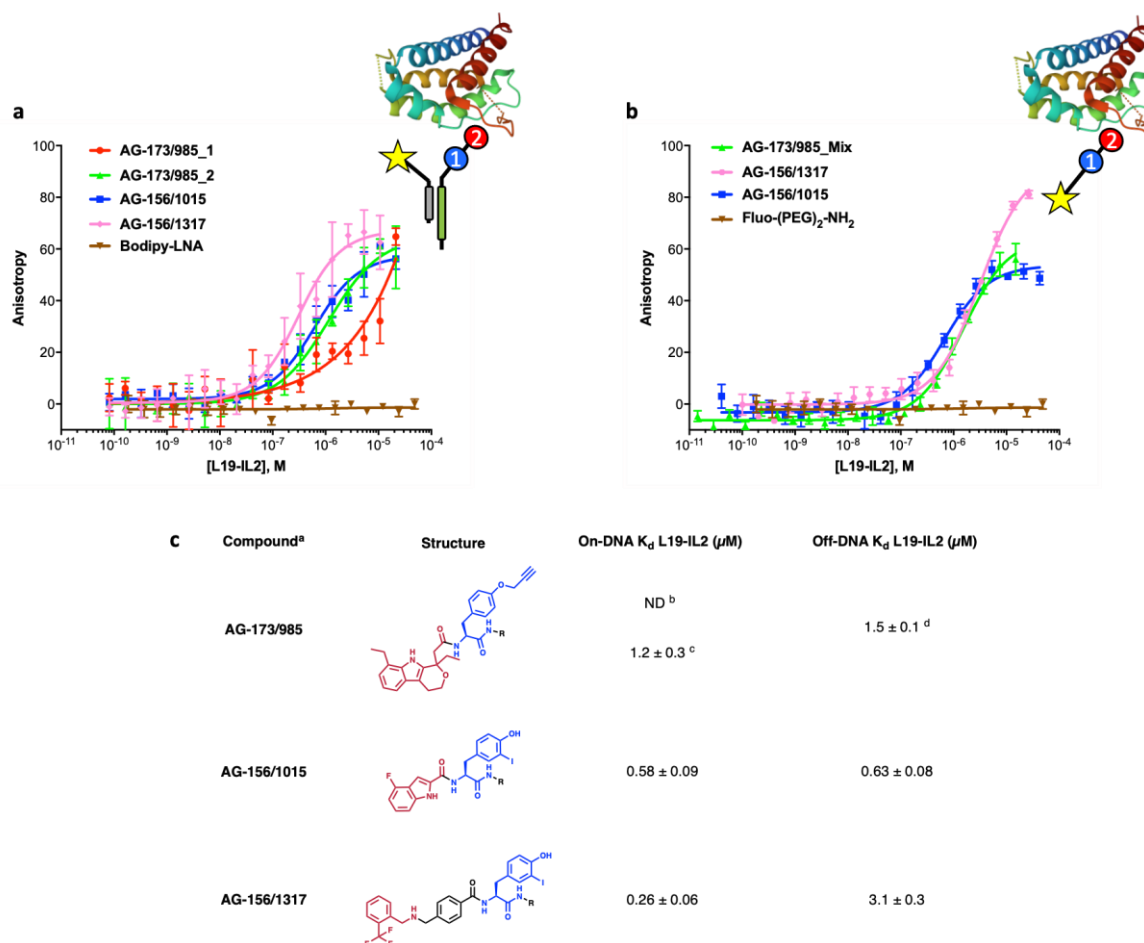
Figure 4.3.3. **a**. On-DNA fluorescence polarization experiments. The cartoon represents the **DNA-Ligand/LNA-Bodipy** duplex setting used. **b**. Off-DNA fluorescence polarization experiments. The cartoon represents the **Ligand-PEG$_2$-Fluorescein** setting used. **c**. Summary table with the On-DNA and Off-DNA dissociation constants (K$_d$) obtained for each hit. Inside the table: [a]Each ligand was synthesized according to the setting used (DNA-Ligand/LNA-Bodipy or Ligand-PEG$_2$-Fluorescein), [b]Isomer 1, [c]Isomer 2, [d]Diastereoisomeric mixture. ND: Non-detectable binding. R: 12-mer oligonucleotide strand or Fluorescein-PEG$_2$-.

Based on the results, we decided to further develop the ligands using a 2-(2-aminoethoxy)-ethylamine (referred to as PEG$_1$) as a linker. To confirm binding of the original ligand with the new linker (Compound **1**) to L19-IL2, we performed different orthogonal validation experiments, together with the L19 antibody alone as a control (FP, and coelution by gel filtration). As described in **Figure 4.3.4**, compound **1** showed a K$_d$ of 0.25 ± 0.03 μM (FP) and coelution with the protein when both species were incubated and eluted on a NAP5 column. Experiments performed with the L19 antibody alone, serving as 0061 negative control of specificity in this setting, confirmed the specific binding of compound **1** to IL2.
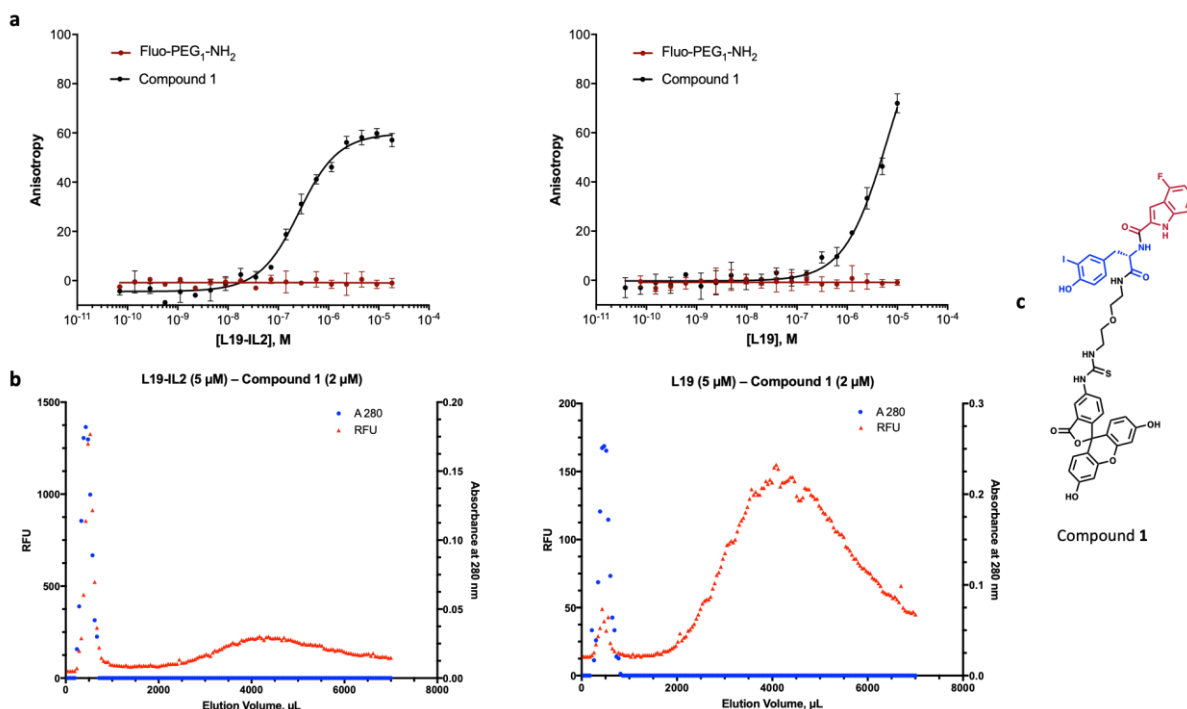
Figure 4.3.4. Orthogonal methodologies for the validation of compound **1** as a binder of IL2. **a**. Fluorescence polarization experiments show binding to the fusion protein L19-IL2 with a dissociation constant of approx. 0.25 μM and weak binding to L19 antibody alone. **b**. Coelution experiments show strong binding between IL2 and compound **1** (fluorescence intensity in the same elution fractions as the protein target), while lower fluorescence intensity can be observed with the L19 antibody. **c**. Compound **1**.
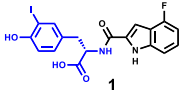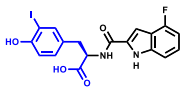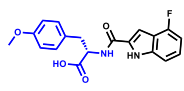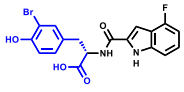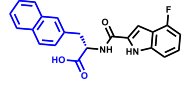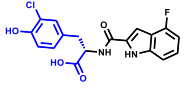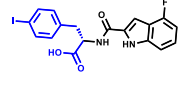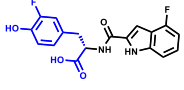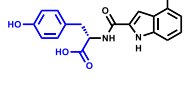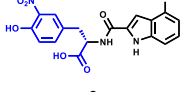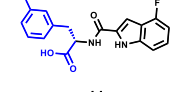
Medicinal Chemistry

With these results in hand, we decided to perform chemical optimization around the ligand. We developed a strategy for the synthesis of different fluorescein-derivatives using solid-phase synthesis. DFPE resin derivatized with an aldehyde was reacted with the PEG$_1$ linker by reductive amination, and subsequently reacted with fluorescein isothiocyanate using the secondary amine formed in the first step (for more details see section 6.4.1). After Fmoc-deprotection of the linker, the synthesis of the molecule was performed using typical conditions for amide bond formation (see detailed procedures in section 6.4.1). **Tables 4.3.1** and **4.3.2** summarize all the synthesized molecules with their affinity against L19-IL2 and Human Serum Albumin (HSA), which constitutes the most abundant protein in plasma.[337–339] On one hand, albumin binding may be desirable to extend the circulatory half-life of IL2 binders, but on the other hand, a too tight interaction in serum could sequester the molecule, preventing distribution to tissue.

We first explored the impact of the chirality on the binding affinity and the selectivity of compound **1** towards L19-IL2. The enantiomer of compound **1** (i.e., compound **2**) showed comparable dissociation constants. Replacing iodine in meta position of **1** with other halogens (-Br, -Cl, and -F) led to a loss of affinity for IL2 by 1.2-fold to 3.7-fold (compounds **3**–**5**). The bromo derivative showed similar dissociation constant for IL2 with certain improvement on the selectivity towards HSA. A series of bromo compounds may be investigated in a follow-up project in order to avoid the potential problematic properties of iodo compounds. The same trend was observed when an

electron-withdrawing group (-NO$_2$) was incorporated in meta position (compound **6**). Elimination of *m*-iodine (compounds **7**–**10**) reduced the IL2 binding affinity by 2.6-fold to 5.6-fold. Compound **11** showed comparable affinity towards IL2 but a higher affinity towards albumin.

Table 4.3.1. Modifications in building block one and their activities

	K_d L19-IL2 (μM)[b]	K_d HSA (μM)[b]
1	0.25 ± 0.03	0.29 ± 0.02

Compound[a]	K_d L19-IL2 (μM)[b]	K_d HSA (μM)[b]	Compound[a]	K_d L19-IL2 (μM)[b]	K_d HSA (μM)[b]
2	0.21 ± 0.02	0.22 ± 0.02	**7**	1.3 ± 0.1	0.43 ± 0.05
3	0.30 ± 0.03	0.78 ± 0.04	**8**	0.75 ± 0.13	0.03 ± 0.01
4	0.59 ± 0.04	0.58 ± 0.07	**9**	0.64 ± 0.13	0.07 ± 0.01
5	0.92 ± 0.07	1.7 ± 0.1	**10**	1.4 ± 0.1	1.5 ± 0.1
6	0.72 ± 0.19	0.31 ± 0.02	**11**	0.25 ± 0.04	0.02 ± 0.01

[a]Compounds were synthesized as Fluo-PEG$_1$-NH derivatives directly on solid-phase. [b]All the dissociation constants were measured by fluorescence polarization and determined by the average values of three replicates.
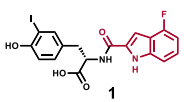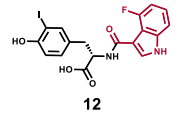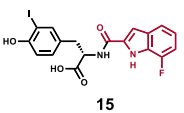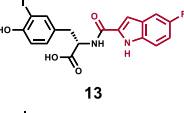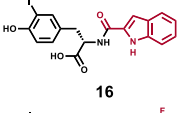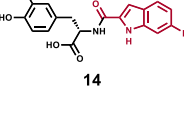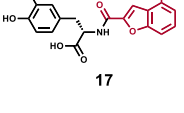
Data obtained using compounds **9** to **11** suggested the importance of iodine in meta position for a higher affinity towards IL2, and the hydroxyl group in para position for an increased selectivity towards albumin. Compound **11** is particularly promising as it does not present phenol groups, chemical moieties which are often not desirable as they are characterized by intrinsic metabolic liabilities (i.e., glucuronidation, oxidation). Initial assessment of the first series of compounds with close analogue designs resulted in a substantial decrease in affinity and comparable selectivity. Therefore, we focused our optimization efforts on the 4-fluoroindole moiety while keeping the first fragment (3-iodo-*L*-tyrosine) constant (**Table 4.3.2**).

Compound **12**, in which a carboxylic acid moiety was placed at the indole 3-position, led to a 2-fold decrease in binding affinity. The study of the fluorine position in the indole moiety (compounds **13**–**15**) resulted in a slight loss of IL2 affinity. By removing the fluorine atom, compound **16** also showed a decrease in the affinity (K_d = 0.42 μM) without any improvement of selectivity. Finally, the benzofuran analogue (compound **17**) demonstrated a significant decrease in the dissociation constant towards IL2 (K_d

= 2.2 μM), thus showing the necessity to have a hydrogen-bond donor to increase affinity.
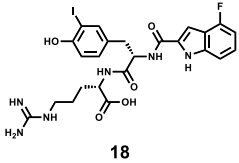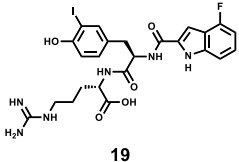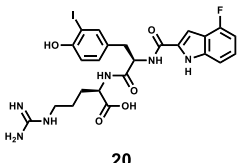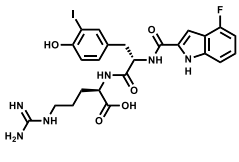
Table 4.3.2. Modifications in building block two and their activities.

	K_d L19-IL2 (μM)[b]	K_d HSA (μM)[b]
1	0.25 ± 0.03	0.29 ± 0.02

Compound[a]	K_d L19-IL2 (μM)[b]	K_d HSA (μM)[b]	Compound[a]	K_d L19-IL2 (μM)[b]	K_d HSA (μM)[b]
12	0.51 ± 0.05	0.82 ± 0.03	**15**	0.39 ± 0.03	0.21 ± 0.02
13	0.33 ± 0.03	0.27 ± 0.02	**16**	0.42 ± 0.04	0.39 ± 0.02
14	0.28 ± 0.03	0.17 ± 0.02	**17**	2.2 ± 0.2	1.0 ± 0.1

[a]Compounds were synthesized as Fluo-PEG$_1$-NH derivatives directly on solid-phase. [b]All the dissociation constants were measured by fluorescence polarization and determined by the average values of three replicates.

The structure-activity relationship (SAR) study presented in this paper brought us to the conclusion that the affinity of the ligands could not be improved with straightforward substitutions. With the aim of improving selectivity, we decided to decrease the lipophilicity of compound **1**, which gave the best binding affinity for IL2 with an initial K_d of 0.25 μM. It is well known that HSA has poor affinity towards positively charged molecules at physiological pH, therefore we suspected that a positively charged group may give us the desired selectivity.[337,338] We synthesized compound **18** (**Table 4.3.3**) bearing an additional arginine moiety. FP results confirmed our hypothesis showing a preferential binding towards IL2, with no significant change in the dissociation constant, while the affinity for HSA decreased by almost 10-fold. In addition, we tested the binding properties of this molecule towards Alpha-1-acid glycoprotein (AGP), since it represents the second most abundant protein in blood.[339] Interestingly, compound **18** also demonstrated a weak dissociation constant with AGP (3.0 μM). These results encouraged us to study the influence of the two chiral center of molecule **18**, with an *S,S* configuration. Therefore, we proceeded with the synthesis of compounds (*S,R*)-**19**, (*R,R*)-**20**, and (*R,S*)-**21**. **Table 4.3.3** summarizes binding affinities of the four ligands (**18**–**21**) against IL2, HSA, and AGP. In contrast to what we observed previously with **1** and **2**, the chiral centers configuration of **18** did influence both the selectivity and the affinity towards IL2. Compound **18** exhibited a higher affinity towards IL2, compared to HSA and AGP (K_d values of 0.34, 2.0, and 3.4 μM respectively). The ionizable character of this molecule could become a problem if cell penetration is desired. Nevertheless, the foreseeable application for the compound would be to bind IL2 and modulate its biological activity outside of cells.

Table 4.3.3. Selectivity study of the different diastereoisomers

Compound[a]	Stereochemistry	K_d L19-IL2 (μM)[b]	K_d HSA (μM)[b]	K_d AGP (μM)[b]
18	S, S	0.34 ± 0.03	2.0 ± 0.1	3.4 ± 0.2
19	S, R	1.2 ± 0.1	3.3 ± 0.2	> 10
20	R, R	0.71 ± 0.05	7.2 ± 0.4	4.0 ± 0.6
21	R, S	0.87 ± 0.08	9.6 ± 0.7	3.0 ± 0.2

[a]Compounds were synthesized as Fluo-PEG$_1$-NH derivatives directly on solid-phase. [b]All the dissociation constants were measured by fluorescence polarization and determined by the average values of three replicates.

To finish our selectivity study, we used compound **18** in a series of FP measurements with different proteins. To confirm that compound **18** was superior to previously described IL2 binders in the same experimental setting, we resynthesized **Ro26-4550** as fluorescein conjugate. **Figure 4.3.5** shows a comparison of the dissociation constants of compounds **1**, **18**, and **Ro26-4550** against a panel of 10 protein controls. **Ro26-4550** showed a K_d = 1.5 μM against IL2, 4.0 μM against HAS, and 4.9 μM against AGP.

In order to discriminate the possible contribution of the L19 antibody to the binding, the affinity of these compounds was also investigated against the L19 antibody alone as a control. Compound **1** showed a 30-fold selectivity towards L19-IL2, while compounds **18**, and **Ro26-4550** did not show apparent binding to the antibody alone. Compound **18** also did not bind to non-related cytokines such as Tumor Necrosis Factor (TNF) and IL15. Gel-filtration experiments with L19 and L19-IL2 showed comparable results in terms of complex stability. Nevertheless, some stickiness can be observed with compounds **1** and **18** towards the matrix of the column in the experimental setting used (**Figure 6.4.49**).
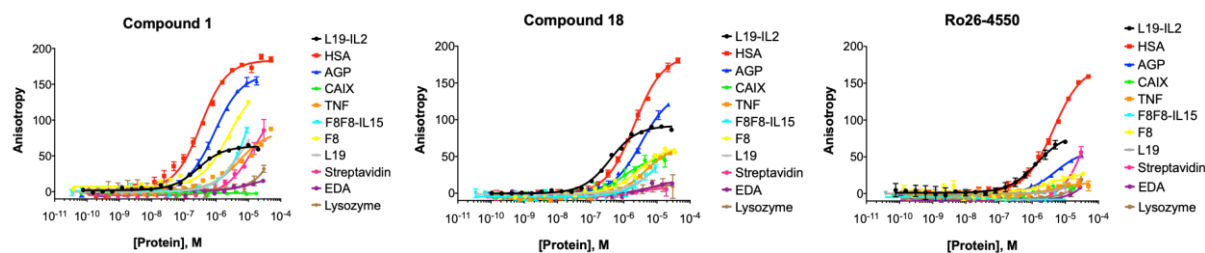
Figure 4.3.5. Selectivity comparison between compounds **1**, **18** and **Ro26-4550**.

Moreover, confirmation of compound **18** binding to the epitope on IL2 involved in CD25 recognition was performed by competition studies via ELISA in the presence of NARA1, an anti-IL2 Fab antibody fragment whose binding properties had previously been characterized by X-Ray crystallography.[378] The binding of NARA1 to IL2 was abrogated in the presence of different concentrations of compound **18**, giving and IC_{50} = 3.4 μM (**Figure 6.4.50**).

4.3.4 Conclusions

As previously discussed in chapter 4.1.1, we have synthesized, a new compact DNA-encoded library composed of 669,240 small molecules, which could be screened in different formats (*de novo* ssDNA or dsDNA, and affinity maturation ESAC type).[225] This library has been screened against multiple proteins often yielding hits with at least single-digit micromolar potency. This confirms that the library design, originally reported by Leimbacher *et al*. offers good opportunities for finding small organic ligands towards challenging therapeutic targets.

From the initial screening of our AG-DEL, we were able to identify compound **1**, whose activity towards IL2 has been confirmed by different orthogonal methodologies, giving a good dissociation constant of 0.25 μM, but which also binds to albumin with comparable affinity. After chemical optimization around the ligand, insertion of arginine moiety led to compound **18** which retains its affinity towards IL2 and improves selectivity towards HSA and AGP by almost 10-fold. On the other hand, competition experiments using the anti-IL2 Fab antibody fragment NARA1 have confirmed that compound **18** binds to the epitope of IL2 involved in CD25 recognition.

The isolation of small organic ligands to cytokines is a formidable challenge, as these proteins of high pharmaceutical value have only been drugged by antibody-based products. There is hope that with additional medicinal chemistry one may reach potency comparable to antibodies. Until now, only antibody fragments and site-specific PEGylation have been considered for the industrial development of not-alpha Interleukin-2 therapeutics. It would be conceivable that compound **18**, or an affinity matured derivative, could be used in complex with IL2, thus masking the biding site for CD25. Interestingly, if the small molecule was to be used to mask the IL2 moiety in a tumor-targeting antibody-IL2 fusion protein (such as L19-IL2), it should be possible to generate a novel class of biopharmaceuticals-small molecule complexes, that do not bind to T_{regs}, selectively localize at the tumor site and progressively lose the small molecule inhibitor at the site of disease, thus regaining full activity. The development of cytokine-based pharmaceuticals with "activity on demand" has been postulated as one of the new horizons of cytokine research for cancer therapy.[379,380]

5. Conclusions and Outlook

During the last two decades, DNA-Encoded Library technology has been established as a powerful tool for the identification of new small-molecule ligands towards pharmaceutically and biologically relevant targets. The power of this technology relies on the possibility to individually and uniquely encode small molecules with oligonucleotide fragments, thus allowing the interrogation of libraries of unprecedented size in an efficient manner and subsequent hit identification by high-throughput sequencing. Notwithstanding the progress in the field has exponentially increased during the last few years, the technology still faces several challenges.

In this work, advances in the field have been achieved, and the utility of DEL technology has been proven with the efficient identification of new small organic ligands towards particularly challenging targets.

The first part of this thesis was focused on the design and synthesis of new DELs using different formats. The utility and modularity of DELs in single-stranded format have already been proven with several reports from our group and others. This format allows for the implementation of different screening methodologies, such as photo-crosslinking mediated affinity selections; and the possibility to create *de novo* and affinity maturation libraries using the encoded self-assembling chemical library technology. A new compact single-pharmacophore DEL, based on the combinatorial assembly of two sets of building blocks, was synthesized. The new AG-DEL, composed of 669,240 members, was screened against multiple therapeutically relevant targets. Different small molecules were identified using conventional solid phase affinity-mediated selection procedures, which may deserve additional investigation to characterize their properties. The new AG-DEL was combined with a new complementary library composed of 256 different building blocks in an ESAC fashion. The combinatorial self-assembly of both sub-libraries delivered a new ESAC 2+1 library composed of more than 171 million encoded small molecules. The ESAC 2+1 library was also screened against two different targets. Carbonic anhydrase IX (CAIX), a very well-characterized tumor-associated antigen, has served for the validation of these libraries. Aromatic sulfonamides are a known class of CAIX ligands which display dissociation constants in the micro to the nanomolar range, and some of them were included during library construction. On the other hand, both libraries were screened against L19-IL2, a clinical-stage antibody fusion protein for the treatment of different tumors, yielding preferentially enriched combinations which were subsequently studied and described in the third part of this thesis. In the last part of this chapter, a new ESAC format, called ESAC Plus, based on the covalent linkage between both ESAC sub-libraries, was designed and patented. A library of 41,020 members was synthesized and, like the previous ones, it was characterized by high-throughput DNA sequencing, revealing a homogeneous distribution of every library member. Moreover, positive control selections against CAIX were performed, revealing a clear difference in enrichment factors and combinations between the non-cyclized ESAC and the final ESAC Plus library. These results may suggest a critical contribution of the three-dimensional structure in protein recognition, thus highlighting the novelty and importance of the new ESAC Plus design for the efficient identification of conformationally restrained ligands. This new ESAC Plus library may serve as an efficient tool for the identification of ligands towards classical "undruggable" or surface-extended targets.

Motivated by the recently patented ESAC Plus library format, the possibility of reutilizing *in-house* building blocks to enhance the diversity of the library was hypothesized. One of the remaining challenges of DEL technology is the efficient implementation of classical and novel organic chemistry transformations to improve the diversity and cover a broader chemical space. The restrictions imposed by the nature of the oligonucleotide tags have limited the implementation of important reactions which make use of extremely acidic or oxidizing conditions. Moreover, the use of metal catalysts has already been proven (e.g., Suzuki, Sonogashira, Buchwald reactions) for the synthesis of DELs. Nevertheless, certain degradation of the DNA codes, by complexation with metals, may affect the overall performance of DEL synthesis and screening. To this extent, a classical transformation, which was not yet described in the context of DELs was the diazo-transfer reaction. In the second experimental part of this work, this transformation was deeply investigated and implemented. The reaction proceeded at relatively low temperatures, in slightly basic conditions without the use of metal catalysts. The optimized reaction conditions were applied for the efficient transformation of 20 different primary aliphatic amines. To assess the suitability of this protocol for the synthesis of DELs, a complete synthetic sequence including the ligation of the nascent oligonucleotide to a new encoding fragment was performed, yielding the full construct without apparent DNA degradation. The implementation of this new reaction has allowed our research group to synthesize a second macrocyclic ESAC Plus library, composed of more than 10 million members.

In parallel to the construction of ESAC 2+1 and ESAC Plus libraries and the implementation of the diazo-transfer reaction, several affinity selection experiments were performed using the newly synthesized AG-DEL. The most promising fingerprints were those obtained for L19-IL2. Interleukin-2 is a proinflammatory cytokine that has attracted much attention during the last decades for the treatment of certain types of tumors. Indeed, IL2 has already received marketing authorization for the treatment of metastatic melanoma and renal cell carcinoma. Nevertheless, its therapeutic use has been limited due to strong side effects mainly related to the high doses necessary to achieve a pharmacological effect. The therapeutic potential of IL2 is limited by the preferential expression of its alpha subunit receptor (CD25) on immunosuppressive T_{regs}. Therefore, it would be desirable to develop therapeutic approaches which may limit the interaction with CD25 and enhance the antitumor response. After a careful analysis of the selection results using AG-DEL, several hits were resynthesized and validated. On-DNA hit validation is a rapid and efficient manner to confirm hits from affinity selection experiments using the same synthetic protocols used for the library construction. The annealing of the On-DNA resynthesized hits with an LNA-Bodipy conjugate allowed the measurement of dissociation constants via fluorescence polarization techniques. Two of the validated compounds (**AG-156/1015** and **AG-156/1317**) displayed sub-micromolar affinities, and one of them (**AG-173/985**) had a single-digit micromolar affinity in a stereochemical selective manner. After On-DNA hit validation, the ligands were resynthesized using classical solid-phase organic synthesis and further confirmed. One of the ligands, **AG-156/1015**, was selected for further explorations. Medicinal chemistry activities served to characterize the important features of this molecule towards binding IL2. These activities rendered a selective ligand, compound **18**, which retains its affinity towards IL2 and improves selectivity over the most abundant proteins in plasma (human serum albumin, HSA; and alpha-1-acid glycoprotein, AGP) and non-related cytokines such as IL15 and TNF. To confirm the potential of this newly

synthesized molecule, the compound was tested in ELISA competition experiments using the anti-IL2 antibody NARA1. NARA1 has been characterized as a CD25-mimobody, therefore it mimics all the important interactions between IL2 and CD25 thus avoiding the binding. Competition experiments showed that compound **18** can inhibit the binding of NARA1 to IL2 with an IC_{50} of 3.4 μM, thus confirming the binding of the small molecule to the CD25 recognition site of IL2. Such a ligand, or an affinity matured derivative, may serve as a potential starting point for the development of new potent and selective inhibitors of the IL2/IL2Rα interaction. In principle, using one of these ligands, it may be possible to design a novel class of biopharmaceutical-small molecule complexes that may bring activity on demand, masking the CD25 binding epitope of IL2 and regaining activity at the tumor site.

In summary, the discovery of new small-molecule ligands for pharmaceutical and therapeutic applications remains one of the major challenges in drug discovery programs. The implementation of efficient screening platforms, such as DNA-encoded libraries, has promised to accelerate drug discovery campaigns and deliver ligands towards challenging targets. Nevertheless, the technology is still improving, and many avenues are still open for DEL to become the best technology for ligand identification. During this work, I have faced some of these challenges aiming at improving DEL technology and finding new molecular entities which may be useful for the treatment of important diseases.

6. Appendix

6.1 General remarks

Starting materials, solvents and reagents: Unless otherwise noted, all the solvents were used as supplied by VWR (Pennsylvania, United States). The standard reagents and building blocks were acquired from different suppliers including Enamine (Princeton, United States), ABCR (Karlsruhe, Germany), Sigma-Aldrich (Saint-Louis, United States), Chem-Impex (Illinois, United States) and Fluorochem Ltd (Hadfield, United Kingdom) as enantiopure reagents unless otherwise noted. The oligonucleotides were provided by LGC Biosearch Technologies (Risskov, Denmark) and Eurofins Genomics (Ebersberg, Germany) and the sequences are described in their corresponding section. Ligation buffer, T4 DNA-ligase, DNA polymerase I large (Klenow) fragment, and high-fidelity Phusion DNA polymerase were purchased from New England Biolabs (Massachusetts, United States). PCR purification and gel extraction kits were purchased from Qiagen (Hilden, Germany).

Chromatography, spectrometry and instruments: Mass spectrometry (LC-ESI-MS) spectra were recorded on an Agilent 6100 Series Single Quadrupole MS system combined with an Agilent 1260 Series LC. Specifically, for DNA samples, an ACQUITY UPLC Oligonucleotide BEH C18 column (130 Å, 1.7 μm, 2.1 x 50 mm) was used and eluted with a mixture of eluent A (15 mM TEA, 400 mM HFIP in H_2O) and eluent B (MeOH); gradient from 5% B to 95% B in 12 min or 5% B to 65% B in 18 min. For small molecule samples, an InfinityLab Poroshell 120 EC-C18 column (120 Å, 2.7 μm, 4.6 x 50 mm, Agilent) was used and compounds were eluted using a gradient of eluent A (H_2O, 0.1% Formic acid) and eluent B (MeCN, 0.1% Formic acid) gradient from 0 to 100% B. Yields were calculated by examination of the UV (260 nm) of LCMS chromatograms. High Resolution Mass Spectrometry analysis (HRMS) was done as direct infusion with a Q-Exactive Orbitrap coupled to an Ion Max HESI source (Thermo Fisher), with the following parameters: capillary voltage 3.5 kV; capillary temperature 320 °C; Sheath gas 5 units: S-lens RF level of 55. The detector was working in positive ion mode with a scan range of 400-1700 m/z, and a resolution of 70000 FWHM (at 400 m/z). Reverse-phase high-performance liquid chromatography (RP-HPLC) purification of the DNA-conjugated Fmoc-amino acids was performed on an Agilent 1200 Series with an XTerra Shield RP18 OBD Preparative column (125 Å, 5 μm, 10 x 150 mm) using a gradient of eluent A (100 mM TEAA in H_2O) and eluent B (100 mM TEAA in 80% MeCN); gradient from 10% B to 90% B in 22 min. Ion-exchange high-performance liquid chromatography (IE-HPLC) purification of the final Pool 2 and the Elib 6 pool was performed on an Agilent 1200 Series with an DNAPac PA200 BioLC analytical column (125 Å, 8 μm, 4 x 250 mm) using a gradient of eluent A (25 mM Tris-HCl, 6M Urea, pH = 8 in H_2O) and eluent B (25 mM Tris-HCl, 6M Urea, 400 mM $NaClO_4$, pH = 8 in H_2O); gradient from 0% B to 35% B in 0.5 min, then to 62% B in 9.5 min and to 100% B in 0.5 min. Semi-preparative high-performance liquid chromatography of small molecules was performed on a Synergi Polar-RP column (80 Å, 4 μm, 10 x 150 mm) using a gradient of eluent A (H_2O, 0.1% TFA) and eluent B (MeCN, 0.1% TFA) gradient from 30 to 100% B. The fractions containing the products were combined and lyophilized overnight. The concentration of DNA samples was determined by UV absorbance at 260 nm using a Nanodrop 2000 instrument (Thermo Fisher). The concentration of fluorescein-labelled small molecule samples was determined by UV absorbance at 495 nm using a Nanodrop 2000 instrument (Thermo

Fisher). Preparative medium pressure liquid chromatography (MPLC) was performed on CombiFlash NextGen 300+. (Teledyne ISCO). Affinity selections were performed robotically on a KingFisher Magnetic Particle Processor (Thermo Fisher). The selection fingerprints were analyzed using *in-house* implemented software, based on Matlab (Mathworks). Fluorescence polarization measurements, fluorescence intensity measurements and ELISA plate analyses were performed using Tecan Spark (Tecan).

6.2 Design, synthesis and screening of different DELs

6.2.1 Single-pharmacophore AG-DEL

6.2.1.1 Materials and methods

General procedures for On-DNA reactions

Amide bond formation: Method 1: the corresponding Fmoc-amino acid/carboxylic acid (12.5 μL, 200 mM in DMSO, 50 equiv) was diluted with DMSO (32.5 μL, neat) and 4-(4,6-dimethoxy-1,3,5-triazin-2-yl)-4-methyl-morpholinium hydrochloride (DMT-MM HCl) (8.5 μL, 300 mM in H_2O, 50 equiv) was added. The mixture was incubated for 15 min at 30 °C. The activated Fmoc-amino acid/carboxylic acid solution was added to the amino-modified oligonucleotide (71 μL, 0.7 mM in 50 mM MOPS buffer, pH 8.0, 500 mM NaCl) and the reaction was let to proceed overnight at 37 °C.

Method 2: the corresponding Fmoc-amino acid/carboxylic acid (12.5 μL, 200 mM in DMSO, 50 equiv) was diluted with DMSO (225 μL, neat) and then 1-ethyl-3-(3-diethylaminopropyl)carbodiimide (EDC) (24 μL, 100mM in DMSO, 48 eq) and N-hydroxysulfosuccinimide sodium salt (s-NHS NaCl) (20 μL, 333 mM in DMSO/H_2O 2:1, 133 equiv) were added. The mixture was incubated for 30 min at 30 °C. The activated Fmoc-amino acid/carboxylic acid solution was added to the amino-modified oligonucleotide (75 μL, 0.67 mM in 50 mM MOPS buffer, pH 8.0, 500 mM NaCl) and the reaction was let to proceed overnight at 30 °C.

Method 3: the corresponding Fmoc-amino acid/carboxylic acid (6.5 μL, 200 mM in DMSO, 26 equiv) was diluted with DMSO (17.5 μL, neat) and incubated with a mixture of 1-ethyl-3-(3-diethylaminopropyl)carbodiimide (EDC), 1-hydroxy-7-azabenzotriazole (HOAt) and N-methylmorpholine (NMM) (6 μL, 100/20/100 mM in DMSO) for 15 min at 37 °C. The activated Fmoc-amino acid/carboxylic acid solution was added to the amino-modified oligonucleotide (20 μL, 2.5 mM in 50 mM MOPS buffer, pH 8.0, 500 mM NaCl) and the reaction was let to proceed for 1 h at room temperature. A second activation and addition was performed and the reaction was let to proceed during 1 h more at room temperature.

Fmoc deprotection: To the Pool 1 (2 mL, 0.2 mM in H_2O, 8 different fractions) was added triethylamine (100 μL, neat, 1800 equiv) The reaction was let to proceed overnight at 37 °C.

(thio)urea formation: The corresponding iso(thio)cyanate (10.5 μL, 100 mM in MeCN, 750 equiv) was added to a fraction of the deprotected and codified Pool 1 (31 μL, 0.05 in 400 mM borate buffer, pH 9.4, 1 equiv) and the reaction was let to proceed overnight at 40 °C.

Coupling of 4-formylbenzoic acid: 4-formylbenzoic acid (12.5 μL, 200 mM in DMSO, 1785 equiv) was diluted with DMSO (32.5 μL, neat) and DMT-MM (8.5 μL, 300 mM in H$_2$O, 1820 equiv) was added. The mixture was incubated for 15 min at 30 °C. The activated carboxylic acid solution was add-ed to a fraction of the deprotected and codified Pool 1 (30 μL, 0.05 mM in 50 mM MOPS buffer, pH 8.0, 500 mM NaCl) and the reaction was let to proceed overnight at 37 °C.

Reductive amination: The corresponding amine (25 μL, 100 mM in DMSO, 1785 equiv) was added to 4-formylbenzoic acid-modified fraction of codified Pool 1 (11 μL, 0.127 mM in 1M phosphate buffer, pH 5.5) and the mixture was incubated for 4 h at 40 °C. Then, sodium cyanoborohydride (NaCNBH$_3$) (3.5 μL, 400 mM in MeCN, 1000 equiv) was added to the formed imine and the reaction was let to proceed overnight at 40 °C.

Coupling of succinic anhydride: Succinic anhydride (15 μL, 200 mM in DMSO) followed by 4-dimethylaminopyridine (DMAP) (1.25 μL, 200 mM in DMSO) were added to a fraction of the deprotected and codified Pool 1 (15 μL, 0.1 mM in 300 mM TEA HCl, pH 10, 1 equiv) and the reaction was let to proceed for 3 h at 60 °C.

Reverse amide bond formation: The corresponding amine (15 μL, 100 mM in DMSO, 1000 equiv), DMT-MM (12 μL, 200 mM in H$_2$O, 1700 equiv) and DMSO (15 μL, neat) were added to a succinic acid-modified fraction of Pool 1 (35 μL, 0.05 mM in 100 mM MOPS buffer, pH 8.0, 500 mM NaCl) and the mixture was incubated overnight at 37 °C.

Sulfonylation: The corresponding sulfonyl chloride (10.5 μL, 100 mM in MeCN, 750 equiv) was added to a fraction of the deprotected codified Pool 1 (31 μL, 0.05 mM in 400 mM borate buffer, pH 9.4, 1 equiv) and the reaction was let to proceed overnight at 40 °C.

Optimized protocol for Splint-mediated ligation in AG-DEL

A fraction of deprotected Pool 1 (1.4 μL, 1 mM in H$_2$O, 1 equiv), the corresponding 5'-phosphorylated oligonucleotide (Code 2) (2.1 μL, 1 mM in H$_2$O, 1.5 equiv) and the DNA adaptor (1.4 μL, 2 mM in H$_2$O, 2 eq) were mixed and incubated for 1 h at room temperature. In a separate vial, a master mix of the corresponding amount of 10x T4 DNA-ligase buffer (1.75 μL, New England Biolabs), H$_2$O (0.15 μL) and T4 DNA-ligase (0.2 μL, 400 U/μL, New England Biolabs) was prepared and added to the oligo mixture. The ligation was let to proceed for 16 h at 16 °C without shaking, before inactivating the ligase for 10 min at 65 °C. The formation of the desired product was confirmed by gel electrophoresis analysis. The mixture was dried under vacuum and the DNA pellets were directly used for the coupling of the second building block (BB2).

General procedure for Klenow polymerization and double strand formation

The single-stranded single-pharmacophore library (31.7 μL, 3.2 μM) and Code 3 (2 μL, 50 μM) were dissolved in H$_2$O (50.3 μL) and NEB Buffer 10x (10 μL). A pre-hybridization step was performed for 2 min at 95 °C and the mixture was allowed to cool down at room temperature. The DNA Polymerase I, Large (Klenow) Fragment (2 μL, New England Biolabs) and deoxynucleotides solution mix (4 μL, 5 mM) were

added and incubated for 1 h at room temperature. The reaction was checked by gel electrophoresis analysis on Novex™ TBE-Urea Gels 15% (Invitrogen). The library was purified by QIAquick PCR Purification Kit (Qiagen), redissolved in 100 µL, and the concentration evaluated by absorbance at 260 nm using a Nanodrop 2000 instrument (Thermo Fisher).

General procedure for affinity selections

Affinity selections were performed in double stranded (ds) format using 10^6 copies of individual library members for each selection. Each selection was performed in duplicate or triplicate depending on the availability of the protein. The library was diluted to 100 nM in protein-specific buffer, containing also 0.05% tween-20 and 20 µg/mL herring sperm DNA (100 µL). Biotinylated proteins were immobilized on Dynabeads MyOne streptavidin (Thermo Fisher), and the remaining streptavidin was blocked by addition of biotin. The selections were performed with the automated system King Fisher (Thermo Fisher) as reported by Decurtins *et al.*[95]

6.2.1.2 Supplementary information

Oligonucleotides and library sequences

Fmoc-amino acids were coupled to their corresponding amino-modified oligonucleotide **Code 1** (468). Phosphorylated oligonucleotides **Code 2** (1430) were ligated to the Pool 1 fractions using a **DNA adaptor**.

Code 1:

`NH₂-C6-5'-GGAGCTTCTGAATTCTGTGTGCTGXXXXXXCGAGTCCCATGGCGC-3'` being XXXXXX the encoding region for each code

Code 2:

`Phospho-5'-CGGATCGACGYYYYYYYGCGTCAGGCAGC-3'` being YYYYYYY the encoding region for each code

DNA adaptor:

`5'-CGTCGATCCGGCGCCATGGGACTCG-3'`

Klenow Fill-in Code 3 for dsDNA screenings:

`5'-GCTCTGCACGGTCGCCGTCTAAGCTGCCTGACGC-3'`

PCR1 Forward primers for ssDNA screenings:

`5'-TACACGACGCTCTTCCGATCT``ACACAC``GGAGCTTCTGAATTCTGTGTG-3'` marked in red the encoding region of each primer

PCR1 Reverse primers for ssDNA screenings:

`5'-CAGACGTGTGCTCTTCCGATC``CGATAT``GCTGCTGCCTGACGC-3'` marked in red the encoding region of each primer

PCR1 Forward primer for dsDNA screenings:

5'-TACACGACGCTCTTCCGATCT<mark>ACACAC</mark>GGAGCTTCTGAATTCTGTGTG-3' marked in blue the encoding region of each primer

PCR1 Reverse primer for dsDNA screenings:

5'-CAGACGTGTGCTCTTCCGATC<mark>CGATAT</mark>GCTCTGCACGGTCGC-3' marked in blue the encoding region of each primer

PCR2 Illumina Forward primer:

5'-AATGATACGGCGACCACCGAGATCTACACTCTTTCCCTACACGACGCTCTTCCGATCT-3'

PCR2 Illumina Reverse primer:

5'-CAAGCAGAAGACGGCATACGAGAT333333GTGACTGGAGTTCAGACGTGTGCTCTTCCGATC-3'

PCR1 product example for ssDNA screenings:

5'–TACACGACGCTCTTCCGATCTACACACGGAGCTTCTGAATTCTGTGTGCTGTATCCACGAGTCCCATGGCGCCGGATCGACGGTCTCACGCGTCAGGCAGCAGCATATCGGATCGGAAGAGCACACGTCTG–3'

3'–ATGTGCTGCGAGAAGGCTAGATGTGTGCCTCGAAGACTTAAGACACACGACATAGGTGCTCAGGGTACCGCGGCCTAGCTGCCAGAGTGCGCAGTCCGTCGTCGTATAGCCTAGCCTTCTCGTGTGCAGAC–5'

PCR2 product example for ssDNA screenings:

5'–AATGATACGGCGACCACCGAGATCTACACTCTTTCCCTACACGACGCTCTTCCGATCTACACACGGAGCTTCTGAATTCTGTGTGCTGTATCCACGAGTCCCATGGCGCCGGATCGACGGTCTCACGCGTCAGGCAGCAGCATATCGGATCGGAAGAGCACACGTCTGAACTCCAGTCACGCCAATATCTCGTATGCCGTCTTCTGCTTG–3'

3'–TTACTATGCCGCTGGTGGCTCTAGATGTGAGAAAGGGATGTGCTGCGAGAAGGCTAGATGTGTGCCTCGAAGACTTAAGACACACGACATAGGTGCTCAGGGTACCGCGGCCTAGCTGCCAGAGTGCGCAGTCCGTCGTCGTATAGCCTAGCCTTCTCGTGTGCAGACTTGAGGTCAGTGCGGTTATAGAGCATACGGCAGAAGACGAAC–5'

PCR1 product example for dsDNA screenings:

5'–TACACGACGCTCTTCCGATCTACACACGGAGCTTCTGAATTCTGTGTGCTGTATCCACGAGTCCCATGGCGCCGGATCGACGGTCTCACGCGTCAGGCAGCTTAGACGGCGACCGTGCAGAGCATATCGGATCGGAAGAGCACACGTCTG–3'

3'–ATGTGCTGCGAGAAGGCTAGATGTGTGCCTCGAAGACTTAAGACACACGACATAGGTGCTCAGGGTACCGCGGCCTAGCTGCCAGAGTGCGCAGTCCGTCGAATCTGCCGCTGGCACGTCTCGTATAGCCTAGCCTTCTCGTGTGCAGAC–5'

PCR2 product example for dsDNA screenings:

5'–AATGATACGGCGACCACCGAGATCTACACTCTTTCCCTACACGACGCTCTTCCGATCTACACACGGAGCTTCTGAATTCTGTGTGCTGTATCCACGAGTCCCATGGCGCCGGATCGACGGTCTCACGCGTCAGGCAGCTTAGACGGCGACCGTGCAGAGCATATCGGATCGGAAGAGCACACGTCTGAACTCCAGTCACTACGTAATCTCGTATGCCGTCTTCTGCTTG–3'

3'–TTACTATGCCGCTGGTGGCTCTAGATGTGAGAAAGGGATGTGCTGCGAGAAGGCTAGATGTGTGCCTCGAAGACTTAAGACACACGACATAGGTGCTCAGGGTACCGCGGCCTAGCTGCCAGAGTGCGCAGTCCGTCGAATCTGCCGCTGGCACGTCTCGTATAGCCTAGCCTTCTCGTGTGCAGACTTGAGGTCAGTGATGCATTAGAGCATACGGCAGAAGACGAAC–5'

5'–Amino-modified-12mer DNA:

NH$_2$–C6–5'–TAGTAGCCATCC–3'

3'–Amino-modified-8mer LNA:

5'–GGCTACTA–3'–C6–NH$_2$

LC-MS analysis of splint mediated ligation between Pool 1 and Code 2
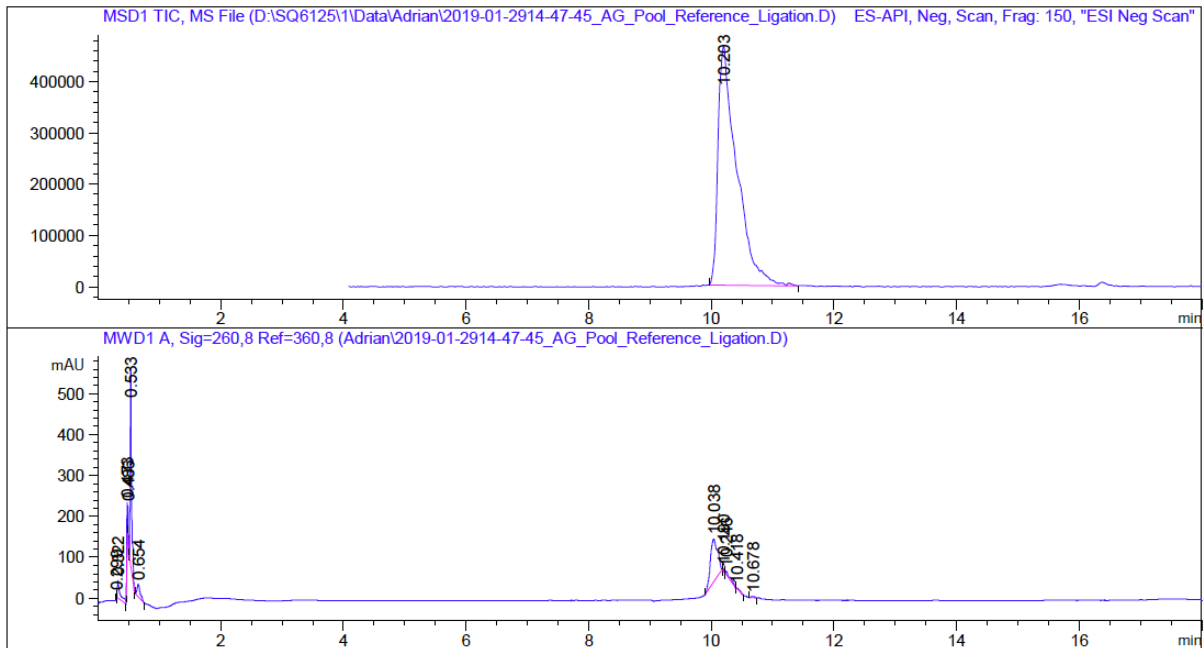
Figure 6.2.1. UV and MS traces of deprotected Pool 1 run on a different method serving as reference for ligation analysis.
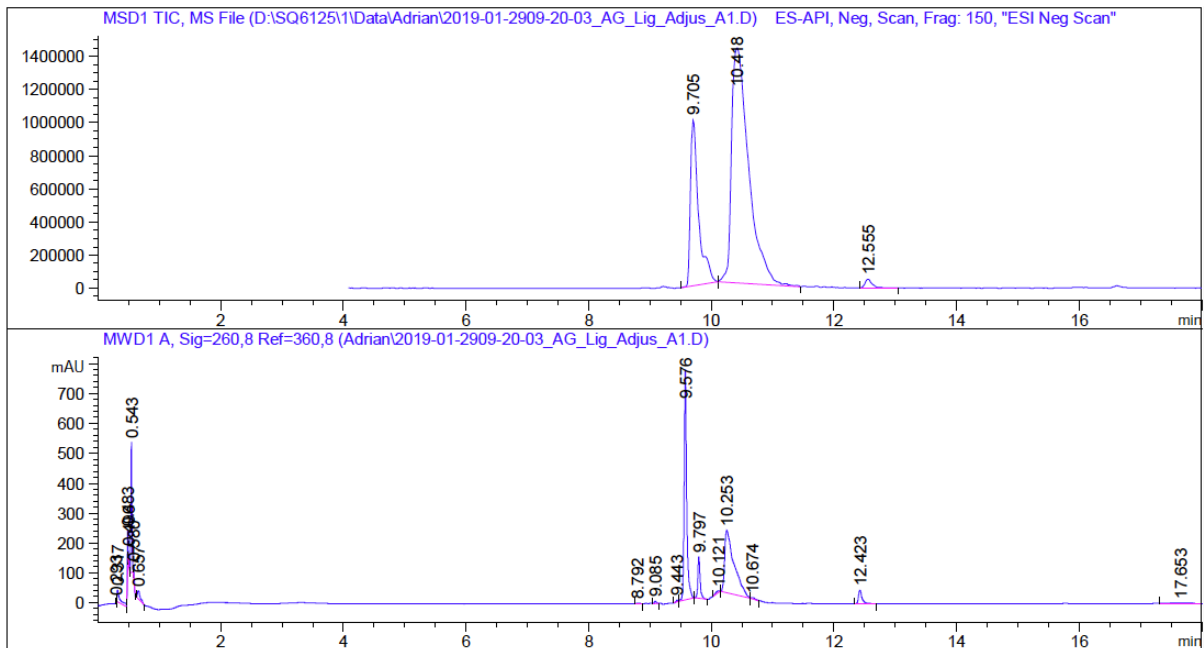
Figure 6.2.2. UV and MS traces of a representative example of splint-mediated ligation of Code 2 to Pool 1.

110
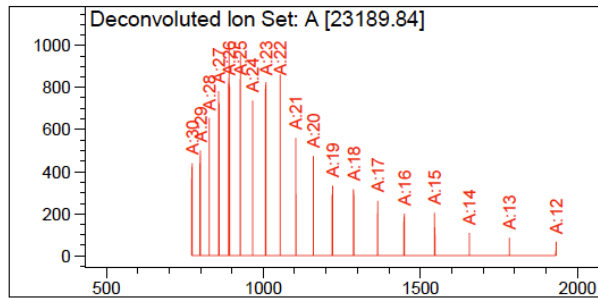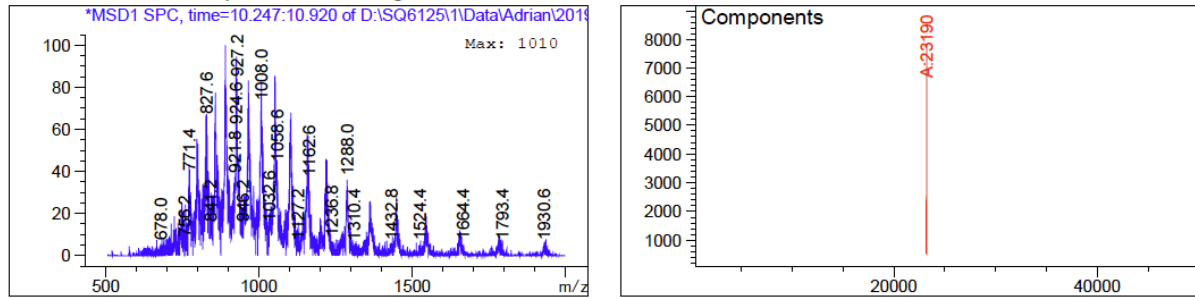
Figure 6.2.3. Deconvoluted MS spectrum of a representative example of splint-mediated ligation of Code 2 to Pool 1.
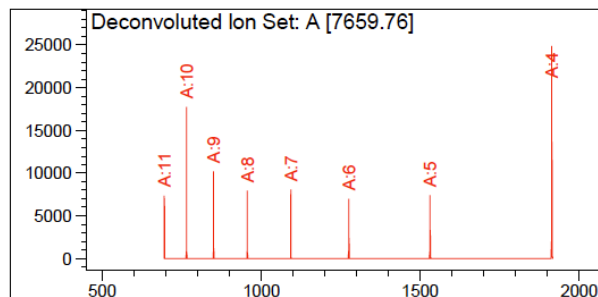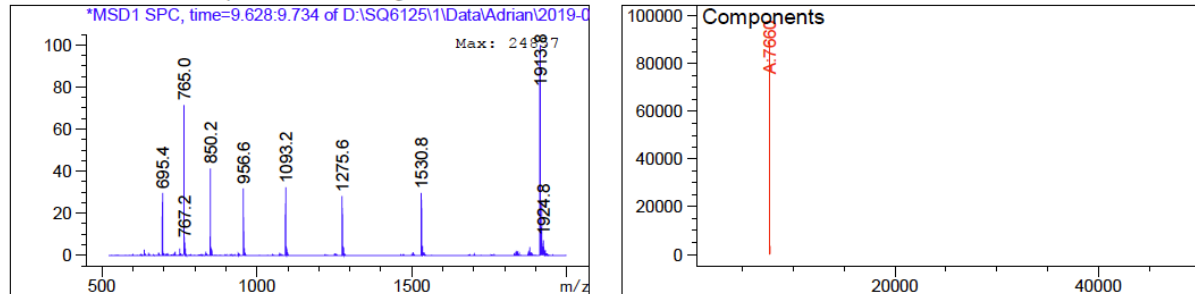
Figure 6.2.4. Deconvoluted MS spectrum of the DNA adaptor fraction.

111
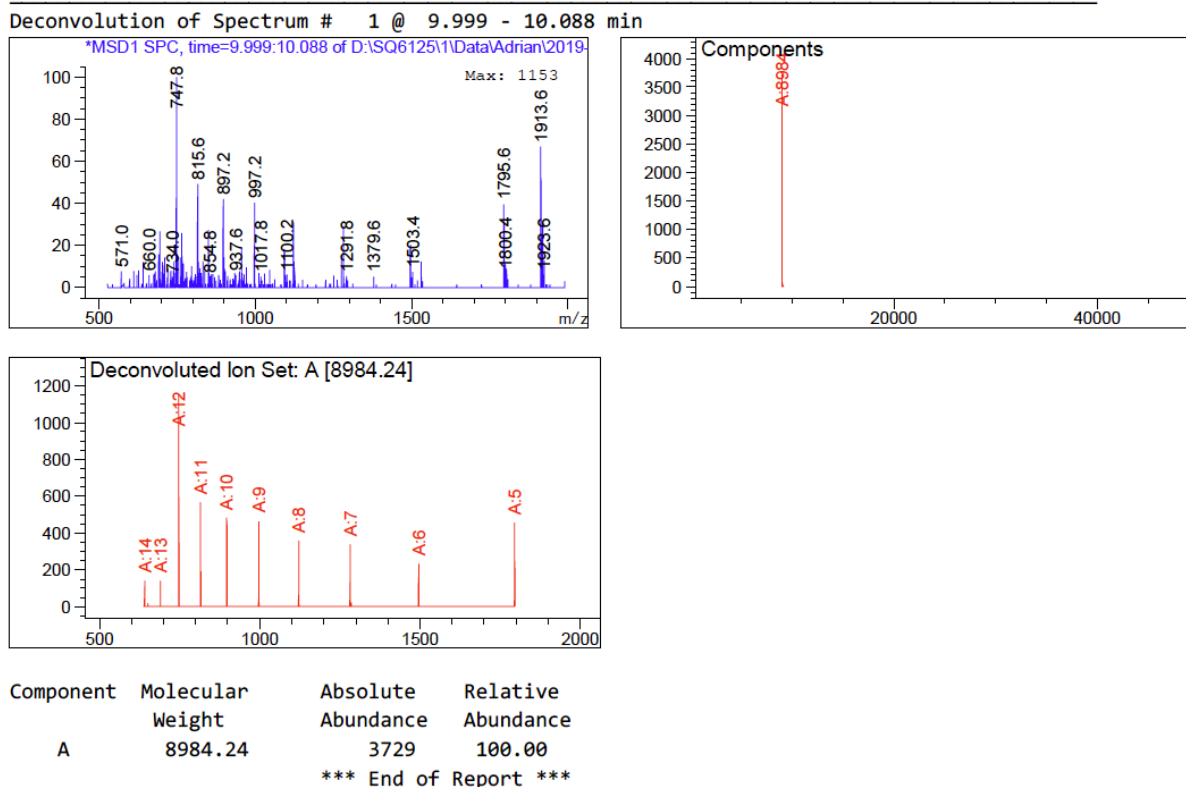
Figure 6.2.5. Deconvoluted MS spectrum of the Code 2 fraction.

Gel electrophoresis analysis of AG-DEL in dsDNA format after Klenow
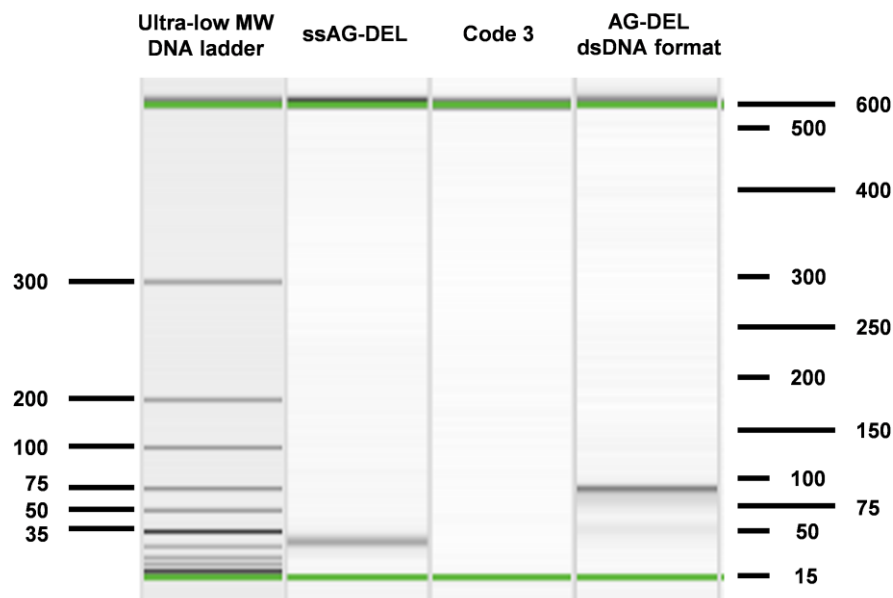
Figure 6.2.6. Gel electrophoresis analysis of AG-DEL after Klenow Polymerization with Code 3. The analysis was performed using a QIAxcel Advanced instrument. Ultra-low molecular weight (MW) DNA ladder was run as a sample to compare the bands with those obtained using pre-casted 15% TBE-Urea gels. As expected, final AG-DEL in dsDNA format shows a band below 100 bp (final library size 96 bp).

Affinity selection experiments replicate fingerprints

No Protein controls:
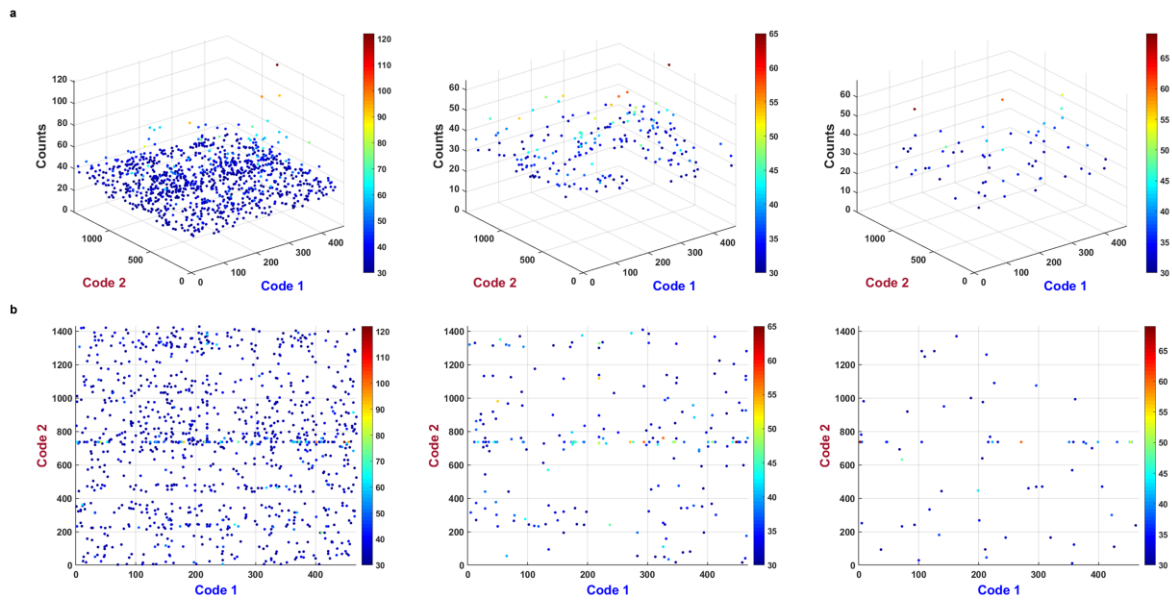
Figure 6.2.7. Affinity selection replicates against empty beads "No Protein" control. **a**. 3D plots. **b**. 2D plots.

CAIX:

Counts (C)	Total Counts (T)	Library Size (S)	"Noise" (N)	Enrichment Factor (EF)	BB1	BB2
10258	581246	669240	0.87	11810	356	586
10195	581246	669240	0.87	11738	201	586
4456	581246	669240	0.87	5130	105	586
3889	581246	669240	0.87	4477	80	586
3805	581246	669240	0.87	4381	146	586
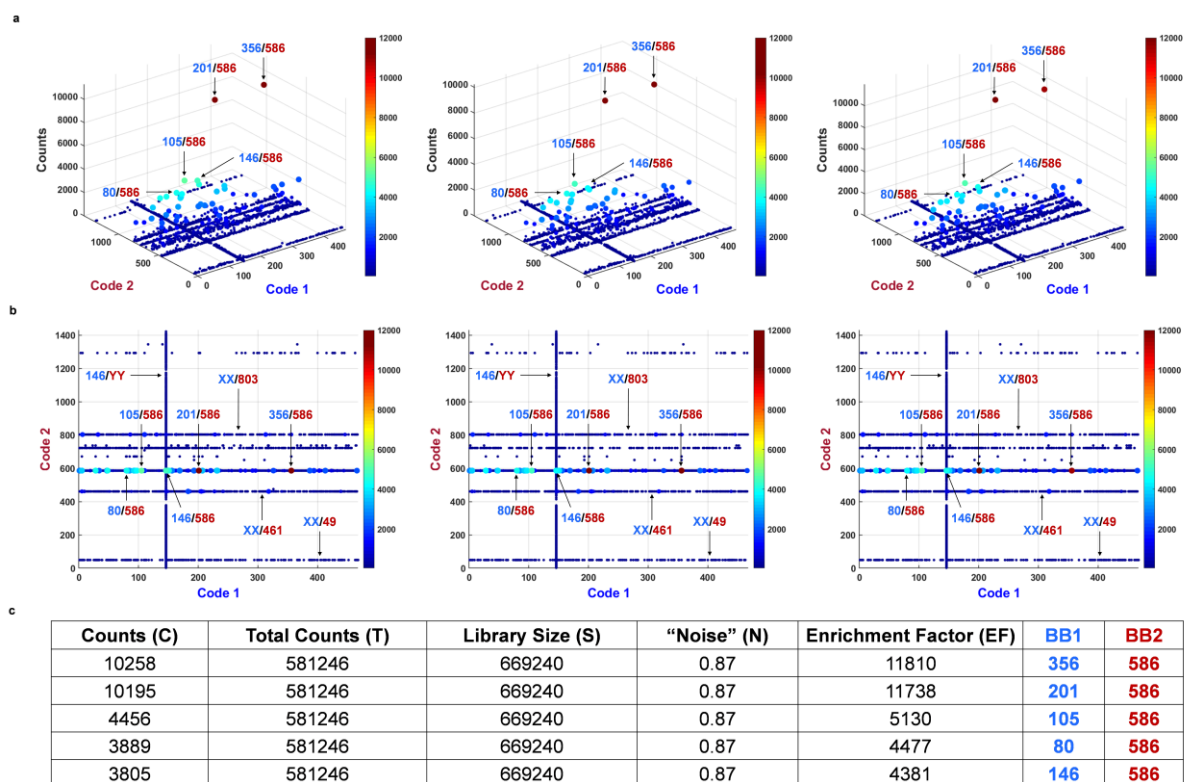
$$EF = \frac{C}{N} = \frac{C}{(T/S)}$$

Figure 6.2.8. Affinity selection replicates against CAIX. **a**. 3D plots. **b**. 2D plots. **c**. Enrichment factors (EFs) of the 5 most enriched compounds calculated with the indicated equation. Enrichment factors are consistent between both replicates.

114

AASS full construct:

Counts (C)	Total Counts (T)	Library Size (S)	"Noise" (N)	Enrichment Factor (EF)	BB1	BB2
262	735687	669240	1.1	238	326	232
241	735687	669240	1.1	219	13	1013
225	735687	669240	1.1	205	326	722
223	735687	669240	1.1	203	234	722
201	735687	669240	1.1	183	234	973
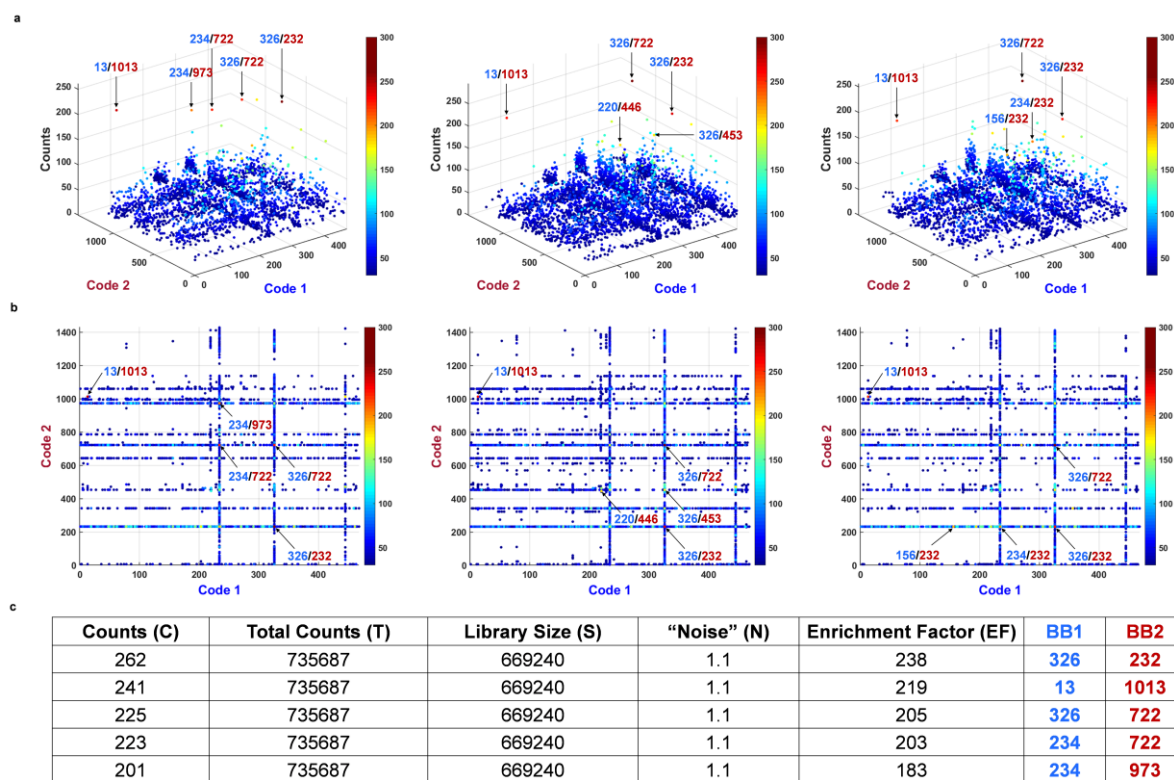
$$EF = \frac{C}{N} = \frac{C}{(T/S)}$$

Figure 6.2.9. Affinity selection replicates against AASS full construct. **a**. 3D plots. **b**. 2D plots. **c**. Enrichment factors (EFs) of the 5 most enriched compounds calculated with the indicated equation. Enrichment factors are consistent between both replicates.

115

AASS$_{454-926}$ (saccharopine dehydrogenase domain):

Counts (C)	Total Counts (T)	Library Size (S)	"Noise" (N)	Enrichment Factor (EF)	BB1	BB2
338	1085216	669240	1.6	208	326	232
297	1085216	669240	1.6	183	326	722
287	1085216	669240	1.6	177	326	453
246	1085216	669240	1.6	152	326	342
217	1085216	669240	1.6	134	326	786
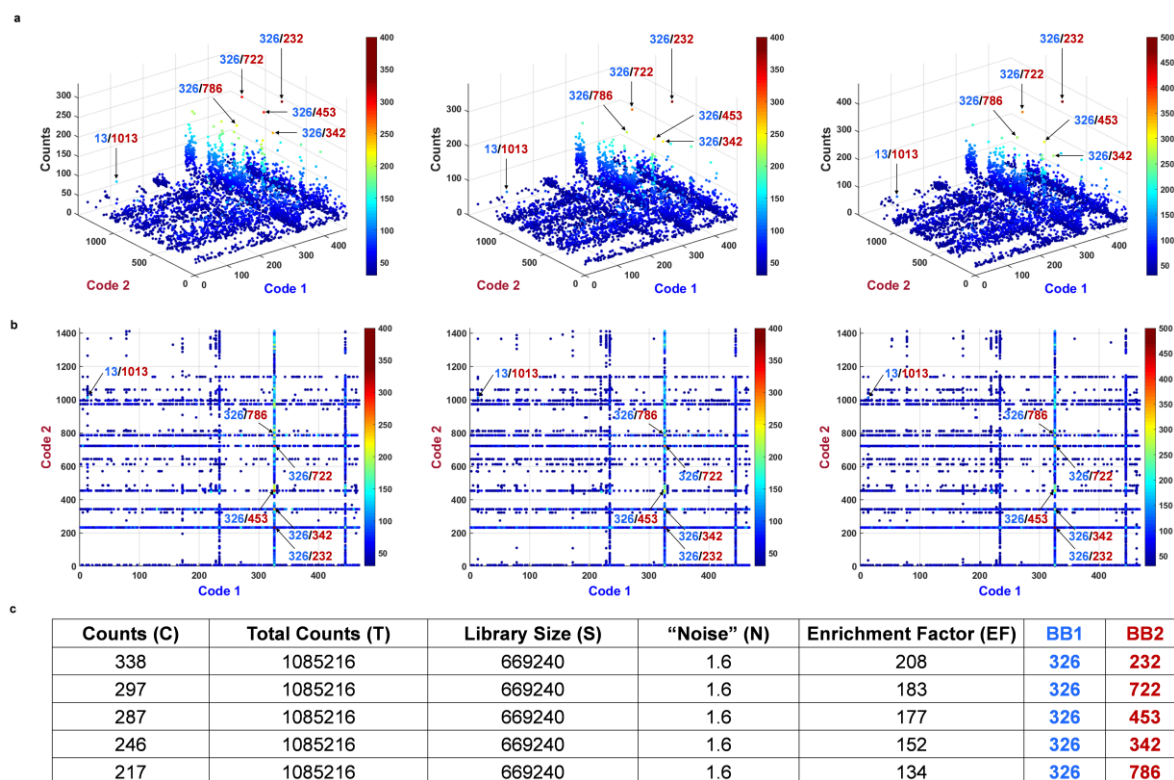
$$EF = \frac{C}{N} = \frac{C}{(T/S)}$$

Figure 6.2.10. Affinity selection replicates against AASS$_{454-926}$, (saccharopine dehydrogenase domain). **a**. 3D plots. **b**. 2D plots. **c**. Enrichment factors (EFs) of the 5 most enriched compounds calculated with the indicated equation. Enrichment factors are consistent between both replicates.

CEA:

Counts (C)	Total Counts (T)	Library Size (S)	"Noise" (N)	Enrichment Factor (EF)	BB1	BB2
570	733881	669240	1.1	520	44	722
510	733881	669240	1.1	465	336	722
500	733881	669240	1.1	456	403	722
490	733881	669240	1.1	447	118	722
480	733881	669240	1.1	438	359	722
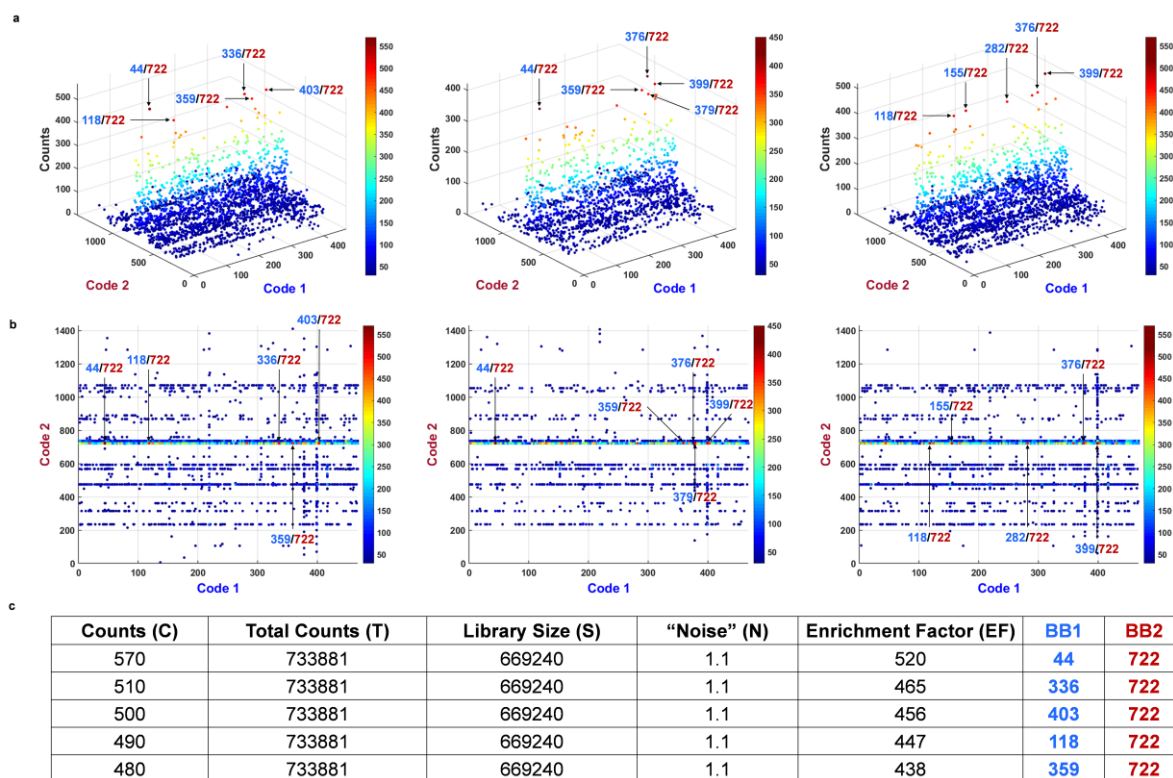
$$EF = \frac{C}{N} = \frac{C}{(T/S)}$$

Figure 6.2.11. Affinity selection replicates against CEA. **a**. 3D plots. **b**. 2D plots. **c**. Enrichment factors (EFs) of the 5 most enriched compounds calculated with the indicated equation. Enrichment factors are consistent between both replicates.

117

HSA:

$$EF = \frac{C}{N} = \frac{C}{(T/S)}$$

Counts (C)	Total Counts (T)	Library Size (S)	"Noise" (N)	Enrichment Factor (EF)	BB1	BB2
976	79171	669240	0.12	8133	214	484
871	79171	669240	0.12	7258	251	448
571	79171	669240	0.12	4758	214	884
435	79171	669240	0.12	3625	251	884
376	79171	669240	0.12	3133	214	616
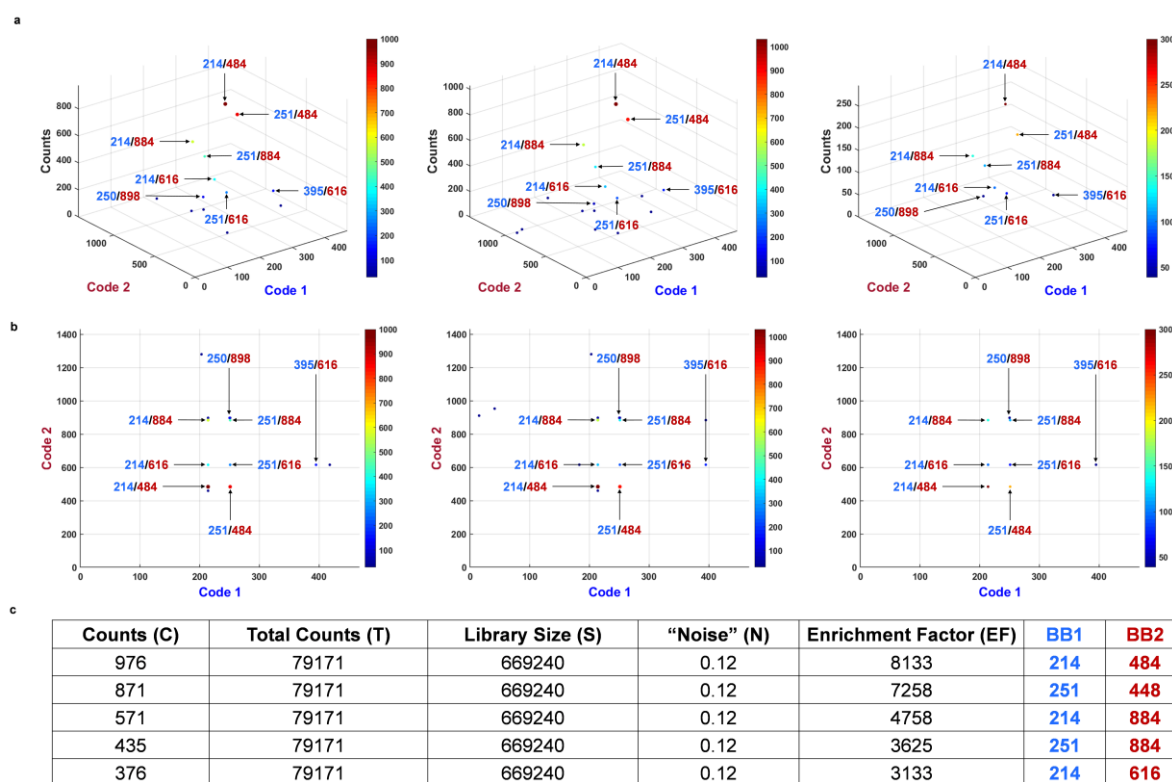
Figure 6.2.12. Affinity selection replicates against HSA. **a**. 3D plots. **b**. 2D plots. **c**. Enrichment factors (EFs) of the 5 most enriched compounds calculated with the indicated equation. Enrichment factors are consistent between both replicates.

6.2.2 Dual-pharmacophore ESAC 2+1

6.2.2.1 Materials and methods

Optimized protocol for Splint-mediated ligation in Elib6 sub-library

The corresponding d-spacer conjugate (1.4 μL, 1 mM in H_2O, 1 equiv), the 3'-phosphorylated 65-mer oligonucleotide (Elib6 code) (2.1 μL, 1 mM in H_2O, 1.5 equiv) and the DNA adaptor (1.4 μL, 2 mM in H_2O, 2 eq) were mixed and incubated for 1 h at room temperature. In a separate vial, a master mix of the corresponding amount of 10x T4 DNA-ligase buffer (1.75 μL, New England Biolabs), H_2O (0.15 μL) and T4 DNA-ligase (0.2 μL, 400 U/μL, New England Biolabs) was prepared and added to the oligo mixture. The ligation was let to proceed for 16 h at 16 °C without shaking, before inactivating the ligase for 10 min at 65 °C. The formation of the desired product was confirmed by gel electrophoresis analysis.

General procedure for the final assembly of ESAC 2+1 library

The single-stranded single-pharmacophore AG-DEL (31.7 μL, 3.2 μM) and the Elib6 sub-library (2 μL, 50 μM) were dissolved in H_2O (50.3 μL) and NEB Buffer 10x

(10 μL). A pre-hybridization step was performed for 2 min at 95 °C and the mixture was allowed to cool down at room temperature. The DNA Polymerase I, Large (Klenow) fragment (2 μL, New England Biolabs) and deoxynucleotides solution mix (4 μL, 5 mM) were added and incubated for 1 h at room temperature. The reaction was checked by gel electrophoresis analysis on Novex™ TBE-Urea Gels 15% (Invitrogen). The library was purified by QIAquick PCR Purification Kit (Qiagen), redissolved in 100 μL and the concentration evaluated by absorbance at 260 nm using a Nanodrop 2000 instrument (Thermo Fisher).

6.2.2.2 Supplementary information

Oligonucleotide sequences

AG-DEL sequences are the ones described in section 6.2.1.2

Elib6 sequences

d-spacer:

NH$_2$-C6-3'-CCTCGAAGACTTAAGACACACGACddddddGCTCAGGGTAC-5'-Phospho
being dddddd the abasic portion.

d-Spacer2-Code3:

3'-CGCGGCCTAGCTGCdddddddCGCAGTCCGTCGCACTAGGATGZZZZZZZCGCTGGCACGTCTCG-5' being ddddddd the second abasic portion and ZZZZZZZ the encoding region for each code.

Elib6 DNA adaptor:

5'-CGAGTCCCATGGCGCCGGATCGACG-3'

PCR1 Forward primer:

5'-TACACGACGCTCTTCCGATCTACACACGGAGCTTCTGAATTCTGTGTG-3' marked in blue the encoding region of each primer

PCR1 Reverse primer:

5'-CAGACGTGTGCTCTTCCGATCCGATATGCTCTGCACGGTCGC-3' marked in blue the encoding region of each primer

PCR2 Illumina Forward primer:

5'-AATGATACGGCGACCACCGAGATCTACACTCTTTCCCTACACGACGCTCTTCCGATCT-3'

PCR2 Illumina Reverse primer:

5'-CAAGCAGAAGACGGCATACGAGAT333333GTGACTGGAGTTCAGACGTGTGCTCTTCCGATC-3'

Gel electrophoresis analysis of the ESAC 2+1 library after Klenow
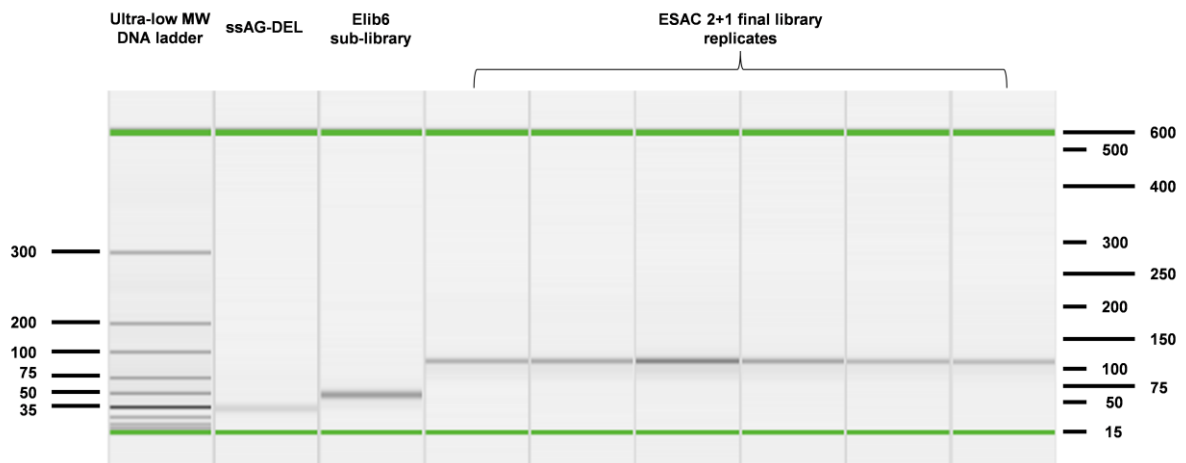
Figure 6.2.13. Gel electrophoresis analysis of the final ESAC 2+1 library after Klenow Polymerization. The analysis was performed using a QIAxcel Advanced instrument. Ultra-low molecular weight (MW) DNA ladder was run as a sample to compare the bands with those obtained using pre-casted 15% TBE-Urea gels. As expected, the final ESAC 2+1 library shows a band above 100 bp (final library size 106 bp).

Affinity selection experiments replicate fingerprints

No Protein controls:
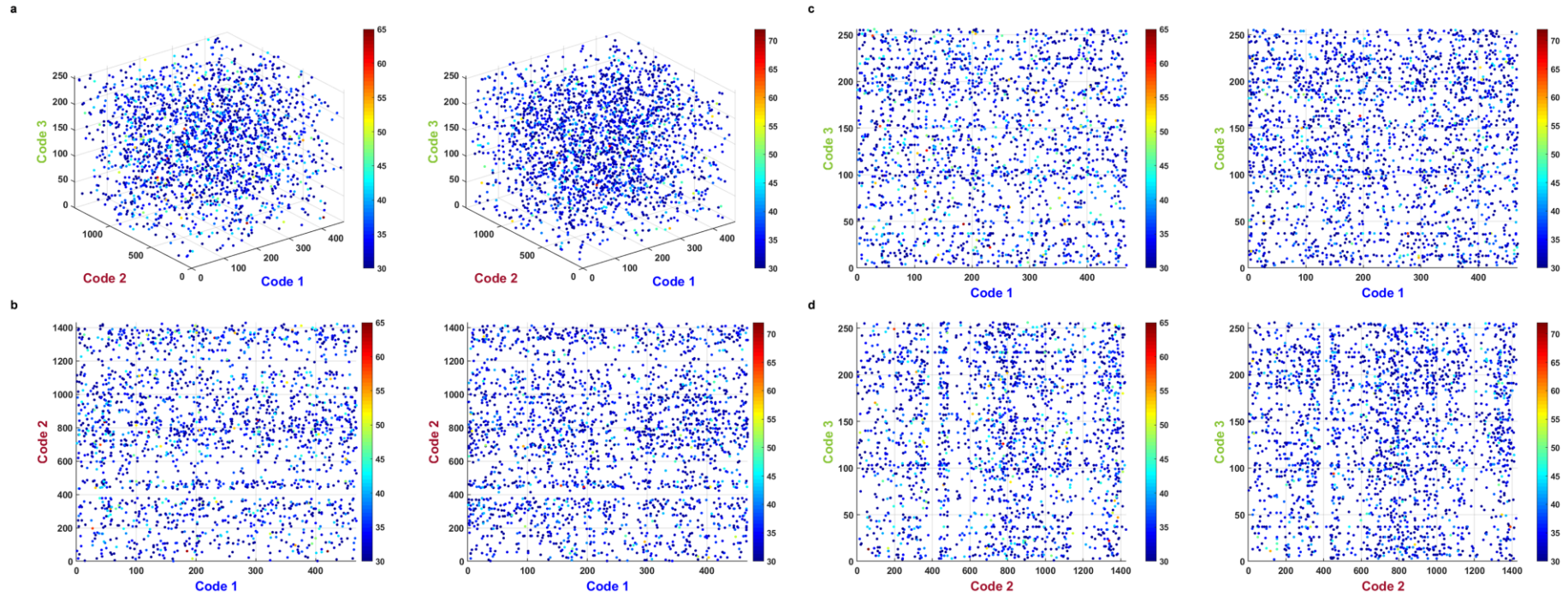
Figure 6.2.14. Affinity selection replicates against empty beads "No Protein" controls. **a**. 3D plots. **b**. Code1/Code2 2D plots. **c**. Code1/Code3 2D plots. **d**. Code2/Code3 2D plots.
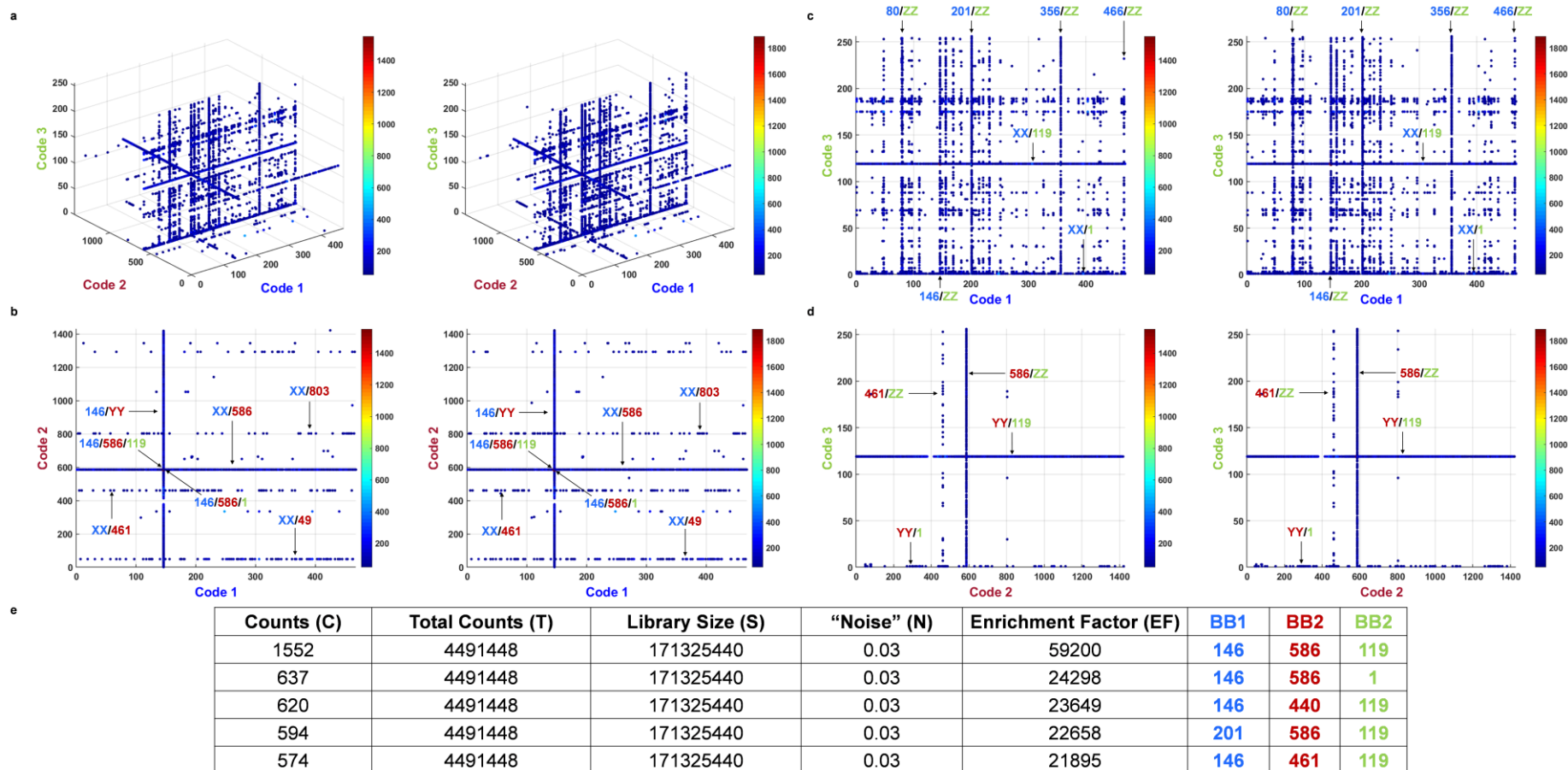
CAIX:

Figure 6.2.15. Affinity selection replicates against CAIX. **a**. 3D plots. **b**. Code1/Code2 2D plots. **c**. Code1/Code3 2D plots. **d**. Code2/Code3 2D plots. **e**. Enrichment factors (EFs) of the 5 most enriched compounds calculated with the indicated equation. Enrichment factors are consistent between both replicates.

Counts (C)	Total Counts (T)	Library Size (S)	"Noise" (N)	Enrichment Factor (EF)	BB1	BB2	BB2
1552	4491448	171325440	0.03	59200	146	586	119
637	4491448	171325440	0.03	24298	146	586	1
620	4491448	171325440	0.03	23649	146	440	119
594	4491448	171325440	0.03	22658	201	586	119
574	4491448	171325440	0.03	21895	146	461	119

$$EF = \frac{C}{N} = \frac{C}{(T/S)}$$

122
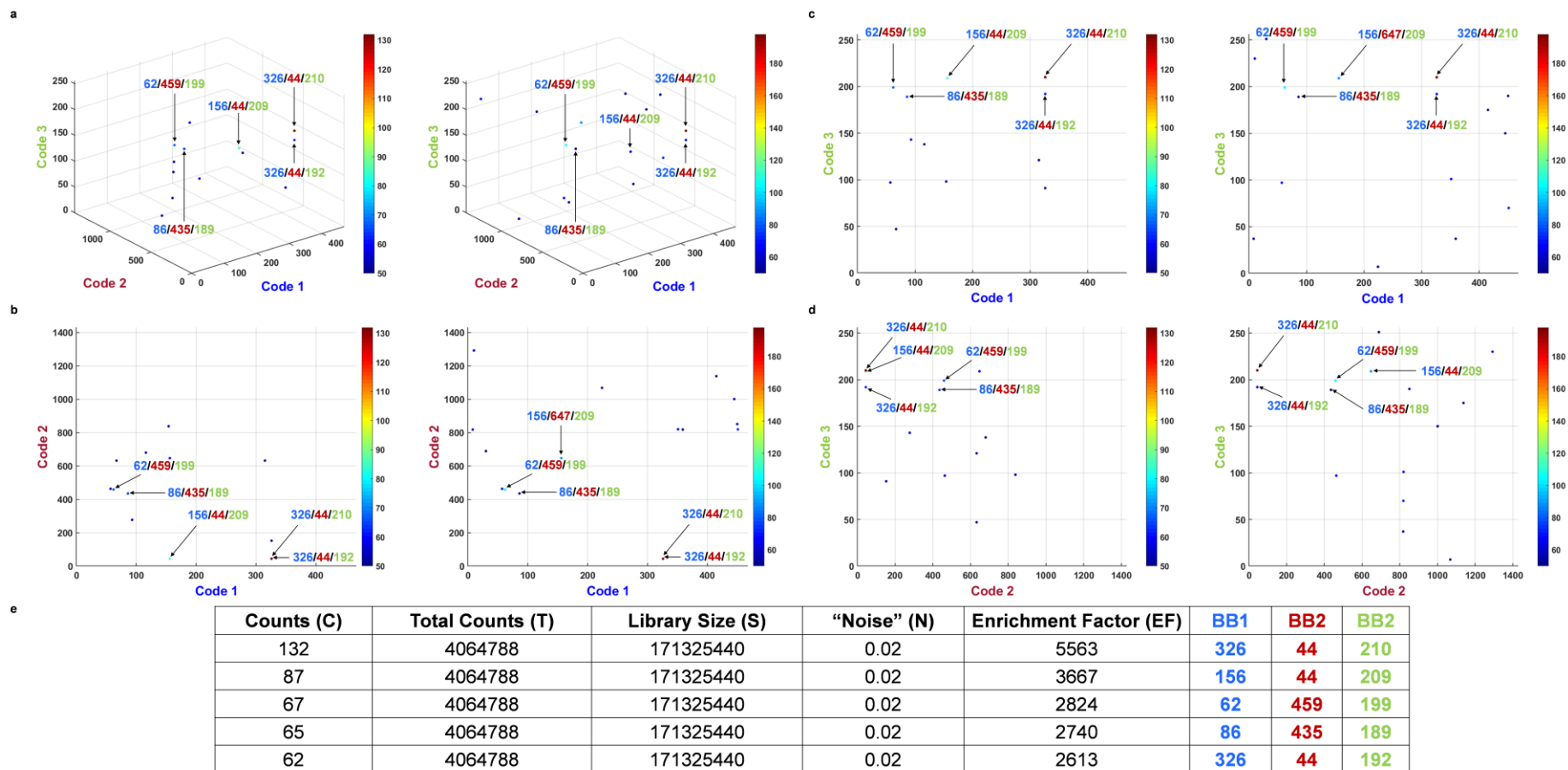
L19-IL2:

$$EF = \frac{C}{N} = \frac{C}{(T/S)}$$

Figure 6.2.16. Affinity selection replicates against L19-IL2. **a**. 3D plots. **b**. Code1/Code2 2D plots. **c**. Code1/Code3 2D plots. **d**. Code2/Code3 2D plots. **e**. Enrichment factors (EFs) of the 5 most enriched compounds calculated with the indicated equation. Enrichment factors are consistent between both replicates.

123

6.2.3 Dual-pharmacophore ESAC Plus

6.2.3.1 Materials and methods

General procedures for On-DNA reactions

General procedures for the synthesis of DNA-conjugated azides and alkynes are described in section 6.2.1.1 (amide bond formation)

General procedure for Copper(I)-catalyzed azide-alkyne cycloaddition (CuAAC) click reaction: DNA-conjugated azide and DNA-conjugated alkyne, in equimolar amount, were dissolved in borate buffer (250 mM, pH 9.4). TBTA (3 μL, 50 mM in DMSO), $CuSO_4$ (2 μL, 50 mM in H_2O) and (+)-Sodium *L*-ascorbate (4 μL, 50 mM in H_2O) were subsequently added in this order and the reaction was allowed to proceed for 2 h at room temperature.

6.2.3.2 Supplementary information

Oligonucleotide sequences

Sequences of oligonucleotides used for test reactions.

Elib2 Code:

```
NH₂-C6-5'-GGAGCTTCTGAATTCTGTGTGCTGXXXXXXCGAGTCCCATGGCGCAGC-3',
```
being XXXXXX the encoding region

d-spacer:

```
NH₂-C6-3'-CCTCGAAGACTTAAGACACACGACddddddGCTCAGGGTAC-5'-Phospho
```
being dddddd the abasic portion.

Elib4 Code:

```
3'-CGCGTCGACGYYYYYYYYGTGCCTAGGTAAGCTACGTCC-5'
```

Chimeric DNA/RNA adaptor:

```
5'-CGA-rG-5-Me-U-rC-CCATGGC-rG-rC-rA-rG-CTGC-3'
```

Oligonucleotide sequences used for the synthesis of the -ESAC Plus library were the same used for ESAC 2+1
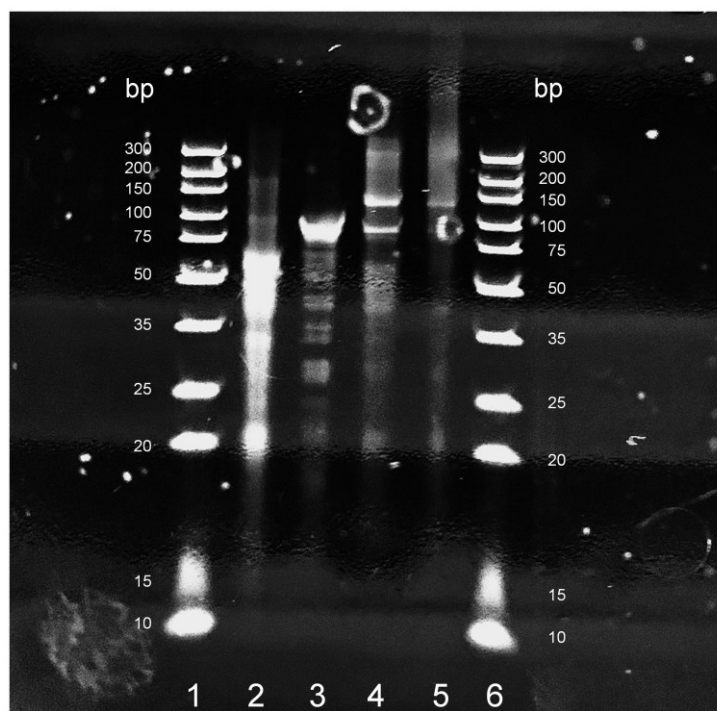
Figure 6.2.17. 15% TBE gel electrophoresis analysis of the final ESAC Plus library after Klenow Polymerization and CuAAC reaction. Lane 1, DNA ladder (size expressed in base-pairs); lane 2, Elib5 sub-library, lane 3, Elib6 sub-library; lane 4, the mixture of Elib5 and Elib6 sub-libraries before Klenow polymerization and CuAAC reaction; lane 5, final ESAC Plus library after Klenow Polymerization and CuAAC reaction; lane 6, DNA-ladder. As expected, the final ESAC Plus library (lane 5) shows a band above 100 bp (final library size 106 bp). Lane 4 shows strong annealing of both sub-libraries even before Klenow polymerization.

Affinity selection experiments replicate fingerprints
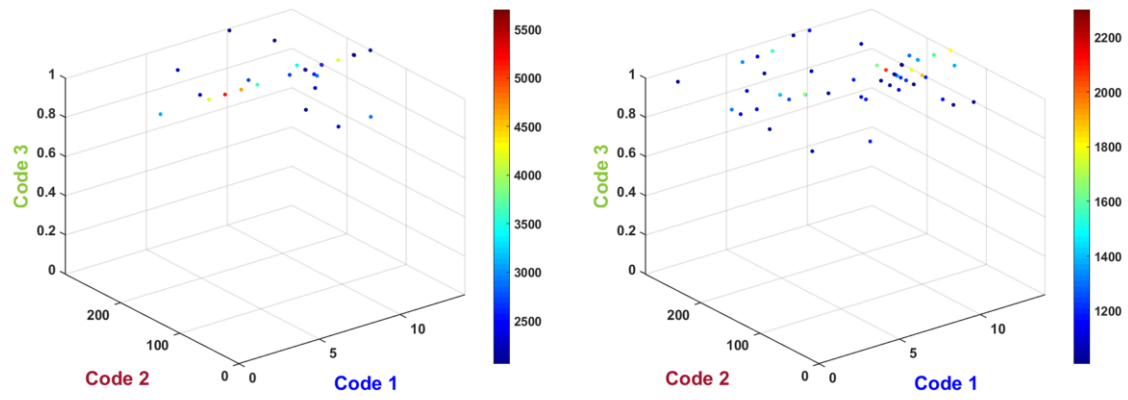
No Protein Controls:
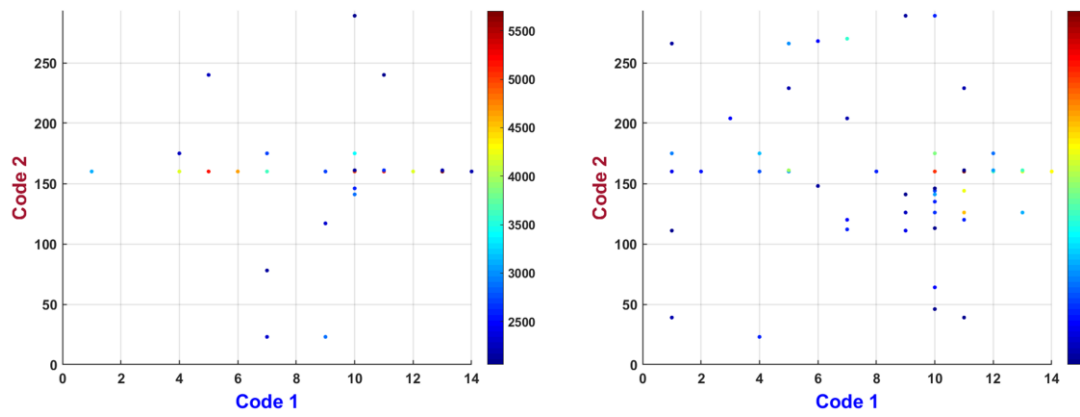
Figure 6.2.18. Affinity selection replicates of Elib5 sub-library against empty beads "No Protein" controls. **a**. 3D plots. **b**. 2D plots.
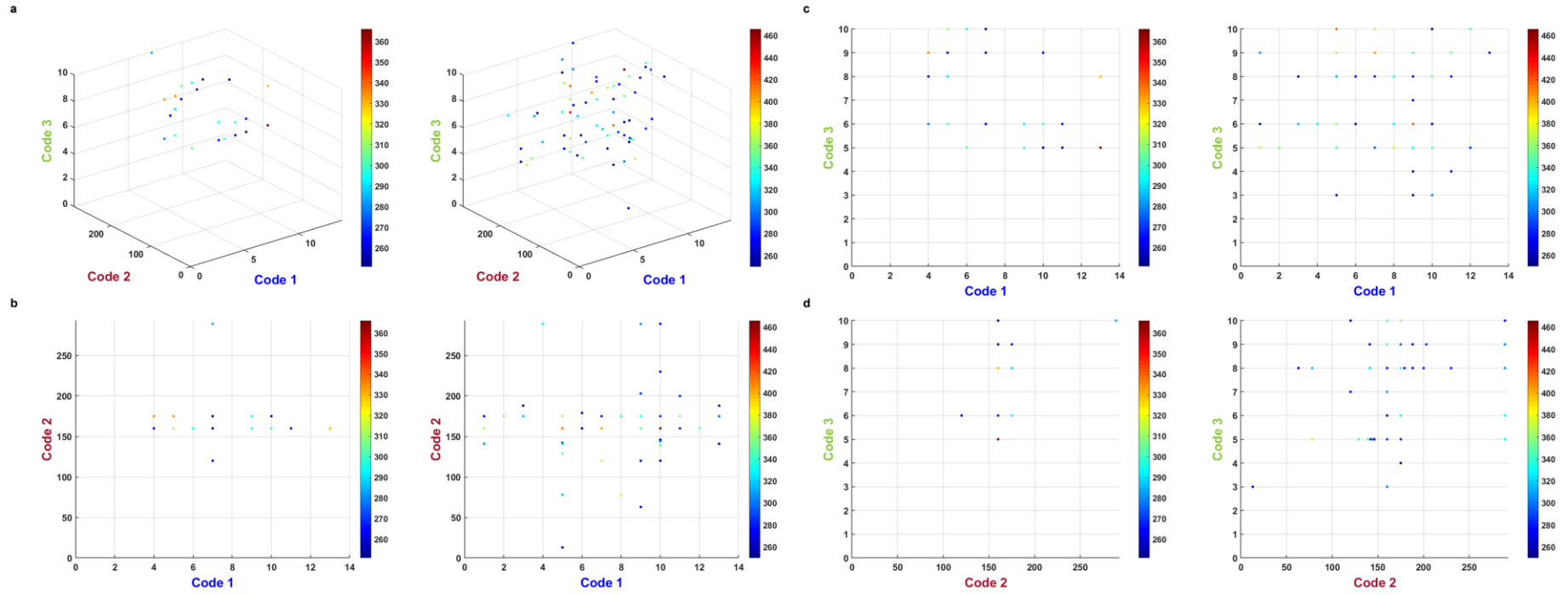
Figure 6.2.19. Affinity selection replicates of non-cyclized ESAC library against empty beads "No Protein" controls. **a**. 3D plots. **b**. Code1/Code2 2D plots. **c**. Code1/Code3 2D plots. **d**. Code2/Code3 2D plots.
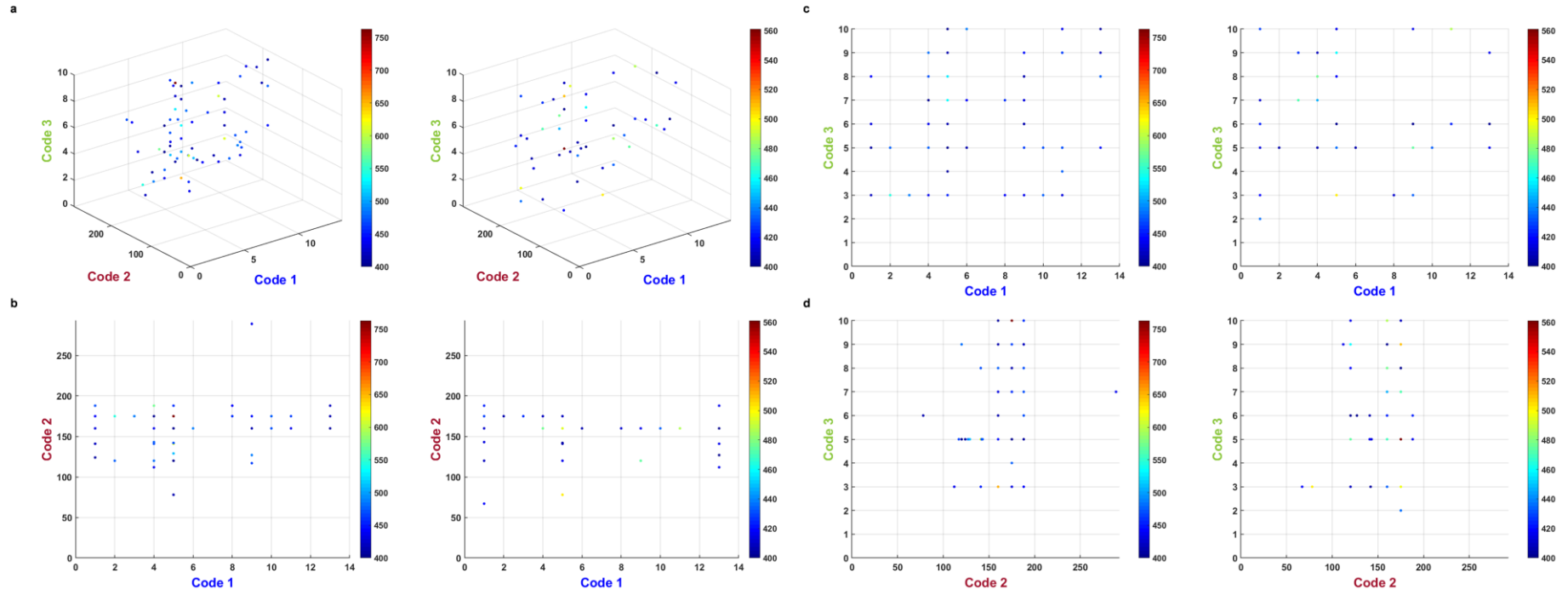
Figure 6.2.20. Affinity selection replicates of ESAC Plus library against empty beads "No Protein" controls. **a**. 3D plots. **b**. Code1/Code2 2D plots. **c**. Code1/Code3 2D plots. **d**. Code2/Code3 2D plots.

CAIX:

Counts (C)	Total Counts (T)	Library Size (S)	"Noise" (N)	Enrichment Factor (EF)	BB1	BB2
65169	1202907	4102	293	222	4	53
65079	1202907	4102	293	222	13	53
58290	1202907	4102	293	199	12	53
56878	1202907	4102	293	194	5	53
52779	1202907	4102	293	180	6	53
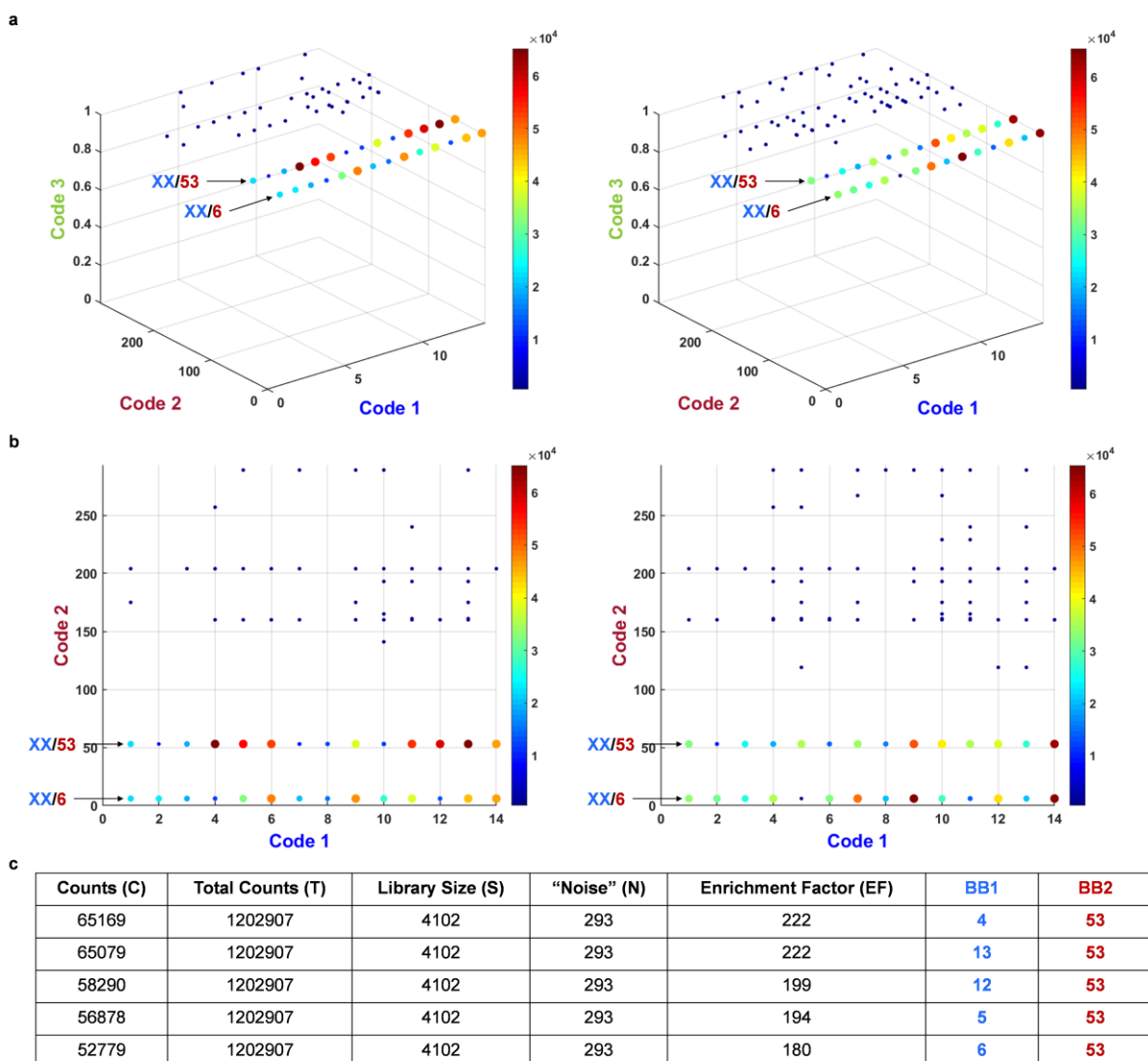
$$EF = \frac{C}{N} = \frac{C}{(T/S)}$$

Figure 6.2.21. Affinity selection replicates of Elib5 sub-library against CAIX. **a**. 3D plots. **b**. 2D plots. **c**. Enrichment factors (EFs) of the 5 most enriched compounds calculated with the indicated equation. Preferentially enriched combinations bearing BB2_6 and 62 (corresponding to aromatic sulfonamides) can be observed. Enrichment factors are consistent between both replicates.

Figure 6.2.22. Affinity selection replicates of non-cyclized ESAC library against CAIX. **a**. 3D plots. **b**. Code1/Code2 2D plots. **c**. Code1/Code3 2D plots. **d**. Code2/Code3 2D plots. **e**. Enrichment factors (EFs) of the 5 most enriched compounds calculated with the indicated equation. Preferentially enriched combinations bearing BB2_6 (corresponding to an aromatic sulfonamide) can be observed. Enrichment factors are consistent between both replicates.

The table in panel **e**:
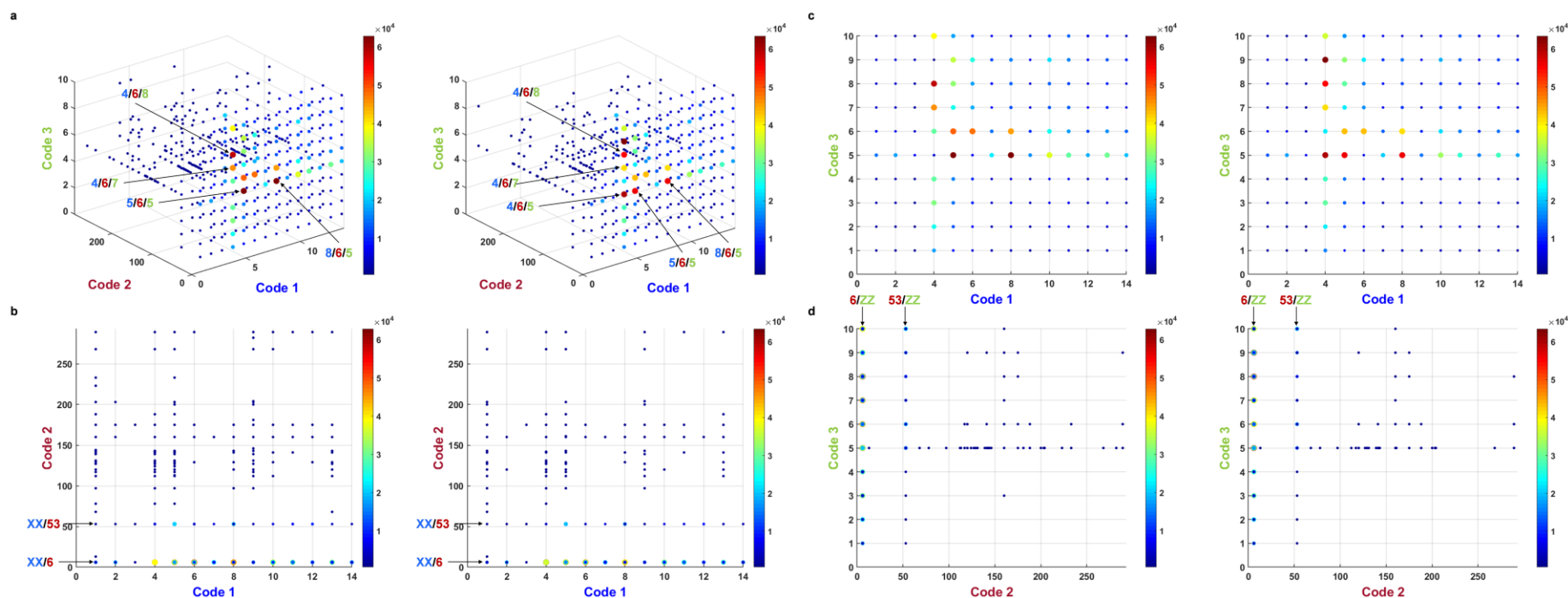
Counts (C)	Total Counts (T)	Library Size (S)	"Noise" (N)	Enrichment Factor (EF)	BB1	BB2	BB2
63480	5859614	41020	143	444	4	6	9
60344	5859614	41020	143	422	4	6	5
56403	5859614	41020	143	395	8	6	5
55864	5859614	41020	143	391	5	6	5
55184	5859614	41020	143	386	4	6	8

$$EF = \frac{C}{N} = \frac{C}{(T/S)}$$

130
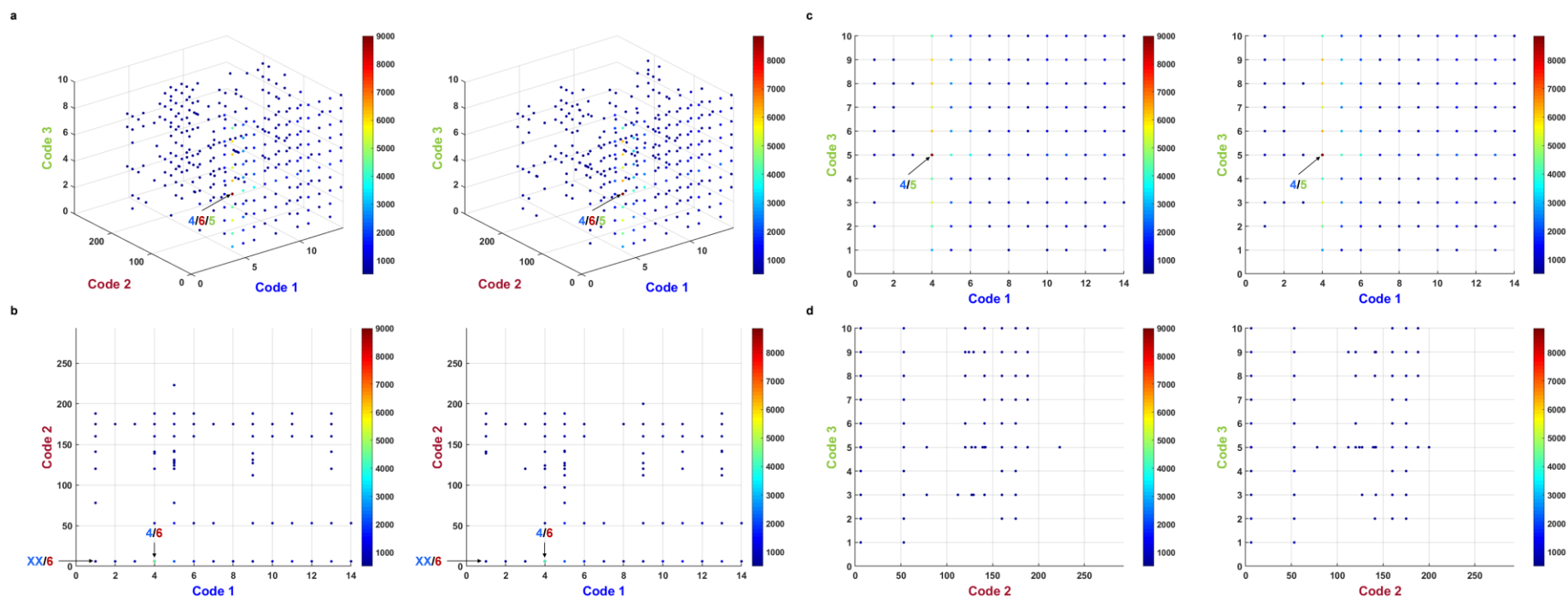
Counts (C)	Total Counts (T)	Library Size (S)	"Noise" (N)	Enrichment Factor (EF)	BB1	BB2	BB2
8851	4638696	41020	113	78	4	6	5
6292	4638696	41020	113	56	4	6	6
6197	4638696	41020	113	55	4	6	9
5998	4638696	41020	113	53	4	6	8
5386	4638696	41020	113	48	4	6	3

$$EF = \frac{C}{N} = \frac{C}{(T/S)}$$

Figure 6.2.23. Affinity selection replicates of ESAC Plus library against CAIX. **a**. 3D plots. **b**. Code1/Code2 2D plots. **c**. Code1/Code3 2D plots. **d**. Code2/Code3 2D plots. **e**. Enrichment factors (EFs) of the 5 most enriched compounds calculated with the indicated equation. Preferentially enriched combinations lock both BB1_4 and BB2_6 which may suggest an important influence from the three-dimensional conformation of the binding molecules. Enrichment factors are consistent between both replicates.

6.3 DNA-compatible diazo-transfer reaction in aqueous media suitable for DNA-encoded chemical library synthesis

6.3.1 Supplementary information

Screening conditions with DNA-Conjugated glycine
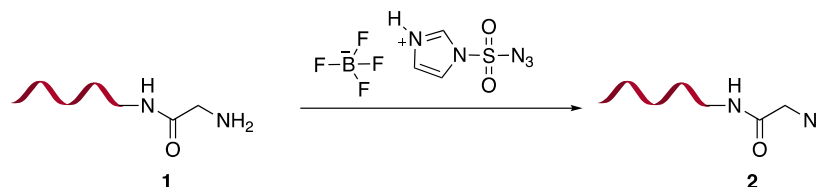
Table 6.3.1. Reaction optimization for DNA-compatible diazo-transfer reaction[a].

entry	diazo-transfer reagent (equiv)	copper sulfate (equiv)	buffer (pH)	temperature (°C)	conversion (%)[b]	time[c] (h)
1	120	120	MOPS (8.0)	60	95*	16
2	120	-	MOPS (8.0)	60	95*	16
3	60	60	MOPS (8.0)	60	95*	16
4	60	-	MOPS (8.0)	60	95*	16
5	60	-	MOPS (8.0)	37	95	3
6	40	-	MOPS (8.0)	37	95*	3
7	20	-	MOPS (8.0)	37	95*	16
8	120	120	Borate (9.4)	60	95*	16
9	120	-	Borate (9.4)	60	95*	16
10	60	60	Borate (9.4)	60	95*	16
11	60	-	Borate (9.4)	60	95*	16
12	60	-	Borate (9.4)	37	95	1
13	40	-	Borate (9.4)	37	95	1
14	20	-	Borate (9.4)	37	95	1
15	120	120	Carbonate (11.5)	60	95*	16
16	120	-	Carbonate (11.5)	60	95*	16
17	60	60	Carbonate (11.5)	60	95*	16
18	60	-	Carbonate (11.5)	60	95*	16

[a]All the reactions were conducted at 0.4 mM in 2 nmol scale. [b]Conversion observed by LC-ESI-MS. [c]Time to completion. *DNA degradation observed by mass spectrometry.

From all the conditions tested, borate buffer and MOPS buffer gave the best results. The conversion was comparable under all the different experimental conditions enumerated above. The addition of Cu (II) source did not have a significant impact on the reactivity. In addition, the deconvoluted mass spectrum showed unclear profile, meaning possible DNA damage. The same trend was observed when basic buffer such as carbonate (pH 11.5) was employed.

General procedures

*General Procedure 1: Ethanol precipitation (**GP1**).* To aqueous DNA solutions, 10% (v/v) of 5 M NaCl was added, followed by 2.5-3 volumes of cold EtOH. The suspension was allowed to seat for 2−16 h at -20 °C and then centrifuged at 15000 rpm. for 15−60 min at 4 °C. The resulting supernatant was discarded, and the pellet was rinsed once with cold 80% EtOH. After centrifugation for another 5 min at 4 °C at 15000 rpm., the supernatant was discarded, and the pellet was dried under vacuum using a SpeedVac. The recovered samples were dissolved in the appropriate buffer for subsequent reactions or analysis. The crude mixture was filtered out using Silica Spin Columns before HPLC purification. **GP1** was generally performed after each chemical reaction.

Amide bond formation method with s-NHS/EDC. Fmoc-amino acid (5 μL, 200 mM in DMSO) was incubated with EDC (2.5 μL, 400 mM DMSO) and s-NHS sodium salt (6.6 μL, 133 mM DMSO/H_2O (2:1)) for 25 min at 30 °C. The amino-modified oligonucleotide "DEL01" (20 nmol) in Borate Buffer (20 μL, 250 mM, pH 9.4) was then added to the mixture and the reaction was let to proceed for 3 hours at 30 °C. The DNA was precipitated following the procedure **GP1** and was purified by RP-HPLC using a gradient of eluent A (TEAA 100 mM in H_2O) and eluent B (TEAA 100 mM in 80% MeCN). The fractions containing the product were combined and lyophilized overnight.

Fmoc deprotection. The purified product was dissolved in H_2O (100 μL) and Piperidine (5 μL, Neat) was added for 2 h at room temperature. The DNA was precipitated following the procedure **GP1** and the final DNA-Conjugated amino acid (**1**, **4**–**22**) was dissolved in H_2O (100 μL). The concentration was determined by Nanodrop.

Optimized diazo-transfer reaction. DNA-Conjugated amino acid (**1**, **4**–**22**; 2 nmol) was dissolved in Borate buffer (4 μL, 250 mM, pH 9.4) followed by ISA·HBF_4 (**2**; 1 μL, 40 mM H_2O) and stirred for 1 h at 37 °C. The reaction was monitored by LC-ESI-MS at 1, 3, and 16 h.

Reduction of the DNA-Conjugated azido-glycine (control experiment). The DNA-conjugated azido-glycine (2 nmol) was dissolved in a solution of TCEP (100 μL, 30 mM in Tris-HCl 500 mM, pH 7.4). The reaction was let to proceed for 3 h at 30 °C. The DNA was precipitated following the procedure **GP1** and the resulting pellet was re-dissolved in H_2O (100 μL) for analysis.

*Ligation procedure (synthesis of oligonucleotide **D**).* Oligonucleotide **B** (20 μL, 200 μM H_2O) bearing the Azido-modified Glycine (BB1), oligonucleotide **C** (30 μl, 200 μM H_2O) and adaptor (32 μL, 200 μM H_2O), were mixed and heated up to 90 °C for 2 min. The mixture was allowed to cool down to room temperature and 10x T4 DNA-ligase buffer (10 μl, New England Biolabs) and T4 DNA-ligase (1 μL, 400 U/μL, New England Biolabs) was then added. The ligation process was left at 16 °C for 16 hours. DNA was precipitated following protocol **GP1**. The resulting mixture was checked by LC-ESI-MS to confirm the desired ligated product. LC-ESI-MS: 23065.21 m/z, found: 23066.62 m/z.

Copper(I)-catalyzed alkyne-azide cycloaddition (CuAAC) "click" reaction procedure. The DNA-conjugated azido-glycine (**45**) (8 μL, 500 μM H_2O) was diluted in Borate buffer (8 μL, 500 mM, pH 9.4). Hex-5-ynoic acid (**46**) (4 μL, 40 mM DMSO), TBTA (4 μL, 60 mM DMSO), $CuSO_4 \cdot 5 H_2O$ (4 μL, 50 mM H_2O) and (+)-Sodium *L*-ascorbate (4 μL, 70 mM H_2O) were subsequently added and the reaction was let to proceed for 3 h at 30 °C. DNA was precipitated following protocol **GP1**. The final pellet was dissolved in H_2O (20 μL) and then checked by LC-ESI-MS to confirm the desired product. LC-ESI-MS: 23177.34 m/z, found: 23177.17 m/z.

Oligonucleotide Sequences

Fmoc-amino acids were coupled to amino modified Oligonucleotide **A** and used for the study of the diazo-transfer reaction. Amino modified Oligonucleotide **B** and phosphorylated Oligonucleotide **C** were used for the validation of the process (**Scheme 4.2.1**, chapter 4.2).

*Oligonucleotide **A**:*

5'-(NH$_2$-C6)-GGAGCTTGTGAATTCTGGATCTTAGGACGTGTGTGAATTGTC-3'

Modification: 5'–C6–Amino linker

MW = 13239.71 Da

*Oligonucleotide **B**:*

5'-(NH$_2$-C6)-GGAGCTTCTGAATTCTGTGTGCTGTCCGACCGAGTCCCATGGCGC-3'

Modification: 5'–C6–Amino linker

MW = 14015.13 Da

*Oligonucleotide **C**:*

5'-Phospho-CGGATCGACGGTCTCACGCGTCAGGCAGC-3'

Modification: 5'–Phosphorylated

MW = 8984.77 Da

DNA adaptor:

5'-CGATCCGGCGCCAT-3'

MW = 4224.78 Da

*Oligonucleotide **D**:*

```
5'-(NH₂-C6)-GGAGCTTCTGAATTCTGTGTGCTGTCCGACCGAGTCCCATGGCGCCGGATCGACGGTCTCACGCGTCAGGCAGC-3'
```

MW = 22981.90 Da


```
5'-(Alkyne/Azide)-GGAGCTTCTGAATTCTGTGTGCTGTCCGACCGAGTCCCATGGCGCCGGATCGACGGTCTCACGCGTCAGGCAGC-3'
                                               3'-TACCGCGGCCTAGC-5'
```

Scheme 6.3.1. DNA-encoding scheme of the validation process of the diazo-transfer reaction. Ligation extension is needed to encode the building blocks at diversity elements -1/2 (BB- 1/2). Oligonucleotide **B** (red) contains the code (Code 1; green) for the first building block (glycine) and a 5'-terminal amine for modification with the encoded small molecule compound. Oligonucleotide **C** (blue) contains the code (Code 2; yellow) for the second building block (Alkyne). Both Oligonucleotide **B** and Oligonucleotide **C** are annealed with the DNA adaptor through a 7-nucleotide annealing sequence. Oligonucleotide **D** is then obtained upon addition of T4 DNA-ligase.

LC-ESI-MS chromatograms

*DNA-Conjugated amino acids (**1**, **4**–**22**)*
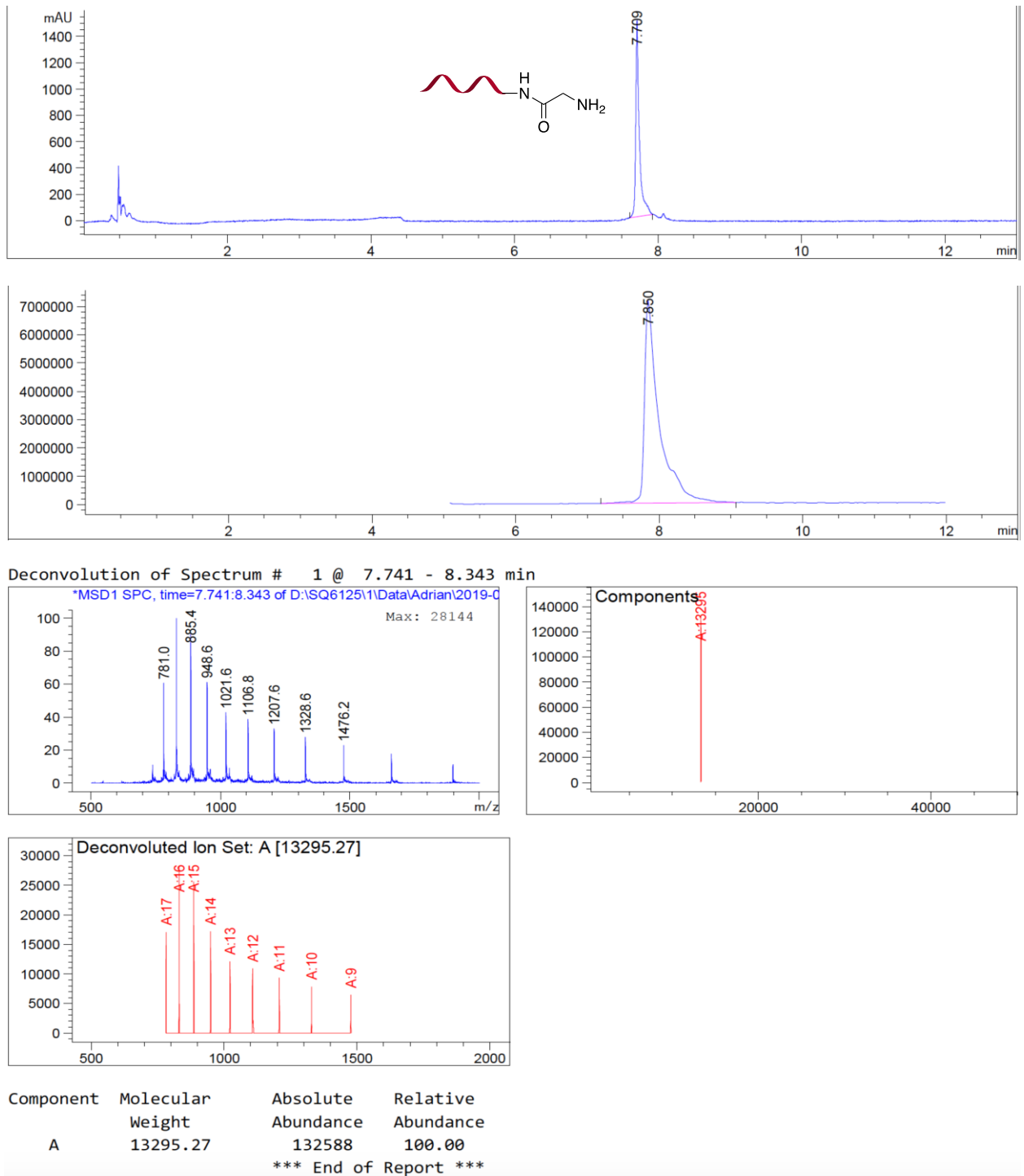
Figure 6.3.1. LC-ESI-MS chromatogram of compound **1**, t_R: 7.709 min (DAD), 7.850 min (TIC). Expected mass 13297.02, observed 13295.27.
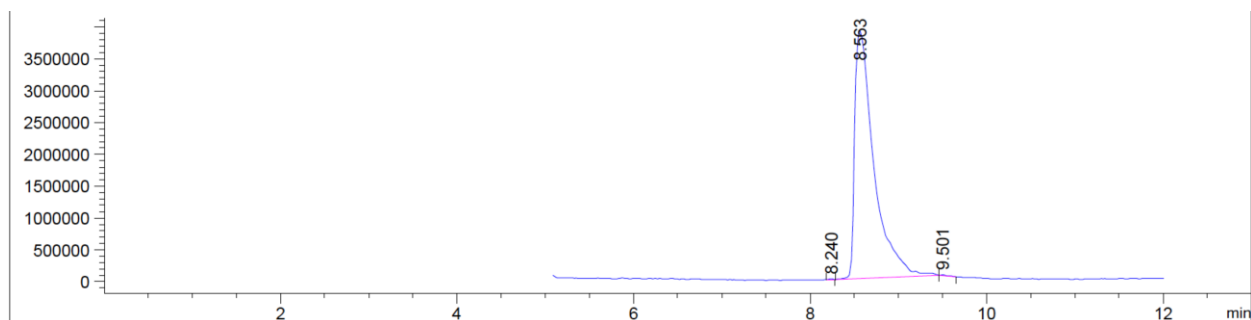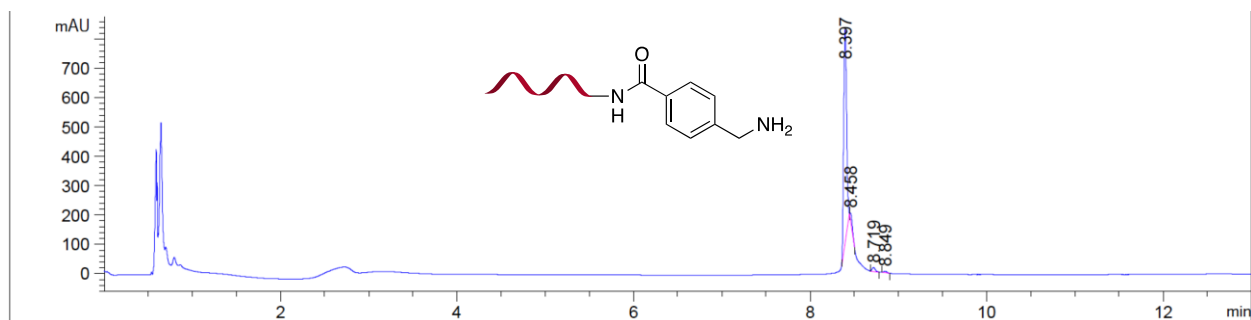
137
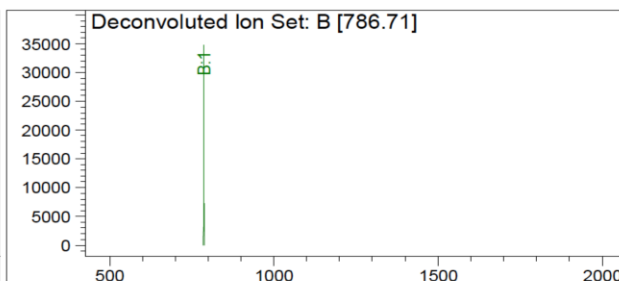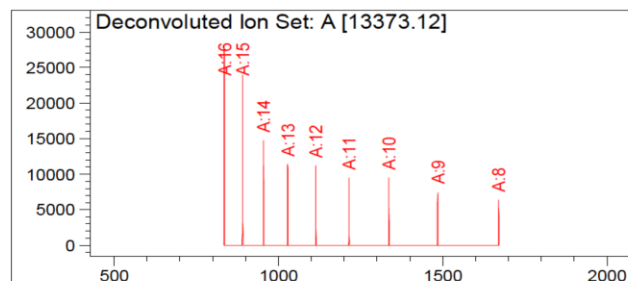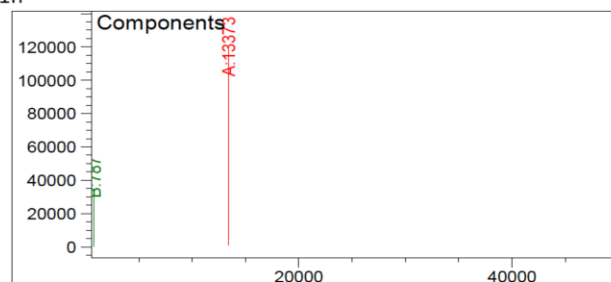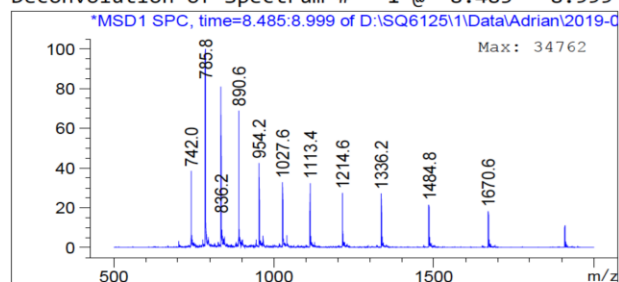
Figure 6.3.2. LC-ESI-MS chromatogram of compound **4**, t_R: 8.397 min (DAD), 8.563 min (TIC). Expected mass 13373.11, observed 13373.12.
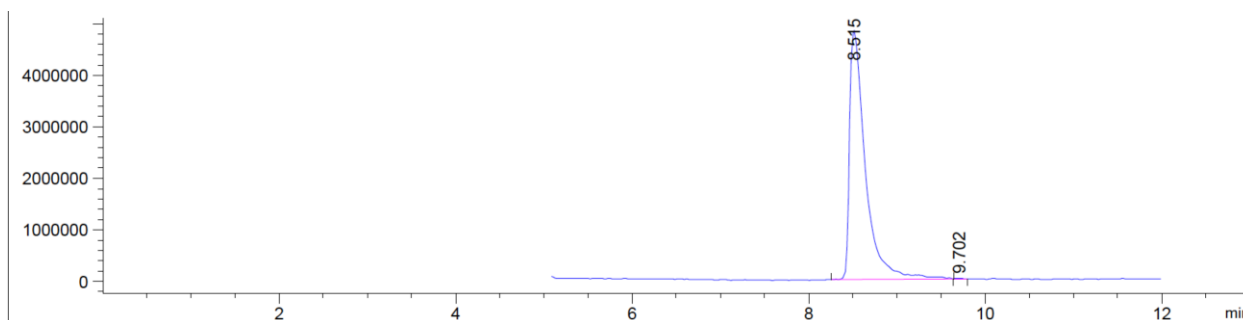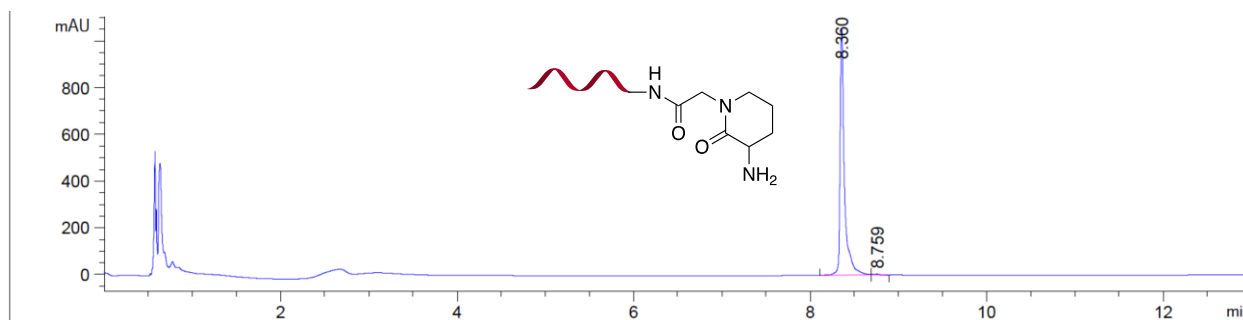
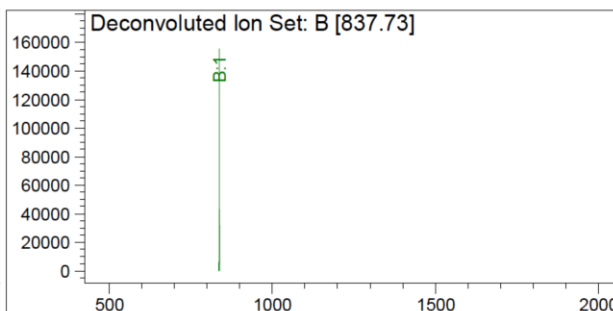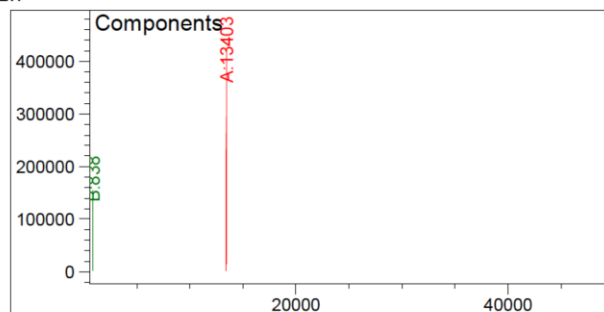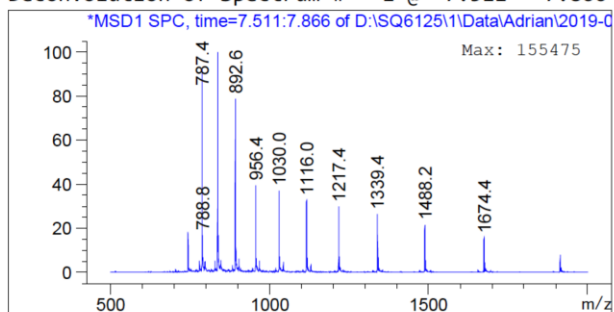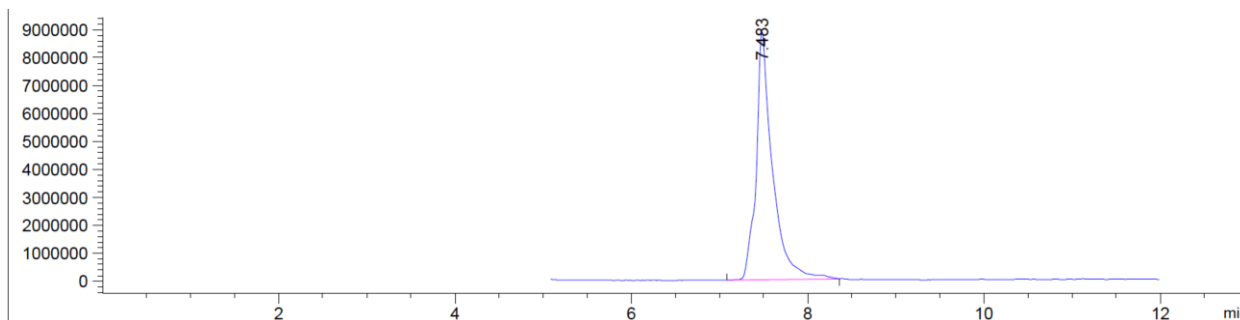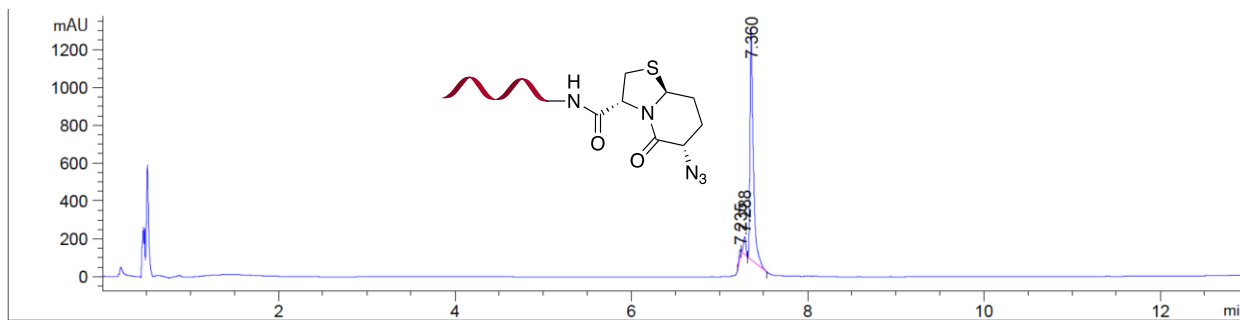**Deconvolution of Spectrum # 1 @ 8.432 - 8.751 min**
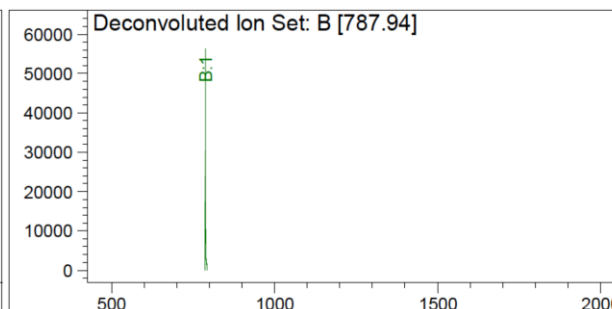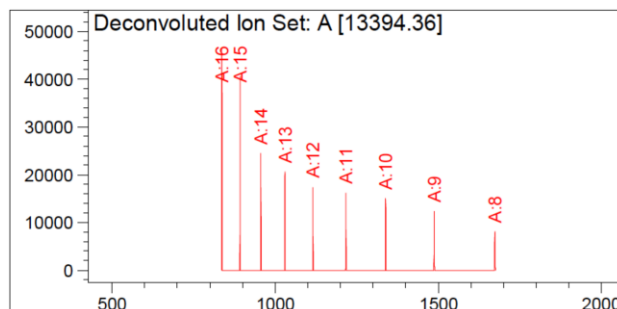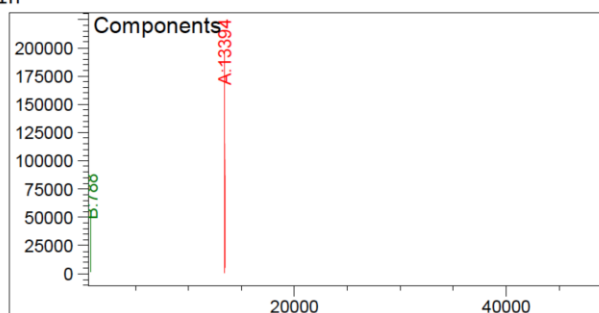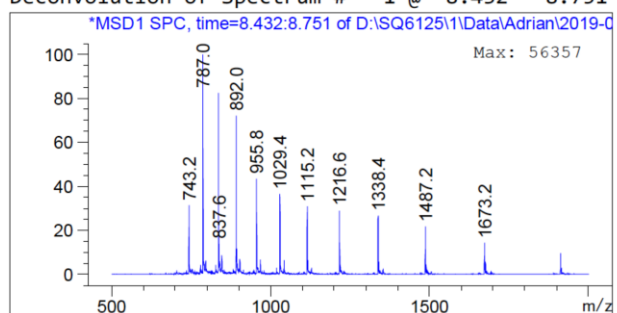
Component	Molecular Weight	Absolute Abundance	Relative Abundance
A	13394.36	196741	100.00
B	787.94	56357	28.65

*** End of Report ***

Figure 6.3.3. LC-ESI-MS chromatogram of compound **5**, t_R: 8.360 min (DAD), 8.515 min (TIC). Expected mass 13394.14, observed 13394.36.
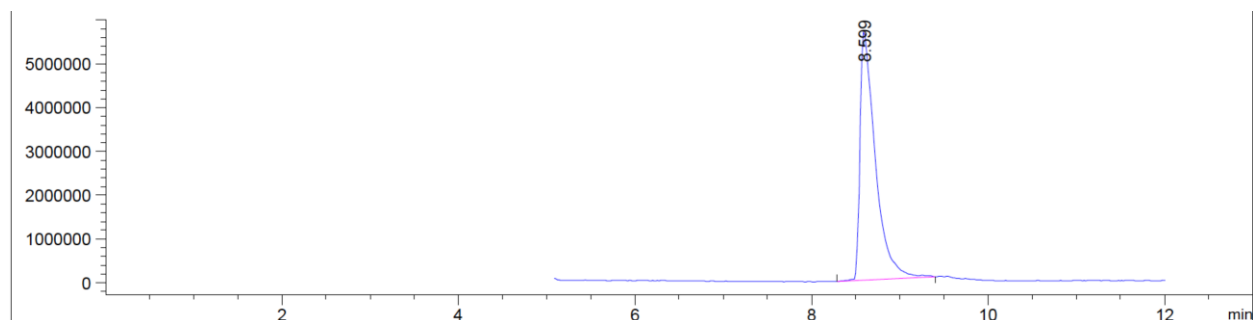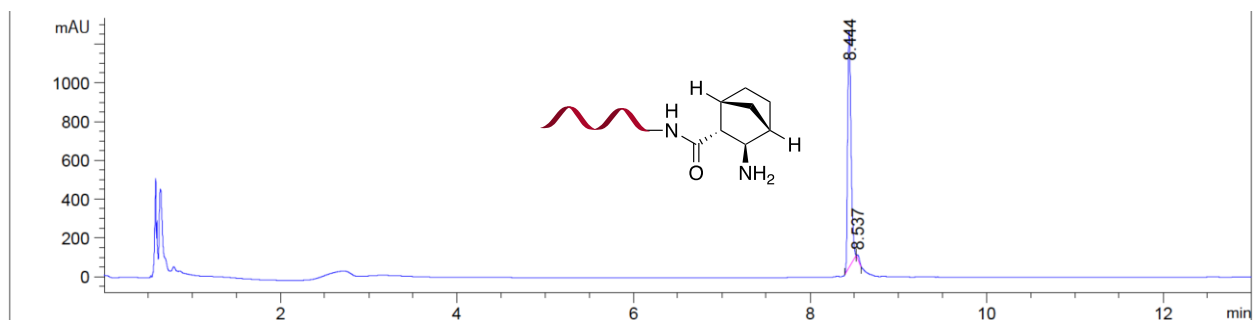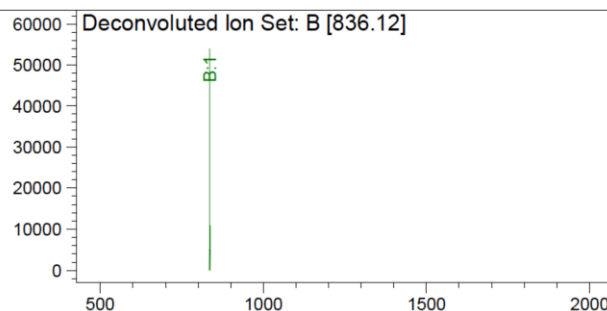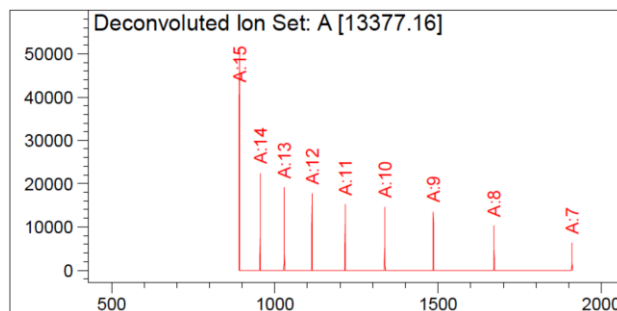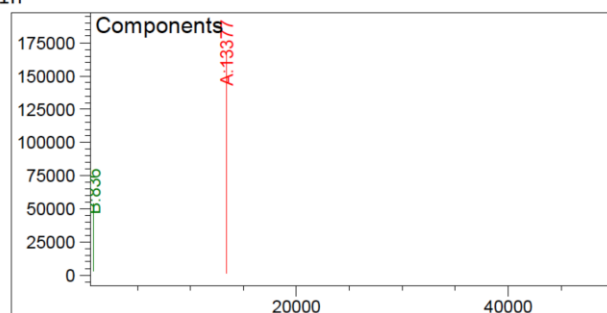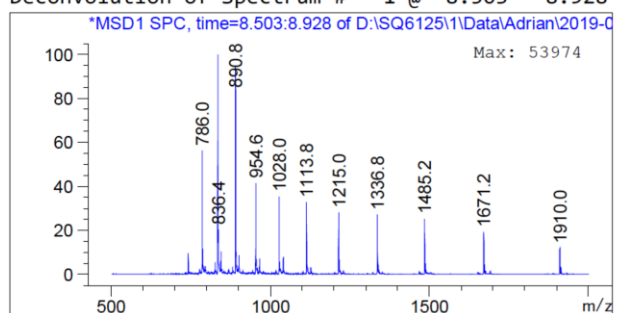
Figure 6.3.4. LC-ESI-MS chromatogram of compound **6**, t_R: 8.444 min (DAD), 8.599 min (TIC). Expected mass 13377.11, observed 13377.16.
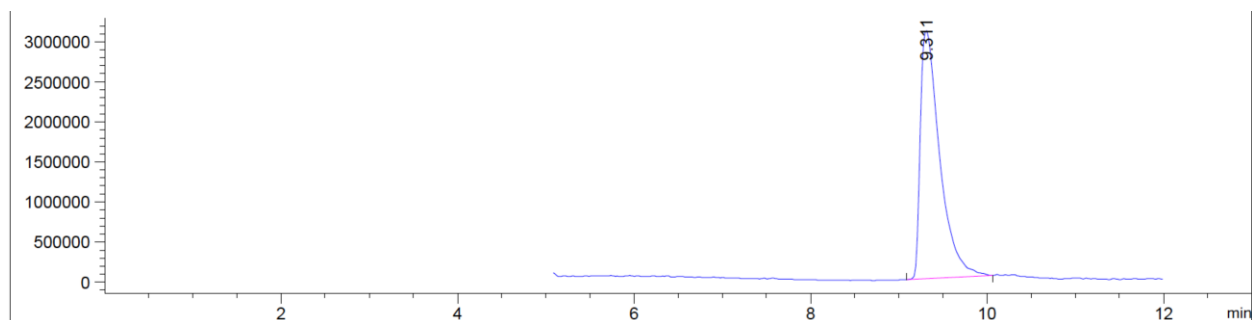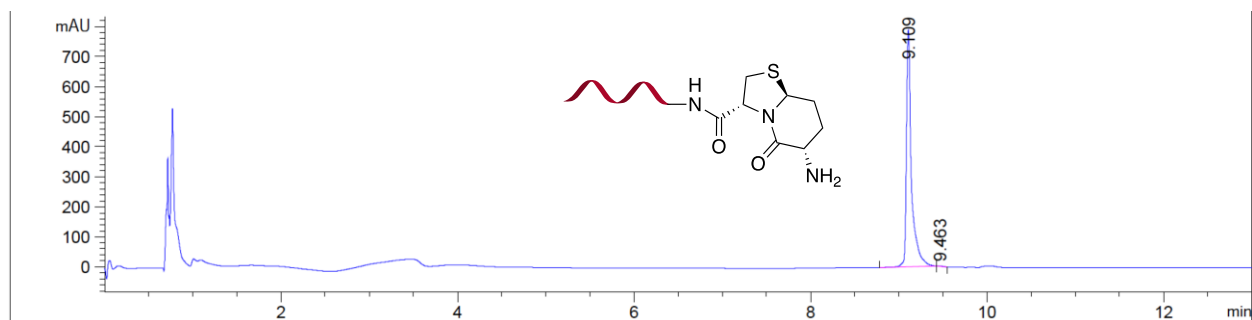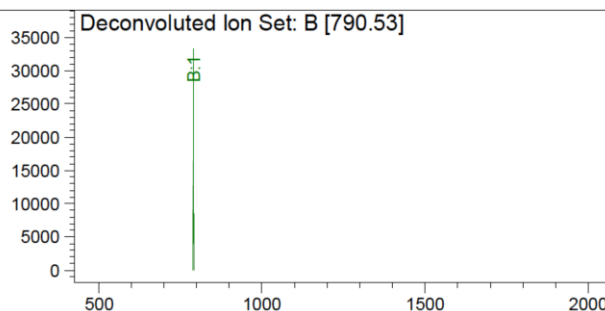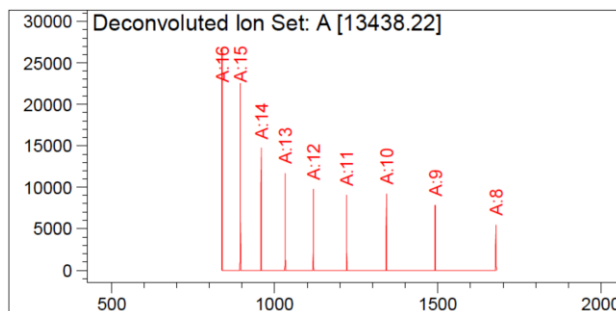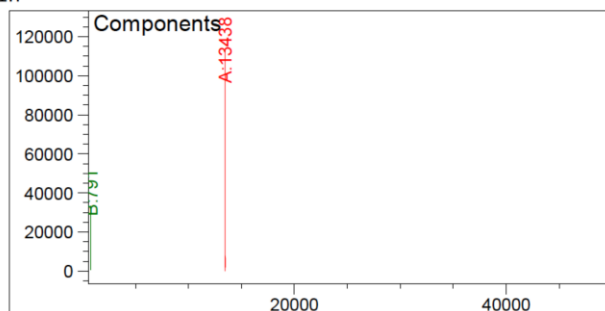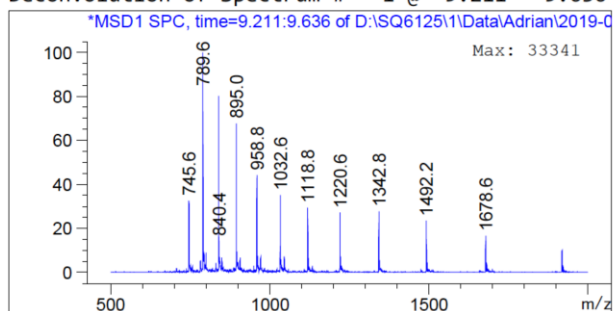
Figure 6.3.5. LC-ESI-MS chromatogram of compound **7**, t_R: 9.109 min (DAD), 9.311 min (TIC). Expected mass 13438.21, observed 13438.22.
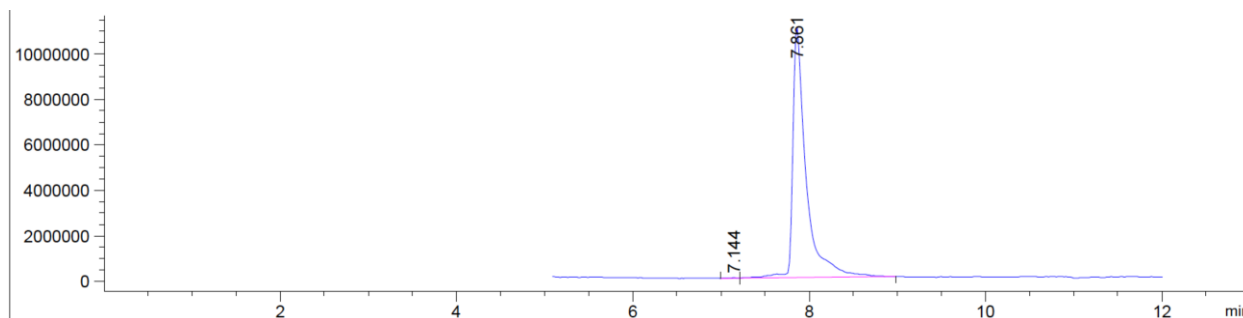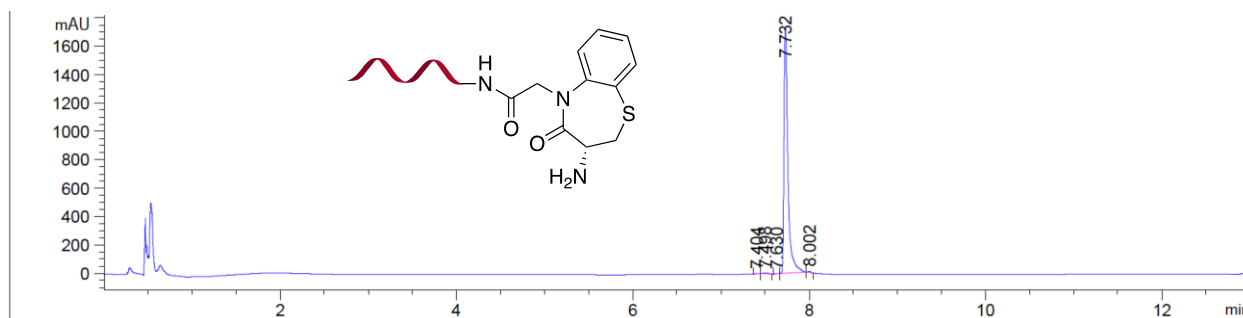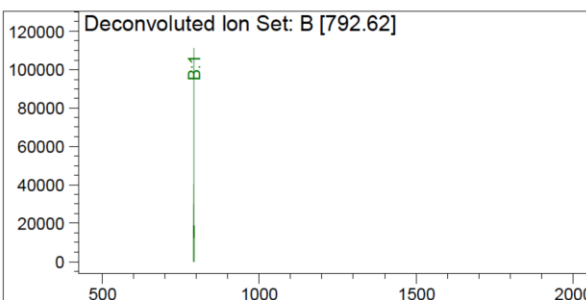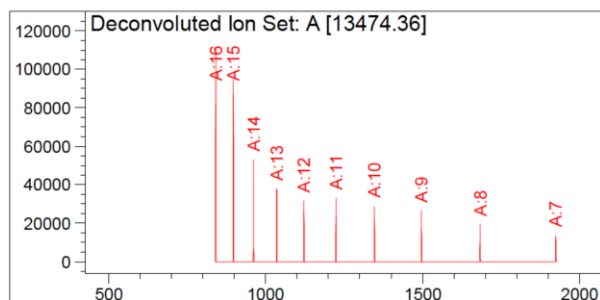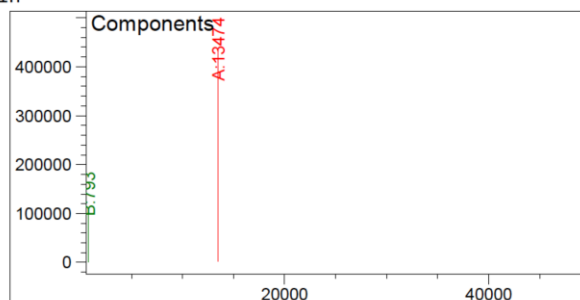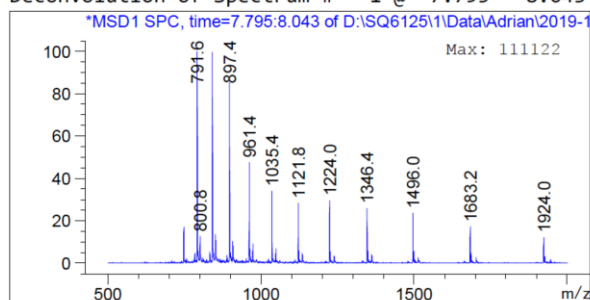
Figure 6.3.6. LC-ESI-MS chromatogram of compound **8**, t_R: 7.732 min (DAD), 7.861 min (TIC). Expected mass 13474.24, observed 13474.36.
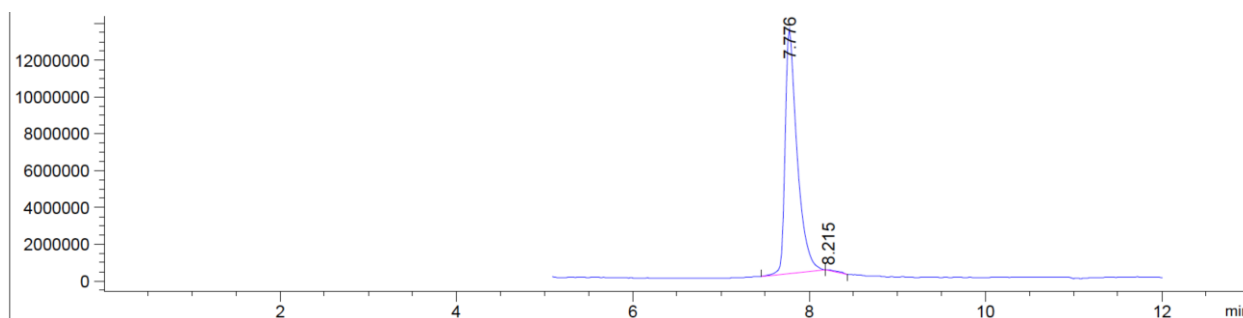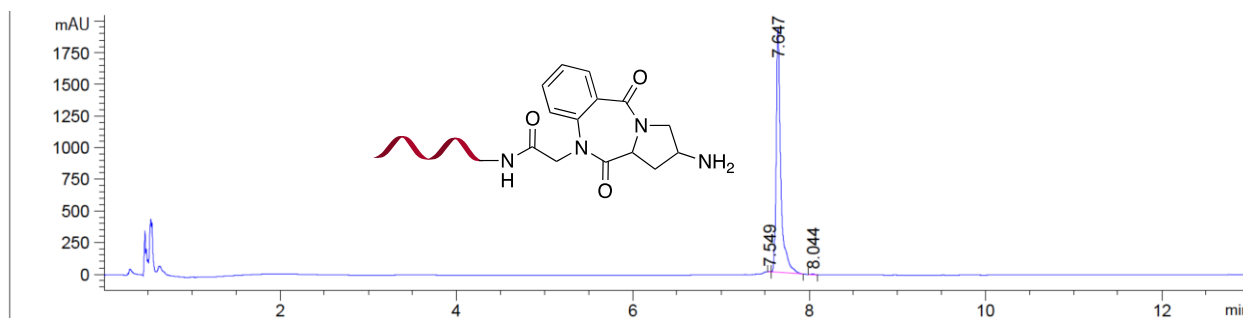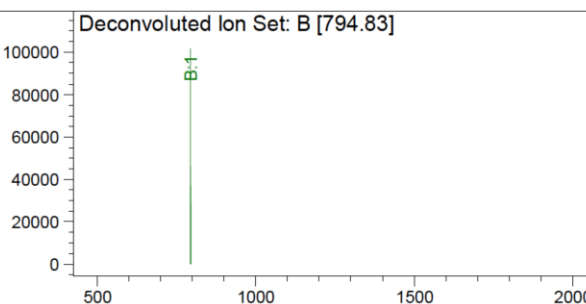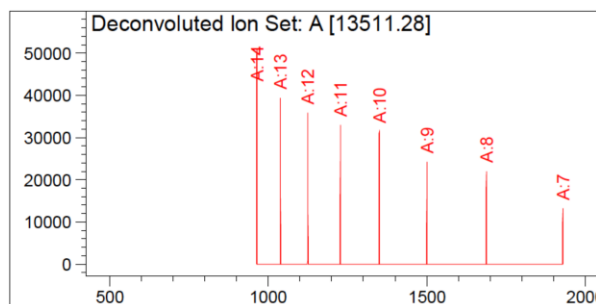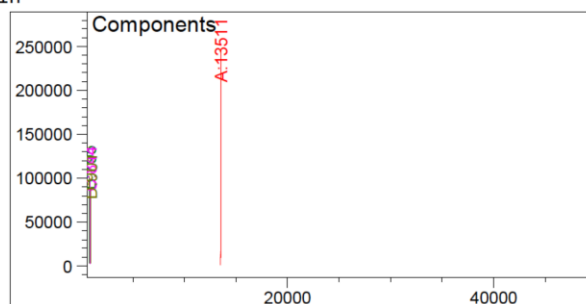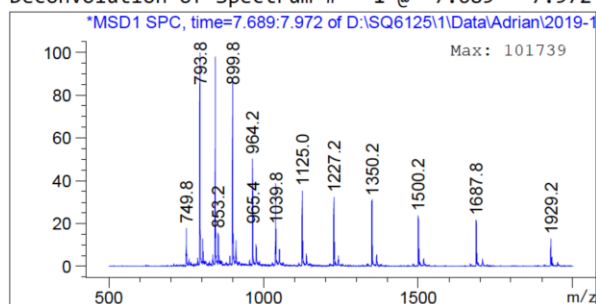
Figure 6.3.7. LC-ESI-MS chromatogram of compound **9**, t_R: 7.647 min (DAD), 7.776 min (TIC). Expected mass 13511.24, observed 13511.28.
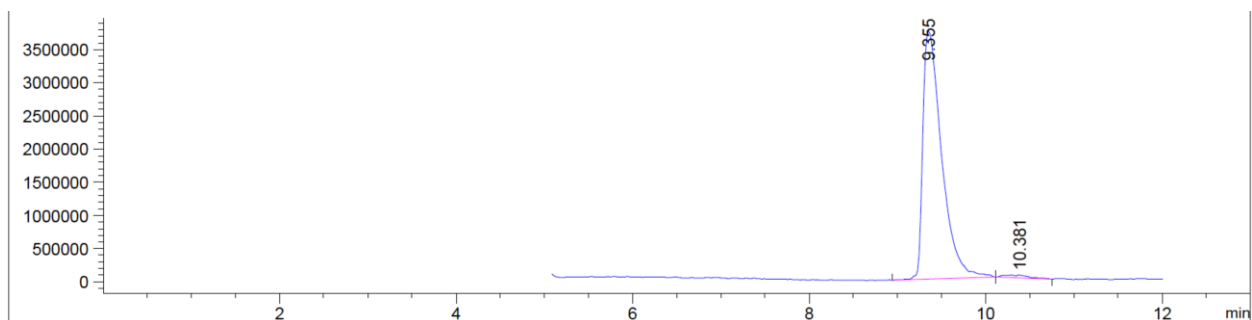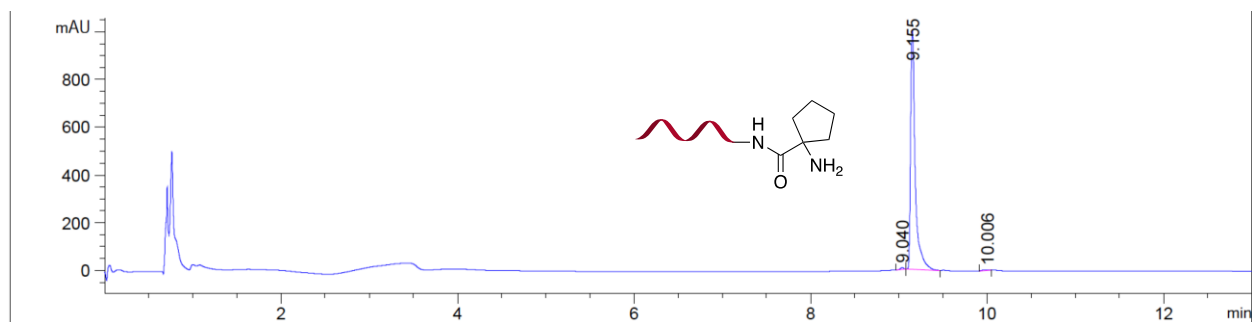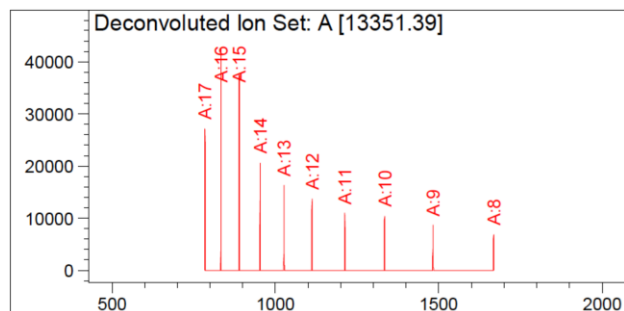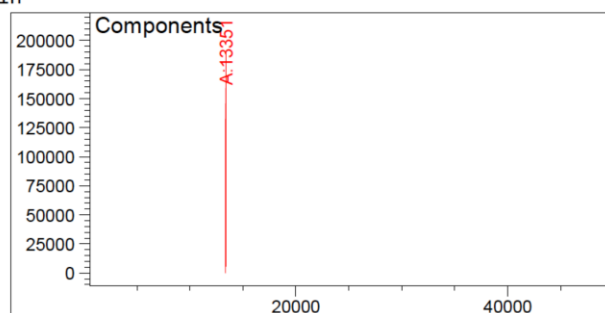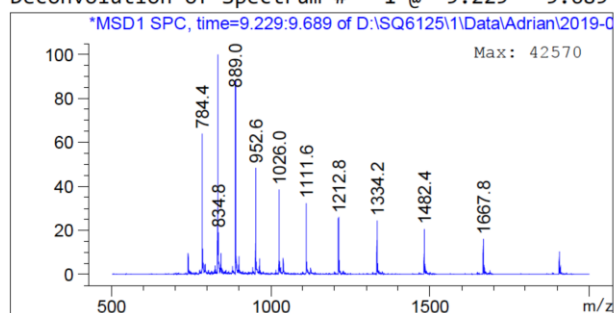
Figure 6.3.8. LC-ESI-MS chromatogram of compound **10**, t_R: 9.155 min (DAD), 9.355 min (TIC). Expected mass 13351.11, observed 13351.39.
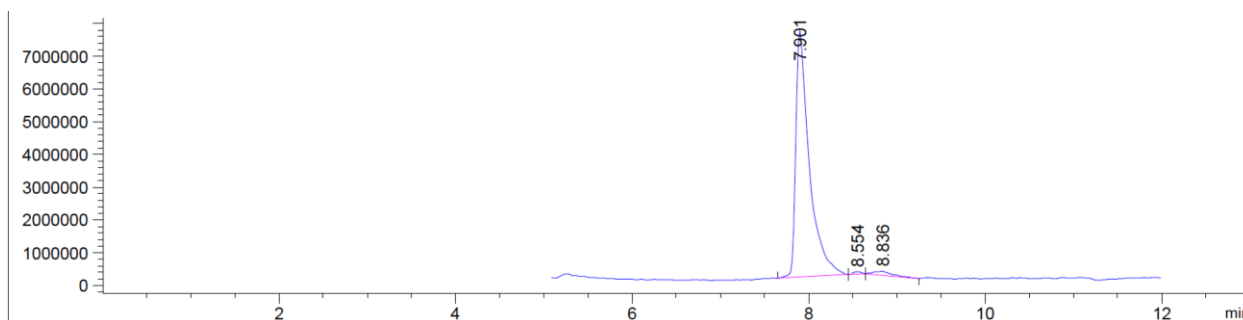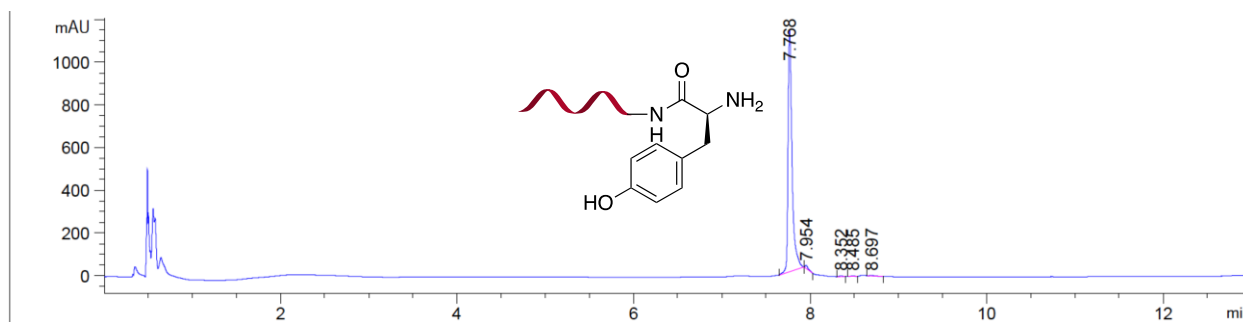
Deconvolution of Spectrum #   1 @   7.812 - 8.220 min
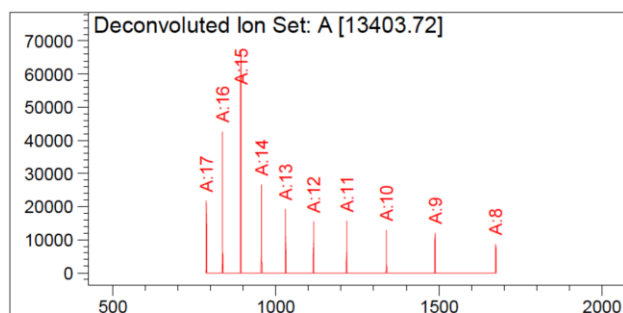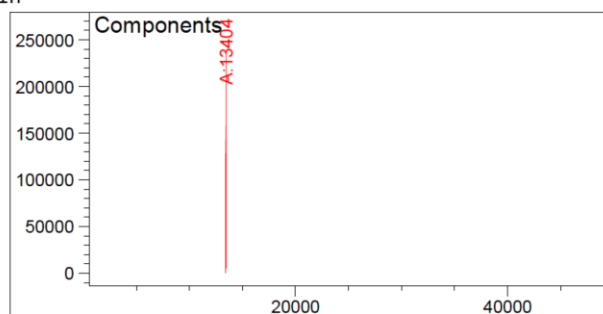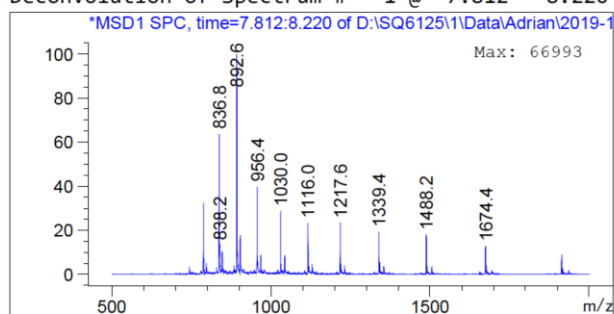
Component	Molecular Weight	Absolute Abundance	Relative Abundance
A	13403.72	237846	100.00

*** End of Report ***

Figure 6.3.9. LC-ESI-MS chromatogram of compound **11**, t_R: 7.768 min (DAD), 7.901 min (TIC). Expected mass 13403.14, observed 13403.72.
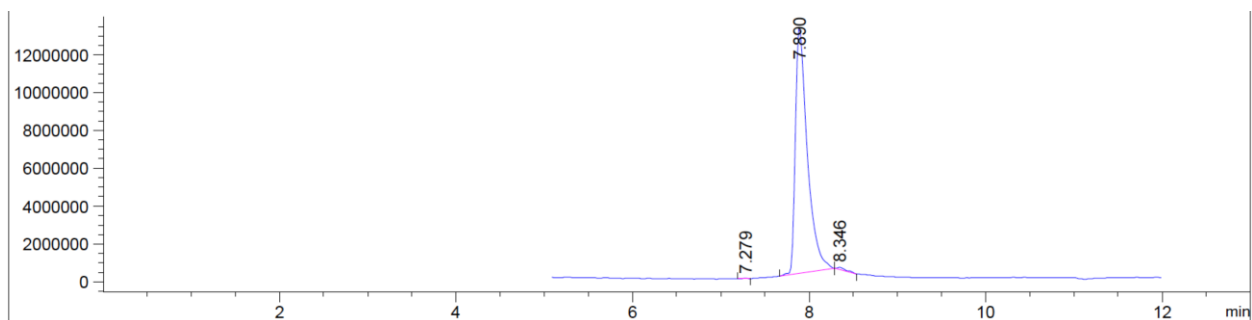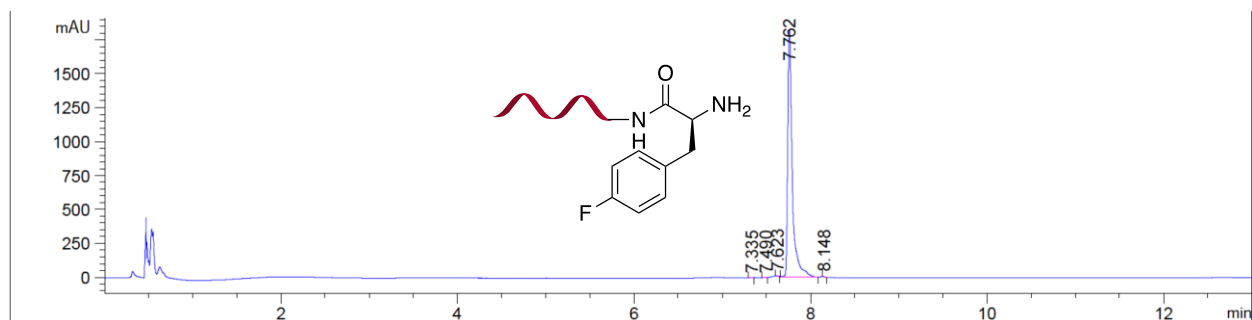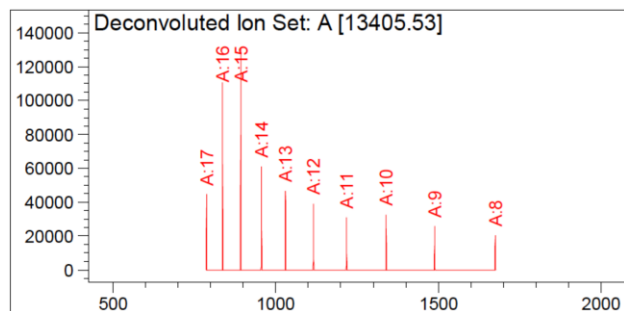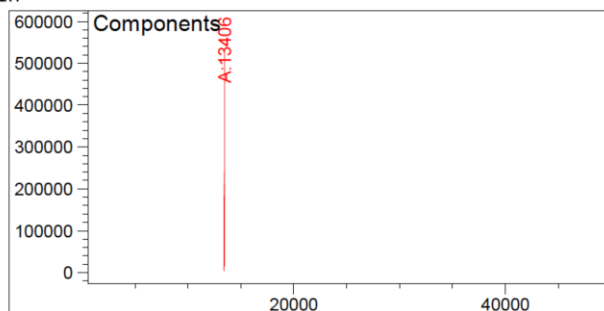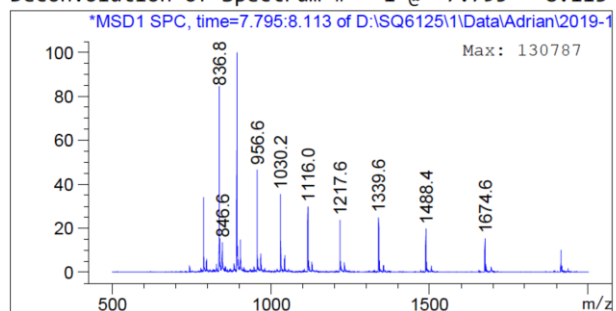
Figure 6.3.10. LC-ESI-MS chromatogram of compound **12**, t_R: 7.762 min (DAD), 7.890 min (TIC). Expected mass 13405.14, observed 13405.53.
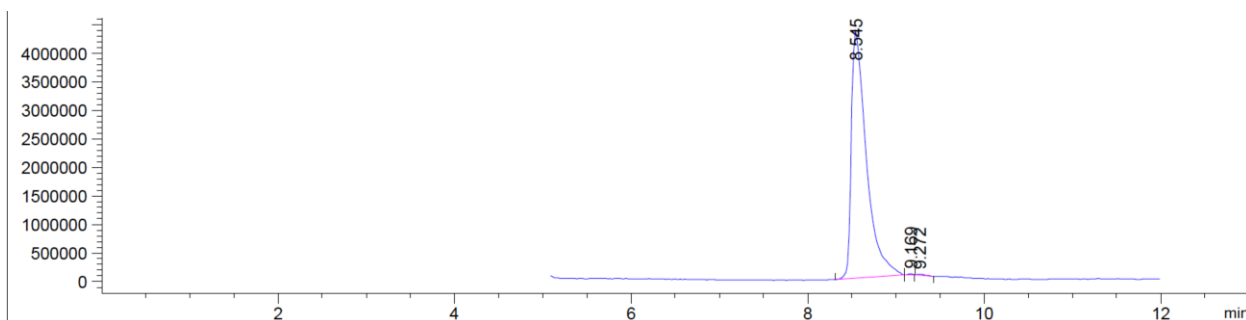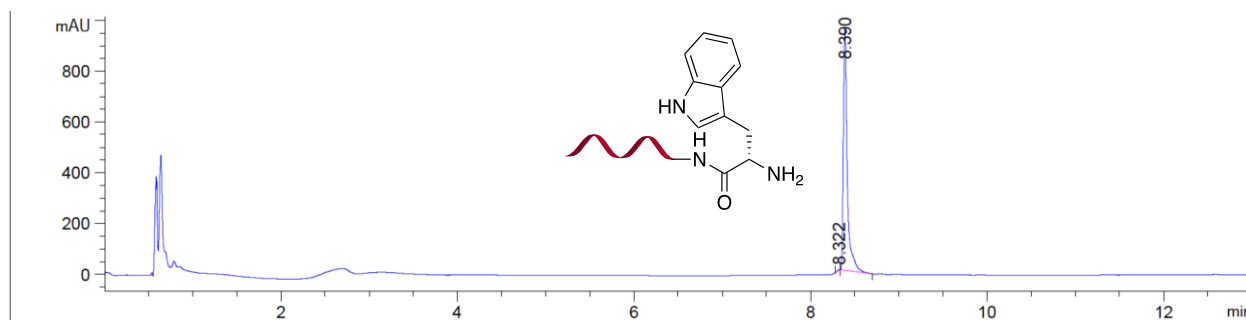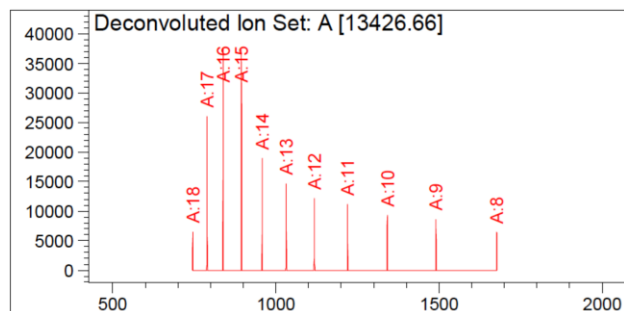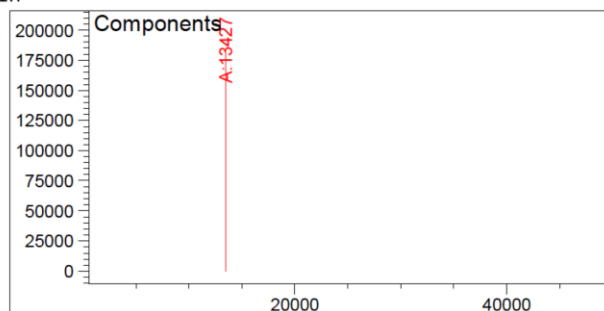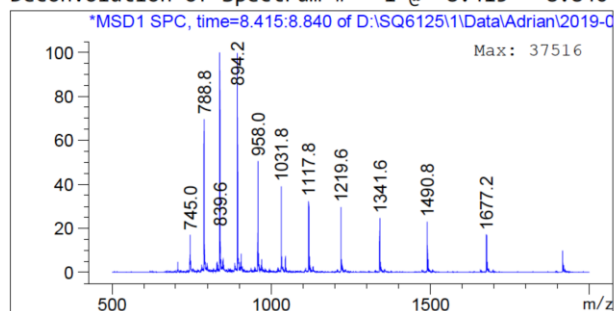
Figure 6.3.11. LC-ESI-MS chromatogram of compound **13**, t_R: 8.390 min (DAD), 8.545 min (TIC). Expected mass 13426.18, observed 13426.66.
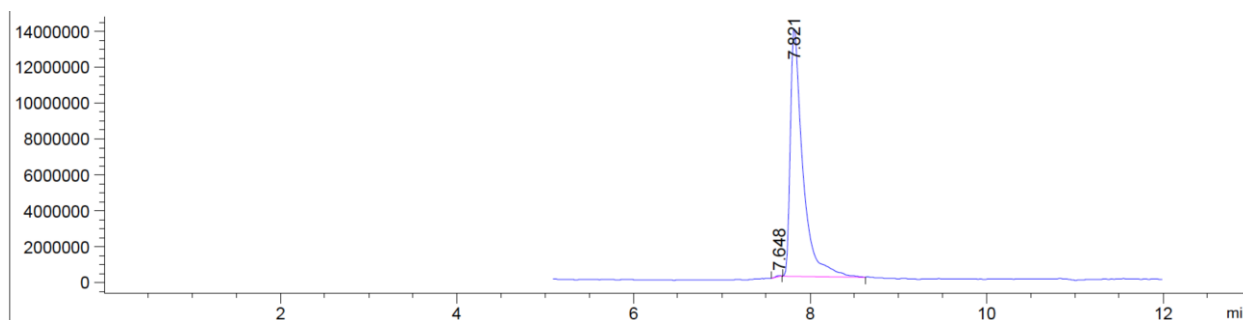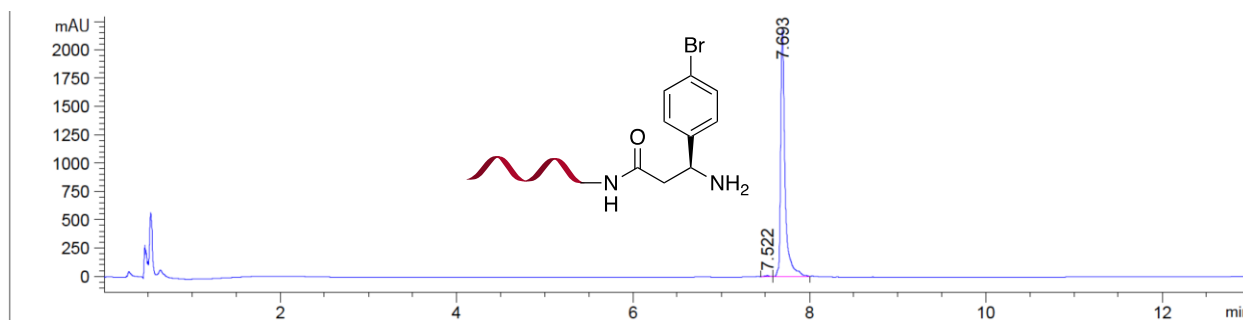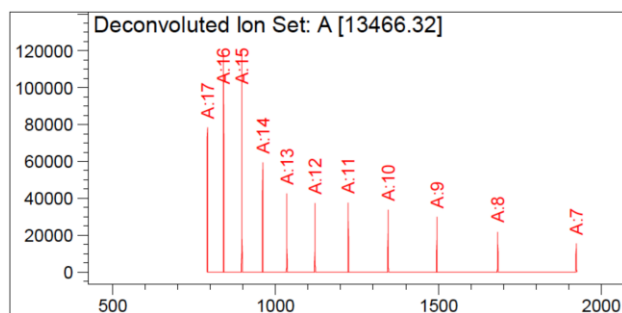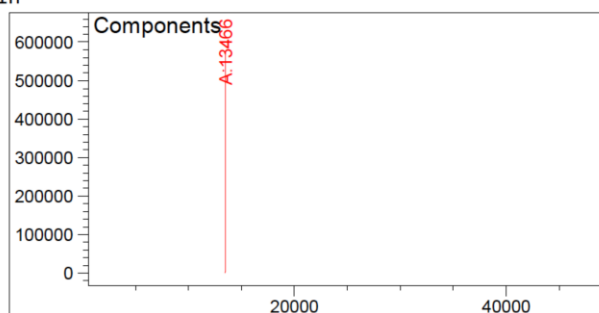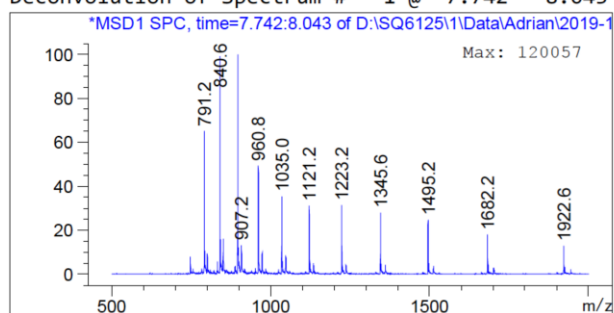
Figure 6.3.12. LC-ESI-MS chromatogram of compound **14**, t_R: 7.693 min (DAD), 7.821 min (TIC). Expected mass 13465.03, observed 13466.32.
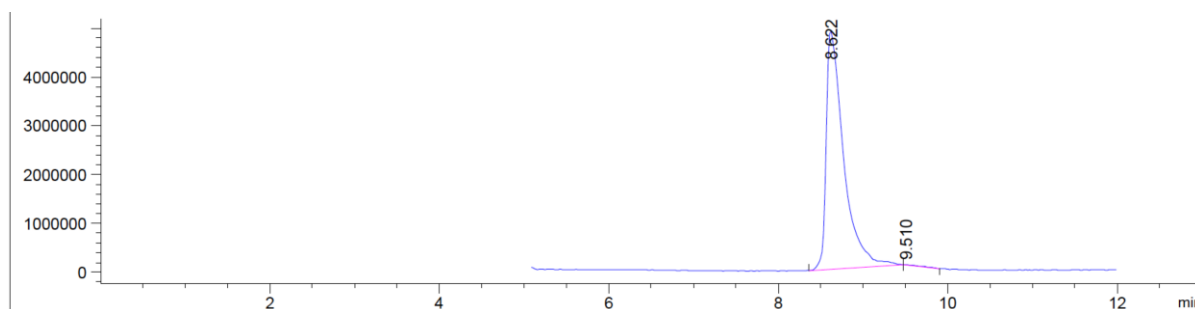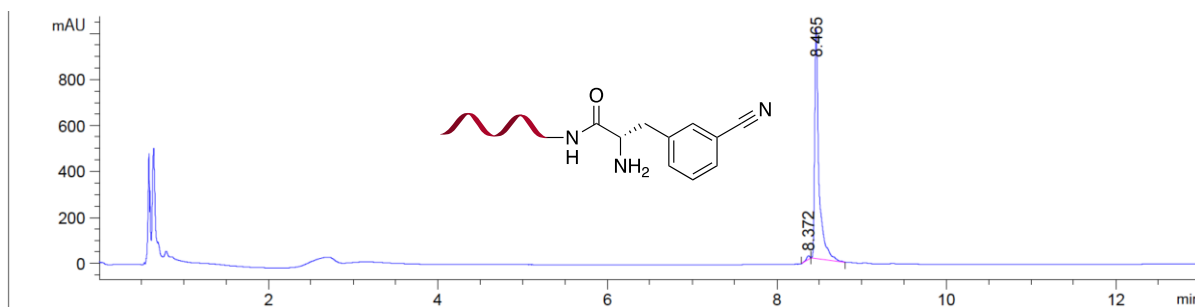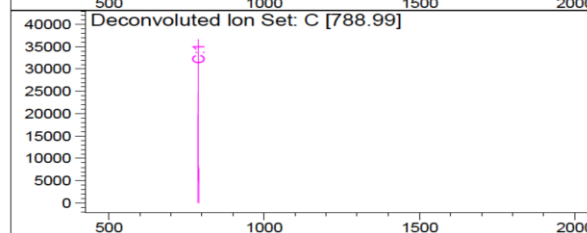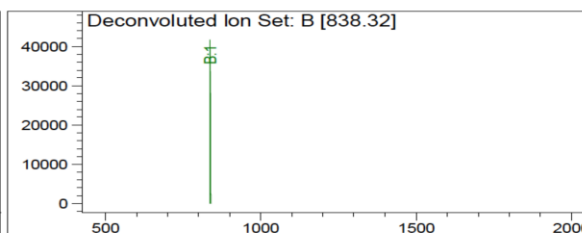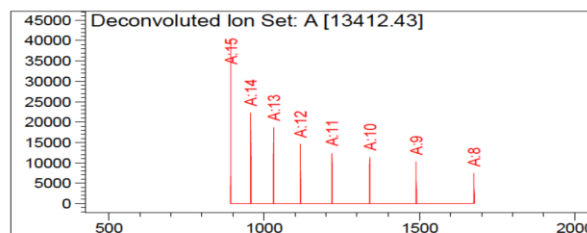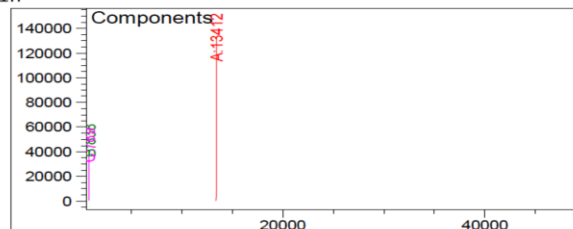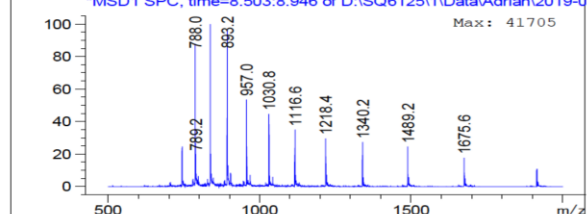
Figure 6.3.13. LC-ESI-MS chromatogram of compound **15**, t_R: 8.465 min (DAD), 8.622 min (TIC). Expected mass 13412.16, observed 13412.43.
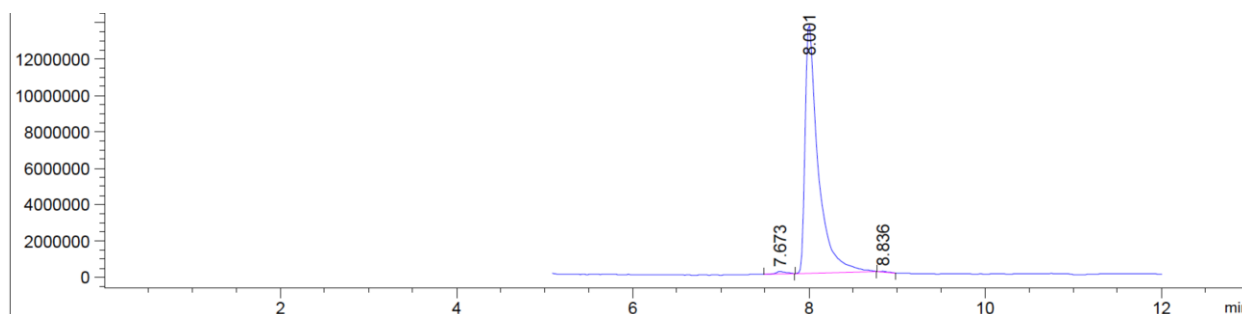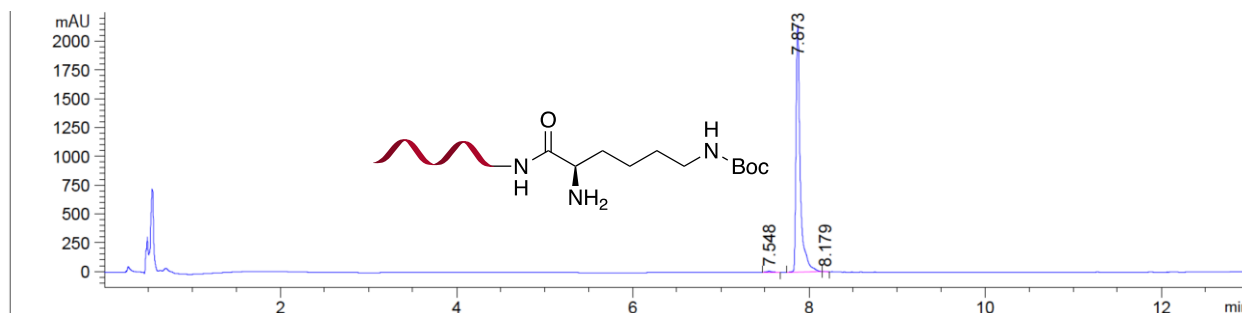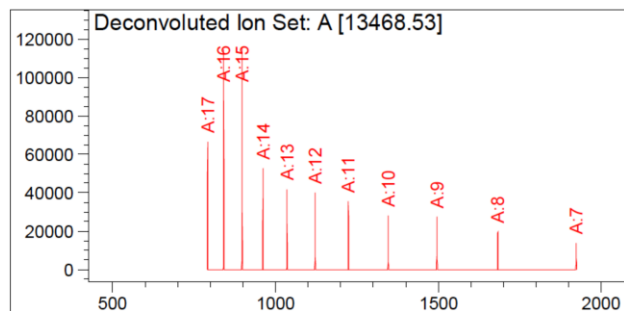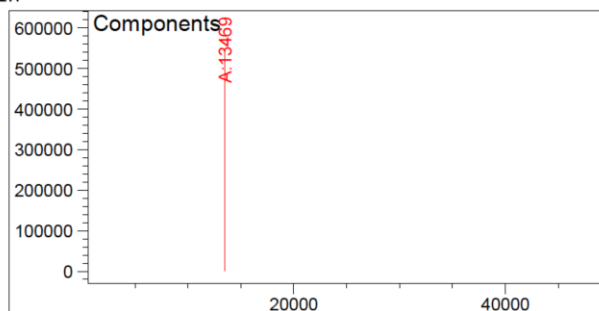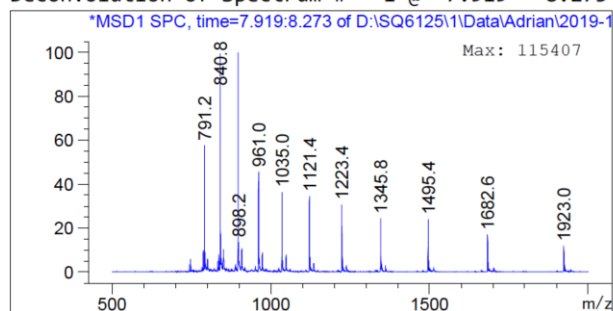
Figure 6.3.14. LC-ESI-MS chromatogram of compound **16**, t_R: 7.873 min (DAD), 8.001 min (TIC). Expected mass 13468.26, observed 13468.53.
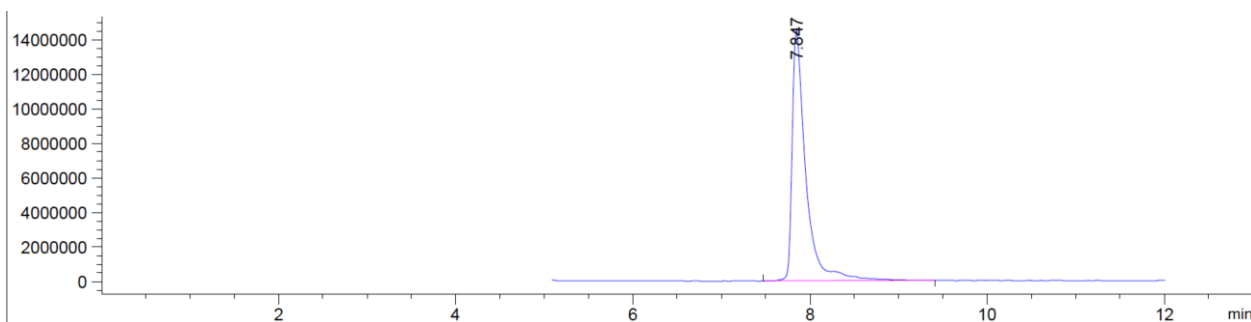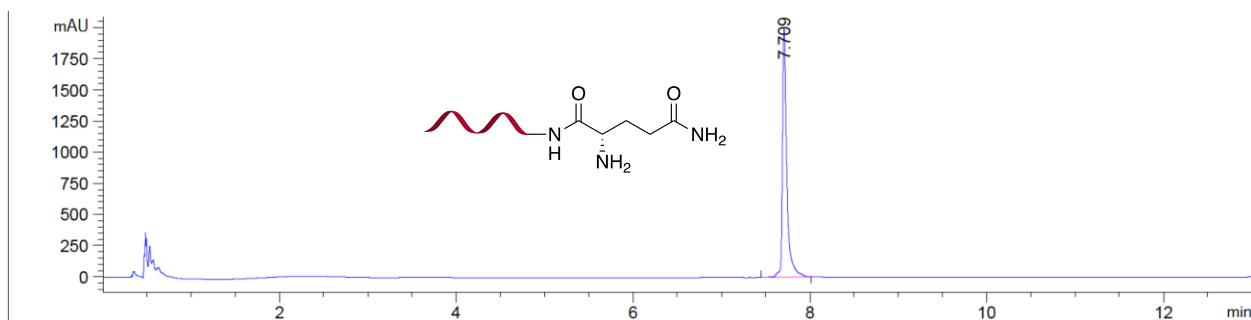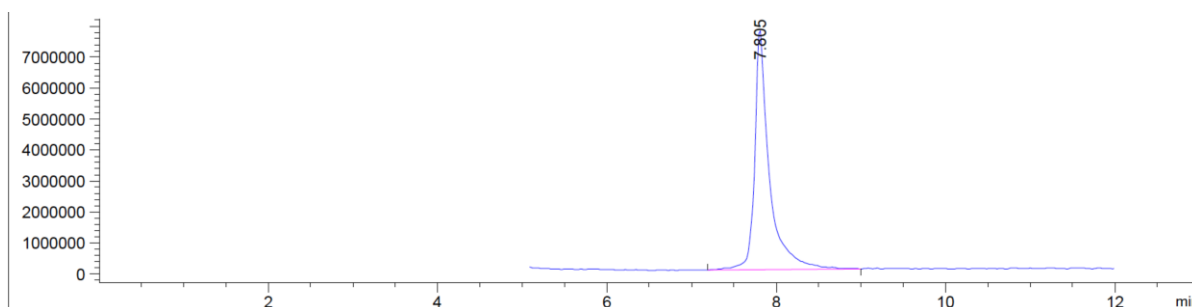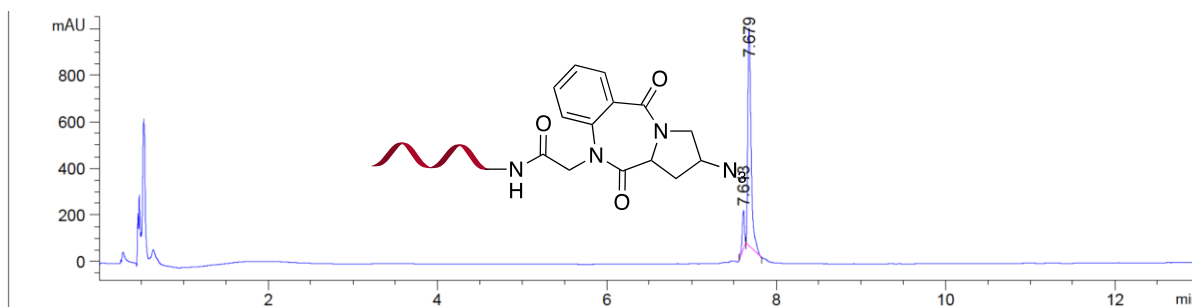
Deconvolution of Spectrum # 1 @ 7.759 - 8.042 min
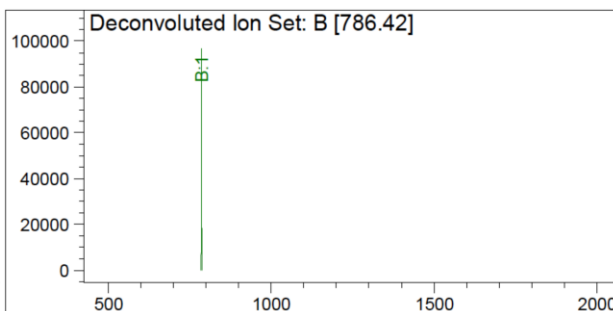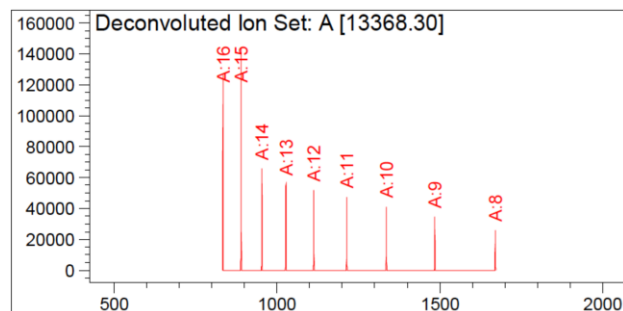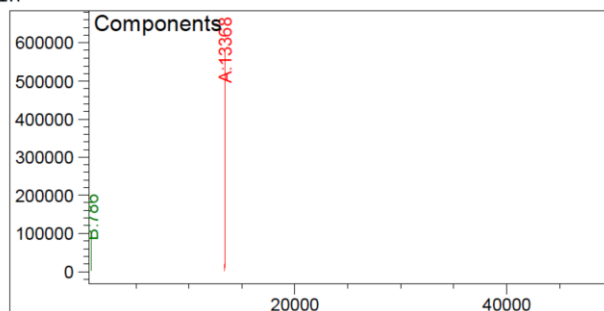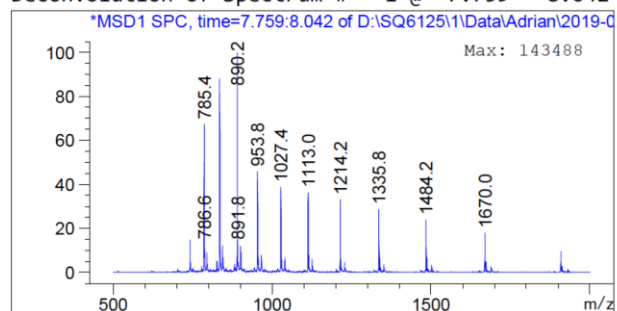
Component   Molecular   Absolute   Relative
             Weight   Abundance   Abundance
    A   13368.30   582873   100.00
    B   786.42   96706   16.59
                 *** End of Report ***

Figure 6.3.15. LC-ESI-MS chromatogram of compound **17**, t_R: 7.709 min (DAD), 7.847 min (TIC). Expected mass 13368.1, observed 13368.33.
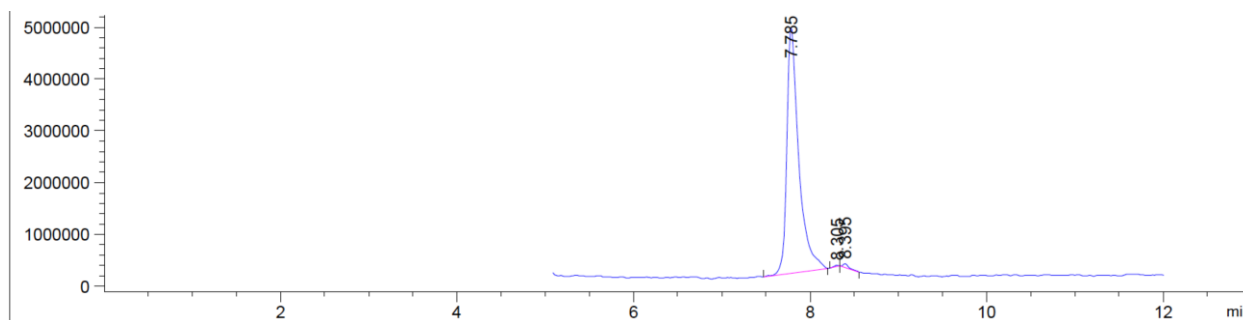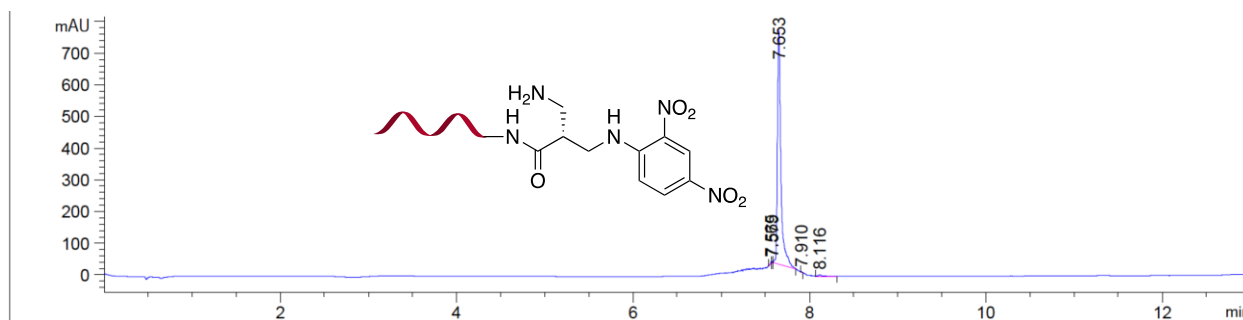
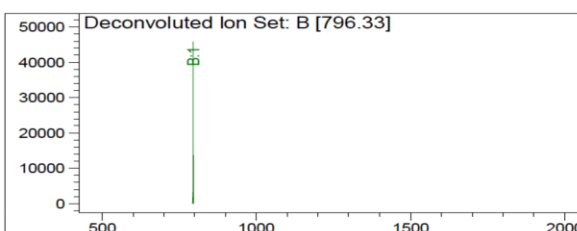**Deconvolution of Spectrum #   1 @   7.706 - 7.883 min**
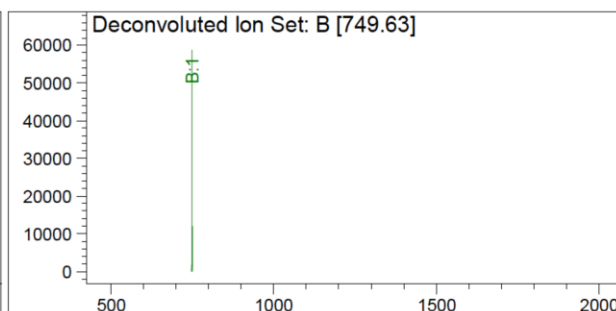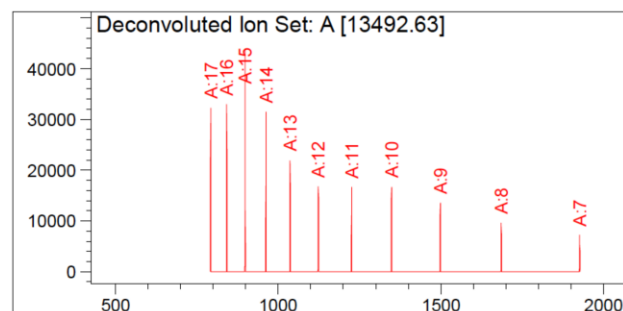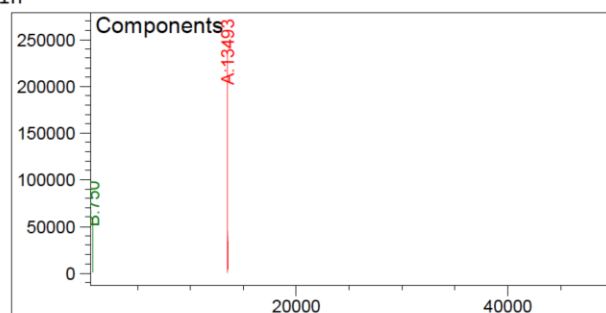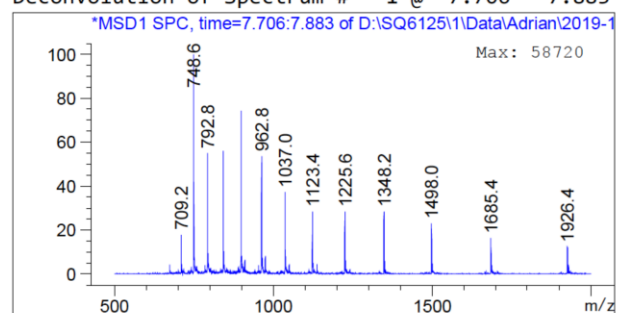
Component	Molecular Weight	Absolute Abundance	Relative Abundance
A	13492.63	237411	100.00
B	749.63	58720	24.73

*** End of Report ***

Figure 6.3.16. LC-ESI-MS chromatogram of compound **18**, t_R: 7.653 min (DAD), 7.785 min (TIC). Expected mass 13492.15, observed 13492.63.
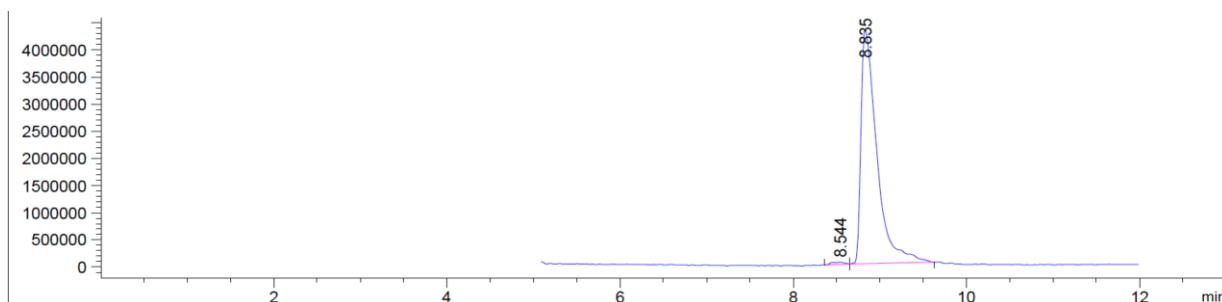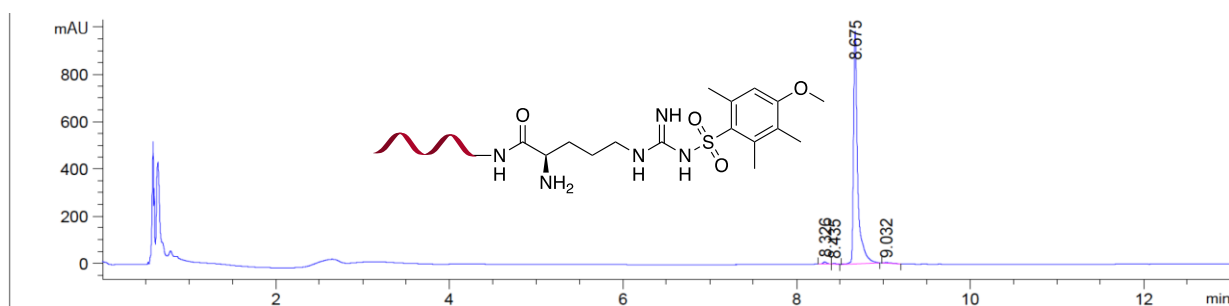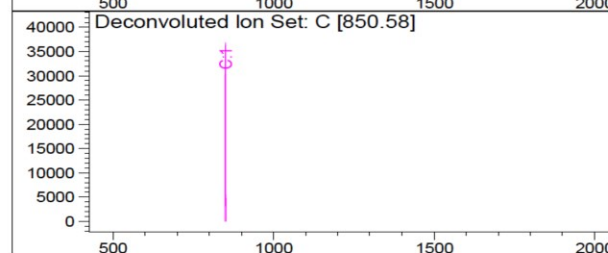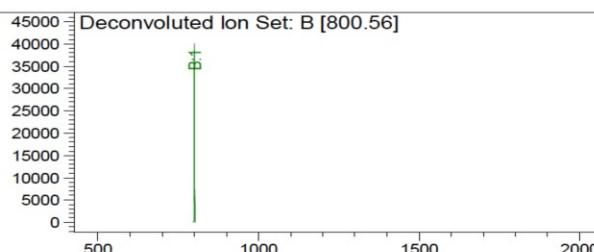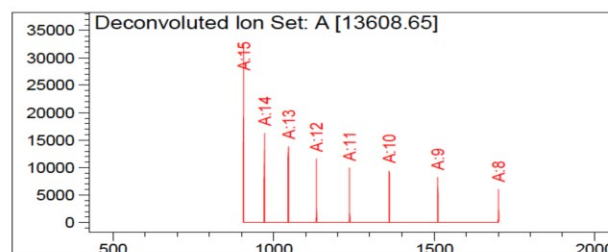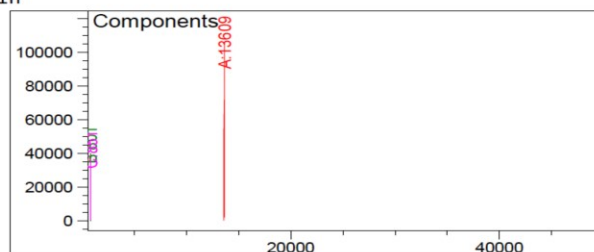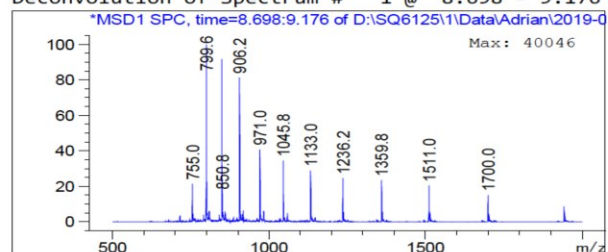
Figure 6.3.17. LC-ESI-MS chromatogram of compound **19**, t_R: 8.675 min (DAD), 8.835 min (TIC). Expected mass 13608.42, observed 13608.65.
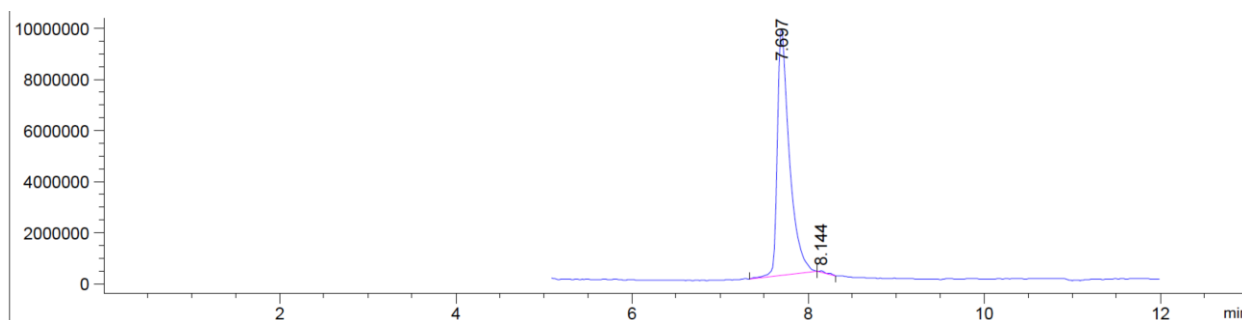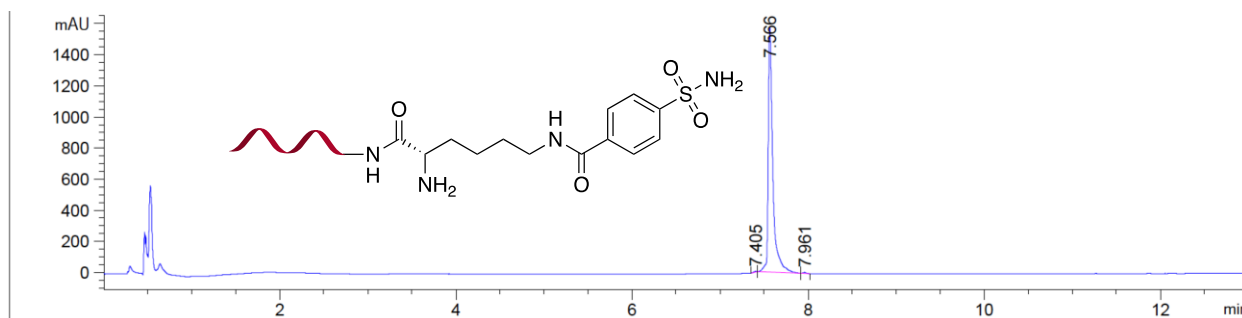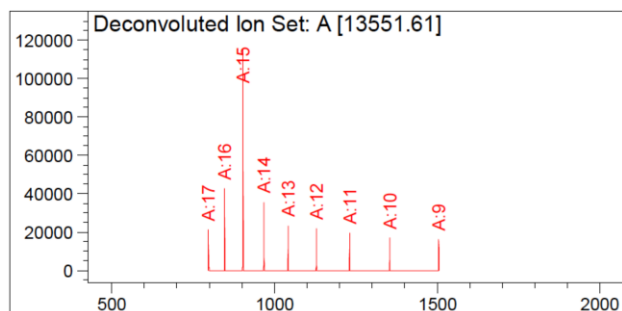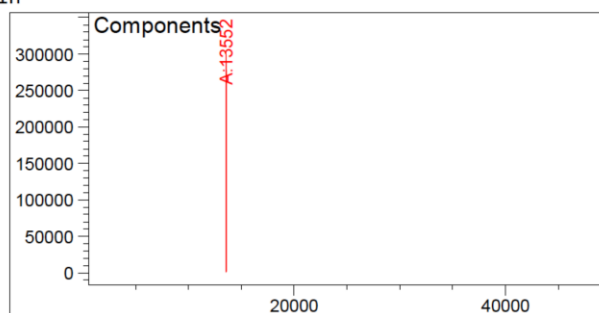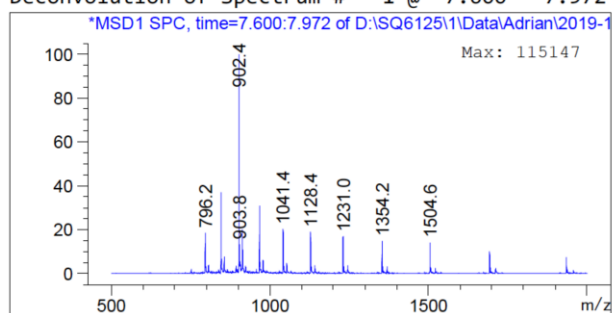
Figure 6.3.18. LC-ESI-MS chromatogram of compound **20**, t_R: 7.566 min (DAD), 7.697 min (TIC). Expected mass 13551.32, observed 13551.61.
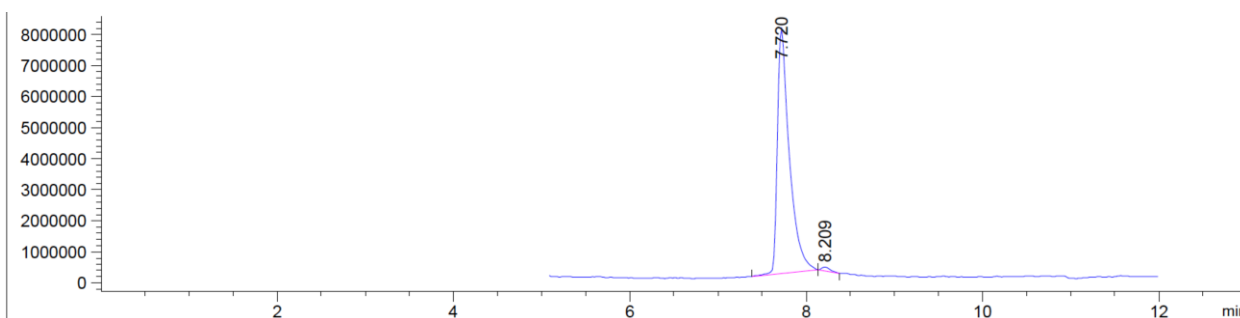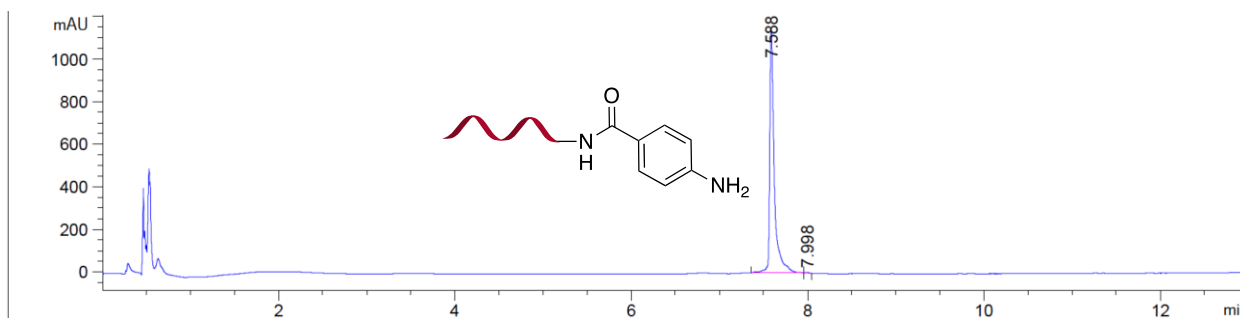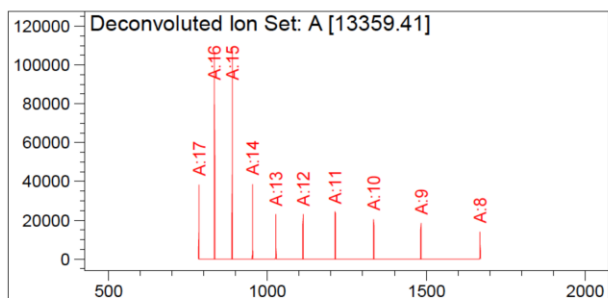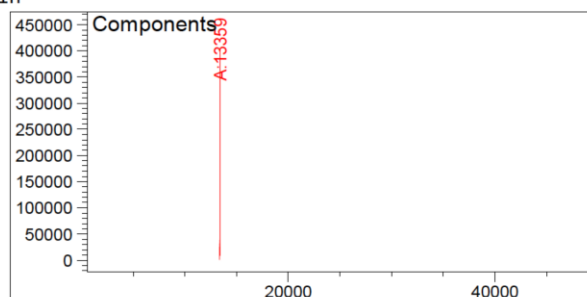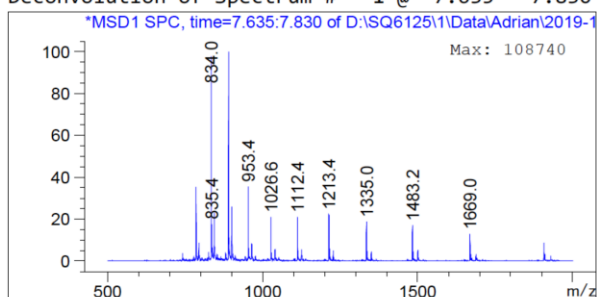
Figure 6.3.19. LC-ESI-MS chromatogram of compound **21**, t_R: 7.588 min (DAD), 7.720 min (TIC). Expected mass 13359.09, observed 13359.41.
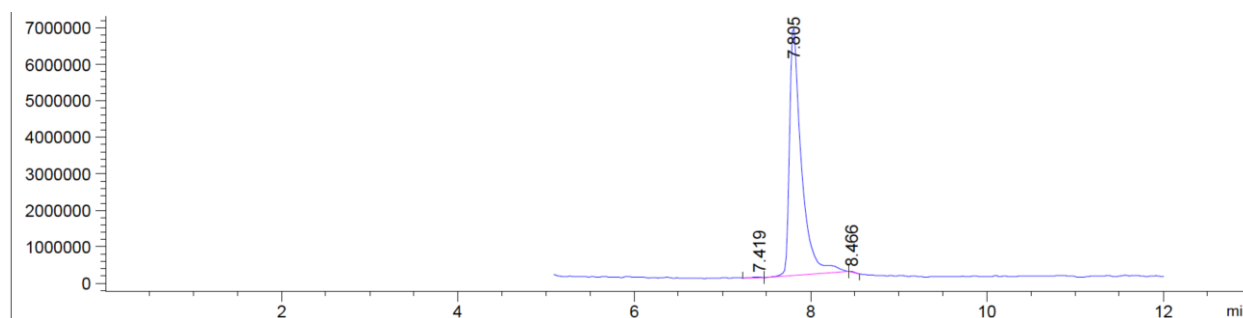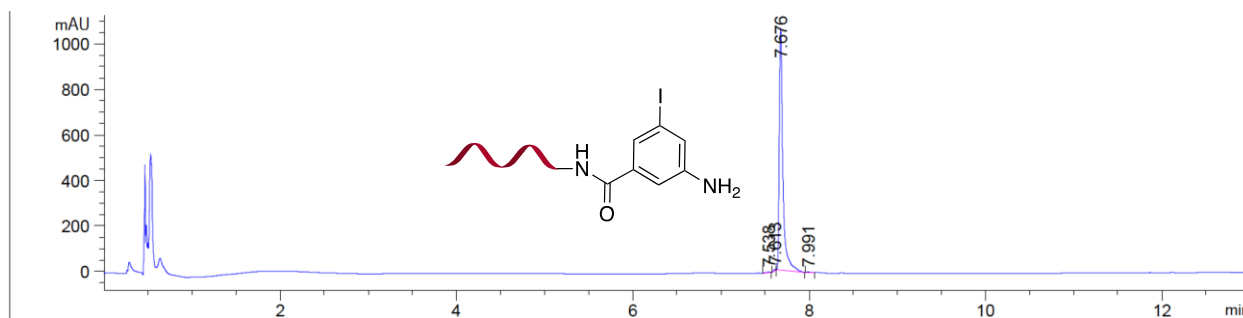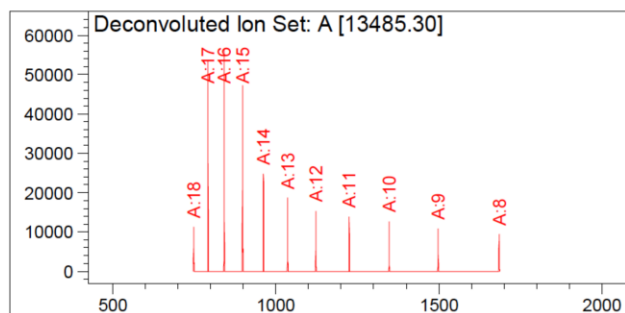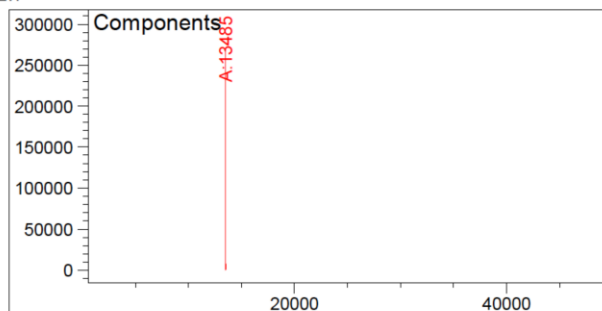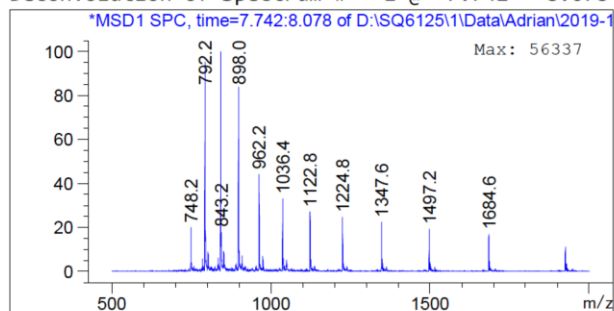
Figure 6.3.20. LC-ESI-MS chromatogram of compound **22**, t_R: 7.676 min (DAD), 7.805 min (TIC). Expected mass 13484.99, observed 13485.30.

DNA-Conjugated Azides (3, 23–41)
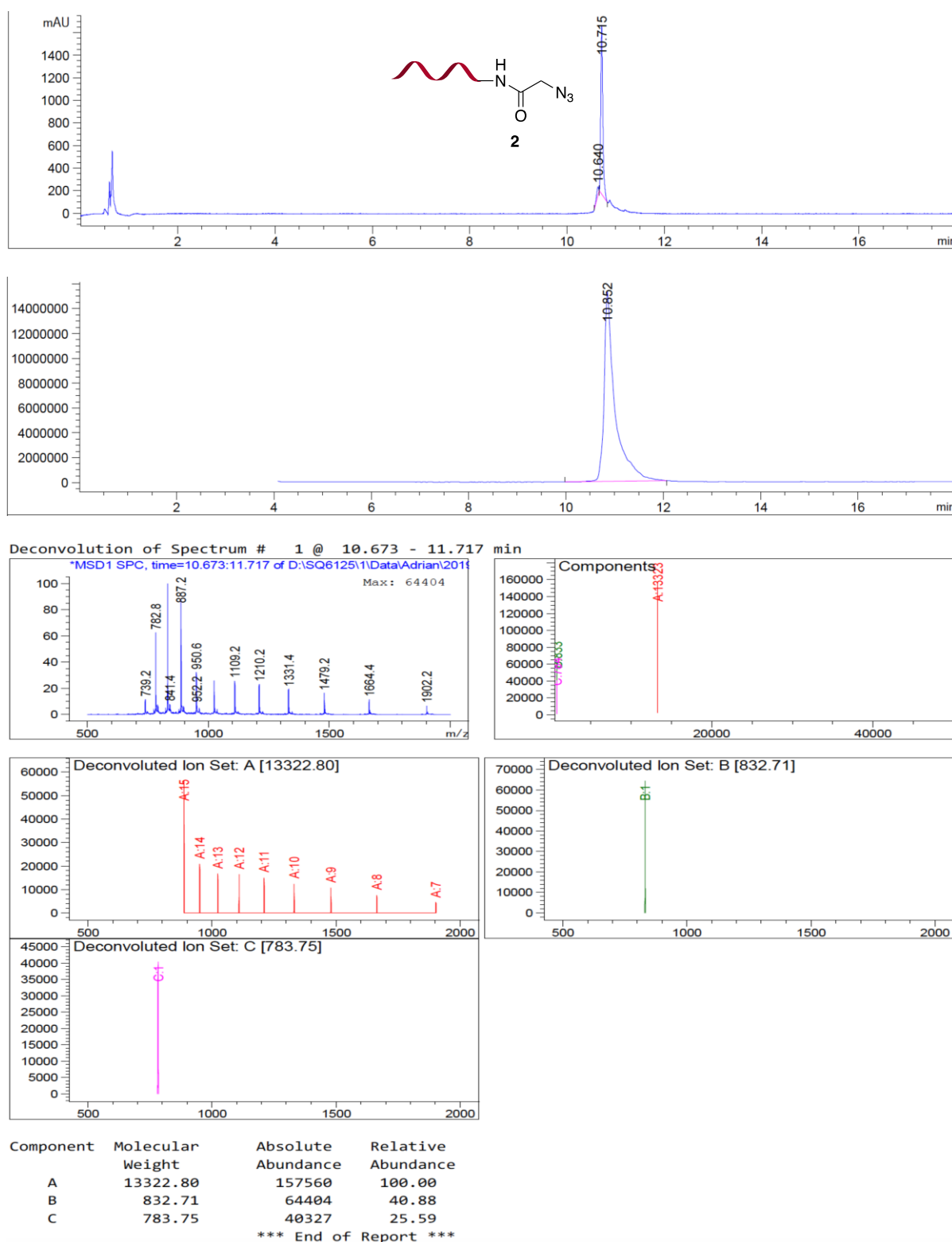
Figure 6.3.21. LC-ESI-MS chromatogram of compound **3**, t_R: 10.715 min (DAD), 10.852 min (TIC). Expected mass 13323.02, observed 13322.80.
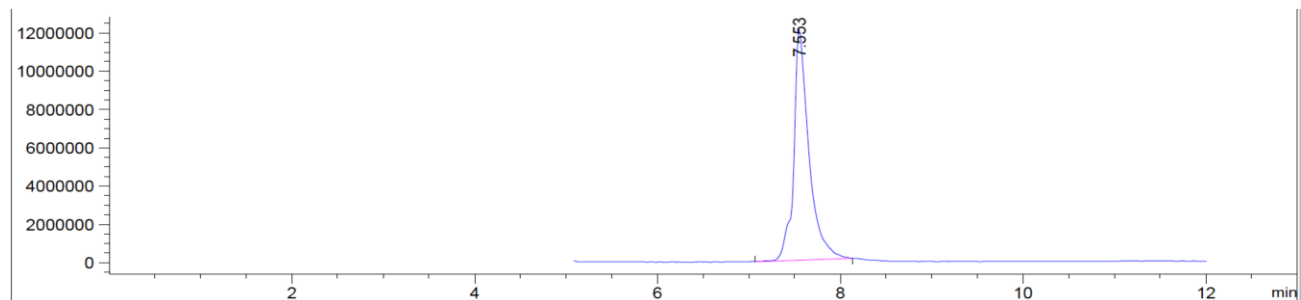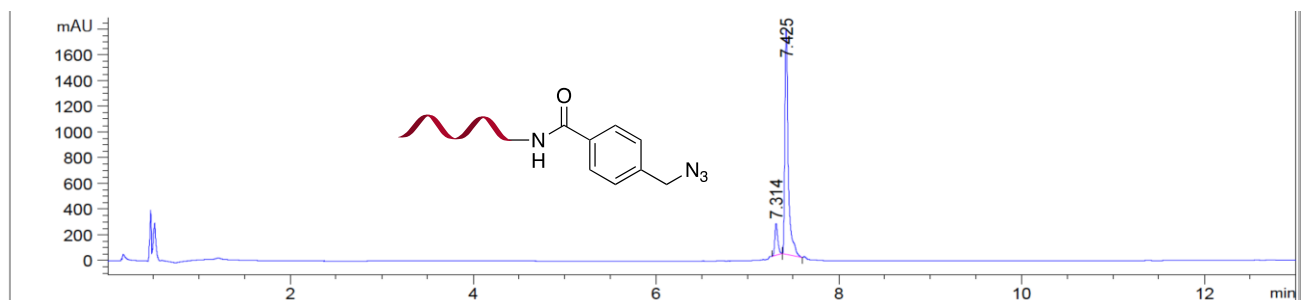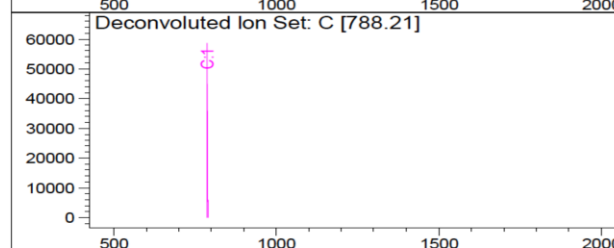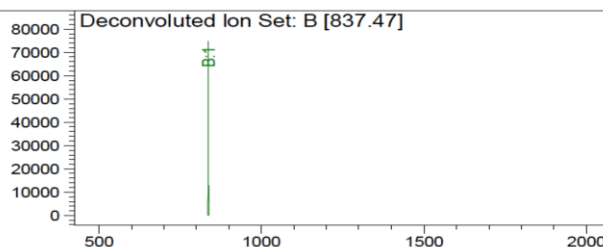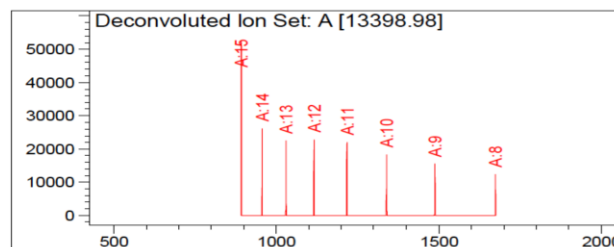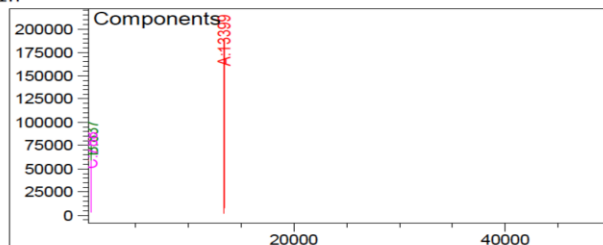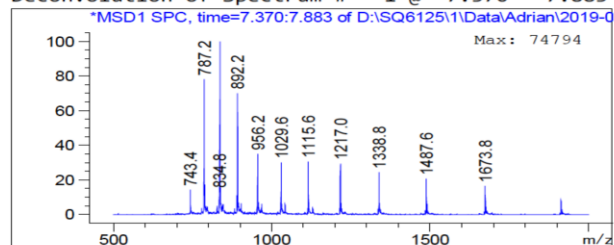
Figure 6.3.22. LC-ESI-MS chromatogram of compound **23**, t_R: 7.425 min (DAD), 7.553 min (TIC). Expected mass 13399.11, observed 13398.98.
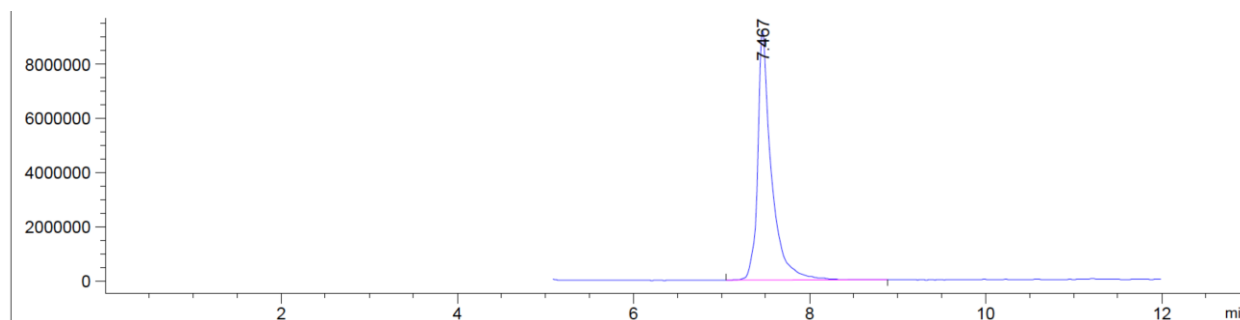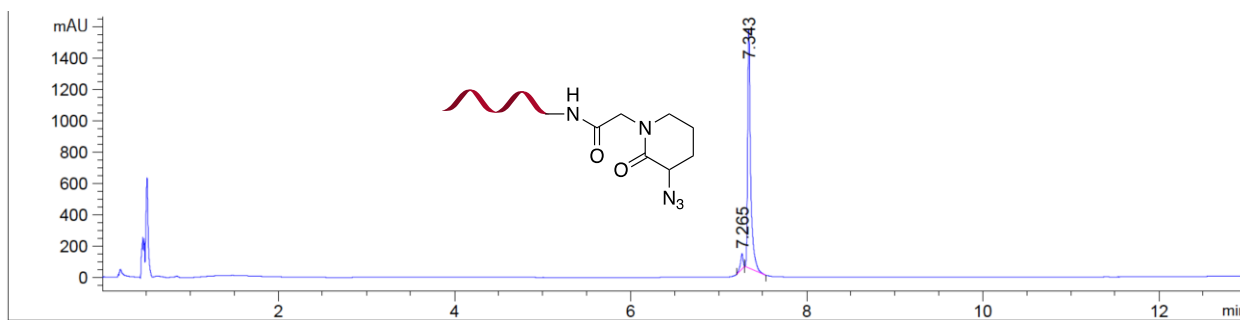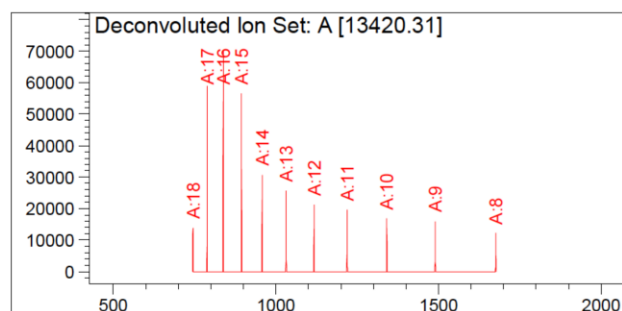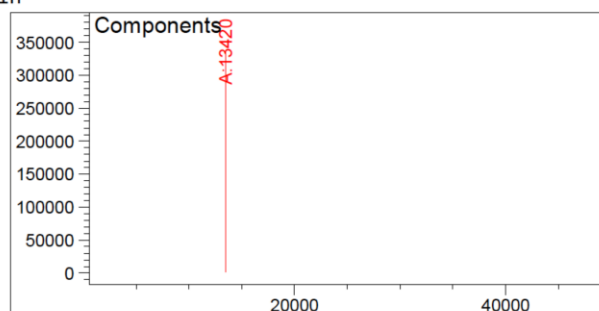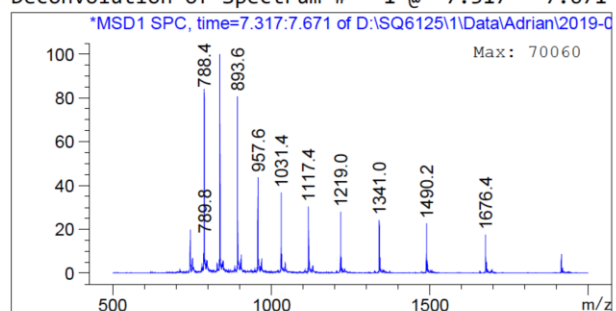
Figure 6.3.23. LC-ESI-MS chromatogram of compound **24**, t_R: 7.343 min (DAD), 7.467 min (TIC). Expected mass 13420.14, observed 13420.31.
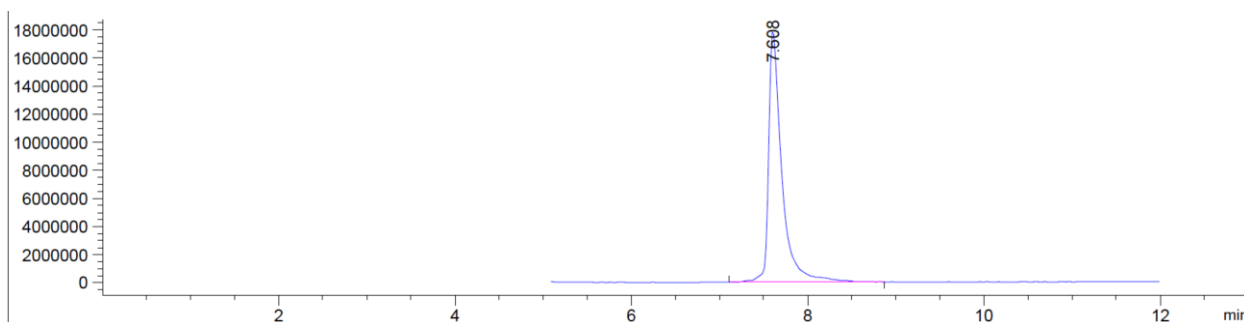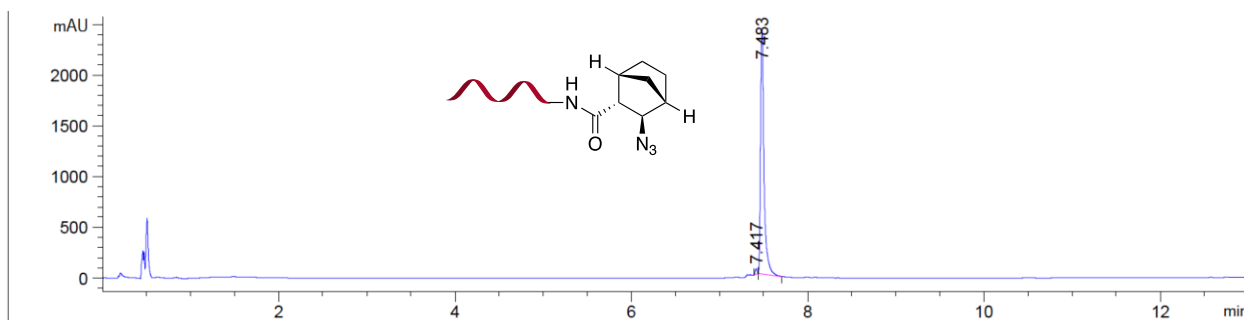
Deconvolution of Spectrum # 1 @ 7.511 - 7.866 min
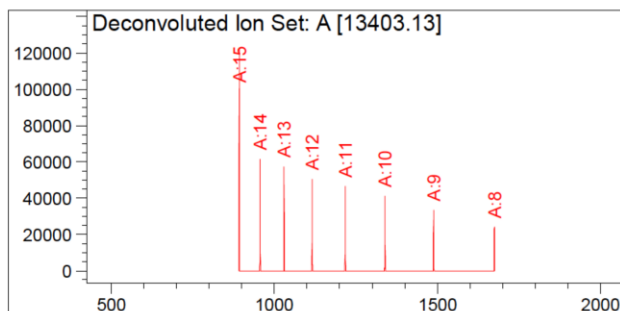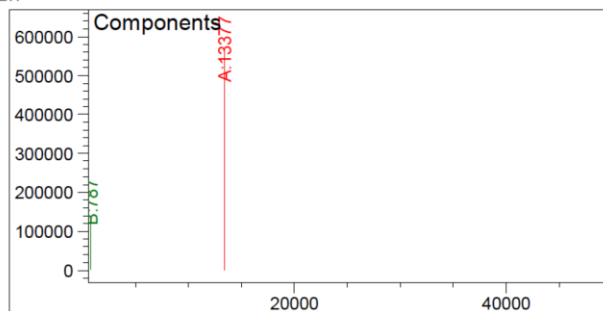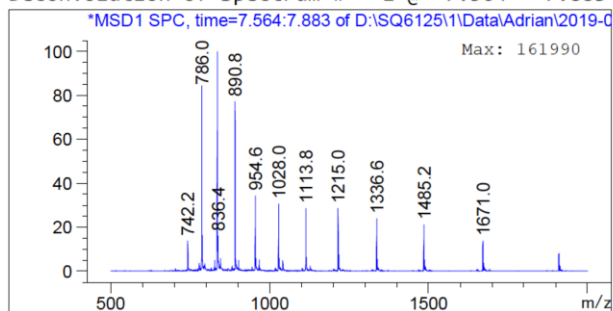
Component	Molecular Weight	Absolute Abundance	Relative Abundance
A	13403.13	423389	100.00
B	837.73	155475	36.72

*** End of Report ***

Figure 6.3.24. LC-ESI-MS chromatogram of compound **25**, t_R: 7.483 min (DAD), 7.608 min (TIC). Expected mass 13403.11, observed 13403.13.
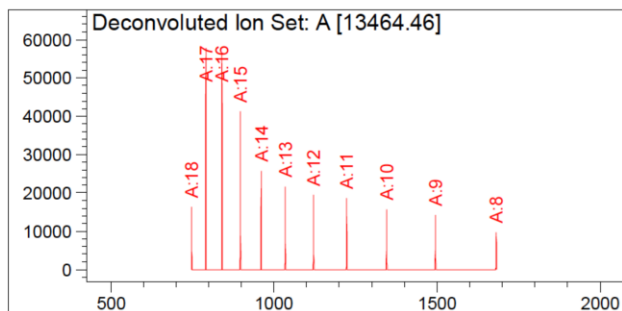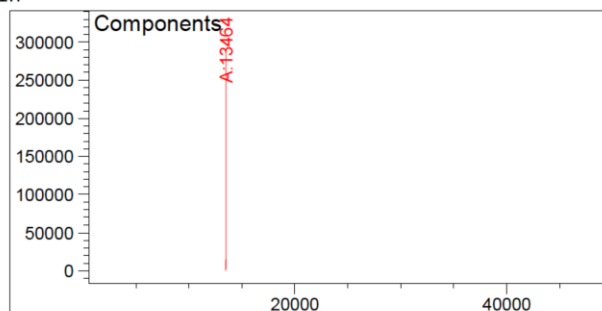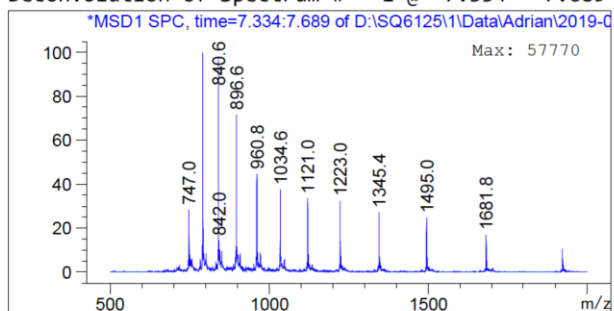
Figure 6.3.25. LC-ESI-MS chromatogram of compound **26**, t_R: 7.360 min (DAD), 7.483 min (TIC): Expected mass 13464.21, observed 13464.46.
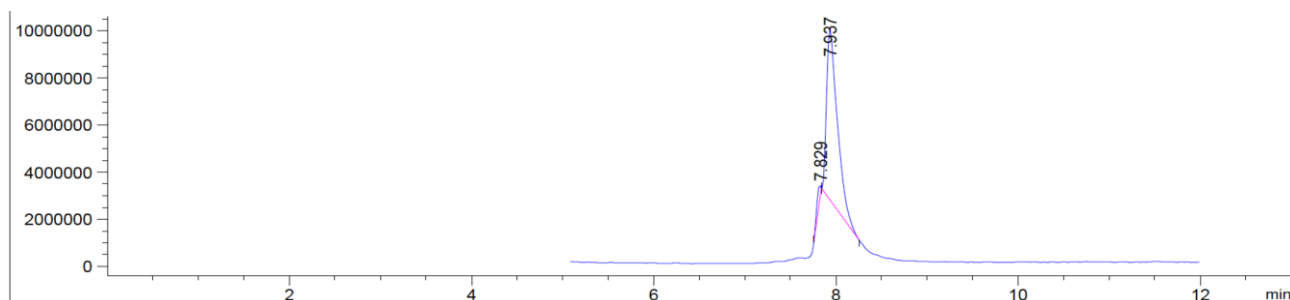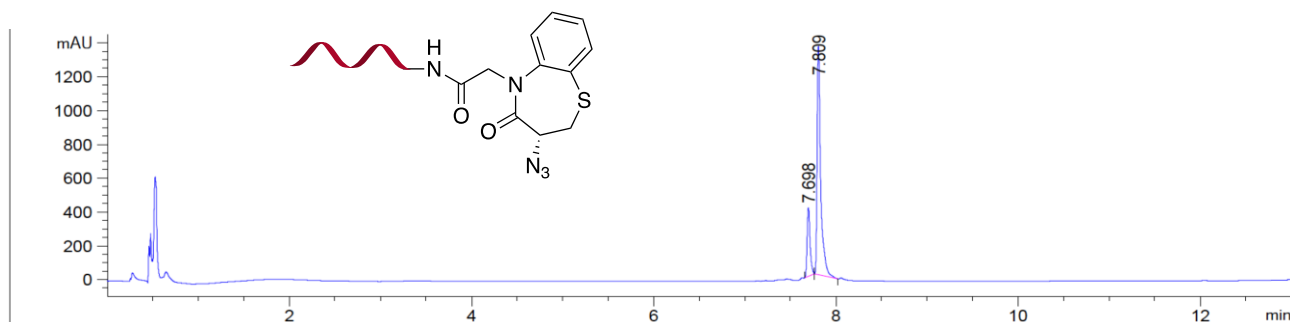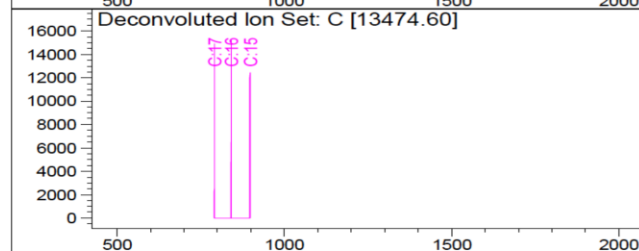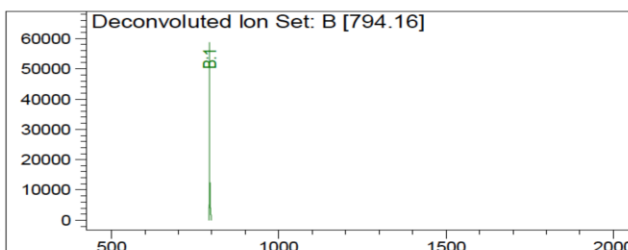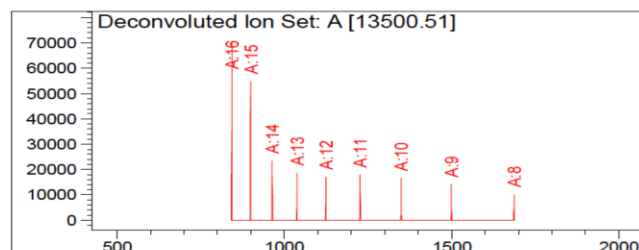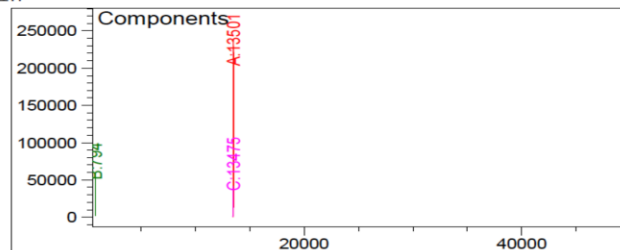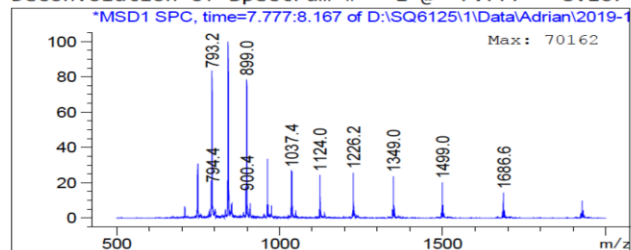
Figure 6.3.26. LC-ESI-MS chromatogram of compound **27**, t_R: 7.009 min (DAD), 7.937 min (TIC). Expected mass 13500.24, observed 13500.51. 3 h reaction time.
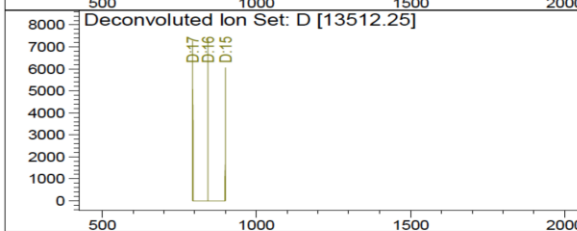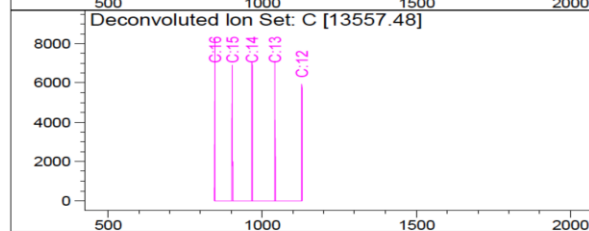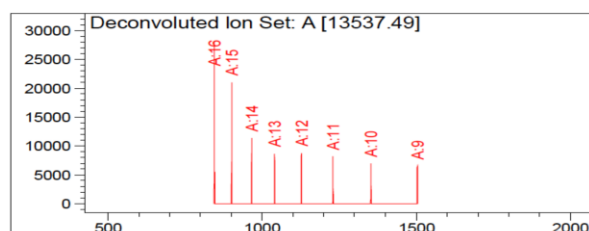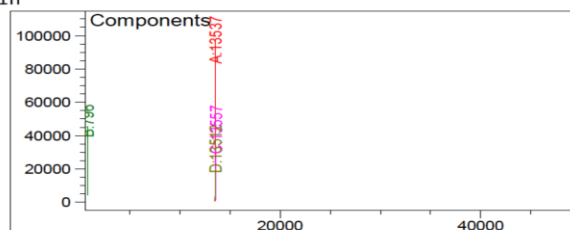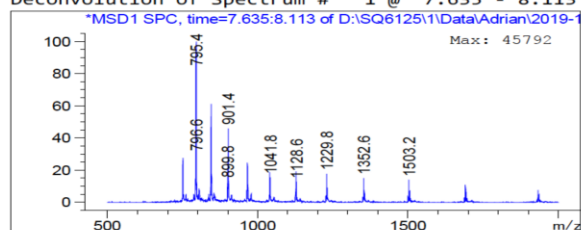
Figure 6.3.27. LC-ESI-MS chromatogram of compound **28**, t_R: 7.679 min (DAD), 7.805 min (TIC). Expected mass 13537.24, observed 13537.49.
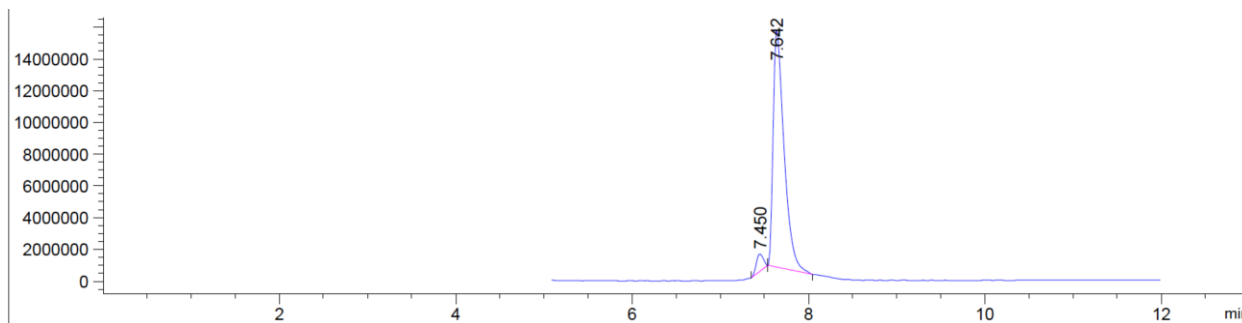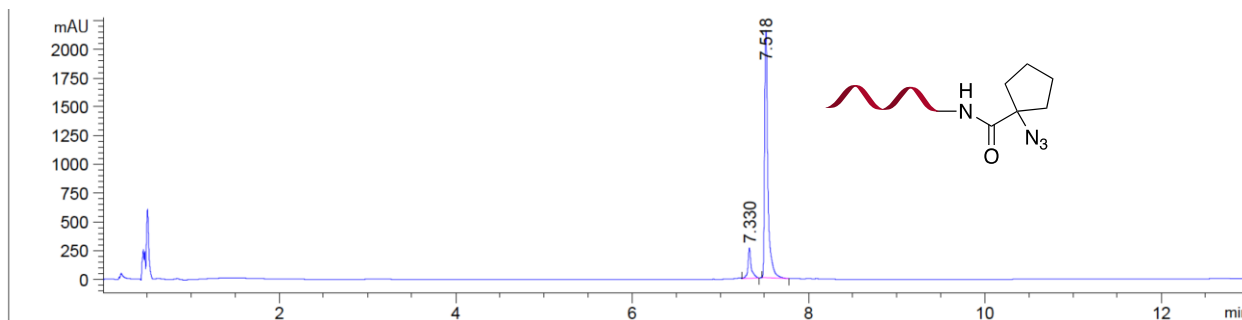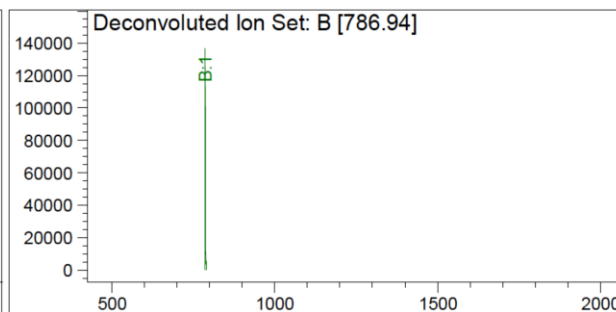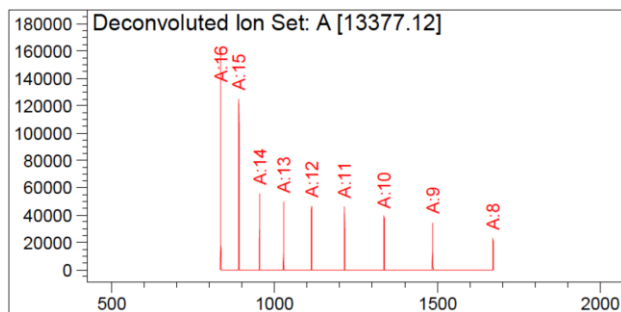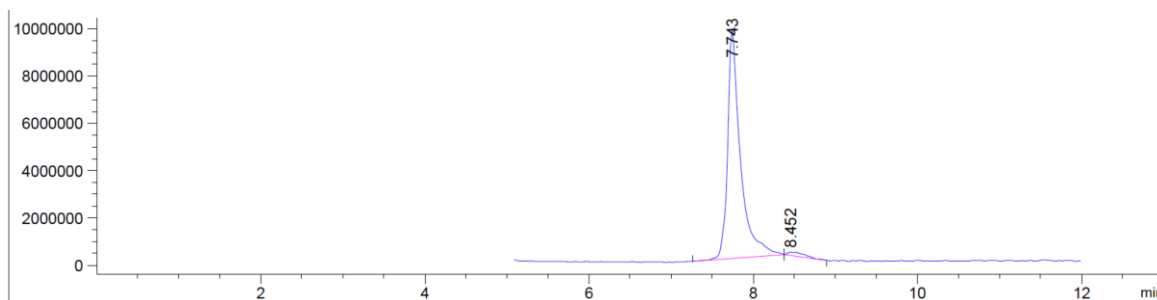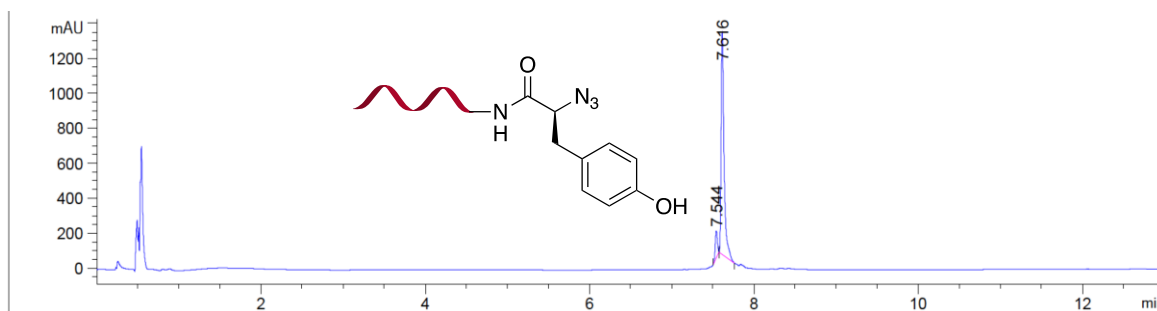
Figure 6.3.28. LC-ESI-MS chromatogram of compound **29**, t_R: 7.518 min (DAD), 7.642 min (TIC): Expected mass 13377.11, observed 13377.12.
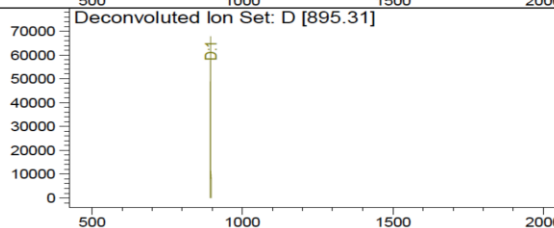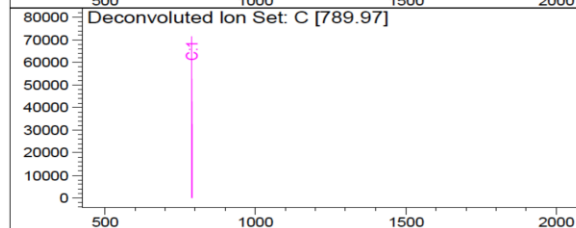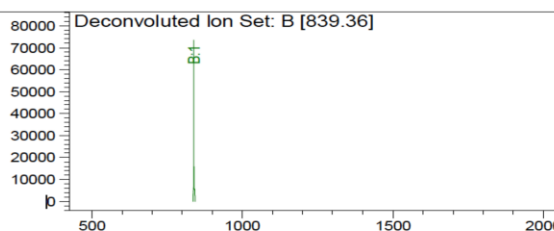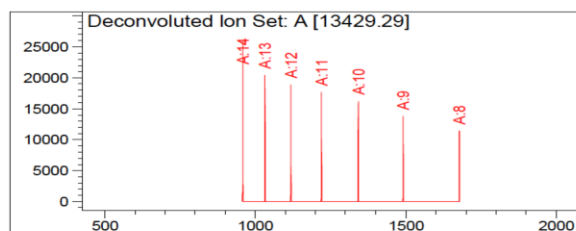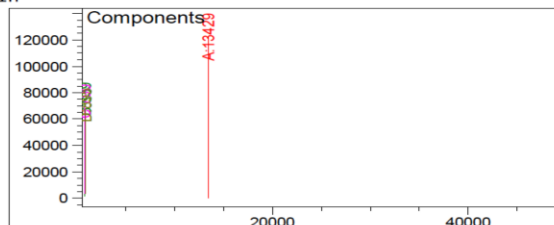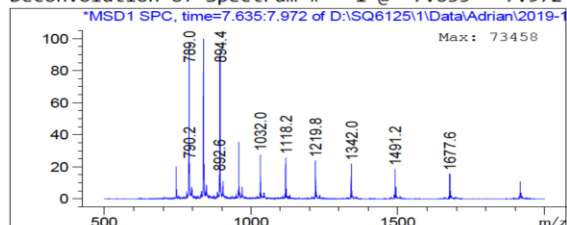
164

Figure 6.3.29. LC-ESI-MS chromatogram of compound **30**, t_R: 7.616 min (DAD), 7.743 min (TIC). Expected mass 13429.14, observed 13429.29.
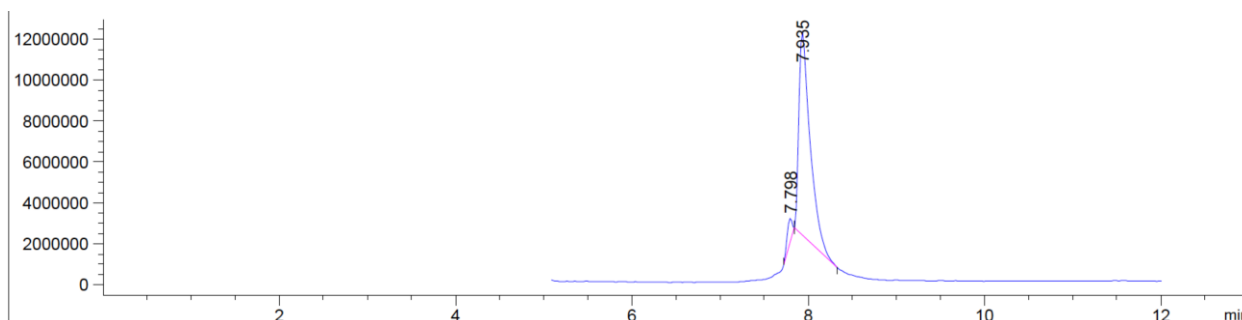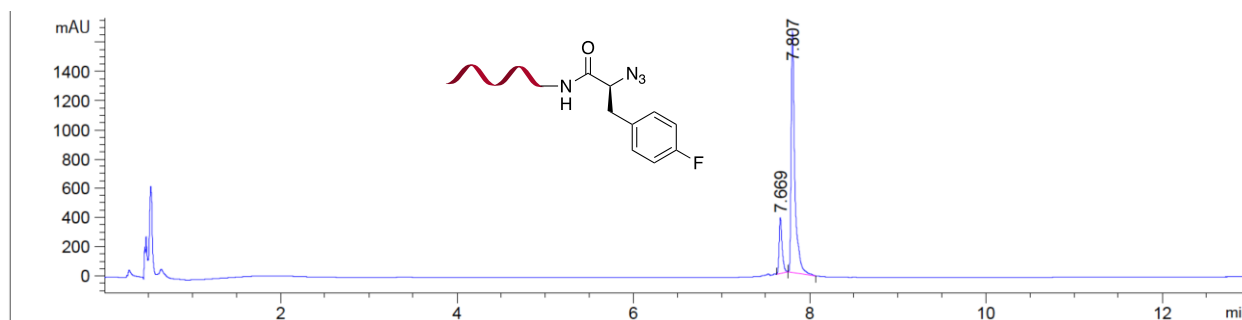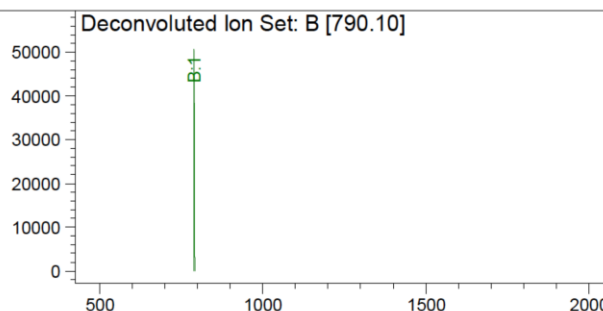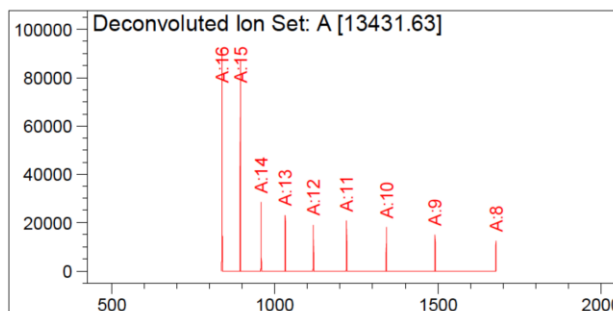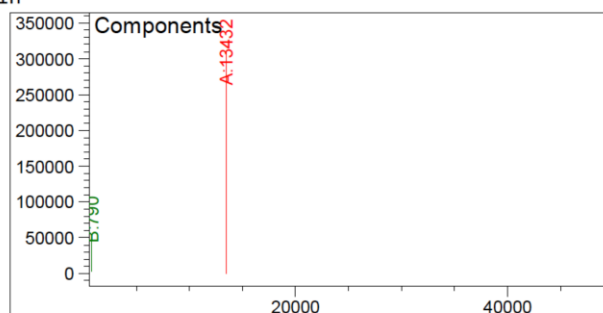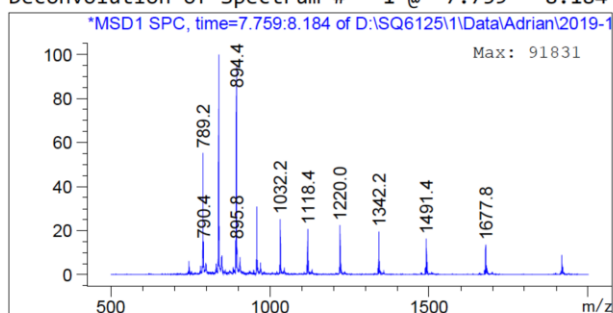
Figure 6.3.30. LC-ESI-MS chromatogram of compound **31**, t_R: 7.807 min (DAD), 7.935 min (TIC). Expected mass 13431.14, observed 13431.63.
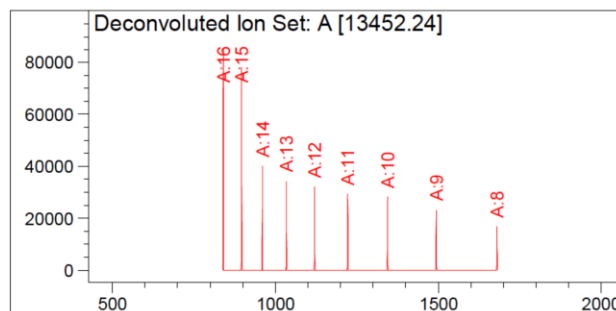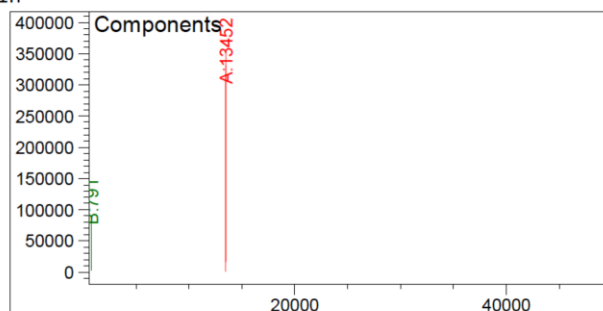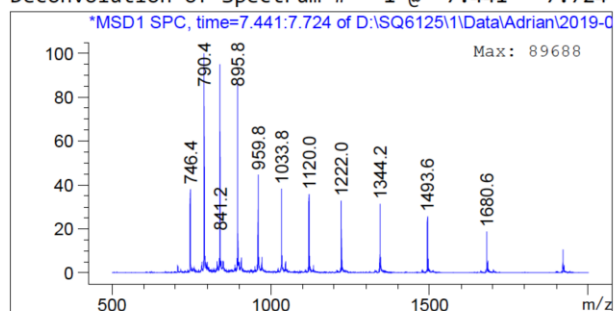
Figure 6.3.31. LC-ESI-MS chromatogram of compound **32**, t_R: 7.410 min (DAD), 7.534 min (TIC). Expected mass 13452.14, observed 13452.24.
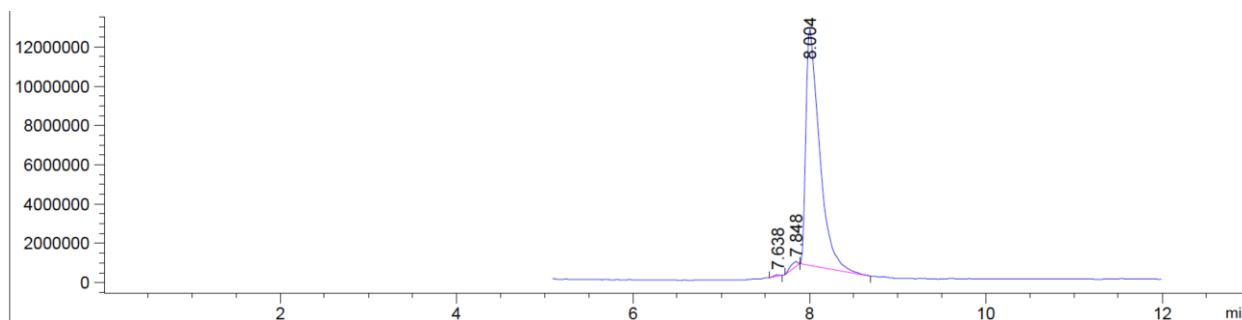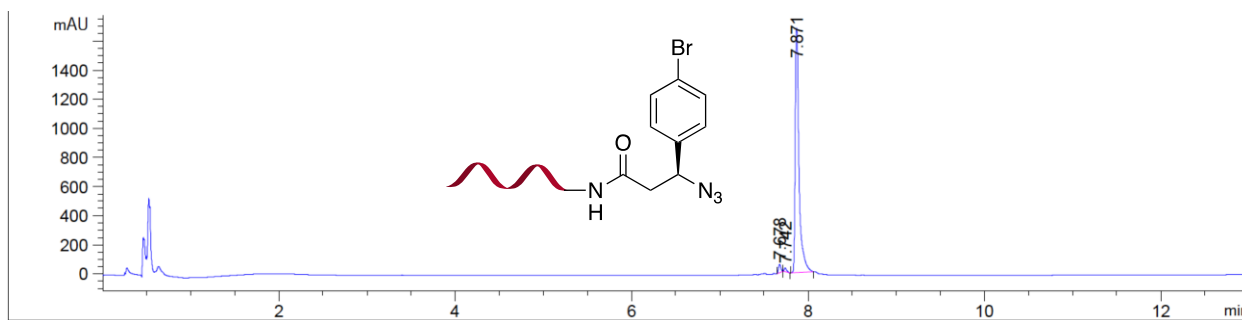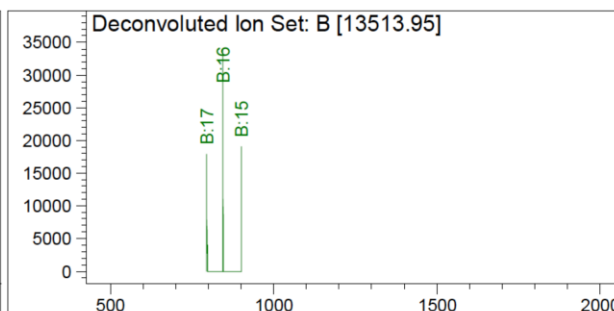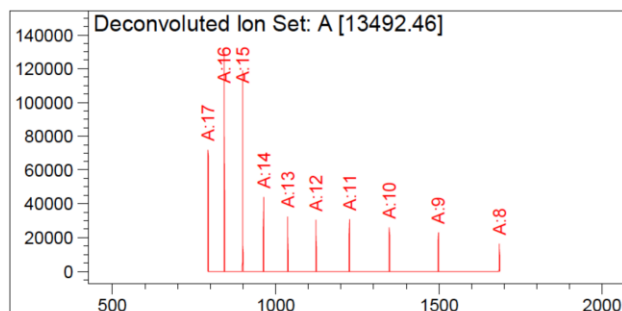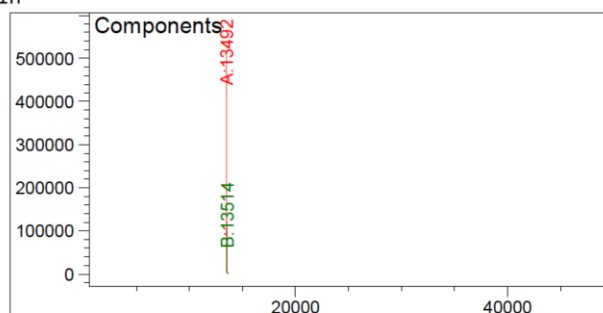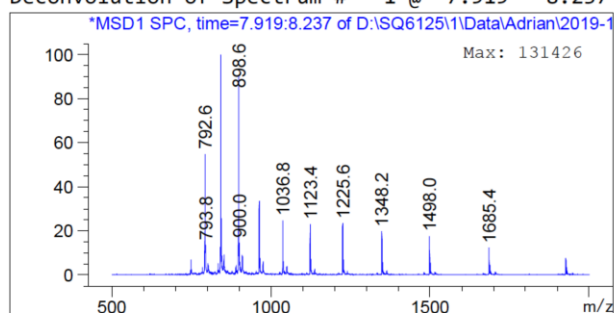
Figure 6.3.32. LC-ESI-MS chromatogram of compound **33**, t_R: 7.871 min (DAD), 8.004 min (TIC). Expected mass 13491.03, observed 13492.46.
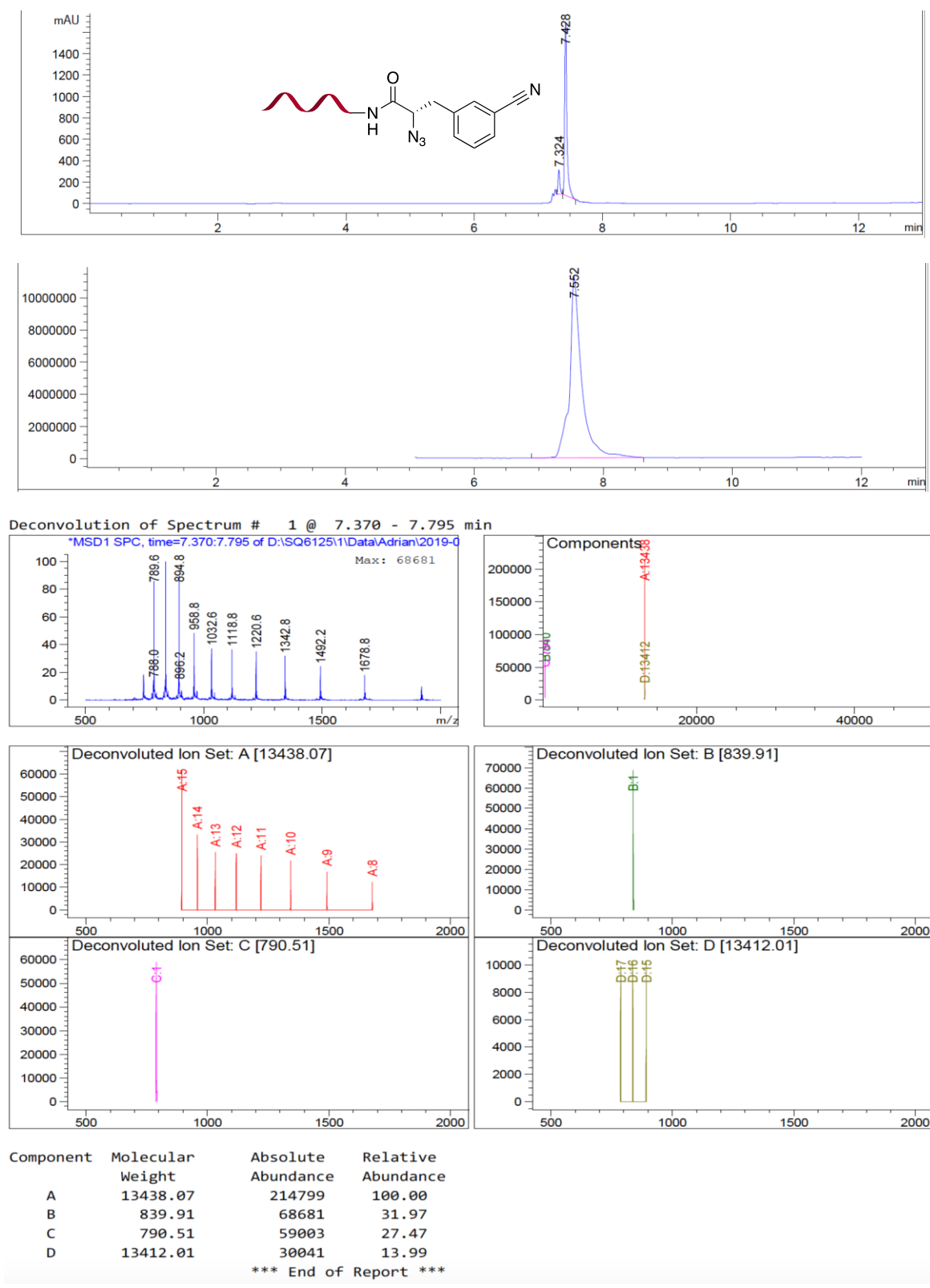
Figure 6.3.33. LC-ESI-MS chromatogram of compound **34**, t_R: 7.428 min (DAD), 7.552 min (TIC). Expected mass 13438.16, observed 13438.07.
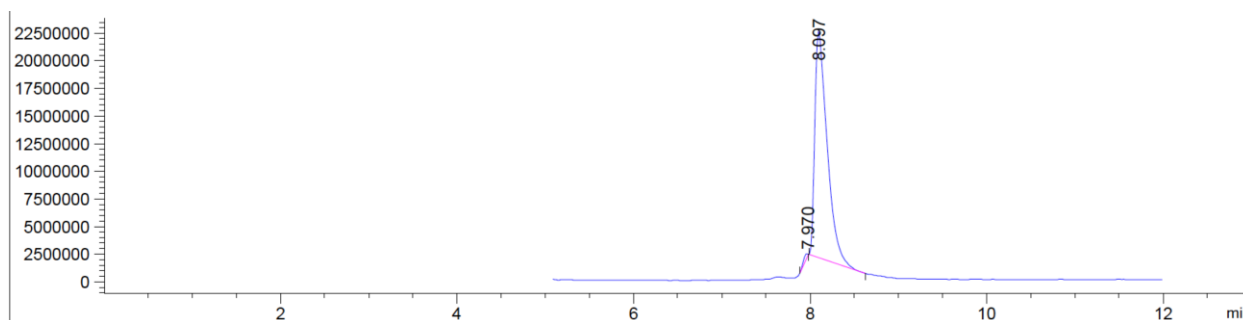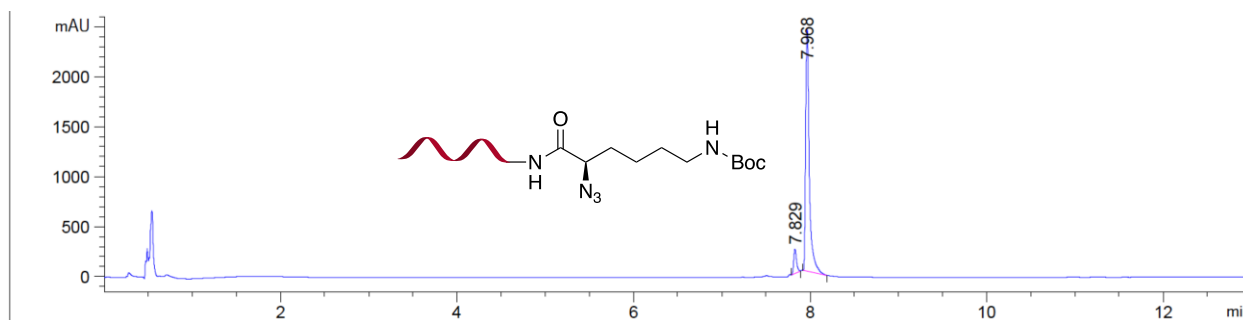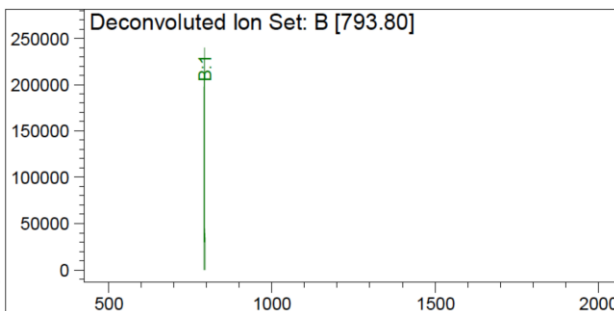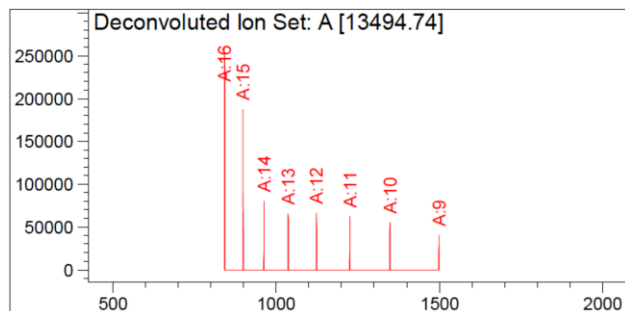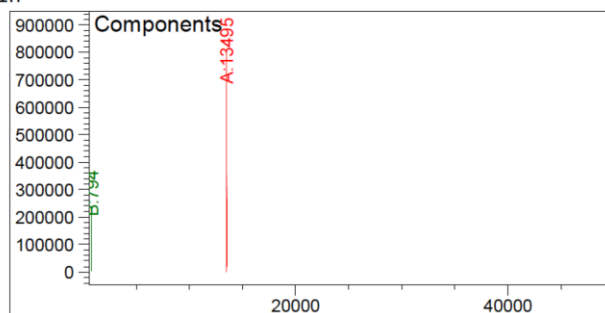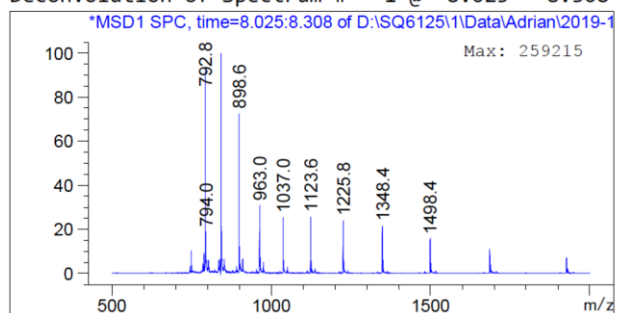
Figure 6.3.34. LC-ESI-MS chromatogram of compound **35**, t_R: 7.968 min (DAD), 8.097 min (TIC). Expected mass 13494.26, observed 13494.74.
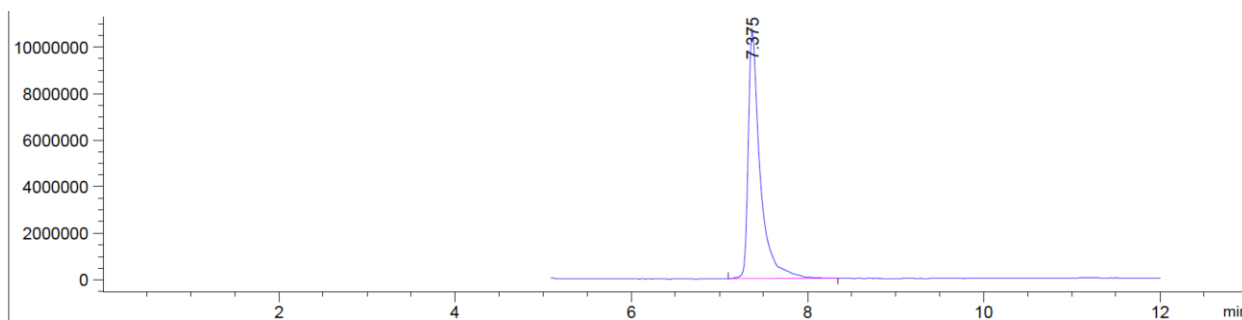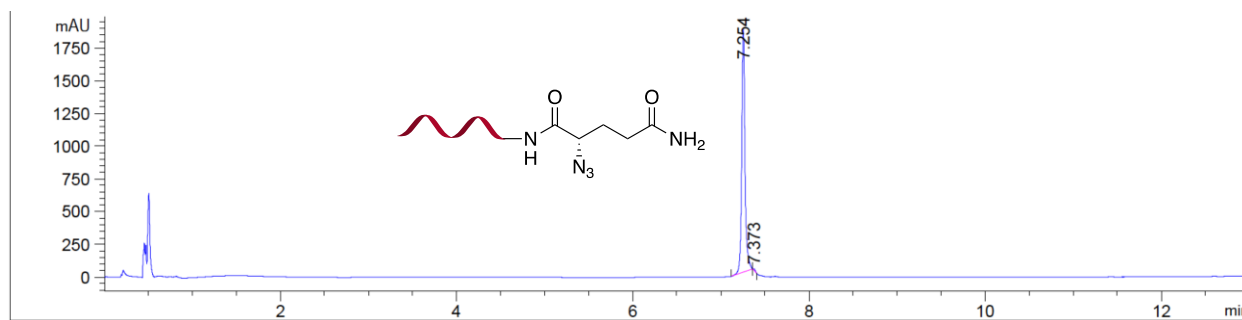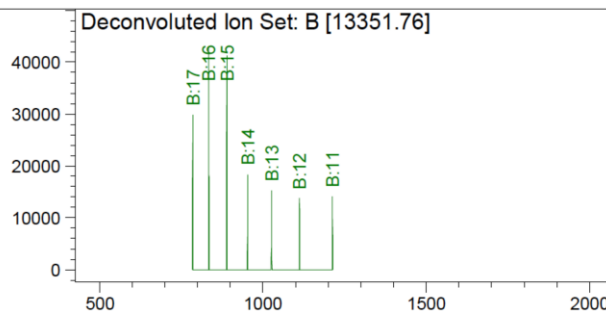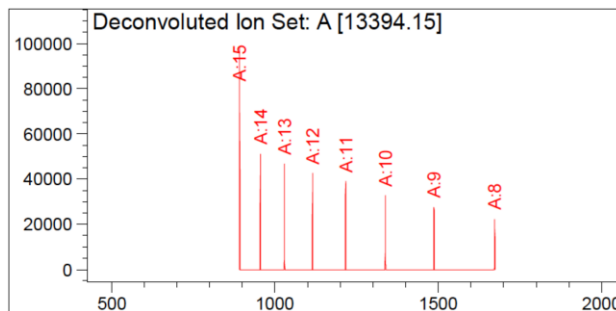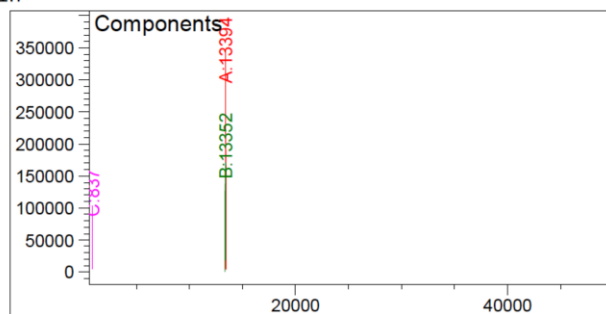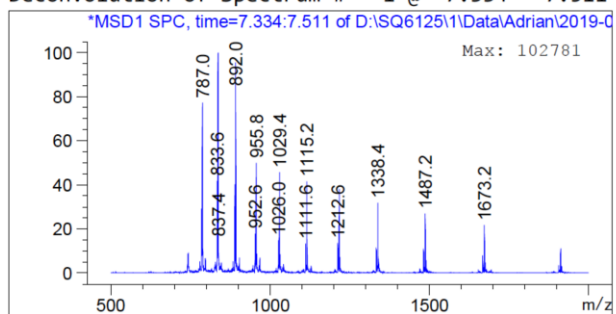
Figure 6.3.35. LC-ESI-MS chromatogram of compound **36**, t_R: 7.254 min (DAD), 7.375 min (TIC). Expected mass 13394.10, observed 13394.15.
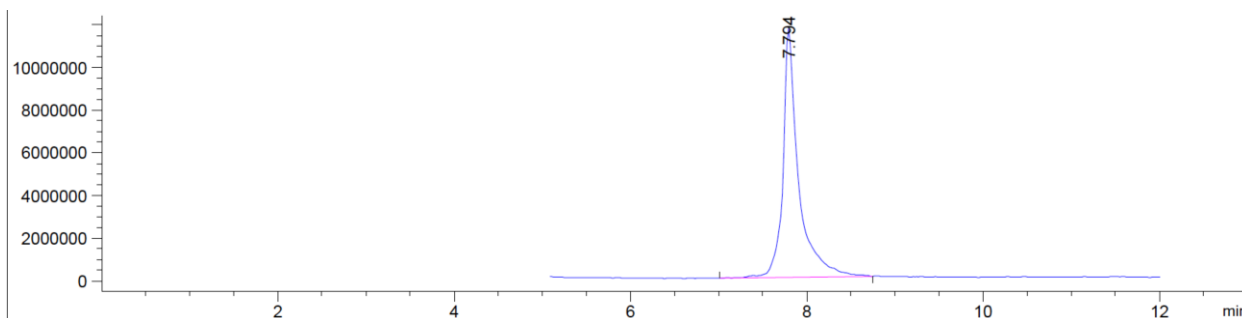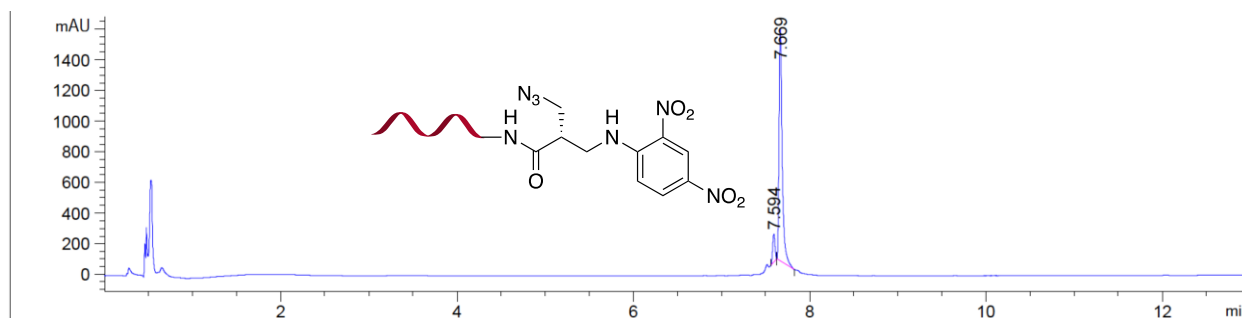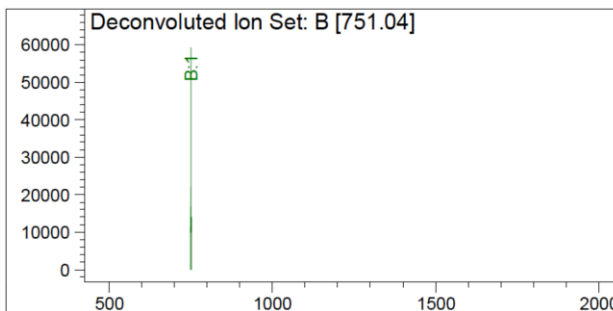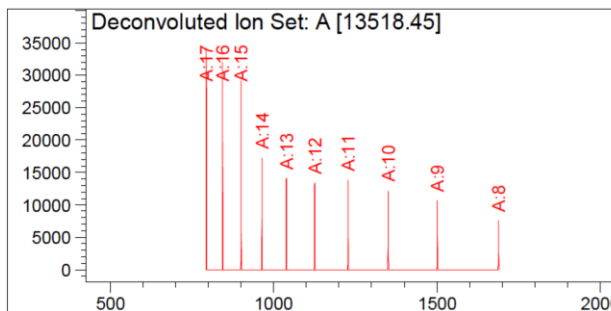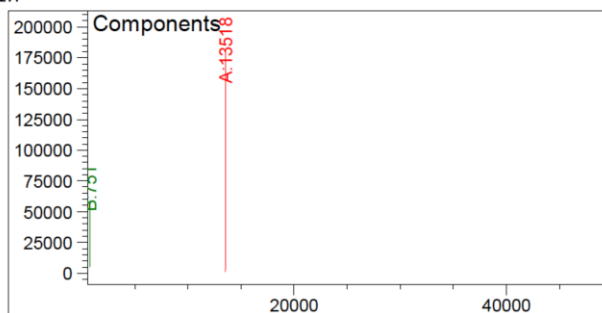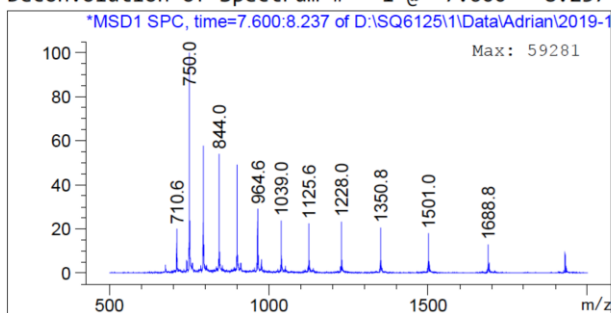
Figure 6.3.36. LC-ESI-MS chromatogram of compound **37**, t_R: 7.669 min (DAD), 7.794 min (TIC). Expected mass 13518.15, observed 13518.45. 3 h reaction time.
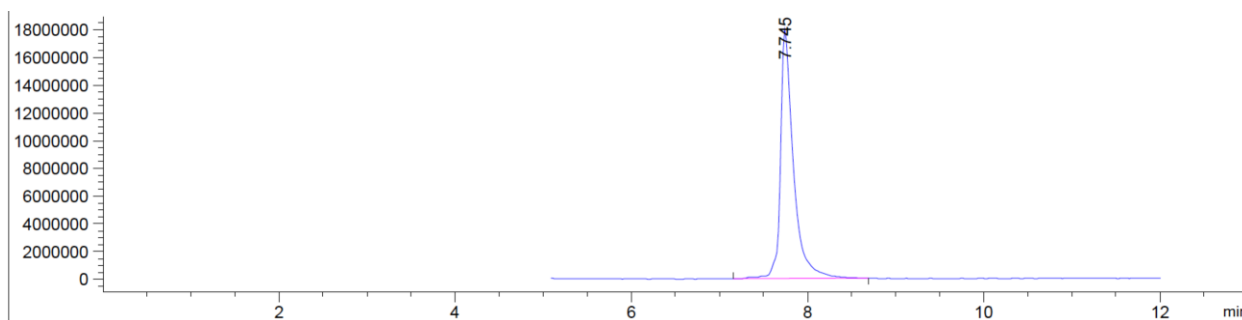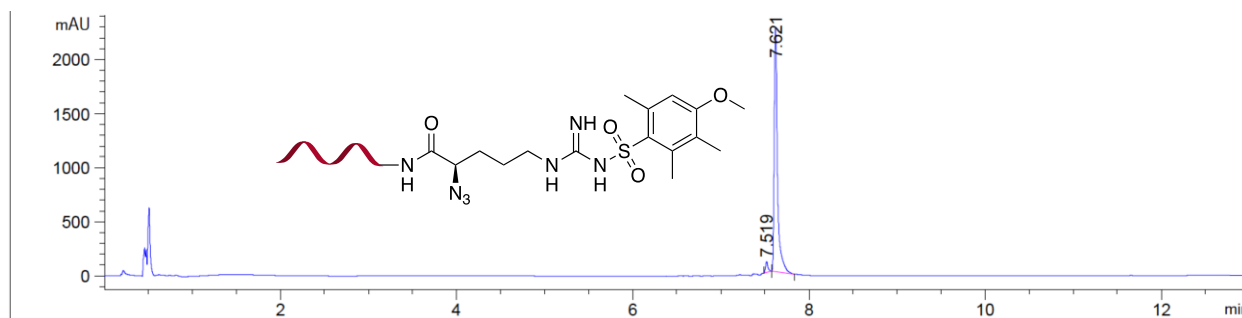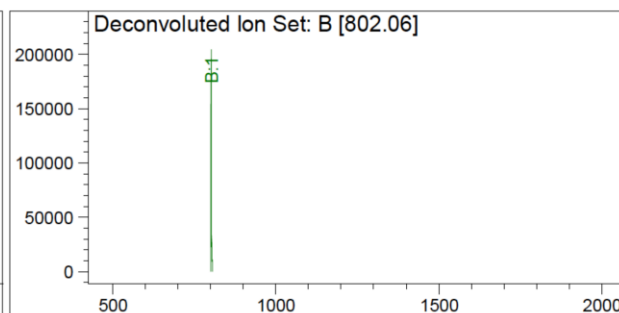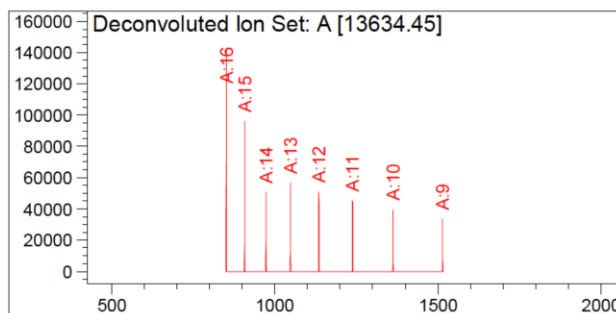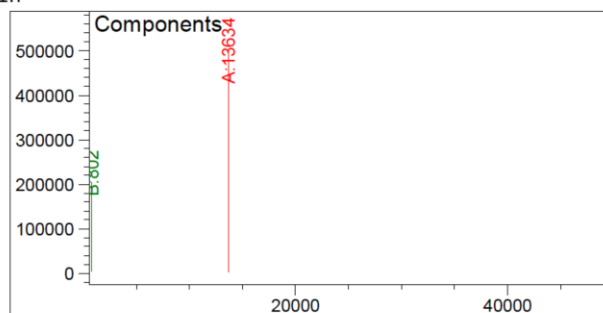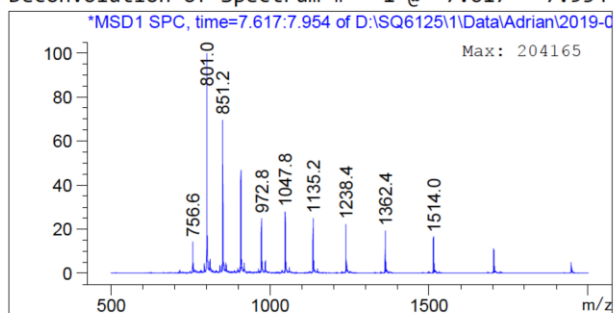
Figure 6.3.37. LC-ESI-MS chromatogram of compound **38**, t_R: 7.621 min (DAD), 7.745 min (TIC). Expected mass 13634.42, observed 13634.45.
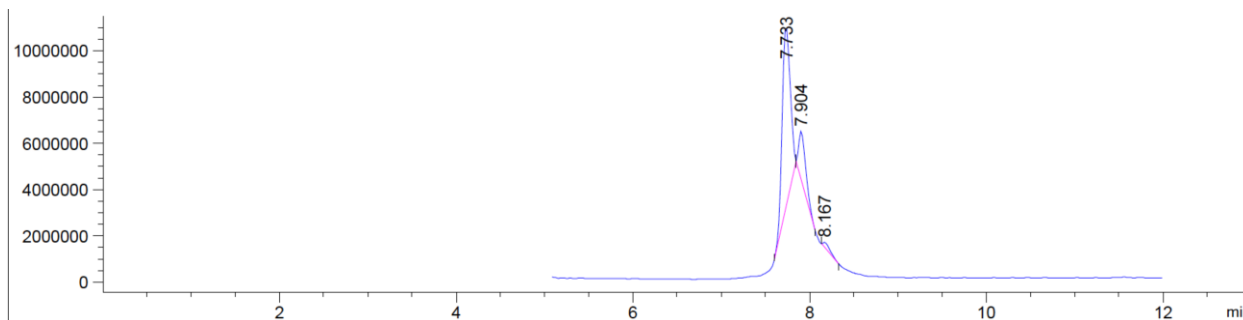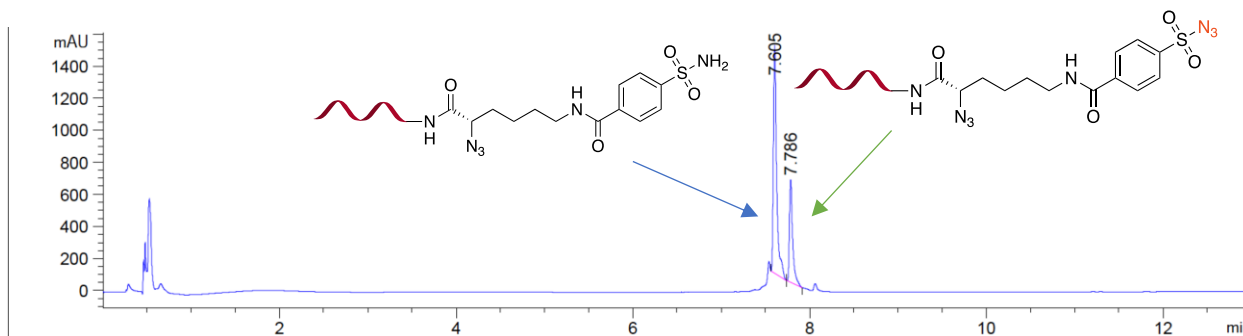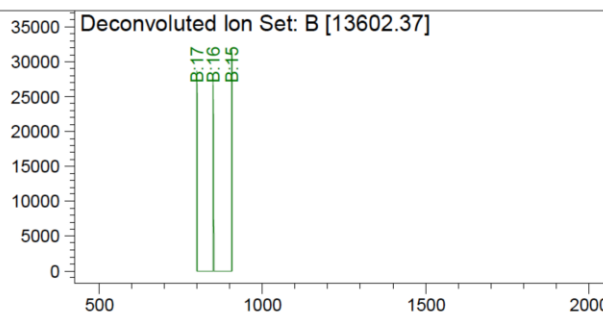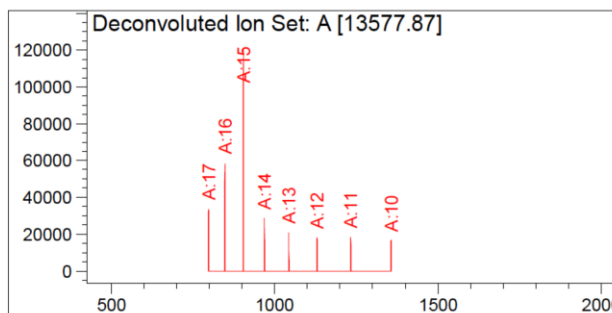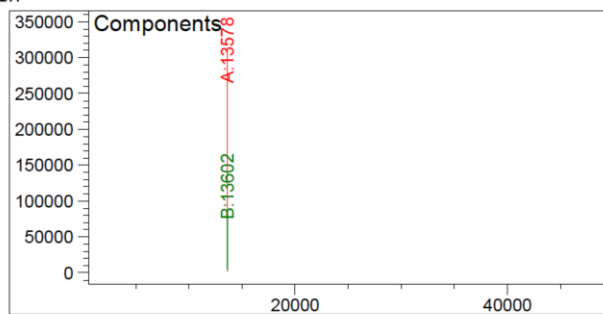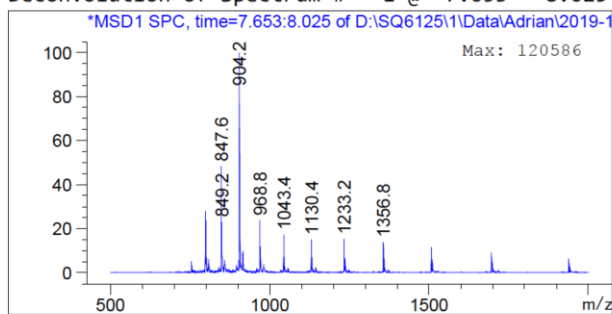
Figure 6.3.38. LC-ESI-MS chromatogram of compound **39**, t_R: 7.605 min (DAD), 7.786 min (TIC). Expected mass 13577.32, observed 13577.87. 30% formation of sulfonyl azide by-product observed.
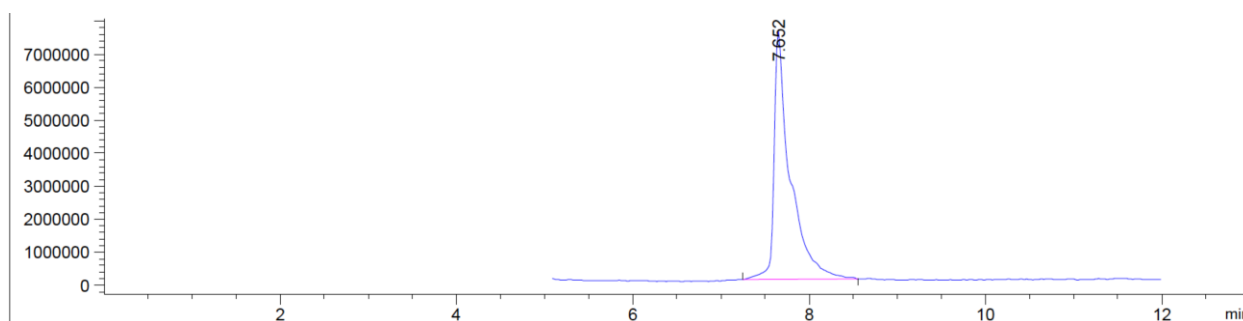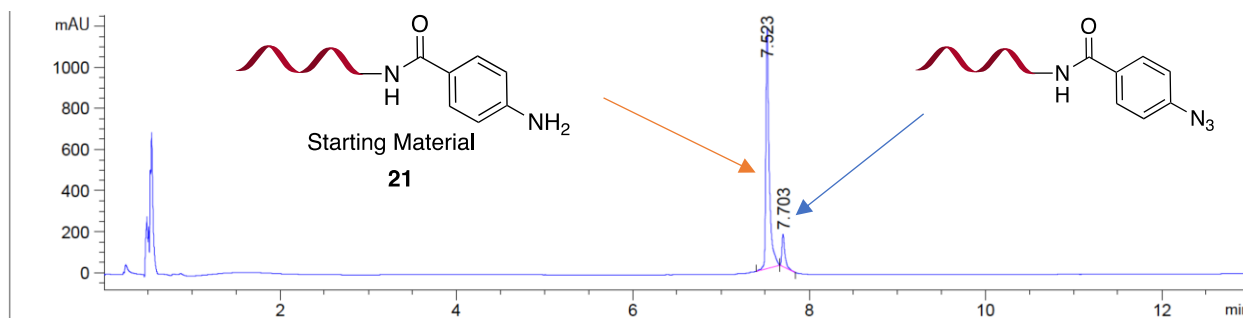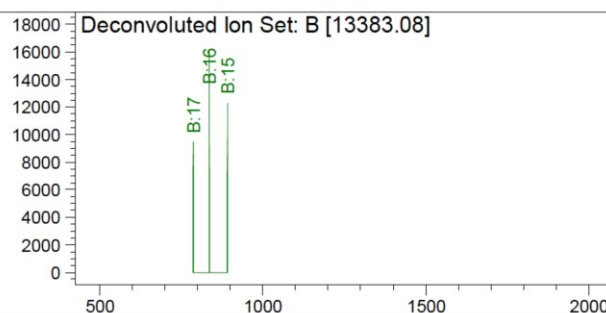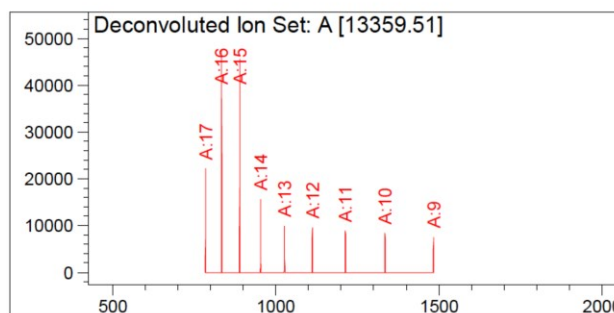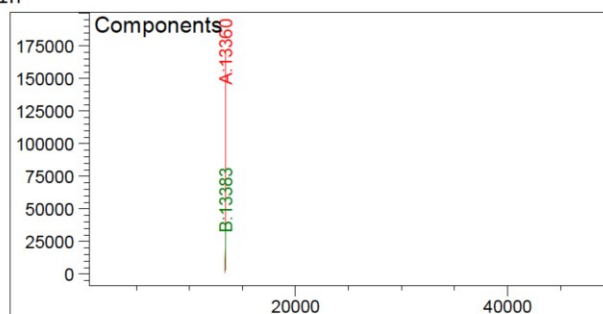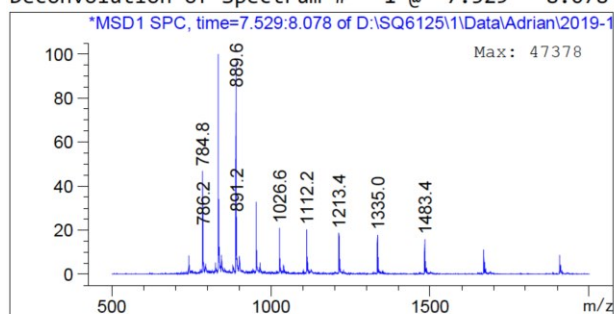
Figure 6.3.39. LC-ESI-MS chromatogram of compound **40**, t_R: 7.703 min (DAD), 7.652 min (TIC). Expected mass 13385.09, observed 13383.08. 16 h reaction time.
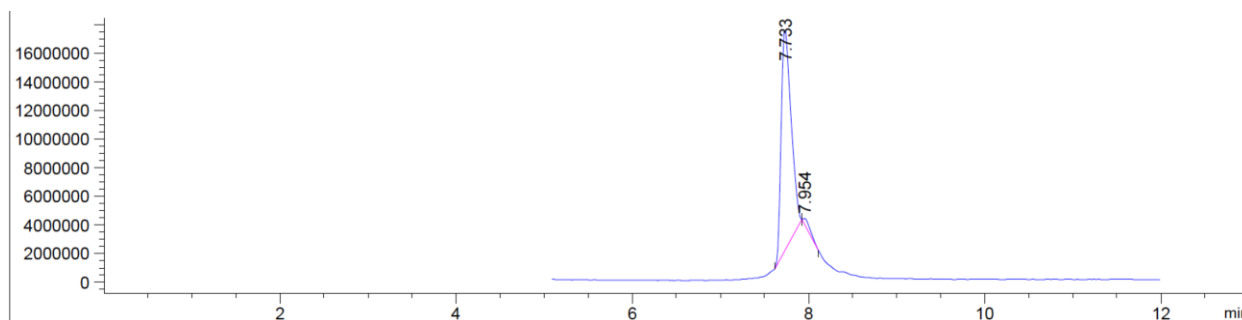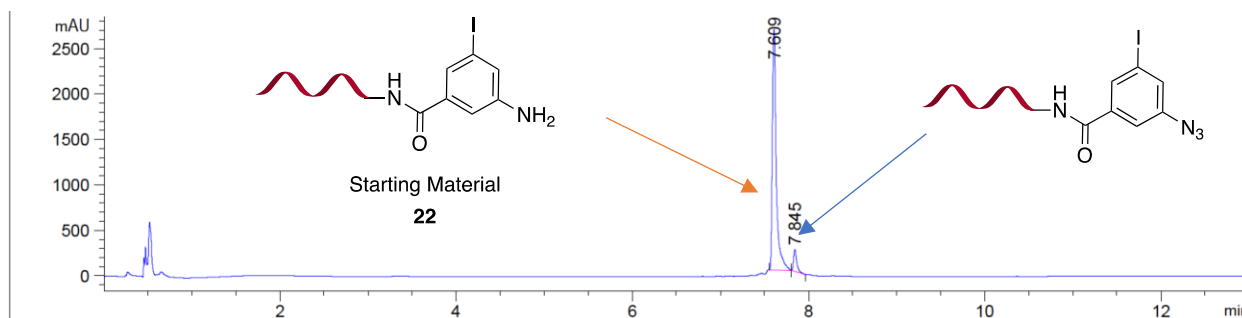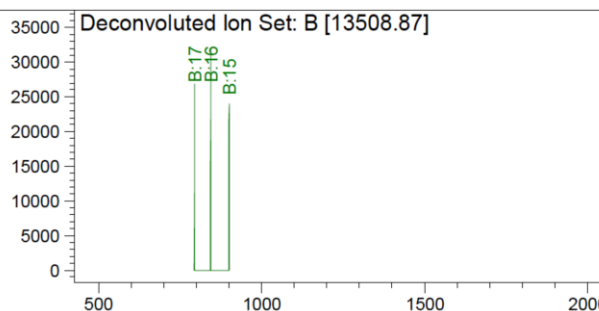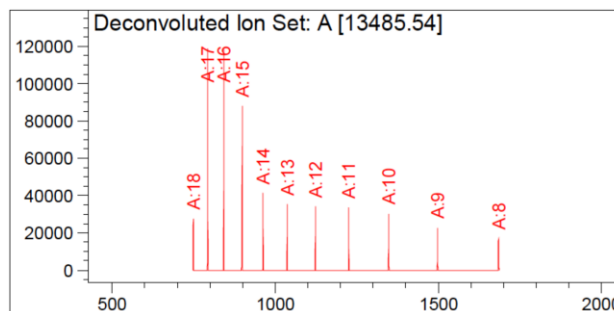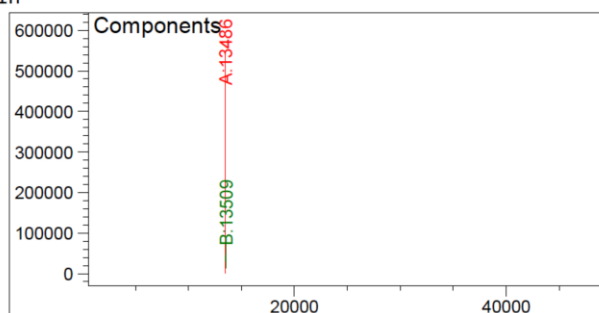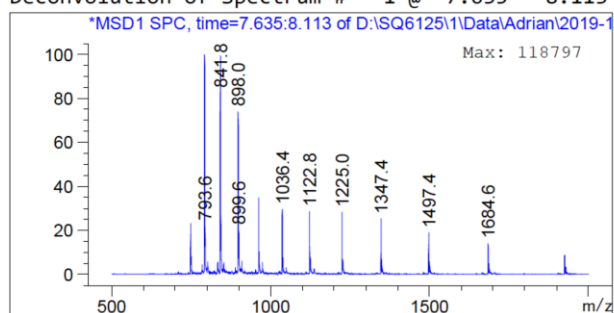
Figure 6.3.40. LC-ESI-MS chromatogram of compound **41**, t_R: 7.845 min (DAD), 7.954 min (TIC). Expected mass 13510.99, observed 13508.87. 16 h reaction time.

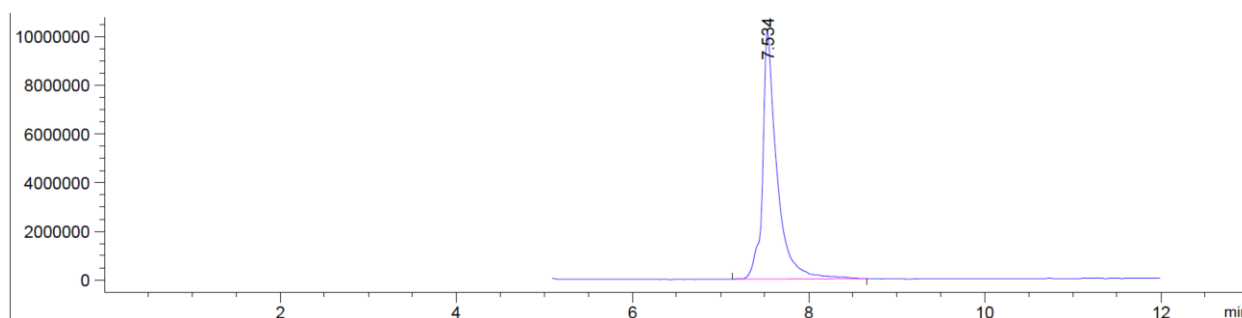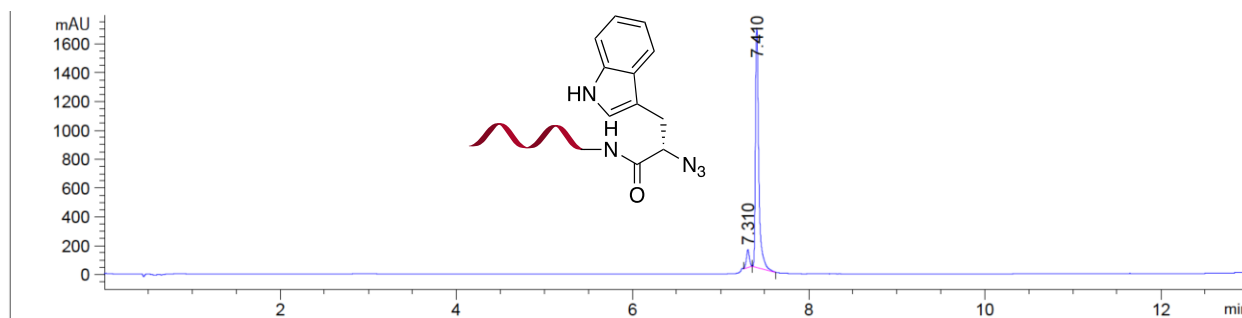*Azide Reduction Control Experiment.*
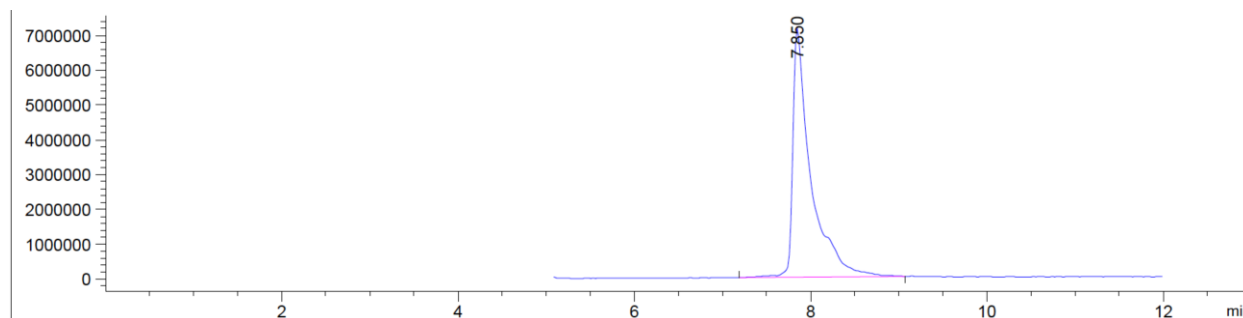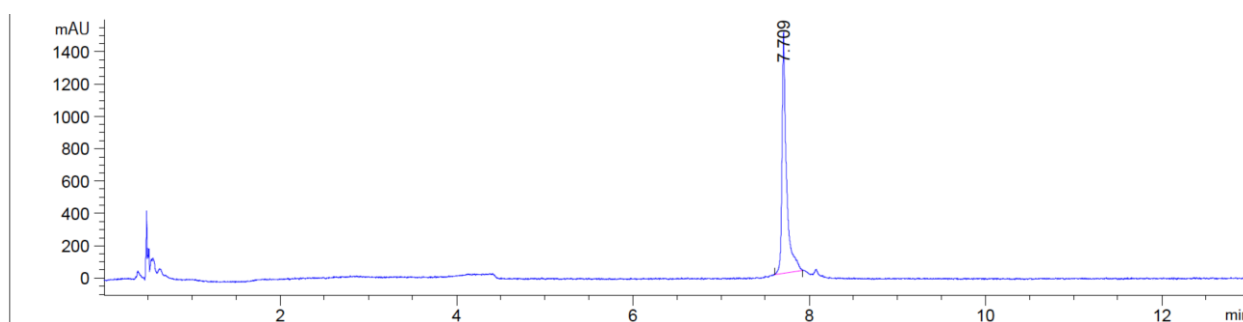
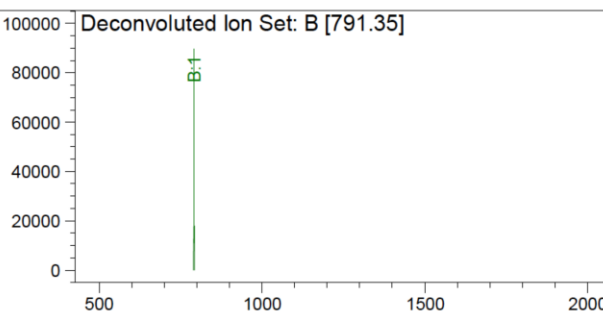Deconvolution of Spectrum # 1 @ 7.741 - 8.343 min
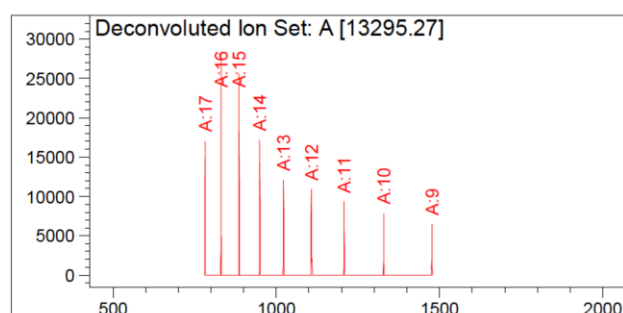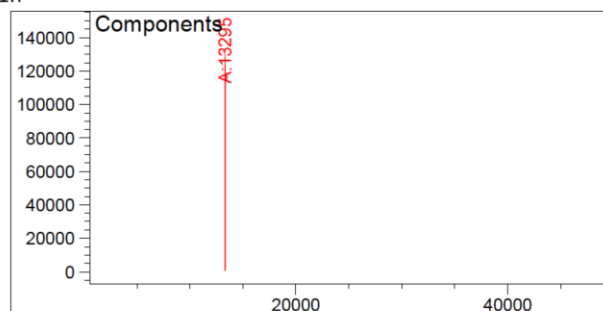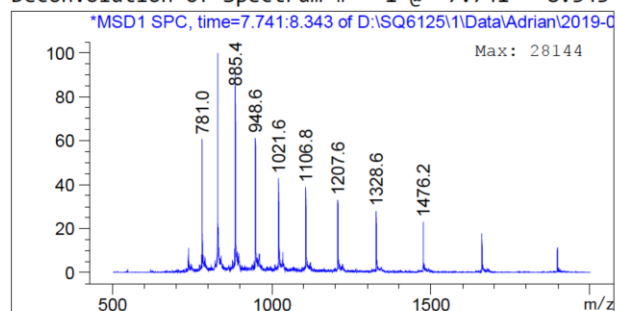
Component	Molecular Weight	Absolute Abundance	Relative Abundance
A	13295.27	132588	100.00

*** End of Report ***

Figure 6.3.41. LC-ESI-MS chromatogram of compound **3**, t_R: 7.709 min (DAD), 7.850 min (TIC). Expected mass 13297.02, observed 13295.27.
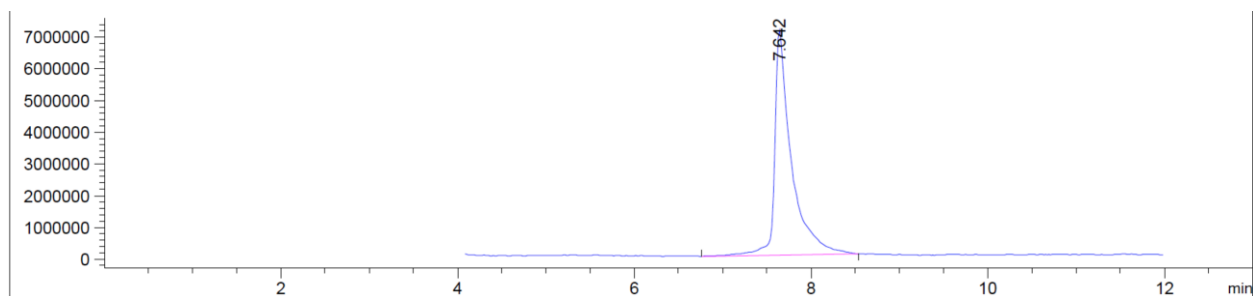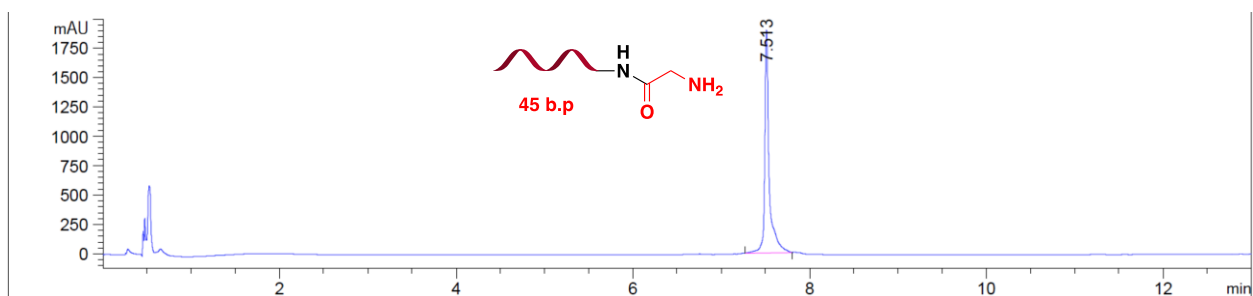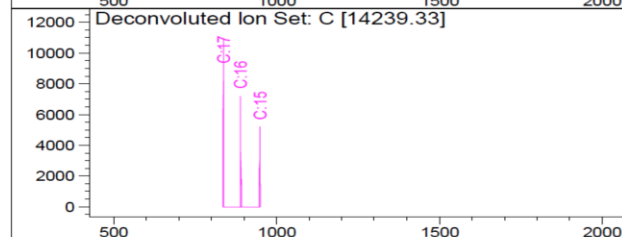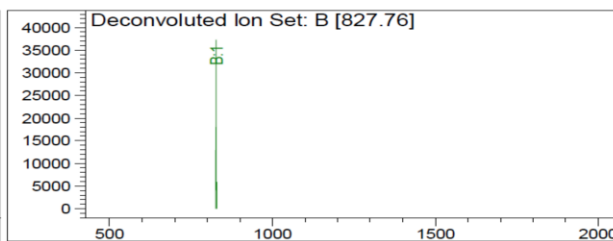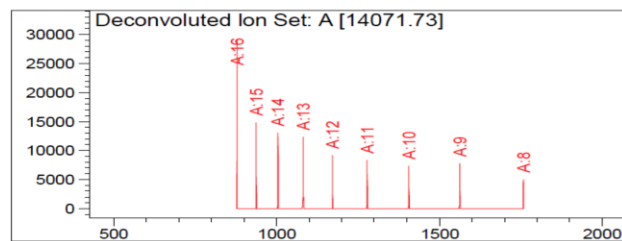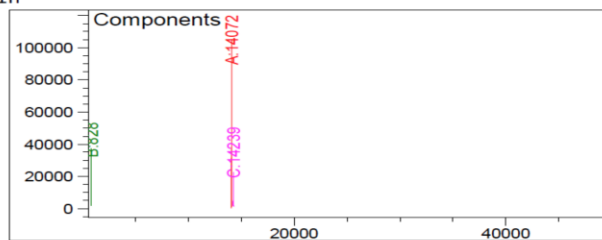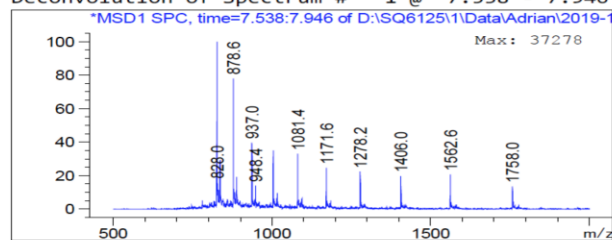
Figure 6.3.42. LC-ESI-MS chromatogram of compound **43**, t_R: 7.513 min (DAD), 7.642 min (TIC). Expected mass 14072.44, observed 14071.73.
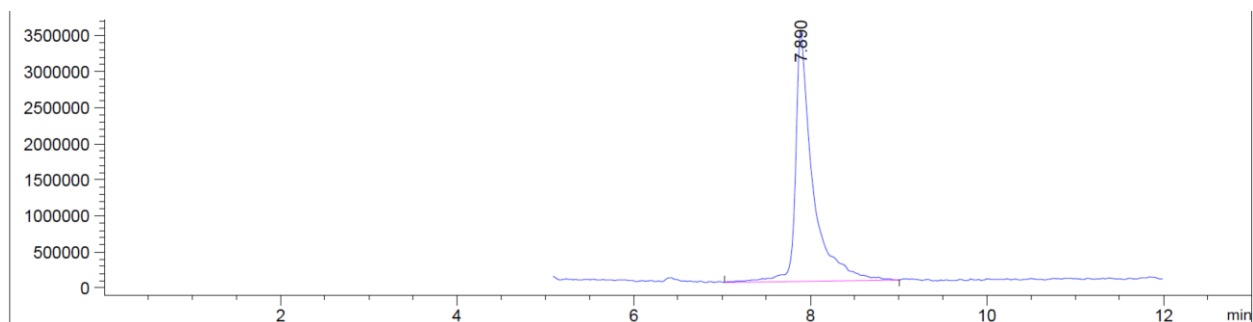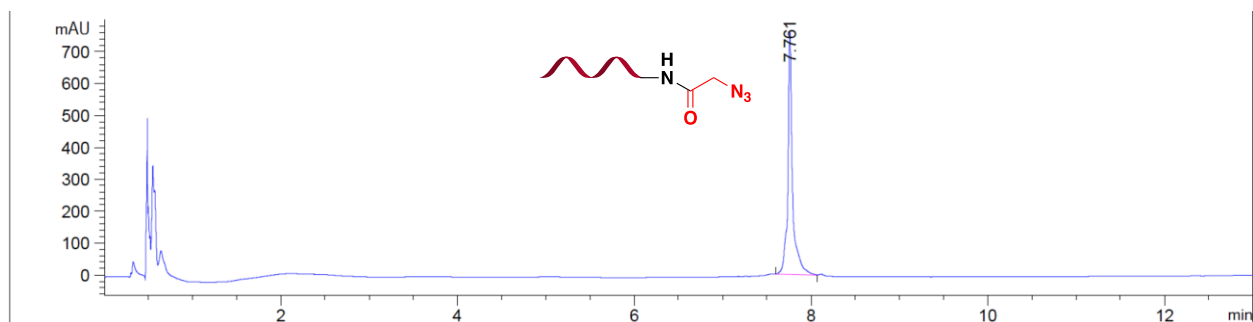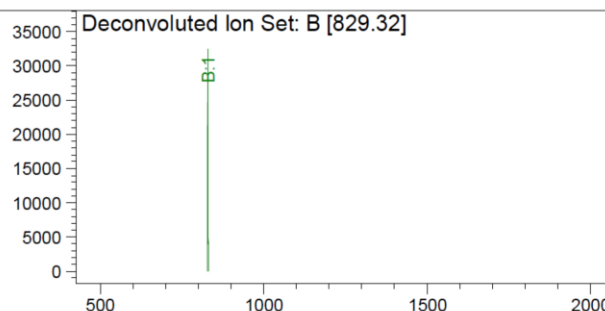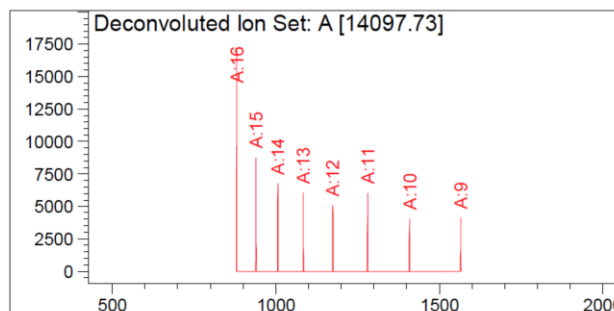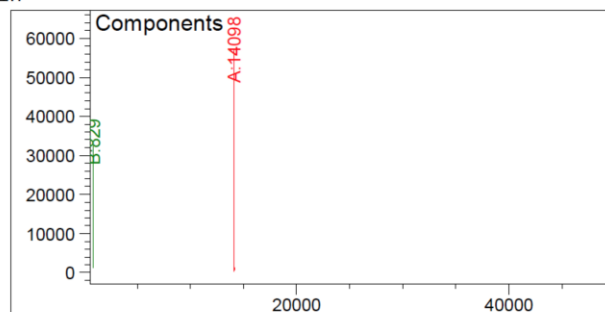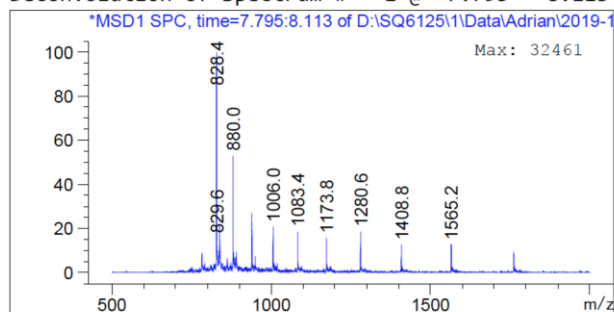
Figure 6.3.43. LC-ESI-MS chromatogram of compound **44**, t_R: 7.761 min (DAD), 7.890 min (TIC). Expected mass 14098.44, observed 14097.73.
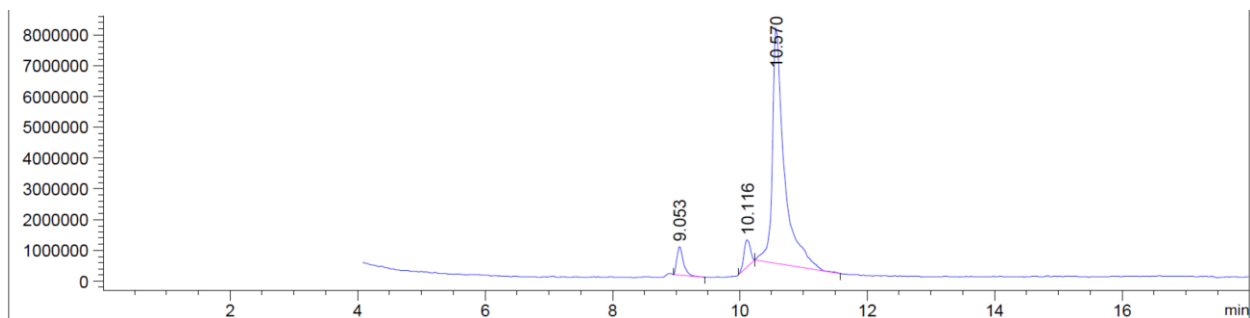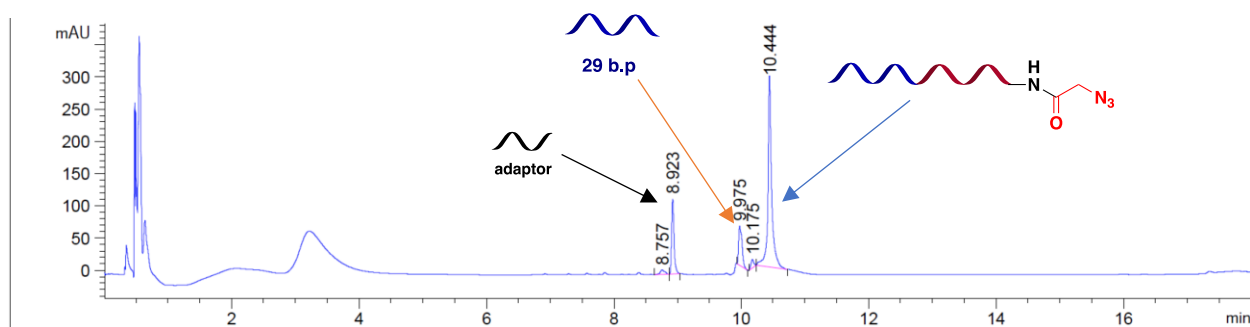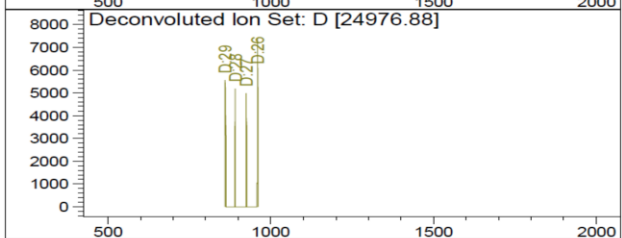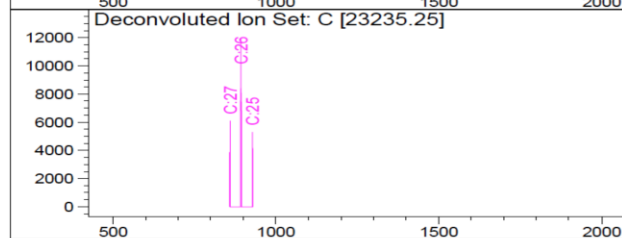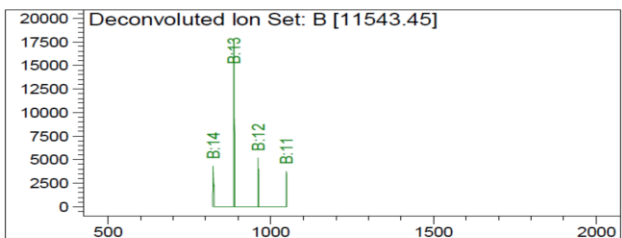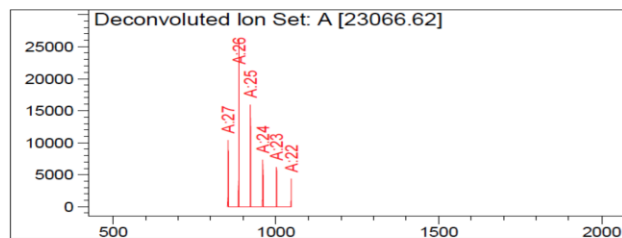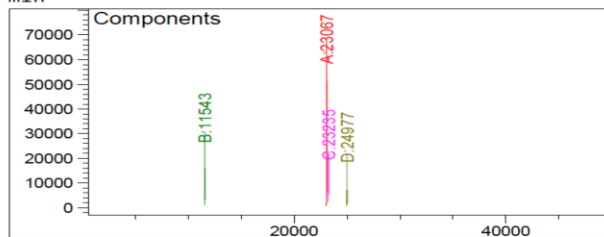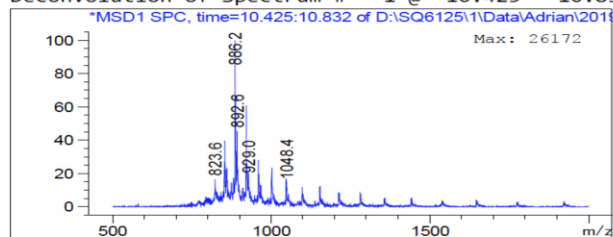
Figure 6.3.44. LC-ESI-MS chromatogram of compound **45**, t_R: 10.444 min (DAD), 10.570 min (TIC). Expected mass 23065.21, observed 23066.62.
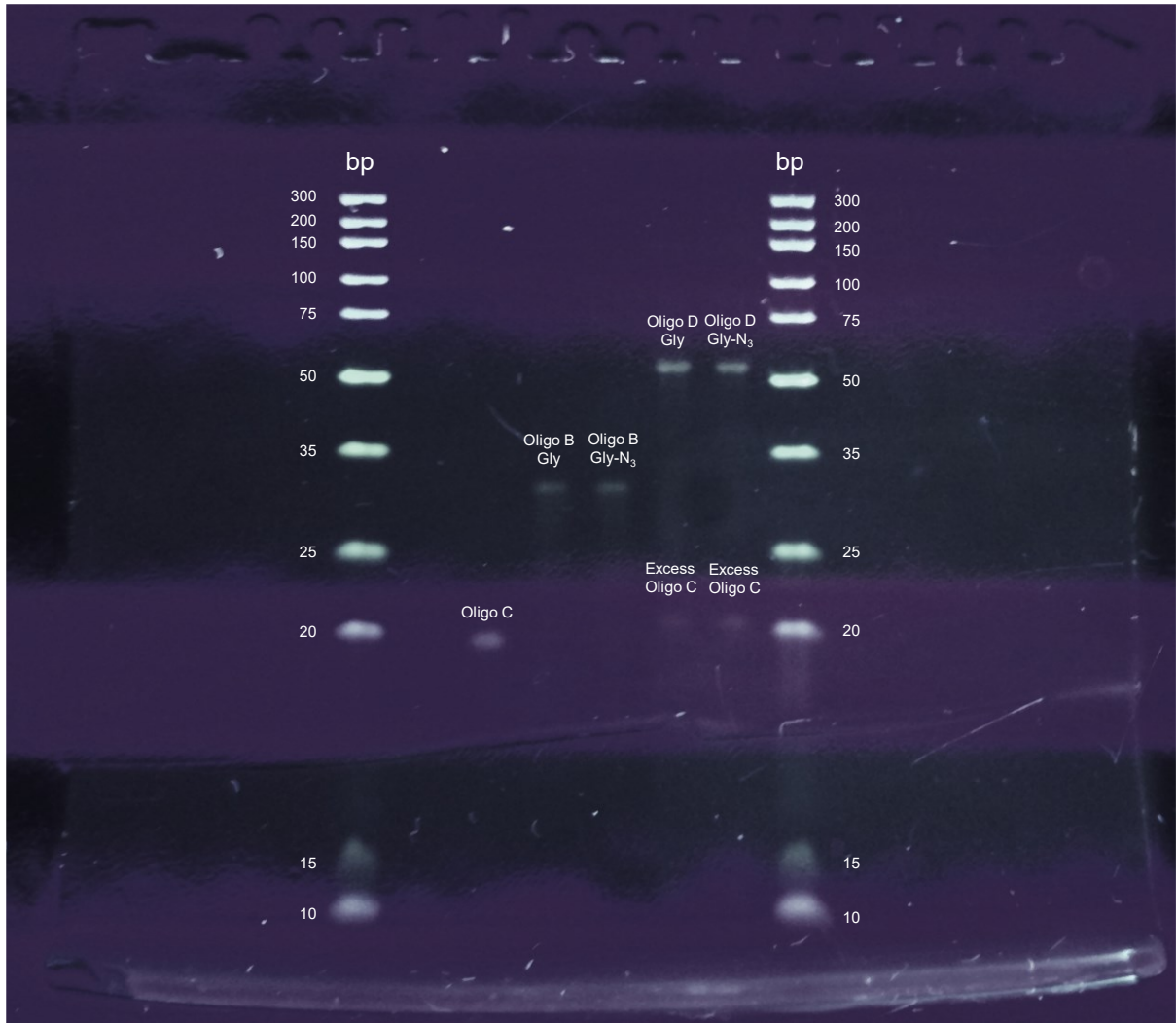
Figure 6.3.45. Gel electrophoresis analysis after ligation. The ligation of the Oligonucleotide **B,** bearing both Glycine and its azido derivative was performed in order to check the integrity of the DNA. As shown in the picture the reaction proceeded until completion (Lanes 5 and 6) with small excess of the Oligonucleotide **C.**

Figure 6.3.46. LC-ESI-MS chromatogram of compound **47**, t_R: 10.479 min (DAD), 10.610 min (TIC). Expected mass 23177.34, observed 23177.17.

6.4 Identification and validation of new interleukin-2 ligands sing DNA-encoded libraries

6.4.1 Materials and methods

Bodipy labelling of amino-modified-8mer LNA

3'-amino-modified 8-mer LNA (30 μL, 0.81 mM in water) was diluted in sodium borate buffer (240 μL, 100 mM, pH 8.5). To the solution was added a stock solution of BODIPY-TMR-X NHS ester (48.6 μL, 10 mM in DMSO) and the reaction was let to proceed overnight at room temperature. Solvents were removed by using a Speedvac and the solid was redissolved in water and excess of BODIPY- TMR-X NHS ester was removed by using a SephadexTM PD-Minitrap-G10 column (GE Healthcare). The recovered fractions were finally purified by RP-HPLC.

On-DNA fluorescence polarization experiments

Fluorescence polarization experiments were performed in triplicates for each of the desired compounds, in 384-well black plates. A stock solution of the desired protein (at the highest concentration) was serially diluted (1:1 in PBS) in order to have 15 μL/well. Then, a preformed DNA/LNA double strand hybrid between the corresponding compound and Bodipy was diluted to 20 nM concentration and added to the serial dilution of the protein (15 μL/well) reaching 10 nM final concentration of compound. Measurements were per-formed right after the addition of the compound (time 0) and after keeping the solution for 30 min at room temperature (time 1) and 60 min (time 2) in the dark to confirm reproducibility. The mean anisotropy values of the three replicates were fitted to **Equation 1** using Prism 7 (GraphPad), where A is the anisotropy, $[P]_0$ the total protein concentration, $[L]_0$ the total concentration of the fluorescently labeled ligand and K_d the dissociation constant.

Equation 1:

$$A = \frac{1}{2}\{([P]_0 + [L]_0 + K_d) - \sqrt{([P]_0 + [L]_0 + K_d)^2 - 4[P]_0[L]_0}\}$$

General procedures for Off-DNA resynthesis

All the compounds were resynthesized using commercially available building blocks unless otherwise noted. All compounds are >95% pure by HPLC analysis.

Synthesis of BB2 1317: In a 25 mL round bottom flask, 4-formylbenzic acid (150 mg, 1 mmol, 1 equiv) was suspended in a mixture of 2,2,2-trifluoroethanol and ether (3 mL, 2:1) for 10 min at 40 °C. 2-(trifluoromethyl) benzylamine (175 mg, 1 mmol, 1 equiv) was added to the suspension and the imine was let to be formed for 10 min at 40 °C. Sodium borohydride (45.6 mg, 1.2 mmol, 1.2 equiv) was slowly added to the mixture and the reaction was let to proceed for 1 h at 40 °C. The reaction was washed with water and extracted three times with ether. The water phase was then concentrated under vacuum to obtain the mixture of the mono- and di-alkylated resulting amines which were subsequently separated by flash chromatography using a gradient 9:1 of DCM/MeOH. The fractions with the desired product were combined and dried under vacuum to obtain the final product as a white powder. Final amount

74 mg, 24% yield. This product was used without further purification for the synthesis of the final compound **AG-156/1317**.

*Synthesis of compounds **AG-173/985; AG-156/1317** and **AG-156/1015***:

*Note: Building block 985 was used as a racemic mixture.

O-Bis-(amino-ethyl)ethylene glycol trityl resin (Novabiochem, 0.64 mmol/g loading capacity, 50 mg, 0.032 mmol, 1 equiv) was swollen in DMF (500 μL, neat) for 30 min at room temperature. A solution of the corresponding Fmoc-amino acid (0.064 mmol, 2 equiv), 1-[Bis(dimethylamino)methylene]-1H-1,2,3-triazolo[4,5-b]pyridinium-3-oxide hexafluorophosphate (HATU) (24.3 mg, 0.064 mmol, 2 equiv) HOAt (8.7 mg, 0.064 mmol, 2 equiv) and NMM (21 μL, 0.19 mmol, 6 equiv) in DMF (500 μL, neat) was added and the reaction was let to proceed for 1 h at room temperature. The resin was washed several times with DMF. Fmoc deprotection was performed by addition of piperidine (20% in DMF, 500 μL), twice for 7 and 3 min respectively. A solution of the corresponding carboxylic acid (0.064 mmol, 2 equiv) HATU (24.3 mg, 0.064 mmol, 2 equiv) HOAt (8.7 mg, 0.064 mmol, 2 equiv) and NMM (21 μL, 0.19 mmol, 6 equiv) in DMF (500 μL, neat) was added and the reaction was let to proceed for 1 h at room temperature. The resin was washed with DMF and DCM and then the product was cleaved using a solution of TFA:DCM:TIPS:H_2O (63:30:3.5:3.5), twice for 45 min. The liquids were recovered, the resin was washed with DCM and the solution of the cleaved product was evaporated under vacuum. The crude was washed with toluene 3 to 5 times to evaporate the rest of TFA. The crude was dissolved in DMF to obtain a 40 to 60 mM solution. Triethylamine was added until the pH was checked to be above 9, then fluorescein isothiocyanate isomer I (1.5 equiv) was added to the mixture and the reaction was let to proceed between 2 and 16 h at room temperature in the dark, checking the formation of the product by LCMS. The final products were purified by RP-HPLC. The fractions containing the product were mixed and lyophilized overnight. The obtained powder was re-dissolved in a random amount of DMSO (neat), and the concentration was checked by absorbance at 495 nm using a Nanodrop 2000 instrument (Thermo Fisher) with a 1:100 dilution in PBS. The solutions were then adjusted to 1 mM in DMSO (neat) and stored at -20 °C.

Synthesis of Fluorescein-PEG$_1$-Fmoc protected modified DFPE resin: Aldehyde-modified DFPE resin (300 mg, 0.192 mmol) was swollen in dimethylformamide (3 mL, neat) for 30 minutes at room temperature. Then, a solution of Fmoc-2-(2-aminoethoxy)-ethylamine hydrochloride in DCE (1.5 equiv, 1.5 mL) was added to the filtered resin and the formation of the imine was allowed to proceed for 1 h at room temperature. Afterwards, a solution of sodium triacetoxyborohydride (NaBH(OAc)$_3$) (3 equiv) acetic acid (10 equiv) and MeOH (6% v.v.) in dichloroethane (DCE) (1.5 mL) was added to the mixture and the reaction was let to proceed overnight at room temperature. The resin was carefully washed with DMF, DCE, DCM, MeOH and DMF. Afterwards, a solution of fluorescein isothiocyanate isomer I in DMF (1.5 equiv 3 mL) was added to the resin and the reaction was let to proceed for 2 h at room temperature. The formation of the product was confirmed by LCMS of a small cleaved fraction. The resin was carefully washed with DMF, DCM, MeOH and Et$_2$O and dried under vacuum. The final loading was calculated to be 0.64 mmol/g and the resin was stored at -20 °C protected from light.

*Synthesis of compounds **1** to **17***: The Fluorescein-PEG$_1$-Fmoc-protected functionalized resin (5 to 10 mg, 0.0032 to 0.0064 mmol, 1 equiv) was swollen in DMF (50 to 100 μL, neat) for 30 min at room temperature. Fmoc deprotection was performed by addition of piperidine (20% in DMF, 50 to 100 μL), twice for 7 and 3 min respectively. After washing the resin several times with DMF, a solution of the corresponding Fmoc-amino acid (0.0064 to 0.0128 mmol, 2 equiv) HATU (2.43 to 4.86 mg, 0.0064 to 0.0128 mmol, 2 equiv) HOAt (0.87 to 1.74 mg, 0.0064 to 0.0128 mmol, 2 equiv) and NMM (2 to 4 μL, 0.0192 to 0.0384 mmol, 6 equiv) in DMF (50 to 100 μL, neat) was added and the reaction was let to proceed for 1 h at room temperature. The resin was washed several times with DMF and Fmoc deprotection was performed as indicated before. Then, a solution of the corresponding carboxylic acid (0.0064 to 0.0128 mmol, 2 equiv) HATU (2.43 to 4.86 mg, 0.0064 to 0.0128 mmol, 2 equiv) HOAt (0.87 to 1.74 mg, 0.0064 to 0.0128 mmol, 2 equiv) and NMM (2 to 4 μL, 0.0192 to 0.0384 mmol, 6 equiv) in DMF (50 to 100 μL, neat) was added and the reaction was let to proceed for 1 h at room temperature. The resin was washed with DMF and DCM and then the product was cleaved using a solution of TFA:DCM (3:1), twice for 45 min. The liquids were recovered, the resin was washed with DCM and the solution of the cleaved product was evaporated under vacuum. The crude was washed with toluene 3 to 5 times to evaporate the rests of TFA. The final products were purified by RP-HPLC. The fractions containing the product were mixed and lyophilized overnight. The obtained powder was re-dissolved in a random amount of DMSO (neat) and the concentration was checked by absorbance at 495 nm using a Nanodrop 2000 instrument (Thermo Fisher) with a 1:100 dilution in PBS. HPLC purity of each compound: Compound (**1**), 100%; compound (**2**), 100%; compound (**3**), 99.2%; compound (**4**), 95.5%; compound (**5**), 100%; compound (**6**), 100%; compound (**7**), 96%; compound (**8**), 98.6%; compound (**9**), 96%; compound (**10**), 95%; compound (**11**), 100%; compound (**12**), 100%; compound (**13**), 100%; compound (**14**), 97.6%; compound (**15**), 100%; compound (**16**), 96.4% and compound (**17**), 100%. The solutions were then adjusted to 1 mM in DMSO (neat) and stored at -20 °C protected from light.

*Synthesis of compounds **18** to **21***: The Fluorescein-PEG$_1$-Fmoc protected functionalized resin (100 mg, 0.064 mmol, 1 equiv) was swollen in DMF (1 mL, neat) for 30 min at room temperature. Fmoc deprotection was performed by addition of piperidine (20% in DMF, 1 mL), twice for 3 and 7 min respectively. After washing the resin several times with DMF, a solution of the corresponding Fmoc-arginine isomer (0.128 mmol, 2 equiv) HATU (48.7 mg, 0.128 mmol, 2 equiv) HOAt (17.4 mg, 0.128 mmol, 2 equiv) and NMM (42.2 μL, 0.384 mmol, 6 equiv) in DMF (1 mL, neat) was added and the reaction was let to proceed for 1 h at room temperature. The resin was washed several times with DMF and Fmoc deprotection was performed as indicated before. Then, a solution of the corresponding Fmoc 3-iodotyrosine isomer (67.7 mg, 0.128 mmol, 2 equiv) HATU (48.7 mg, 0.128 mmol, 2 equiv) HOAt (17.4 mg, 0.128 mmol, 2 equiv) and NMM (42.2 μL, 0.384 mmol, 6 equiv) in DMF (1 mL, neat) was added and the reaction was let to proceed for 1 h at room temperature. The resin was washed several times with DMF and Fmoc deprotection was performed as indicated before. Then, a solution of 4-fluoro-1H-indole-2-carboxylic acid (22.9 mg, 0.128 mmol, 2 equiv) HATU (48.7 mg, 0.128 mmol, 2 equiv) HOAt (17.4 mg, 0.128 mmol, 2 equiv) and NMM (42.2 μL, 0.384 mmol, 6 equiv) in DMF (1 mL, neat) was added and the reaction was let to proceed for 1 h at room temperature The resin was washed with DMF and DCM and then the product was cleaved using a solution of TFA:DCM (3:1),

185

twice for 45 min. The liquids were recovered, the resin was washed with DCM and the solution of the cleaved product was evaporated under vacuum. The crude was washed with toluene 3 to 5 times to evaporate the rests of TFA. The final products were purified by RP-HPLC. The fractions containing the product were mixed and lyophilized overnight. The obtained powder was re-dissolved in a random amount of DMSO (neat) and the concentration was checked by absorbance at 495 nm using a Nanodrop 2000 instrument (Thermo Fisher) with a 1:100 dilution in PBS. HPLC purity of each compound: Compound (**18**), 100%; compound (**19**), 97.2%; compound (**20**), 100%; compound (**21**), 100%. The solutions were then adjusted to 1 mM in DMSO (neat) and stored at -20 °C protected from light.

Synthesis of N-Fmoc-4-(2-phenylethynyl)-L-Phenylalanine: In a 25 mL round bottom flask, *N*-Fmoc-4-iodo-*L*-Phenylalanine (200 mg; 0.39 mmol, 1 equiv), phenylacetylene (128.4 μL, 1.17 mmol, 3 equiv), 4-dimethylaminopyridine (143 mg, 1.17 mmol, 3 equiv) triphenylphosphine (10.24 mg, 0.039 mmol, 0.1 equiv) copper (I) bromide (5.6 mg, 0.039 mmol, 0.1 equiv) and Palladium (II) bis-triphenylphosphine chloride (13.7 mg, 0.0195 mmol, 0.05 equiv) were added, followed by the addition of pre-degassed anhydrous THF. The reaction was stirred vigorously at 50 °C under argon atmosphere. After 4 h the reaction was washed with HCl (1M). The precipitate was filtered off and the mother liquids were extracted with ethyl acetate. The aqueous phase was washed three times with ethyl acetate. The organic phases were combined, dry over sodium sulfate and evaporated to dryness to obtain 223 mg of crude which shows 80% purity by LC-MS. The product was used, without further purification, for the synthesis of the Fluorescein-PEG$_1$-Ro26-4550.

*Synthesis of Fluorescein-PEG$_1$-Ro26-4550 (**Ro26-4550**)*: The synthesis of the free amino derivative of the Fluorescein-PEG$_1$-Ro26-4550 (**Ro26-4550**) was performed following the same procedures as for compounds 1 to 17. After cleavage from the resin, the crude was washed 5 times with toluene and redissolved in DMF (500 μL, neat). 1-amidinopyrazole hydrochloride (16 μL, 16 equiv 1M in DMF) was added to the crude and the reaction was stirred over 72 hours at room temperature to obtain the final guanidino derivative. The reaction was stopped by dilution with water and the product directly purified by HPLC. The fractions containing the product were mixed and lyophilized overnight. The obtained powder was re-dissolved in a random amount of DMSO (neat) and the concentration was checked by absorbance at 495 nm using a Nanodrop 2000 instrument (Thermo Fisher) with a 1:100 dilution in PBS. HPLC purity: 98.3%. The solution was then adjusted to 1 mM in DMSO (neat) and stored at -20 °C protected from light.

Off-DNA fluorescence polarization experiments

Fluorescence polarization experiments were performed in triplicates for each of the desired compounds, in 384-well black plates. A stock solution of the desired protein (at the highest concentration) was serially diluted (1:1 in PBS) in order to have 15 μL/well. Then, a solution of the corresponding Fluo-PEG$_2$- or Fluo-PEG$_1$- ligand (15 μL/well) was added to the protein reaching 100 nM final concentration of compound. Measurements were done right after the addition of the compound (time 0) and after keeping the solution for 30 min at room temperature (time 1) and 60 min (time 2) in the dark to confirm reproducibility. The mean anisotropy values of the three replicates were fitted to **Equation 1** using Prism 7 (GraphPad), where A is the anisotropy, $[P]_0$

the total protein concentration, $[L]_0$ the total concentration of the fluorescently labeled ligand and K_d the dissociation constant.

Gel filtration coelution experiments

A solution of the corresponding protein (5 μM final concentration) and the corresponding Fluo-PEG$_1$-ligand (2 μM final concentration) in PBS (2% DMSO final) was incubated for 5 min at room temperature in the dark. The solution was then added to a Shepadex pre-packed NAP5 column (Cytiva) and the complex was eluted by subsequent additions of PBS 2% DMSO (500 μL each) collecting one drop per fraction in 96-well plates, for a total volume of 7 mL. Concentration of protein was determined by UV absorbance at 280 nm in a Nanodrop 2000 instrument and fluorescence intensity was measured in a Tecan Spark instrument (TECAN) and plotted together as a function of the elution volume.

ELISA competition experiments

96-well MaxiSorp plates (Thermo Fisher) were coated with NARA1 Fab format (100 nM, 100 μL in PBS) for 16 h at 4 °C. Wells were washed three times with PBS after every step described in this protocol. Blocking solution (2% Milk in PBS, 200 μL) was added to each well and incubated for 1 h at room temperature. Different dilutions of the corresponding Fluo-PEG$_1$-ligand were prepared in DMSO, added to a solution of 10 nM L19-IL2 in PBS (2% DMSO final), and incubated for 15 min at room temperature in the dark. The preincubated solutions were added to the wells to let them interact with the pre-coated NARA1 for 1h at room temperature in the dark. The unbound L19-IL2 was removed by washing with PBS. Protein A HRP-conjugated (Sigma Aldrich, 100 μL, dil. 1:1000) binds the variable heavy chain of the L19 and was used as a detection method. After 1h at room temperature in the dark the wells were extensively washed with PBS containing 0.1% Tween-20 and then with PBS. The 3,3',5,5'-tetramethylbenzidine substrate (TMB, 60 μL, Roche) was added to each well and after 1.5 min the reaction was stopped by addition of sulfuric acid (40 μL, 1M solution). The absorbance was measured at 450 and 620 nm and the inhibition of bound L19-IL2 was plotted as a function of compound concentration.

Recombinant proteins production

All the recombinant proteins including: L19 and F8 antibodies in diabody format (recognizing the extracellular domain A and B of fibronectin, respectively); F8F8-IL15 fusion protein, NARA1 in Fab format (recognizing the CD25 binding epitope of IL2), TNF, CAIX and EDA were produced in CHO mammalian cells. The sequences and quality controls can be found in the supplementary information (section 6.4.2).

6.4.2 Supplementary information

Affinity selection experiments replicate fingerprints

L19-IL2:

Counts (C)	Total Counts (T)	Library Size (S)	"Noise" (N)	Enrichment Factor (EF)	BB1	BB2
303	445983	669240	0.67	455	173	985
251	445983	669240	0.67	377	156	722
212	445983	669240	0.67	318	156	1317
202	445983	669240	0.67	303	156	1316
178	445983	669240	0.67	267	156	1015
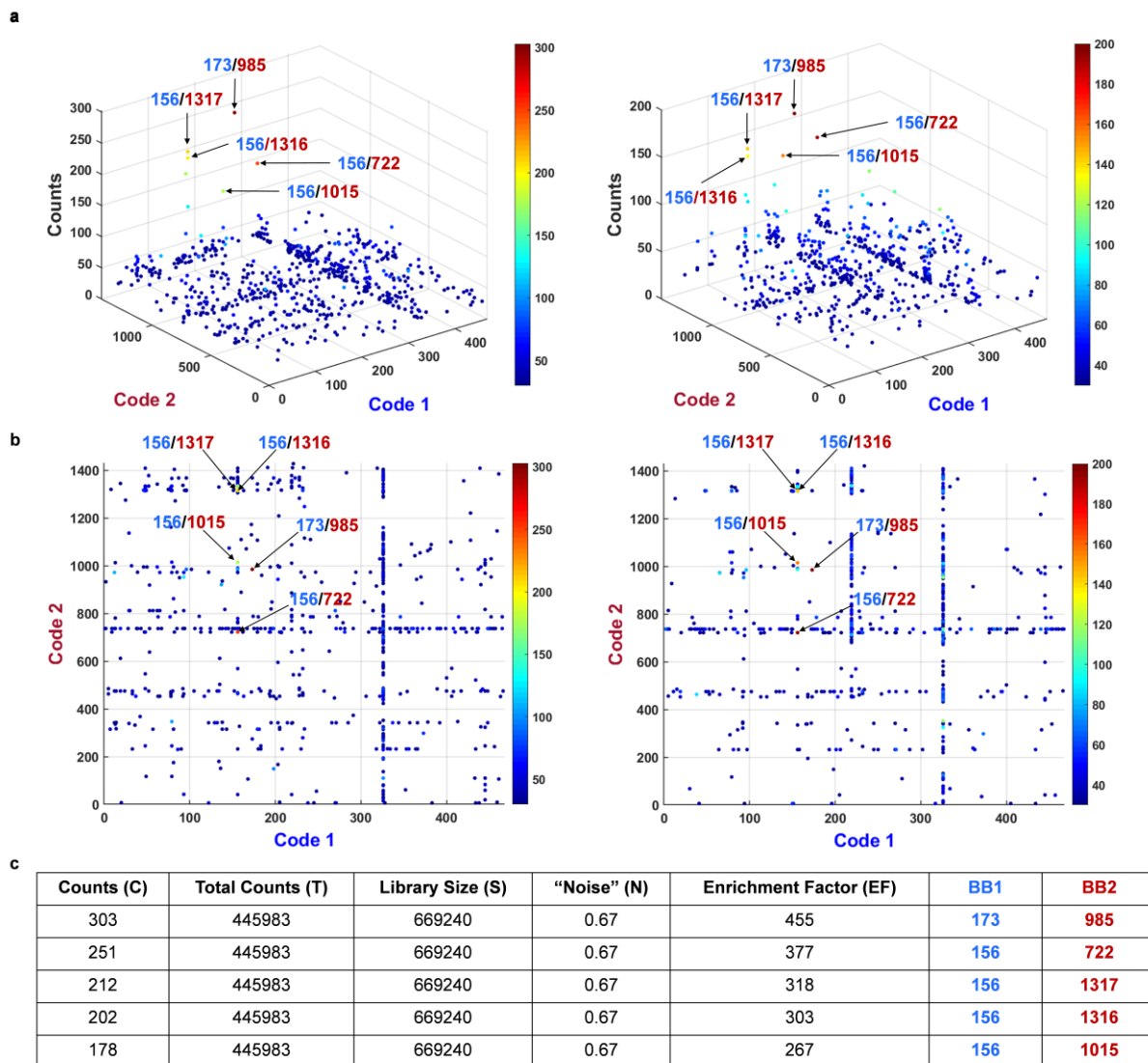
$$EF = \frac{C}{N} = \frac{C}{(T/S)}$$

Figure 6.4.1. Affinity selection replicates of AG-DEL against L19-IL2. **a**. 3D plots. **b**. 2D plots. **c**. Enrichment factors (EFs) of the 5 most enriched compounds calculated with the indicated equation. Enrichment factors are consistent between both replicates.

On-DNA resynthesis
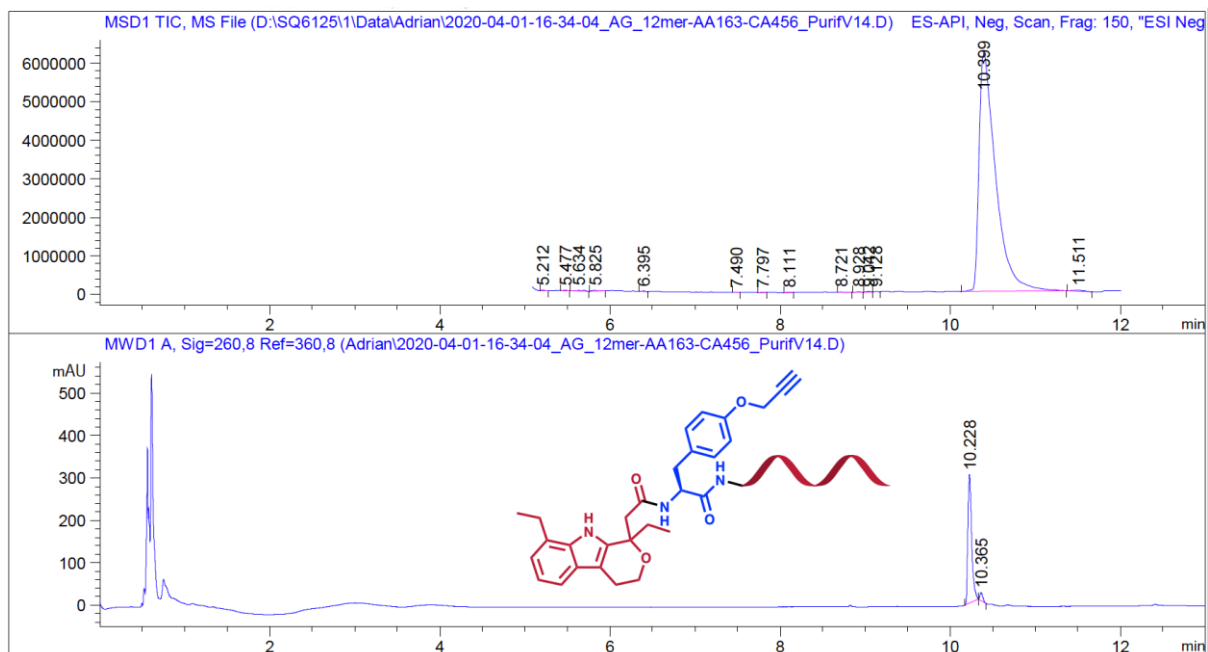
Deconvolution of Spectrum #   1 @ 10.575 - 10.876 min
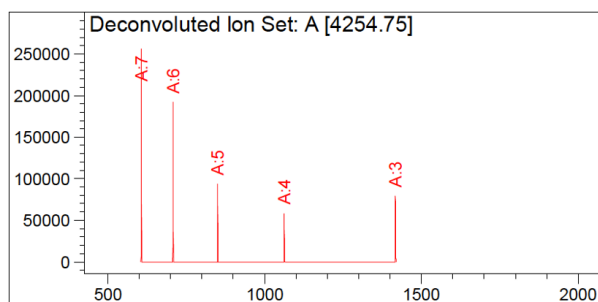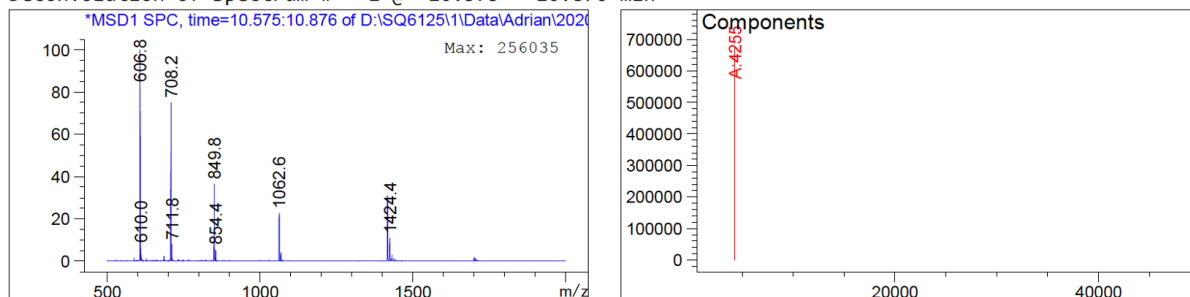
Component	Molecular Weight	Absolute Abundance	Relative Abundance
A	4254.75	675633	100.00

*** End of Report ***

Figure 6.4.2. LC-ESI-MS chromatogram of compound **AG-173/985 Isomer 1**, t_R:10.228 min (DAD), 10.399 min (TIC). Expected mass 4255.18, observed 4254.75.
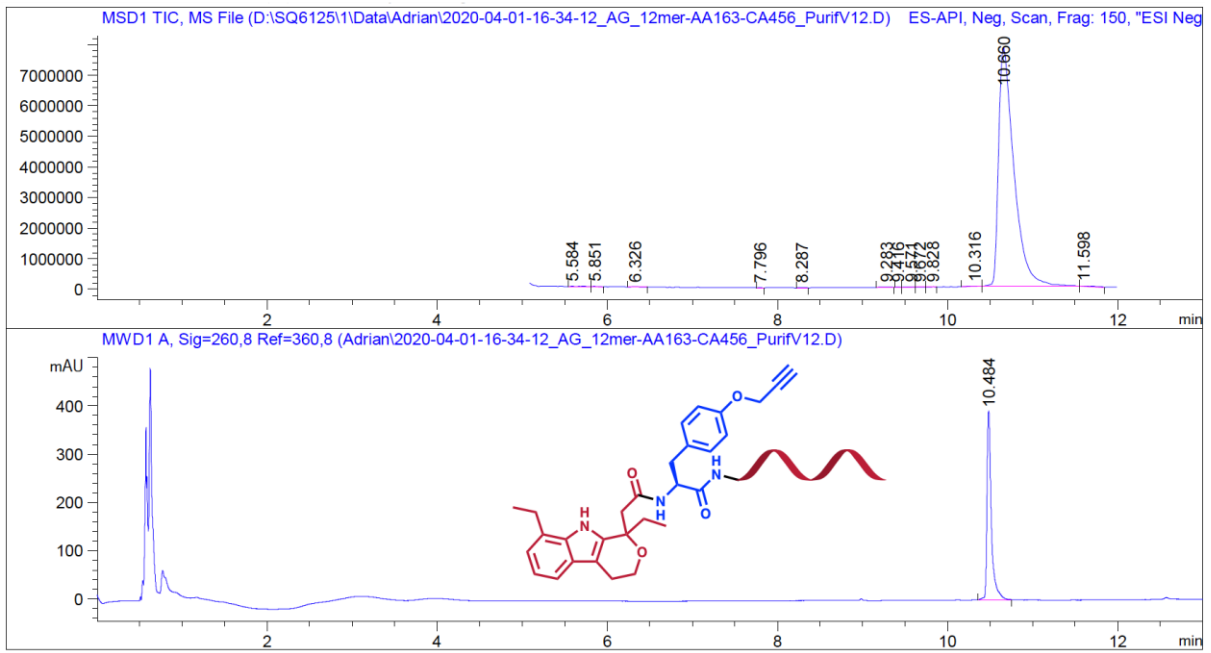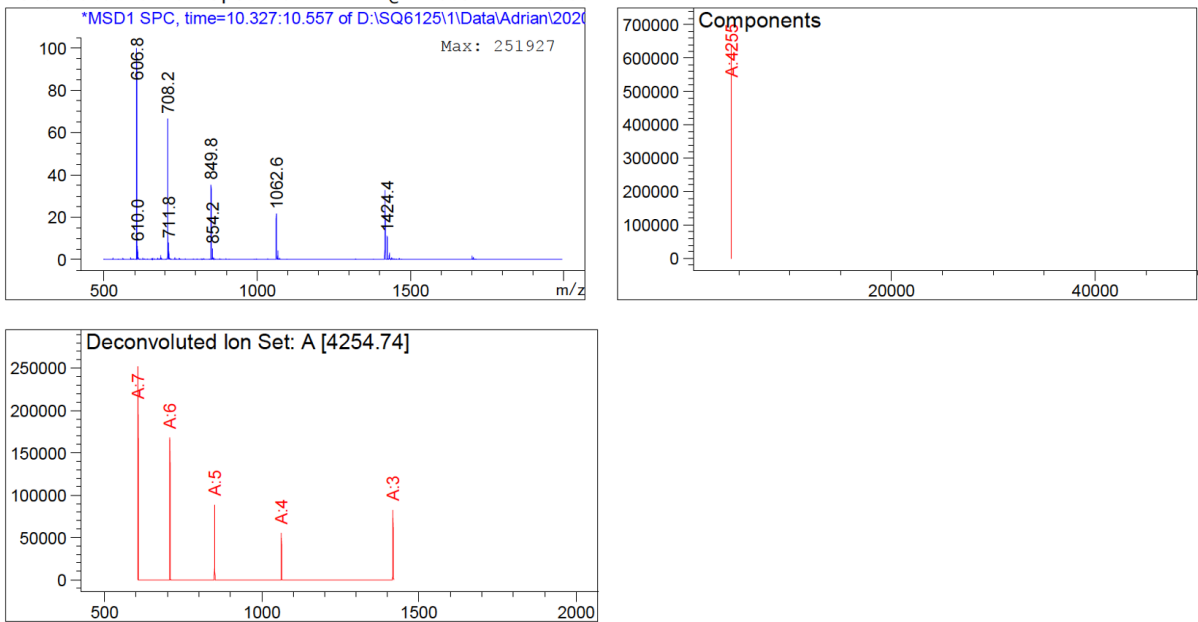
Figure 6.4.3. LC-ESI-MS chromatogram of compound **AG-173/985 Isomer 2**, t_R:10.484 min (DAD), 10.660 min (TIC). Expected mass 4255.18, observed 4254.74.
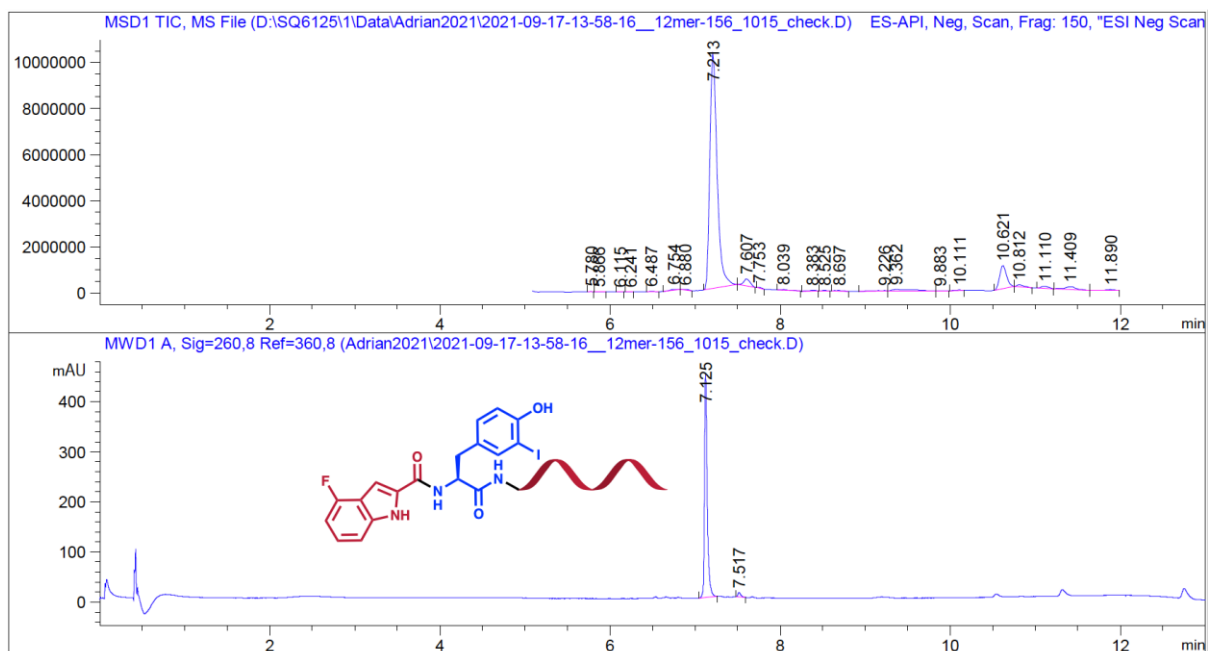
Deconvolution of Spectrum # 1 @ 7.175 - 7.263 min
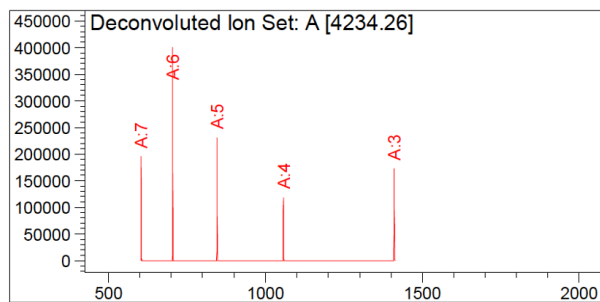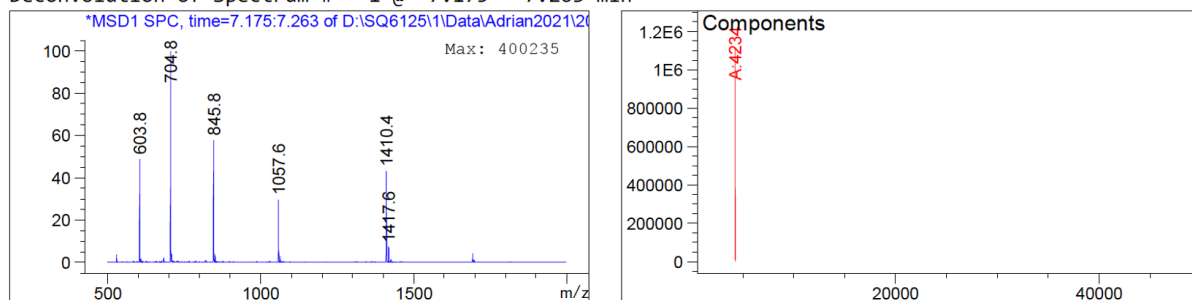
Component	Molecular Weight	Absolute Abundance	Relative Abundance
A	4234.26	1113278	100.00

*** End of Report ***

Figure 6.4.4. LC-ESI-MS chromatogram of compound **AG-156/1015**, t_R:7.125 min (DAD), 7.213 min (TIC). Expected mass 4234.82, observed 4234.26.
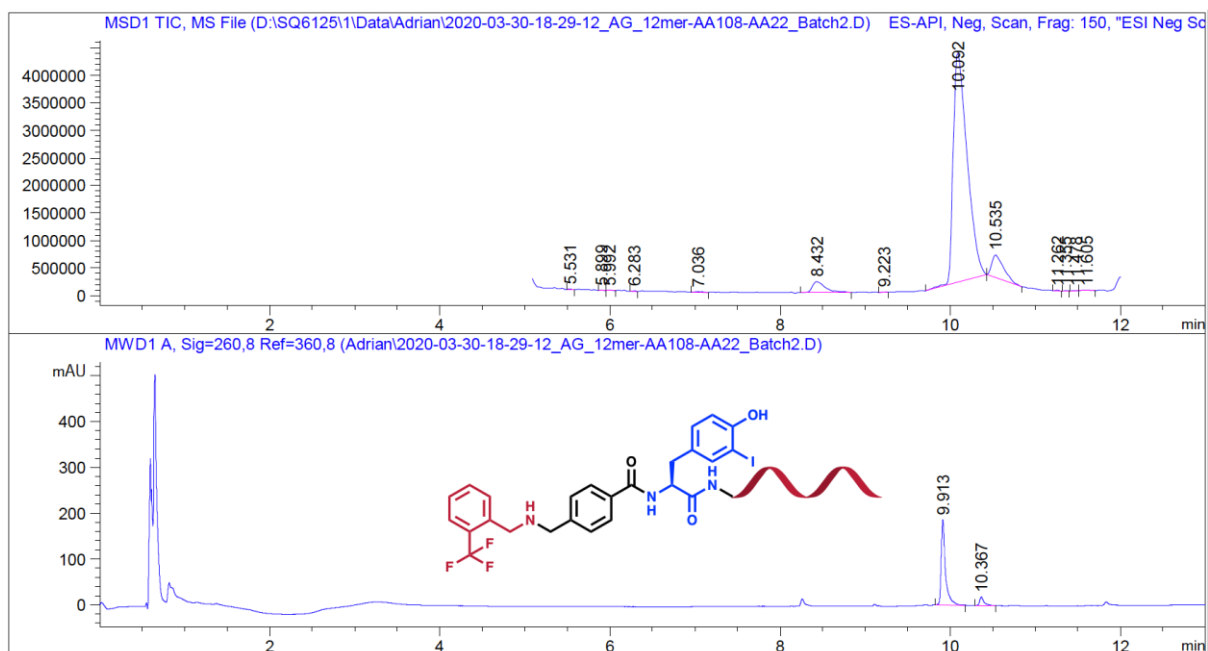
Deconvolution of Spectrum #   1 @ 10.026 - 10.274 min
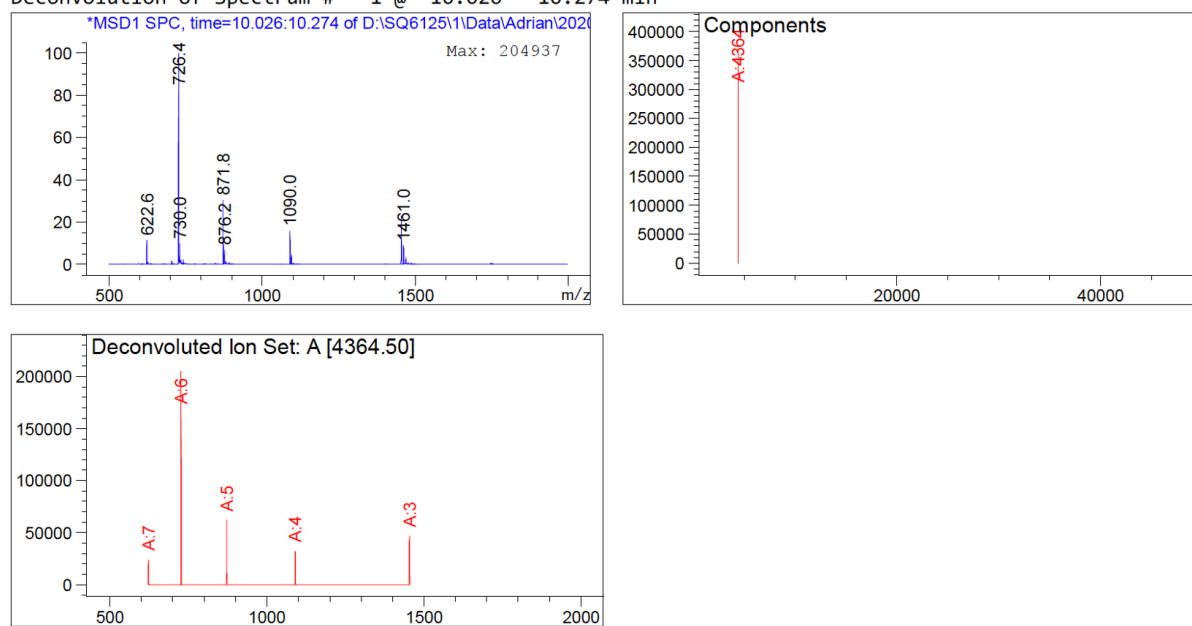
Component	Molecular Weight	Absolute Abundance	Relative Abundance
A	4364.50	368249	100.00

*** End of Report ***

Figure 6.4.5. LC-ESI-MS chromatogram of compound **AG-156/1317**, t_R:9.913 min (DAD), 10.092 min (TIC). Expected mass 4364.96, observed 4364.50.
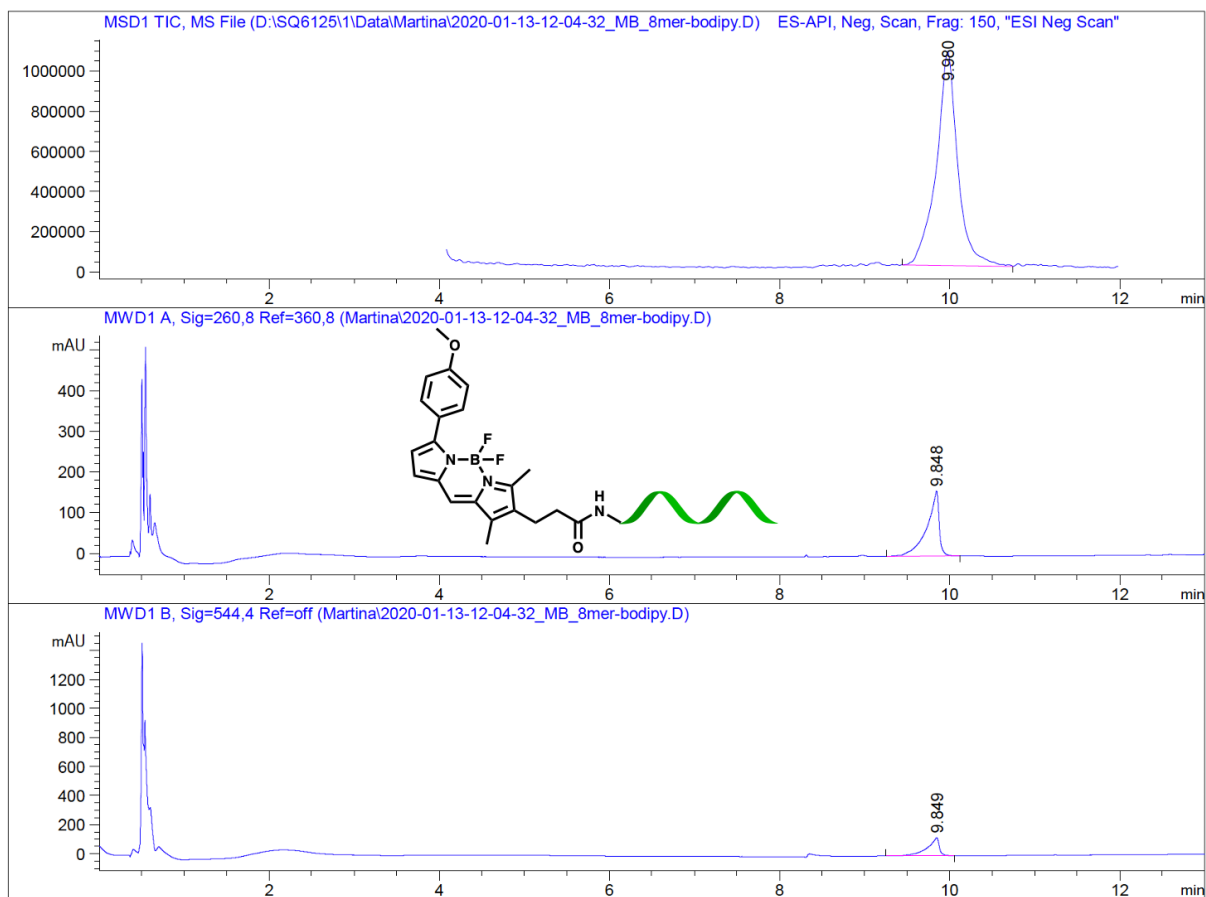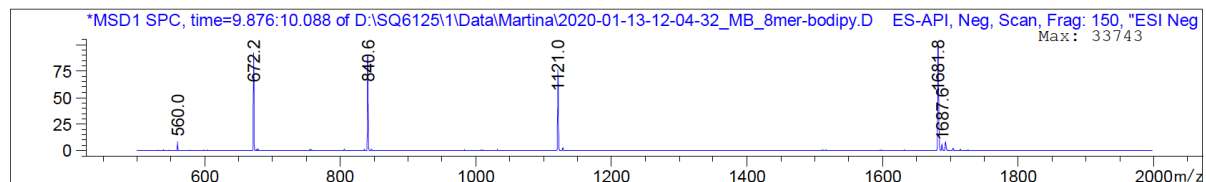
Figure 6.4.6. LC-ESI-MS chromatogram of compound **8-mer LNA-BODIPY**, t_R:9.848 min (DAD), 9.980 min (TIC). Expected mass 3366.05, observed 3366.08.

Off-DNA resynthesis
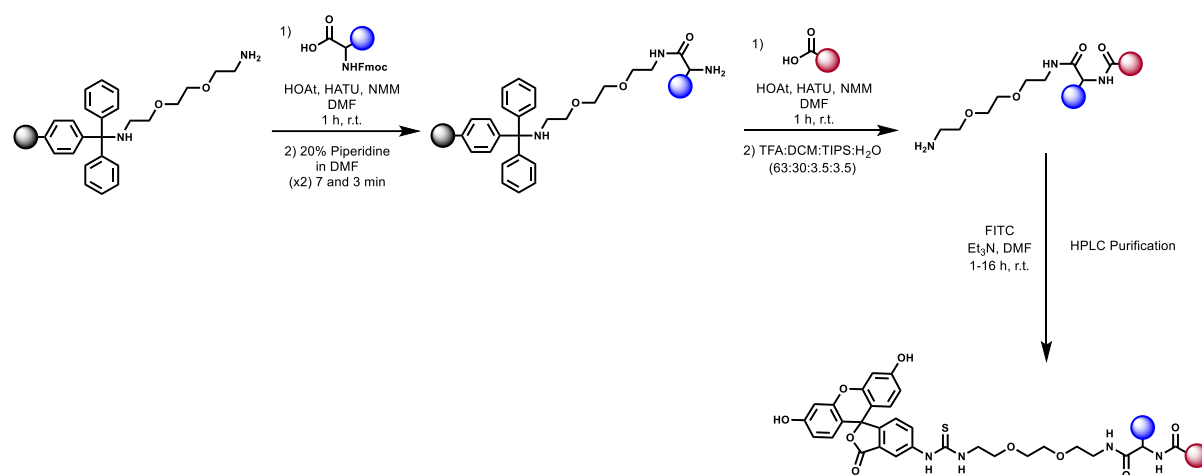
Scheme 6.4.1. Synthetic route for the synthesis of compounds **AG-173/985**, **AG-156/1317** and **AG-156/1015**. The grey ball represents the solid support, the blue ball represents the building block 1 and the red ball represents the building block 2.
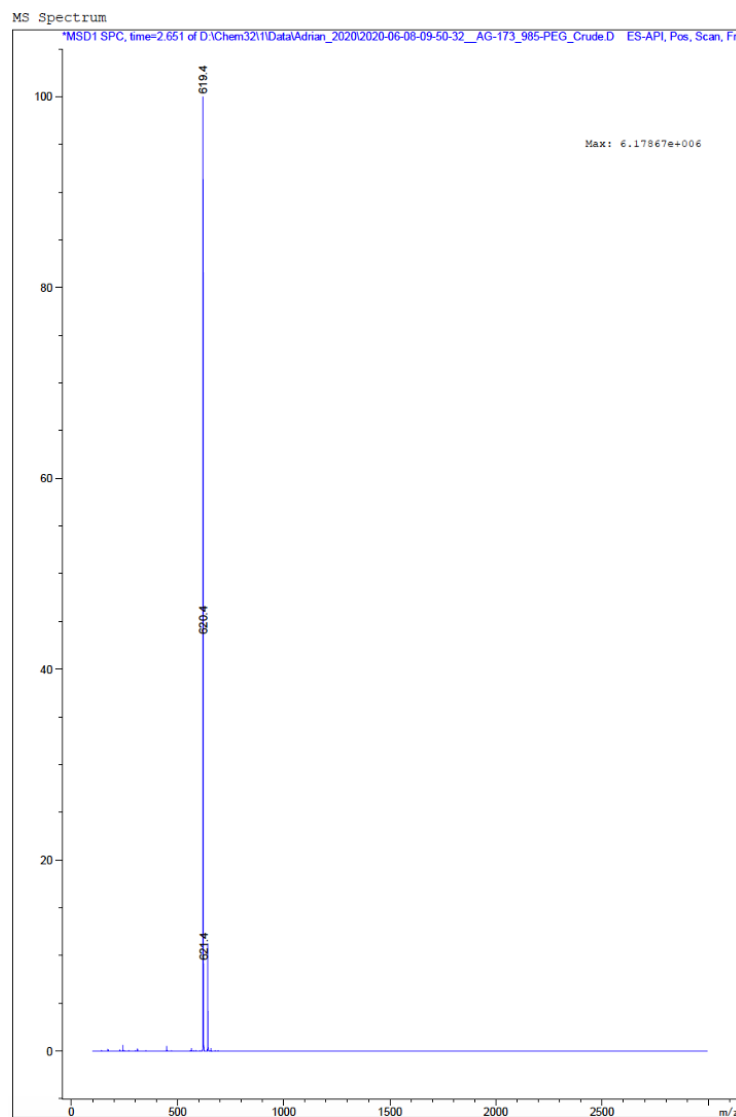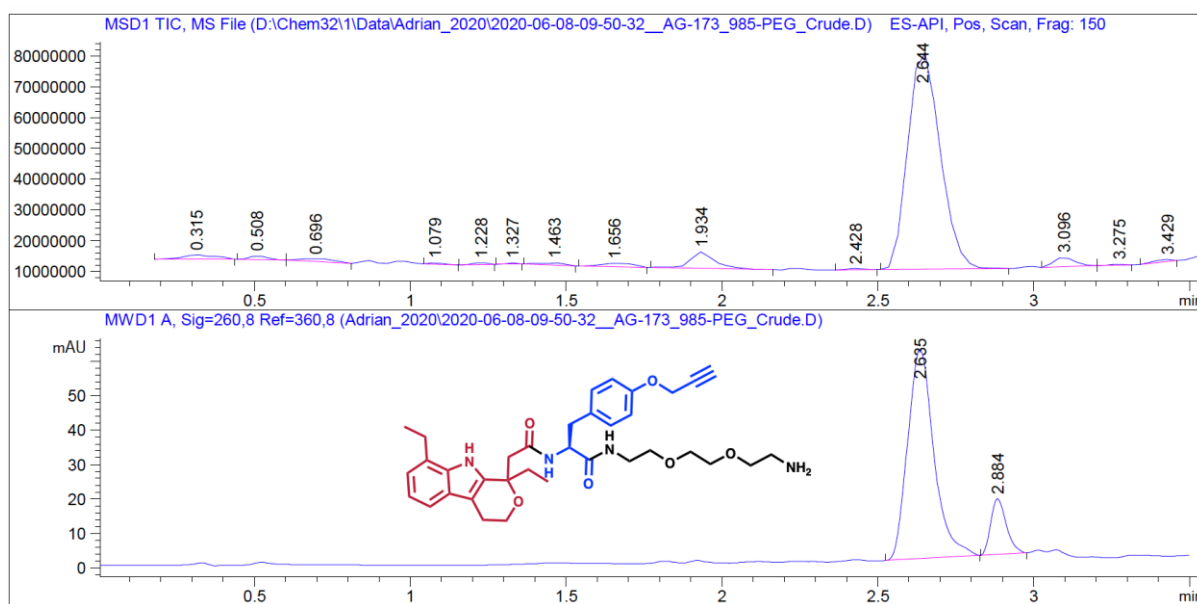
Figure 6.4.7. LC-ESI-MS chromatogram of compound **AG-173/985-PEG₂-NH₂**, t_R:2.635 min (DAD), 2.644 min (TIC). Expected mass 618.3, observed 619.4.
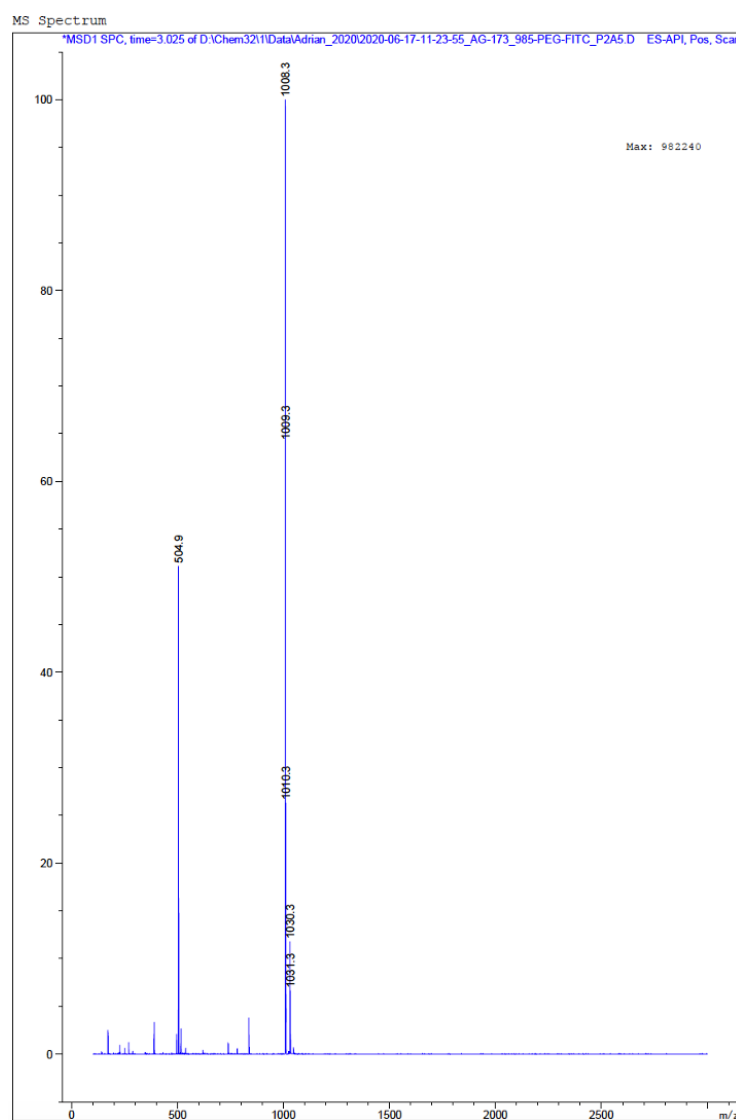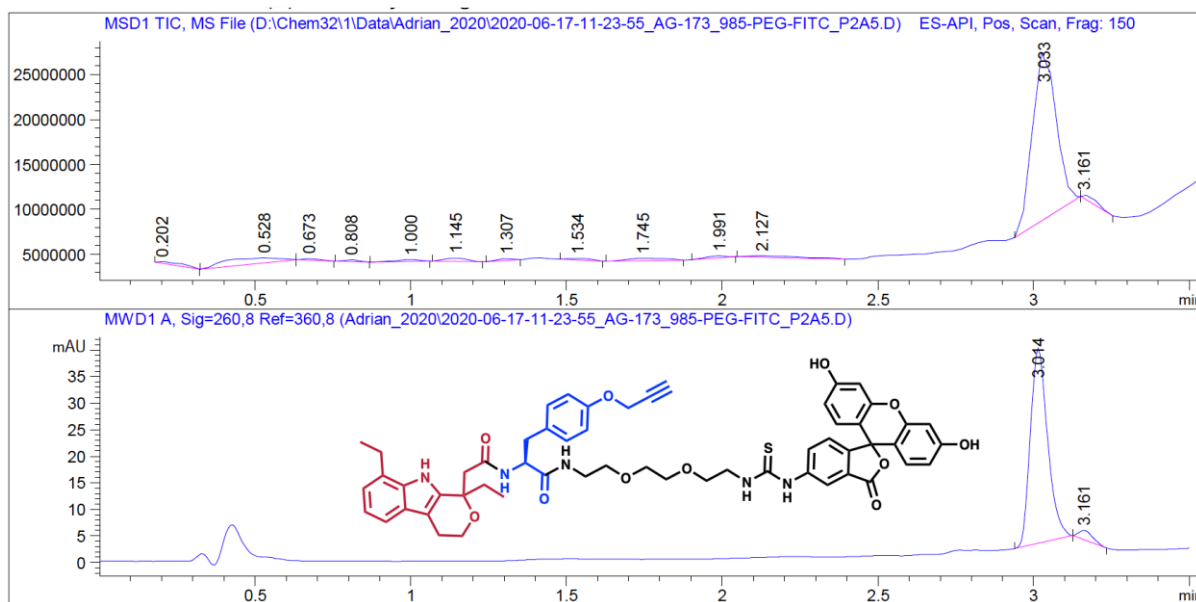
Figure 6.4.8. LC-ESI-MS chromatogram of compound **AG-173/985**, t_R:3.014 min (DAD), 3.033 min (TIC). Expected mass 1007.4, observed 1008.3.
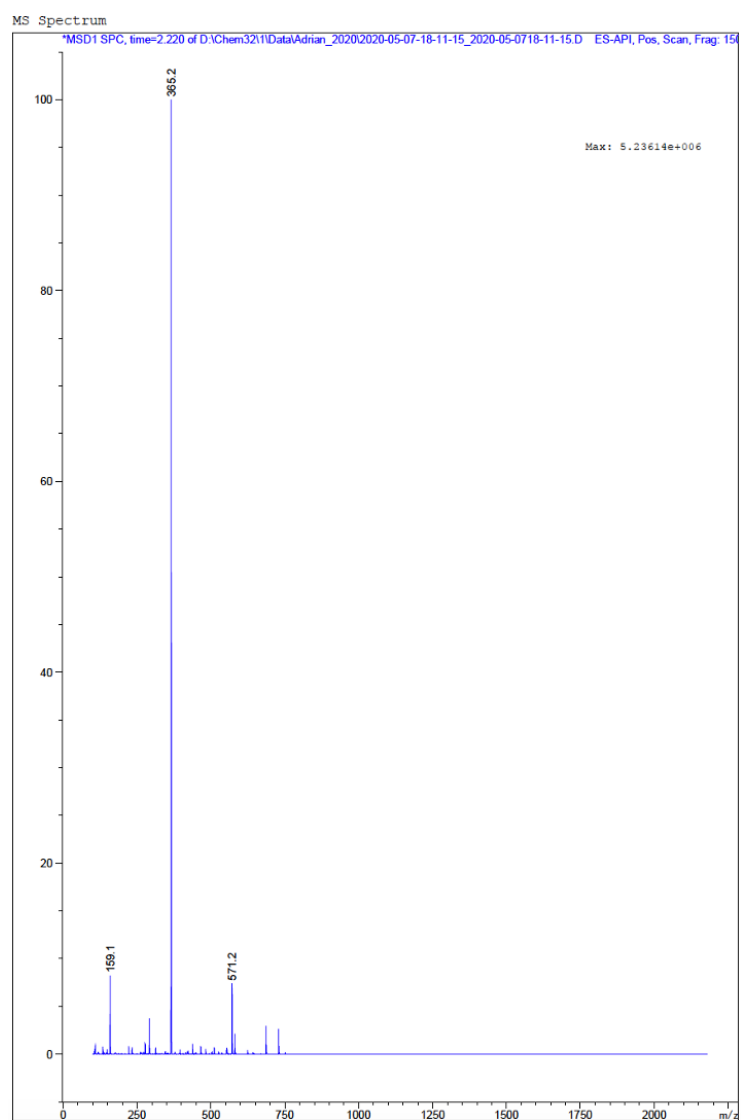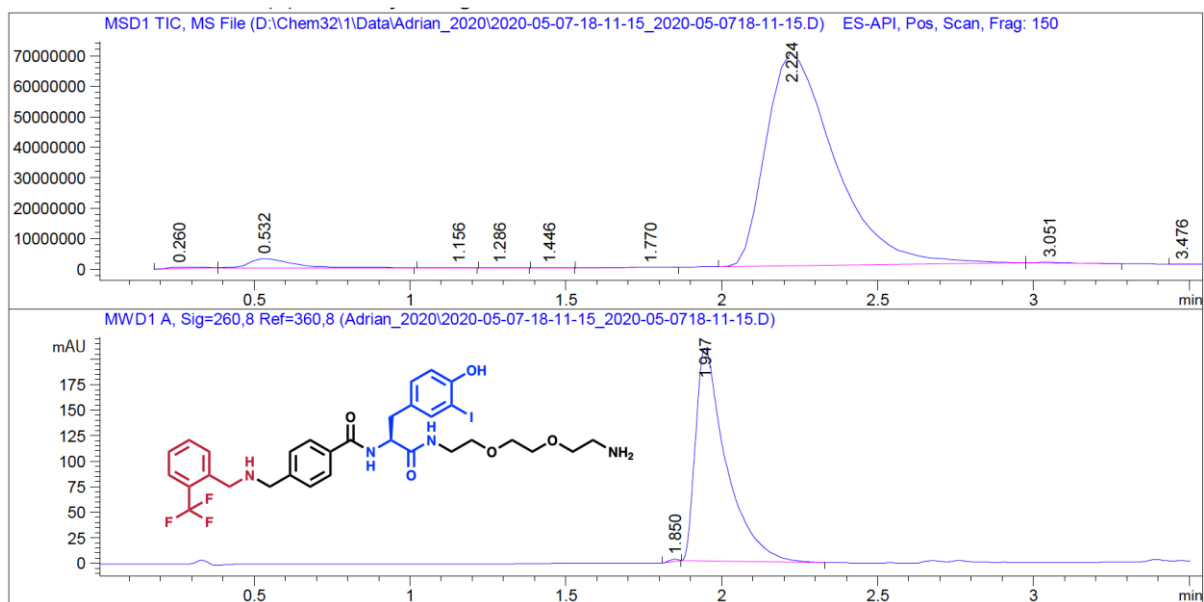
Figure 6.4.9. LC-ESI-MS chromatogram of compound **AG-156/1317-PEG$_2$-NH$_2$**, t_R:1.947 min (DAD), 2.224 min (TIC). Expected mass 728.2, observed 365.2 (z=2) corresponding to 729.4.

197
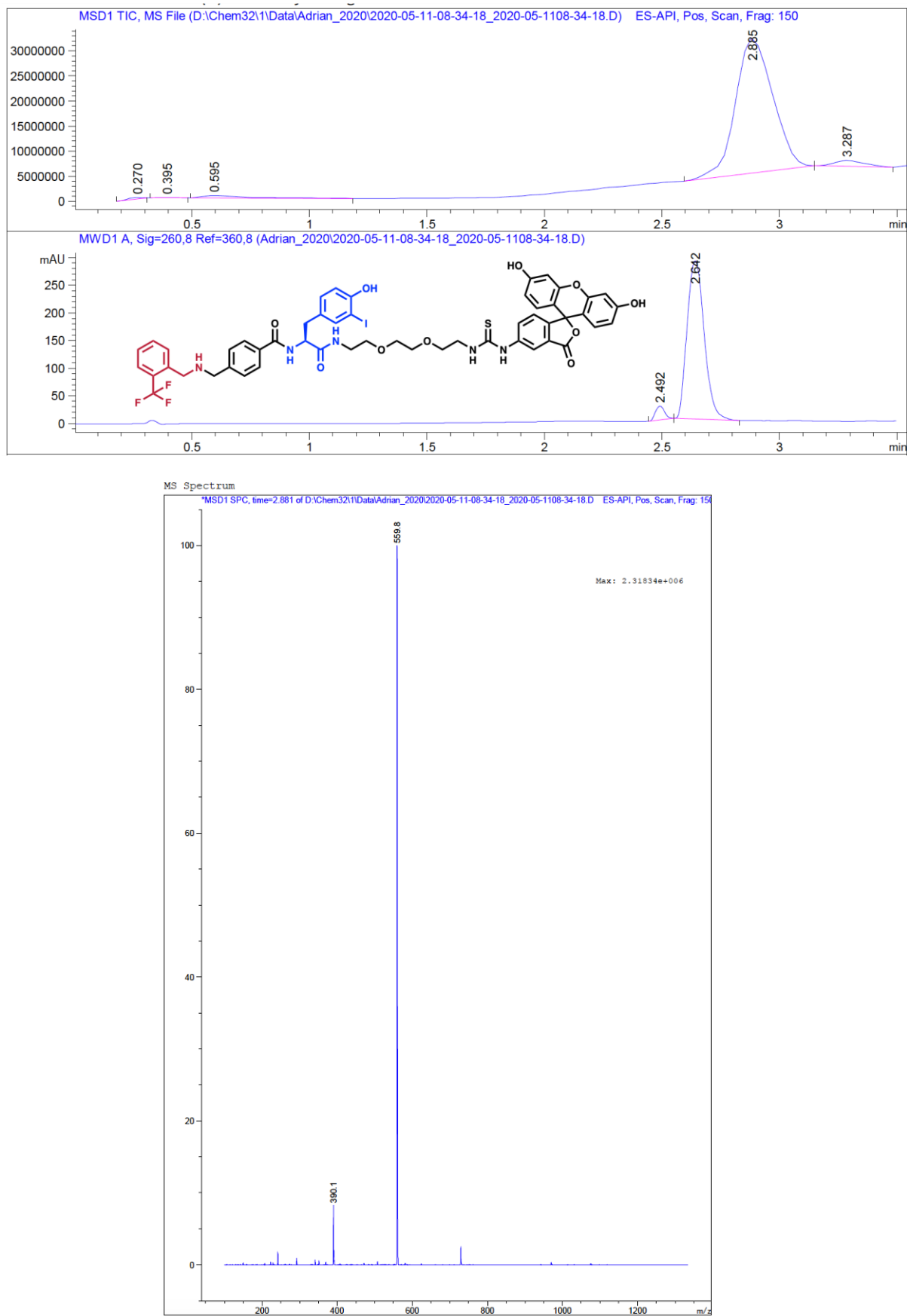
Figure 6.4.10. LC-ESI-MS chromatogram of compound **AG-156/1317**, t_R:2.642 min (DAD), 2.885 min (TIC). Expected mass 1117.2, observed 559.8 (z=2) corresponding to 1118.6.
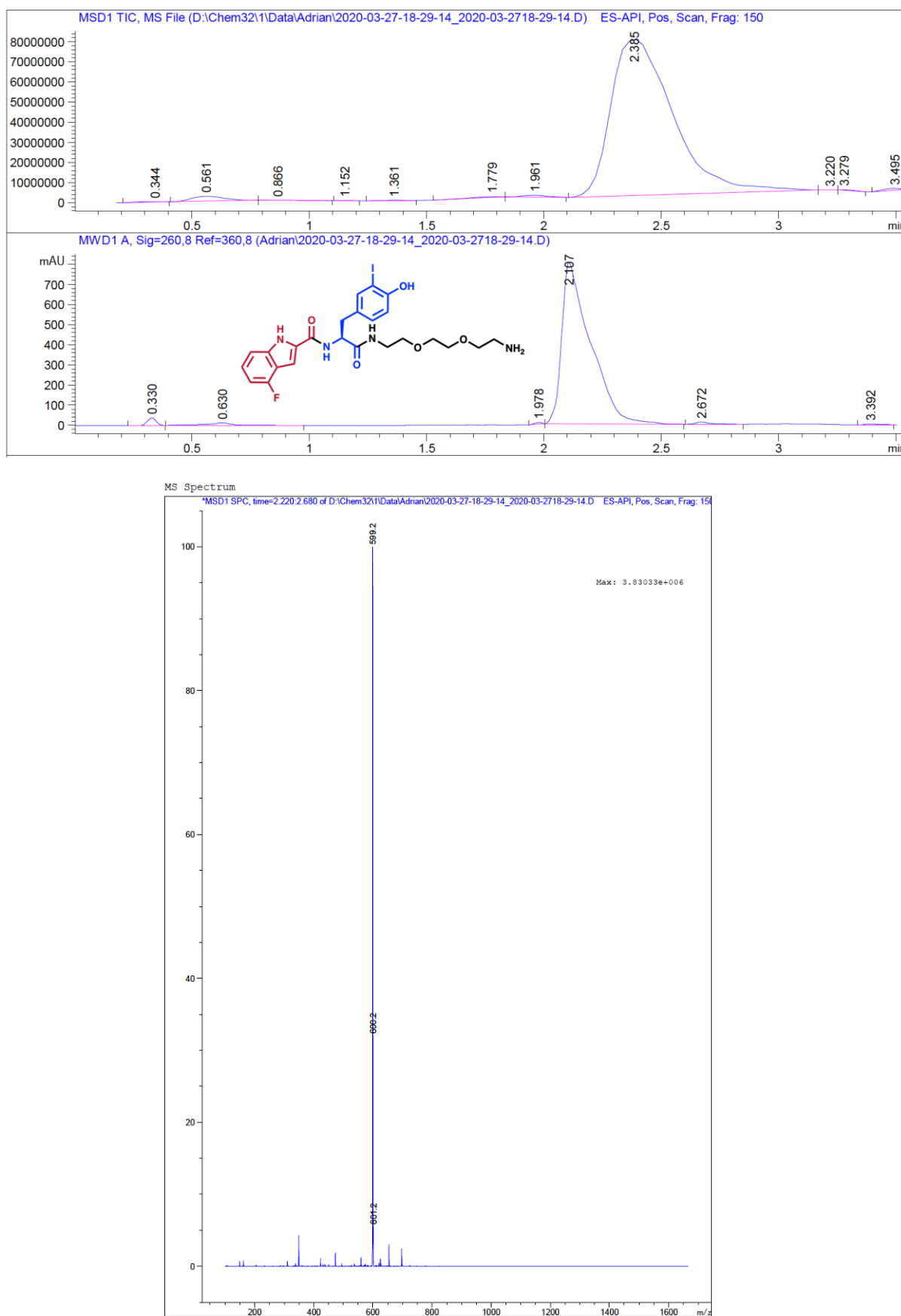
Figure 6.4.11. LC-ESI-MS chromatogram of compound **AG-156/1015-PEG$_2$-NH$_2$**, t_R:2.107 min (DAD), 2.385 min (TIC). Expected mass 598.1, observed 599.2.
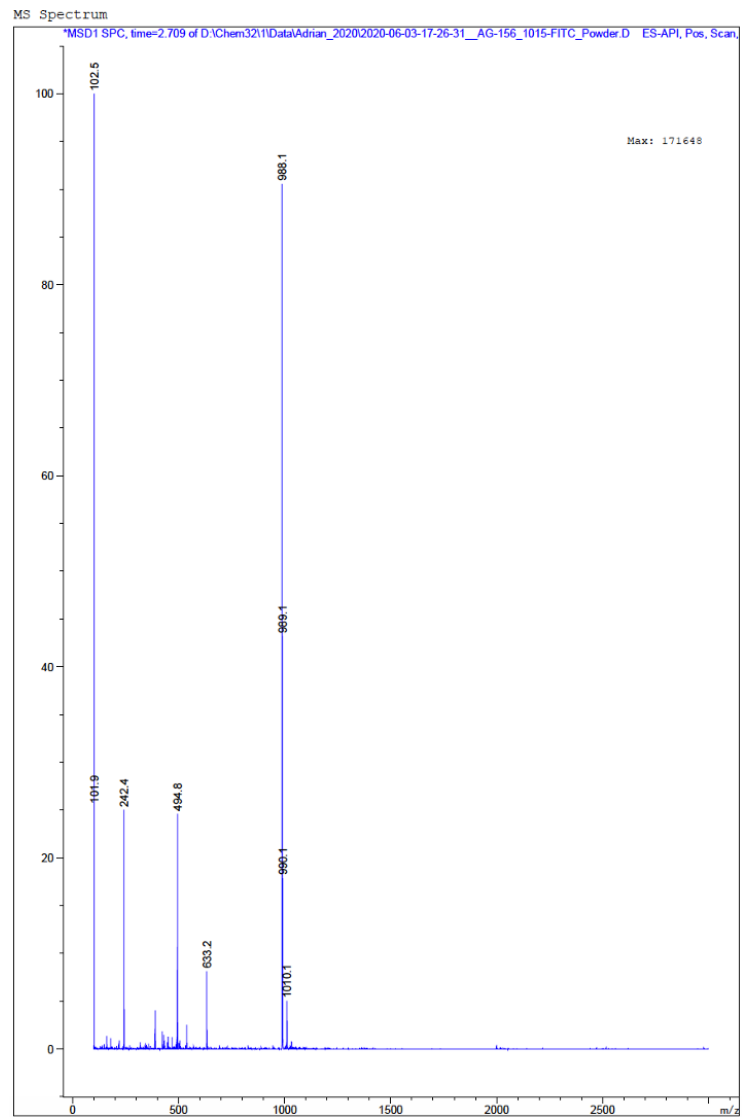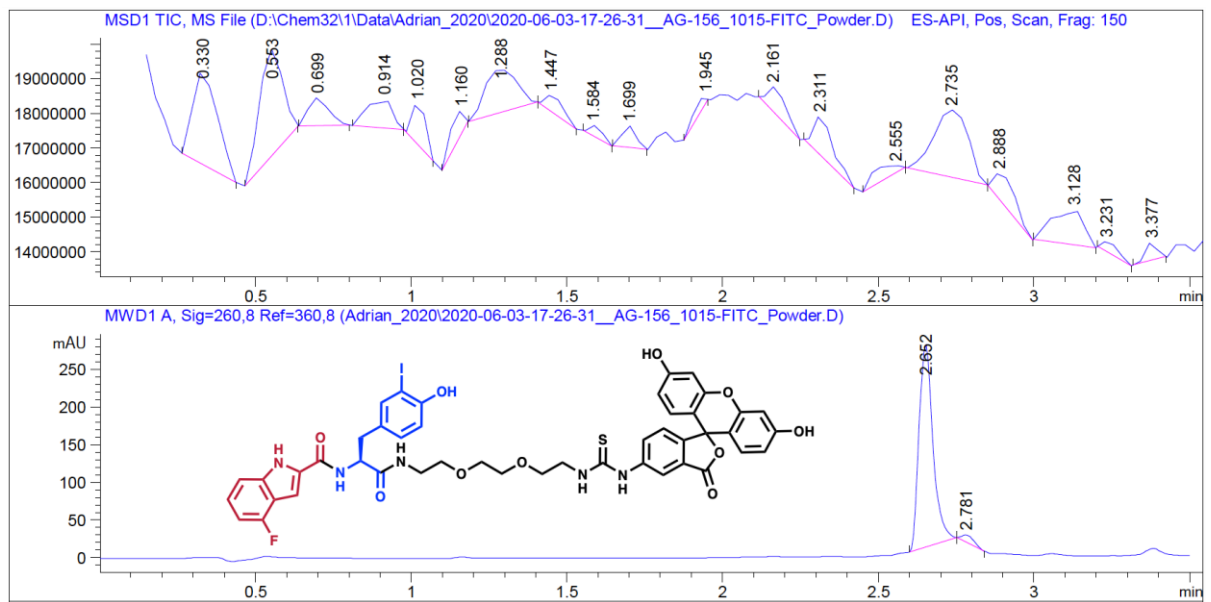
Figure 6.4.12. LC-ESI-MS chromatogram of compound **AG-156/1015**, t_R:2.652 min (DAD), 2.735 min (TIC). Expected mass 987.1, observed 988.1.
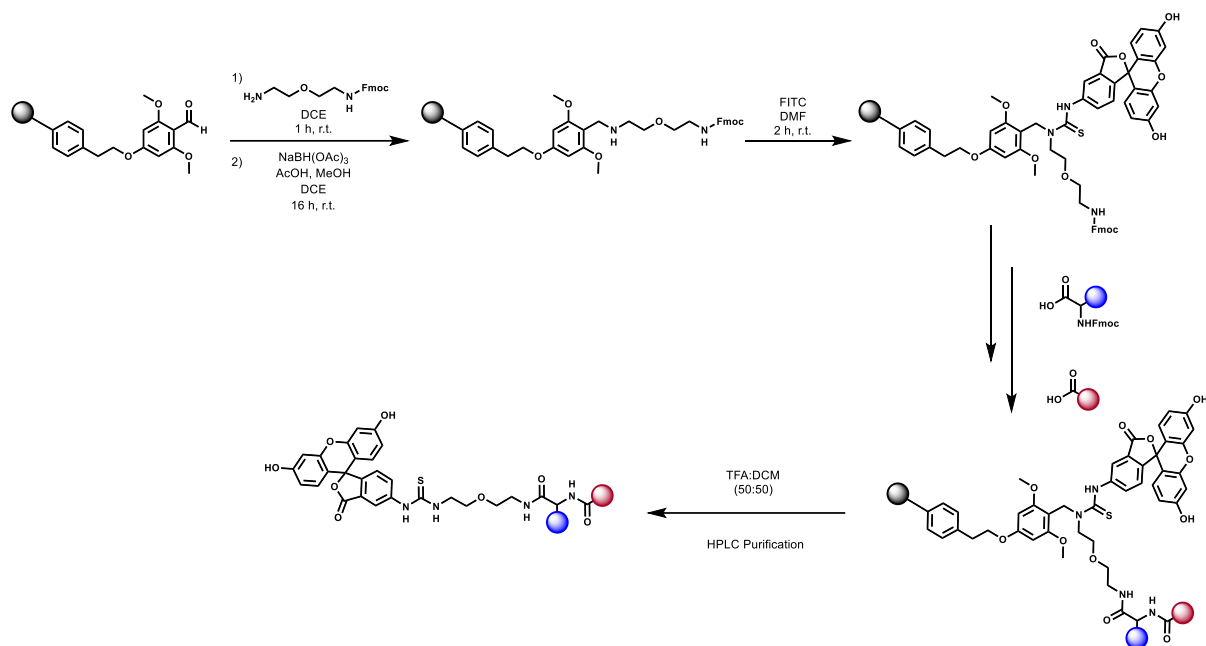
Scheme 6.4.2. Synthetic route for the synthesis of compounds **1-17** and **Ro26-4550**. The grey ball represents the solid support, the blue ball represents the building block 1 and the red ball represents the building block 2.
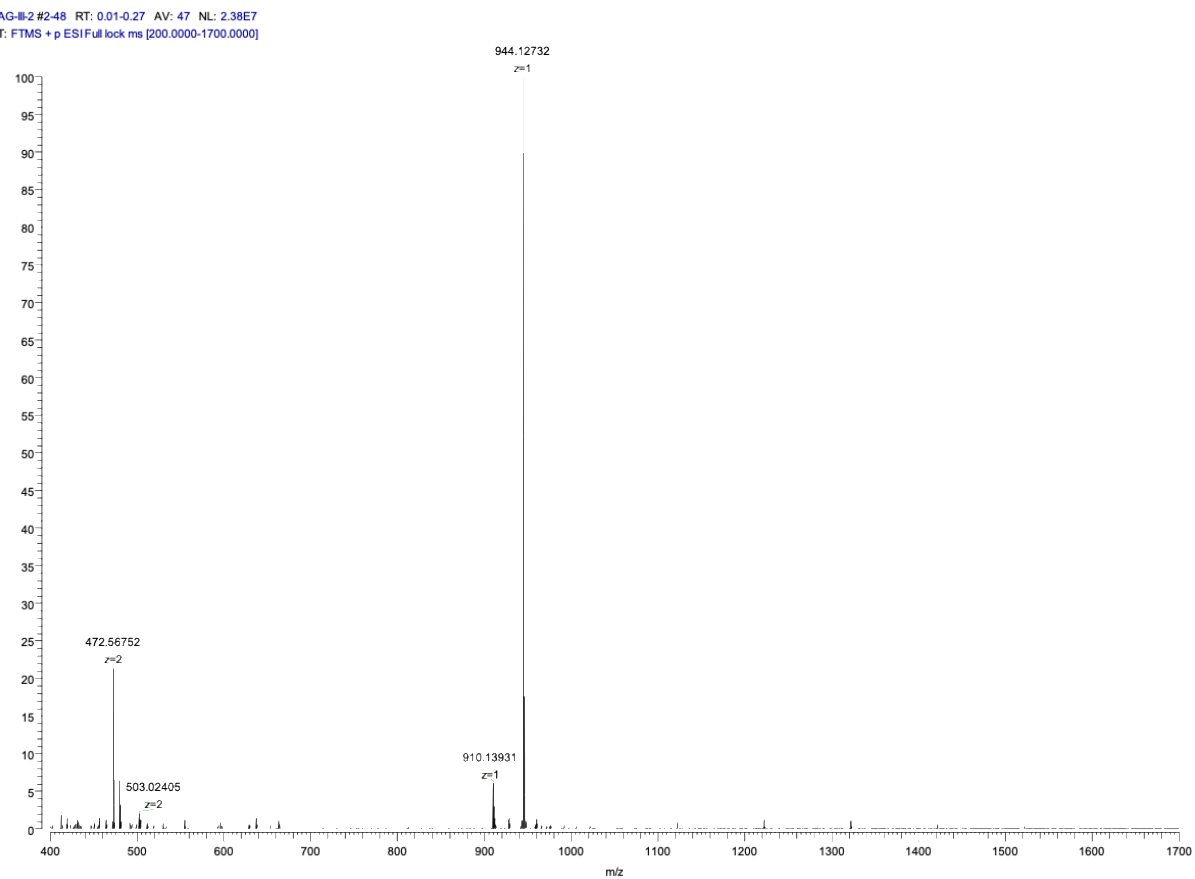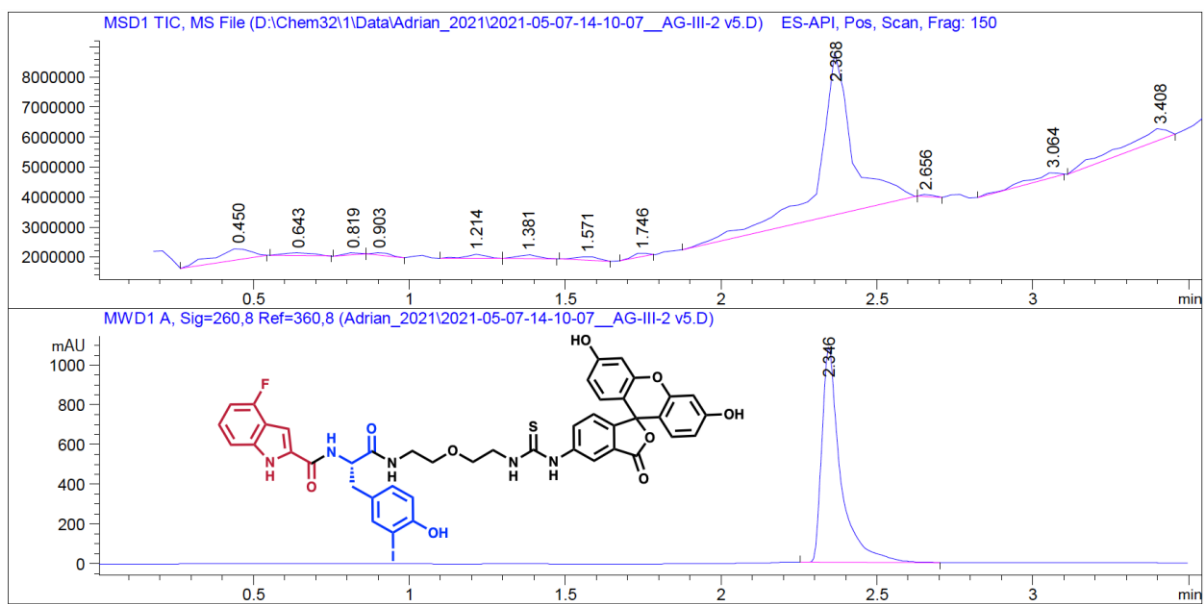
Figure 6.4.13. LC-HRMS chromatogram of compound **1**, t_R:2.346 min (DAD). Expected mass 943.11842, observed 944.12732.
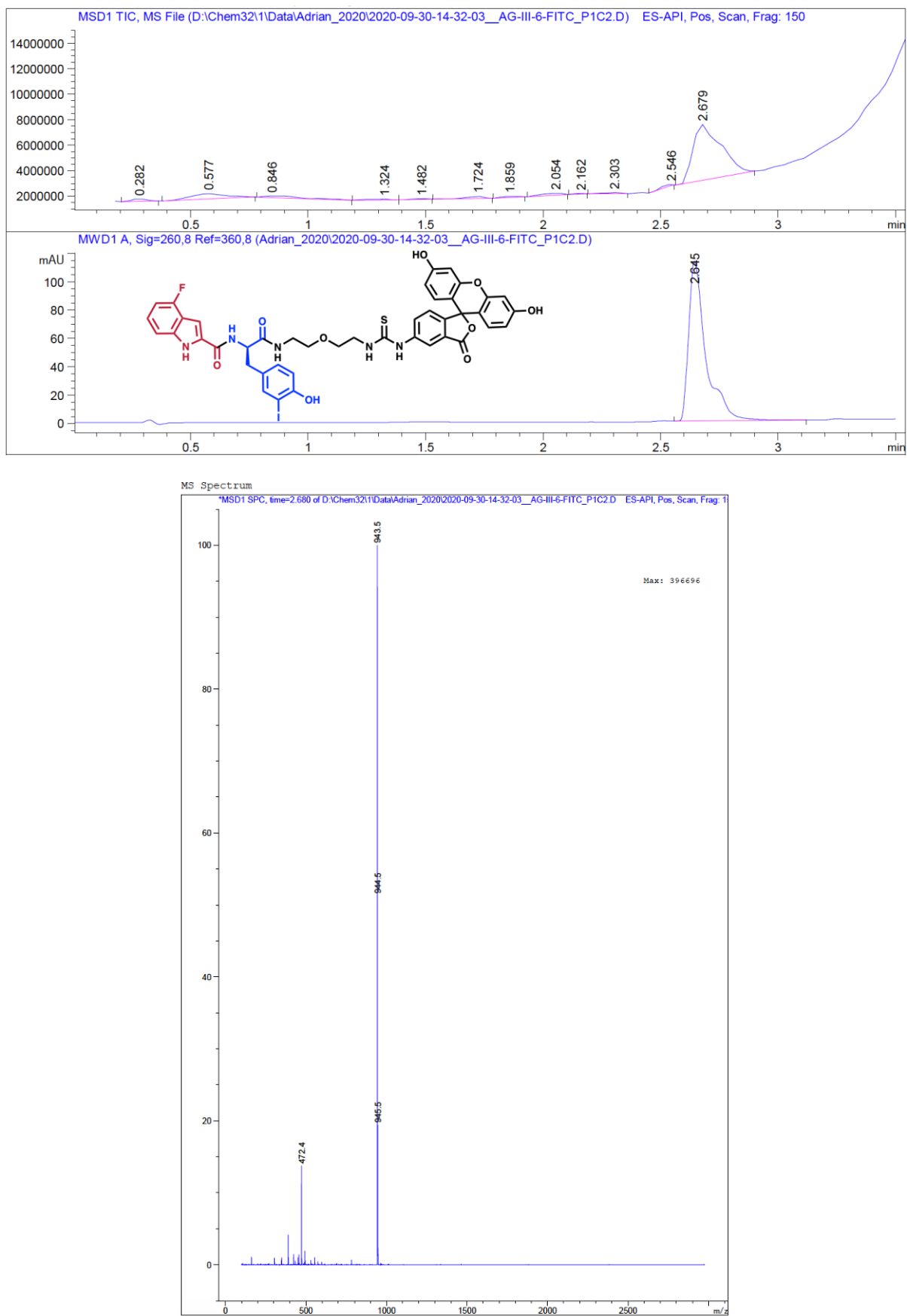
Figure 6.4.14. LC-ESI-MS chromatogram of compound **2**, t_R:2.645 min (DAD), 2.679 min (TIC). Expected mass 943.1, observed 943.5.
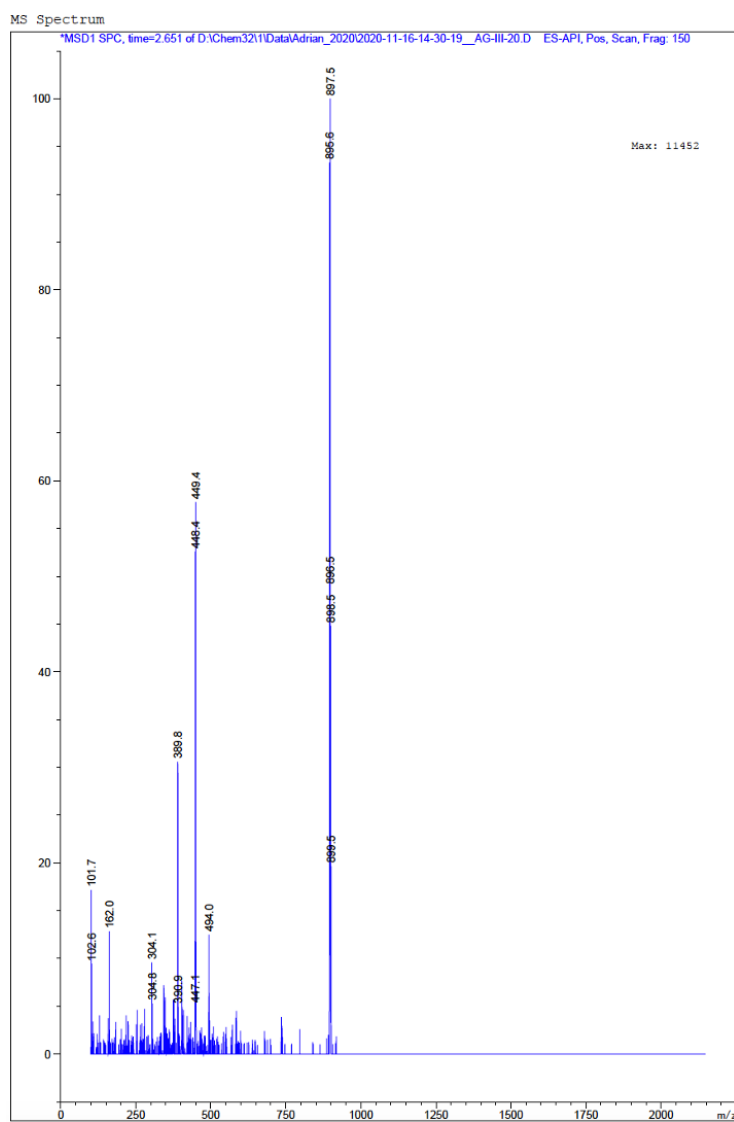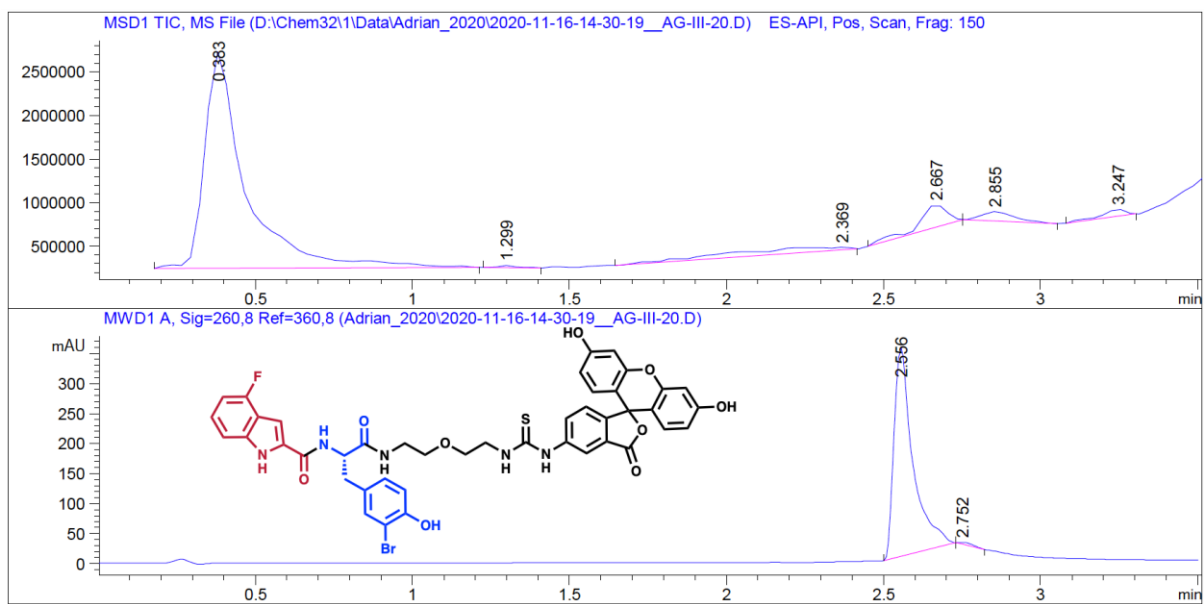
Figure 6.4.15. LC-ESI-MS chromatogram of compound **3**, t_R:2.556 min (DAD), 2.667 min (TIC). Expected mass 895.1, observed 897.5.
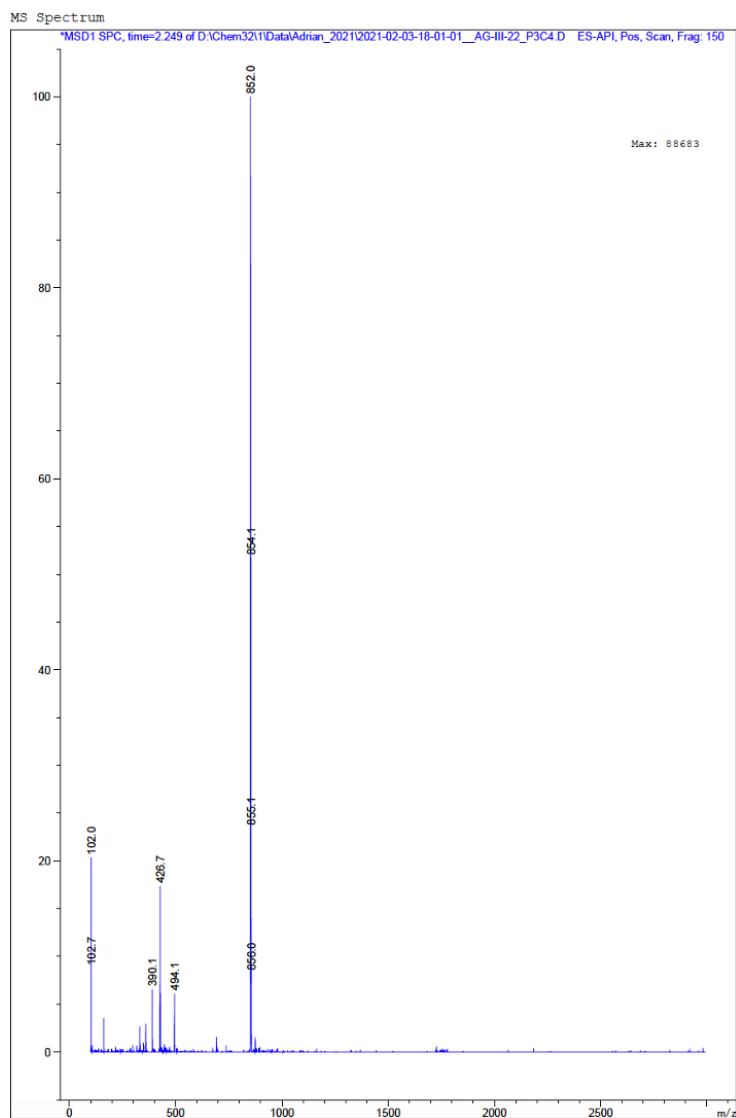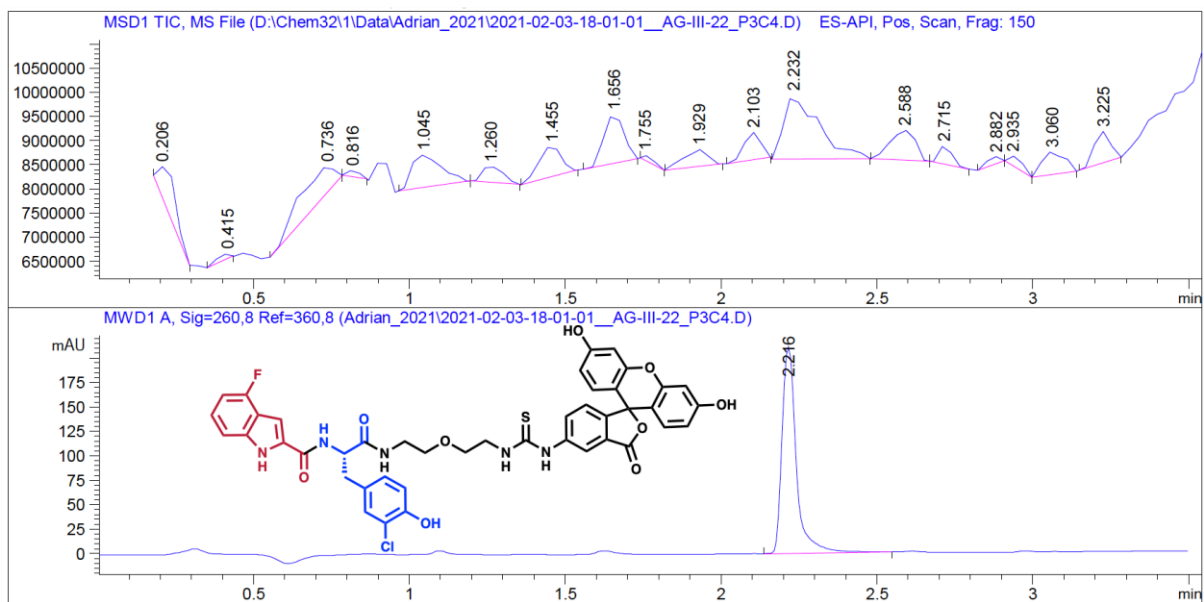
Figure 6.4.16. LC-ESI-MS chromatogram of compound **4**, t_R:2.216 min (DAD), 2.232 min (TIC). Expected mass 851.2, observed 852.0.
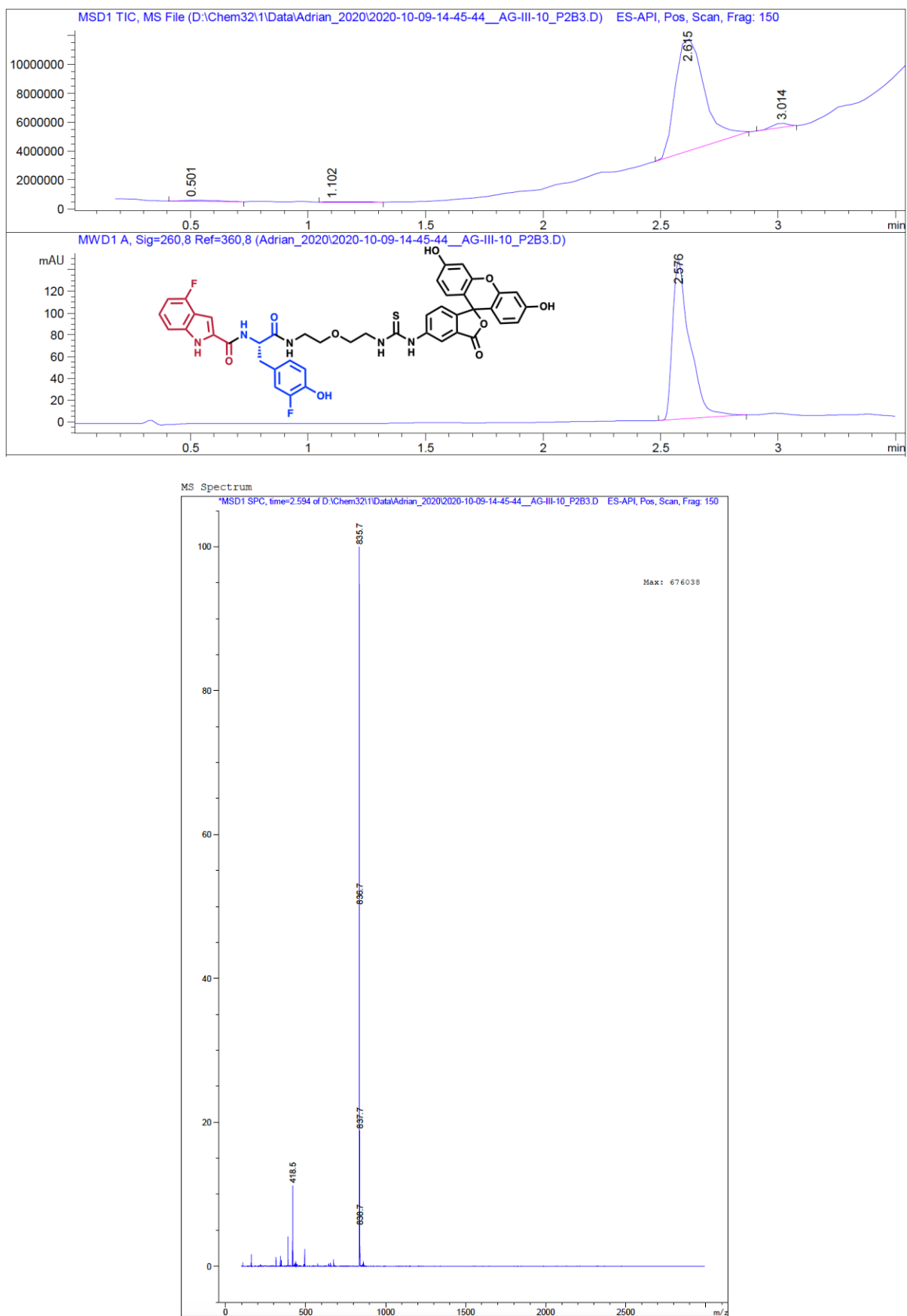
Figure 6.4.17. LC-ESI-MS chromatogram of compound **5**, t_R:2.576 min (DAD), 2.615 min (TIC). Expected mass 835.2, observed 835.7.
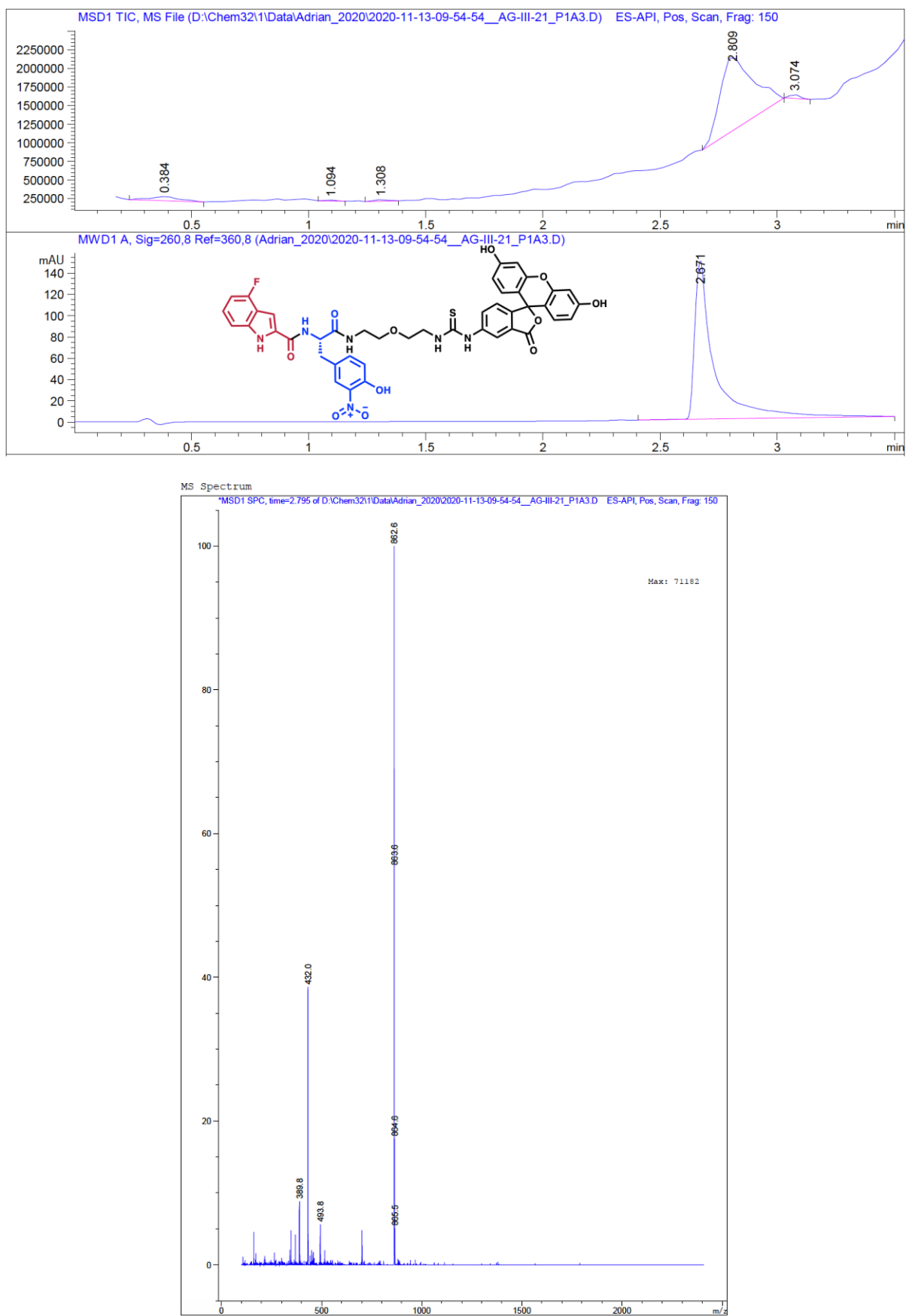
Figure 6.4.18. LC-ESI-MS chromatogram of compound **6**, t_R:2.671 min (DAD), 2.809 min (TIC). Expected mass 862.2, observed 862.6.
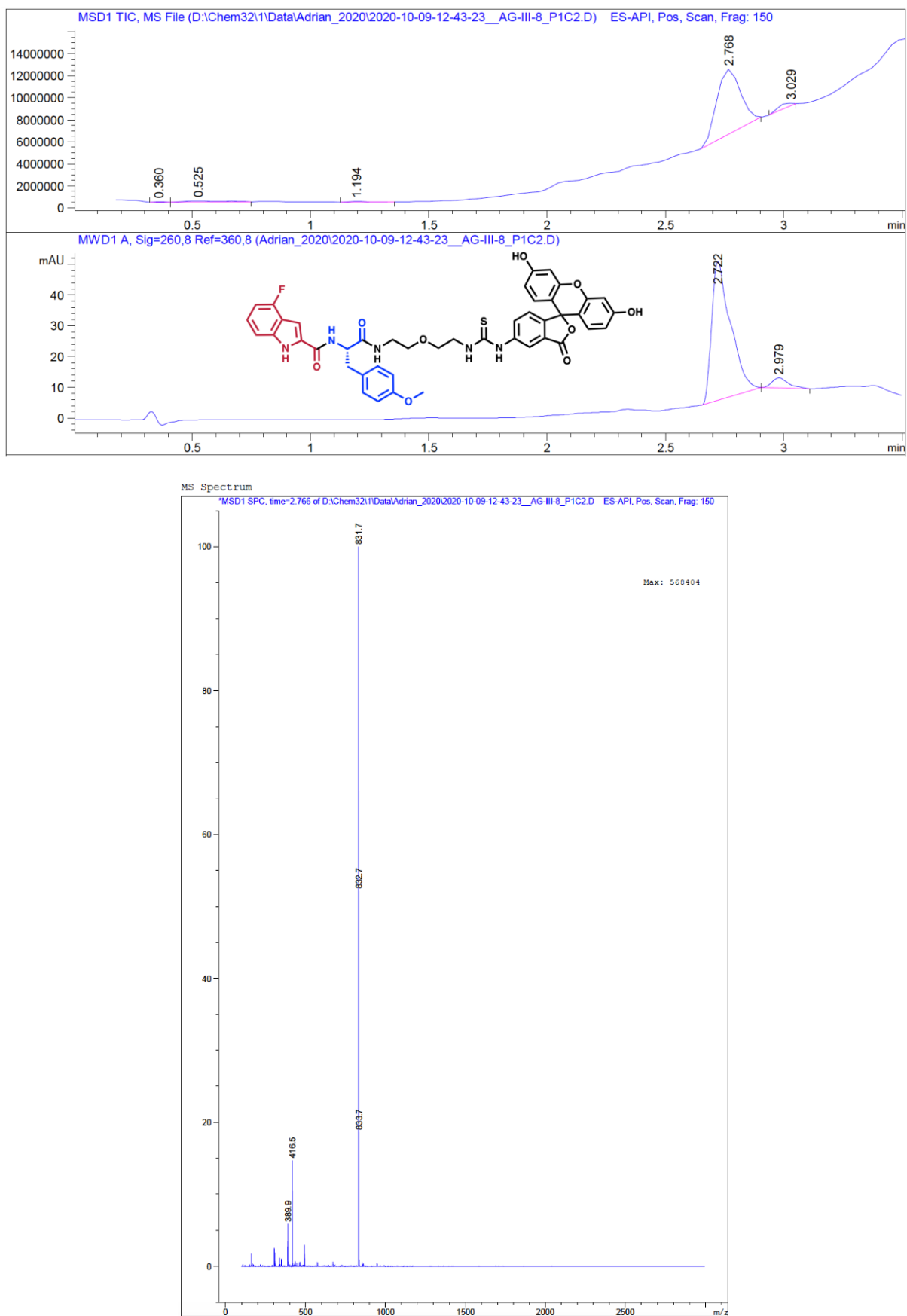
Figure 6.4.19. LC-ESI-MS chromatogram of compound **7**, t_R:2.722 min (DAD), 2.768 min (TIC). Expected mass 831.2, observed 831.7.
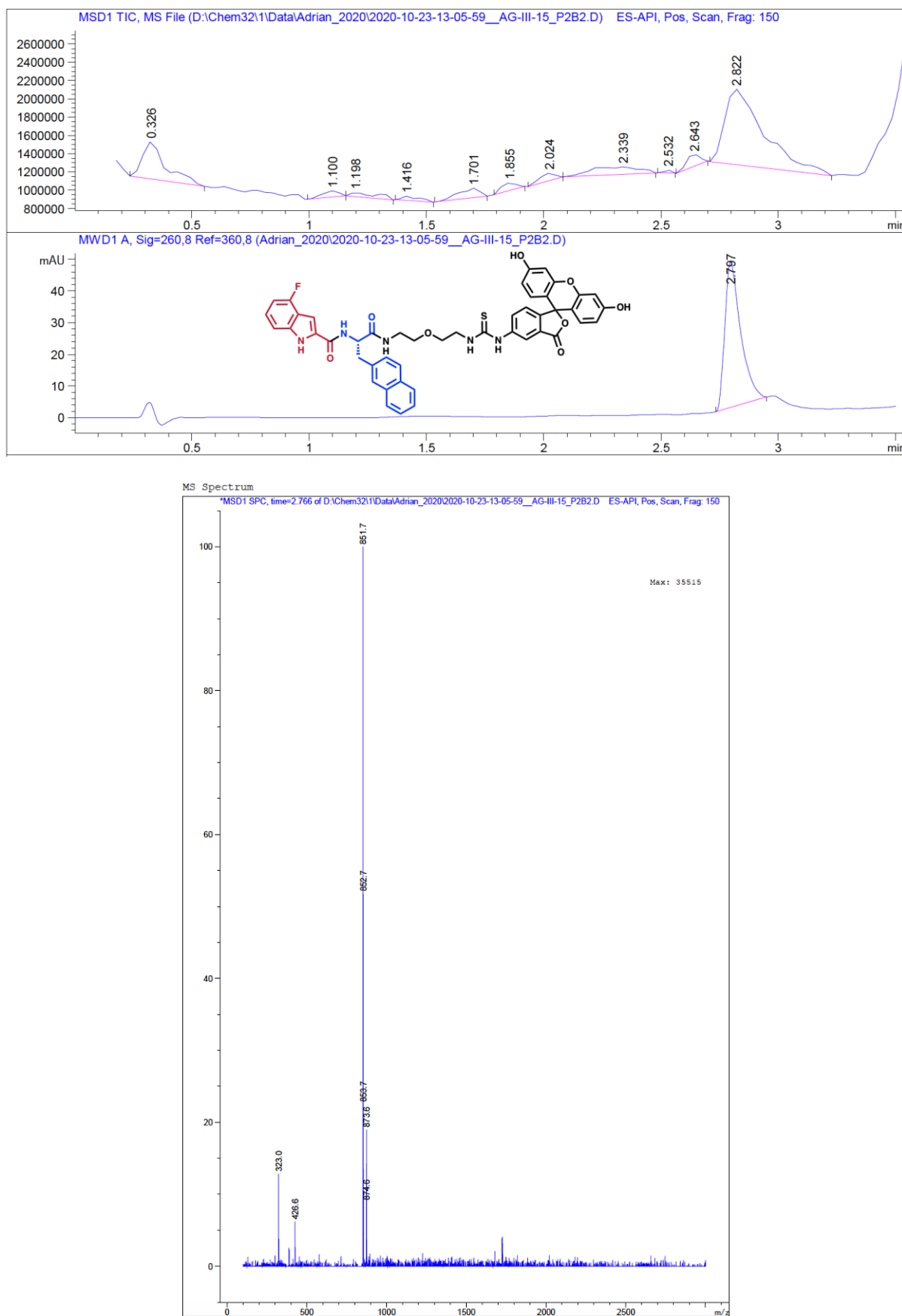
Figure 6.4.20. LC-ESI-MS chromatogram of compound **8**, t_R:2.797 min (DAD), 2.822 min (TIC). Expected mass 851.2, observed 851.7.
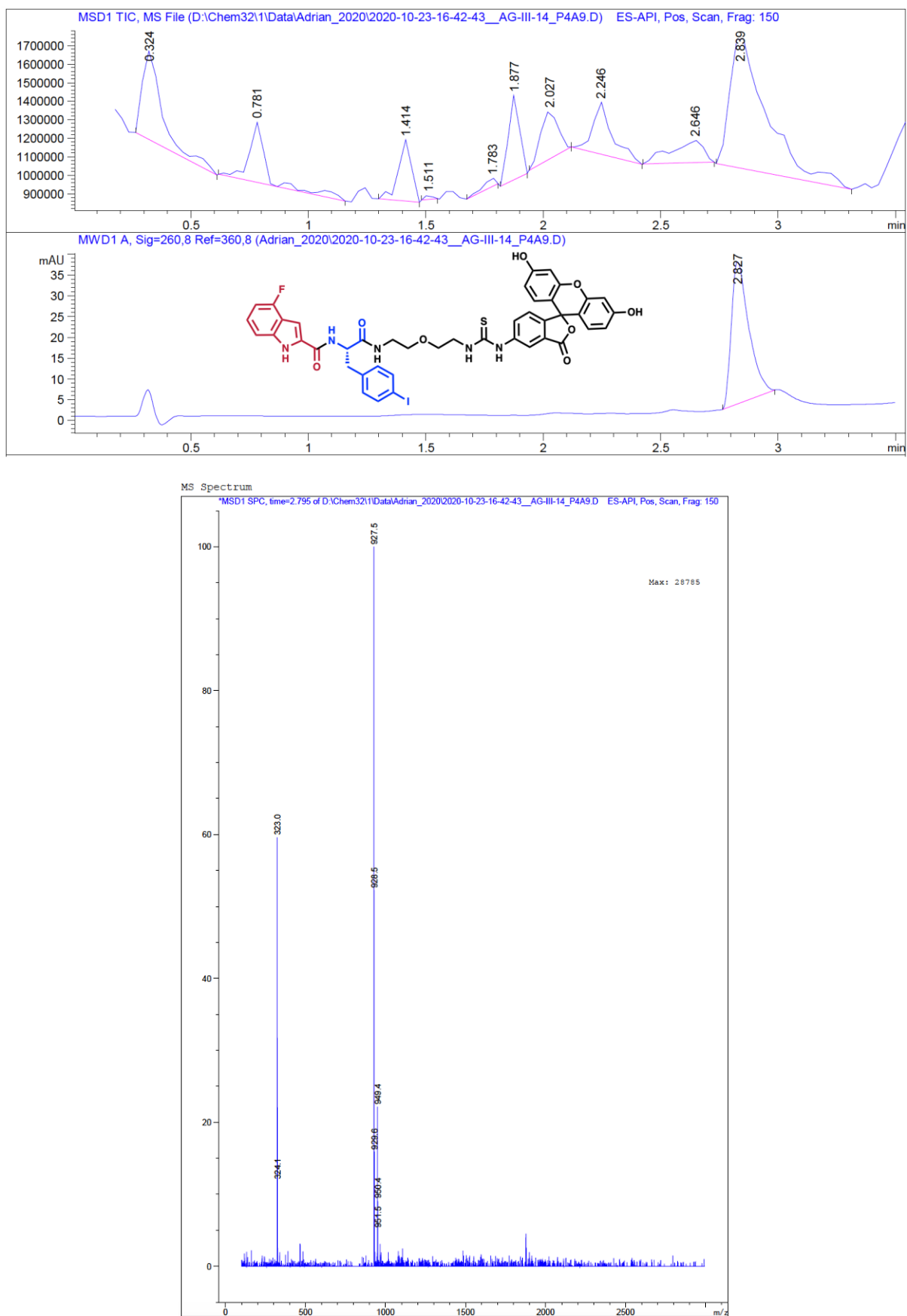
Figure 6.4.21. LC-ESI-MS chromatogram of compound **9**, t_R:2.827 min (DAD), 2.839 min (TIC). Expected mass 927.1, observed 927.5.
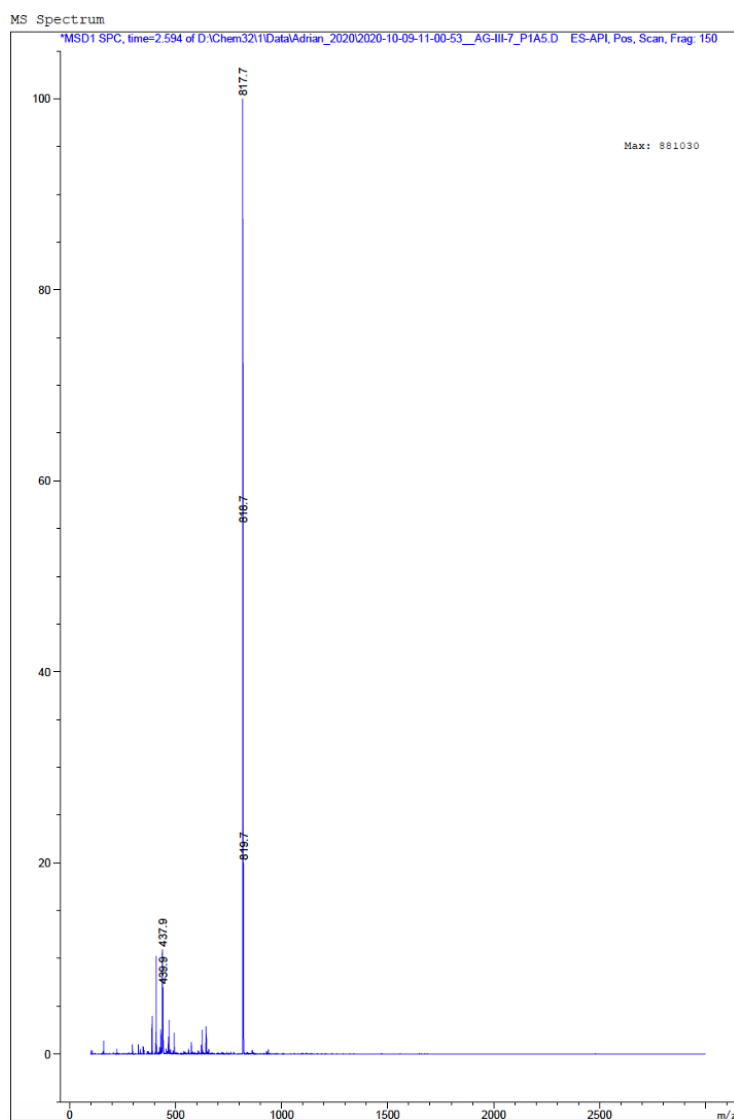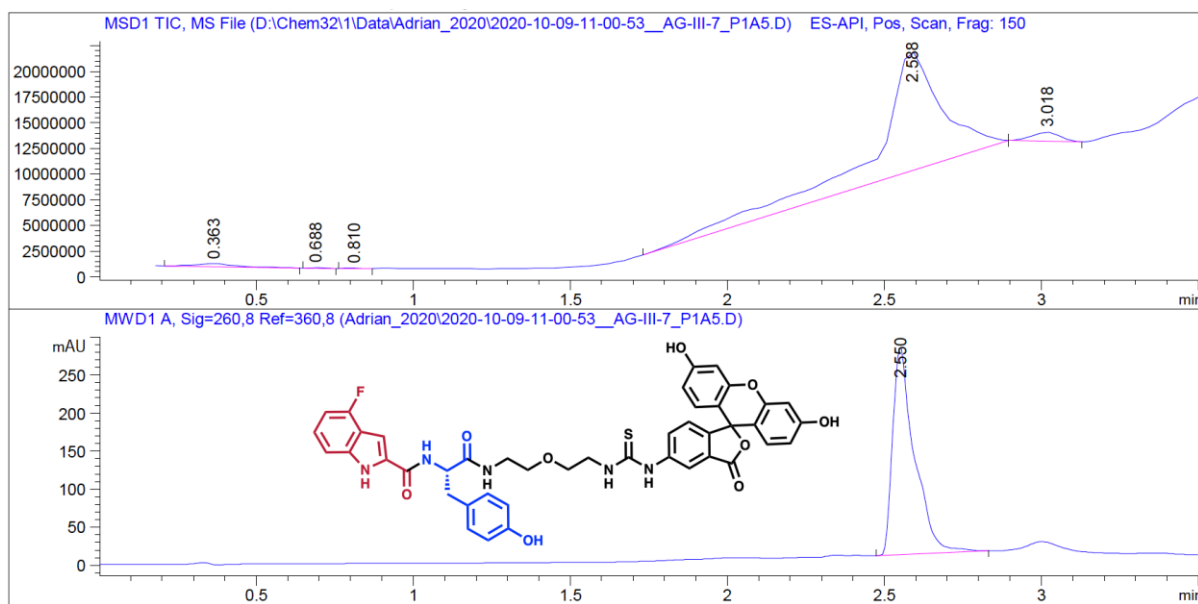
Figure 6.4.22. LC-ESI-MS chromatogram of compound **10**, t_R:2.550 min (DAD), 2.588 min (TIC). Expected mass 817.2, observed 817.7.
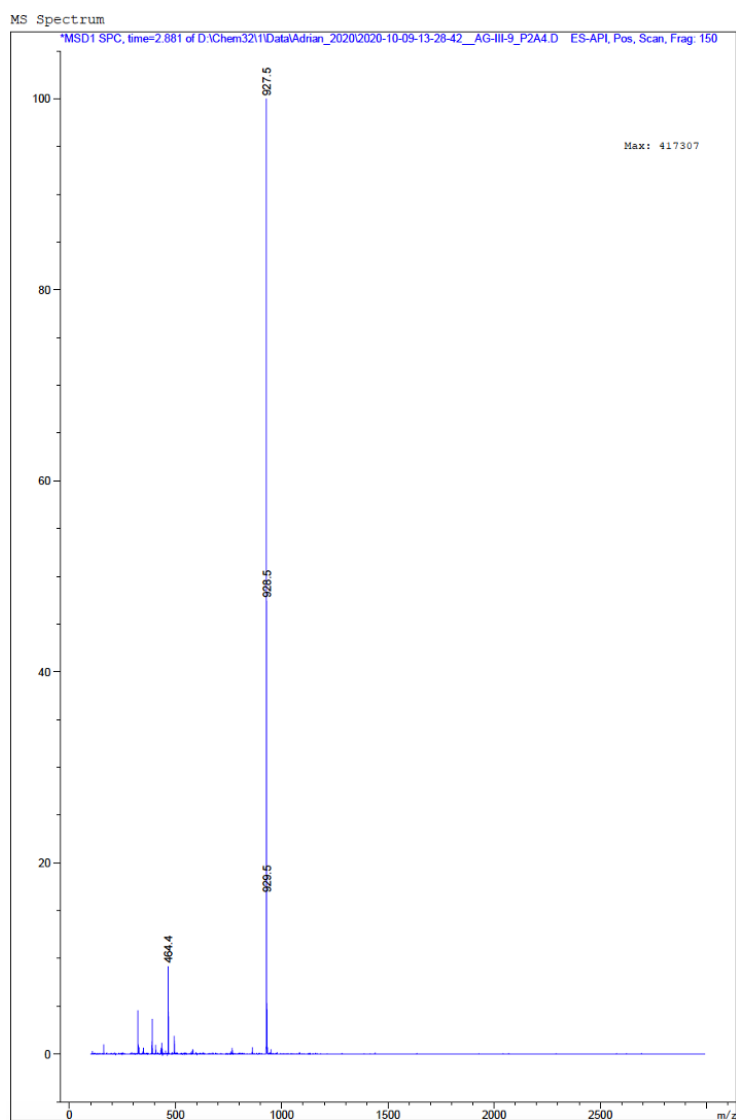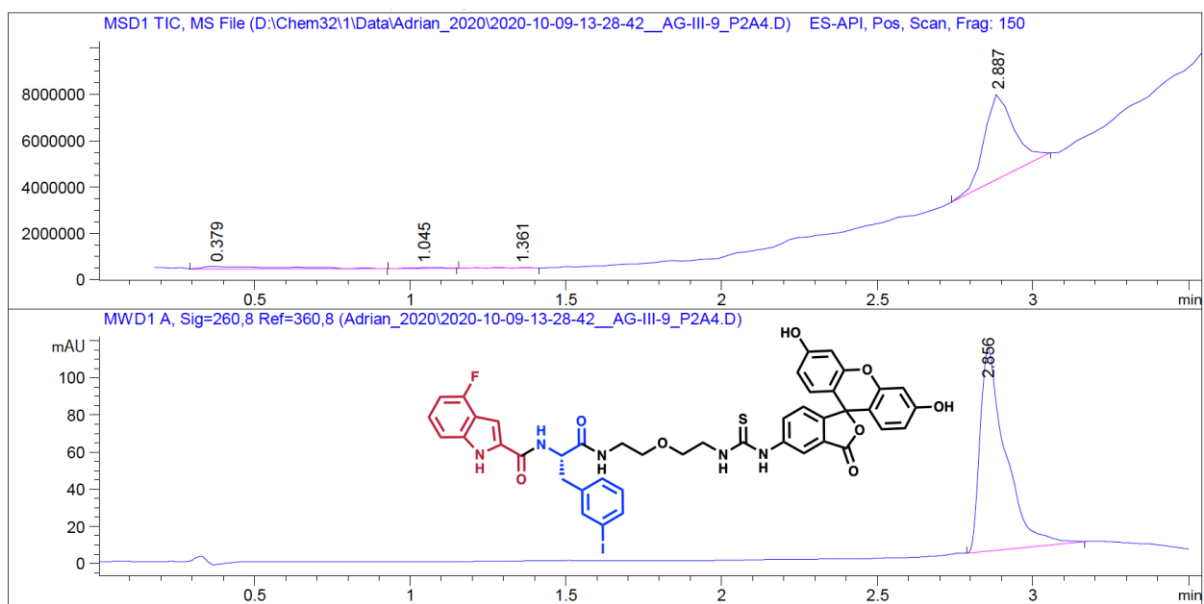
Figure 6.4.23. LC-ESI-MS chromatogram of compound **11**, t_R:2.856 min (DAD), 2.887 min (TIC). Expected mass 927.1, observed 927.5.
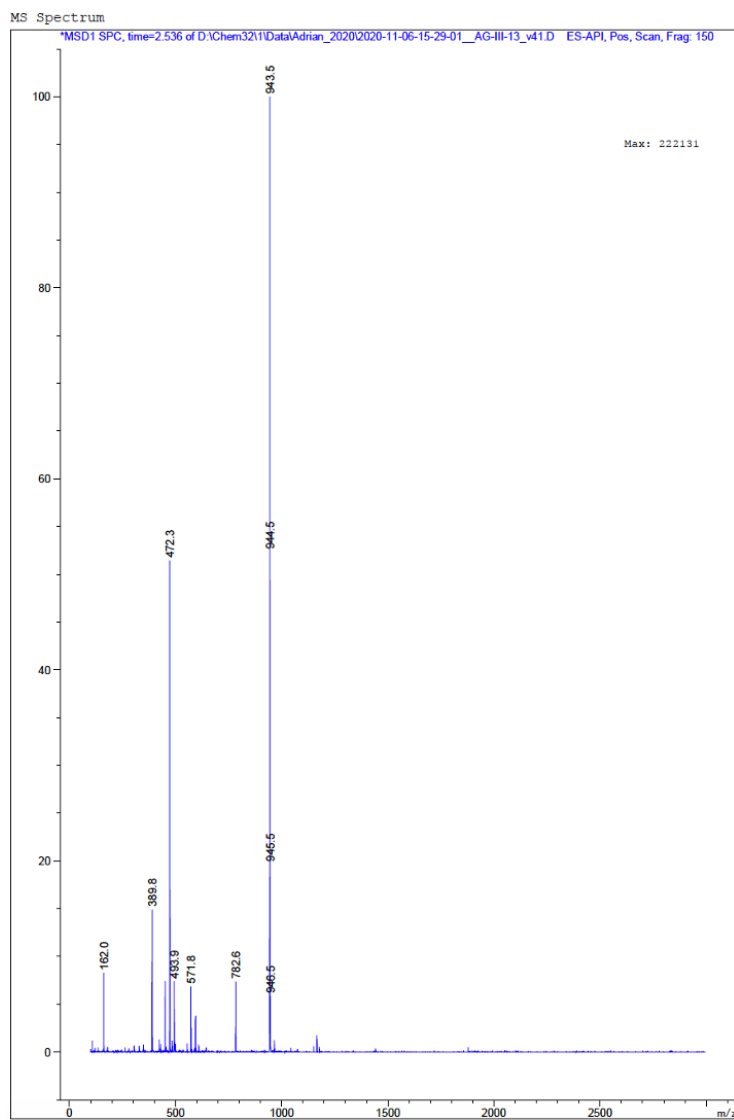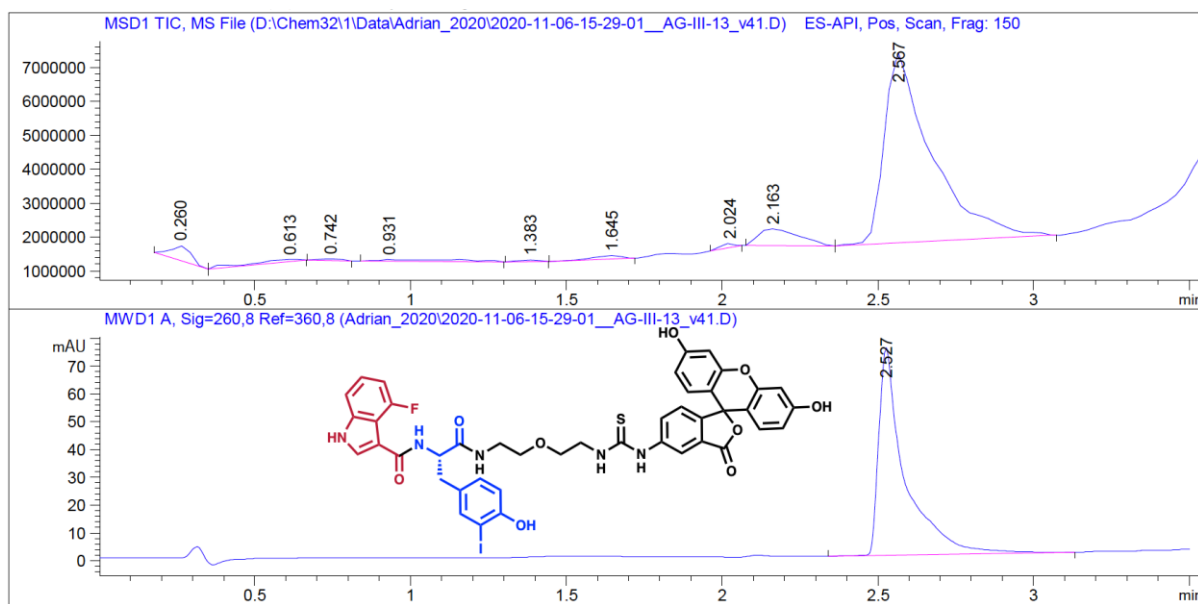
Figure 6.4.24. LC-ESI-MS chromatogram of compound **12**, t_R:2.527 min (DAD), 2.567 min (TIC). Expected mass 943.1, observed 943.5.
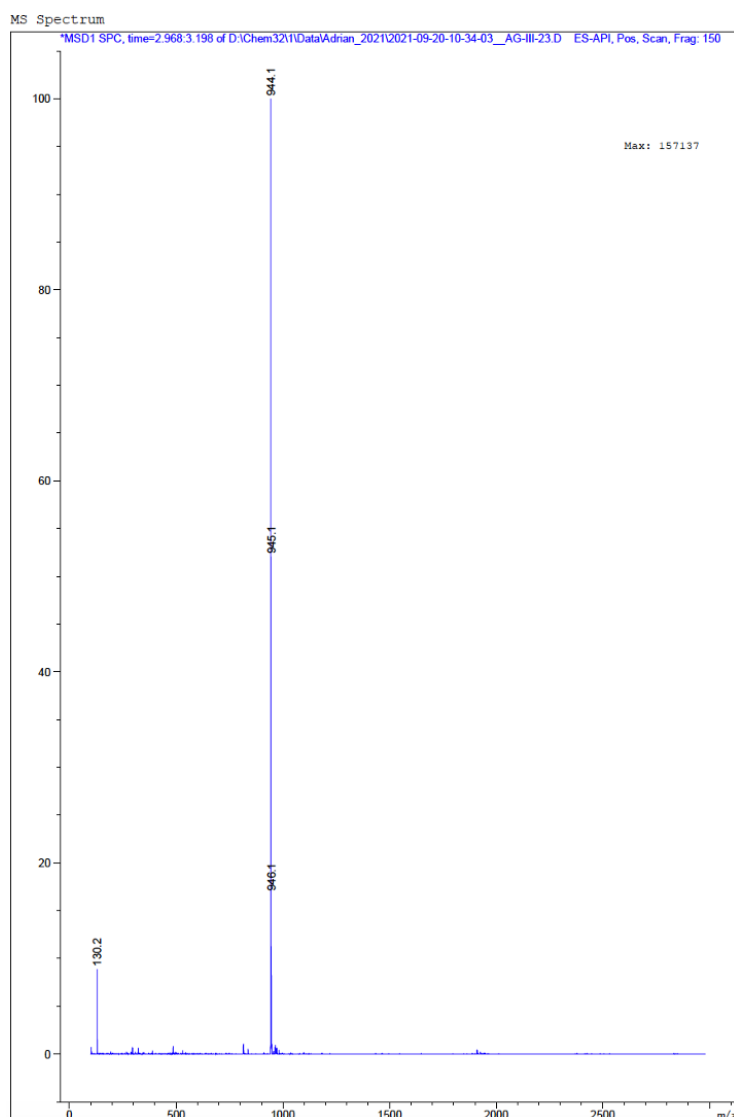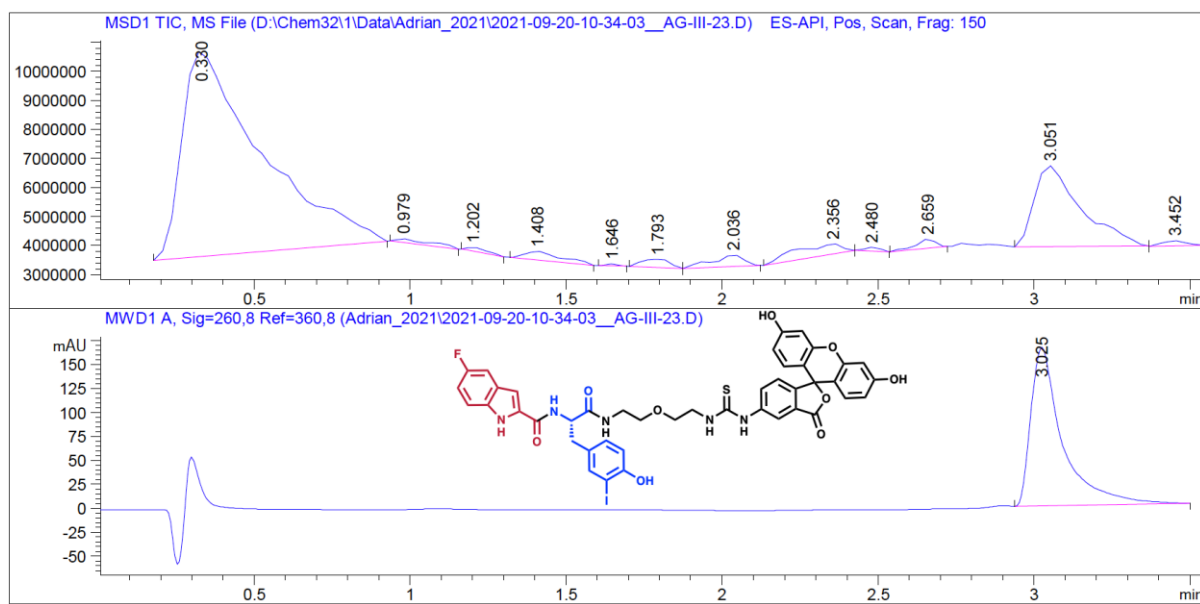
Figure 6.4.25. LC-ESI-MS chromatogram of compound **13**, t_R:3.025 min (DAD), 3.051 min (TIC). Expected mass 943.1, observed 944.1.
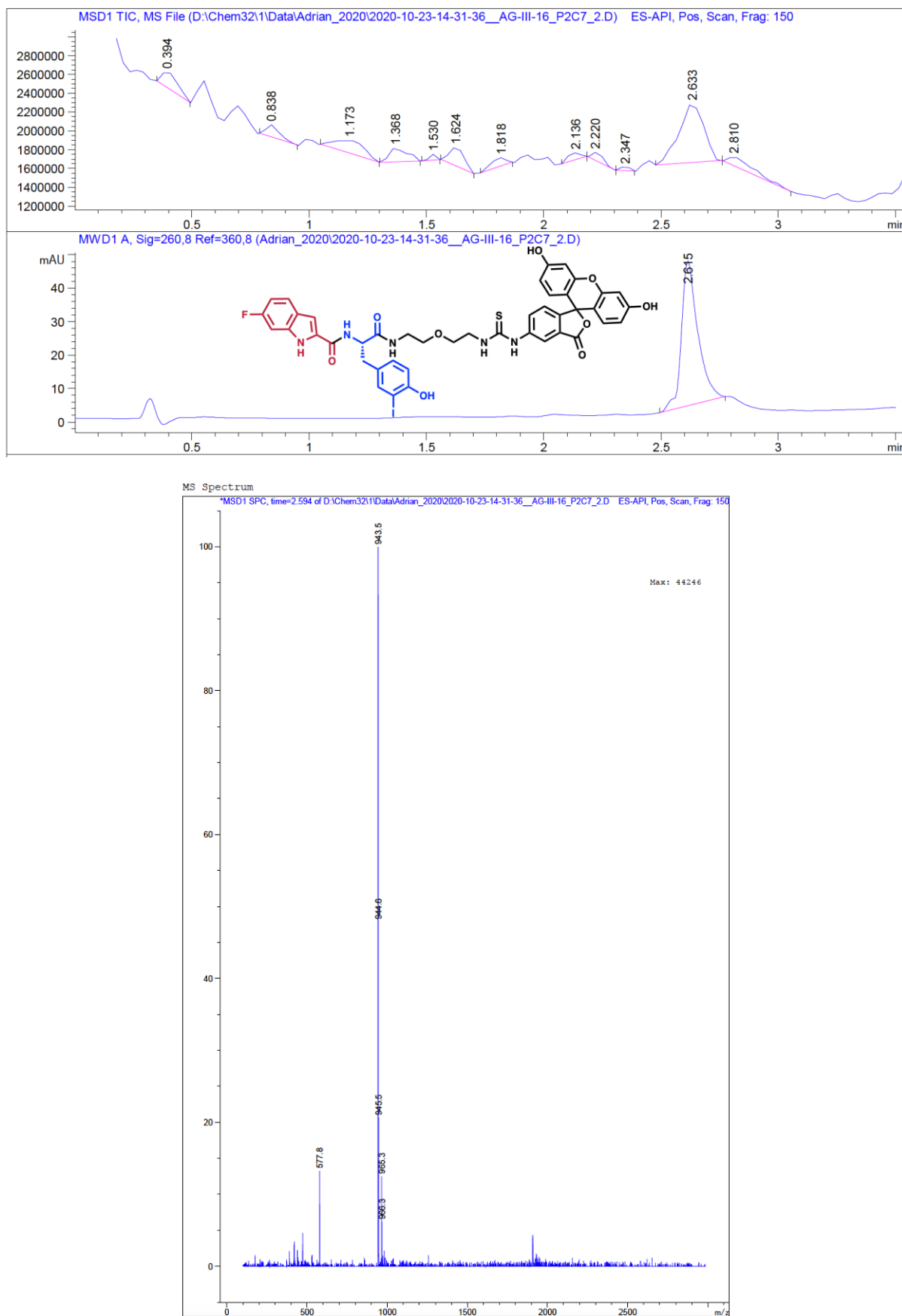
Figure 6.4.26. LC-ESI-MS chromatogram of compound **14**, t_R:2.615 min (DAD), 2.633 min (TIC). Expected mass 943.1, observed 943.5.
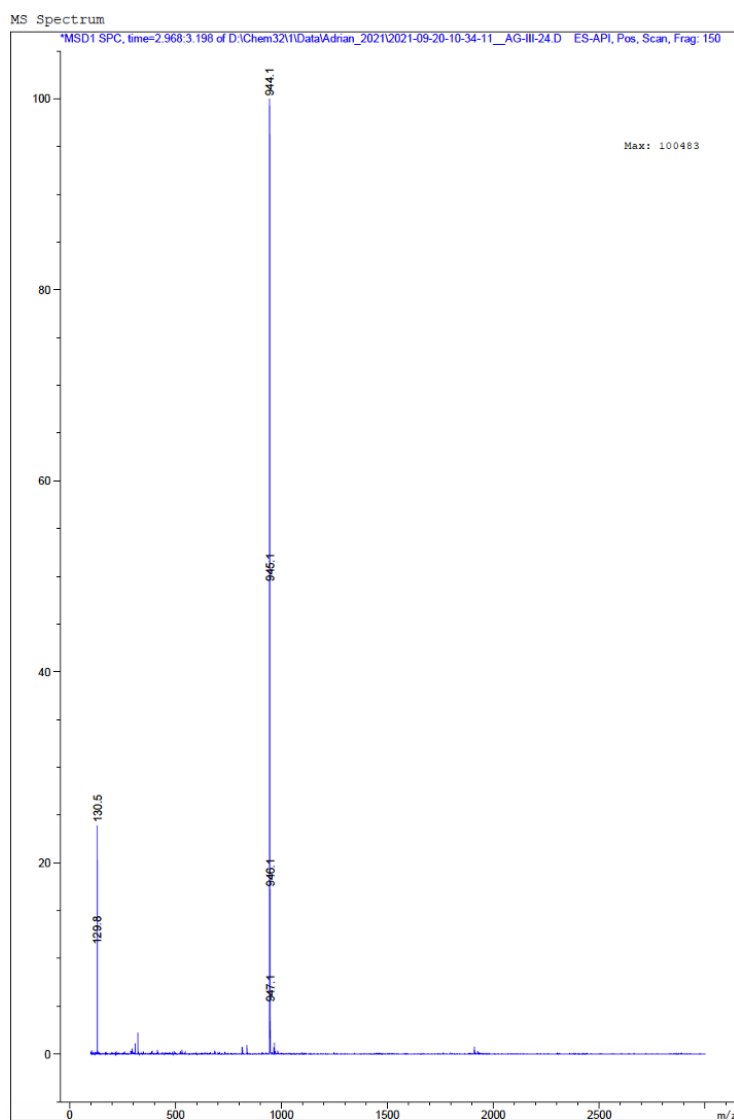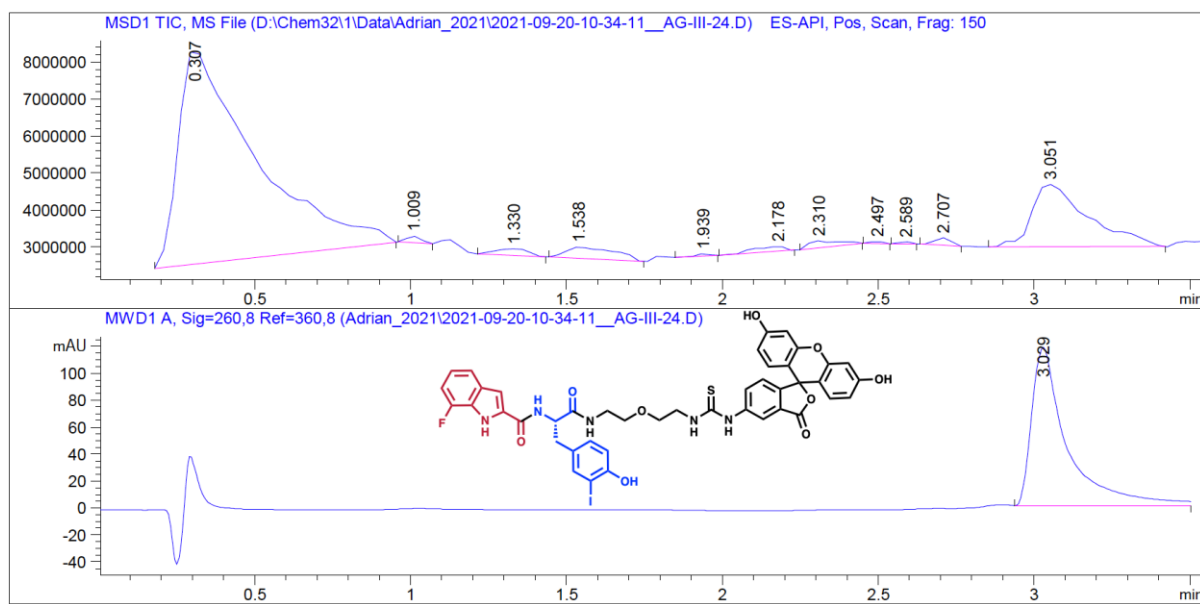
Figure 6.4.27. LC-ESI-MS chromatogram of compound **15**, t_R:3.029 min (DAD), 3.051 min (TIC). Expected mass 943.1, observed 944.1.
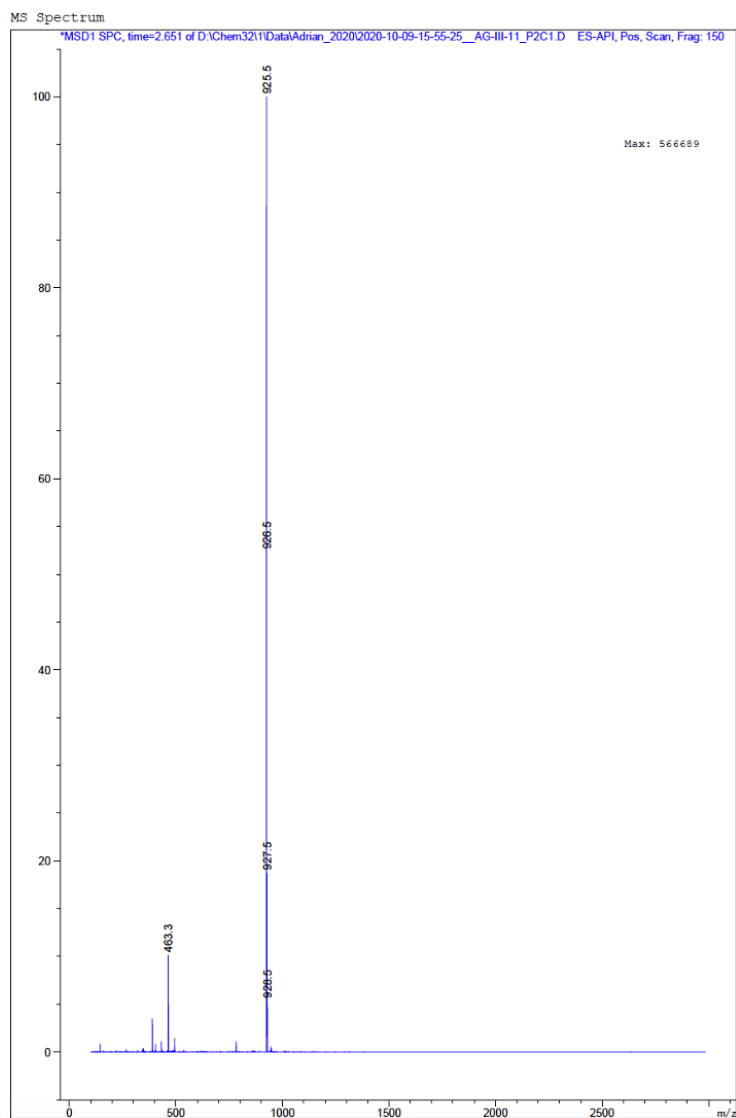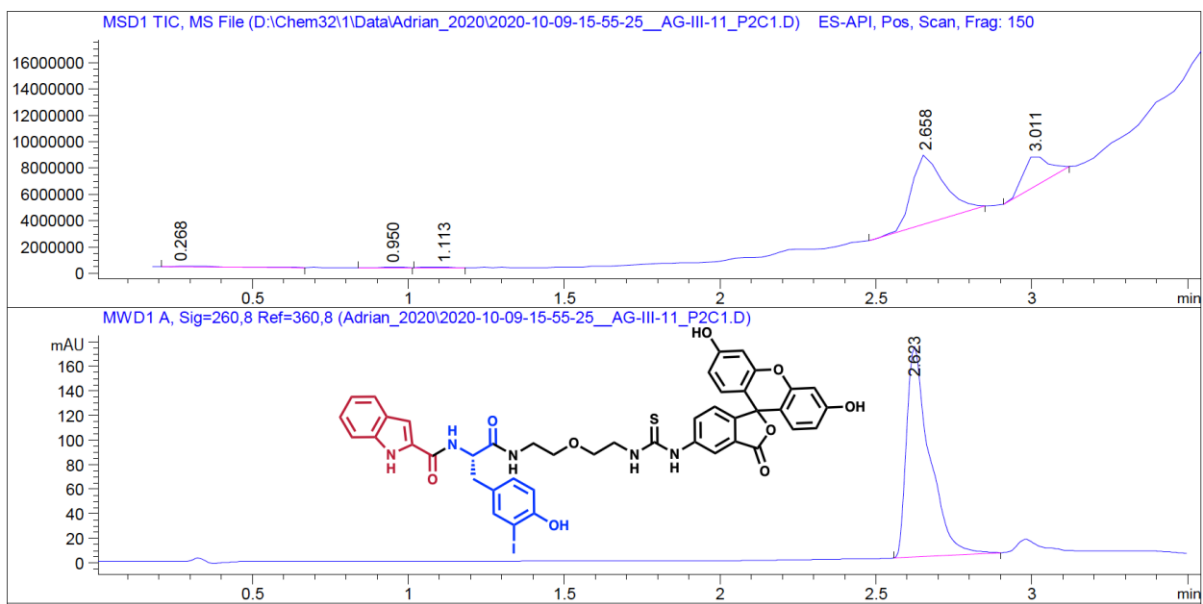
Figure 6.4.28. LC-ESI-MS chromatogram of compound **16**, t_R:2.623 min (DAD), 2.658 min (TIC). Expected mass 925.1, observed 925.5.
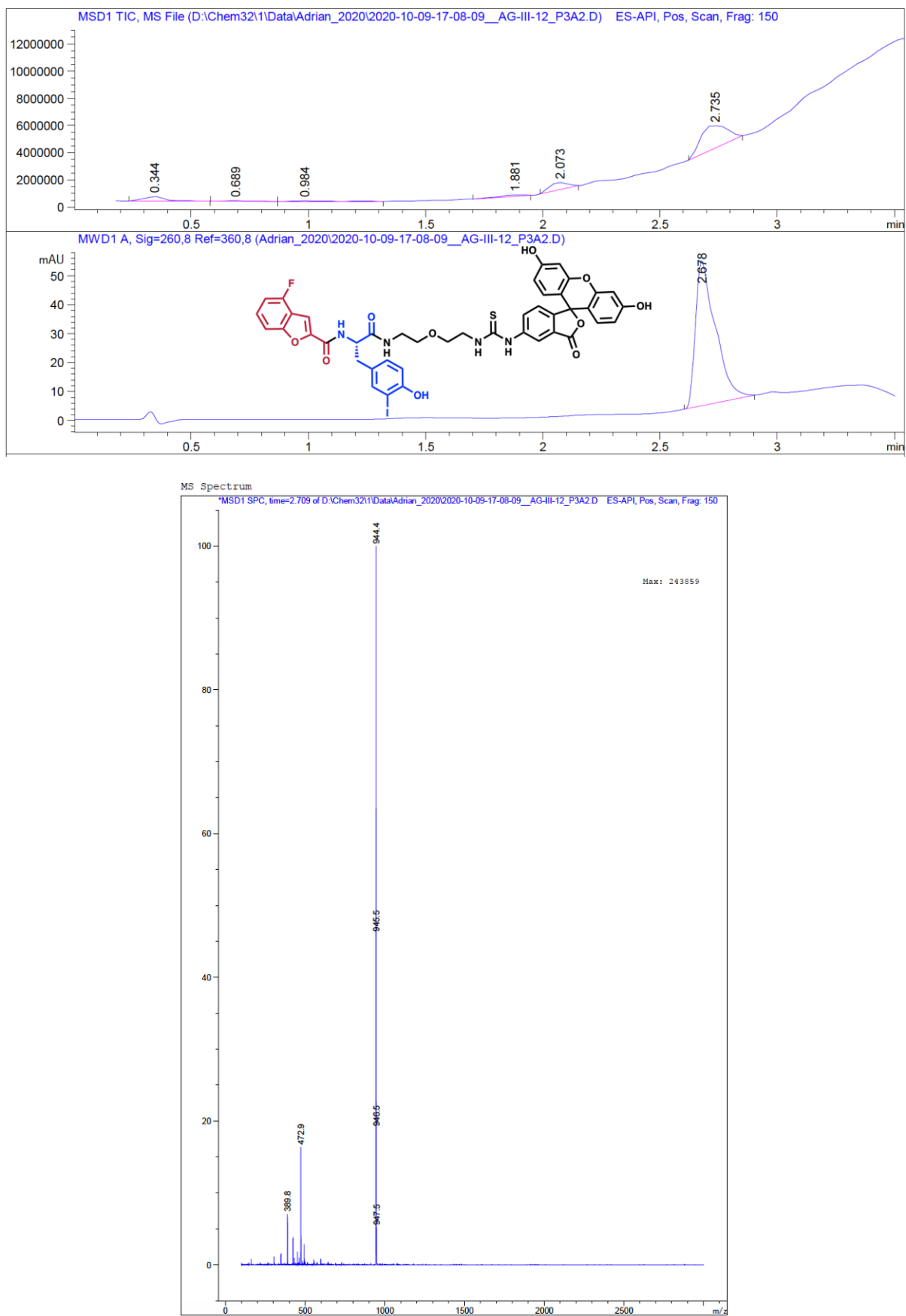
Figure 6.4.29. LC-ESI-MS chromatogram of compound **17**, t_R:2.678 min (DAD), 2.735 min (TIC). Expected mass 944.1, observed 944.4.
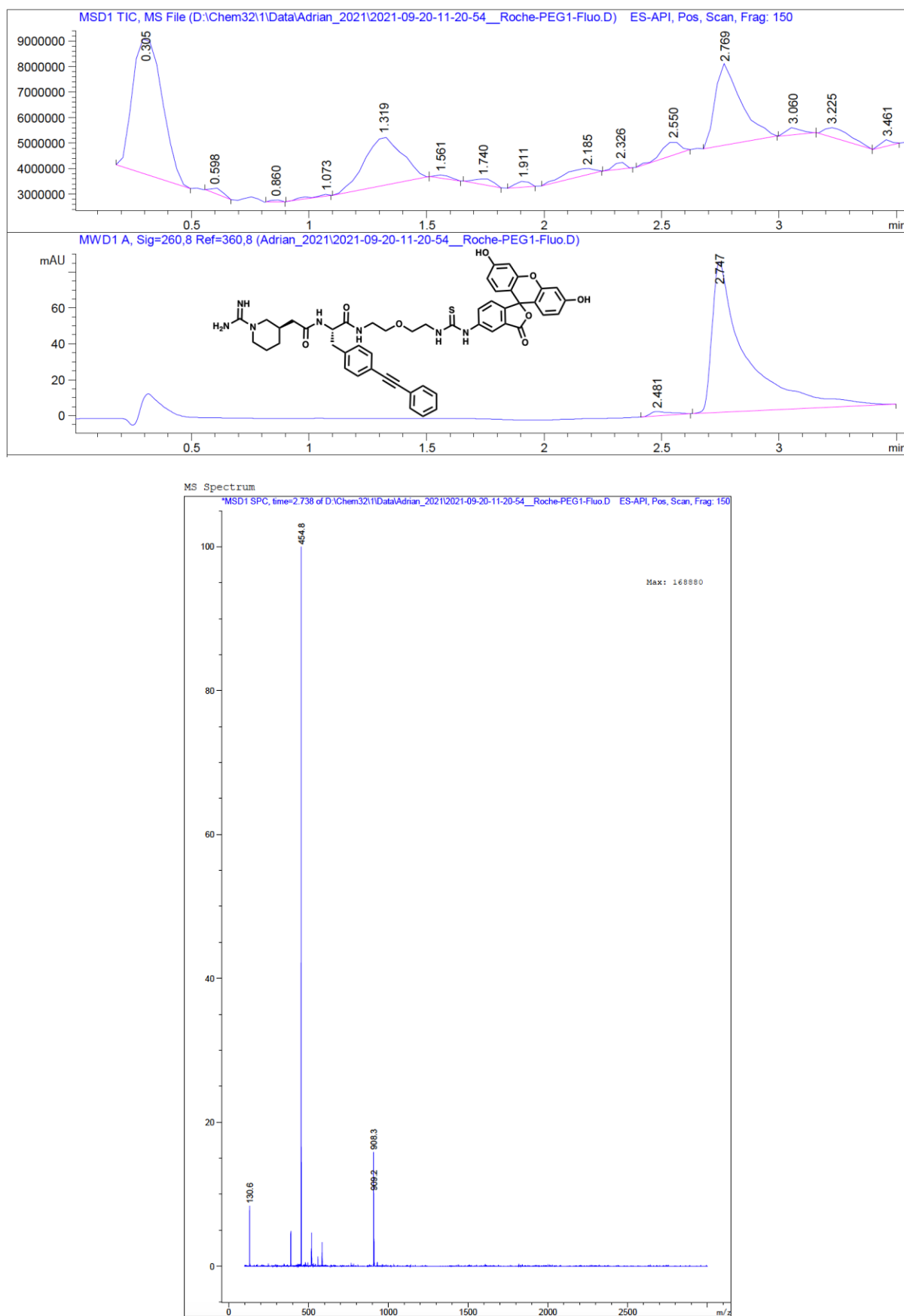
Figure 6.4.30. LC-ESI-MS chromatogram of compound **Ro26-4550**, t_R:2.747 min (DAD), 2.769 min (TIC). Expected mass 907.3, observed 908.3.
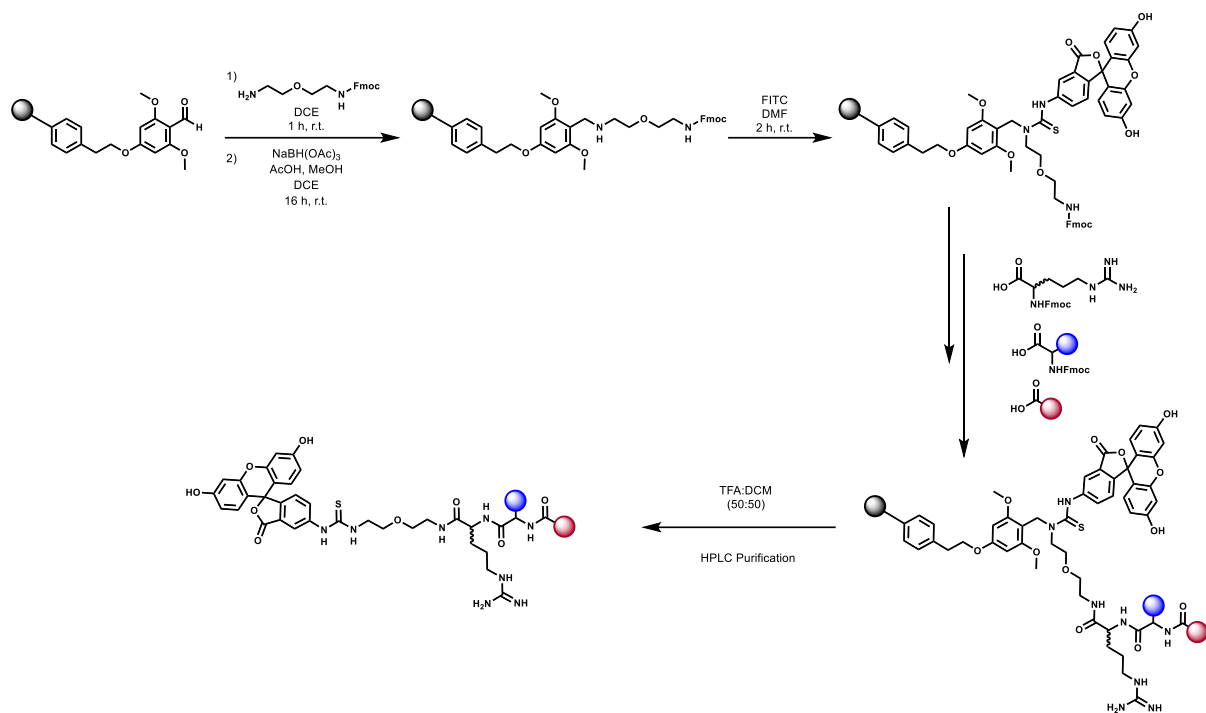
Scheme 6.4.3. Synthetic route for the synthesis of compounds **18-21**. The grey ball represents the solid support, the blue ball represents the building block 1 and the red ball represents the building block 2.
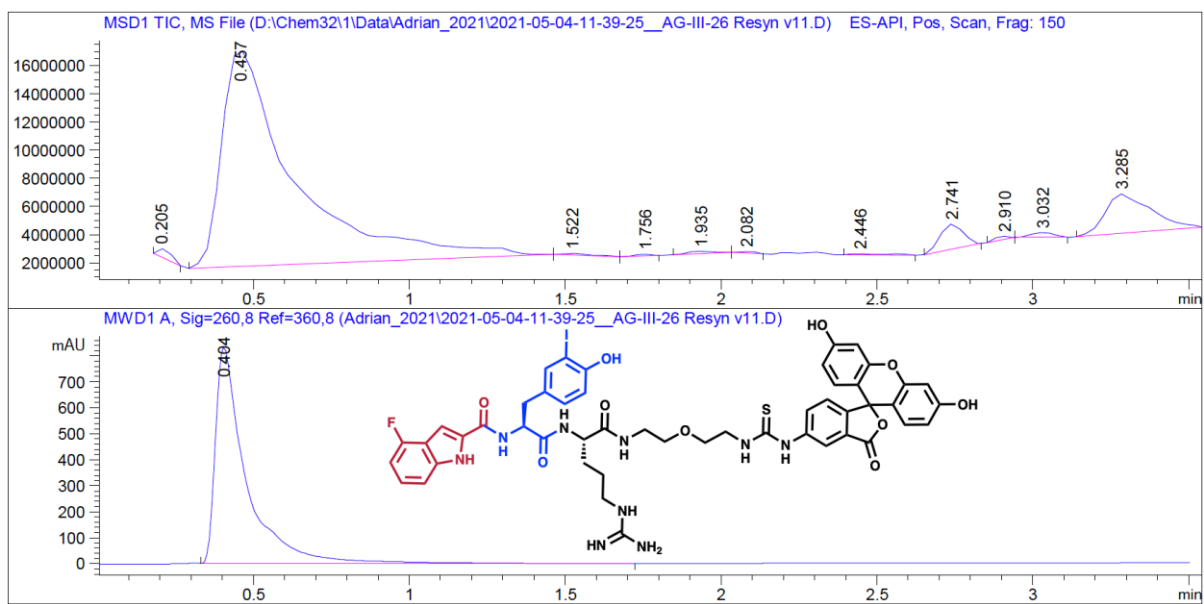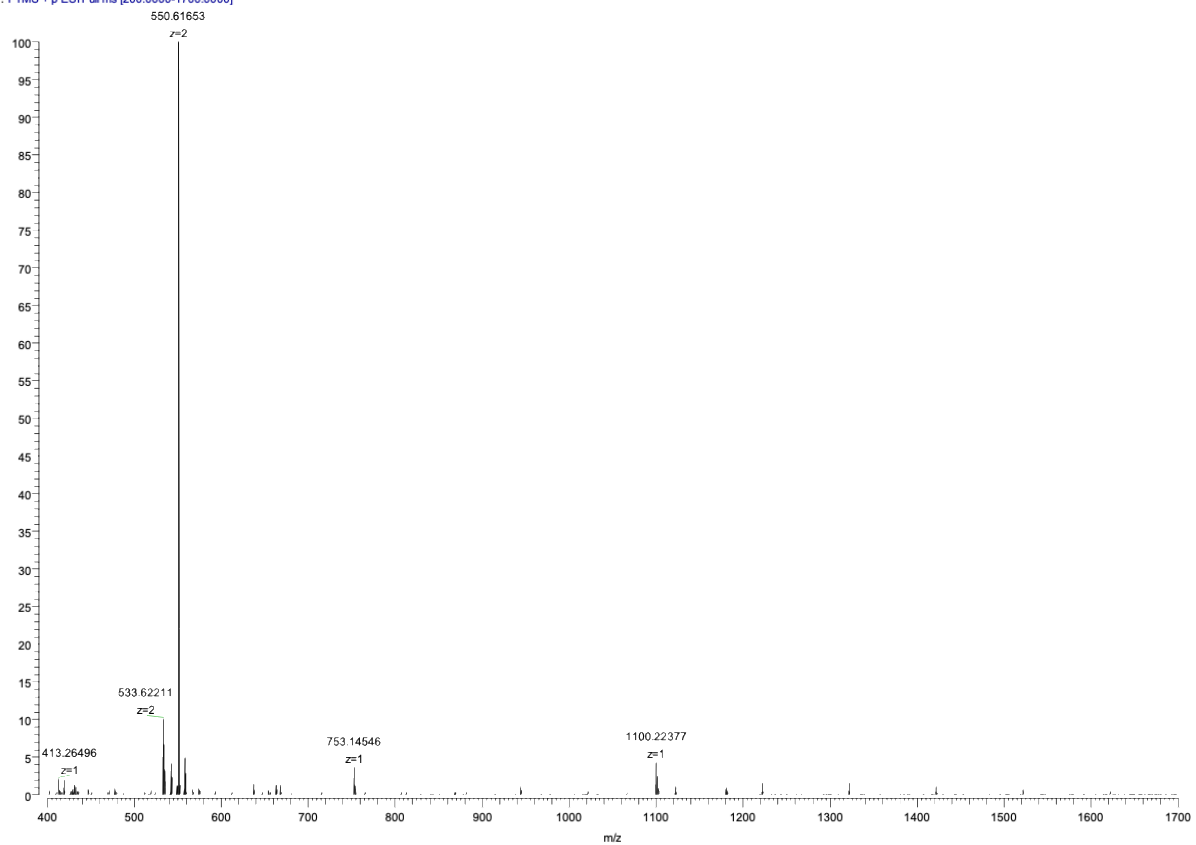
Figure 6.4.31. LC-HRMS chromatogram of compound **18**, t_R:0.457 min (DAD). Expected mass 1099.21953, observed 1100.22377.
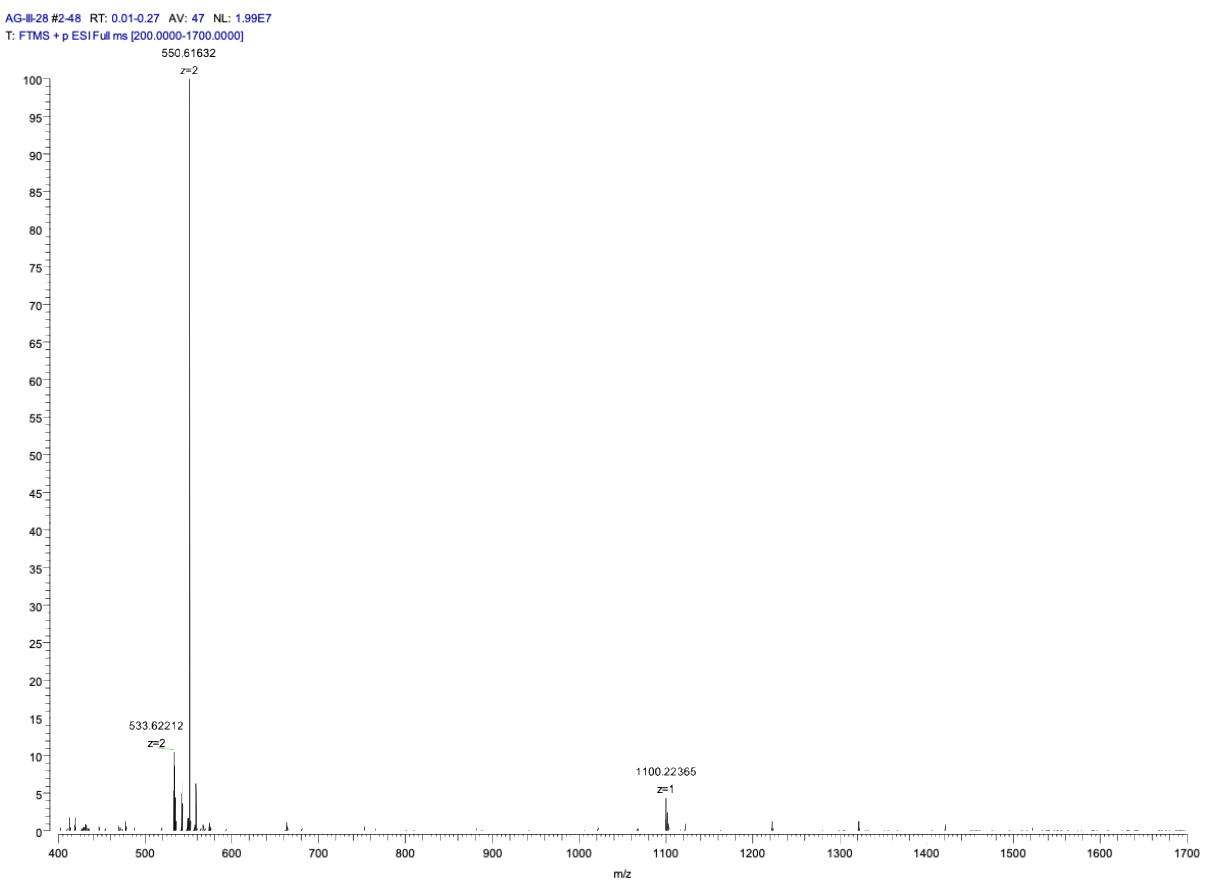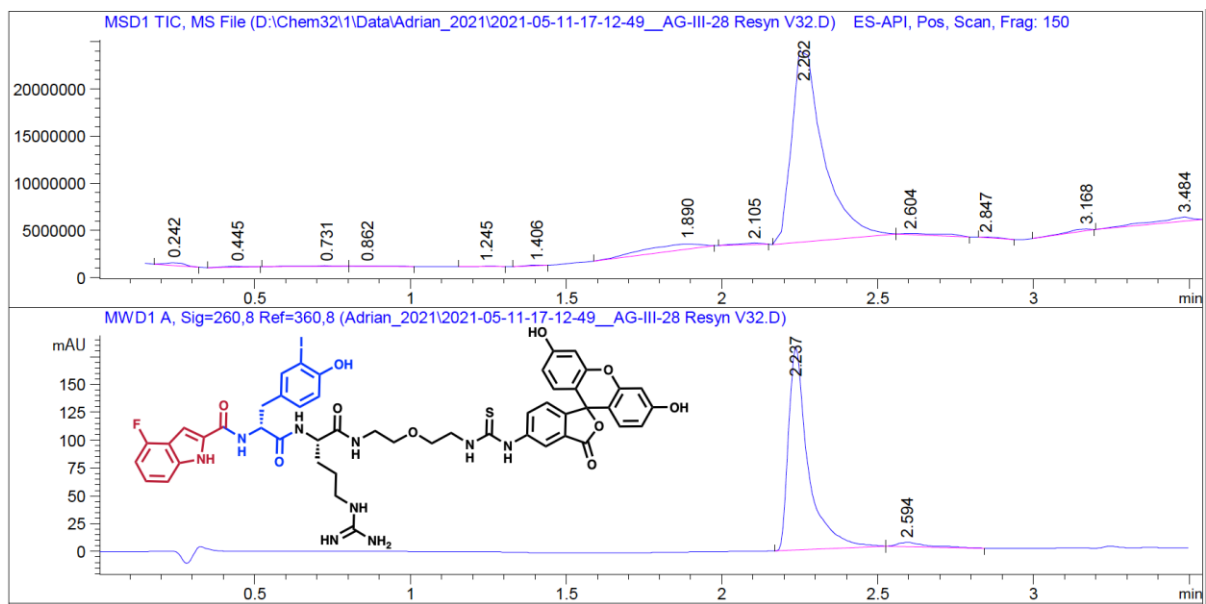
Figure 6.4.32. LC-HRMS chromatogram of compound **19**, t_R:2.237 min (DAD). Expected mass 1099.21953, observed 1100.22365.
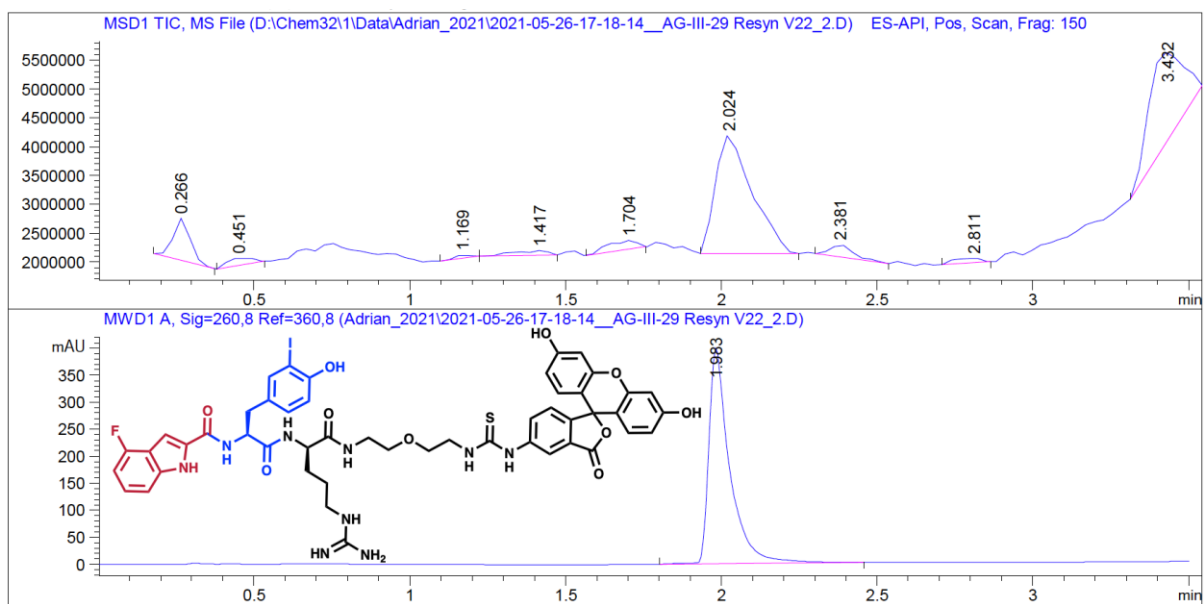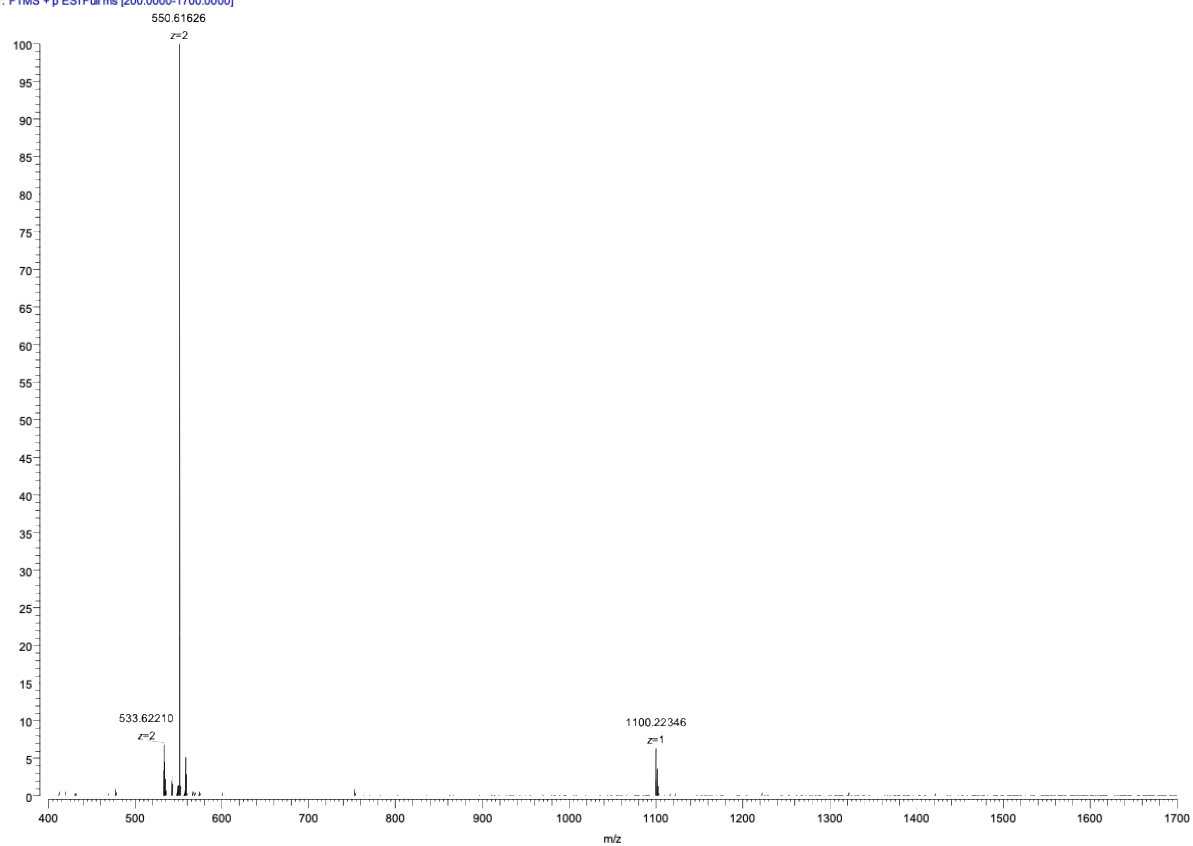
Figure 6.4.33. LC-HRMS chromatogram of compound **20**, t_R:1.983 min (DAD). Expected mass 1099.21953, observed 1100.22346.
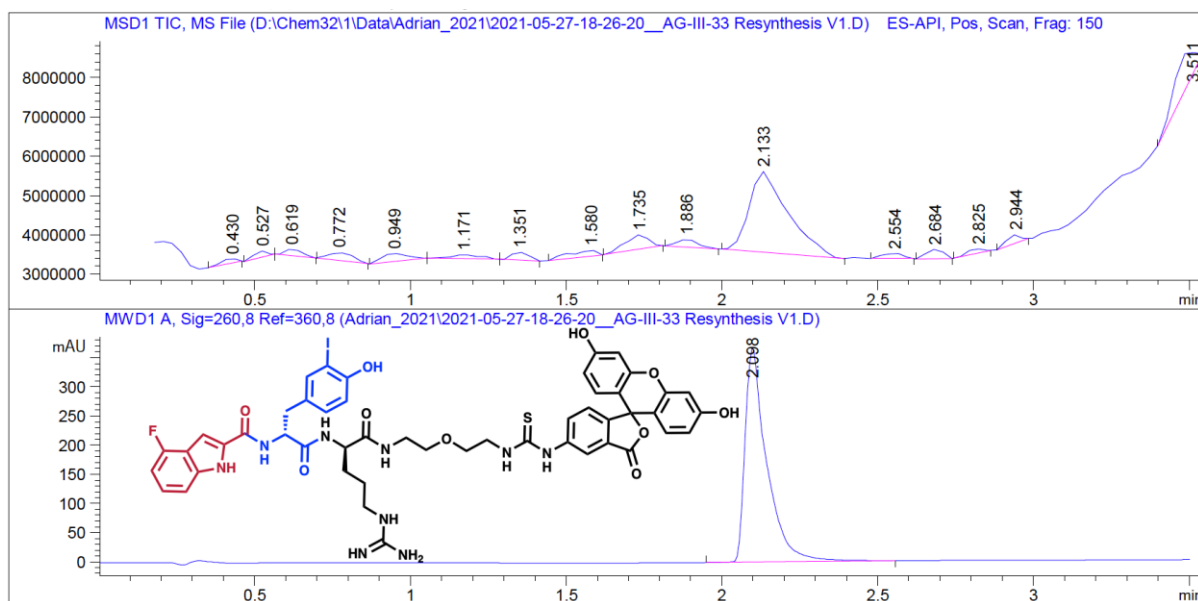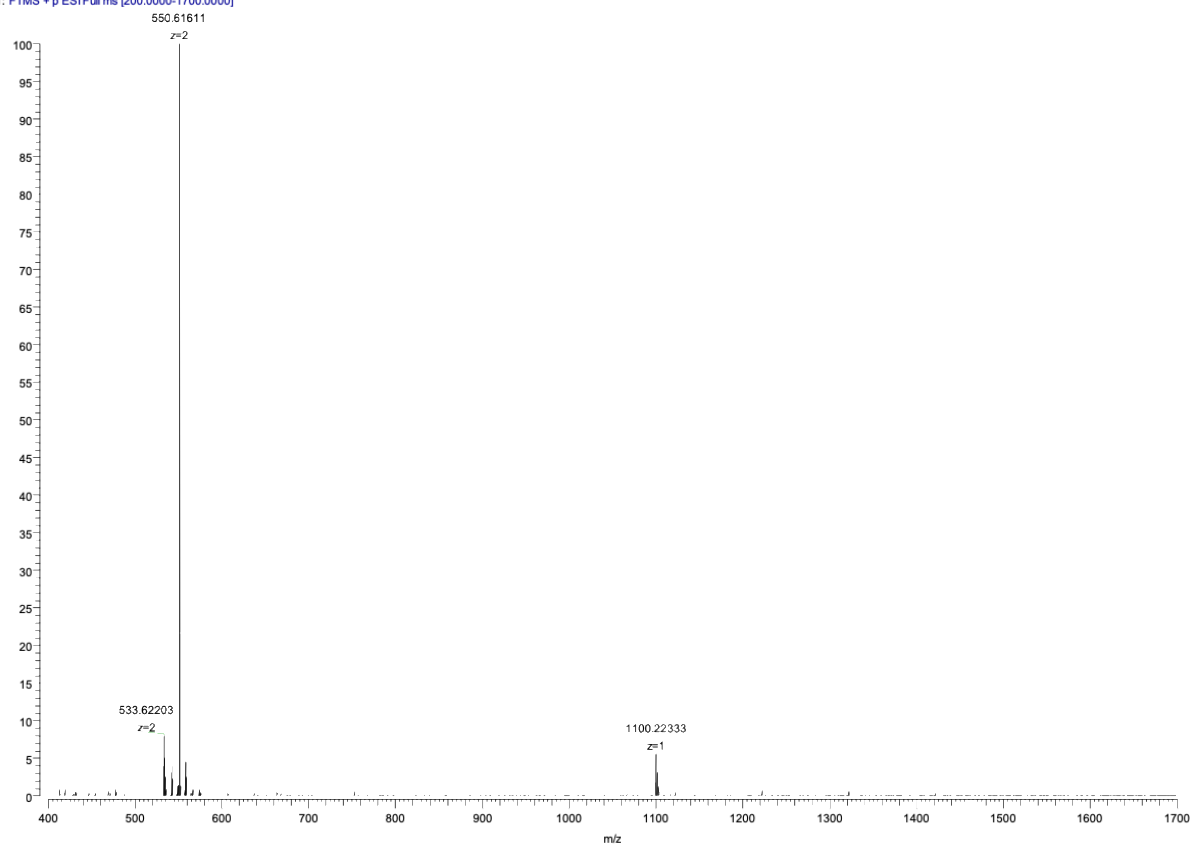
Figure 6.4.34. LC-HRMS chromatogram of compound **21**, t_R:2.098 min (DAD). Expected mass 1099.21953, observed 1100.22333.

Recombinant proteins. Sequences and quality control

NARA1 anti-IL2 antibody Fab format:

Nara-1 (Fab): <mark>VL</mark> – mCL

<mark>DIVLTQSPASLAVSLGQRATISCKASQSVDYDGDSYMNWYQQKPGQPPKLLIYAAS
NLESGIPARFSGSGSGTDFTLNIHPVEEEDAATYYCQQSNEDPYTFGGGTKLEIK</mark>RA
DAAPTVSIFPPSSEQLTSGGASVVCFLNNFYPKDINVKWKIDGSERQNGVLNSWTD
QDSKDSTYSMSSTLTLTKDEYERHNSYTCEATHKTSTSPIVKSFNRNEC

Nara-1 (Fab): <mark style="background-color:#00ff00">VH</mark> – mCH1

<mark style="background-color:#00ff00">QVQLQQSGAELVRPGTSVKVSCKASGYAFTNYLIEWVKQRPGQGLEWIGVINPGS
GGTNYNEKFKGKATLTADKSSSTAYMQLSSLTSDDSAVYFCARWRGDGYYAYFDV
WGAGTTVTVSS</mark>AKTTAPSVYPLAPVCGDTTGSSVTLGCLVKGYFPEPVTLTWNSG
SLSSGVHTFPAVLQSDLYTLSSSVTVTSSTWPSQSITCNVAHPASSTKVDKKIEPRG
PTHHHHHH
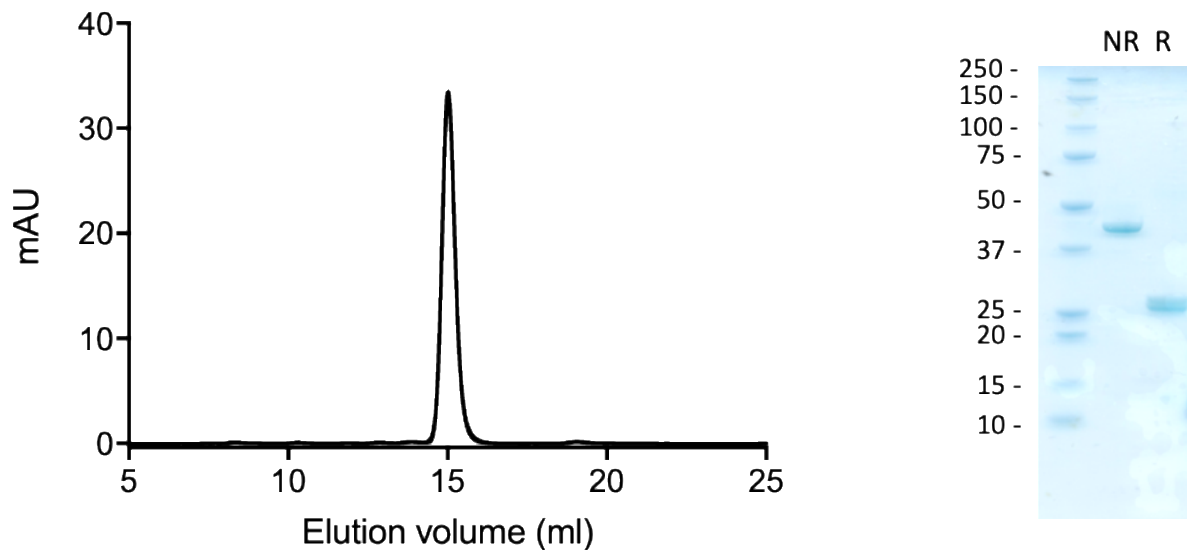
Figure 6.4.35. Size exclusion chromatography profile and Sodium Dodecyl Sulfate Polyacrylamide Gel Electrophoresis (SDS-PAGE) of NARA1. The size corresponds to the predicted molecular weight based on the sequence (48.47 kDa). As expected, under reducing conditions the Fab antibody format presents a single band on SDS-PAGE.

L19-IL2 fusion protein:

The protein was obtained from our GMP production plant in Siena. The sequence is indicated below, and a MS spectrum serves as quality control for chemical biotinylation.

VH(L19) – *linker* – VL(L19) – <u>linker</u> – **IL2**

EVQLLESGGGLVQPGGSLRLSCAASGFTFSSFSMSWVRQAPGKGLEWVSSISGS
SGTTYYADSVKGRFTISRDNSKNTLYLQMNSLRAEDTAVYYCAKPFPYFDYWGQG
TLVTVSS*GDGSSGGSGGAS*EIVLTQSPGTLSLSPGERATLSCRASQSVSSSFLAWY
QQKPGQAPRLLIYYASSRATGIPDRFSGSGSGTDFTLTISRLEPEDFAVYYCQQTG
RIPPTFGQGTKVEIK<u>EFSSSSGSSSSGSSSSG</u>**APTSSSTKKTQLQLEHLLLDLQMIL
NGINNYKNPKLTRMLTFKFYMPKKATELKHLQCLEEELKPLEEVLNLAQSKNFHL
RPRDLISNINVIVLELKGSETTFMCEYADETATIVEFLNRWITFCQSIISTLT**

biot-L19-IL2 fusion protein:
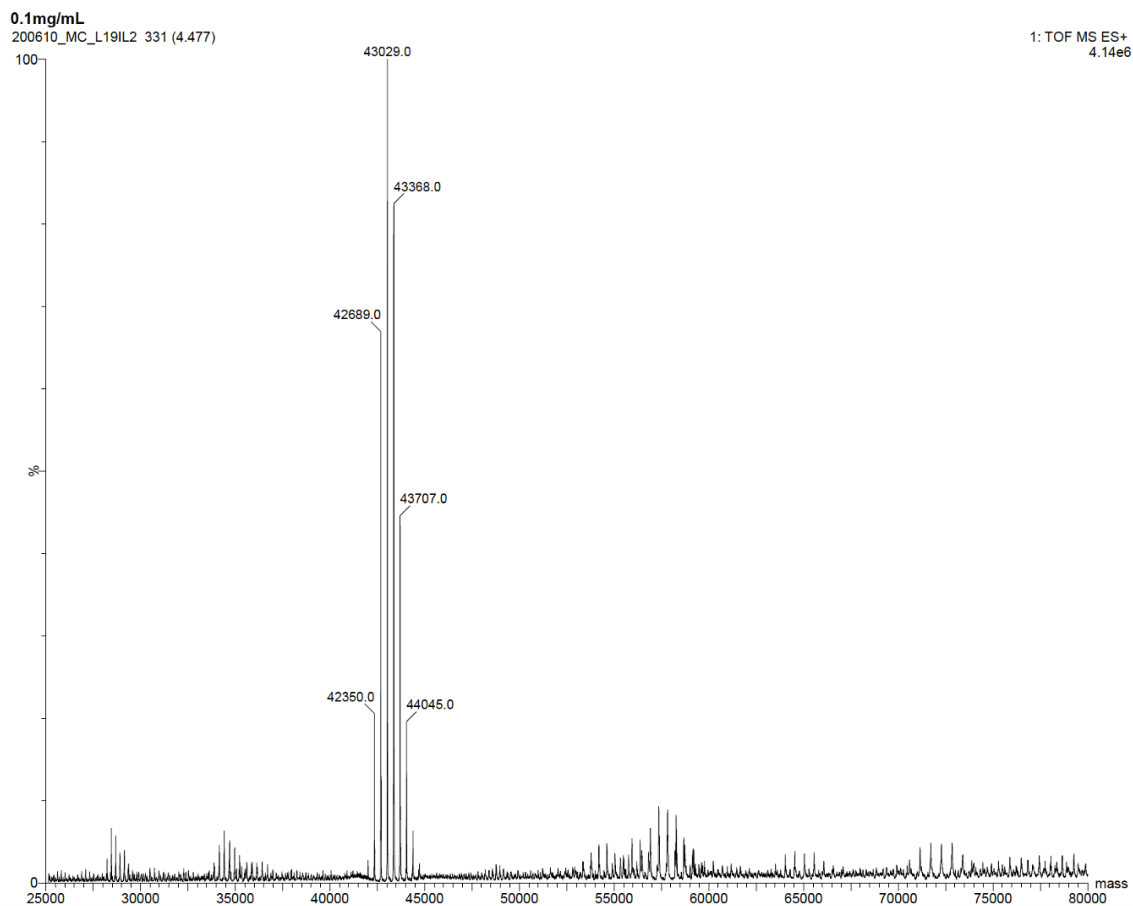
Figure 6.4.36. MS spectrum of biotinylated L19-IL2. Up to six biotin molecules can be observed.

Carbonic Anhydrase IX (CAIX):

CAIX – HisTag

GDPQEPQNNAHRDKEGDDQSHWRYGGDPPWPRVSPACAGRFQSPVDIRPQLA AFCPALRPLELLGFQLPPLPELRLRNNGHSVQLTLPPGLEMALGPGREYRALQLH LHWGAAGRPGSEHTVEGHRFPAEIHVVHLSTAFARVDEALGRPGGLAVLAAFLE EGPEENSAYEQLLSRLEEIAEEGSETQVPGLDISALLPSDFSRYFQYEGSLTTPPC AQGVIWTVFNQTVMLSAKQLHTLSDTLWGPGDSRLQLNFRATQPLNGRVIEASFP AGVDSSHHHHHH
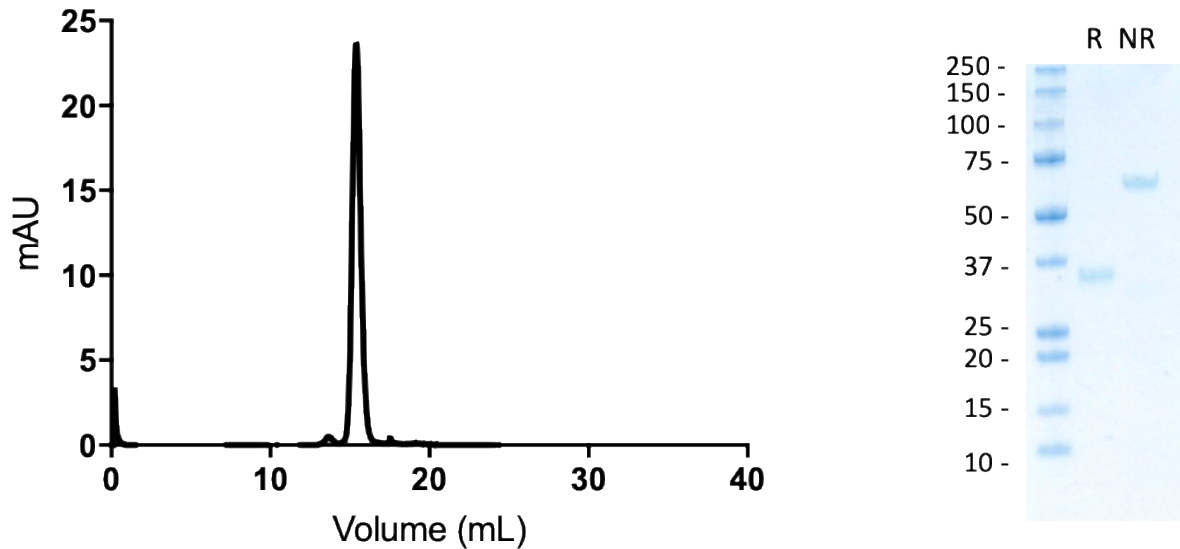
Figure 6.4.37. Size exclusion chromatography profile and Sodium Dodecyl Sulfate Polyacrylamide Gel Electrophoresis (SDS-PAGE) of CAIX. The size corresponds to the predicted molecular weight based on the sequence (Homodimer 62.47 kDa). As expected, under reducing conditions the disulfide-bridged homodimer presents a single band on SDS-PAGE.

Tumor Necrosis Factor (TNF):

TNF – HisTag

MGSHHHHHH**RTPSDKPVAHVVANPQAEGQLQWLNRRANALLANGVELRDNQLV
VPSEGLYLIYSQVLFKGQGCPSTHVLLTHTISRIAVSYQTKVNLLSAIKSPCQRETP
EGAEAKPWYEPIYLGGVFQLEKGDRLSAEINRPDYLDFAESGQVYFGIIAL**
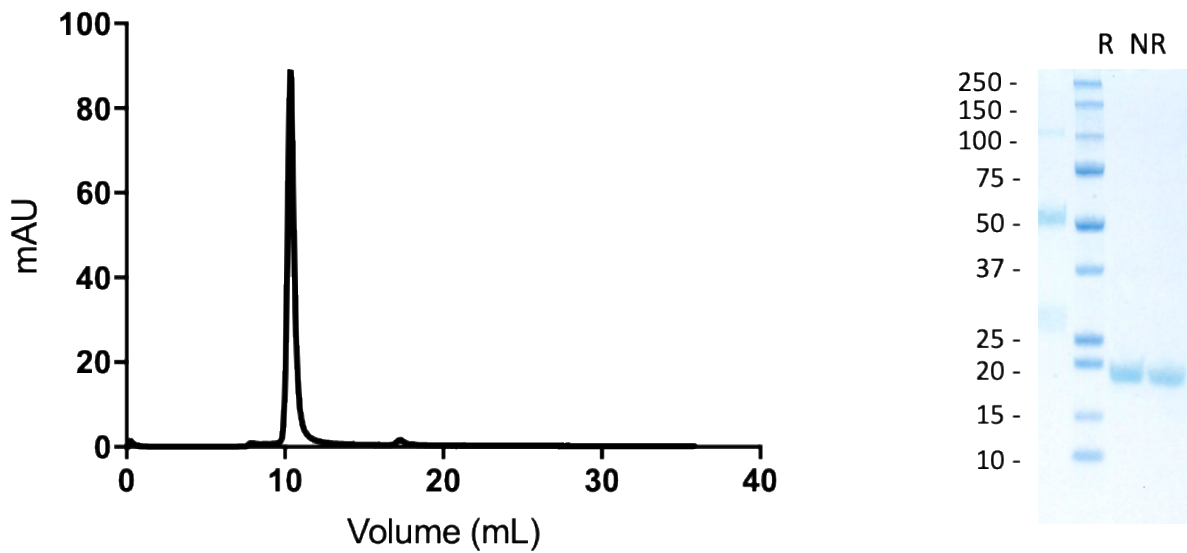
Figure 6.4.38. Size exclusion chromatography profile and Sodium Dodecyl Sulfate Polyacrylamide Gel Electrophoresis (SDS-PAGE) of TNF. The size corresponds to the predicted molecular weight based on the sequence (17.93 kDa). As expected, reducing and non-reducing conditions give the same bands on SDS-PAGE.

F8 anti-EDA antibody (diabody format):

VH(F8) – linker – VL(F8)

EVQLLESGGGLVQPGGSLRLSCAASGFTFSLFTMSWVRQAPGKGLEWVSAISGSG
GSTYYADSVKGRFTISRDNSKNTLYLQMNSLRAEDTAVYYCAKSTHLYLFDYWGQ
GTLVTVSSGGSGGEIVLTQSPGTLSLSPGERATLSCRASQSVSMPFLAWYQQKPG
QAPRLLIYGASSRATGIPDRFSGSGSGTDFTLTISRLEPEDFAVYYCQQMRGRPPT
FGQGTKVEIK
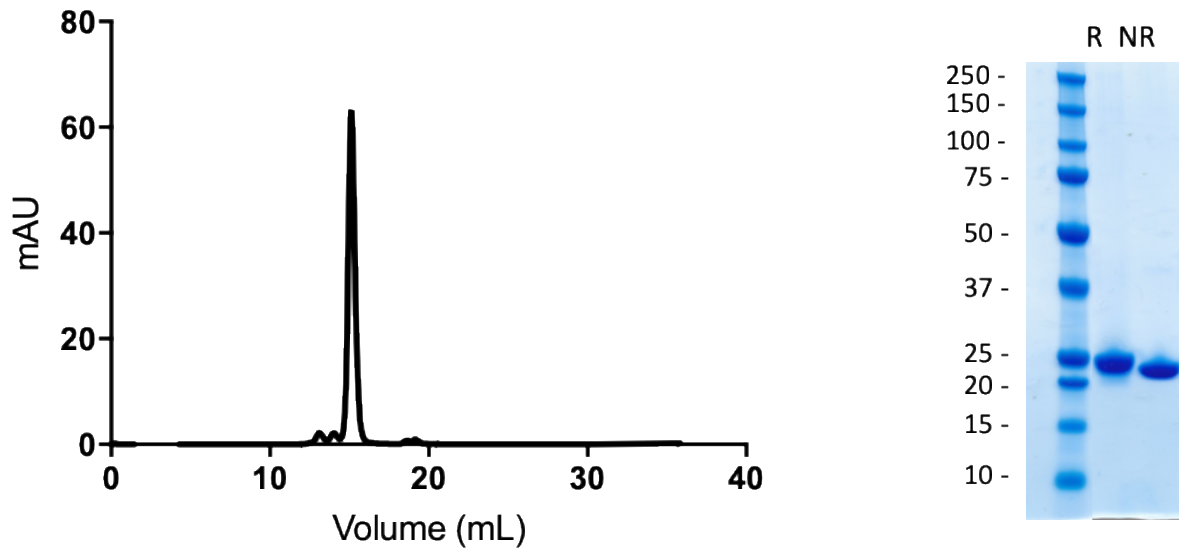
Figure 6.4.39. Size exclusion chromatography profile and Sodium Dodecyl Sulfate Polyacrylamide Gel Electrophoresis (SDS-PAGE) of F8. The size corresponds to the predicted molecular weight based on the sequence (24.79 kDa). As expected, reducing and non-reducing conditions give the same bands on SDS-PAGE.

Extra domain A of Fibronectin (EDA):

EDA – HisTag

**MRGSYRTEIDKPSQMQVTDVQDNSISVKWLPSSSPVTGYRVTTTPKNGPGPTKTK
TAGPDQTEMTIEGLQPTVEYVVSVYAQNPSGESQPLVQTAVTNIDRPKGLAFTDV
DVDSIKIAWESPQGQVSRYRVTYSSPEDGIHELFPAPDGEEDTAELQGLRPGSEY
TVSVVALHDDMESQPLIGTQSTAIPAPTDLKFTQVTPTSLSAQWTPPNVQLTGYRV
RVTPKEKTGPMKEINLAPDSSSVVVSGLMVATKYEVSVYALKDTLTSRPAQGVVT
TLENVRSHHHHHH**
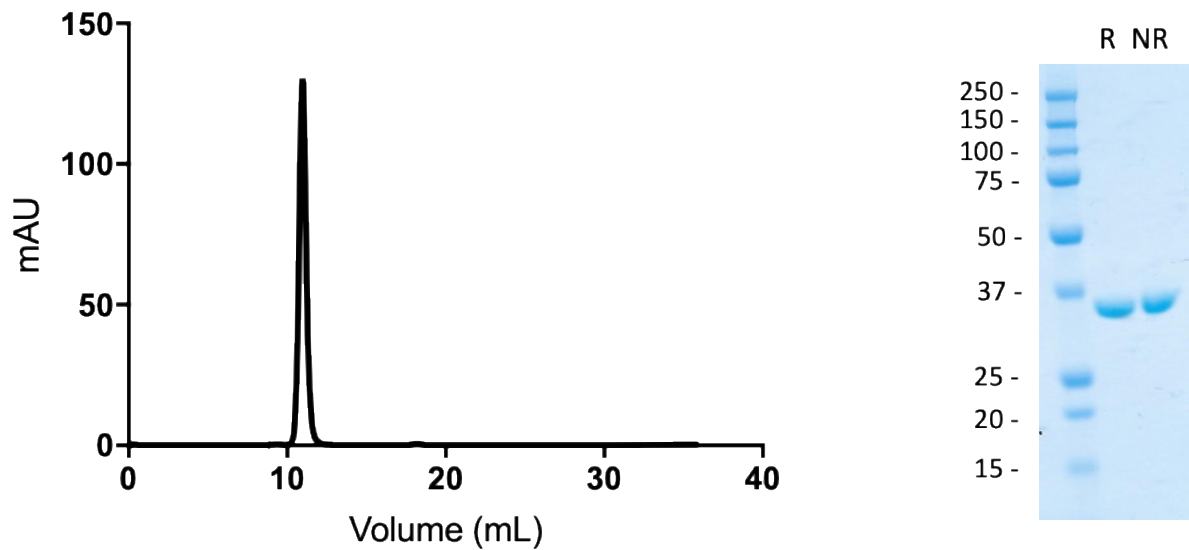
Figure 6.4.40. Size exclusion chromatography profile and Sodium Dodecyl Sulfate Polyacrylamide Gel Electrophoresis (SDS-PAGE) of EDA. The size corresponds to the predicted molecular weight based on the sequence (31.45 kDa). As expected, reducing and non-reducing conditions give the same bands on SDS-PAGE.

F8F8-IL15 fusion protein:

VH(F8) – linker – VL(F8) – <u>linker</u> – VH(F8) – linker – VL(F8) – *linker* – **IL15**

MGWSLILLFLVAVATGVHSEVQLLESGGGLVQPGGSLRLSCAASGFTFSLFTMSW
VRQAPGKGLEWVSAISGSGGSTYYADSVKGRFTISRDNSKNTLYLQMNSLRAEDT
AVYYCAKSTHLYLFDYWGQGTLVTVSSGGSGGEIVLTQSPGTLSLSPGERATLSCR
ASQSVSMPFLAWYQQKPGQAPRLLIYGASSRATGIPDRFSGSGSGTDFTLTISRLE
PEDFAVYYCQQMRGRPPTFGQGTKVEIK<u>SSSSGSSSSGSSSSG</u>EVQLLESGGGLV
QPGGSLRLSCAASGFTFSLFTMSWVRQAPGKGLEWVSAISGSGGSTYYADSVKG
RFTISRDNSKNTLYLQMNSLRAEDTAVYYCAKSTHLYLFDYWGQGTLVTVSSGGS
GGEIVLTQSPGTLSLSPGERATLSCRASQSVSMPFLAWYQQKPGQAPRLLIYGASS
RATGIPDRFSGSGSGTDFTLTISRLEPEDFAVYYCQQMRGRPPTFGQGTKVEIK*GD*
*GSSGGSGGAS***NWVNVISDLKKIEDLIQSMHIDATLYTESDVHPSCKVTAMKCFLLE**
LQVISLESGDASIHDTVENLIILANNSLSSNGNVTESGCKECEELEEKNIKEFLQSFV
HIVQMFINTS
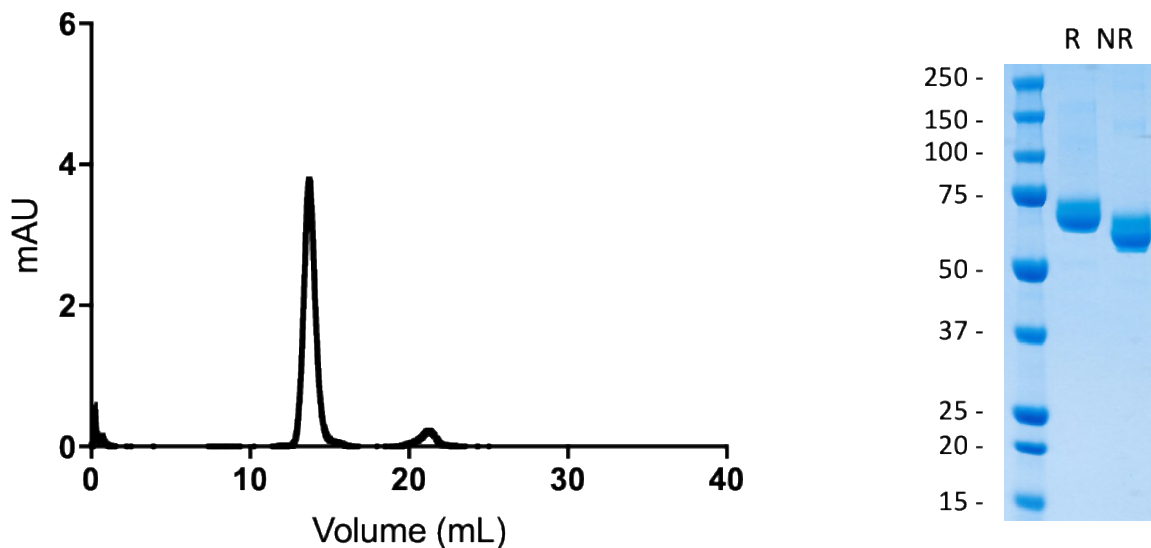
Figure 6.4.41. Size exclusion chromatography profile and Sodium Dodecyl Sulfate Polyacrylamide Gel Electrophoresis (SDS-PAGE) of F8F8-IL15. The size corresponds to the predicted molecular weight based on the sequence (66.40 kDa). As expected, reducing and non-reducing conditions give the same bands on SDS-PAGE.

L19 anti-EDB antibody (diabody format):

VH(L19) – linker – VL(L19)

EVQLLESGGGLVQPGGSLRLSCAASGFTFSSFSMSWVRQAPGKGLEWVSSISGS
SGTTYYADSVKGRFTISRDNSKNTLYLQMNSLRAEDTAVYYCAKPFPYFDYWGQG
TLVTVSSGSSGGEIVLTQSPGTLSLSPGERATLSCRASQSVSSSFLAWYQQKPGQ
APRLLIYYASSRATGIPDRFSGSGSGTDFTLTISRLEPEDFAVYYCQQTGRIPPTFG
QGTKVEIK
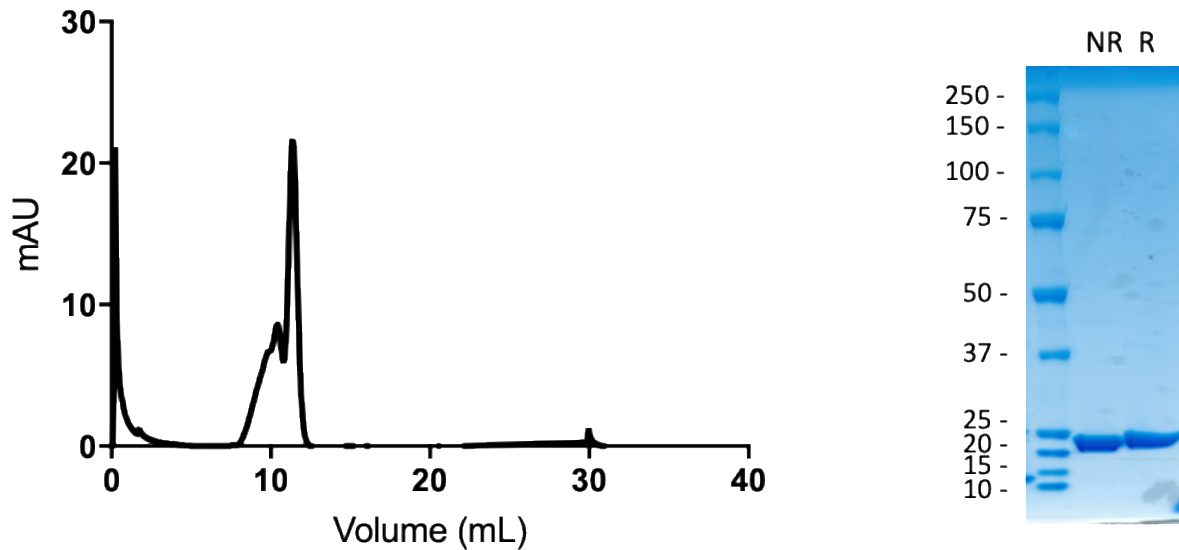
Figure 6.4.42. Size exclusion chromatography profile and Sodium Dodecyl Sulfate Polyacrylamide Gel Electrophoresis (SDS-PAGE) of L19. The size corresponds to the predicted molecular weight based on the sequence (24.61 kDa). As expected, reducing and non-reducing conditions give the same bands on SDS-PAGE.

Coelution by gel filtration
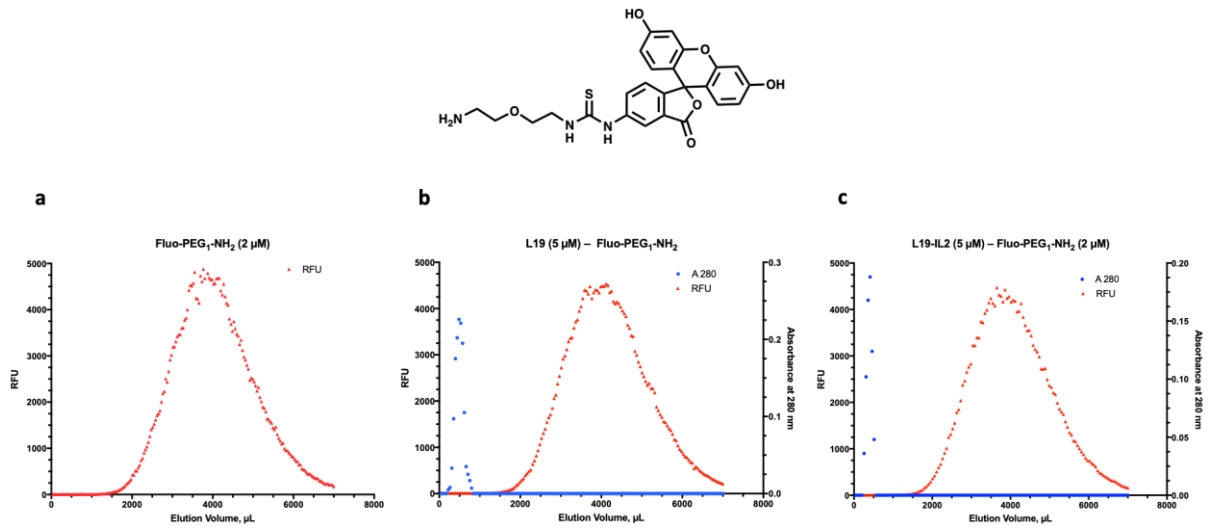
Figure 6.4.43. Gel filtration experiments using the negative control Fluo-PEG$_1$-NH$_2$. In blue absorbance at 280 nm (protein concentration); in red relative fluorescence units (ligand detection). **a.** Ligand alone, **b.** Preincubation with L19 antibody, **c.** Preincubation with L19-IL2.
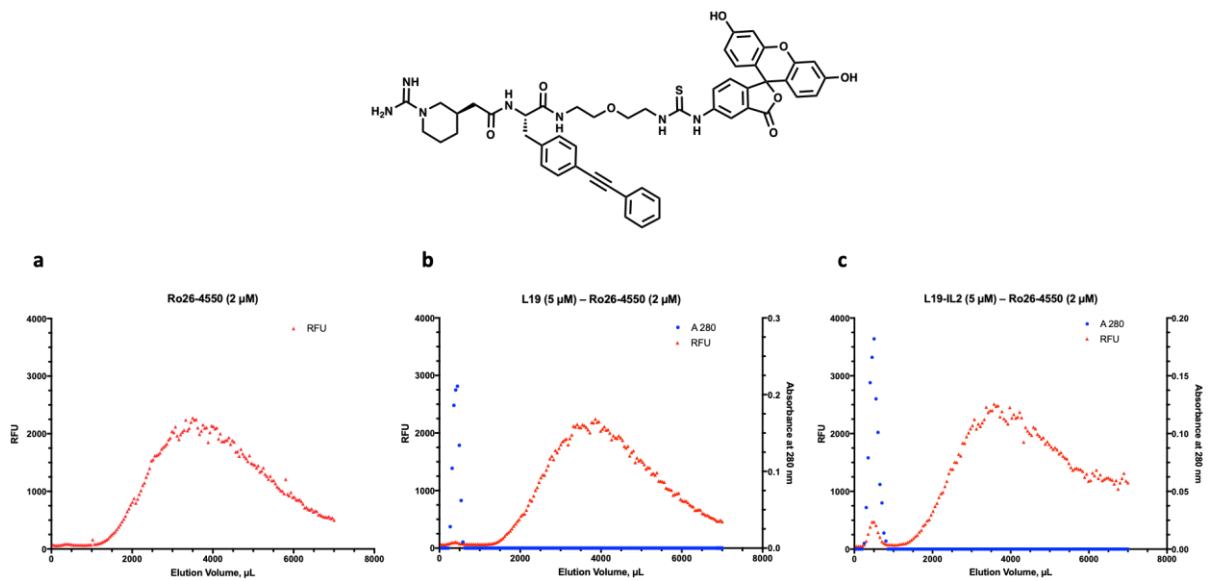
Figure 6.4.44. Gel filtration experiments using the positive control **Ro26-4550** as fluorescein conjugate. In blue absorbance at 280 nm (protein concentration); in red relative fluorescence units (ligand detection). **a.** Ligand alone, **b.** Preincubation with L19 antibody, **c.** Preincubation with L19-IL2.
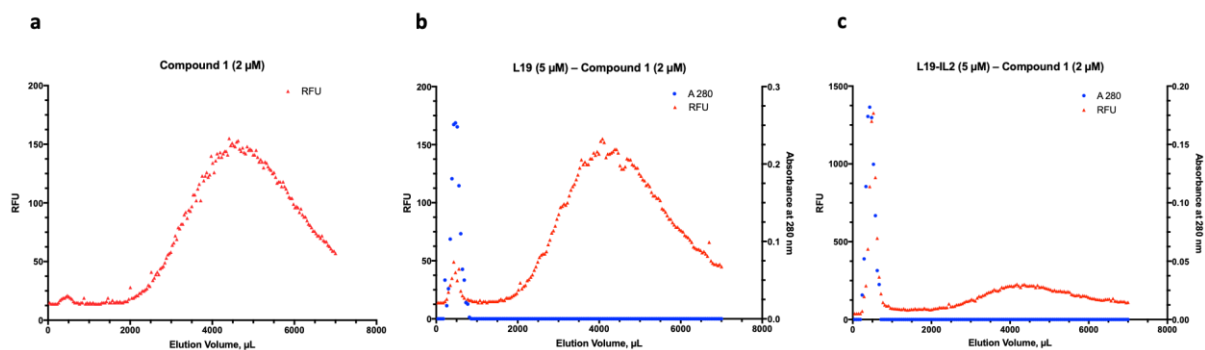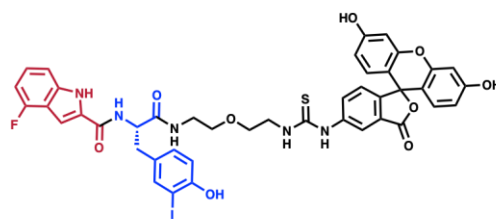
Figure 6.4.45. Gel filtration experiments using the positive control compound **1**. In blue absorbance at 280 nm (protein concentration); in red relative fluorescence units (ligand detection). **a.** Ligand alone, **b.** Preincubation with L19 antibody, **c.** Preincubation with L19-IL2.
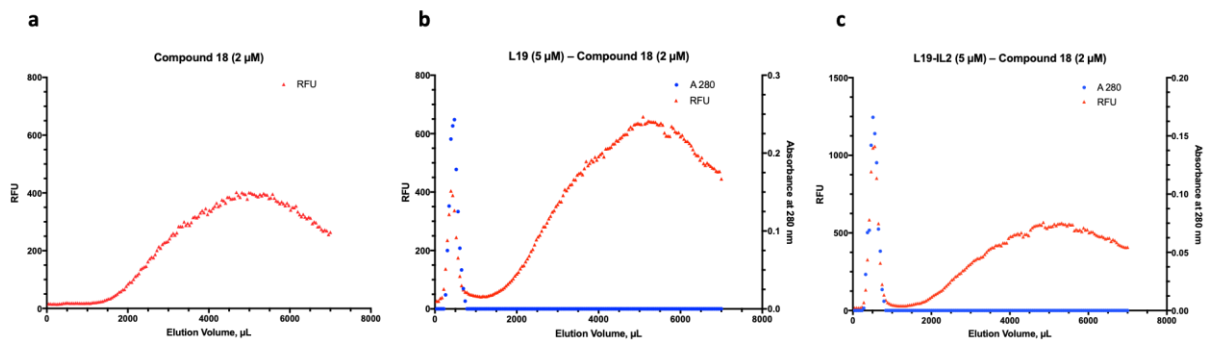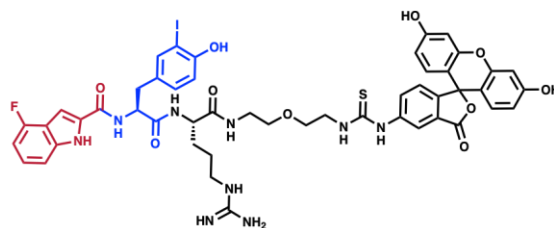
Figure 6.4.46. Gel filtration experiments using the positive control compound **18**. In blue absorbance at 280 nm (protein concentration); in red relative fluorescence units (ligand detection). **a.** Ligand alone, **b.** Preincubation with L19 antibody, **c.** Preincubation with L19-IL2.
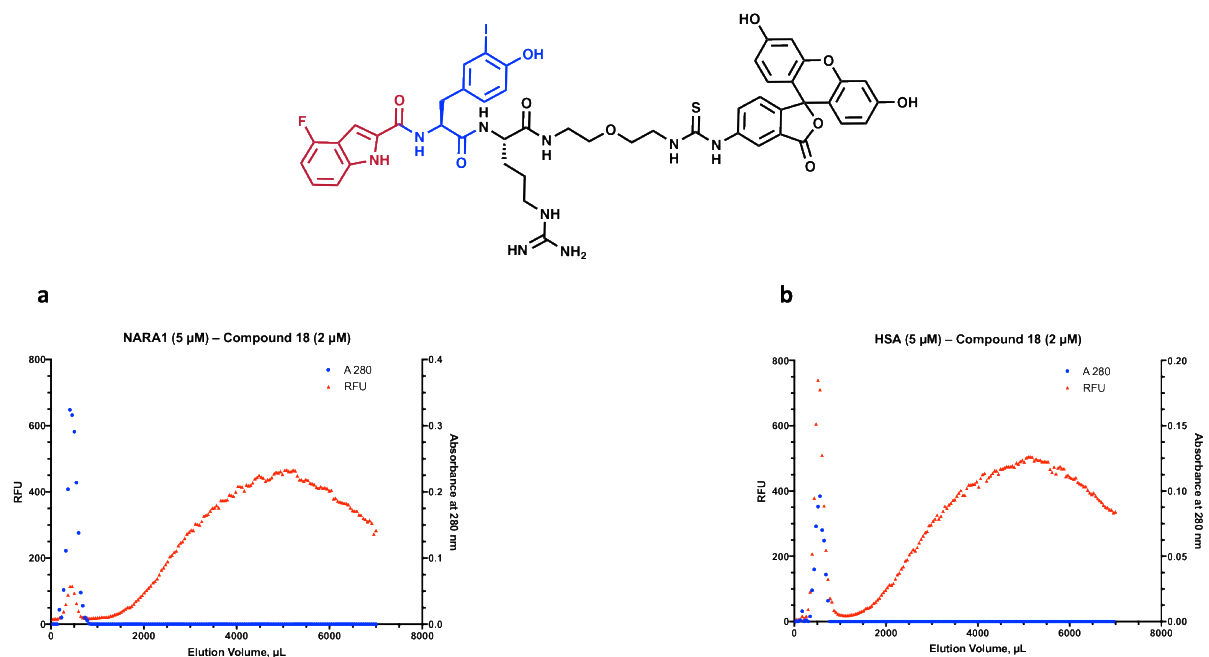
Figure 6.4.47. Gel filtration experiments using the positive control compound **18**. In blue absorbance at 280 nm (protein concentration); in red relative fluorescence units (ligand detection). **a.** Preincubation with NARA1 antibody, **b.** Preincubation with HSA.
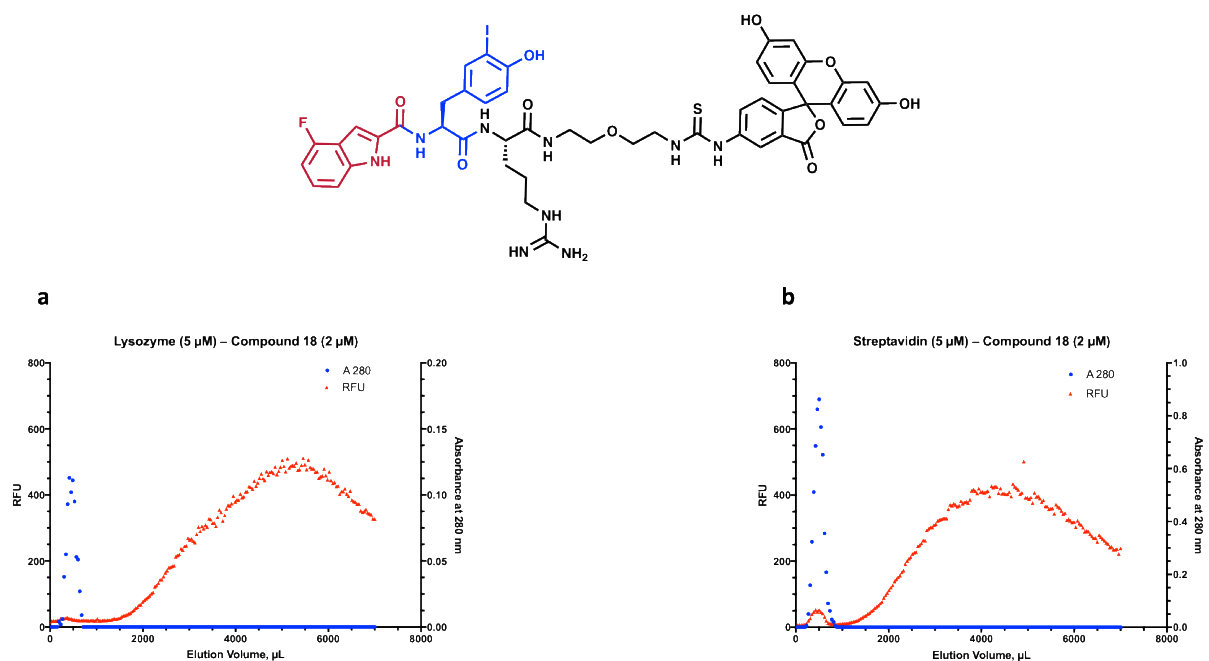
Figure 6.4.48. Gel filtration experiments using the positive control compound **18**. In blue absorbance at 280 nm (protein concentration); in red relative fluorescence units (ligand detection). **a.** Preincubation with Lysozyme, **b.** Preincubation with Streptavidin.

235
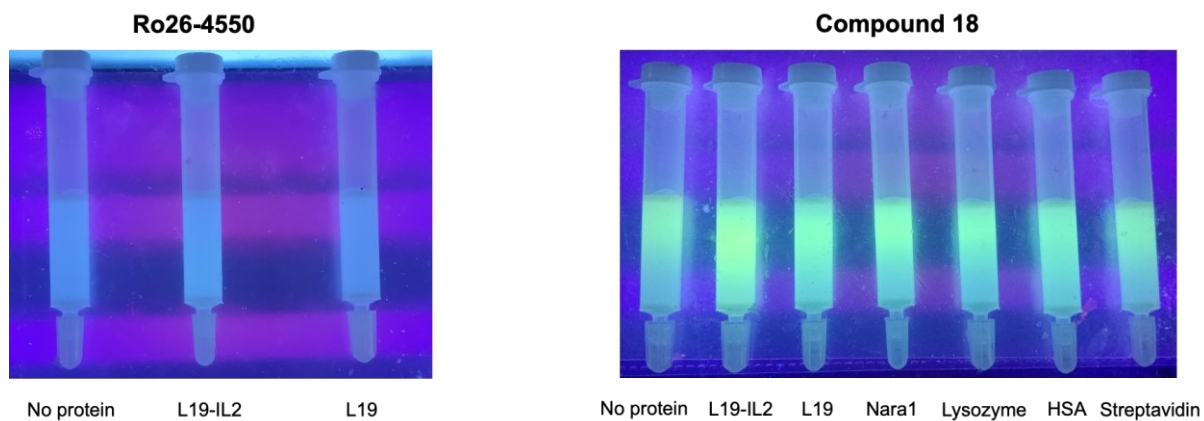
Figure 6.4.49. UV light pictures of the NAP5 columns after gel filtration experiments. Excess of compound **18** was trapped in the matrix of the column. As shown in the picture, a better affinity constant between the corresponding protein and compound **18** makes the small molecule run more efficiently.

Competition Experiment via ELISA
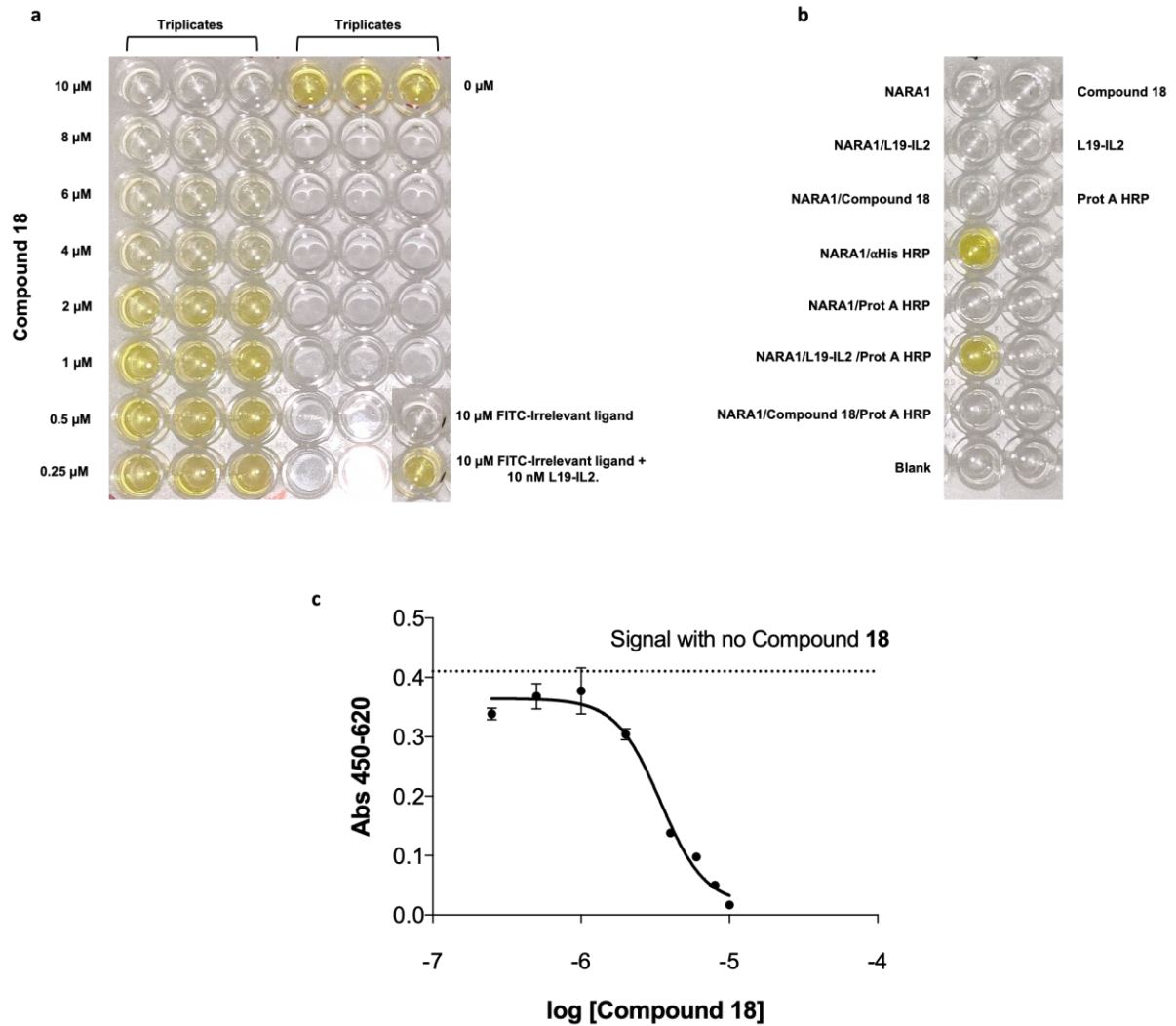
Figure 6.4.50. ELISA competition experiments. **a.** Experimental plate, **b.** Controls, **c.** Plotted data of the ELISA competition experiment. Data shows that compound **18** inhibits the interaction between IL2 and NARA1 with an inhibition constant (IC_{50}) of approximately 3.4 μM.

7. References

(1)   Mackenbach, J. P. The Origins of Human Disease: A Short Story on "Where Diseases Come From." *J. Epidemiol. Community Health* **2006**, *60* (1), 81–86. https://doi.org/10.1136/JECH.2005.038661.

(2)   Wolfe, N. D.; Dunavan, C. P.; Diamond, J. Origins of Major Human Infectious Diseases. *Nature* **2007**, *447* (7142), 279–283. https://doi.org/10.1038/nature05775.

(3)   Bernardini, S.; Tiezzi, A.; Laghezza Masci, V.; Ovidi, E. Natural Products for Human Health: An Historical Overview of the Drug Discovery Approaches. *Nat. Prod. Res.* **2018**, *32* (16), 1926–1950. https://doi.org/10.1080/14786419.2017.1356838.

(4)   Atanasov, A. G.; Zotchev, S. B.; Dirsch, V. M.; Orhan, I. E.; Banach, M.; Rollinger, J. M.; Barreca, D.; Weckwerth, W.; Bauer, R.; Bayer, E. A.; Majeed, M.; Bishayee, A.; Bochkov, V.; Bonn, G. K.; Braidy, N.; Bucar, F.; Cifuentes, A.; D'Onofrio, G.; Bodkin, M.; Diederich, M.; Dinkova-Kostova, A. T.; Efferth, T.; El Bairi, K.; Arkells, N.; Fan, T. P.; Fiebich, B. L.; Freissmuth, M.; Georgiev, M. I.; Gibbons, S.; Godfrey, K. M.; Gruber, C. W.; Heer, J.; Huber, L. A.; Ibanez, E.; Kijjoa, A.; Kiss, A. K.; Lu, A.; Macias, F. A.; Miller, M. J. S.; Mocan, A.; Müller, R.; Nicoletti, F.; Perry, G.; Pittalà, V.; Rastrelli, L.; Ristow, M.; Russo, G. L.; Silva, A. S.; Schuster, D.; Sheridan, H.; Skalicka-Woźniak, K.; Skaltsounis, L.; Sobarzo-Sánchez, E.; Bredt, D. S.; Stuppner, H.; Sureda, A.; Tzvetkov, N. T.; Vacca, R. A.; Aggarwal, B. B.; Battino, M.; Giampieri, F.; Wink, M.; Wolfender, J. L.; Xiao, J.; Yeung, A. W. K.; Lizard, G.; Popp, M. A.; Heinrich, M.; Berindan-Neagoe, I.; Stadler, M.; Daglia, M.; Verpoorte, R.; Supuran, C. T. Natural Products in Drug Discovery: Advances and Opportunities. *Nat. Rev. Drug Discov.* **2021**, *20* (3), 200–216. https://doi.org/10.1038/s41573-020-00114-z.

(5)   Drews, J. Drug Discovery: A Historical Perspective. *Science* **2000**, *287* (5460), 1960–1964. https://doi.org/10.1126/SCIENCE.287.5460.1960.

(6)   Berdigaliyev, N.; Aljofan, M. An Overview of Drug Discovery and Development. *Future Med. Chem.* **2020**, *12* (10), 939–947. https://doi.org/10.4155/fmc-2019-0307.

(7)   Lombardino, J. G.; Lowe, J. A. The Role of the Medicinal Chemist in Drug Discovery - Then and Now. *Nat. Rev. Drug Discov.* **2004**, *3* (10), 853–862. https://doi.org/10.1038/nrd1523.

(8)   Wouters, O. J.; McKee, M.; Luyten, J. Estimated Research and Development Investment Needed to Bring a New Medicine to Market, 2009-2018. *JAMA - J. Am. Med. Assoc.* **2020**, *323* (9), 844–853. https://doi.org/10.1001/jama.2020.1166.

(9)   Wong, C. H.; Siah, K. W.; Lo, A. W. Estimation of Clinical Trial Success Rates and Related Parameters. *Biostatistics* **2019**, *20* (2), 273–286. https://doi.org/10.1093/BIOSTATISTICS/KXX069.

(10)   Paul, S. M.; Mytelka, D. S.; Dunwiddie, C. T.; Persinger, C. C.; Munos, B. H.; Lindborg, S. R.; Schacht, A. L. How to Improve RD Productivity: The Pharmaceutical Industry's Grand Challenge. *Nat. Rev. Drug Discov.* **2010**, *9* (3), 203–214. https://doi.org/10.1038/nrd3078.

(11)   Pammolli, F.; Righetto, L.; Abrignani, S.; Pani, L.; Pelicci, P. G.; Rabosio, E. The Endless Frontier? The Recent Increase of R&D Productivity in Pharmaceuticals. *J. Transl. Med.* **2020**, *18* (1). https://doi.org/10.1186/s12967-020-02313-z.

(12)   Blanco, M.-J.; Gardinier, K. M. New Chemical Modalities and Strategic Thinking in Early Drug Discovery. *ACS Med. Chem. Lett.* **2020**, *11* (3), 228–231. https://doi.org/10.1021/acsmedchemlett.9b00582.

(13)   Wan, H. An Overall Comparison of Small Molecules and Large Biologics in ADME Testing. *ADMET DMPK* **2016**, *4* (1), 1–22. https://doi.org/10.5599/admet.4.1.276.

(14)   Erlanson, D. A.; Fesik, S. W.; Hubbard, R. E.; Jahnke, W.; Jhoti, H. Twenty Years on: The Impact of Fragments on Drug Discovery. *Nat. Rev. Drug Discov.* **2016**, *15* (9), 605–619. https://doi.org/10.1038/nrd.2016.109.

(15)   Madsen, D.; Azevedo, C.; Micco, I.; Petersen, L. K.; Hansen, N. J. V. An Overview of DNA-Encoded Libraries: A Versatile Tool for Drug Discovery. In *Progress in Medicinal Chemistry*; Elsevier B.V., 2020; Vol. 59, pp 181–249. https://doi.org/10.1016/bs.pmch.2020.03.001.

(16)   Gironda-Martínez, A.; Donckele, E. J.; Samain, F.; Neri, D. DNA-Encoded Chemical Libraries: A Comprehensive Review with Succesful Stories and Future Challenges. *ACS Pharmacol. Transl. Sci.* **2021**, *4* (4), 1265–1279. https://doi.org/10.1021/acsptsci.1c00118.

(17)   Maia, E. H. B.; Assis, L. C.; de Oliveira, T. A.; da Silva, A. M.; Taranto, A. G. Structure-Based Virtual Screening: From Classical to Artificial Intelligence. *Front. Chem.* **2020**, *8*, 343. https://doi.org/10.3389/fchem.2020.00343.

(18)   Brown, D. G.; Boström, J. Where Do Recent Small Molecule Clinical Development Candidates Come From? *J. Med. Chem.* **2018**, *61* (21), 9442–9468. https://doi.org/10.1021/acs.jmedchem.8b00675.

(19)   Lipinski, C. A.; Lombardo, F.; Dominy, B. W.; Feeney, P. J. Experimental and Computational Approaches to Estimate Solubility and Permeability in Drug Discovery and Development Settings. *Adv. Drug Deliv. Rev.* **1997**, *23* (1), 3–25. https://doi.org/10.1016/S0169-409X(96)00423-1.

(20)   Shultz, M. D. Two Decades under the Influence of the Rule of Five and the Changing Properties of Approved Oral Drugs. *J. Med. Chem.* **2019**, *62* (4), 1701–1714. https://doi.org/10.1021/acs.jmedchem.8b00686.

(21)   Sioud, M. Phage Display Libraries: From Binders to Targeted Drug Delivery and Human Therapeutics. *Mol. Biotechnol.* **2019**, *61* (4), 286–303. https://doi.org/10.1007/s12033-019-00156-8.

(22)   Galán, A.; Comor, L.; Horvatić, A.; Kuleš, J.; Guillemin, N.; Mrljak, V.; Bhide, M. Library-Based Display Technologies: Where Do We Stand? *Mol. Biosyst.* **2016**, *12* (8), 2342–2358. https://doi.org/10.1039/C6MB00219F.

(23)   Kong, X.-D.; Moriya, J.; Carle, V.; Pojer, F.; Abriata, L. A.; Deyle, K.; Heinis, C. De Novo Development of Proteolytically Resistant Therapeutic Peptides for Oral Administration. *Nat. Biomed. Eng.* **2020**, *4* (5), 560–571. https://doi.org/10.1038/s41551-020-0556-3.

(24)   Urquhart, L. Top Companies and Drugs by Sales in 2020. *Nat. Rev. Drug Discov.* **2021**, *20* (4), 253–253. https://doi.org/10.1038/d41573-021-00050-6.

(25)   The top 20 drugs by worldwide sales in 2020 https://www.fiercepharma.com/special-report/top-20-drugs-by-2020-sales (accessed 2021 -10 -30).

(26)   MacArron, R.; Banks, M. N.; Bojanic, D.; Burns, D. J.; Cirovic, D. A.; Garyantes, T.; Green, D. V. S.; Hertzberg, R. P.; Janzen, W. P.; Paslay, J. W.; Schopfer, U.; Sittampalam, G. S. Impact of High-Throughput Screening in Biomedical Research. *Nat. Rev. Drug Discov.* **2011**, *10* (3), 188–195. https://doi.org/10.1038/nrd3368.

(27)   Lyu, J.; Wang, S.; Balius, T. E.; Singh, I.; Levit, A.; Moroz, Y. S.; O'Meara, M. J.; Che, T.; Algaa, E.; Tolmachova, K.; Tolmachev, A. A.; Shoichet, B. K.; Roth, B. L.; Irwin, J. J. Ultra-Large Library Docking for Discovering New Chemotypes. *Nature* **2019**, *566* (7743), 224–229. https://doi.org/10.1038/s41586-019-0917-9.

(28)   Wildey, M. J.; Haunso, A.; Tudor, M.; Webb, M.; Connick, J. H. High-Throughput Screening. In *Annual Reports in Medicinal Chemistry*; Elsevier, 2017; Vol. 50, pp 149–195. https://doi.org/10.1016/bs.armc.2017.08.004.

(29)   Lloyd, M. D. High-Throughput Screening for the Discovery of Enzyme Inhibitors. *J. Med. Chem.* **2020**, *63* (19), 10742–10772. https://doi.org/10.1021/acs.jmedchem.0c00523.

(30)   Blay, V.; Tolani, B.; Ho, S. P.; Arkin, M. R. High-Throughput Screening: Today's Biochemical and Cell-Based Approaches. *Drug Discov. Today* **2020**, *25* (10), 1807–1821. https://doi.org/10.1016/j.drudis.2020.07.024.

(31)   Fragment-based Drug Discovery: Lessons and Outlook | Wiley https://www.wiley.com/en-us/Fragment+based+Drug+Discovery%3A+Lessons+and+Outlook-p-9783527337750 (accessed 2021 -10 -31).

(32)   Li, Q. Application of Fragment-Based Drug Discovery to Versatile Targets. *Front. Mol. Biosci.* **2020**, *7*, 180. https://doi.org/10.3389/fmolb.2020.00180.

(33)   Kirsch, P.; Hartman, A. M.; Hirsch, A. K. H.; Empting, M. Concepts and Core Principles of Fragment-Based Drug Design. *Molecules* **2019**, *24* (23), 4309. https://doi.org/10.3390/molecules24234309.

(34)   Jhoti, H.; Williams, G.; Rees, D. C.; Murray, C. W. The "rule of Three" for Fragment-Based Drug Discovery: Where Are We Now? *Nat. Rev. Drug Discov.* **2013**, *12* (8), 644–644. https://doi.org/10.1038/nrd3926-c1.

(35)   Baker, M. Fragment-Based Lead Discovery Grows Up. *Nat. Rev. Drug Discov.* **2013**, *12* (1), 5–7. https://doi.org/10.1038/nrd3926.

(36)   Erlanson, D. A.; Davis, B. J.; Jahnke, W. Fragment-Based Drug Discovery: Advancing Fragments in the Absence of Crystal Structures. *Cell Chem. Biol.* **2019**, *26* (1), 9–15. https://doi.org/10.1016/j.chembiol.2018.10.001.

(37)   Miyake, Y.; Itoh, Y.; Hatanaka, A.; Suzuma, Y.; Suzuki, M.; Kodama, H.; Arai, Y.; Suzuki, T. Identification of Novel Lysine Demethylase 5-Selective Inhibitors by Inhibitor-Based Fragment Merging Strategy. *Bioorg. Med. Chem.* **2019**, *27* (6), 1119–1129. https://doi.org/10.1016/j.bmc.2019.02.006.

(38)   Ichihara, O.; Barker, J.; Law, R. J.; Whittaker, M. Compound Design by Fragment-Linking. *Mol. Inform.* **2011**, *30* (4), 298–306. https://doi.org/10.1002/minf.201000174.

(39)   Mondal, M.; Radeva, N.; Fanlo-Virgós, H.; Otto, S.; Klebe, G.; Hirsch, A. K. H. Fragment Linking and Optimization of Inhibitors of the Aspartic Protease Endothiapepsin: Fragment-Based Drug Design Facilitated by Dynamic Combinatorial Chemistry. *Angew. Chem. Int. Ed.* **2016**, *55* (32), 9422–9426. https://doi.org/10.1002/anie.201603074.

(40)   Merrifield, R. B. Solid Phase Peptide Synthesis. I. The Synthesis of a Tetrapeptide. *J. Am. Chem. Soc.* **1963**, *85* (14), 2149–2154. https://doi.org/10.1021/ja00897a025.

(41)   FURKA, Á.; SEBESTYÉN, F.; ASGEDOM, M.; DIBÓ, G. General Method for Rapid Synthesis of Multicomponent Peptide Mixtures. *Int. J. Pept. Protein Res.* **1991**, *37* (6), 487–493. https://doi.org/10.1111/j.1399-3011.1991.tb00765.x.

(42)   Schreiber, S. L. Target-Oriented and Diversity-Oriented Organic Synthesis in Drug Discovery. *Science* **2000**, *287* (5460), 1964–1969. https://doi.org/10.1126/science.287.5460.1964.

(43)   Burke, M. D.; Berger, E. M.; Schreiber, S. L. Generating Diverse Skeletons of Small Molecules Combinatorially. *Science* **2003**, *302* (5645), 613–618. https://doi.org/10.1126/science.1089946.

(44)   Burke, M. D.; Schreiber, S. L. A Planning Strategy for Diversity-Oriented Synthesis. *Angew. Chem. Int. Ed.* **2004**, *43* (1), 46–58. https://doi.org/10.1002/anie.200300626.

(45)   Letsinger, R. L.; Mahadevan, V. Oligonucleotide Synthesis on a Polymer Support1,2. *J. Am. Chem. Soc.* **1965**, *87* (15), 3526–3527. https://doi.org/10.1021/ja01093a058.

(46)   Schuerch, C.; Frechet, J. M. Solid-Phase Synthesis of Oligosaccharides. I. Preparation of the Solid Support. Poly[p-(1-Propen-3-Ol-1-Yl)Styrene]. *J. Am. Chem. Soc.* **1971**, *93* (2), 492–496. https://doi.org/10.1021/ja00731a031.

(47)   Bunin, B. A.; Ellman, J. A. A General and Expedient Method for the Solid-Phase Synthesis of 1,4-Benzodiazepine Derivatives. *J. Am. Chem. Soc.* **1992**, *114* (27), 10997–10998. https://doi.org/10.1021/ja00053a067.

(48)   Toy, P. H.; Lam, Y. *Solid-Phase Organic Synthesis: Concepts, Strategies, and Applications*; John Wiley & Sons, 2012.

(49)   Houghten, R. A.; Pinilla, C.; Blondelle, S. E.; Appel, J. R.; Dooley, C. T.; Cuervo, J. H. Generation and Use of Synthetic Peptide Combinatorial Libraries for Basic Research and Drug Discovery. *Nature* **1991**, *354* (6348), 84–86. https://doi.org/10.1038/354084a0.

(50)   Lam, K. S.; Salmon, S. E.; Hersh, E. M.; Hruby, V. J.; Kazmierski, W. M.; Knapp, R. J. A New Type of Synthetic Peptide Library for Identifying Ligand-Binding Activity. *Nature* **1991**, *354* (6348), 82–84. https://doi.org/10.1038/354082a0.

(51)   Ohlmeyer, M. H.; Swanson, R. N.; Dillard, L. W.; Reader, J. C.; Asouline, G.; Kobayashi, R.; Wigler, M.; Still, W. C. Complex Synthetic Chemical Libraries Indexed with Molecular Tags. *Proc. Natl. Acad. Sci. U. S. A.* **1993**, *90* (23), 10922–10926. https://doi.org/10.1073/pnas.90.23.10922.

(52)   Li, M. Applications of Display Technology in Protein Analysis. *Nat. Biotechnol.* **2000**, *18* (12), 1251–1256. https://doi.org/10.1038/82355.

(53)   Bradbury, A. R. M.; Sidhu, S.; Dübel, S.; McCafferty, J. Beyond Natural Antibodies: The Power of in Vitro Display Technologies. *Nat. Biotechnol.* **2011**, *29* (3), 245–254. https://doi.org/10.1038/nbt.1791.

(54)   Hudson, E. P.; Uhlen, M.; Rockberg, J. Multiplex Epitope Mapping Using Bacterial Surface Display Reveals Both Linear and Conformational Epitopes. *Sci. Rep.* **2012**, *2* (1), 706. https://doi.org/10.1038/srep00706.

(55)   Boder, E. T.; Wittrup, K. D. Yeast Surface Display for Screening Combinatorial Polypeptide Libraries. *Nat. Biotechnol.* **1997**, *15* (6), 553–557. https://doi.org/10.1038/nbt0697-553.

(56)   Wang, H.; Liu, R. Advantages of MRNA Display Selections over Other Selection Techniques for Investigation of Protein–Protein Interactions. *Expert Rev. Proteomics* **2011**, *8* (3), 335–346. https://doi.org/10.1586/epr.11.15.

(57)   Kawasaki, G. Cell-Free Synthesis and Isolation of Novel Genes and Polypeptides. EP0494955B1, July 15, 1998.

(58)   Feldhaus, M. J.; Siegel, R. W.; Opresko, L. K.; Coleman, J. R.; Feldhaus, J. M. W.; Yeung, Y. A.; Cochran, J. R.; Heinzelman, P.; Colby, D.; Swers, J.; Graff, C.; Wiley, H. S.; Wittrup, K. D. Flow-Cytometric Isolation of Human Antibodies from a Nonimmune Saccharomyces Cerevisiae Surface Display Library. *Nat. Biotechnol.* **2003**, *21* (2), 163–170. https://doi.org/10.1038/nbt785.

(59)   Josephson, K.; Ricardo, A.; Szostak, J. W. MRNA Display: From Basic Principles to Macrocycle Drug Discovery. *Drug Discov. Today* **2014**, *19* (4), 388–399. https://doi.org/10.1016/j.drudis.2013.10.011.

(60)   Mattheakis, L. C.; Bhatt, R. R.; Dower, W. J. An in Vitro Polysome Display System for Identifying Ligands from Very Large Peptide Libraries. *Proc. Natl. Acad. Sci. U. S. A.* **1994**, *91* (19), 9022–9026. https://doi.org/10.1073/pnas.91.19.9022.

(61) Zaccolo, M.; Williams, D. M.; Brown, D. M.; Gherardi, E. An Approach to Random Mutagenesis of DNA Using Mixtures of Triphosphate Derivatives of Nucleoside Analogues. *J. Mol. Biol.* **1996**, *255* (4), 589–603. https://doi.org/10.1006/jmbi.1996.0049.

(62) Metzker, M. L. Sequencing Technologies — the next Generation. *Nat. Rev. Genet.* **2010**, *11* (1), 31–46. https://doi.org/10.1038/nrg2626.

(63) Smith, G. P. Filamentous Fusion Phage: Novel Expression Vectors That Display Cloned Antigens on the Virion Surface. *Science* **1985**, *228* (4705), 1315–1317.

(64) McCafferty, J.; Griffiths, A. D.; Winter, G.; Chiswell, D. J. Phage Antibodies: Filamentous Phage Displaying Antibody Variable Domains. *Nature* **1990**, *348* (6301), 552–554. https://doi.org/10.1038/348552a0.

(65) Clackson, T.; Hoogenboom, H. R.; Griffiths, A. D.; Winter, G. Making Antibody Fragments Using Phage Display Libraries. *Nature* **1991**, *352* (6336), 624–628. https://doi.org/10.1038/352624a0.

(66) Marks, J. D.; Hoogenboom, H. R.; Bonnert, T. P.; McCafferty, J.; Griffiths, A. D.; Winter, G. By-Passing Immunization. Human Antibodies from V-Gene Libraries Displayed on Phage. *J. Mol. Biol.* **1991**, *222* (3), 581–597. https://doi.org/10.1016/0022-2836(91)90498-U.

(67) Winter, G.; Griffiths, A. D.; Hawkins, R. E.; Hoogenboom, H. R. Making Antibodies by Phage Display Technology. *Annu. Rev. Immunol.* **1994**, *12*, 433–455. https://doi.org/10.1146/annurev.iy.12.040194.002245.

(68) Jespers, L.; Schon, O.; Famm, K.; Winter, G. Aggregation-Resistant Domain Antibodies Selected on Phage by Heat Denaturation. *Nat. Biotechnol.* **2004**, *22* (9), 1161–1165. https://doi.org/10.1038/nbt1000.

(69) Griffiths, A. D.; Duncan, A. R. Strategies for Selection of Antibodies by Phage Display. *Curr. Opin. Biotechnol.* **1998**, *9* (1), 102–108. https://doi.org/10.1016/S0958-1669(98)80092-X.

(70) Schreuder, M. P.; Mooren, A. T. A.; Toschka, H. Y.; Theo Verrips, C.; Klis, F. M. Immobilizing Proteins on the Surface of Yeast Cells. *Trends Biotechnol.* **1996**, *14* (4), 115–120. https://doi.org/10.1016/0167-7799(96)10017-2.

(71) Hanes, J.; Plückthun, A. In Vitro Selection and Evolution of Functional Proteins by Using Ribosome Display. *Proc. Natl. Acad. Sci. U. S. A.* **1997**, *94* (10), 4937–4942. https://doi.org/10.1073/pnas.94.10.4937.

(72) Makeyev, E. V.; Kolb, V. A.; Spirin, A. S. Enzymatic Activity of the Ribosome-Bound Nascent Polypeptide. *FEBS Lett.* **1996**, *378* (2), 166–170. https://doi.org/10.1016/0014-5793(95)01438-1.

(73) Bencurova, E.; Pulzova, L.; Flachbartova, Z.; Bhide, M. A Rapid and Simple Pipeline for Synthesis of MRNA–Ribosome–VHH Complexes Used in Single-Domain

Antibody Ribosome Display. *Mol. Biosyst.* **2015**, *11* (6), 1515–1524. https://doi.org/10.1039/C5MB00026B.

(74)   Hoogenboom, H. R. Selecting and Screening Recombinant Antibody Libraries. *Nat. Biotechnol.* **2005**, *23* (9), 1105–1116. https://doi.org/10.1038/nbt1126.

(75)   Roberts, R. W.; Szostak, J. W. RNA-Peptide Fusions for the in Vitro Selection of Peptides and Proteins. *Proc. Natl. Acad. Sci. U. S. A.* **1997**, *94* (23), 12297–12302. https://doi.org/10.1073/pnas.94.23.12297.

(76)   Takahashi, T. T.; Austin, R. J.; Roberts, R. W. MRNA Display: Ligand Discovery, Interaction Analysis and Beyond. *Trends Biochem. Sci.* **2003**, *28* (3), 159–165. https://doi.org/10.1016/S0968-0004(03)00036-7.

(77)   Josephson, K.; Hartman, M. C. T.; Szostak, J. W. Ribosomal Synthesis of Unnatural Peptides. *J. Am. Chem. Soc.* **2005**, *127* (33), 11727–11735. https://doi.org/10.1021/ja0515809.

(78)   Kawakami, T.; Murakami, H.; Suga, H. Messenger RNA-Programmed Incorporation of Multiple N-Methyl-Amino Acids into Linear and Cyclic Peptides. *Chem. Biol.* **2008**, *15* (1), 32–42. https://doi.org/10.1016/j.chembiol.2007.12.008.

(79)   Guillen Schlippe, Y. V.; Hartman, M. C. T.; Josephson, K.; Szostak, J. W. In Vitro Selection of Highly Modified Cyclic Peptides That Act as Tight Binding Inhibitors. *J. Am. Chem. Soc.* **2012**, *134* (25), 10469–10477. https://doi.org/10.1021/ja301017y.

(80)   Hayashi, Y.; Morimoto, J.; Suga, H. In Vitro Selection of Anti-Akt2 Thioether-Macrocyclic Peptides Leading to Isoform-Selective Inhibitors. *ACS Chem. Biol.* **2012**, *7* (3), 607–613. https://doi.org/10.1021/cb200388k.

(81)   Heinis, C.; Rutherford, T.; Freund, S.; Winter, G. Phage-Encoded Combinatorial Chemical Libraries Based on Bicyclic Peptides. *Nat. Chem. Biol.* **2009**, *5* (7), 502–507. https://doi.org/10.1038/nchembio.184.

(82)   Heinis, C.; Winter, G. Encoded Libraries of Chemically Modified Peptides. *Gener. Ther.* **2015**, *26*, 89–98. https://doi.org/10.1016/j.cbpa.2015.02.008.

(83)   Jorgensen, W. L. The Many Roles of Computation in Drug Discovery. *Science* **2004**, *303* (5665), 1813–1818. https://doi.org/10.1126/science.1096361.

(84)   Lazo, J. S.; Sharlow, E. R. Drugging Undruggable Molecular Cancer Targets. *Annu. Rev. Pharmacol. Toxicol.* **2016**, *56* (1), 23–40. https://doi.org/10.1146/annurev-pharmtox-010715-103440.

(85)   Dang, C. V.; Reddy, E. P.; Shokat, K. M.; Soucek, L. Drugging the "undruggable" Cancer Targets. *Nat. Rev. Cancer* **2017**, *17* (8), 502–508. https://doi.org/10.1038/nrc.2017.36.

(86)   Brenner, S.; Lerner, R. A. Encoded Combinatorial Chemistry. *Proc. Natl. Acad. Sci. U. S. A.* **1992**, *89* (12), 5381–5383. https://doi.org/10.1073/pnas.89.12.5381.

(87) Lerner, R. A.; Neri, D. Reflections on DNA-Encoded Chemical Libraries. *Biochem. Biophys. Res. Commun.* **2020**, *527* (3), 757–759. https://doi.org/10.1016/j.bbrc.2020.04.080.

(88) Neri, D.; Lerner, R. A. DNA-Encoded Chemical Libraries: A Selection System Based on Endowing Organic Compounds with Amplifiable Information. *Annu. Rev. Biochem.* **2018**, *87* (1), 479–502. https://doi.org/10.1146/annurev-biochem-062917-012550.

(89) Favalli, N.; Bassi, G.; Scheuermann, J.; Neri, D. DNA-Encoded Chemical Libraries – Achievements and Remaining Challenges. *FEBS Lett.* **2018**, *592* (12), 2168–2180. https://doi.org/10.1002/1873-3468.13068.

(90) Dickson, P.; Kodadek, T. Chemical Composition of DNA-Encoded Libraries, Past Present and Future. *Org. Biomol. Chem.* **2019**, *17* (19), 4676–4688. https://doi.org/10.1039/c9ob00581a.

(91) Flood, D. T.; Kingston, C.; Vantourout, J. C.; Dawson, P. E.; Baran, P. S. DNA Encoded Libraries: A Visitor's Guide. *Isr. J. Chem.* **2020**, *60* (3–4), 268–280. https://doi.org/10.1002/ijch.201900133.

(92) Goodnow, R. A.; Dumelin, C. E.; Keefe, A. D. DNA-Encoded Chemistry: Enabling the Deeper Sampling of Chemical Space. *Nat. Rev. Drug Discov.* **2017**, *16* (2), 131–147. https://doi.org/10.1038/nrd.2016.213.

(93) Castañón, J.; Román, J. P.; Jessop, T. C.; de Blas, J.; Haro, R. Design and Development of a Technology Platform for DNA-Encoded Library Production and Affinity Selection. *SLAS Discov.* **2018**, *23* (5), 387–396. https://doi.org/10.1177/2472555217752091.

(94) Conole, D.; H Hunter, J.; J Waring, M. The Maturation of DNA Encoded Libraries: Opportunities for New Users. *Future Med. Chem.* **2021**, *13* (2), 173–191. https://doi.org/10.4155/fmc-2020-0285.

(95) Decurtins, W.; Wichert, M.; Franzini, R. M.; Buller, F.; Stravs, M. A.; Zhang, Y.; Neri, D.; Scheuermann, J. Automated Screening for Small Organic Ligands Using DNA-Encoded Chemical Libraries. *Nat. Protoc.* **2016**, *11* (4), 764–780. https://doi.org/10.1038/nprot.2016.039.

(96) Needels, M. C.; Jones, D. G.; Tate, E. H.; Heinkel, G. L.; Kochersperger, L. M.; Dower, W. J.; Barrett, R. W.; Gallop, M. A. Generation and Screening of an Oligonucleotide-Encoded Synthetic Peptide Library. *Proc. Natl. Acad. Sci. U. S. A.* **1993**, *90* (22), 10700–10704. https://doi.org/10.1073/pnas.90.22.10700.

(97) Nielsen, J.; Brenner, S.; Janda, K. D. Synthetic Methods for the Implementation of Encoded Combinatorial Chemistry. *J. Am. Chem. Soc.* **1993**, *115* (21), 9812–9813. https://doi.org/10.1021/ja00074a063.

(98) Kinoshita, Y.; Nishigaki, K. Enzymatic Synthesis of Code Regions for Encoded Combinatorial Chemistry (ECC). *Nucleic Acids Symp. Ser.* **1995**, No. 34, 201—202.

(99)   Gartner, Z. J.; Tse, B. N.; Grubina, R.; Doyon, J. B.; Snyder, T. M.; Liu, D. R. DNA-Templated Organic Synthesis and Selection of a Library of Macrocycles. *Science* **2004**, *305* (5690), 1601–1605. https://doi.org/10.1126/science.1102629.

(100) Melkko, S.; Scheuermann, J.; Dumelin, C. E.; Neri, D. Encoded Self-Assembling Chemical Libraries. *Nat Biotechnol* **2004**, *22* (5), 568–574. https://doi.org/10.1038/nbt961.

(101) Halpin, D. R.; Harbury, P. B. DNA Display I. Sequence-Encoded Routing of DNA Populations. *PLoS Biol.* **2004**, *2* (7), 1015–1021. https://doi.org/10.1371/journal.pbio.0020173.

(102) Halpin, D. R.; Harbury, P. B. DNA Display II. Genetic Manipulation of Combinatorial Chemistry Libraries for Small-Molecule Evolution. *PLoS Biol.* **2004**, *2* (7), 1022–1030. https://doi.org/10.1371/journal.pbio.0020174.

(103) Halpin, D. R.; Lee, J. A.; Wrenn, S. J.; Harbury, P. B. DNA Display III. Solid-Phase Organic Synthesis on Unprotected DNA. *PLoS Biol.* **2004**, *2* (7). https://doi.org/10.1371/journal.pbio.0020175.

(104) Mannocci, L.; Zhang, Y.; Scheuermann, J.; Leimbacher, M.; De Bellis, G.; Rizzi, E.; Dumelin, C.; Melkko, S.; Neri, D. High-Throughput Sequencing Allows the Identification of Binding Molecules Isolated from DNA-Encoded Chemical Libraries. *Proc. Natl. Acad. Sci. U. S. A.* **2008**, *105* (46), 17670–17675. https://doi.org/10.1073/pnas.0805130105.

(105) Clark, M. A.; Acharya, R. A.; Arico-Muendel, C. C.; Belyanskaya, S. L.; Benjamin, D. R.; Carlson, N. R.; Centrella, P. A.; Chiu, C. H.; Creaser, S. P.; Cuozzo, J. W.; Davie, C. P.; Ding, Y.; Franklin, G. J.; Franzen, K. D.; Gefter, M. L.; Hale, S. P.; Hansen, N. J. V.; Israel, D. I.; Jiang, J.; Kavarana, M. J.; Kelley, M. S.; Kollmann, C. S.; Li, F.; Lind, K.; Mataruse, S.; Medeiros, P. F.; Messer, J. A.; Myers, P.; O'Keefe, H.; Oliff, M. C.; Rise, C. E.; Satz, A. L.; Skinner, S. R.; Svendsen, J. L.; Tang, L.; Van Vloten, K.; Wagner, R. W.; Yao, G.; Zhao, B.; Morgan, B. A. Design, Synthesis and Selection of DNA-Encoded Small-Molecule Libraries. *Nat. Chem. Biol.* **2009**, *5* (9), 647–654. https://doi.org/10.1038/nchembio.211.

(106) Goodnow, R. A. A Handbook for DNA-Encoded Chemistry: Theory and Applications for Exploring Chemical Space and Drug Discovery, First Edition. Edited A BRIEF HISTORY OF THE DEVELOPMENT OF COMBINATORIAL CHEMISTRY AND THE EMERGING NEED FOR DNA-ENCODED CHEMISTRY. **2014**, 19–43.

(107) Li, Y.; de Luca, R.; Cazzamalli, S.; Pretto, F.; Bajic, D.; Scheuermann, J.; Neri, D. Versatile Protein Recognition by the Encoded Display of Multiple Chemical Elements on a Constant Macrocyclic Scaffold. *Nat. Chem.* **2018**, *10* (4), 1–8. https://doi.org/10.1038/s41557-018-0017-8.

(108) Leimbacher, M.; Zhang, Y.; Mannocci, L.; Stravs, M.; Geppert, T.; Scheuermann, J.; Schneider, G.; Neri, D. Discovery of Small-Molecule Interleukin-2 Inhibitors from a DNA-Encoded Chemical Library. *Chem. - Eur. J.* **2012**, *18* (25), 7729–7737. https://doi.org/10.1002/chem.201200952.

(109) Litovchick, A.; Clark, M. A.; Keefe, A. D. Universal Strategies for the DNA-Encoding of Libraries of Small Molecules Using the Chemical Ligation of Oligonucleotide Tags. *Artif. DNA PNA XNA* **2014**, *5* (1), e27896-1-e27896-11. https://doi.org/10.4161/adna.27896.

(110) Li, Y.; Zhao, P.; Zhang, M.; Zhao, X.; Li, X. Multistep DNA-Templated Synthesis Using a Universal Template. *J. Am. Chem. Soc.* **2013**, *135* (47), 17727–17730. https://doi.org/10.1021/ja409936r.

(111) Hansen, M. H.; Blakskjaer, P.; Petersen, L. K.; Hansen, T. H.; Hoøjfeldt, J. W.; Gothelf, K. V.; Hansen, N. J. V. A Yoctoliter-Scale DNA Reactor for Small-Molecule Evolution. *J. Am. Chem. Soc.* **2009**, *131* (3), 1322–1327. https://doi.org/10.1021/ja808558a.

(112) Blakskjaer, P.; Heitner, T.; Hansen, N. J. V. Fidelity by Design: Yoctoreactor and Binder Trap Enrichment for Small-Molecule DNA-Encoded Libraries and Drug Discovery. *Curr. Opin. Chem. Biol.* **2015**, *26*, 62–71. https://doi.org/10.1016/j.cbpa.2015.02.003.

(113) Neri, D.; Melkko, S. Encoded Self-Assembling Chemical Libraries (Esachel). WO 2003/076943, September 18, 2003.

(114) Scheuermann, J.; Dumelin, C. E.; Melkko, S.; Zhang, Y.; Mannocci, L.; Jaggi, M.; Sobek, J.; Neri, D. DNA-Encoded Chemical Libraries for the Discovery of MMP-3 Inhibitors. *Bioconjug. Chem.* **2008**, *19* (3), 778–785. https://doi.org/10.1021/bc7004347.

(115) Wichert, M.; Krall, N.; Decurtins, W.; Franzini, R. M.; Pretto, F.; Schneider, P.; Neri, D.; Scheuermann, J. Dual-Display of Small Molecules Enables the Discovery of Ligand Pairs and Facilitates Affinity Maturation. *Nat. Chem.* **2015**, 7 (3), 241–249. https://doi.org/10.1038/nchem.2158.

(116) Bigatti, M.; Dal Corso, A.; Vanetti, S.; Cazzamalli, S.; Rieder, U.; Scheuermann, J.; Neri, D.; Sladojevich, F. Impact of a Central Scaffold on the Binding Affinity of Fragment Pairs Isolated from DNA-Encoded Self-Assembling Chemical Libraries. *ChemMedChem* **2017**, *12* (21), 1748–1752. https://doi.org/10.1002/cmdc.201700569.

(117) Zimmermann, G.; Li, Y.; Rieder, U.; Mattarella, M.; Neri, D.; Scheuermann, J. Hit-Validation Methodologies for Ligands Isolated from DNA-Encoded Chemical Libraries. *ChemBioChem* **2017**, *18* (9), 853–857. https://doi.org/10.1002/cbic.201600637.

(118) Prati, L.; Bigatti, M.; Donckele, E. J.; Neri, D.; Samain, F. On-DNA Hit Validation Methodologies for Ligands Identified from DNA-Encoded Chemical Libraries. *Biochem. Biophys. Res. Commun.* **2020**, *533* (2), 235–240. https://doi.org/10.1016/j.bbrc.2020.04.030.

(119) Reddavide, F. V.; Lin, W.; Lehnert, S.; Zhang, Y. DNA-Encoded Dynamic Combinatorial Chemical Libraries. *Angew. Chem. Int. Ed.* **2015**, *54* (27), 7924–7928. https://doi.org/10.1002/anie.201501775.

(120) Zhou, Y.; Li, C.; Peng, J.; Xie, L.; Meng, L.; Li, Q.; Zhang, J.; Li, X. D.; Li, X.; Huang, X.; Li, X. DNA-Encoded Dynamic Chemical Library and Its Applications in Ligand Discovery. *J. Am. Chem. Soc.* **2018**, *140* (46), 15859–15867. https://doi.org/10.1021/jacs.8b09277.

(121) Reddavide, F. V.; Cui, M.; Lin, W.; Fu, N.; Heiden, S.; Andrade, H.; Thompson, M.; Zhang, Y. Second Generation DNA-Encoded Dynamic Combinatorial Chemical Libraries. *Chem. Commun.* **2019**, *55* (26), 3753–3756. https://doi.org/10.1039/c9cc01429b.

(122) Zambaldo, C.; Barluenga, S.; Winssinger, N. PNA-Encoded Chemical Libraries. *Curr. Opin. Chem. Biol.* **2015**, *26*, 8–15. https://doi.org/10.1016/j.cbpa.2015.01.005.

(123) Gorska, K.; Huang, K. T.; Chaloin, O.; Winssinger, N. DNA-Templated Homo- and Heterodimerization of Peptide Nucleic Acid Encoded Oligosaccharides That Mimick the Carbohydrate Epitope of HIV. *Angew. Chem. Int. Ed.* **2009**, *48* (41), 7695–7700. https://doi.org/10.1002/anie.200903328.

(124) Fitzgerald, P. R.; Paegel, B. M. DNA-Encoded Chemistry: Drug Discovery from a Few Good Reactions. *Chem. Rev.* **2021**, *121* (12), 7155–7177. https://doi.org/10.1021/acs.chemrev.0c00789.

(125) Franzini, R. M.; Randolph, C. Chemical Space of DNA-Encoded Libraries: Miniperspective. *J. Med. Chem.* **2016**, *59* (14), 6629–6644. https://doi.org/10.1021/acs.jmedchem.5b01874.

(126) Tomberg, A.; Boström, J. Can Easy Chemistry Produce Complex, Diverse, and Novel Molecules? *Drug Discov. Today* **2020**, *25* (12), 2174–2181. https://doi.org/10.1016/j.drudis.2020.09.027.

(127) Götte, K.; Chines, S.; Brunschweiger, A. Reaction Development for DNA-Encoded Library Technology: From Evolution to Revolution? *Tetrahedron Lett.* **2020**, *61* (22). https://doi.org/10.1016/j.tetlet.2020.151889.

(128) Zabolotna, Y.; Pikalyova, R.; Volochnyuk, D.; Horvath, D.; Marcou, G.; Varnek, A. Exploration of the Chemical Space of DNA-Encoded Libraries. **2021**. https://doi.org/10.33774/chemrxiv-2021-dpbdx.

(129) Martín, A.; Nicolaou, C. A.; Toledo, M. A. Navigating the DNA Encoded Libraries Chemical Space. *Commun. Chem.* **2020**, *3* (1), 127. https://doi.org/10.1038/s42004-020-00374-1.

(130) Malone, M. L.; Paegel, B. M. What Is a "DNA-Compatible" Reaction? *ACS Comb. Sci.* **2016**, *18* (4), 182–187. https://doi.org/10.1021/acscombsci.5b00198.

(131) Ratnayake, A. S.; Flanagan, M. E.; Foley, T. L.; Smith, J. D.; Johnson, J. G.; Bellenger, J.; Montgomery, J. I.; Paegel, B. M. A Solution Phase Platform to Characterize Chemical Reaction Compatibility with DNA-Encoded Chemical Library Synthesis. *ACS Comb. Sci.* **2019**, *21* (10), 650–655. https://doi.org/10.1021/acscombsci.9b00113.

(132) Sauter, B.; Schneider, L.; Stress, C.; Gillingham, D. An Assessment of the Mutational Load Caused by Various Reactions Used in DNA Encoded Libraries. *Bioorg. Med. Chem.* **2021**, *52*, 116508. https://doi.org/10.1016/j.bmc.2021.116508.

(133) Satz, A. L.; Hochstrasser, R.; Petersen, A. C. Analysis of Current DNA Encoded Library Screening Data Indicates Higher False Negative Rates for Numerically Larger Libraries. *ACS Comb. Sci.* **2017**, *19* (4), 234–238. https://doi.org/10.1021/acscombsci.7b00023.

(134) Fair, R. J.; Walsh, R. T.; Hupp, C. D. The Expanding Reaction Toolkit for DNA-Encoded Libraries. *Bioorg. Med. Chem. Lett.* **2021**, *51*. https://doi.org/10.1016/j.bmcl.2021.128339.

(135) Hunter, J. H.; Prendergast, L.; Valente, L. F.; Madin, A.; Pairaudeau, G.; Waring, M. J. High Fidelity Suzuki-Miyaura Coupling for the Synthesis of DNA Encoded Libraries Enabled by Micelle Forming Surfactants. *Bioconjug. Chem.* **2020**, *31* (1), 149–155. https://doi.org/10.1021/acs.bioconjchem.9b00838.

(136) Flood, D. T.; Zhang, X.; Fu, X.; Zhao, Z.; Asai, S.; Sanchez, B. B.; Sturgell, E. J.; Vantourout, J. C.; Richardson, P.; Flanagan, M. E.; Piotrowski, D. W.; Kölmel, D. K.; Wan, J.; Tsai, M.-H.; Chen, J. S.; Baran, P. S.; Dawson, P. E. RASS-Enabled S/P−C and S−N Bond Formation for DEL Synthesis. *Angew. Chem. Int. Ed.* **2020**, *59* (19), 7377–7383. https://doi.org/10.1002/anie.201915493.

(137) Ruff, Y.; Martinez, R.; Pellé, X.; Nimsgern, P.; Fille, P.; Ratnikov, M.; Berst, F. An Amphiphilic Polymer-Supported Strategy Enables Chemical Transformations under Anhydrous Conditions for DNA-Encoded Library Synthesis. *ACS Comb. Sci.* **2020**, *22* (3), 120–128. https://doi.org/10.1021/acscombsci.9b00164.

(138) Hunter, J. H.; Anderson, M. J.; Castan, I. F. S. F.; Graham, J. S.; Salvini, C. L. A.; Stanway-Gordon, H. A.; Crawford, J. J.; Madin, A.; Pairaudeau, G.; Waring, M. J. Highly Efficient On-DNA Amide Couplings Promoted by Micelle Forming Surfactants for the Synthesis of DNA Encoded Libraries. *Chem. Sci.* **2021**, *12* (27), 9475–9484. https://doi.org/10.1039/d1sc03007h.

(139) Gerry, C. J.; Wawer, M. J.; Clemons, P. A.; Schreiber, S. L. DNA Barcoding a Complete Matrix of Stereoisomeric Small Molecules. *J. Am. Chem. Soc.* **2019**, *141* (26), 10225–10235. https://doi.org/10.1021/jacs.9b01203.

(140) Xu, H.; Ma, F.; Wang, N.; Hou, W.; Xiong, H.; Lu, F.; Li, J.; Wang, S.; Ma, P.; Yang, G.; Lerner, R. A. DNA-Encoded Libraries: Aryl Fluorosulfonates as Versatile Electrophiles Enabling Facile On-DNA Suzuki, Sonogashira, and Buchwald Reactions. *Adv. Sci.* **2019**, *6* (23). https://doi.org/10.1002/advs.201901551.

(141) Favalli, N.; Bassi, G.; Bianchi, D.; Scheuermann, J.; Neri, D. Large Screening of DNA-Compatible Reaction Conditions for Suzuki and Sonogashira Cross-Coupling Reactions and for Reverse Amide Bond Formation. *Bioorg. Med. Chem.* **2021**, *41*. https://doi.org/10.1016/j.bmc.2021.116206.

(142) De Pedro Beato, E.; Priego, J.; Gironda-Martínez, A.; González, F.; Benavides, J.; Blas, J.; Martín-Ortega, M. D.; Toledo, M. Á.; Ezquerra, J.; Torrado, A. Mild and

Efficient Palladium-Mediated C-N Cross-Coupling Reaction between DNA-Conjugated Aryl Bromides and Aromatic Amines. *ACS Comb. Sci.* **2019**, *21* (2). https://doi.org/10.1021/acscombsci.8b00142.

(143) Chen, Y. C.; Faver, J. C.; Ku, A. F.; Miklossy, G.; Riehle, K.; Bohren, K. M.; Ucisik, M. N.; Matzuk, M. M.; Yu, Z.; Simmons, N. C-N Coupling of DNA-Conjugated (Hetero)Aryl Bromides and Chlorides for DNA-Encoded Chemical Library Synthesis. *Bioconjug. Chem.* **2020**, *31* (3), 770–780. https://doi.org/10.1021/acs.bioconjchem.9b00863.

(144) Kölmel, D. K.; Loach, R. P.; Knauber, T.; Flanagan, M. E. Employing Photoredox Catalysis for DNA-Encoded Chemistry: Decarboxylative Alkylation of α-Amino Acids. *ChemMedChem* **2018**, *13* (20), 2159–2165. https://doi.org/10.1002/cmdc.201800492.

(145) Kölmel, D. K.; Meng, J.; Tsai, M. H.; Que, J.; Loach, R. P.; Knauber, T.; Wan, J.; Flanagan, M. E. On-DNA Decarboxylative Arylation: Merging Photoredox with Nickel Catalysis in Water. *ACS Comb. Sci.* **2019**, *21* (8), 588–597. https://doi.org/10.1021/acscombsci.9b00076.

(146) Kölmel, D. K.; Ratnayake, A. S.; Flanagan, M. E. Photoredox Cross-Electrophile Coupling in DNA-Encoded Chemistry. *Biochem. Biophys. Res. Commun.* **2020**, *533*, 201–208. https://doi.org/10.1016/j.bbrc.2020.04.028.

(147) Wu, R.; Du, T.; Sun, W.; Shaginian, A.; Gao, S.; Li, J.; Wan, J.; Liu, G. Functionalization of DNA-Tagged Alkenes Enabled by Visible-Light-Induced C-H Activation of N-Aryl Tertiary Amines. *Org. Lett.* **2021**, *23* (9), 3486–3490. https://doi.org/10.1021/acs.orglett.1c00924.

(148) Badir, S. O.; Sim, J.; Billings, K.; Csakai, A.; Zhang, X.; Dong, W.; Molander, G. A. Multifunctional Building Blocks Compatible with Photoredox-Mediated Alkylation for DNA-Encoded Library Synthesis. *Org. Lett.* **2020**, *22* (3), 1046–1051. https://doi.org/10.1021/acs.orglett.9b04568.

(149) Phelan, J. P.; Lang, S. B.; Sim, J.; Berritt, S.; Peat, A. J.; Billings, K.; Fan, L.; Molander, G. A. Open-Air Alkylation Reactions in Photoredox-Catalyzed DNA-Encoded Library Synthesis. *J. Am. Chem. Soc.* **2019**, *141* (8), 3723–3732. https://doi.org/10.1021/jacs.9b00669.

(150) Wen, X.; Duan, Z.; Liu, J.; Lu, W.; Lu, X. On-DNA Cross-Dehydrogenative Coupling Reaction toward the Synthesis of Focused DNA-Encoded Tetrahydroisoquinoline Libraries. *Org. Lett.* **2020**, *22* (15), 5721–5725. https://doi.org/10.1021/acs.orglett.0c01565.

(151) Gao, H.; Lin, S.; Zhang, S.; Chen, W.; Liu, X.; Yang, G.; Lerner, R. A.; Xu, H.; Zhou, Z.; Yi, W. Gem-Difluoromethylene Alkyne-Enabled Diverse C−H Functionalization and Application to the on-DNA Synthesis of Difluorinated Isocoumarins. *Angew. Chem. Int. Ed.* **2021**, *60* (4), 1959–1966. https://doi.org/10.1002/anie.202013052.

(152) Zhang, J.; Li, X.; Wei, H.; Li, Y.; Zhang, G.; Li, Y. Sequential DNA-Encoded Building Block Fusion for the Construction of Polysubstituted Pyrazoline Core Libraries. *Org. Lett.* **2021**, *23* (21), 8429–8433. https://doi.org/10.1021/acs.orglett.1c03145.

(153) Potowski, M.; Lüttig, R.; Vakalopoulos, A.; Brunschweiger, A. Copper(I/II)-Promoted Diverse Imidazo[1,2-α]Pyridine Synthesis on Solid-Phase Bound DNA Oligonucleotides for Encoded Library Design. *Org. Lett.* **2021**, *23* (14), 5480–5484. https://doi.org/10.1021/acs.orglett.1c01834.

(154) Park, J. H.; Wang, H. M.; Shin, M. H.; Lim, H. S. Synthesis of a DNA-Encoded Library of Pyrrolo[2,3-d]Pyrimidines. *Bull. Korean Chem. Soc.* **2021**, *42* (4), 691–698. https://doi.org/10.1002/bkcs.12243.

(155) Liu, S.; Qi, J.; Lu, W.; Wang, X.; Lu, X. Synthetic Studies toward DNA-Encoded Heterocycles Based on the on-DNA Formation of α,β-Unsaturated Ketones. *Org. Lett.* **2021**, *23* (3), 908–913. https://doi.org/10.1021/acs.orglett.0c04118.

(156) Qi, J.; Liu, S.; Seydimemet, M.; Wang, X.; Lu, X. A General Set of DNA-Compatible Reactions for Preparing DNA-Tagged Multisubstituted Pyrroles. *Bioconjug. Chem.* **2021**, *32* (11), 2290–2294. https://doi.org/10.1021/acs.bioconjchem.1c00427.

(157) Wu, R.; Gao, S.; Du, T.; Cai, K.; Cheng, X.; Fan, J.; Feng, J.; Shaginian, A.; Li, J.; Wan, J.; Liu, G. Exploring Aldol Reactions on DNA and Applications to Produce Diverse Structures: An Example of Expanding Chemical Space of DNA-Encoded Compounds by Diversity-Oriented Synthesis. *Chem. - Asian J.* **2020**, *15* (23), 4033–4037. https://doi.org/10.1002/asia.202001105.

(158) Ma, F.; Li, J.; Zhang, S.; Gu, Y.; Tan, T.; Chen, W.; Wang, S.; Ma, P.; Xu, H.; Yang, G.; Lerner, R. A. DNA-Encoded Libraries: Hydrazide as a Pluripotent Precursor for On-DNA Synthesis of Various Azole Derivatives. *Chem. - Eur. J.* **2021**, *27* (31), 8214–8220. https://doi.org/10.1002/chem.202100850.

(159) Du, H. C.; Bangs, M. C.; Simmons, N.; Matzuk, M. M. Multistep Synthesis of 1,2,4-Oxadiazoles via DNA-Conjugated Aryl Nitrile Substrates. *Bioconjug. Chem.* **2019**, *30* (5), 1304–1308. https://doi.org/10.1021/acs.bioconjchem.9b00188.

(160) Qu, Y.; Wen, H.; Ge, R.; Xu, Y.; Gao, H.; Shi, X.; Wang, J.; Cui, W.; Su, W.; Yang, H.; Kuai, L.; Satz, A. L.; Peng, X. Copper-Mediated DNA-Compatible One-Pot Click Reactions of Alkynes with Aryl Borates and TMS-N3. *Org. Lett.* **2020**, *22* (11), 4146–4150. https://doi.org/10.1021/acs.orglett.0c01219.

(161) Potowski, M.; Esken, R.; Brunschweiger, A. Translation of the Copper/Bipyridine-Promoted Petasis Reaction to Solid Phase-Coupled DNA for Encoded Library Synthesis. *Bioorg. Med. Chem.* **2020**, *28* (9). https://doi.org/10.1016/j.bmc.2020.115441.

(162) Kunig, V. B. K.; Ehrt, C.; Dömling, A.; Brunschweiger, A. Isocyanide Multicomponent Reactions on Solid-Phase-Coupled DNA Oligonucleotides for

Encoded Library Synthesis. *Org. Lett.* **2019**, *21* (18), 7238–7243. https://doi.org/10.1021/acs.orglett.9b02448.

(163) Tran-Hoang, N.; Kodadek, T. Solid-Phase Synthesis of β-Amino Ketones Via DNA-Compatible Organocatalytic Mannich Reactions. *ACS Comb. Sci.* **2018**, *20* (2), 55–60. https://doi.org/10.1021/acscombsci.7b00151.

(164) Monty, O. B. C.; Simmons, N.; Chamakuri, S.; Matzuk, M. M.; Young, D. W. Solution-Phase Fmoc-Based Peptide Synthesis for DNA-Encoded Chemical Libraries: Reaction Conditions, Protecting Group Strategies, and Pitfalls. *ACS Comb. Sci.* **2020**, *22* (12), 833–843. https://doi.org/10.1021/acscombsci.0c00144.

(165) Stress, C. J.; Sauter, B.; Schneider, L. A.; Sharpe, T.; Gillingham, D. A DNA-Encoded Chemical Library Incorporating Elements of Natural Macrocycles. *Angew. Chem. Int. Ed.* **2019**, *58* (28), 9570–9574. https://doi.org/10.1002/anie.201902513.

(166) Ling, X.; Lu, W.; Miao, L.; Marcaurelle, L. A.; Wang, X.; Ding, Y.; Lu, X. Divergent On-DNA Transformations from DNA-Linked Piperidones. *J. Org. Chem.* **2021**. https://doi.org/10.1021/acs.joc.1c00670.

(167) Liu, W.; Huang, W.; Lin, Q.; Tsai, M. H.; Zhang, R.; Fan, L.; Scott, J. D.; Liu, G.; Wan, J. Development of DNA-Compatible Hydroxycarbonylation Reactions Using Chloroform as a Source of Carbon Monoxide. *Bioorg. Med. Chem.* **2021**, *38*. https://doi.org/10.1016/j.bmc.2021.116118.

(168) Priego, J.; De Pedro Beato, E.; Benavides, J.; Gironda-Martínez, A.; González, F.; Blas, J.; Martín-Ortega, M. D.; Rama-Garda, R.; Ezquerra, J.; Toledo, M. A.; Torrado, A. On-DNA Palladium-Catalyzed Hydrogenation-like Reaction Suitable for DNA-Encoded Library Synthesis. *Bioconjug. Chem.* **2021**, *32* (1), 88–93. https://doi.org/10.1021/acs.bioconjchem.0c00566.

(169) Dawadi, S.; Simmons, N.; Miklossy, G.; Bohren, K. M.; Faver, J. C.; Ucisik, M. N.; Nyshadham, P.; Yu, Z.; Matzuk, M. M. Discovery of Potent Thrombin Inhibitors from a Protease-Focused DNA-Encoded Chemical Library. *Proc. Natl. Acad. Sci. U. S. A.* **2020**, *117* (29), 16782. https://doi.org/10.1073/pnas.2005447117.

(170) Gironda-Martínez, A.; Neri, D.; Samain, F.; Donckele, E. J. DNA-Compatible Diazo-Transfer Reaction in Aqueous Media Suitable for DNA-Encoded Chemical Library Synthesis. *Org. Lett.* **2019**, *21* (23), 9555–9558. https://doi.org/10.1021/acs.orglett.9b03726.

(171) Ede, S.; Schenk, M.; Bierer, D.; Weinmann, H.; Graham, K. Improved Diazo-Transfer Reaction for DNA-Encoded Chemistry and Its Potential Application for Macrocyclic DEL-Libraries. *Molecules* **2021**, *26* (6). https://doi.org/10.3390/molecules26061790.

(172) DNA-Compatible Conversion of Primary Amines into Azides. *Synfacts* **2020**, *16* (02), 0221. https://doi.org/10.1055/s-0039-1691634.

(173) Chan, A. I.; McGregor, L. M.; Liu, D. R. Novel Selection Methods for DNA-Encoded Chemical Libraries. *Curr. Opin. Chem. Biol.* **2015**, *26*, 55–61. https://doi.org/10.1016/j.cbpa.2015.02.010.

(174) Huang, Y.; Li, X. Recent Advances on the Selection Methods of DNA-Encoded Libraries. *ChemBioChem* **2021**, *22* (14), 2384–2397. https://doi.org/10.1002/cbic.202100144.

(175) Harris, P. A.; King, B. W.; Bandyopadhyay, D.; Berger, S. B.; Campobasso, N.; Capriotti, C. A.; Cox, J. A.; Dare, L.; Dong, X.; Finger, J. N.; Grady, L. S. C.; Hoffman, S. J.; Jeong, J. U.; Kang, J.; Kasparcova, V.; Lakdawala, A. S.; Lehr, R.; McNulty, D. E.; Nagilla, R.; Ouellette, M. T.; Pao, C. S.; Rendina, A. R.; Schaeffer, M. C.; Summerfield, J. D.; Swift, B. A.; Totoritis, R. D.; Ward, P.; Zhang, A.; Zhang, D.; Marquis, R. W.; Bertin, J.; Gough, P. J. DNA-Encoded Library Screening Identifies Benzo[b][1,4]Oxazepin-4-Ones as Highly Potent and Monoselective Receptor Interacting Protein 1 Kinase Inhibitors. *J. Med. Chem.* **2016**, *59* (5), 2163–2178. https://doi.org/10.1021/acs.jmedchem.5b01898.

(176) Harris, P. A.; Berger, S. B.; Jeong, J. U.; Nagilla, R.; Bandyopadhyay, D.; Campobasso, N.; Capriotti, C. A.; Cox, J. A.; Dare, L.; Dong, X.; Eidam, P. M.; Finger, J. N.; Hoffman, S. J.; Kang, J.; Kasparcova, V.; King, B. W.; Lehr, R.; Lan, Y.; Leister, L. K.; Lich, J. D.; MacDonald, T. T.; Miller, N. A.; Ouellette, M. T.; Pao, C. S.; Rahman, A.; Reilly, M. A.; Rendina, A. R.; Rivera, E. J.; Schaeffer, M. C.; Sehon, C. A.; Singhaus, R. R.; Sun, H. H.; Swift, B. A.; Totoritis, R. D.; Vossenkämper, A.; Ward, P.; Wisnoski, D. D.; Zhang, D.; Marquis, R. W.; Gough, P. J.; Bertin, J. Discovery of a First-in-Class Receptor Interacting Protein 1 (RIP1) Kinase Specific Clinical Candidate (GSK2982772) for the Treatment of Inflammatory Diseases. *J. Med. Chem.* **2017**, *60* (4), 1247–1261. https://doi.org/10.1021/acs.jmedchem.6b01751.

(177) Ding, Y.; Belyanskaya, S.; DeLorey, J. L.; Messer, J. A.; Joseph Franklin, G.; Centrella, P. A.; Morgan, B. A.; Clark, M. A.; Skinner, S. R.; Dodson, J. W.; Li, P.; Marino, J. P.; Israel, D. I. Discovery of Soluble Epoxide Hydrolase Inhibitors through DNA-Encoded Library Technology (ELT). *Bioorg. Med. Chem.* **2021**, *41*. https://doi.org/10.1016/j.bmc.2021.116216.

(178) Belyanskaya, S. L.; Ding, Y.; Callahan, J. F.; Lazaar, A. L.; Israel, D. I. Discovering Drugs with DNA-Encoded Library Technology: From Concept to Clinic with an Inhibitor of Soluble Epoxide Hydrolase. *ChemBioChem* **2017**, *18* (9), 837–842. https://doi.org/10.1002/cbic.201700014.

(179) Wong, L. S.; Khan, F.; Micklefield, J. Selective Covalent Protein Immobilization: Strategies and Applications. *Chem. Rev.* **2009**, *109* (9), 4025–4053. https://doi.org/10.1021/cr8004668.

(180) Kimple, M. E.; Brill, A. L.; Pasker, R. L. Overview of Affinity Tags for Protein Purification. *Curr. Protoc. Protein Sci.* **2013**, No. SUPPL.73. https://doi.org/10.1002/0471140864.ps0909s73.

(181) The Enzymatic Biotinylation of Proteins. a Post-Translational Modification of Exceptional Specificity. Chapman-Smith and Cronan. 1999. TIBS.

(182) Block, H.; Maertens, B.; Spriestersbach, A.; Brinker, N.; Kubicek, J.; Fabis, R.; Labahn, J.; Schäfer, F. Chapter 27 Immobilized-Metal Affinity Chromatography (IMAC). A Review. In *Methods in Enzymology*; Academic Press Inc., 2009; Vol. 463, pp 439–473. https://doi.org/10.1016/S0076-6879(09)63027-5.

(183) Cull, M. G.; Schatz, P. J. [26] Biotinylation of Proteins in Vivo and in Vitro Using Small Peptide Tags. In *Methods in Enzymology*; Academic Press, 2000; Vol. 326, pp 430–440. https://doi.org/10.1016/S0076-6879(00)26068-0.

(184) Spriestersbach, A.; Kubicek, J.; Schäfer, F.; Block, H.; Maertens, B. Purification of His-Tagged Proteins. In *Methods in Enzymology*; Academic Press Inc., 2015; Vol. 559, pp 1–15. https://doi.org/10.1016/bs.mie.2014.11.003.

(185) Arnau, J.; Lauritzen, C.; Petersen, G. E.; Pedersen, J. Current Strategies for the Use of Affinity Tags and Tag Removal for the Purification of Recombinant Proteins. *Protein Expr. Purif.* **2006**, *48* (1), 1–13. https://doi.org/10.1016/j.pep.2005.12.002.

(186) Dumelin, C. E.; Scheuermann, J.; Melkko, S.; Neri, D. Selection of Streptavidin Binders from a DNA-Encoded Chemical Library. *Bioconjug. Chem.* **2006**, *17* (2), 366–370. https://doi.org/10.1021/bc050282y.

(187) Sannino, A.; Gabriele, E.; Bigatti, M.; Mulatto, S.; Piazzi, J.; Scheuermann, J.; Neri, D.; Donckele, E. J.; Samain, F. Quantitative Assessment of Affinity Selection Performance by Using DNA-Encoded Chemical Libraries. *ChemBioChem* **2019**, *20* (7), 955–962. https://doi.org/10.1002/cbic.201800766.

(188) McGregor, L. M.; Gorin, D. J.; Dumelin, C. E.; Liu, D. R. Interaction-Dependent PCR: Identification of Ligand-Target Pairs from Libraries of Ligands and Libraries of Targets in a Single Solution-Phase Experiment. *J. Am. Chem. Soc.* **2010**, *132* (44), 15522–15524. https://doi.org/10.1021/ja107677q.

(189) McGregor, L. M.; Jain, T.; Liu, D. R. Identification of Ligand-Target Pairs from Combined Libraries of Small Molecules and Unpurified Protein Targets in Cell Lysates. *J. Am. Chem. Soc.* **2014**, *136* (8), 3264–3270. https://doi.org/10.1021/ja412934t.

(190) Chan, A. I.; McGregor, L. M.; Jain, T.; Liu, D. R. Discovery of a Covalent Kinase Inhibitor from a DNA-Encoded Small-Molecule Library × Protein Library Selection. *J. Am. Chem. Soc.* **2017**, *139* (30), 10192–10195. https://doi.org/10.1021/jacs.7b04880.

(191) Zhao, P.; Chen, Z.; Li, Y.; Sun, D.; Gao, Y.; Huang, Y.; Li, X. Selection of DNA-Encoded Small Molecule Libraries against Unmodified and Non-Immobilized Protein Targets. *Angew. Chem. Int. Ed.* **2014**, *53* (38), 10056–10059. https://doi.org/10.1002/anie.201404830.

(192) Li, G.; Liu, Y.; Yu, X.; Li, X. Multivalent Photoaffinity Probe for Labeling Small Molecule Binding Proteins. *Bioconjug. Chem.* **2014**, *25* (6), 1172–1180. https://doi.org/10.1021/bc500195w.

(193) Li, G.; Liu, Y.; Liu, Y.; Chen, L.; Wu, S.; Liu, Y.; Li, X. Photoaffinity Labeling of Small-Molecule-Binding Proteins by DNA-Templated Chemistry. *Angew. Chem. Int. Ed.* **2013**, *52* (36), 9544–9549. https://doi.org/10.1002/anie.201302161.

(194) Sannino, A.; Gironda-Martínez, A.; Gorre, É. M. D.; Prati, L.; Piazzi, J.; Scheuermann, J.; Neri, D.; Donckele, E. J.; Samain, F. Critical Evaluation of Photo-Cross-Linking Parameters for the Implementation of Efficient DNA-Encoded Chemical Library Selections. *ACS Comb. Sci.* **2020**, *22* (4), 204–212. https://doi.org/10.1021/acscombsci.0c00023.

(195) Wu, Z.; Graybill, T. L.; Zeng, X.; Platchek, M.; Zhang, J.; Bodmer, V. Q.; Wisnoski, D. D.; Deng, J.; Coppo, F. T.; Yao, G.; Tamburino, A.; Scavello, G.; Franklin, G. J.; Mataruse, S.; Bedard, K. L.; Ding, Y.; Chai, J.; Summerfield, J.; Centrella, P. A.; Messer, J. A.; Pope, A. J.; Israel, D. I. Cell-Based Selection Expands the Utility of DNA-Encoded Small-Molecule Library Technology to Cell Surface Drug Targets: Identification of Novel Antagonists of the NK3 Tachykinin Receptor. *ACS Comb. Sci.* **2015**, *17* (12), 722–731. https://doi.org/10.1021/acscombsci.5b00124.

(196) Cai, B.; Kim, D.; Akhand, S.; Sun, Y.; Cassell, R. J.; Alpsoy, A.; Dykhuizen, E. C.; Van Rijn, R. M.; Wendt, M. K.; Krusemark, C. J. Selection of DNA-Encoded Libraries to Protein Targets within and on Living Cells. *J. Am. Chem. Soc.* **2019**, *141* (43), 17057–17061. https://doi.org/10.1021/jacs.9b08085.

(197) Huang, Y.; Meng, L.; Nie, Q.; Zhou, Y.; Chen, L.; Yang, S.; Fung, Y. M. E.; Li, X.; Huang, C.; Cao, Y.; Li, Y.; Li, X. Selection of DNA-Encoded Chemical Libraries against Endogenous Membrane Proteins on Live Cells. *Nat. Chem.* **2021**, *13* (1), 77–88. https://doi.org/10.1038/s41557-020-00605-x.

(198) Petersen, L. K.; Christensen, A. B.; Andersen, J.; Folkesson, C. G.; Kristensen, O.; Andersen, C.; Alzu, A.; Sløk, F. A.; Blakskjær, P.; Madsen, D.; Azevedo, C.; Micco, I.; Hansen, N. J. V. Screening of DNA-Encoded Small Molecule Libraries inside a Living Cell. *J. Am. Chem. Soc.* **2021**, *143* (7), 2751–2756. https://doi.org/10.1021/jacs.0c09213.

(199) Buller, F.; Steiner, M.; Scheuermann, J.; Mannocci, L.; Nissen, I.; Kohler, M.; Beisel, C.; Neri, D. High-Throughput Sequencing for the Identification of Binding Molecules from DNA-Encoded Chemical Libraries. *Bioorg. Med. Chem. Lett.* **2010**, *20* (14), 4188–4192. https://doi.org/10.1016/j.bmcl.2010.05.053.

(200) Melkko, S.; Dumelin, C. E.; Scheuermann, J.; Neri, D. On the Magnitude of the Chelate Effect for the Recognition of Proteins by Pharmacophores Scaffolded by Self-Assembling Oligonucleotides. *Chem. Biol.* **2006**, *13* (2), 225–231. https://doi.org/10.1016/j.chembiol.2005.12.006.

(201) Satz, A. L. DNA Encoded Library Selections and Insights Provided by Computational Simulations. *ACS Chem. Biol.* **2015**, *10* (10), 2237–2245. https://doi.org/10.1021/acschembio.5b00378.

(202) McCarthy, K. A.; Franklin, G. J.; Lancia, D. R.; Olbrot, M.; Pardo, E.; O'Connell, J. C.; Kollmann, C. S. The Impact of Variable Selection Coverage on Detection of Ligands from a DNA-Encoded Library Screen. *SLAS Discov.* **2020**, *25* (5), 515–522. https://doi.org/10.1177/2472555220908240.

(203) Bassi, G.; Favalli, N.; Oehler, S.; Martinelli, A.; Catalano, M.; Scheuermann, J.; Neri, D. Comparative Evaluation of DNA-Encoded Chemical Selections Performed Using DNA in Single-Stranded or Double-Stranded Format. *Biochem. Biophys. Res. Commun.* **2020**, *533* (2), 223–229. https://doi.org/10.1016/j.bbrc.2020.04.035.

(204) Kuai, L.; O'Keeffe, T.; Arico-Muendel, C. Randomness in DNA Encoded Library Selection Data Can Be Modeled for More Reliable Enrichment Calculation. *SLAS Discov.* **2018**, *23* (5), 405–416. https://doi.org/10.1177/2472555218757718.

(205) MacConnell, A. B.; Paegel, B. M. Poisson Statistics of Combinatorial Library Sampling Predict False Discovery Rates of Screening. *ACS Comb. Sci.* **2017**, *19* (8), 524–532. https://doi.org/10.1021/acscombsci.7b00061.

(206) Faver, J. C.; Riehle, K.; Lancia, D. R.; Milbank, J. B. J.; Kollmann, C. S.; Simmons, N.; Yu, Z.; Matzuk, M. M. Quantitative Comparison of Enrichment from DNA-Encoded Chemical Library Selections. *ACS Comb. Sci.* **2019**, *21* (2), 75–82. https://doi.org/10.1021/acscombsci.8b00116.

(207) Kómár, P.; Kalinić, M. Denoising DNA Encoded Library Screens with Sparse Learning. *ACS Comb. Sci.* **2020**, *22* (8), 410–421. https://doi.org/10.1021/acscombsci.0c00007.

(208) Rama-Garda, R.; Amigo, J.; Priego, J.; Molina-Martin, M.; Cano, L.; Domínguez, E.; Loza, M. I.; Rivera-Sagredo, A.; de Blas, J. Normalization of DNA Encoded Library Affinity Selection Results Driven by High Throughput Sequencing and HPLC Purification. *Bioorg. Med. Chem.* **2021**, *40*. https://doi.org/10.1016/j.bmc.2021.116178.

(209) Chen, Q.; Cheng, X.; Zhang, L.; Li, X.; Chen, P.; Liu, J.; Zhang, L.; Wei, H.; Li, Z.; Dou, D. Exploring the Lower Limit of Individual DNA-Encoded Library Molecules in Selection. *SLAS Discov.* **2020**, *25* (5), 523–529. https://doi.org/10.1177/2472555219893949.

(210) Buller, F.; Zhang, Y.; Scheuermann, J.; Schäfer, J.; Bühlmann, P.; Neri, D. Discovery of TNF Inhibitors from a DNA-Encoded Chemical Library Based on Diels-Alder Cycloaddition. *Chem. Biol.* **2009**, *16* (10), 1075–1086. https://doi.org/10.1016/j.chembiol.2009.09.011.

(211) Amigo, J.; Rama-Garda, R.; Bello, X.; Sobrino, B.; de Blas, J.; Martín-Ortega, M.; Jessop, T. C.; Carracedo, Á.; Loza, M. I. G.; Domínguez, E. TagFinder: A Novel Tag Analysis Methodology That Enables Detection of Molecules from DNA-Encoded Chemical Libraries. *SLAS Discov.* **2018**, *23* (5), 397–404. https://doi.org/10.1177/2472555217753840.

(212) Hall, J.; Foley, T. L.; Chen, Q.; Israel, D. I.; Xu, Y.; Ford, K. F.; Xie, P.; Fan, J.; Wan, J. A Simple Method for Determining Compound Affinity and Chemical Yield from DNA-Encoded Library Selections. *Biochem. Biophys. Res. Commun.* **2020**, *527* (1), 250–256. https://doi.org/10.1016/j.bbrc.2020.04.024.

(213) Chen, Q.; Hall, J.; Foley, T. L.; Wan, J.; Li, Y.; Israel, D. I. A Method for Estimating Binding Affinity from Primary DEL Selection Data. *Biochem. Biophys. Res. Commun.* **2020**, *533* (2), 249–255. https://doi.org/10.1016/j.bbrc.2020.04.029.

(214) Samain, F.; Ekblad, T.; Mikutis, G.; Zhong, N.; Zimmermann, M.; Nauer, A.; Bajic, D.; Decurtins, W.; Scheuermann, J.; Brown, P. J.; Hall, J.; Gräslund, S.; Schüler, H.; Neri, D.; Franzini, R. M. Tankyrase 1 Inhibitors with Drug-like Properties Identified by Screening a DNA-Encoded Chemical Library. *J. Med. Chem.* **2015**, *58* (12), 5143–5149. https://doi.org/10.1021/acs.jmedchem.5b00432.

(215) Ding, Y.; O'Keefe, H.; DeLorey, J. L.; Israel, D. I.; Messer, J. A.; Chiu, C. H.; Skinner, S. R.; Matico, R. E.; Murray-Thompson, M. F.; Li, F.; Clark, M. A.; Cuozzo, J. W.; Arico-Muendel, C.; Morgan, B. A. Discovery of Potent and Selective Inhibitors for ADAMTS-4 through DNA-Encoded Library Technology (ELT). *ACS Med. Chem. Lett.* **2015**, *6* (8), 888–893. https://doi.org/10.1021/acsmedchemlett.5b00138.

(216) Petersen, L. K.; Blakskjær, P.; Chaikuad, A.; Christensen, A. B.; Dietvorst, J.; Holmkvist, J.; Knapp, S.; Kořínek, M.; Larsen, L. K.; Pedersen, A. E.; Röhm, S.; Sløk, F. A.; Hansen, N. J. V. Novel P38α MAP Kinase Inhibitors Identified from YoctoReactor DNA-Encoded Small Molecule Library. *MedChemComm* **2016**, *7* (7), 1332–1339. https://doi.org/10.1039/c6md00241b.

(217) Usanov, D. L.; Chan, A. I.; Maianti, J. P.; Liu, D. R. Second-Generation DNA-Templated Macrocycle Libraries for the Discovery of Bioactive Small Molecules. *Nat. Chem.* **2018**, *10* (7), 704–714. https://doi.org/10.1038/s41557-018-0033-8.

(218) Gilmartin, A. G.; Faitg, T. H.; Richter, M.; Groy, A.; Seefeld, M. A.; Darcy, M. G.; Peng, X.; Federowicz, K.; Yang, J.; Zhang, S. Y.; Minthorn, E.; Jaworski, J. P.; Schaber, M.; Martens, S.; McNulty, D. E.; Sinnamon, R. H.; Zhang, H.; Kirkpatrick, R. B.; Nevins, N.; Cui, G.; Pietrak, B.; Diaz, E.; Jones, A.; Brandt, M.; Schwartz, B.; Heerding, D. A.; Kumar, R. Allosteric Wip1 Phosphatase Inhibition through Flap-Subdomain Interaction. *Nat. Chem. Biol.* **2014**, *10* (3), 181–187. https://doi.org/10.1038/nchembio.1427.

(219) Taylor, D. M.; Anglin, J.; Park, S.; Ucisik, M. N.; Faver, J. C.; Simmons, N.; Jin, Z.; Palaniappan, M.; Nyshadham, P.; Li, F.; Campbell, J.; Hu, L.; Sankaran, B.; Prasad, B. V. V.; Huang, H.; Matzuk, M. M.; Palzkill, T. Identifying Oxacillinase-48 Carbapenemase Inhibitors Using DNA-Encoded Chemical Libraries. *ACS Infect. Dis.* **2020**, *6* (5), 1214–1227. https://doi.org/10.1021/acsinfecdis.0c00015.

(220) Ahn, S.; Pani, B.; Kahsai, A. W.; Olsen, E. K.; Husemoen, G.; Vestergaard, M.; Jin, L.; Zhao, S.; Wingler, L. M.; Rambarat, P. K.; Simhal, R. K.; Xu, T. T.; Sun, L. D.; Shim, P. J.; Staus, D. P.; Huang, L. Y.; Franch, T.; Chen, X.; Lefkowitz, R. J. Small-Molecule Positive Allosteric Modulators of the b 2 -Adrenoceptor Isolated from DNA-Encoded Libraries. *Mol. Pharmacol.* **2018**, *94* (2), 850–861. https://doi.org/10.1124/mol.118.111948.

(221) Ye, N.; Chen, C. H.; Chen, T.; Song, Z.; He, J. X.; Huan, X. J.; Song, S. S.; Liu, Q.; Chen, Y.; Ding, J.; Xu, Y.; Miao, Z. H.; Zhang, A. Design, Synthesis, and Biological Evaluation of a Series of Benzo[de][1,7]Naphthyridin-7(8H)-Ones Bearing a Functionalized Longer Chain Appendage as Novel PARP1 Inhibitors. *J. Med. Chem.* **2013**, *56* (7), 2885–2903. https://doi.org/10.1021/jm301825t.

(222) Cuozzo, J. W.; Clark, M. A.; Keefe, A. D.; Kohlmann, A.; Mulvihill, M.; Ni, H.; Renzetti, L. M.; Resnicow, D. I.; Ruebsam, F.; Sigel, E. A.; Thomson, H. A.; Wang, C.; Xie, Z.; Zhang, Y. Novel Autotaxin Inhibitor for the Treatment of Idiopathic Pulmonary Fibrosis: A Clinical Candidate Discovered Using DNA-Encoded Chemistry. *J. Med. Chem.* **2020**, *63* (14), 7840–7856. https://doi.org/10.1021/acs.jmedchem.0c00688.

(223) Kunig, V. B. K.; Potowski, M.; Akbarzadeh, M.; Klika Škopić, M.; dos Santos Smith, D.; Arendt, L.; Dormuth, I.; Adihou, H.; Andlovic, B.; Karatas, H.; Shaabani, S.;

Zarganes-Tzitzikas, T.; Neochoritis, C. G.; Zhang, R.; Groves, M.; Guéret, S. M.; Ottmann, C.; Rahnenführer, J.; Fried, R.; Dömling, A.; Brunschweiger, A. TEAD–YAP Interaction Inhibitors and MDM2 Binders from DNA-Encoded Indole-Focused Ugi Peptidomimetics. *Angew. Chem. Int. Ed.* **2020**, *59* (46), 20338–20342. https://doi.org/10.1002/anie.202006280.

(224) Shin, M. H.; Lee, K. J.; Lim, H. S. DNA-Encoded Combinatorial Library of Macrocyclic Peptoids. *Bioconjug. Chem.* **2019**, *30* (11), 2931–2938. https://doi.org/10.1021/acs.bioconjchem.9b00628.

(225) Bassi, G.; Favalli, N.; Vuk, M.; Catalano, M.; Martinelli, A.; Trenner, A.; Porro, A.; Yang, S.; Tham, C. L.; Moroglu, M.; Yue, W. W.; Conway, S. J.; Vogt, P. K.; Sartori, A. A.; Scheuermann, J.; Neri, D. A Single-Stranded DNA-Encoded Chemical Library Based on a Stereoisomeric Scaffold Enables Ligand Discovery by Modular Assembly of Building Blocks. *Adv. Sci.* **2020**, *2001970*, 1–10. https://doi.org/10.1002/advs.202001970.

(226) Koesema, E.; Roy, A.; Paciaroni, N. G.; Kodadek, T. Synthesis and Screening of A DNA-Encoded Library of Non-Peptidic Macrocycles. **2020**. https://doi.org/10.26434/chemrxiv.13490151.v1.

(227) Chamakuri, S.; Lu, S.; Nihan Ucisik, M.; Bohren, K. M.; Chen, Y.-C.; Du, H.-C.; Faver, J. C.; Jimmidi, R.; Li, F.; Li, J.-Y.; Nyshadham, P.; Palmer, S. S.; Pollet, J.; Qin, X.; Ronca, S. E.; Sankaran, B.; Sharma, K. L.; Tan, Z.; Versteeg, L.; Yu, Z.; Matzuk, M. M.; Palzkill, T.; Young, D. W.; McLean, M. DNA-Encoded Chemistry Technology Yields Expedient Access to SARS-CoV-2 M pro Inhibitors. https://doi.org/10.1073/pnas.2111172118/-/DCSupplemental.

(228) Onda, Y.; Bassi, G.; Elsayed, A.; Ulrich, F.; Oehler, S.; Plais, L.; Scheuermann, J.; Neri, D. A DNA-Encoded Chemical Library Based on Peptide Macrocycles. *Chem. Eur. J.* **2021**, *27* (24), 7160–7167. https://doi.org/10.1002/chem.202005423.

(229) Zhu, Z.; Shaginian, A.; Grady, L. C.; O'Keeffe, T.; Shi, X. E.; Davie, C. P.; Simpson, G. L.; Messer, J. A.; Evindar, G.; Bream, R. N.; Thansandote, P. P.; Prentice, N. R.; Mason, A. M.; Pal, S. Design and Application of a DNA-Encoded Macrocyclic Peptide Library. *ACS Chem. Biol.* **2018**, *13* (1), 53–59. https://doi.org/10.1021/acschembio.7b00852.

(230) Kennedy, A. J.; Sundström, L.; Geschwindner, S.; Poon, E. K. Y.; Jiang, Y.; Chen, R.; Cooke, R.; Johnstone, S.; Madin, A.; Lim, J.; Liu, Q.; Lohman, R. J.; Nordqvist, A.; Fridén-Saxin, M.; Yang, W.; Brown, D. G.; Fairlie, D. P.; Dekker, N. Protease-Activated Receptor-2 Ligands Reveal Orthosteric and Allosteric Mechanisms of Receptor Inhibition. *Commun. Biol.* **2020**, *3* (1). https://doi.org/10.1038/s42003-020-01504-0.

(231) Richter, H.; Satz, A. L.; Bedoucha, M.; Buettelmann, B.; Petersen, A. C.; Harmeier, A.; Hermosilla, R.; Hochstrasser, R.; Burger, D.; Gsell, B.; Gasser, R.; Huber, S.; Hug, M. N.; Kocer, B.; Kuhn, B.; Ritter, M.; Rudolph, M. G.; Weibel, F.; Molina-David, J.; Kim, J. J.; Santos, J. V.; Stihle, M.; Georges, G. J.; Bonfil, R. D.; Fridman, R.; Uhles, S.; Moll, S.; Faul, C.; Fornoni, A.; Prunotto, M. DNA-Encoded Library-Derived DDR1 Inhibitor Prevents Fibrosis and Renal Function Loss in a

Genetic Mouse Model of Alport Syndrome. *ACS Chem. Biol.* **2019**, *14* (1), 37–49. https://doi.org/10.1021/acschembio.8b00866.

(232) Cazzamalli, S.; Dal Corso, A.; Neri, D. Acetazolamide Serves as Selective Delivery Vehicle for Dipeptide-Linked Drugs to Renal Cell Carcinoma. *Mol. Cancer Ther.* **2016**, *15* (12), 2926–2935. https://doi.org/10.1158/1535-7163.MCT-16-0283.

(233) Cazzamalli, S.; Ziffels, B.; Widmayer, F.; Murer, P.; Pellegrini, G.; Pretto, F.; Wulhfard, S.; Neri, D. Enhanced Therapeutic Activity of Non-Internalizing Small-Molecule-Drug Conjugates Targeting Carbonic Anhydrase IX in Combination with Targeted Interleukin-2. *Clin. Cancer Res.* **2018**, *24* (15), 3656–3667. https://doi.org/10.1158/1078-0432.CCR-17-3457.

(234) Cazzamalli, S.; Dal Corso, A.; Widmayer, F.; Neri, D. Chemically Defined Antibody- and Small Molecule-Drug Conjugates for in Vivo Tumor Targeting Applications: A Comparative Analysis. *J. Am. Chem. Soc.* **2018**, *140* (5), 1617–1621. https://doi.org/10.1021/jacs.7b13361.

(235) Kulterer, O. C.; Pfaff, S.; Wadsak, W.; Garstka, N.; Remzi, M.; Vraka, C.; Nics, L.; Mitterhauser, M.; Bootz, F.; Cazzamalli, S.; Krall, N.; Neri, D.; Haug, A. R. A Microdosing Study with 99mTc-PHC-102 for the SPECT/CT Imaging of Primary and Metastatic Lesions in Renal Cell Carcinoma Patients. *J. Nucl. Med. Off. Publ. Soc. Nucl. Med.* **2021**, *62* (3), 360–365. https://doi.org/10.2967/jnumed.120.245530.

(236) Wishart, D. S.; Feunang, Y. D.; Guo, A. C.; Lo, E. J.; Marcu, A.; Grant, J. R.; Sajed, T.; Johnson, D.; Li, C.; Sayeeda, Z.; Assempour, N.; Iynkkaran, I.; Liu, Y.; Maciejewski, A.; Gale, N.; Wilson, A.; Chin, L.; Cummings, R.; Le, Di.; Pon, A.; Knox, C.; Wilson, M. DrugBank 5.0: A Major Update to the DrugBank Database for 2018. *Nucleic Acids Res.* **2018**, *46* (D1), D1074–D1082. https://doi.org/10.1093/nar/gkx1037.

(237) The human proteome in druggable - The Human Protein Atlas https://www.proteinatlas.org/humanproteome/tissue/druggable (accessed 2021 -10 - 28).

(238) Santos, R.; Ursu, O.; Gaulton, A.; Bento, A. P.; Donadi, R. S.; Bologa, C. G.; Karlsson, A.; Al-Lazikani, B.; Hersey, A.; Oprea, T. I.; Overington, J. P. A Comprehensive Map of Molecular Drug Targets. *Nat. Rev. Drug Discov.* **2016**, *16* (1), 19–34. https://doi.org/10.1038/nrd.2016.230.

(239) Wang, Y.; Zhang, S.; Li, F.; Zhou, Y.; Zhang, Y.; Wang, Z.; Zhang, R.; Zhu, J.; Ren, Y.; Tan, Y.; Qin, C.; Li, Y.; Li, X.; Chen, Y.; Zhu, F. Therapeutic Target Database 2020: Enriched Resource for Facilitating Research and Early Development of Targeted Therapeutics. *Nucleic Acids Res.* **2020**, *48* (D1), D1031–D1041. https://doi.org/10.1093/nar/gkz981.

(240) Cheng, A. C.; Coleman, R. G.; Smyth, K. T.; Cao, Q.; Soulard, P.; Caffrey, D. R.; Salzberg, A. C.; Huang, E. S. Structure-Based Maximal Affinity Model Predicts Small-Molecule Druggability. *Nat. Biotechnol.* **2007**, *25* (1), 71–75. https://doi.org/10.1038/nbt1273.

(241) Owens, J. Determining Druggability. *Nat. Rev. Drug Discov.* **2007**, *6* (3), 187. https://doi.org/10.1038/nrd2275.

(242) Hajduk, P. J.; Huth, J. R.; Tse, C. Predicting Protein Druggability. *Drug Discov. Today* **2005**, *10* (23–24), 1675–1682. https://doi.org/10.1016/S1359-6446(05)03624-X.

(243) Duffy, M. J.; Crown, J. Drugging "Undruggable" Genes for Cancer Treatment: Are We Making Progress? *Int. J. Cancer* **2021**, *148* (1), 8–17. https://doi.org/10.1002/IJC.33197.

(244) Coleman, N.; Rodon, J. Taking Aim at the Undruggable. *Am. Soc. Clin. Oncol. Educ. Book* **2021**, No. 41, e145–e152. https://doi.org/10.1200/edbk_325885.

(245) Mészáros, B.; Simon, I.; Dosztányi, Z. The Expanding View of Protein-Protein Interactions: Complexes Involving Intrinsically Disordered Proteins. *Phys. Biol.* **2011**, *8* (3). https://doi.org/10.1088/1478-3975/8/3/035003.

(246) Lu, H.; Zhou, Q.; He, J.; Jiang, Z.; Peng, C.; Tong, R.; Shi, J. Recent Advances in the Development of Protein–Protein Interactions Modulators: Mechanisms and Clinical Trials. *Signal Transduct. Target. Ther.* **2020**, *5* (1). https://doi.org/10.1038/s41392-020-00315-3.

(247) Mabonga, L.; Kappo, A. P. Protein-Protein Interaction Modulators: Advances, Successes and Remaining Challenges. *Biophys. Rev.* **2019**, *11* (4), 559–581. https://doi.org/10.1007/s12551-019-00570-x.

(248) Arkin, M. R.; Tang, Y.; Wells, J. A. Small-Molecule Inhibitors of Protein-Protein Interactions: Progressing toward the Reality. *Chem. Biol.* **2014**, *21* (9), 1102–1114. https://doi.org/10.1016/j.chembiol.2014.09.001.

(249) Scott, D. E.; Bayly, A. R.; Abell, C.; Skidmore, J. Small Molecules, Big Targets: Drug Discovery Faces the Protein-Protein Interaction Challenge. *Nat. Rev. Drug Discov.* **2016**, *15* (8), 533–550. https://doi.org/10.1038/nrd.2016.29.

(250) Arkin, M. M. R.; Wells, J. A. Small-Molecule Inhibitors of Protein-Protein Interactions: Progressing towards the Dream. *Nat. Rev. Drug Discov.* **2004**, *3* (4), 301–317. https://doi.org/10.1038/nrd1343.

(251) Wilson, C. G. M.; Arkin, M. R. Small-Molecule Inhibitors of IL-2/IL-2R: Lessons Learned and Applied. In *Small-Molecule Inhibitors of Protein-Protein Interactions*; Vassilev, L., Fry, D., Eds.; Springer Berlin Heidelberg: Berlin, Heidelberg, 2011; pp 25–59. https://doi.org/10.1007/82_2010_93.

(252) Struntz, N. B.; Chen, A.; Deutzmann, A.; Wilson, R. M.; Stefan, E.; Evans, H. L.; Ramirez, M. A.; Liang, T.; Caballero, F.; Wildschut, M. H. E.; Neel, D. V.; Freeman, D. B.; Pop, M. S.; McConkey, M.; Muller, S.; Curtin, B. H.; Tseng, H.; Frombach, K. R.; Butty, V. L.; Levine, S. S.; Feau, C.; Elmiligy, S.; Hong, J. A.; Lewis, T. A.; Vetere, A.; Clemons, P. A.; Malstrom, S. E.; Ebert, B. L.; Lin, C. Y.; Felsher, D. W.; Koehler, A. N. Stabilization of the Max Homodimer with a Small Molecule Attenuates Myc-Driven Transcription. *Cell Chem. Biol.* **2019**, *26* (5), 711-723.e14. https://doi.org/10.1016/j.chembiol.2019.02.009.

(253) Oltersdorf, T.; Elmore, S. W.; Shoemaker, A. R.; Armstrong, R. C.; Augeri, D. J.; Belli, B. A.; Bruncko, M.; Deckwerth, T. L.; Dinges, J.; Hajduk, P. J.; Joseph, M. K.; Kitada, S.; Korsmeyer, S. J.; Kunzer, A. R.; Letai, A.; Li, C.; Mitten, M. J.; Nettesheim, D. G.; Ng, S. C.; Nimmer, P. M.; O'Connor, J. M.; Oleksijew, A.; Petros, A. M.; Reed, J. C.; Shen, W.; Tahir, S. K.; Thompson, C. B.; Tomaselli, K. J.; Wang, B.; Wendt, M. D.; Zhang, H.; Fesik, S. W.; Rosenberg, S. H. An Inhibitor of Bcl-2 Family Proteins Induces Regression of Solid Tumours. *Nature* **2005**, *435* (7042), 677–681. https://doi.org/10.1038/nature03579.

(254) Kapoor, I.; Bodo, J.; Hill, B. T.; Hsi, E. D.; Almasan, A. Targeting BCL-2 in B-Cell Malignancies and Overcoming Therapeutic Resistance. *Cell Death Dis.* **2020**, *11* (11). https://doi.org/10.1038/s41419-020-03144-y.

(255) Ostrem, J. M.; Peters, U.; Sos, M. L.; Wells, J. A.; Shokat, K. M. K-Ras(G12C) Inhibitors Allosterically Control GTP Affinity and Effector Interactions. *Nature* **2013**, *503* (7477), 548–551. https://doi.org/10.1038/nature12796.

(256) Kessler, D.; Gmachl, M.; Mantoulidis, A.; Martin, L. J.; Zoephel, A.; Mayer, M.; Gollner, A.; Covini, D.; Fischer, S.; Gerstberger, T.; Gmaschitz, T.; Goodwin, C.; Greb, P.; Häring, D.; Hela, W.; Hoffmann, J.; Karolyi-Oezguer, J.; Knesl, P.; Kornigg, S.; Koegl, M.; Kousek, R.; Lamarre, L.; Moser, F.; Munico-Martinez, S.; Peinsipp, C.; Phan, J.; Rinnenthal, J.; Sai, J.; Salamon, C.; Scherbantin, Y.; Schipany, K.; Schnitzer, R.; Schrenk, A.; Sharps, B.; Siszler, G.; Sun, Q.; Waterson, A.; Wolkerstorfer, B.; Zeeb, M.; Pearson, M.; Fesik, S. W.; McConnell, D. B. Drugging an Undruggable Pocket on KRAS. *Proc. Natl. Acad. Sci. U. S. A.* **2019**, *116* (32), 15823–15829. https://doi.org/10.1073/PNAS.1904529116.

(257) Hong, D. S.; Fakih, M. G.; Strickler, J. H.; Desai, J.; Durm, G. A.; Shapiro, G. I.; Falchook, G. S.; Price, T. J.; Sacher, A.; Denlinger, C. S.; Bang, Y.-J.; Dy, G. K.; Krauss, J. C.; Kuboki, Y.; Kuo, J. C.; Coveler, A. L.; Park, K.; Kim, T. W.; Barlesi, F.; Munster, P. N.; Ramalingam, S. S.; Burns, T. F.; Meric-Bernstam, F.; Henary, H.; Ngang, J.; Ngarmchamnanrith, G.; Kim, J.; Houk, B. E.; Canon, J.; Lipford, J. R.; Friberg, G.; Lito, P.; Govindan, R.; Li, B. T. KRAS G12C Inhibition with Sotorasib in Advanced Solid Tumors. *N. Engl. J. Med.* **2020**, *383* (13), 1207–1217. https://doi.org/10.1056/nejmoa1917239.

(258) Moore, A. R.; Rosenberg, S. C.; McCormick, F.; Malek, S. RAS-Targeted Therapies: Is the Undruggable Drugged? *Nat. Rev. Drug Discov.* **2020**, *19* (8), 533–552. https://doi.org/10.1038/s41573-020-0068-6.

(259) Tilley, J. W.; Chen, L.; Fry, D. C.; Emerson, S. D.; Powers, G. D.; Biondi, D.; Varnell, T.; Trilles, R.; Guthrie, R.; Mennona, F.; Kaplan, G.; LeMahieu, R. A.; Carson, M.; Han, R. J.; Liu, C. M.; Palermo, R.; Ju, G. Identification of a Small Molecule Inhibitor of the IL-2/IL-2Rα Receptor Interaction Which Binds to IL-2. *J. Am. Chem. Soc.* **1997**, *119* (32), 7589–7590. https://doi.org/10.1021/ja970702x.

(260) Braisted, A. C.; Oslob, J. D.; Delano, W. L.; Hyde, J.; McDowell, R. S.; Waal, N.; Yu, C.; Arkin, M. R.; Raimundo, B. C. Discovery of a Potent Small Molecule IL-2 Inhibitor through Fragment Assembly. *J. Am. Chem. Soc.* **2003**, *125* (13), 3714–3715. https://doi.org/10.1021/ja034247i.

(261) Hyde, J.; Braisted, A. C.; Randal, M.; Arkin, M. R. Discovery and Characterization of Cooperative Ligand Binding in the Adaptive Region of Interleukin-2. *Biochemistry* **2003**, *42* (21), 6475–6483. https://doi.org/10.1021/bi034138g.

(262) De Paula, V. S.; Jude, K. M.; Nerli, S.; Glassman, C. R.; Garcia, K. C.; Sgourakis, N. G. Interleukin-2 Druggability Is Modulated by Global Conformational Transitions Controlled by a Helical Capping Switch. *Proc. Natl. Acad. Sci. U. S. A.* **2020**, *117* (13), 7183–7192. https://doi.org/10.1073/pnas.2000419117.

(263) Rochman, Y.; Spolski, R.; Leonard, W. J. New Insights into the Regulation of T Cells by Γc Family Cytokines. *Nat. Rev. Immunol.* **2009**, *9* (7), 480–490. https://doi.org/10.1038/nri2580.

(264) Leonard, W. J.; Lin, J. X.; O'Shea, J. J. The γ c Family of Cytokines: Basic Biology to Therapeutic Ramifications. *Immunity* **2019**, *50* (4), 832–850. https://doi.org/10.1016/j.immuni.2019.03.028.

(265) Scott, L. J. Tocilizumab: A Review in Rheumatoid Arthritis. *Drugs* **2017**, *77* (17), 1865–1879. https://doi.org/10.1007/s40265-017-0829-7.

(266) Burness, C. B.; McKeage, K. Adalimumab: A Review in Chronic Plaque Psoriasis. *Drugs* **2015**, *75* (18), 2119–2130. https://doi.org/10.1007/s40265-015-0503-x.

(267) Blair, H. A. Secukinumab: A Review in Psoriatic Arthritis. *Drugs* **2021**, *81* (4), 483–494. https://doi.org/10.1007/s40265-021-01476-3.

(268) Schliemann, C.; Hemmerle, T.; Berdel, A. F.; Angenendt, L.; Kerkhoff, A.; Hering, J. P.; Heindel, W.; Hartmann, W.; Wardelmann, E.; Chawla, S. P.; de Braud, F.; Lenz, G.; Neri, D.; Kessler, T.; Berdel, W. E. Dose Escalation and Expansion Phase I Studies with the Tumour-Targeting Antibody-Tumour Necrosis Factor Fusion Protein L19TNF plus Doxorubicin in Patients with Advanced Tumours, Including Sarcomas. *Eur. J. Cancer* **2021**, *150*, 143–154. https://doi.org/10.1016/j.ejca.2021.03.038.

(269) Danielli, R.; Patuzzo, R.; Di Giacomo, A. M.; Gallino, G.; Maurichi, A.; Di Florio, A.; Cutaia, O.; Lazzeri, A.; Fazio, C.; Miracco, C.; Giovannoni, L.; Elia, G.; Neri, D.; Maio, M.; Santinami, M. Intralesional Administration of L19-IL2/L19-TNF in Stage III or Stage IVM1a Melanoma Patients: Results of a Phase II Study. *Cancer Immunol. Immunother.* **2015**, *64* (8), 999–1009. https://doi.org/10.1007/s00262-015-1704-6.

(270) A Study to Evaluate Safety and Efficacy of L19TNF Plus Lomustine in Patients With Glioblastoma at First Progression - Full Text View - ClinicalTrials.gov https://clinicaltrials.gov/ct2/show/NCT04573192 (accessed 2021 -10 -29).

(271) Efficacy and Safety of L19TNF in Previously Treated Patients With Advanced Stage or Metastatic Soft-tissue Sarcoma - Full Text View - ClinicalTrials.gov https://clinicaltrials.gov/ct2/show/NCT04733183 (accessed 2021 -10 -29).

(272) Dakhel, S.; Ongaro, T.; Gouyou, B.; Matasci, M.; Villa, A.; Neri, D.; Cazzamalli, S. Targeted Enhancement of the Therapeutic Window of L19-TNF by Transient and Selective Inhibition of RIPK1-Signaling Cascade. *Oncotarget* **2019**, *10*, 6678–6690.

(273) Arenas-Ramirez, N.; Woytschak, J.; Boyman, O. Interleukin-2: Biology, Design and Application. *Trends Immunol.* **2015**, *36* (12), 763–777. https://doi.org/10.1016/j.it.2015.10.003.

(274) Taniguchi, T.; Minami, Y. The IL-2 IL-2 Receptor System: A Current Overview. *Cell* **1993**, *73* (1), 5–8. https://doi.org/10.1016/0092-8674(93)90152-G.

(275) Rickert, M.; Wang, X.; Boulanger, M. J.; Goriatcheva, N.; Garcia, K. C. Structural Biology: The Structure of Interleukin-2 Complexed with Its Alpha Receptor. *Science* **2005**, *308* (5727), 1477–1480. https://doi.org/10.1126/science.1109745.

(276) Wang, X.; Rickert, M.; Garcia, K. C. Structure of the Quaternary Complex of Interleukin-2 with Its α, ß, and Γc Receptors. *Science* **2005**, *310* (5751), 1159–1163. https://doi.org/10.1126/SCIENCE.1117893.

(277) Boyman, O.; Sprent, J. The Role of Interleukin-2 during Homeostasis and Activation of the Immune System. *Nat. Rev. Immunol.* **2012**, *12* (3), 180–190. https://doi.org/10.1038/nri3156.

(278) Malek, T. R.; Castro, I. Interleukin-2 Receptor Signaling: At the Interface between Tolerance and Immunity. *Immunity* **2010**, *33* (2), 153–165. https://doi.org/10.1016/j.immuni.2010.08.004.

(279) Zelante, T.; Fric, J.; Wong, A. Y. W.; Ricciardi-Castagnoli, P. Interleukin-2 Production by Dendritic Cells and Its Immuno-Regulatory Functions. *Front. Immunol.* **2012**, *3* (JUN), 1–5. https://doi.org/10.3389/fimmu.2012.00161.

(280) Yu, A.; Olosz, F.; Choi, C. Y.; Malek, T. R. Efficient Internalization of IL-2 Depends on the Distal Portion of the Cytoplasmic Tail of the IL-2R Common γ-Chain and a Lymphoid Cell Environment. *J. Immunol.* **2000**, *165* (5), 2556–2562. https://doi.org/10.4049/jimmunol.165.5.2556.

(281) Liao, W.; Lin, J. X.; Leonard, W. J. Interleukin-2 at the Crossroads of Effector Responses, Tolerance, and Immunotherapy. *Immunity* **2013**, *38* (1), 13–25. https://doi.org/10.1016/j.immuni.2013.01.004.

(282) Zubler, R. H.; Lowenthal, J. W.; Erard, F.; Hashimoto, N.; Devos, R.; MacDonald, H. R. Activated B Cells Express Receptors for, and Proliferate in Response to, Pure Interleukin 2. *J. Exp. Med.* **1984**, *160* (4), 1170–1183. https://doi.org/10.1084/jem.160.4.1170.

(283) Roediger, B.; Kyle, R.; Yip, K. H.; Sumaria, N.; Guy, T. V.; Kim, B. S.; Mitchell, A. J.; Tay, S. S.; Jain, R.; Forbes-Blom, E.; Chen, X.; Tong, P. L.; Bolton, H. A.; Artis, D.; Paul, W. E.; de St Groth, B. F.; Grimbaldeston, M. A.; Le Gros, G.; Weninger, W. Cutaneous Immunosurveillance and Regulation of Inflammation by Group 2 Innate Lymphoid Cells. *Nat. Immunol. 2013 146* **2013**, *14* (6), 564–573. https://doi.org/10.1038/ni.2584.

(284) Krieg, C.; Létourneau, S.; Pantaleo, G.; Boyman, O. Improved IL-2 Immunotherapy by Selective Stimulation of IL-2 Receptors on Lymphocytes and Endothelial Cells. *Proc. Natl. Acad. Sci. U. S. A.* **2010**, *107* (26), 11906–11911. https://doi.org/10.1073/PNAS.1002569107.

(285) Aoki, C. A.; Roifman, C. M.; Lian, Z. X.; Bowlus, C. L.; Norman, G. L.; Shoenfeld, Y.; Mackay, I. R.; Eric Gershwin, M. IL-2 Receptor Alpha Deficiency and Features of Primary Biliary Cirrhosis. *J. Autoimmun.* **2006**, *27* (1), 50–53. https://doi.org/10.1016/J.JAUT.2006.04.005.

(286) Caudy, A. A.; Reddy, S. T.; Chatila, T.; Atkinson, J. P.; Verbsky, J. W. CD25 Deficiency Causes an Immune Dysregulation, Polyendocrinopathy, Enteropathy, X-Linked–like Syndrome, and Defective IL-10 Expression from CD4 Lymphocytes. *J. Allergy Clin. Immunol.* **2007**, *119* (2), 482–487. https://doi.org/10.1016/J.JACI.2006.10.007.

(287) Gregersen, P. K.; Olsson, L. M. Recent Advances in the Genetics of Autoimmune Disease. *Annu. Rev. Immunol.* **2009**, *27* (1), 363–391. https://doi.org/10.1146/annurev.immunol.021908.132653.

(288) Yu, A.; Snowhite, I.; Vendrame, F.; Rosenzwajg, M.; Klatzmann, D.; Pugliese, A.; Malek, T. R. Selective IL-2 Responsiveness of Regulatory T Cells Through Multiple Intrinsic Mechanisms Supports the Use of Low-Dose IL-2 Therapy in Type 1 Diabetes. *Diabetes* **2015**, *64* (6), 2172–2183. https://doi.org/10.2337/DB14-1322.

(289) Azzi, J. R.; Sayegh, M. H.; Mallat, S. G. Calcineurin Inhibitors: 40 Years Later, Can't Live Without …. *J. Immunol.* **2013**, *191* (12), 5785–5791. https://doi.org/10.4049/jimmunol.1390055.

(290) Alva, A.; Daniels, G. A.; Wong, M. K. K.; Kaufman, H. L.; Morse, M. A.; McDermott, D. F.; Clark, J. I.; Agarwala, S. S.; Miletello, G.; Logan, T. F.; Hauke, R. J.; Curti, B.; Kirkwood, J. M.; Gonzalez, R.; Amin, A.; Fishman, M.; Agarwal, N.; Lowder, J. N.; Hua, H.; Aung, S.; Dutcher, J. P. Contemporary Experience with High-Dose Interleukin-2 Therapy and Impact on Survival in Patients with Metastatic Melanoma and Metastatic Renal Cell Carcinoma. *Cancer Immunol. Immunother.* **2016**, *65* (12), 1533–1544. https://doi.org/10.1007/s00262-016-1910-x.

(291) Pachella, L. A.; Madsen, L. T.; Dains, J. E. The Toxicity and Benefit of Various Dosing Strategies for Interleukin-2 in Metastatic Melanoma and Renal Cell Carcinoma. *J Adv Pr. Oncol* **2015**, *6*, 212–221. https://doi.org/10.6004/jadpro.2015.6.3.3.

(292) Waldhauer, I.; Gonzalez-Nicolini, V.; Freimoser-Grundschober, A.; Nayak, T. K.; Fahrni, L.; Hosse, R. J.; Gerrits, D.; Geven, E. J. W.; Sam, J.; Lang, S.; Bommer, E.; Steinhart, V.; Husar, E.; Colombetti, S.; Van Puijenbroek, E.; Neubauer, M.; Cline, J. M.; Garg, P. K.; Dugan, G.; Cavallo, F.; Acuna, G.; Charo, J.; Teichgräber, V.; Evers, S.; Boerman, O. C.; Bacac, M.; Moessner, E.; Umaña, P.; Klein, C. Simlukafusp Alfa (FAP-IL2v) Immunocytokine Is a Versatile Combination Partner for Cancer Immunotherapy. *mAbs* **2021**, *13*. https://doi.org/10.1080/19420862.2021.1913791.

(293) Xue, D.; Hsu, E.; Fu, Y.-X.; Peng, H. Next-Generation Cytokines for Cancer Immunotherapy. *Antib. Ther.* **2021**, *4* (2), 123–133. https://doi.org/10.1093/ABT/TBAB014.

(294) Van Limbergen, E. J.; Hoeben, A.; Lieverse, R. I. Y.; Houben, R.; Overhof, C.; Postma, A.; Zindler, J.; Verhelst, F.; Dubois, L. J.; De Ruysscher, D.; Troost, E. G. C.; Lambin, P. Toxicity of L19-Interleukin 2 Combined with Stereotactic Body Radiation

Therapy: A Phase 1 Study. *Int. J. Radiat. Oncol.* **2021**, *109* (5), 1421–1430. https://doi.org/10.1016/J.IJROBP.2020.11.053.

(295) Rekers, N. H.; Olivo Pimentel, V.; Yaromina, A.; Lieuwes, N. G.; Biemans, R.; Zegers, C. M. L.; Germeraad, W. T. V.; Van Limbergen, E. J.; Neri, D.; Dubois, L. J.; Lambin, P. The Immunocytokine L19-IL2: An Interplay between Radiotherapy and Long-Lasting Systemic Anti-Tumour Immune Responses. *OncoImmunology* **2018**, *7* (4), e1414119. https://doi.org/10.1080/2162402X.2017.1414119.

(296) Carnemolla, B.; Borsi, L.; Balza, E.; Castellani, P.; Meazza, R.; Berndt, A.; Ferrini, S.; Kosmehl, H.; Neri, D.; Zardi, L. Enhancement of the Antitumor Properties of Interleukin-2 by Its Targeted Delivery to the Tumor Blood Vessel Extracellular Matrix. *Blood* **2002**, *99* (5), 1659–1665. https://doi.org/10.1182/blood.V99.5.1659.

(297) Hu, P.; Hornick, J. L.; Glasky, M. S.; Yun, A.; Milkie, M. N.; Khawli, L. A.; Anderson, P. M.; Epstein, A. L. A Chimeric Lym-1/Interleukin 2 Fusion Protein for Increasing Tumor Vascular Permeability and Enhancing Antibody Uptake. *Cancer Res.* **1996**, *56* (21), 4998–5004.

(298) Reisfeld, R. A.; Gillies, S. D. Antibody-Interleukin 2 Fusion Proteins: A New Approach to Cancer Therapy. *J. Clin. Lab. Anal.* **1996**, *10* (3), 160–166. https://doi.org/10.1002/(SICI)1098-2825(1996)10:3<160::AID-JCLA9>3.0.CO;2-F.

(299) Dela Cruz, J. S.; Trinh, K. R.; Chen, H. W.; Ribas, A.; Morrison, S. L.; Penichet, M. L. Anti-HER2/Neu IgG3-(IL-2) and Anti-HER2/Neu IgG3-(GM-CSF) Promote HER2/Neu Processing and Presentation by Dendritic Cells: Implications in Immunotherapy and Vaccination Strategies. *Mol. Immunol.* **2006**, *43* (6), 667–676. https://doi.org/10.1016/j.molimm.2005.04.007.

(300) Klein, C.; Waldhauer, I.; Nicolini, V. G.; Freimoser-Grundschober, A.; Nayak, T.; Vugts, D. J.; Dunn, C.; Bolijn, M.; Benz, J.; Stihle, M.; Lang, S.; Roemmele, M.; Hofer, T.; van Puijenbroek, E.; Wittig, D.; Moser, S.; Ast, O.; Brünker, P.; Gorr, I. H.; Neumann, S.; de Vera Mudry, M. C.; Hinton, H.; Crameri, F.; Saro, J.; Evers, S.; Gerdes, C.; Bacac, M.; van Dongen, G.; Moessner, E.; Umaña, P. Cergutuzumab Amunaleukin (CEA-IL2v), a CEA-Targeted IL-2 Variant-Based Immunocytokine for Combination Cancer Immunotherapy: Overcoming Limitations of Aldesleukin and Conventional IL-2-Based Immunocytokines. *OncoImmunology* **2017**, *6* (3), 1–15. https://doi.org/10.1080/2162402X.2016.1277306.

(301) Mullard, A. Restoring IL-2 to Its Cancer Immunotherapy Glory. *Nat. Rev. Drug Discov.* **2021**, *20* (3), 163–165. https://doi.org/10.1038/D41573-021-00034-6.

(302) IL-2 treatment can be dangerous. Here's how drug firms are trying to fix it https://cen.acs.org/pharmaceuticals/biologics/safer-IL2-cancer-immunotherapy-autoimmunity/99/i12 (accessed 2021 -10 -29).

(303) Solomon, I.; Amann, M.; Goubier, A.; Arce Vargas, F.; Zervas, D.; Qing, C.; Henry, J. Y.; Ghorani, E.; Akarca, A. U.; Marafioti, T.; Śledzińska, A.; Werner Sunderland, M.; Franz Demane, D.; Clancy, J. R.; Georgiou, A.; Salimu, J.; Merchiers, P.; Brown, M. A.; Flury, R.; Eckmann, J.; Murgia, C.; Sam, J.; Jacobsen, B.; Marrer-Berger, E.; Boetsch, C.; Belli, S.; Leibrock, L.; Benz, J.; Koll, H.; Sutmuller, R.; Peggs,

K. S.; Quezada, S. A. CD25-Treg-Depleting Antibodies Preserving IL-2 Signaling on Effector T Cells Enhance Effector Activation and Antitumor Immunity. *Nat. Cancer* **2020**, *1* (12), 1153–1166. https://doi.org/10.1038/s43018-020-00133-0.

(304) Diab, A.; Tannir, N. M.; Bentebibel, S. E.; Hwu, P.; Papadimitrakopoulou, V.; Haymaker, C.; Kluger, H. M.; Gettinger, S. N.; Sznol, M.; Tykodi, S. S.; Curti, B. D.; Tagliaferri, M. A.; Zalevsky, J.; Hannah, A. L.; Hoch, U.; Aung, S.; Fanton, C.; Rizwan, A.; Iacucci, E.; Liao, Y.; Bernatchez, C.; Hurwitz, M. E.; Cho, D. C. Bempegaldesleukin (NKTR-214) plus Nivolumab in Patients with Advanced Solid Tumors: Phase I Dose-Escalation Study of Safety, Effi Cacy, and Immune Activation (PIVOT-02). *Cancer Discov.* **2020**, *10* (8), 1158–1173. https://doi.org/10.1158/2159-8290.CD-19-1510.

(305) Sharma, M.; Khong, H.; Fa'ak, F.; Bentebibel, S. E.; Janssen, L. M. E.; Chesson, B. C.; Creasy, C. A.; Forget, M. A.; Kahn, L. M. S.; Pazdrak, B.; Karki, B.; Hailemichael, Y.; Singh, M.; Vianden, C.; Vennam, S.; Bharadwaj, U.; Tweardy, D. J.; Haymaker, C.; Bernatchez, C.; Huang, S.; Rajapakshe, K.; Coarfa, C.; Hurwitz, M. E.; Sznol, M.; Hwu, P.; Hoch, U.; Addepalli, M.; Charych, D. H.; Zalevsky, J.; Diab, A.; Overwijk, W. W. Bempegaldesleukin Selectively Depletes Intratumoral Tregs and Potentiates T Cell-Mediated Cancer Therapy. *Nat. Commun.* **2020**, *11* (1). https://doi.org/10.1038/s41467-020-14471-1.

(306) Parisi, G.; Saco, J. D.; Salazar, F. B.; Tsoi, J.; Krystofinski, P.; Puig-Saus, C.; Zhang, R.; Zhou, J.; Cheung-Lau, G. C.; Garcia, A. J.; Grasso, C. S.; Tavaré, R.; Hu-Lieskovan, S.; Mackay, S.; Zalevsky, J.; Bernatchez, C.; Diab, A.; Wu, A. M.; Comin-Anduix, B.; Charych, D.; Ribas, A. Persistence of Adoptively Transferred T Cells with a Kinetically Engineered IL-2 Receptor Agonist. *Nat. Commun.* **2020**, *11* (1), 1–12. https://doi.org/10.1038/s41467-019-12901-3.

(307) Milla, M. E.; Ptacin, J.; Caffaro, C. E.; Aerni, H. R.; Ma, L.; Koriazova, L.; Joseph, I. B.; Shawver, L. K. THOR-707: Using Synthetic Biology to Reprogram the Therapeutic Activity of Interleukin-2 (IL-2). *J. Clin. Oncol.* **2019**, *37* (15_suppl), 2603. https://doi.org/10.1200/JCO.2019.37.15_suppl.2603.

(308) Ptacin, J. L.; Caffaro, C. E.; Ma, L.; San Jose Gall, K. M.; Aerni, H. R.; Acuff, N. V.; Herman, R. W.; Pavlova, Y.; Pena, M. J.; Chen, D. B.; Koriazova, L. K.; Shawver, L. K.; Joseph, I. B.; Milla, M. E. An Engineered IL-2 Reprogrammed for Anti-Tumor Therapy Using a Semi-Synthetic Organism. *Nat. Commun.* **2021**, *12* (1). https://doi.org/10.1038/s41467-021-24987-9.

(309) Arenas-Ramirez, N.; Zou, C.; Popp, S.; Zingg, D.; Brannetti, B.; Wirth, E.; Calzascia, T.; Kovarik, J.; Sommer, L.; Zenke, G.; Woytschak, J.; Regnier, C. H.; Katopodis, A.; Boyman, O. Improved Cancer Immunotherapy by a CD25-Mimobody Conferring Selectivity to Human Interleukin-2. *Sci. Transl. Med.* **2016**, *8* (367), 1–13. https://doi.org/10.1126/scitranslmed.aag3187.

(310) Sahin, D.; Arenas-Ramirez, N.; Rath, M.; Karakus, U.; Hümbelin, M.; van Gogh, M.; Borsig, L.; Boyman, O. An IL-2-Grafted Antibody Immunotherapy with Potent Efficacy against Metastatic Cancer. *Nat. Commun.* **2020**, *11* (1), 1–12. https://doi.org/10.1038/s41467-020-20220-1.

(311) Brandhuber, B. J.; Boone, T.; Kenney, W. C.; McKay, D. B. Three-Dimensional Structure of Interleukin-2. *Science* **1987**, *238* (4834), 1707–1709. https://doi.org/10.1126/SCIENCE.3500515.

(312) Bazan, J. F. Unraveling the Structure of IL-2. *Science* **1992**, *257* (5068), 410–413. https://doi.org/10.1126/SCIENCE.1631562.

(313) Mott, H. R.; Baines, B. S.; Hall, R. M.; Cooke, R. M.; Driscoll, P. C.; Weir, M. P.; Campbell, I. D. The Solution Structure of the F42A Mutant of Human Interleukin 2. *J. Mol. Biol.* **1995**, *247* (5), 979–994. https://doi.org/10.1006/JMBI.1994.0194.

(314) Sauvé, K.; Nachman, M.; Spence, C.; Bailon, P.; Campbell, E.; Tsien, W. H.; Kondas, J. A.; Hakimi, J.; Ju, G. Localization in Human Interleukin 2 of the Binding Site to the Alpha Chain (P55) of the Interleukin 2 Receptor. *Proc. Natl. Acad. Sci. U. S. A.* **1991**, *88* (11), 4636–4640. https://doi.org/10.1073/PNAS.88.11.4636.

(315) Emerson, S. D. NMR Characterization of Interleukin-2 in Complexes with the IL-2Ralpha Receptor Component, and with Low Molecular Weight Compounds That Inhibit the IL-2/IL-Ralpha Interaction. *Protein Sci.* **2003**, *12* (4), 811–822. https://doi.org/10.1110/ps.0232803.

(316) Erlanson, D. A.; Braisted, A. C.; Raphael, D. R.; Randal, M.; Stroud, R. M.; Gordon, E. M.; Wells, J. A. Site-Directed Ligand Discovery. *Proc. Natl. Acad. Sci. U. S. A.* **2000**, *97* (17), 9367–9372. https://doi.org/10.1073/PNAS.97.17.9367.

(317) Arkin, M. R.; Randal, M.; DeLano, W. L.; Hyde, J.; Luong, T. N.; Oslob, J. D.; Raphael, D. R.; Taylor, L.; Wang, J.; McDowell, R. S.; Wells, J. A.; Braisted, A. C. Binding of Small Molecules to an Adaptive Protein-Protein Interface. *Proc. Natl. Acad. Sci. U. S. A.* **2003**, *100* (4), 1603–1608. https://doi.org/10.1073/pnas.252756299.

(318) Thanos, C. D.; Randal, M.; Wells, J. A. Potent Small-Molecule Binding to a Dynamic Hot Spot on IL-2. *J. Am. Chem. Soc.* **2003**, *125* (50), 15280–15281. https://doi.org/10.1021/ja0382617.

(319) Raimundo, B. C.; Oslob, J. D.; Braisted, A. C.; Hyde, J.; McDowell, R. S.; Randal, M.; Waal, N. D.; Wilkinson, J.; Yu, C. H.; Arkin, M. R. Integrating Fragment Assembly and Biophysical Methods in the Chemical Advancement of Small-Molecule Antagonists of IL-2: An Approach for Inhibiting Protein-Protein Interactions. *J. Med. Chem.* **2004**, *47* (12), 3111–3130. https://doi.org/10.1021/jm049967u.

(320) Waal, N. D.; Yang, W.; Oslob, J. D.; Arkin, M. R.; Hyde, J.; Lu, W.; McDowell, R. S.; Yu, C. H.; Raimundo, B. C. Identification of Nonpeptidic Small-Molecule Inhibitors of Interleukin-2. *Bioorg. Med. Chem. Lett.* **2005**, *15* (4), 983–987. https://doi.org/10.1016/j.bmcl.2004.12.045.

(321) Thanos, C. D.; DeLano, W. L.; Wells, J. A. Hot-Spot Mimicry of a Cytokine Receptor by a Small Molecule. *Proc. Natl. Acad. Sci. U. S. A.* **2006**, *103* (42), 15422–15427. https://doi.org/10.1073/pnas.0607058103.

(322) Samain, F.; Gorre, E.; Millul, J.; Donckele, E.; Gironda, M. A. Nucleic Acid Encoded Chemical Libraries. WO2020128064A1, June 25, 2020.

(323) Catalano, M.; Moroglu, M.; Balbi, P.; Mazzieri, F.; Clayton, J.; Andrews, K. H.; Bigatti, M.; Scheuermann, J.; Conway, S. J.; Neri, D. Selective Fragments for the CREBBP Bromodomain Identified from an Encoded Self-Assembly Chemical Library. *ChemMedChem* **2020**, *15* (18), 1752–1756. https://doi.org/10.1002/cmdc.202000528.

(324) Catalano, M.; Bassi, G.; Rotondi, G.; Khettabi, L.; Dichiara, M.; Murer, P.; Scheuermann, J.; Soler-Lopez, M.; Neri, D. Discovery, Affinity Maturation and Multimerization of Small Molecule Ligands against Human Tyrosinase and Tyrosinase-Related Protein 1. *RSC Med. Chem.* **2021**, *12* (3), 363–369. https://doi.org/10.1039/D0MD00310G.

(325) Buller, F.; Mannocci, L.; Zhang, Y.; Dumelin, C. E.; Scheuermann, J.; Neri, D. Design and Synthesis of a Novel DNA-Encoded Chemical Library Using Diels-Alder Cycloadditions. *Bioorg. Med. Chem. Lett.* **2008**, *18* (22), 5926–5931. https://doi.org/10.1016/j.bmcl.2008.07.038.

(326) Becker, H. M. Carbonic Anhydrase IX and Acid Transport in Cancer. *Br. J. Cancer* **2020**, *122* (2), 157–167. https://doi.org/10.1038/s41416-019-0642-z.

(327) Neri, D.; Supuran, C. T. Interfering with PH Regulation in Tumours as a Therapeutic Strategy. *Nat. Rev. Drug Discov.* **2011**, *10* (10), 767–777. https://doi.org/10.1038/nrd3554.

(328) Wichert, M.; Krall, N. Targeting Carbonic Anhydrase IX with Small Organic Ligands. *Curr. Opin. Chem. Biol.* **2015**, *26*, 48–54. https://doi.org/10.1016/j.cbpa.2015.02.005.

(329) Nocentini, A.; Bua, S.; Lomelino, C. L.; McKenna, R.; Menicatti, M.; Bartolucci, G.; Tenci, B.; Di Cesare Mannelli, L.; Ghelardini, C.; Gratteri, P.; Supuran, C. T. Discovery of New Sulfonamide Carbonic Anhydrase IX Inhibitors Incorporating Nitrogenous Bases. *ACS Med. Chem. Lett.* **2017**, *8* (12), 1314–1319. https://doi.org/10.1021/acsmedchemlett.7b00399.

(330) Supuran, C. T.; Winum, J.-Y. Carbonic Anhydrase IX Inhibitors in Cancer Therapy: An Update. *Future Med. Chem.* **2015**, *7* (11), 1407–1414. https://doi.org/10.4155/fmc.15.71.

(331) Tondo, M.; Calpena, E.; Arriola, G.; Sanz, P.; Martorell, L.; Ormazabal, A.; Castejon, E.; Palacin, M.; Ugarte, M.; Espinos, C.; Perez, B.; Perez-Dueñas, B.; Pérez-Cerda, C.; Artuch, R. Clinical, Biochemical, Molecular and Therapeutic Aspects of 2 New Cases of 2-Aminoadipic Semialdehyde Synthase Deficiency. *Mol. Genet. Metab.* **2013**, *110* (3), 231–236. https://doi.org/10.1016/j.ymgme.2013.06.021.

(332) Pena, I. A.; Marques, L. A.; Laranjeira, Â. B. A.; Yunes, J. A.; Eberlin, M. N.; MacKenzie, A.; Arruda, P. Mouse Lysine Catabolism to Aminoadipate Occurs Primarily through the Saccharopine Pathway; Implications for Pyridoxine Dependent Epilepsy (PDE). *Biochim. Biophys. Acta BBA - Mol. Basis Dis.* **2017**, *1863* (1), 121–128. https://doi.org/10.1016/j.bbadis.2016.09.006.

(333) Crowther, L. M.; Mathis, D.; Poms, M.; Plecko, B. New Insights into Human Lysine Degradation Pathways with Relevance to Pyridoxine-Dependent Epilepsy Due

to Antiquitin Deficiency. *J. Inherit. Metab. Dis.* **2019**, *42* (4), 620–628. https://doi.org/10.1002/jimd.12076.

(334) Hammarström, S. The Carcinoembryonic Antigen (CEA) Family: Structures, Suggested Functions and Expression in Normal and Malignant Tissues. *Semin. Cancer Biol.* **1999**, *9* (2), 67–81. https://doi.org/10.1006/scbi.1998.0119.

(335) Pavlopoulou, A.; Scorilas, A. A Comprehensive Phylogenetic and Structural Analysis of the Carcinoembryonic Antigen (CEA) Gene Family. *Genome Biol. Evol.* **2014**, *6* (6), 1314–1326. https://doi.org/10.1093/gbe/evu103.

(336) Hall, C.; Clarke, L.; Pal, A.; Buchwald, P.; Eglinton, T.; Wakeman, C.; Frizelle, F. A Review of the Role of Carcinoembryonic Antigen in Clinical Practice. *Ann Coloproctol* **2019**, *35* (6), 294–305. https://doi.org/10.3393/ac.2019.11.13.

(337) Fasano, M.; Curry, S.; Terreno, E.; Galliano, M.; Fanali, G.; Narciso, P.; Notari, S.; Ascenzi, P. The Extraordinary Ligand Binding Properties of Human Serum Albumin. *IUBMB Life* **2005**, *57* (12), 787–796. https://doi.org/10.1080/15216540500404093.

(338) Kragh-Hansen, U. Human Serum Albumin: A Multifunctional Protein. In *Albumin in Medicine: Pathological and Clinical Applications*; Otagiri, M., Chuang, V. T. G., Eds.; Springer: Singapore, 2016; pp 1–24. https://doi.org/10.1007/978-981-10-2116-9_1.

(339) Bteich, M. An Overview of Albumin and Alpha-1-Acid Glycoprotein Main Characteristics: Highlighting the Roles of Amino Acids in Binding Kinetics and Molecular Interactions. *Heliyon* **2019**, *5* (11), e02879. https://doi.org/10.1016/j.heliyon.2019.e02879.

(340) Decurtins, W.; Franzini, R.; Neri, D.; Scheuermann, J.; Wichert, M. Production of Encoded Chemical Libraries. WO2015091207A1, June 25, 2015.

(341) Kolb, H. C.; Finn, M. G.; Sharpless, K. B. Click Chemistry: Diverse Chemical Function from a Few Good Reactions. *Angew. Chem. Int. Ed.* **2001**, *40* (11), 2004–2021. https://doi.org/10.1002/1521-3773(20010601)40:11<2004::AID-ANIE2004>3.0.CO;2-5.

(342) Tornøe, C. W.; Christensen, C.; Meldal, M. Peptidotriazoles on Solid Phase: [1,2,3]-Triazoles by Regiospecific Copper(I)-Catalyzed 1,3-Dipolar Cycloadditions of Terminal Alkynes to Azides. *J. Org. Chem.* **2002**, *67* (9), 3057–3064. https://doi.org/10.1021/jo011148j.

(343) Rostovtsev, V. V.; Green, L. G.; Fokin, V. V.; Sharpless, K. B. A Stepwise Huisgen Cycloaddition Process: Copper(I)-Catalyzed Regioselective "Ligation" of Azides and Terminal Alkynes. *Angew. Chem. Int. Ed.* **2002**, *41* (14), 2596–2599. https://doi.org/10.1002/1521-3773(20020715)41:14<2596::AID-ANIE2596>3.0.CO;2-4.

(344) Liang, L.; Astruc, D. The Copper(I)-Catalyzed Alkyne-Azide Cycloaddition (CuAAC) "Click" Reaction and Its Applications. An Overview. *Coord. Chem. Rev.* **2011**, *255* (23), 2933–2945. https://doi.org/10.1016/j.ccr.2011.06.028.

(345) Meldal, M.; Diness, F. Recent Fascinating Aspects of the CuAAC Click Reaction. *Trends Chem.* **2020**, *2* (6), 569–584. https://doi.org/10.1016/j.trechm.2020.03.007.

(346) Yuen, L. H.; Franzini, R. M. Achievements, Challenges, and Opportunities in DNA-Encoded Library Research: An Academic Point of View. *ChemBioChem* **2017**, *18* (9), 829–836. https://doi.org/10.1002/cbic.201600567.

(347) Zhao, G.; Huang, Y.; Zhou, Y.; Li, Y.; Li, X. Future Challenges with DNA-Encoded Chemical Libraries in the Drug Discovery Domain. *Expert Opin. Drug Discov.* **2019**, *14* (8), 735–753. https://doi.org/10.1080/17460441.2019.1614559.

(348) Satz, A. L.; Cai, J.; Chen, Y.; Goodnow, R.; Gruber, F.; Kowalczyk, A.; Petersen, A.; Naderi-Oboodi, G.; Orzechowski, L.; Strebel, Q. DNA Compatible Multistep Synthesis and Applications to DNA Encoded Libraries. *Bioconjug. Chem.* **2015**, *26* (8), 1623–1632. https://doi.org/10.1021/acs.bioconjchem.5b00239.

(349) Du, H.-C.; Huang, H. DNA-Compatible Nitro Reduction and Synthesis of Benzimidazoles. *Bioconjug. Chem.* **2017**, *28* (10), 2575–2580. https://doi.org/10.1021/acs.bioconjchem.7b00416.

(350) Li, J.-Y.; Huang, H. Development of DNA-Compatible Suzuki-Miyaura Reaction in Aqueous Media. *Bioconjug. Chem.* **2018**, *29* (11), 3841–3846. https://doi.org/10.1021/acs.bioconjchem.8b00676.

(351) Wang, X.; Sun, H.; Liu, J.; Dai, D.; Zhang, M.; Zhou, H.; Zhong, W.; Lu, X. Ruthenium-Promoted C–H Activation Reactions between DNA-Conjugated Acrylamide and Aromatic Acids. *Org. Lett.* **2018**, *20* (16), 4764–4768. https://doi.org/10.1021/acs.orglett.8b01837.

(352) Li, H.; Sun, Z.; Wu, W.; Wang, X.; Zhang, M.; Lu, X.; Zhong, W.; Dai, D. Inverse-Electron-Demand Diels–Alder Reactions for the Synthesis of Pyridazines on DNA. *Org. Lett.* **2018**, *20* (22), 7186–7191. https://doi.org/10.1021/acs.orglett.8b03114.

(353) Wang, X.; Sun, H.; Liu, J.; Zhong, W.; Zhang, M.; Zhou, H.; Dai, D.; Lu, X. Palladium-Promoted DNA-Compatible Heck Reaction. *Org. Lett.* **2019**, *21* (3), 719–723. https://doi.org/10.1021/acs.orglett.8b03926.

(354) Gerry, C. J.; Yang, Z.; Stasi, M.; Schreiber, S. L. DNA-Compatible [3 + 2] Nitrone–Olefin Cycloaddition Suitable for DEL Syntheses. *Org. Lett.* **2019**, *21* (5), 1325–1330. https://doi.org/10.1021/acs.orglett.9b00017.

(355) Cai, P.; Yang, G.; Zhao, L.; Wan, J.; Li, J.; Liu, G. Synthesis of C3-Alkylated Indoles on DNA via Indolyl Alcohol Formation Followed by Metal-Free Transfer Hydrogenation. *Org. Lett.* **2019**, *21* (17), 6633–6637. https://doi.org/10.1021/acs.orglett.9b02132.

(356) Favalli, N.; Bassi, G.; Zanetti, T.; Scheuermann, J.; Neri, D. Screening of Three Transition Metal-Mediated Reactions Compatible with DNA-Encoded Chemical Libraries. *Helv. Chim. Acta* **2019**, *102* (4), e1900033. https://doi.org/10.1002/hlca.201900033.

(357) Gerry, C. J.; Schreiber, S. L. Recent Achievements and Current Trajectories of Diversity-Oriented Synthesis. *Gener. Ther.* **2020**, *56*, 1–9. https://doi.org/10.1016/j.cbpa.2019.08.008.

(358) Li, Y.; Gabriele, E.; Samain, F.; Favalli, N.; Sladojevich, F.; Scheuermann, J.; Neri, D. Optimized Reaction Conditions for Amide Bond Formation in DNA-Encoded Combinatorial Libraries. *ACS Comb. Sci.* **2016**, *18* (8), 438–443. https://doi.org/10.1021/acscombsci.6b00058.

(359) Bräse, S.; Gil, C.; Knepper, K.; Zimmermann, V. Organic Azides: An Exploding Diversity of a Unique Class of Compounds. *Angew. Chem. Int. Ed.* **2005**, *44* (33), 5188–5240. https://doi.org/10.1002/anie.200400657.

(360) Huang, D.; Yan, G. Recent Advances in Reactions of Azides. *Adv. Synth. Catal.* **2017**, *359* (10), 1600–1619. https://doi.org/10.1002/adsc.201700103.

(361) Jiang, X.; Hao, X.; Jing, L.; Wu, G.; Kang, D.; Liu, X.; Zhan, P. Recent Applications of Click Chemistry in Drug Discovery. *Expert Opin. Drug Discov.* **2019**, *14* (8), 779–789. https://doi.org/10.1080/17460441.2019.1614910.

(362) Meng, G.; Guo, T.; Ma, T.; Zhang, J.; Shen, Y.; Sharpless, K. B.; Dong, J. Modular Click Chemistry Libraries for Functional Screens Using a Diazotizing Reagent. *Nature* **2019**, *574* (7776), 86–89. https://doi.org/10.1038/s41586-019-1589-1.

(363) Favalli, N.; Biendl, S.; Hartmann, M.; Piazzi, J.; Sladojevich, F.; Gräslund, S.; Brown, P. J.; Näreoja, K.; Schüler, H.; Scheuermann, J.; Franzini, R.; Neri, D. A DNA-Encoded Library of Chemical Compounds Based on Common Scaffolding Structures Reveals the Impact of Ligand Geometry on Protein Recognition. *ChemMedChem* **2018**, *13* (13), 1303–1307. https://doi.org/10.1002/cmdc.201800193.

(364) Škopić, M. K.; Bugain, O.; Jung, K.; Onstein, S.; Brandherm, S.; Kalliokoski, T.; Brunschweiger, A. Design and Synthesis of DNA-Encoded Libraries Based on a Benzodiazepine and a Pyrazolopyrimidine Scaffold. *MedChemComm* **2016**, *7* (10), 1957–1965. https://doi.org/10.1039/c6md00243a.

(365) Ju, Y.; Kumar, D.; Varma, R. S. Revisiting Nucleophilic Substitution Reactions: Microwave-Assisted Synthesis of Azides, Thiocyanates, and Sulfones in an Aqueous Medium. *J. Org. Chem.* **2006**, *71* (17), 6697–6700. https://doi.org/10.1021/jo061114h.

(366) Nyffeler, P. T.; Liang, C.-H.; Koeller, K. M.; Wong, C.-H. The Chemistry of Amine−Azide Interconversion: Catalytic Diazotransfer and Regioselective Azide Reduction. *J. Am. Chem. Soc.* **2002**, *124* (36), 10773–10778. https://doi.org/10.1021/ja0264605.

(367) Liu, Q.; Tor, Y. Simple Conversion of Aromatic Amines into Azides. *Org. Lett.* **2003**, *5* (14), 2571–2572. https://doi.org/10.1021/ol034919+.

(368) Wurz, R. P.; Lin, W.; Charette, A. B. Trifluoromethanesulfonyl Azide: An Efficient Reagent for the Preparation of α-Cyano-α-Diazo Carbonyls and an α-Sulfonyl-α-Diazo Carbonyl. *Tetrahedron Lett.* **2003**, *44* (49), 8845–8848. https://doi.org/10.1016/j.tetlet.2003.09.197.

(369) Lee, C.-T.; Huang, S.; Lipshutz, B. H. Copper-in-Charcoal-Catalyzed, Tandem One-Pot Diazo Transfer-Click Reactions. *Adv. Synth. Catal.* **2009**, *351* (18), 3139–3142. https://doi.org/10.1002/adsc.200900604.

(370) Goddard-Borger, E. D.; Stick, R. V. An Efficient, Inexpensive, and Shelf-Stable Diazotransfer Reagent: Imidazole-1-Sulfonyl Azide Hydrochloride. *Org. Lett.* **2007**, *9* (19), 3797–3800. https://doi.org/10.1021/ol701581g.

(371) Fischer, N.; Goddard-Borger, E. D.; Greiner, R.; Klapötke, T. M.; Skelton, B. W.; Stierstorfer, J. Sensitivities of Some Imidazole-1-Sulfonyl Azide Salts. *J. Org. Chem.* **2012**, *77* (4), 1760–1764. https://doi.org/10.1021/jo202264r.

(372) Castro, V.; Blanco-Canosa, J. B.; Rodriguez, H.; Albericio, F. Imidazole-1-Sulfonyl Azide-Based Diazo-Transfer Reaction for the Preparation of Azido Solid Supports for Solid-Phase Synthesis. *ACS Comb. Sci.* **2013**, *15* (7), 331–334. https://doi.org/10.1021/co4000437.

(373) Potter, G. T.; Jayson, G. C.; Miller, G. J.; Gardiner, J. M. An Updated Synthesis of the Diazo-Transfer Reagent Imidazole-1-Sulfonyl Azide Hydrogen Sulfate. *J. Org. Chem.* **2016**, *81* (8), 3443–3446. https://doi.org/10.1021/acs.joc.6b00177.

(374) Lartia, R.; Murat, P.; Dumy, P.; Defrancq, E. Versatile Introduction of Azido Moiety into Oligonucleotides through Diazo Transfer Reaction. *Org. Lett.* **2011**, *13* (20), 5672–5675. https://doi.org/10.1021/ol202397e.

(375) Zambaldo, C.; Daguer, J.-P.; Saarbach, J.; Barluenga, S.; Winssinger, N. Screening for Covalent Inhibitors Using DNA-Display of Small Molecule Libraries Functionalized with Cysteine Reactive Moieties. *Med Chem Commun* **2016**, *7* (7), 1340–1351. https://doi.org/10.1039/C6MD00242K.

(376) Pandiakumar, A. K.; Sarma, S. P.; Samuelson, A. G. Mechanistic Studies on the Diazo Transfer Reaction. *Tetrahedron Lett.* **2014**, *55* (18), 2917–2920. https://doi.org/10.1016/j.tetlet.2014.03.057.

(377) Lieverse, R. I. Y.; Van Limbergen, E. J.; Oberije, C. J. G.; Troost, E. G. C.; Hadrup, S. R.; Dingemans, A. M. C.; Hendriks, L. E. L.; Eckert, F.; Hiley, C.; Dooms, C.; Lievens, Y.; De Jong, M. C.; Bussink, J.; Geets, X.; Valentini, V.; Elia, G.; Neri, D.; Billiet, C.; Abdollahi, A.; Pasquier, D.; Boisselier, P.; Yaromina, A.; De Ruysscher, D.; Dubois, L. J.; Lambin, P. Stereotactic Ablative Body Radiotherapy (SABR) Combined with Immunotherapy (L19-IL2) versus Standard of Care in Stage IV NSCLC Patients, ImmunoSABR: A Multicentre, Randomised Controlled Open-Label Phase II Trial. *BMC Cancer* **2020**, *20* (1), 1–10. https://doi.org/10.1186/s12885-020-07055-1.

(378) Arenas-Ramirez, N.; Zou, C.; Popp, S.; Zingg, D.; Brannetti, B.; Wirth, E.; Calzascia, T.; Kovarik, J.; Sommer, L.; Zenke, G.; Woytschak, J.; Regnier, C. H.; Katopodis, A.; Boyman, O. Improved Cancer Immunotherapy by a CD25-Mimobody Conferring Selectivity to Human Interleukin-2. *Sci. Transl. Med.* **2016**, *8* (367), 1–13. https://doi.org/10.1126/scitranslmed.aag3187.

(379) Neri, D. Antibody–Cytokine Fusions: Versatile Products for the Modulation of Anticancer Immunity. *Cancer Immunol. Res.* **2019**, *7* (3), 348–354. https://doi.org/10.1158/2326-6066.CIR-18-0622.

(380) Mock, J.; Stringhini, M.; Villa, A.; Weller, M.; Weiss, T.; Neri, D. An Engineered 4-1BBL Fusion Protein with "Activity on Demand." *Proc. Natl. Acad. Sci. U. S. A.* **2020**, *117* (50), 31780–31788. https://doi.org/10.1073/pnas.2013615117.

8. Acknowledgements

I would like to thank my supervisor Prof. Dr. Dario Neri, for giving me the opportunity to perform my PhD studies at Philochem, surrounded by great scientists and human beings. I have learned so much, both professionally and personally speaking, and I will carry this knowledge for the rest of my life.

Special thanks to my lab supervisors during these three and a half years, Dr. Florent Samain and Dr. Etienne J. Donckele. Without your guidance, nothing would have been possible. Thanks for pushing me hard to achieve so many goals, and for not letting my passion for science get lost.

Thanks to Florent, for accepting me as a PhD student in the DEL group, for all your work during these three and a half years, for your invaluable support, and all your "crazy stupid things" and jokes. You will rock it in your new position!

Thanks to Etienne, for being such a professional, humble, and lovely person. All the words I have are not enough to acknowledge you. You were peace in the difficult times. I bring with me all the scientific knowledge I got from you, which is tremendous. Now I know more pK_a than ever before, and the importance of being picky and meticulous with our job. Remember to always take care of yourself and continue to be the amazing person you are. I know you will do amazing things in your career, and I look forward to seeing it!

I would also like to thank Dr. Samuele Cazzamalli, for his guidance during the last period of the PhD, for helping me to finish my last publication, for the correction of this thesis, and his invaluable suggestions throughout these years; and Dr. Gabriele Bassi, for the critical reading and correction of this thesis.

I am very grateful to the former and new Chemistry Team, and the Biology Team: Arnel, Martina, Alessandro, Joffrey, Brenno, Andrea, Lottie, Anne, Baptiste, Ettore, Tiz, Lisa, and Dragana, to name a few. But in particular to:

"The Darker Corner"; Elli, Sir Émile M. D. Gorre, and Jeff "The Boss". Nothing would have been the same without you. Thanks for all the funny moments together, but also the not so funny ones. You were a rock to grab before falling. Keep being so pure and real and do not forget to visit me in Madrid.

Also, to Luca, for all your support and organic chemistry knowledge, for always being there to solve our mess with the HPLC, the LCMS, computers in general, and many other things. Remember to think about yourself and to enjoy your little family more than anything else.

To Andy, for all your biology knowledge, for the coffee breaks and the Magic sessions. I have learned so much from you, scientifically and personally speaking. You also have to remember to visit me in Madrid. We still have many beers to share and many scientific discussions!

To the greatest scientific trio and golf players, Abdullah, Louis, and Fred. I was always honored and happy to solve all your chemistry questions and to have such great moments with you. Thank you for your help in every biology question I had,

thanks for your protein shakes, and for always being there to bring good vibes to the group. Keep training golf, otherwise, I will destroy you the next time we play together.

I would also like to express my gratitude to my colleagues and friends at ETH. Marco Catalano, Marcone, my Broski Seba, Pitti, Christian and Louise. Thank you for all your help when needed, for all the beers we shared, and for so many other moments. Keep being such great people.

Thanks to Sheila, a little piece of Spain in Zurich. Thank you for our parties, for dinners together, for your support and scientific help, for remembering me that being Spanish is something we have to be proud of!

To Dalila. Thank you for being so "annoying" with me (as much as I am with you!), for our parties together, dinners with Jacopo, Marta, and the others, for reminding me that I am a big mess and that I might need a secretary in the near future to organize my life. Keep pushing the PhD, do not give up, do not regret any decision, and love yourself. You deserve everything in life. I have a little piece of Puglia with me. Grazie mille!

I am also very grateful to Aureliano. You are such a nice and funny person. I love your sense of humor and being able to speak in Spanish with you, pendejo! Thanks for teaching me some Italian (including "some" bad words). Keep doing great in science and putting so much effort into your work. You will do whatever you want. I wait for you here in Spain to show you Madrid and to continue having fun together. Te quiero amigo!

Thanks to Marta, another little piece of Spain in Zurich. I am grateful I could help you to enjoy a little bit of your time in Zurich. I am happy that I had the opportunity to meet you and that you became a big part of my life there. Enjoy your time in Switzerland, keep being such a strong woman and I wait for you here in Spain to have more good moments together. Take good care of Jacopino, support each other, and grow together, you have a bright future ahead (maybe in Spain). Gracias tronqui!

Thanks to Corbi (Dr. Riccardo Corbellari, yes, Dr.!). You are such a great human being and an invaluable friend. I will always have you in my life and I thank destiny for the opportunity to meet you. Thank you for being so "empanado", for all your love, for showing me Venice (and letting me get lost there), for laughing at me when I pronounce this invented "E" at the beginning of the English words, and for all our parties together. I still have to kick your ass with my black belt Karate skills. Ti voglio bene caro!

To all of you, as my favorite movie says, "You got a friend in me".

I would like to express my gratitude to someone who has been a pillar in my life in Switzerland. Thank you, Pablito! I will always be grateful to my uncle Ferminator who gave me your contact to start there. Thank you for welcoming me to your place like if I were part of your family. You are part of mine now. Thanks for giving me great life advice, for pushing us to do things during the tough Zurich winters. For your "Cocido Madrileño", your "Fabes", for the "siesta con babilla", our nights in Hive, Vagabundo, Zukunft and so many other places and memories. Te quiero Pablito!

I would also like to thank my friends from Spain. Juan, Miguel, Jorge, Antonio, Cascales, Javi, Matías, Chema y Gon (mis Vergadores); y Kq. Chemistry put us together and nothing will separate us. Thanks for being always there. It has been a tough period separated but I always felt you with me. I am very grateful to have such a bunch of friends like you.

And now, I would like to thank the person who has become my best friend and one of the most important persons in my life. But I want to do it in Spanish since he already has the knowledge to understand every word.

Gracias, Jacopo. No tengo palabras para agradecerte todo lo que has hecho por mí durante estos años. Empezamos como dos desconocidos, nos lanzamos a vivir juntos, ¡y menudo acierto! Hemos vivido muchos momentos juntos, momentos muy buenos, momentos bastante malos con una pandemia mundial de por medio, pero siempre juntos. Gracias por nuestras fiestas, por nuestras cenas (las que tú siempre hacías), por nuestras charlas sobre cualquier tema, por sacarme de casa después de toda la noche bailando en Hive o Zukunft, por el pesto y las galletas "senza lattosio" de tu nonna, el buen parmigiano y el buen salame, por reírte de mí, pero también conmigo, por calmar mi ira y compartir mis lágrimas, por tantos abrazos, por hacerme sentir como en casa fuera de casa y por muchas otras cosas más. Ahora que esta relación se ha forjado, no dejemos que se pierda nunca. Para mí no eres solo mi mejor amigo, eres parte de mi familia, eres un hermano. Gracias siempre. ¡Te quiero muchísimo!

To my family, and I will do it in Spanish again.

Gracias a toda mi familia, mi padre, mi madre, mi hermana, mis abuelas, que, aunque no saben lo que hago sé que están orgullosas de mí, y a mis abuelos que ya no están, pero desde donde quiera que estén sé que también estarán muy orgullosos. Soy el primer graduado, el primer máster y, con suerte, el primer doctor de una familia humilde que me ha demostrado siempre que con esfuerzo y constancia todo se puede conseguir. Han sido más de tres años muy duros, separado de todos vosotros, en los que he aprendido que necesito teneros cerca siempre. ¡A todos vosotros, infinitas gracias!

Gracias, mamá y papá, por habérmelo dado todo aun no teniendo nada, gracias por todo vuestro esfuerzo a lo largo de toda mi vida para darme la educación que vosotros no pudisteis tener. Gracias por cuidarme desde la distancia, gracias por darme siempre buenos consejos, gracias por darme la vida, gracias por ser mis padres; porque no puedo estar más orgulloso de vosotros. ¡Os quiero con toda mi alma!

Mi enana, mi pequeña revolucionaria comunista. Gracias por ser mi hermana, lloré tanto por no tener un hermano o hermana, luego lloré porque tus padres "ya no me querían"; y ahora lloro porque sé que eres lo mejor que tengo en esta vida. Juntos podemos con todo, ya lo sabes. Por nuestras conversaciones interminables sobre cualquier tema, por haberte convertido en un ejemplo de mujer, persona y profesional; porque tú siempre me has tenido a mí como ejemplo de hermano, pero yo te tengo a ti como ejemplo de superación y logro. ¡Te quiero hasta el infinito y más allá!

Y las últimas líneas van para ti, Irene. No tengo palabras suficientes para agradecerte todo lo que has hecho por mí durante este tiempo. Gracias por acompañarme y apoyarme en este duro viaje, por tus consejos y tu paciencia, por no dejarme decaer en los momentos más difíciles, por nuestros viajes alrededor de Suiza (aunque aún nos quedan cosas por ver) y alrededor del mundo (¡y los que nos quedan!). Gracias por sacarme de mi zona de confort y por cuestionar todo lo que digo, aunque lo haga con una seguridad pasmosa. Has hecho de mí una persona más fuerte, y lo haces cada día. Hemos atravesado momentos duros, con una pandemia mundial de por medio, pero hemos conseguido mantenernos vivos y seguir siempre juntos. Ahora es nuestro momento; de vivir juntos, de crecer juntos y de seguir hacia delante siempre. ¡Te quiero muchísimo!

9. Curriculum Vitae

ADRIÁN GIRONDA MARTÍNEZ

PERSONAL INFORMATION

10/01/1990 (Madrid).
Madrid, Spain.
+34 63 553 60 85
adrian.girondamartinez@gmail.com
es.linkedin.com/pub/adrián-gironda-martínez/a6/323/1aa/

PhD student in Biochemistry and Molecular Biology, Master's degree in Drug R&D and Bachelor's degree in Chemistry.
I am fully committed to developing new drugs that could potentially improve the life of people. I believe that new drug discovery technologies will help the scientific community to better understand the biological processes at the disease level and will improve the outcome of drug discovery programs. I consider myself as an interdisciplinary scientist, with deep knowledge in organic chemistry, medicinal chemistry, display technologies, and basic knowledge of biology. I am a very active and dynamic person; I love to propose and develop my own ideas.

EDUCATION

Jun 2018 – **Industrial PhD student in biochemistry and molecular biology.**
Sep 2021   University of Siena. Research conducted at Philochem AG. Zurich, Switzerland.
Supervised by Prof. Dario Neri.
Due for submission December 2021. Due for defense March 2022.

Thesis title: "DNA-Encoded Chemical Libraries: Advances and Applications to Drug Difficult Targets".

Design and synthesis of DNA-Encoded Libraries (DELs) for screening against difficult therapeutic targets.
Optimization and implementation of new DNA-compatible reactions for the synthesis of novel DELs.
Validation and optimization of ligands found during DEL screening campaigns. In particular, ligands for Interleukin-2 (IL2).

Sep 2014 – **Master's degree in drug research and development.**
Jun 2016   Autónoma University of Madrid, Teófilo Hernando Institute and Esame foundation. Madrid, Spain.

Sep 2008 – **Bachelor's degree in chemistry.**
May 2014   Autónoma University of Madrid.
Thesis' research conducted at the Medicinal Chemistry Institute (IQM, CSIC). Madrid, Spain.
Bachelor's thesis title: "Design and Synthesis of new Indazol-3-ol derivatives as potential drugs for Alzheimer's disease".

RESEARCH EXPERIENCE

Jun 2018 – **Research associate/PhD student (DNA-Encoded Libraries).**
Sep 2021 Philochem AG. Zurich, Switzerland.

I was involved in different internal projects and strategic collaborations with other pharmaceutical companies. Activities on DEL screening campaigns, and resynthesis and validation of hits identified from those screenings.

Dec 2017 – **Research associate (DNA-Encoded Libraries).**
May 2018 NovAliX (Insourcing at Eli Lilly and Company). Madrid, Spain.

As a research associate my main focus was the production of DELs. As an experienced researcher in the DEL field I was responsible of teaching other scientists from NovAliX to work on it.

Sep 2015 – **Junior research associate in medicinal chemistry (DNA-Encoded**
Sep 2017 **Libraries).**
Eli Lilly and Company. Madrid, Spain.

During the two years I spent at Eli Lilly I learnt how to work on DNA-Encoded Libraries. Mainly focused on validation of building blocks for DELs construction, optimization of new DNA-compatible reactions, and design and synthesis of new DELs.

Jul 2012 – **Bachelor's internship.**
Aug 2012 Medicinal Chemistry Institute (IQM, CSIC). Madrid, Spain.

Two months non-mandatory internship at the IQM. I had the opportunity to develop my skills as organic/medicinal chemist. I performed the synthesis of new series of compounds, purification and characterization using different analytical techniques.

OTHER WORK EXPERIENCE

May 2015 – **Trainee at quality assurance department.**
Sep 2015 Toll Pharma. Madrid, Spain.

Jun 2007 – **Shop assistant.**
May 2015 Zara Spain (Inditex Group). Madrid, Spain.

Intermittent **Private tutor.**
jobs Chemistry, Physics, Maths and Biology. Madrid, Spain.

COMPLEMENTARY INFORMATION

- **Postgraduate course in medicinal chemistry.** Medicinal Chemistry Institute (IQM, CSIC) Total of 40 hours. 2014.
- **Course in "Web Of Knowledge, Advanced level".** Spanish Foundation for Science and Technology (FECYT). Medicinal Chemistry Institute (IQM, CSIC). 2013.

LANGUAGES

- **English.** Full professional proficiency.
- **French.** Elementary proficency.
- **Spanish.** Native speaker.

INFORMATICS

- Office package, internet environment, software related with scientific environment (GraphPad Prism, bkchem, ChemOffice, TIBCO Spotfire, Agilent Softwares, Tecan softwares).
- Data bases. Reaxys, SciFinder, PubMed, WOK.

PUBLICATIONS

- **Gironda-Martínez, A.**, Gorre, E. M. D., Prati, L., Gosalbes, J-F., Dakhel, S., Cazzamalli, S., Samain, F., Donckele, E. J. and Neri, D. Identification and Validation of New Interleukin-2 Ligands Using DNA-Encoded Libraries. *J. Med. Chem.* **2021**, *64*, 17496–17510.
- **Gironda-Martínez, A.**, Donckele, E., Samain, F. and Neri, D. DNA-Encoded Chemical Libraries: A Comprehensive Review with Successful Stories and Future Challenges. *ACS Pharmacol. Transl. Sci.* **2021**, *4*, 1265–1279**.**
- Priego, J., de Pedro Beato, E., Benavides, J., **Gironda-Martínez, A.**, González, F., Blas, J., Martín-Ortega, M. D., Rama-Garda, R., Ezquerra, J., Toledo, M. A. and Torrado, A. On-DNA Palladium-Catalyzed Hydrogenation-like Reaction Suitable for DNA-Encoded Library Synthesis. *Bioconjugate Chem.* **2021**, *32*, 88–93.
- Sannino, A., **Gironda-Martínez, A.**, Gorre, E. M. D., Prati, L., Piazzi, J., Scheuermann, J., Neri, D., Donckele, E. J. and Samain, F. Critical Evaluation of Photo-cross-linking Parameters for the Implementation of Efficient DNA-Encoded Chemical Library Selections. *ACS Comb. Sci.* **2020**, *22*, 204–212.
- **Gironda-Martínez, A.**, Neri, D., Samain, F. and Donckele, E. J. DNA-Compatible Diazo-Transfer Reaction in Aqueous Media Suitable for DNA-Encoded Chemical Library Synthesis. *Org. Lett.* **2019**, *21*, 9555–9558. **Publication highlighted in Synfacts.**
- de Pedro Beato, E., Priego, J., **Gironda-Martínez, A.**, González, F., Benavides, J., Blas, J., Martín-Ortega, M. D., Toledo, M. A., Ezquerra, J. and Torrado, A. Mild and Efficient Palladium-Mediated C-N Cross-Coupling Reaction between DNA-Conjugated Aryl Bromides and Aromatic Amines. *ACS Comb. Sci.* **2019**, *21*, 69–74.

OTHER SCIENTIFIC CONTRIBUTIONS

- Gironda-Martínez, A., Samain, F., Gorre, E. M. D., Millul, J. and Donckele, E. J. Nucleic Acid Encoded Chemical Libraries. International Publication Number **WO 2020/128064 A1.** June **2020.**
- Oral presentation at the VII Young Researchers Symposium of the Spanish Society of Medicinal Chemistry (SEQT). "The power of big numbers: DNA-Encoded Libraries as a powerful technology in drug discovery". June **2021.**
- Poster presentation at the 9th International Symposium on DNA-Encoded Chemical Libraries. Gironda-Martínez, A., Gorre, E. M. D., Hodžić, A., Bigatti, M., Donckele, E. J., Samain, F., Scheuermann, J. and Neri, D. Encoded Self-Assembling Chemical (ESAC 2+1) Libraries: Expanding the Scope of ESAC Technology. September **2019.**

REFERENCES

- Dario Neri (Professor Department of Chemistry and Applied Biosciences at ETH Zurich; CEO, CSO and President of Scientific Advisory Board of Philogen S.p.A.). dario.neri@pharma.ethz.ch
- Etienne J. Donckele (Senior Scientist in Medicinal Chemistry at Monte Rosa Therapeutics). edonckele@monterosatx.com
- Florent Samain. (Former Head of DNA-Encoded Libraries at Philochem AG). florent@samain.com
- Jesús Ezquerra Carrera. (Retired from Eli Lilly and Company). jezquerra59@gmail.com
- María Alicia Torrado Varela (Principal Research Scientist at Eli Lilly and Company). torrado_alicia@lilly.com